TRW Document No. 2291-6005-RU-00

CR 137504

Systems Design Study of the Pioneer Venus Spacecraft

Final Study Report

Volume I. Technical Analyses and Tradeoffs Sections 1-4 (Part 1 of 4)

29 July 1973

Contract No. NAS2-7249

Prepared for

AMES RESEARCH CENTER
NATIONAL AERONAUTICS AND SPACE ADMINISTRATION

TRW SYSTEMS GROUP

MARTIN MARIETTA

PIONEER VENUS STUDY BOOKMARK

SUBJECT LOCATOR FOR VOLUME 1. TECHNICAL ANALYSES AND TRADEOFFS

SUBJECT	VOLUME 1 LOCATION SECTION	VOLUME 1 LOCATION (PART)	APPENDICES LOCATION (PART)
INTRODUCTION	1	1 OF 4	
SUMMARY	2	1 OF 4	
SCIENCE ANALYSIS AND EVALUATION	3	1 OF 4	1 OF 3
MISSION ANALYSIS AND DESIGN	4	1 OF 4	
SYSTEM CONFIGURATION CONCEPTS AND TRADEOFFS	5	2 OF 4	
SPACECRAFT SYSTEM DEFINITION	6	2 OF 4	1 OF 3
PROBE SUBSYSTEM DEFINITION	7	3 OF 4	2 OF 3
PROBE BUS AND ORBITER SUBSYSTEM DEFINITION AND TRADEOFFS	8	4 OF 4	3 OF 3
NASA/ESRO ORBITER INTERFACE	9	4 OF 4	3 OF 3
MISSION OPERATIONS AND FLIGHT SUPPORT	10	4 OF 4	3 OF 3
LAUNCH VEHICLE-RELATED COST REDUCTIONS	11	4 OF 4	3 OF 3
LONG LEAD ITEMS AND CRITICAL AREAS	12	4 OF 4	

PIONEER VENUS STUDY BOOKMARK

CONFIGURATION SYMBOLS

A/C III A/C IV T/D III	PROBE BUS
A/C III A/C IV T/D III	ORBITER FIXED DISH ANTENNA
A/C III A/C IV T/D III	ORBITER DESPUN REFLECTOR FRANKLIN ARRAY
12 W A/C III 12 W T/D III	ORBITER FANSCAN FRANKLIN ARRAY–12 ω TRANSMITTER POWER
31 W A/C III 31 W T/D III	ORBITER FANSCAN FRANKLIN ARRAY–31 ω TRANSMITTER POWER
A/C III A/C IV T/D III	LARGE PROBE
A/C III A/C IV T/D III	SMALL PROBE

LAUNCH VEHICLES

- A/C – ATLAS/CENTAUR
- T/D – THOR/DELTA

SCIENCE VERSION

- III – DEFINED IN NASA/AMES LETTER 2 NOVEMBER 1972
- IV – DEFINED IN NASA/AMES LETTER 13 APRIL 1973

TRW SYSTEMS GROUP

MARTIN MARIETTA

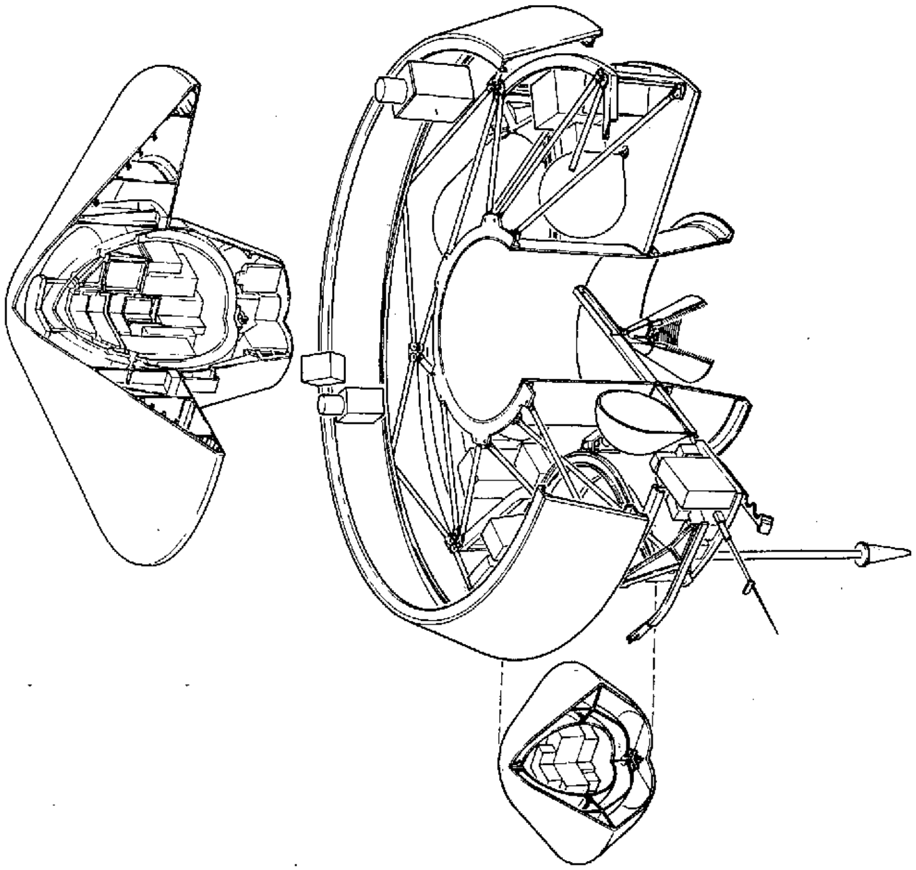

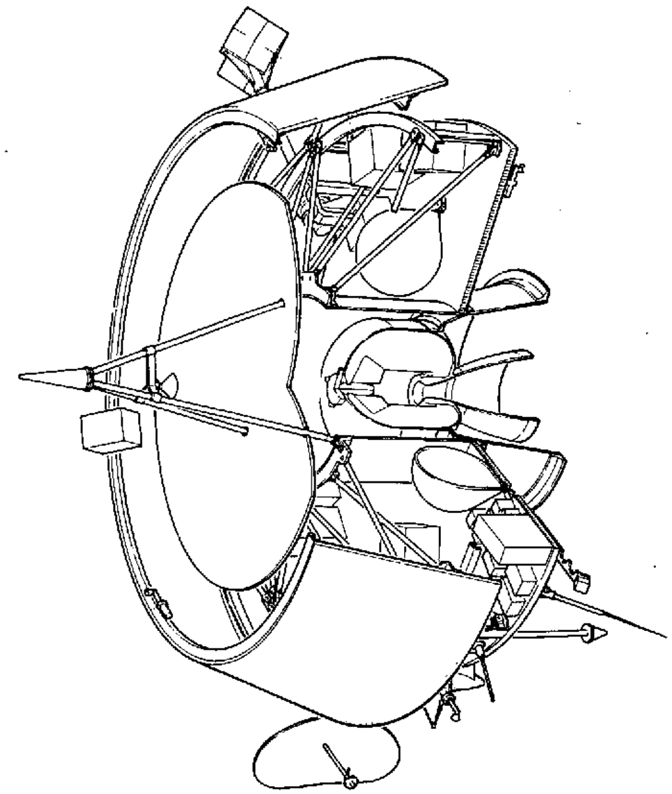

LIST OF VOLUMES

VOLUME I. TECHNICAL ANALYSES AND TRADEOFFS

SECTIONS 1-4 (PART 1 OF 4)

1. Introduction
2. Summary
3. Science Analysis and Evaluation
4. Mission Analysis and Design

VOLUME I. TECHNICAL ANALYSES AND TRADEOFFS

SECTIONS 5-6 (PART 2 OF 4)

5. System Configuration Concepts and Tradeoffs
6. Spacecraft System Definition

VOLUME I. TECHNICAL ANALYSES AND TRADEOFFS

SECTION 7 (PART 3 OF 4)

7. Probe Subsystem Definition

VOLUME I. TECHNICAL ANALYSES AND TRADEOFFS

SECTIONS 8-12 (PART 4 OF 4)

8. Probe Bus and Orbiter Subsystem Definition and Tradeoffs
9. NASA/ESRO Orbiter Interface
10. Mission Operations and Flight Support
11. Launch Vehicle-Related Cost Reductions
12. Long Lead Items and Critical Areas

VOLUME I APPENDICES

SECTIONS 3-6 (PART 1 OF 3)

VOLUME I APPENDICES

SECTION 7 (PART 2 OF 3)

VOLUME I APPENDICES

SECTIONS 8-11 (PART 3 OF 3)

VOLUME II. PRELIMINARY PROGRAM DEVELOPMENT PLAN

VOLUME III. SPECIFICATIONS

CR 137504

[redacted]
TRW Document No. 2291-6005-RU-00

Systems Design Study of the Pioneer Venus Spacecraft

Final Study Report

Volume I. Technical Analyses and Tradeoffs Sections 1-4 (Part 1 of 4)

29 July 1973

Contract No. NAS2-7249

Prepared for

AMES RESEARCH CENTER
NATIONAL AERONAUTICS AND SPACE ADMINISTRATION

TRW SYSTEMS GROUP

MARTIN MARIETTA

CONTENTS

	Page
1. INTRODUCTION	1-1
2. SUMMARY	2-1
2.1 Design	2-8
2.2 Major Tradeoffs: Probe Bus and Orbiter	2-23
2.3 Major Tradeoffs: Large and Small Probes	2-27
2.4 Atlas/Centaur Versus Thor/Delta	2-30
2.5 NASA/ESRO Orbiter Interface	2-32
2.6 Development Costs	2-36
3. SCIENCE ANALYSIS AND EVALUATION	3.1-1
3.1 Probe Science, Atlas/Centaur	3.1-1
3.1.1 Science Requirements and Impact on Mission and System Design	3.1-1
3.1.1.1 Science Objectives and Guidelines	3.1-1
3.1.1.2 Probe Targeting Guidelines and Tradeoffs	3.1-6
3.1.1.3 Entry Measurement Requirement and Tradeoffs	3.1-10
3.1.1.4 Descent Measurement Requirements and Trades	3.1-14
3.1.2 Instrument Accommodation Studies	3.1-24
3.1.2.1 Large Probe Instrument Accommodation Concepts	3.1-25
3.1.2.2 Other Candidate Instrument Accommodation	3.1-41
3.1.2.3 Small Probe Instrument Accommodation Concepts	3.1-46
3.1.2.4 Other Candidate Instrument Accommodation	3.1-56
3.1.2.5 Instrument Accommodation Studies	3.1-58
3.1.2.6 Payload Conflicts and Problem Areas	3.1-71
References	3.1-89
3.2 Probe Science, Thor/Delta	3.2-1
3.2.1 Science Requirements and Impact on Mission and System Design	3.2-1
3.2.1.1 Probe Targeting Guidelines and Mission Trades, 1977	3.2-1
3.2.1.2 Entry Measurement Requirements and Trades, Thor/Delta	3.2-4
3.2.1.3 Descent Measurement Requirements and Trades, Thor/Delta	3.2-8

CONTENTS (Continued)

		Page
3.2.2	Science Instrument Accommodation Studies	3.2-16
3.2.2.1	Large Probe Instrument Accommodation Concepts	3.2-16
3.2.2.2	Small Probe Instrument Accommodation Concepts	3.2-27
3.2.2.3	Other Candidate Instrument Accommodations	3.2-32
3.2.2.4	Payload Conflicts and Problem Areas	3.2-35
3.2.2.5	Engineering Experiments to Improve Future Probe Design	3.2-39
3.3	Probe Bus Science	3.3-1
3.3.1	Science-Related System Requirements Analysis	3.3-2
3.3.1.1	Target Considerations	3.3-2
3.3.1.2	Targeting Update for 1978 Probe Mission	3.3-4
3.3.1.3	Spin Axis Orientation	3.3-5
3.3.1.4	Demise of the Bus	3.3-6
3.3.1.5	Probe Bus Measurement Resolution for the 1977 Probe Mission	3.3-6
3.3.1.6	Probe Bus Measurement Resolution for the 1978 Probe Mission and New Atlas/Centaur Science Payload Version IV	3.3-7
3.3.1.7	Spacecraft Differential Charging	3.3-8
3.3.1.8	Considerations to Minimize Instrument Contamination	3.3-20
3.3.2	Probe Bus Instrument Interfaces	3.3.28
3.3.2.1	Summary of Preferred Science Accommodations for New Atlas/Centaur Version IV Science Payload	3.3-28
3.3.2.2	Details of Science Requirements and Accommodations	3.3-33
	References	3.3-66
3.4	Orbiter Science, Atlas/Centaur and Thor/Delta	3.4-1
3.4.1	Science-Related System Requirements Analysis	3.4-2
3.4.1.1	Orbit and Spin Axis Orientation	3.4-2
3.4.1.2	Gimballing of Scientific Instruments	3.4-23
3.4.1.3	Spacecraft Differential Charging	3.4-24
3.4.1.4	Considerations to Minimize Instrument Contamination	3.4-25

CONTENTS (Continued)

Page

3.4.2 Orbiter Instrument Interfaces 3.4-26

3.4.2.1 Summary of Preferred Science Accommodations for the Atlas/Centaur Orbiter, Version IV Science Payload 3.4-26
3.4.2.2 Mechanical, Thermal, and Power Requirements and Accommodations 3.4-31
3.4.2.3 Data Handling Requirements and Accommodations 3.4-44
3.4.2.4 Signals to Instruments Requirements and Accommodation for All Versions of the Science Payload 3.4-49
3.4.2.5 RF Science Requirements, Studies, and Accommodations 3.4-50
3.4.2.6 Spacecraft Charging Considerations, Version IV Science Payload 3.4-62
3.4.2.7 Magnetic Control 3.4-62

4. MISSION ANALYSIS AND DESIGN 4.1-1

4.1 Mission Analysis Summary 4.1-2

4.1.1 Probe Mission Profile 4.1-2

4.1.1.1 Launch Profile 4.1-2
4.1.1.2 Interplanetary Cruise 4.1-3
4.1.1.3 Probe Release and Planetary Approach 4.1-4
4.1.1.4 Probe Mission Entry and Descent Sequence 4.1-6
4.1.1.5 Probe Entry and Descent Profiles 4.1-8
4.1.1.6 Probe Mission Doppler Profiles 4.1-11

4.1.2 Orbiter Mission Profile 4.1-12

4.1.2.1 Accommodation with Probe Mission 4.1-12
4.1.2.2 Launch Profile 4.1-14
4.1.2.3 Interplanetary Phase 4.1-14
4.1.2.4 Orbit Insertion 4.1-16
4.1.2.5 Insertion Dispersions and Initial Trim 4.1-16
4.1.2.6 Orbiter Profiles 4.1-16

4.2 Mission Opportunity Analysis 4.2-1

4.2.1 Standard Ballistic Transfers 4.2-1

4.2.1.1 1978 Probe Mission 4.2-1
4.2.1.2 1978 Orbiter Mission 4.2-4
4.2.1.3 1977 Probe Mission 4.2-7

4.2.2 Nonstandard Transfers 4.2-8

CONTENTS (Continued)

		Page
4.2.3	Launch Vehicle Constraints and Flight Profiles	4.2-10
4.2.3.1	Thor/Delta	4.2-10
4.2.3.2	Atlas/Centaur	4.2-11
4.3	Probe Mission Studies	4.3-1
4.3.1	Launch, Cruise and Midcourse Corrections	4.3-1
4.3.1.1	Launch Analysis	4.3-1
4.3.1.2	Cruise Analysis	4.3-2
4.3.1.3	Midcourse Analysis	4.3-2
4.3.2	Probe Targeting and Separation Sequence	4.3-6
4.3.2.1	Probe Targeting for 1978	4.3-7
4.3.2.2	Sequential vs Simultaneous Release	4.3-9
4.3.2.3	Mission Implications	4.3-10
4.3.2.4	Bus Requirements	4.3-11
4.3.2.5	Small Probe Requirements	4.3-17
4.3.2.6	Tracking and Operational Considerations	4.3-20
4.3.3	Probe Entry Analyses	4.3-27
4.3.3.1	Peak Entry Deceleration, 1978 Mission	4.3-27
4.3.3.2	Entry Dynamics Analysis, 1978 Mission	4.3-28
4.3.3.3	Large Probe Parachute Deployment Conditions, 1978 Mission	4.3-31
4.3.3.4	Small Probe Descent Science Deployment, 1978 Mission	4.3-32
4.3.3.5	Entry Dispersion Analysis, 1978 Mission	4.3-34
4.3.3.6	Entry Ballistic Coefficient Range, 1977 Mission	4.3-34
4.3.3.7	Entry Flight Path Angle Implications 1977 Mission	4.3-35
4.3.3.8	Entry Dynamics Analysis, 1977 Mission	4.3-36
4.3.3.9	Large Probe Parachute Deployment, 1977 Mission	4.3-38
4.3.3.10	Small Probe Descent Science Deployment, 1977 Mission	4.3-39
4.3.3.11	Entry Dispersion Analysis, 1977 Mission	4.3-39
4.3.4	Probe Descent Analysis	4.3-41
4.3.4.1	Probe Weight Sensitivity	4.3-41
4.3.4.2	Descent Trajectory Sensitivity	4.3-43
4.3.4.3	Dynamic Response to Winds	4.3-44
4.3.4.4	Probe Descent Tracking	4.3-46

CONTENTS (Continued)

		Page
4.3.5	Probe Bus Targeting	4.3-51
4.3.5.1	1978 Bus Targeting	4.3-51
4.3.5.2	1977 Bus Targeting	4.3-53
4.3.6	Entry and Demise of the Probe Bus	4.3-54
4.3.6.1	Bus Aerodynamic Characteristics	4.3-55
4.3.6.2	Entry Trajectories	4.3-57
4.3.6.3	Aerodynamic Heating	4.3-59
4.3.6.4	Communications Blackout	4.3-63
4.3.6.5	Flow Regimes and Molecular Flux Identification	4.3-67
4.3.6.6	Altitude History of Bus Entry Phenomena	4.3-71
4.3.6.7	Entry Behavior of 1978 Atlas/ Centaur Probe Bus	4.3-73
4.4	Orbiter Mission Studies	4.4-1
4.4.1	Launch, Cruise, and Midcourse Corrections	4.4-1
4.4.1.1	Launch Analysis	4.4-1
4.4.1.2	Cruise Analysis	4.4-2
4.4.1.3	Midcourse Analysis	4.4-2
4.4.1.4	Approach Orbit Determination	4.4-7
4.4.2	Orbit Selection	4.4-9
4.4.2.1	Type I Versus Type II	4.4-9
4.4.2.2	Orbital Inclination	4.4-10
4.4.2.3	Orbit Periapsis	4.4-11
4.4.2.4	Orbit Period	4.4-12
4.4.3	Orbit Insertion Analysis	4.4-12
4.4.3.1	Normal Requirements	4.4-12
4.4.3.2	Arrival Condition Variations	4.4-13
4.4.3.3	Insertion Dispersions	4.4-13
4.4.4	Orbit Perturbations and Trim Periapsis Maintenance	4.4-15
4.4.4.1	Perturbative Forces	4.4-15
4.4.4.2	Periapsis Altitude Maintenance	4.4-16
4.4.4.3	Initial Orbit Trims	4.4-16
4.4.5	In-Orbit Tracking	4.4-17
4.4.5.1	Maneuver Implications	4.4-17
4.4.5.2	Celestial Mechanics Measurements	4.4-18
4.4.6	Mission Options	4.4-18
4.4.6.1	Drag Circularization	4.4-18
4.4.6.2	Station Synchronous Orbits	4.4-19
References		4.4-21

ILLUSTRATIONS

		Page
1-1	Definition of Configuration Symbols	1-3
2-1	Preferred Spacecraft Configurations	2-3
2-2	Preferred Probe Configurations	2-3
2-3	Probe Mission Profile	2-5
2-4	Orbiter Mission Profile	2-7
2-5	Key Design Concepts: Probe Bus	2-9
2-6	Key Large Probe Design Concepts	2-11
2-7	Key Small Probe Design Concepts	2-13
2-8	Key Design Concepts: Orbiter	2-15
2-9	Probe Bus and Orbiter Design Summary	2-17
2-10	Equipment Derivation and Commonality: Probe Bus and Orbiter	2-19
2-11	Equipment Derivation and Commonality: Probes	2-21
2-12	Large and Small Probe Design Summary	2-22
2-13	Configuration Options: Probe Bus and Orbiter	2-25
2-14	Major Tradeoffs: Large and Small Probes	2-29
2-15	Thor/Delta and Atlas/Centaur Tradeoffs	2-31
2-16	ESRO Hardware Participation	2-33
2-17	Preferred Prototype/Flight Integration Test and Launch Flow Diagrams	2-37
3-1	Venus Atmosphere Structure	3.1-3
3-2	SSG Recommended Probe Target Areas	3.1-7
3-3	Definition of Probe Entry Angle (γ) and Probe-Earth Communications Angle (θ)	3.1-7
3-4	Contours of Constant Entry Flight Path Angle (γ) and Communications Angles (θ) for 1978 Probe Mission	3.1-8
3-5	Large Probe Altitude Profile versus Time from 50 g Acceleration Level for $\gamma_E = -35^o$	3.1-12
3-6	Small Probe Altitude Profiles versus Time from 50 g Acceleration Level for $\gamma_E = -25^o$ (- -) and $\gamma_E = -60^o$ (——)	3.1-12
3-7	Baseline Large Probe Axial Acceleration Profile During Entry	3.1-13
3-8	Small Probe Altitude versus Entry Flight Path Angle and Time from 50 g Increasing	3.1-17

PRECEDING PAGE BLANK NOT FILMED

ILLUSTRATIONS (CONTINUED)

		Page
3-9	Small Probe Entry Angle Range and Deployment Conditions at Fixed Times after 50 g, Above 66 km	3.1-18
3-10A	Small Probe Version IV Science Data Requirements	3.1-18
3-10B	Baseline Small Probe Altitude Sampling Interval Profile Compared to Requirements	3.1-19
3-11	Large Probe Science Data Rate Requirements versus Ballistic Coefficients	3.1-20
3-12	Maximum Required Science Data Rates Below 44 km (at 29 km) Chute Release at 43 km	3.1-20
3-13	Large Probe Ballistic Coefficient Combinations for Various Descent Times Below 66 km and Formatting Efficiencies	3.1-21
3-14	Large Probe Descent Profiles Showing Alternative Gas Chromatograph Readout Schemes	3.1-22
3-15A	Large Probe Science Data Collection Rates Required to Meet Sampling Interval Requirements	3.1-23
3-15B	Baseline Large Probe Altitude Sampling Interval Profile Compared to Requirements	3.1-23
3-16	Equipment Ring Assembly Concept	3.1-25
3-17	Planetary Flux Radiometer Window	3.1-26
3-18	Single Window Solar Radiometer Configuration	3.1-28
3-19	Two Telescope Solar Radiometer	3.1-29
3-20	Solar Radiometer	3.1-30
3-21	Cloud Particle Size Analyzer	3.1-30
3-22	Mass Spectrometer Accommodation	3.1-31
3-23	Wind Altitude Radar Antenna and Pressure Inlet	3.1-33
3-24	Hygrometer Mounting	3.1-34
3-25	Gas Chromatograph Inlet Configuration	3.1-35
3-26	Plan View of Equipment Ring Assembly Showing Instrument Electrical Feedthroughs	3.1-39
3-27	Light Pipe to Solar Radiometer	3.1-40
3-28	X-Ray Fluorescence Experiment	3.1-42
3-29	Attenuated Total Reflectance Spectrometer Window Assembly	3.1-43
3-30	Aureole Detector Accommodation	3.1-44
3-31	Shock Layer Radiometer Accommodation	3.1-45

ILLUSTRATIONS (CONTINUED)

		Page
3-32	Battery and Thermal Control Weight Increases for Additional Science Data	3.1-46
3-33	Small Probe Temperature and Pressure Gauge Mechanisms	3.1-47
3-34	Dual Penetration Nephelometer Configuration	3.1-49
3-35	Concentric Window Nephelometer	3.1-50
3-36	Small Probe IR Flux Detector	3.1-52
3-37	General Arrangement of Small Probe	3.1-55
3-38	RF Altimeter Antenna	3.1-57
3-39	Window Configuration Concepts	3.1-59
3-40	Heat Transfer Tradeoffs of Venus Probe Windows	3.1-60
3-41	Conical Window Configuration	3.1-61
3-42	Thermal Test of Window Heating During Simulated Venus Descent	3.1-63
3-43	Window Joule Heating Approach	3.1-64
3-44	Thermoelectric Heater Concept	3.1-64
3-45	Chemical Window Heater	3.1-64
3-46	Removable Window (Pyrotechnic Shear Ring)	3.1-65
3-47	Removable Window (Phase Change Release)	3.1-65
3-48	Ballast Volume Inlet System	3.1-67
3-49	Proposed Pioneer Venus Mass Spectrometer Inlet	3.1-68
3-50	Schematic of Noble Gas Enriching Inlet	3.1-69
3-51	1977 Probe Mission Targeting Geometry	3.2-2
3-52	1977 Baseline Probe Mission Targeting Capability	3.2-2
3-53	Large Probe Entry Science Data Requirements	3.2-4
3-54	Small Probe Entry Science Data Requirements	3.2-6
3-55	Baseline Large Probe Entry Measurement Profile	3.2-6
3-56	Baseline Small Probe Entry Accelerometer Measurement Profiles	3.2-7
3-57	Number of Accelerometer Measurements per Pressure Scale Height During Entry for Baseline Thor/Delta Large Probe [γ_E = -37.5°, B_H = 70.7 kg/m^2 (0.45 slugs/ft^2)]	3.2-7
3-58	Number of Single Axis Accelerometer Measurements per Pressure Scale Height During Entry for Baseline Thor/Delta Small Probes [B_H = 141.4 kg/m^2 (0.9 slugs/ft^2)]	3.2-7

ILLUSTRATIONS (CONTINUED)

		Page
3-59	Altitude of Chute Deployment for Large Probe vs Entry Angle and Ballistic Coefficient Nominal $B_H = 78.5 \pm 7.85$ kg/m^2 [0.50 ($\pm$0.05) slug/ft^2]	3.2-8
3-60	Altitude of Descent Instrument Deployment for Small Proves vs Entry Angle and Ballistic Coefficient Nominal $B_H = 125.7$ ($\pm$12.6) kg/m^2 [0.80 ($\pm$0.08) slug/ft^2]	3.2-8
3-61	Total (Measured) Temperatures Compared to Ambient Temperature During High-Velocity Periods of Descent	3.2-9
3-62	Stagnation (Measured) Pressures Compared to Ambient Pressure During High Velocity Periods of Descent	3.2-9
3-63	Large Probe Descent Science Data Rate Requirements	3.2-10
3-64	Small Probe Descent Science Data Rate Requirements	3.2-10
3-65	Thor/Delta Bit Rate and Mass Trades	3.2-10
3-66	Descent Time Sensitivity to Chute Release Altitude and Lower Stage Ballistic Coefficient for 0.12 slug/sq ft Upper Stage	3.2-11
3-67	Large and Small Probe Baseline Altitude Resolutions During Descent	3.2-12
3-68	Mass Spectrometer Altitude Resolution	3.2-13
3-69	Cloud Particle Size Analyzer Measurement Sensitivity to Large Probe Ballistic Coefficients and Chute Release Altitudes	3.2-14
3-70	Wind Velocity Determination with DLBI Technique, 1977 Mission	3.2-15
3-71	Equipment Ring Assembly Concept	3.2-16
3-72	Optical Designs for Probe Penetrations	3.2-18
3-73	Nephelometer Accommodation	3.2-19
3-74	Cloud Particle Size Spectrometer	3.2-20
3-75	Aureole Extinction Detector Accommodation	3.2-21
3-76	Mass Spectrometer and Pressure Gauges Accommodation	3.2-22
3-77	Accelerometer Sensor and Electronics Locations	3.2-22
3-78	Shock Layer Radiometer Accommodation	3.2-23

ILLUSTRATIONS (CONTINUED)

		Page
3-79	Plan View of Equipment Ring Assembly Showing Instrument Electrical Feedthroughs	3.2-27
3-80	Small Probe Configuration for Thor/Delta Launch Vehicle	3.2-28
3-81	Upper Hemispher Cos θ Response Flux Detection for Solar Radiometer	3.2-33
3-82	Attenuated Total Reflectance Spectrometer Window Assembly Design Concept and Optical Configuration	3.2-33
3-83	1977 Probe Mission Bus Targeting	3.3-3
3-84	1978 Bus Targeting (Mercator Projection)	3.3-4
3-85	Time to Descend from 1000 km	3.3-5
3-86	1977 Probe Bus Measurement Resolution	3.3-7
3-87	1978 Mission and Version IV Payload Probe Measurement Resolution	3.3-8
3-88	Ratio of Saturation Current Densities to and from Surface versus Potential Function $[e\Phi/xT_e]$	3.3-13
3-89	Atlas/Centaur Probe Mission Nominal Science and Equipment Layout, Version IV Science Payload	3.3-30
3-90	Atlas/Centaur Probe Mission Science Equipment Layout with Other Candidate Instruments	3.3-31
3-91	Thor/Delta Probe Mission Science and Equipment Layout	3.3-36
3-92	Atlas/Centaur Probe Mission Science and Equipment Layout, Version III Science Payload	3.3-37
3-93	Baseline Probe Bus Capability for Additional Instruments	3.3-38
3-94	Atlas/Centaur Probe Mission Science and Equipment Layout (Including Other Candidate Instruments) Version III Science Payload	3.3-40
3-95	Science Instrument Requirements	3.3-45
3-96	Payload Capability of Baseline Bus	3.3-50
3-97	Magnetic Field of Spacecraft After 25×10^{-4} Tesla Perm	3.3-57
3-98	Magnetic Field of Spacecraft Post Deperm	3.3-57
3-99	Magnetic Field Due to Currents	3.3-57
3-100	Post-Launch Magnetic Field Due to Magnetized Material on Spacecraft	3.3-60
3-101	Angle of Attack	3.4-5

ILLUSTRATIONS (CONTINUED)

		Page
3-102	Spin View Planetary Considerations	3.4-6
3-103	Spin View Coverage	3.4-7
3-104	Spin View Range Considerations	3.4-8
3-105	Venus Aspect Angle	3.4-10
3-106	NVOP Latitude Coverage of Normal Limb Scan if Slit is Rotatable ±1.57 Radians (±90 Degrees) (1000 km and Lower)	3.4-11
3-107	Limb Scan Geometry	3.4-12
3-108	Angles for Normal Limb Scan (200 kilometers altitude)	3.4-13
3-109	Angles for Normal Limb Scan (600 kilometers altitude)	3.4-14
3-110	Angles for Normal Limb Scan (1000 kilometers altitude)	3.4-14
3-111	Maximum and Minimum Venus Aspect, Earth-Pointing Configuration (Type II, θ_{AIM} = 2.09 Rad (120 Deg))	3.4-15
3-112	Maximum and Minimum Venus Aspect Earth-Pointing Configuration (Type II, θ_{AIM} = 2.36 Rad (135 Deg), Inclination = 2.30 Rad (132 Deg) 8.84 Rad/48 Deg)	3.4-16
3-113	Slit Angle for Normal Limb Scan	3.4-17
3-114	Slit Angle for Normal Limb Scan	3.4-18
3-115	Slit Angle for Normal Limb Scan	3.4-19
3-116	Slit Angle for Normal Limb Scan	3.4-19
3-117	Slit Angle for Normal Limb Scan	3.4-19
3-118	Slit Angle for Normal Limb Scan	3.4-19
3-119	Science Interface Ram Gimbal Angles, Earth-Pointing Configuration	3.4-25
3-120	Gimbal Angles, Spin Axis Normal-to-Venus Orbit Plane	3.4-25
3-121	Atlas/Centaur Orbiter Instruments and Equipment, Version IV Science Payload	3.4-27
3-122	Atlas/Centaur Orbiter Instruments and Equipment (plus Other Candidate Instruments), Version IV Science Payload	3.4-28
3-123	Thor/Delta Orbiter, Version I Science Payload and Equipment Layout	3.4-33

ILLUSTRATIONS (CONTINUED)

		Page
3-124	Atlas/Centaur Orbiter, Version II Science Payload and Equipment Layout	3.4-34
3-125	Baseline Orbiter Capability for Additional Instruments	3.4-36
3-126	Atlas/Centaur Orbiter Equipment Layout (plus Other Candidate Instruments)	3.4-38
3-127	Orbiter Data Acquisition	3.4-45
3-128	Earth Occultation History	3.4-45
3-129	Basic Refracted Ray Tracing Program	3.4-52
3-130	Final Geometry of Ray Where θ is the Sum of the ΔV_i	3.4-54
3-131	α Measured in Earth-Venus-Spacecraft Plane	3.4-54
3-132	α Versus True Anomaly	3.4-55
3-133	γ Versus True Anomaly	3.4-55
3-134	Orbiter Occultation Experiments Refraction Tracking Angles	3.4-55
3-135	RF Attenuation Data (Insertion + 0 Days) from Dr. A. J. Kliore and Dr. G. Fjeldbo of JPL	3.4-55
3-136	RF Attenuation Data (Insertion + 35 Days) from Dr. A. J. Kliore and Dr. G. Fjeldbo of JPL	3.4-55
3-137	Transient Response of Pioneer 10 and 11 Power Control Unit	3.4-57
3-138	Mode 1 Transient Amplitude (Shunt to Discharge)	3.4-58
3-139	Radar Altimeter Electronics as Steady Load	3.4-58
3-140	Pioneers 10 and 11 Type PCU Response to Transients	3.4-59
3-141	Filter Circuit and Design Criteria	3.4-59
3-142	Filter Network Design Selection Delta V and Capacitance Versus Filter Weight	3.4-60

ILLUSTRATIONS

		Page
4-1	Probe Mission Departure Geometry	4. 1-3
4-2	Interplanetary Transfer	4. 1-3
4-3	Preferred Target Sites for 1978 Probe Mission	4. 1-4
4-4	Release Sequence and Approach Profile	4. 1-5
4-5	Probe Mission Entry and Descent Sequence	4. 1-7
4-6	Large Probe Entry Profile	4. 1-8
4-7	Large Probe Parachute Deployment and Aeroshell Release	4. 1-9
4-8	Aeroshell Release Dynamics	4. 1-10
4-9	Large Probe Descent Profile	4. 1-10
4-10	Small Probe Entry Profile ($25^{o}\gamma_{E}$)	4. 1-13
4-11	Small Probe Entry Profile ($60^{o}\gamma_{E}$)	4. 1-13
4-12	Small Probe Descent Profile, γ_E = -60 Degrees	4. 1-13
4-13	Large Probe Preentry Doppler Rates	4. 1-13
4-14	Large Probe Descent Doppler Rates	4. 1-13
4-15	Small Probe 3 Descent Doppler Rates	4. 1-13
4-16	Dual Mission Sequencing	4. 1-13
4-17	1978 Orbiter Type 2 Departure Geometry (May 26 Launch 14:15:00 GMT)	4. 1-14
4-18	Interplanetary Transfer	4. 1-15
4-19	Interplanetary Cruise Parameters	4. 1-15
4-20	Tracking Station Coverage for Orbital Mission	4. 1-15
4-21	Initial Orbit	4. 1-16
4-22	In-Orbit Cruise Geometry	4. 1-17
4-23	Earth-Venus Parameters During Orbit Phase	4. 1-19
4-24	Periapsis Altitude Profile	4. 1-19
4-25	Orbiter Attitude Profile	4. 1-19
4-26	Angle-of-Attack Profile	4. 1-19
4-27	Occulted Regions	4. 1-19
4-28	Occultation Duration	4. 1-19
4-29	Launch Performance for Thor/Delta and Atlas/Centaur Vehicles	4. 2-2
4-30	1978 Mission Contours	4. 2-2
4-31	1978 Mission Probe Targeting	4. 2-4

ILLUSTRATIONS (CONTINUED)

		Page
4-32	Operational Time Lines for Type I and Type II-E Options	4.2-6
4-33	1977 Mission Contours	4.2-7
4-34	1977 Mission Probe Targeting	4.2-8
4-35	Broken Plane Performance	4.2-9
4-36	1978 Looper Mission	4.2-10
4-37	Launch Windows and Parking Orbit Coast Times	4.3-2
4-38	Injection Locations for Type II Window	4.3-3
4-39	Time History of Earth Aspect and Altitude for Near-Earth Trajectory	4.3-3
4-40	1978 Probe Mission	4.3-3
4-41	1978 First Midcourse Requirements	4.3-5
4-42	1978 Probe Mission Trajecting Geometry	4.3-7
4-43	1978 Candidate Target Site Sets	4.3-8
4-44	Simultaneous Release Parametrics	4.3-10
4-45	Solar Aspect Angles at Entry at Zero Angle of Attack	4.3-20
4-46	Solar Aspect Angles During Coast	4.3-20
4-47	Solar Pressure Precession	4.3-20
4-48	Earth Aspect Angles During Coast	4.3-20
4-49	Tracking Characteristics, 1978 Probe Mission	4.3-22
4-50	1977 Reference Probe Mission	4.3-25
4-51	Tracking Characteristics of 1977 Mission	4.3-27
4-52	Peak Entry Deceleration, 1978 Mission	4.3-27
4-53	Atlas/Centaur Small Probe Total Angle of Attack Envelope	4.3-28
4-54	Atlas/Centaur Small Probe Lateral Acceleration Envelopes	4.3-29
4-55	Atlas/Centaur Small Probe Roll Rate Variations	4.3-30
4-56	Atlas/Centaur Large Probe Entry Dynamics Summary	4.3-31
4-57	Large Probe Drogue Parachute Deployment Condition	4.3-32
4-58	Small Probe Science Deployment Conditions	4.3-33
4-59	Peak Entry Deceleration-1977 Mission	4.3-35
4-60	Peak-Stagnation Pressure	4.3-36
4-61	Altitude at Mach 1	4.3-36

ILLUSTRATIONS (Continued)

		Page
4-62	Small Probe Entry Dynamics	4.3-37
4-63	Small Probe Entry Dynamic Environment	4.3-37
4-64	Small Probe Entry Spin Rate Dynamics	4.3-38
4-65	Large Probe Parachute Deployment	4.3-38
4-66	Small Probe Science Deployment	4.3-39
4-67	Large Probe Total Descent Time	4.3-42
4-68	Atlas/Centaur Large Probe Thermal Control Weight Sensitivity	4.3-42
4-69	Weight Sensitivity to B_{CH}	4.3-42
4-70	Weight Sensitivity to B_{DC}	4.3-42
4-71	Small Probe Weight Sensitivity	4.3-43
4-72	Parachute Response to Wind Shear	4.3-44
4-73	Descent Capsule Response to Wind Shear	4.3-44
4-74	Small Probe Response to Wind Shear	4.3-45
4-75	Large and Small Probe Attitude Variations to 0.05 m/s/m Wind Shear	4.3-46
4-76	Probe Descent Tracking with DLPI	4.3-48
4-77	1978 Bus Targeting (Mercator Projections)	4.3-52
4-78	Gamma versus B-Magnitude	4.3-53
4-79	1977 Bus Targeting	4.3-53
4-80	1977 Thor/Delta Probe Mission Bus Entry Configuration	4.3-55
4-81	Free Molecular Flow Aerodynamic Coefficients of Thor/Delta Probe Bus	4.3-57
4-82	Thor/Delta Probe Bus Flight Path Angle Variation	4.3-58
4-83	Thor/Delta Probe Bus Deceleration During Entry	4.3-58
4-84	Thor/Delta Probe Bus Angle of Attack Divergence During Entry (Magnetometer Boom Extended)	4.3-60
4-85	Aerodynamic Heating of Thor/Delta Probe Bus	4.3-61
4-86	Electron Density in Stagnation Region Behind Normal Shock and in Wake After Expansion to Ambient Pressure	4.3-65
4-87	Plasma Attenuation of Electromagnetic Wave Propagation	4.3-65
4-88	Pioneer Venus Bus Entry: Identification of Molecular Flux to Body Stagnation Point	4.3-69
4-89	Distribution of Molecular Fluxes Across Face of Body	4.3-71

ILLUSTRATIONS (Continued)

		Page
4-90	Altitude History of Bus Entry Phenomena	4.3-72
4-91	Free Molecular Flow Aerodynamic Coefficients of Atlas/Centaur Probe Bus	4.3-74
4-92	Launch Windows and Parking Orbit Coast Times	4.4-1
4-93	Ground Locations of Injection Points	4.4-3
4-94	Time History of Earth Aspect and Attitude for Near-Earth Trajectory	4.4-3
4-95	TransVenus Cruise Geometry, 1978 Type II Orbiter	4.4-3
4-96	1978 Type II Orbiter First Midcourse Requirements	4.4-4
4-97	1978 Type I Orbiter First Midcourse Requirements	4.4-4
4-98	First Midcourse Requirement for Thor/Delta	4.4-5
4-99	Geocentric Declinations of Approach	4.4-7
4-100	Approach Orbit Determination	4.4-9
4-101	Comparison of Type I and II Orbit Geometries	4.4-10
4-102	θ_{AIM} versus Inclination	4.4-10
4-103	Orbit Inclination Sensitivities	4.4-11
4-104	Periapsis Altitude Selection	4.4-12
4-105	Orbit Period Selection	4.4-12
4-106	Nominal Insertion Requirements	4.4-13
4-107	Arrival Condition Variations	4.4-13
4-108	Insertion Dispersion Sensitivities	4.4-14
4-109	Periapsis Altitude Control	4.4-16
4-110	In-Orbit Tracking Effectiveness	4.4-18
4-111	Evolving Solution for J_2	4.4-18
4-112	Drage Circularization	4.4-19
4-113	Station-Synchronous Orbits	4.4-19

ACRONYMS AND ABBREVIATIONS

A	ampere analog
abA	abampere
AC	alternating current
A/C	Atlas/Centaur
ADA	avalanche diode amplifier
ADCS	attitude determination and control subsystem
ADPE	automatic data processing equipment
AEHS	advanced entry heating simulator
AEO	aureole/extinction detector
AEDC	Arnold Engineering Development Corporation
AF	audio frequency
AGC	automatic gain control
AgCd	silver-cadmium
AgO	silver oxide
AgZn	silver zinc
ALU	authorized limited usage
AM	amplitude modulation
a.m.	ante meridian
AMP	amplifier
APM	assistant project manager
ARC	Ames Research Center
ARO	after receipt of order
ASK	amplitude shift key
at. wt	atomic weight
ATM	atmosphere
ATRS	attenuated total refractance spectrometer
AU	astronomical unit
AWG	American wire gauge
AWGN	additive white gaussian noise
B	bilevel
B	bus (probe bus)
BED	bus entry degradation

BER	bit error rate
BLIMP	boundary layer integral matrix procedure
BPIS	bus-probe interface simulator
BPL	bandpass limiter
BPN	boron potassium nitrate
bps	bits per second
BTU	British thermal unit
C	Canberra tracking station – NASA DSN
CADM	configuration administration and data management
C&CO	calibration and checkout
CCU	central control unit
CDU	command distribution unit
CEA	control electronics assembly
CFA	crossed field amplifier
cg	centigram
c.g.	center of gravity
CIA	counting/integration assembly
CKAFS	Cape Kennedy Air Force Station
cm	centimeter
c.m.	center of mass
C/M	current monitor
CMD	command
CMO	configuration management office
C-MOS	complementary metal oxide silicon
CMS	configuration management system
const	constant construction
COSMOS	complementary metal oxide silicon
c.p.	center of pressure
CPSA	cloud particle size analyzer
CPSS	cloud particle size spectrometer

CPU	central processing unit
CRT	cathode ray tube
CSU	Colorado State University
CTRF	central transformer rectifier filter
D	digital
DACS	data and command subsystem
DCE	despin control electronics
DDA	despin drive assembly
DDE	despin drive electronics
DDU	digital decoder unit
DDULBI	doubly differenced very long baseline interferometry
DEA	despin electronics assembly
DEHP	di-2-ethylhexyl phthalate
DFG	data format generator
DGB	disk gap band
DHC	data handling and command
DIO	direct input/output
DIOC	direct input/output channel
DIP	dual in-line package
DISS REG	dissipative regulator
DLA	declination of the launch azimuth
DLBI	doubly differenced very long baseline interferometry
DMA	despin mechanical assembly
DOF	degree of freedom
DR	design review
DSCS II	Defense System Communications Satellite II
DSIF	Deep Space Instrumentation Facility
DSL	duration and steering logic
DSN	NASA Deep Space Network
DSP	Defense Support Program
DSU	digital storage unit
DTC	design to cost
DTM	decelerator test model

ACRONYMS AND ABBREVIATIONS (CONTINUED)

DTP	descent timer/programmer
DTU	digital telemetry unit
DVU	design verification unit
E	encounter entry
EDA	electronically despun antenna
EGSE	electrical ground support equipment
EIRP	effective isotropic radiated power
EMC	electromagnetic compatibility
EMI	electromagnetic interference
EO	engineering order
EOF	end of frame
EOM	end of mission
EP	earth pointer
ESA	elastomeric silicone ablator
ESLE	equivalent station error level
ESRO	European Space Research Organization
ETM	electrical test model
ETR	Eastern Test Range
EXP	experiment
FFT	fast Fourier transform
FIPP	fabrication/inspection process procedure
FMEA	failure mode and effects analysis
FOV	field of view
FP	fixed price frame pulse (telemetry)
FS	federal stock
FSK	frequency shift keying
FTA	fixed time of arrival

G	Goldstone Tracking Station - NASA DSN gravitational acceleration
g	gravity
G&A	general and administrative
GCC	ground control console
GFE	government furnished equipment
GHE	ground handling equipment
GMT	Greenwich mean time
GSE	ground support equipment
GSFC	Goddard Space Flight Center
H	Haystack Tracking Station - NASA DSN
HFFB	Ames Hypersonic Free Flight Ballistic Range
HPBW	half-power beamwidth
htr	heater
HTT	heat transfer tunnel
I	current
IA	inverter assembly
IC	integrated circuit
ICD	interface control document
IEEE	Institute of Electrical and Electronics Engineering
IFC	interface control document
IFJ	in-flight jumper
IMP	interplanetary monitoring platform
I/O	input/output
IOP	input/output processor
IR	infrared
IRAD	independent research and development
IRIS	infrared interferometer spectrometer
IST	integrated system test
I&T	integration and test
I-V	current-voltage

ACRONYMS AND ABBREVIATIONS (CONTINUED)

JPL	Jet Propulsion Laboratory
KSC	Kennedy Space Center
L	launch
LD/AD	launch date/arrival date
LP	large probe
LPM	lines per minute
LPTTL MSI	low power transistor-transistor logic medium scale integration
LRC	Langley Research Center
M	Madrid tracking station - NASA DSN
MAG	magnetometer
max	maximum
MEOP	maximum expected operating pressure
MFSK	M'ary frequency shift keying
MGSE	mechanical ground support equipment
MH	mechanical handling
MIC	microwave integrated circuit
min	minimum
MJS	Mariner Jupiter-Saturn
MMBPS	multimission bipropellant propulsion subsystem
MMC	Martin Marietta Corporation
MN	Mach number
mod	modulation
MOI	moment of inertia
MOS LSI	metal over silicone large scale integration
MP	maximum power
MSFC	Marshall Space Flight Center
MPSK	M'ary phase shift keying
MSI	medium scale integration
MUX	multiplexer
MVM	Mariner Venus-Mars

NAD	Naval Ammunition Depot, Crane, Indiana
N/A	not available
NiCd	nickel cadmium
NM/IM	neutral mass spectrometer and ion mass spectrometer
NRZ	non-return to zero
NVOP	normal to Venus orbital plane
OEM	other equipment manufacturers
OGO	Orbiting Geophysical Observatory
OIM	orbit insertion motor
P	power
PAM	pulse amplitude modulation
PC	printed circuit
PCM	pulse code modulation
PCM-PSK-PM	pulse code modulation-phase shift keying-phase modulation
PCU	power control unit
PDA	platform drive assembly
PDM	pulse duration modulation
PI	principal investigator proposed instrument
PJU	Pioneer Jupiter-Uranus
PLL	phase-locked loop
PM	phase modulation
p.m.	post meridian
P-MOS	positive channel metal oxide silicon
PMP	parts, materials, processes
PMS	probe mission spacecraft
PMT	photomultiplier tube
PPM	parts per million pulse position modulation
PR	process requirements
PROM	programmable read-only memory
PSE	program storage and execution assembly

ACRONYMS AND ABBREVIATIONS (CONTINUED)

PSIA	pounds per square inch absolute
PSK	phase shift key
PSU	Pioneer Saturn-Uranus
PTE	probe test equipment
QOI	quality operation instructions
QTM	qualification test model
RCS	reaction control subsystem
REF	reference
RF	radio frequency
RHCP	right hand circularly polarized
RHS	reflecting heat shield
RMP-B	Reentry Measurements Program, Phase B
RMS	root mean square
RMU	remote multiplexer unit
ROM	read only memory rough order of magnitude
RSS	root sum square
RT	retargeting
RTU	remote terminal unit
S	separation
SBASI	single bridgewire Apollo standard initiator
SCP	stored command programmer
SCR	silicon controlled rectifier
SCT	spin control thrusters
SEA	shunt electronics assembly
SFOF	Space Flight Operations Facility
SGLS	space ground link subsystem
SHIV	shock induced vorticity
SLR	shock layer radiometer
SLRC	shock layer radiometer calibration

ACRONYMS AND ABBREVIATIONS (CONTINUED)

SMAA	semimajor axis
SMIA	semiminor axis
SNR	signal to noise ratio
SP	small probe
SPC	sensor and power control
SPSG	spin sector generator
SR	shunt radiator
SRM	solid rocket motor
SSG	Science Steering Group
SSI	small scale integration
STM	structural test model
STM/TTM	structural test model/thermal test model
STS	system test set
sync	synchronous
TBD	to be determined
TCC	test conductor's console
T/D	Thor/Delta
TDC	telemetry data console
TEMP	temperature
TS	test set
TTL MSI	transistor-transistor logic medium scale integration
TLM	telemetry
TOF	time of flight
TRF	tuned radio frequency
TTM	thermal test model
T/V	thermo vacuum
TWT	travelling wave tube
TWTA	travelling wave tube amplifier
UHF	ultrahigh frequency
UV	ultraviolet

ACRONYMS AND ABBREVIATIONS (CONTINUED)

VAC	volts alternating current
VCM	vacuum condensable matter
VCO	voltage controlled oscillator
VDC	volts direct current
VLBI	very long baseline interferometry
VOI	Venus orbit insertion
VOP	Venus orbital plane
VSI	Viking standard initiator
VTA	variable time of arrival
XDS	Xerox Data Systems

1. INTRODUCTION

This volume presents the results of the Pioneer Venus studies by TRW Systems and Martin Marietta Corporation from 2 October 1972 through 30 June 1973. In the course of this work, many missions were considered, involving two launch vehicles and different launch opportunities and spacecraft configurations to meet varying science requirements, all at minimum cost. The sequence of events is described and the specific studies conducted are summarized in Section 2.

Throughout this report, standard symbols are used to denote the configurations which were at one time or another recommended for the probe and orbiter missions. Figure 1-1 defines these symbols. The instruments included under each Roman numeral designation for the science payloads are listed in Table 1-1.

The effects of science payload on mission and spacecraft design are discussed in Section 3, followed by the mission analyses in Section 4. Sections 5 through 8 then cover system and subsystem definitions for the spacecraft and probes. After a review of the work on the NASA/ESRO interface (Section 9), the mission operations and flight support activities are defined in Section 10. The specific cost reductions made possible by the choice of the Atlas/Centaur launch vehicle with the cost/weight tradeoffs related to the use of Thor/Delta versus Atlas/Centaur are summarized in Section 11. The last section identifies those items that require long-lead times for procurement or for which testing requirements are critical.

Table 1-1. Science Payload Identification

VERSION I: REFERS TO THE LIST OF SCIENCE INSTRUMENTS PROVIDED IN NASA/AMES LETTER 242-3 PV-02-181, 22 SEPTEMBER 1972. THIS PAYLOAD WAS USED FOR THOR/DELTA-LAUNCHED SPACECRAFT AND ANTICIPATED A 1977 PROBE MISSION AND 1978 ORBITED MISSION LAUNCHES.

VERSION II: REFERS TO THE LIST PROVIDED IN NASA/AMES LETTER 242-3 PV-02-229, 20 OCTOBER 1972, IDENTICAL TO THAT OF VERSION I, BUT THE WEIGHT AND POWER ALLOWANCES ARE INCREASED TO REFLECT THE ADDED WEIGHT CAPABILITY OF THE ATLAS/CENTAUR LAUNCH VEHICLES.

VERSION III: REFERS TO THE SCIENCE PAYLOAD DEFINED IN NASA/AMES LETTER ASD:244-9/22-278, 2 NOVEMBER 1972, WHICH PROVIDED ADDITIONAL DEFINITION OF THE "DUAL FREQUENCY RF OCCULTATION" EXPERIMENT, TOGETHER WITH SPECIFIC WEIGHT AND POWER ALLOCATIONS FOR THE RADAR ALTIMETER. THERE ARE ACCORDINGLY TWO SETS OF VERSION III INSTRUMENTS, ONE FOR THE THOR/DELTA SPACECRAFT AND THE ONE FOR THE ATLAS/CENTAUR SPACECRAFT.

VERSION IV: REFERS TO THE SCIENCE PAYLOAD AS DEFINED IN NASA/AMES LETTER 242-3 PV-03-90, 13 APRIL 1973, SPECIFICALLY FOR THE ATLAS/CENTAUR-LAUNCHED MISSIONS AND WITH THE PROBE MISSION LAUNCH DATA CHANGED FROM 1977 TO 1978 AND WITH THE POSSIBILITY OF ESRO PARTICIPATION REMOVED.

	VERSION I	II	III	IV
LARGE PROBE				
TEMPERATURE GAUGES	N	N	N	N
PRESSURE GAUGES	N	N	N	N
ACCELEROMETERS	N	N	N	N
NEUTRAL MASS SPECTROMETER	N	N	N	N
CLOUD PARTICAL SIZER ANALYZER	N	N	N	N
SOLAR RADIOMETER	N	N	N	N
INFRARED FLUX DETECTOR	N	N	N	N
AUREOLE/EXTINCTION DETECTOR	N	N	N	O
TRANSPONDER	N	N	N	-
NEPHELOMETER	N	N	N	-
SHOCK LAYER RADIOMETER	N	N	N	O
HYGROMETER	N	N	N	N
WIND DRIFT RADAR	O	O	O	N
FLUORESCENCE SPECTROMETER	O	O	O	-
NOISE DETECTOR	O	O	O	-
SFERICS DETECTOR	O	O	O	-
X-RAY FLUORESCENCE	-	-	-	O
ATR SPECTROMETER	-	-	-	O
TOTAL WEIGHT, NOMINAL INSTRUMENTS (KG)	25	27	27	27
TOTAL WEIGHT, OTHER CANDIDATE INSTRUMENTS (KG)	10	12	12	8
TOTAL POWER, NOMINAL INSTRUMENTS (WATTS)	42	49	49	89
TOTAL POWER, OTHER CANDIDATE INSTRUMENTS (WATTS)	30	47	47	11
SMALL PROBES				
TEMPERATURE GAUGE	N	N	N	N
PRESSURE GAUGE	N	N	N	N
NEPHELOMETER	N	N	N	N
ACCELEROMETER	N	N	N	N
MAGNETOMETER	N	N	N	O
STABLE OSCILLATOR FOR DVLBI	N	N	N	N
INFRARED FLUX DETECTOR	-	-	-	N
RADIO FREQUENCY ALTIMETER	-	-	-	O
TOTAL WEIGHT, NOMINAL INSTRUMENTS (KG)	6	7	7	2
TOTAL WEIGHT, OTHER CANDIDATE INSTRUMENTS (KG)	0	0	0	1
TOTAL POWER, NOMINAL INSTRUMENTS (WATTS)	5	7	7	4
TOTAL POWER, OTHER CANDIDATE INSTRUMENTS (WATTS)	0	0	0	6

	VERSION I	II	III	IV
ORBITER				
MAGNETOMETER	N	N	N	N
ELECTRON TEMPERATURE PROBE	N	N	N	N
NEUTRAL MASS SPECTROMETER	N	N	N	N
ION MASS SPECTROMETER	N	N	N	N
ULTRAVIOLET SPECTROMETER	N	N	N	N
INFRARED RADIOMETER	N	N	N	N
DUAL FREQUENCY RF OCCULTATION (SEE DEFINITIONS)	N	N	O*	N
RADIO FREQUENCY ALTIMETER	N	N	N	N
SOLAR WIND PROBE	O	O	O	N
THERMAL/SUPRATHERMAL PARTICLE DETECTOR	O	O	O	O
ELECTRIC FIELD DETECTOR	O	O	O	O
SOLAR ELECTRON DETECTOR	O	O	O	-
MICROWAVE RADIOMETER	O	O	O	O
SPIN SCAN PHOTOMETER	-	-	-	O
TOTAL WEIGHT, NOMINAL INSTRUMENTS (KG)	28	32	33	40
TOTAL WEIGHT, OTHER CANDIDATE INSTRUMENTS (KG)	15	24	24	23
TOTAL POWER, NOMINAL INSTRUMENTS (WATTS)	56	70	60	90
TOTAL POWER, OTHER CANDIDATE INSTRUMENTS (WATTS)	21	28	28	33
PROBE BUS				
NEUTRAL MASS SPECTROMETER	N	N	N	N
ION MASS SPECTROMETER	N	N	N	N
ELECTRON TEMPERATURE PROBE	N	N	N	N
ULTRAVIOLET FLUORESCENCE	N	N	N	-
ULTRAVIOLET SPECTROMETER	-	-	-	N
MAGNETOMETER	N	N	N	N
RETARDING POTENTIAL ANALYZER	-	-	-	N
DAYGLOW PHOTOMETER	O	O	O	-
SOLAR WIND PROBE	O	O	O	O
TOTAL WEIGHT, NOMINAL INSTRUMENTS (KG)	10	12	12	12
TOTAL WEIGHT, OTHER CANDIDATE INSTRUMENTS (KG)	4	7	7	4
TOTAL POWER, NOMINAL INSTRUMENTS (WATTS)	20	24	24	22
TOTAL POWER, OTHER CANDIDATE INSTRUMENTS (WATTS)	6	8	8	6

LEGEND: N = NOMINAL INSTRUMENT
O = OTHER CANDIDATE INSTRUMENT
* = X-BAND IS OTHER CANDIDATE, S-BAND IS NOMINAL

	VEHICLE	SCIENCE VERSION	LAUNCH VEHICLE	NOMINAL ATTITUDE	OMNI ANTENNAS	HORN ANTENNA	HIGH-GAIN ANTENNA	TRANSMITTER POWER	MAXIMUM DATA RATE AT MAXIMUM RANGE	
									64-METER NET	26-METER NET
A/C IV	PROBE BUS	IV	ATLAS/CENTAUR	EARTH POINTING	FORWARD-AFT	AFT	NONE	6	1024	64
A/C IV	LARGE PROBE	IV	ATLAS/CENTAUR		AFT			36	128	
A/C IV	SMALL PROBE	IV	ATLAS/CENTAUR		AFT			20	64	
A/C IV	ORBITER	IV	ATLAS/CENTAUR	EARTH POINTING	FORWARD-AFT	AFT	1.5-METER (5-FOOT) FIXED DISH	6	1024	64
A/C IV	ORBITER	IV	ATLAS/CENTAUR	NORMAL*	AFT	NONE	DESPUN REFLECTOR FRANKLIN ARRAY	12	1024	128
T/D III	PROBE BUS	III	THOR/DELTA	EARTH POINTING	FORWARD-AFT	AFT	NONE	6	1024	64
T/D III	LARGE PROBE	III	THOR/DELTA		AFT			36	128	
T/D III	SMALL PROBES	III	THOR/DELTA		AFT			20	16	
A/C III	PROBE BUS	III	ATLAS/CENTAUR	EARTH POINTING	FORWARD-AFT	AFT	NONE	6	1024	64
A/C III	LARGE PROBE	III	ATLAS/CENTAUR		AFT			36	128	
A/C III	SMALL PROBES	III	ATLAS/CENTAUR		AFT			20	16	
T/D III	ORBITER	III	THOR/DELTA	EARTH POINTING	FORWARD-AFT	AFT	FIXED DISH	6	1024	128
31 W A/C III	ORBITER	III	THOR/DELTA	NORMAL	AFT	NONE	FANSCAN FRANKLIN ARRAY	31	128	8
T/D III	ORBITER	III	THOR/DELTA	NORMAL	AFT	NONE	DESPUN REFLECTOR FRANKLIN ARRAY	12	1024	128
12 W T/D III	ORBITER	III	THOR/DELTA	NORMAL	AFT	NONE	FANSCAN FRANKLIN ARRAY	12	64	0
A/C III	ORBITER	III	ATLAS/CENTAUR	EARTH POINTING	FORWARD-AFT	AFT	FIXED DISH	6	1024	128
31 W T/D III	ORBITER	III	ATLAS/CENTAUR	NORMAL	AFT	NONE	FANSCAN FRANKLIN ARRAY	31	128	8
A/C III	ORBITER	III	ATLAS/CENTAUR	NORMAL	AFT	NONE	DESPUN REFLECTOR FRANKLIN ARRAY	12	1024	128
12 W A/C III	ORBITER	III	ATLAS/CENTAUR	NORMAL	AFT	NONE	FANSCAN FRANKLIN ARRAY	12	64	0

*"NORMAL" MEANS THAT THE NOMINAL SPIN AXIS ATTITUDE IS NORMAL TO THE SPACECRAFT-EARTH LINE WITH LINE NORMAL TO BOTH THE SPIN AXIS AND THE EARTH LINE LYING IN THE ORBIT PLANE OF VENUS. THIS IS SOMETIMES LOOSELY REFERRED TO AS BEING NORMAL TO THE VENUS ORBIT PLANE.

Figure 1-1. Definition of Configuration Symbols

FOLDOUT FRAME

FOLDOUT FRAME

2

2. SUMMARY

The objective of this study has been to attain the lowest-cost, reliable spacecraft to accomplish the mission. The study has been in the framework of a sequence of definitions of the complement of scientific instruments and includes two parallel studies, one using the Thor/Delta launch vehicle and the other, the Atlas/Centaur.

The program includes an Atmospheric-Entry Multiple Probe Flight Mission, originally scheduled for the 1976-77 launch opportunity but subsequently changed to the 1978 opportunity, and an Aeronomy, Fields and Particles, and Mapping Orbiter Mission, also during the 1978 opportunity.

The study shows a definite cost advantage when the Atlas/Centaur is used for the probe mission. The relief of weight and volume constraints allows a substantial use of existing and proven hardware and technology for the probes and increases the commonality of the hardware between the large probe and the three small probes and between the probes and the probe bus. Test costs are also low because of greater design margins. These savings, and the associated savings in scientific instrument development, are significantly greater than the cost differential between the Atlas/Centaur and Thor/Delta launch vehicles. (NASA/ARC provided a value of $9 million per launch for study purposes.)

For the orbiter, however, the savings are much less since for that mission developed hardware and technology can be used within the weight and volume limits of the Thor/Delta. Using the Atlas/Centaur for the probe and Thor/Delta for the orbiter results in increased cost because of loss of commonality between probe bus and orbiter structure, a tight weight control program for the orbiter, and the loss of scientific instrument savings from relaxation of weight, volume, and power constraints. However, these factors constitute only a fraction of the $9 million differential in launch vehicle cost; and at the midterm we therefore recommended a split launch: Atlas/Centaur for the probe mission and Thor/Delta for the orbiter.

Additional factors are therefore involved in NASA's selection of Atlas/Centaur for both missions. Some of these may be:

- Savings from the use of a common launch vehicle for two launches 3 months apart, i.e., launch vehicle procurement, management costs, and reduced launch operations cost
- Uncertainty in the definition of the orbiter's scientific instruments and their requirements and lack of margin in the Thor/Delta orbiter to meet possible increased requirements
- The desire to avoid the development of a spacecraft that is too constrained to be useful in possible follow-on missions to Venus or Mars.

Within the framework of the Atlas/Centaur selection, our preferred system design for each mission is illustrated in Figure 2-1 for the spacecraft and in Figure 2-2 for the probes. These configurations represent the synthesis of several years of work; they meet the requirements of the Version IV science payload in the most cost-effective fashion.

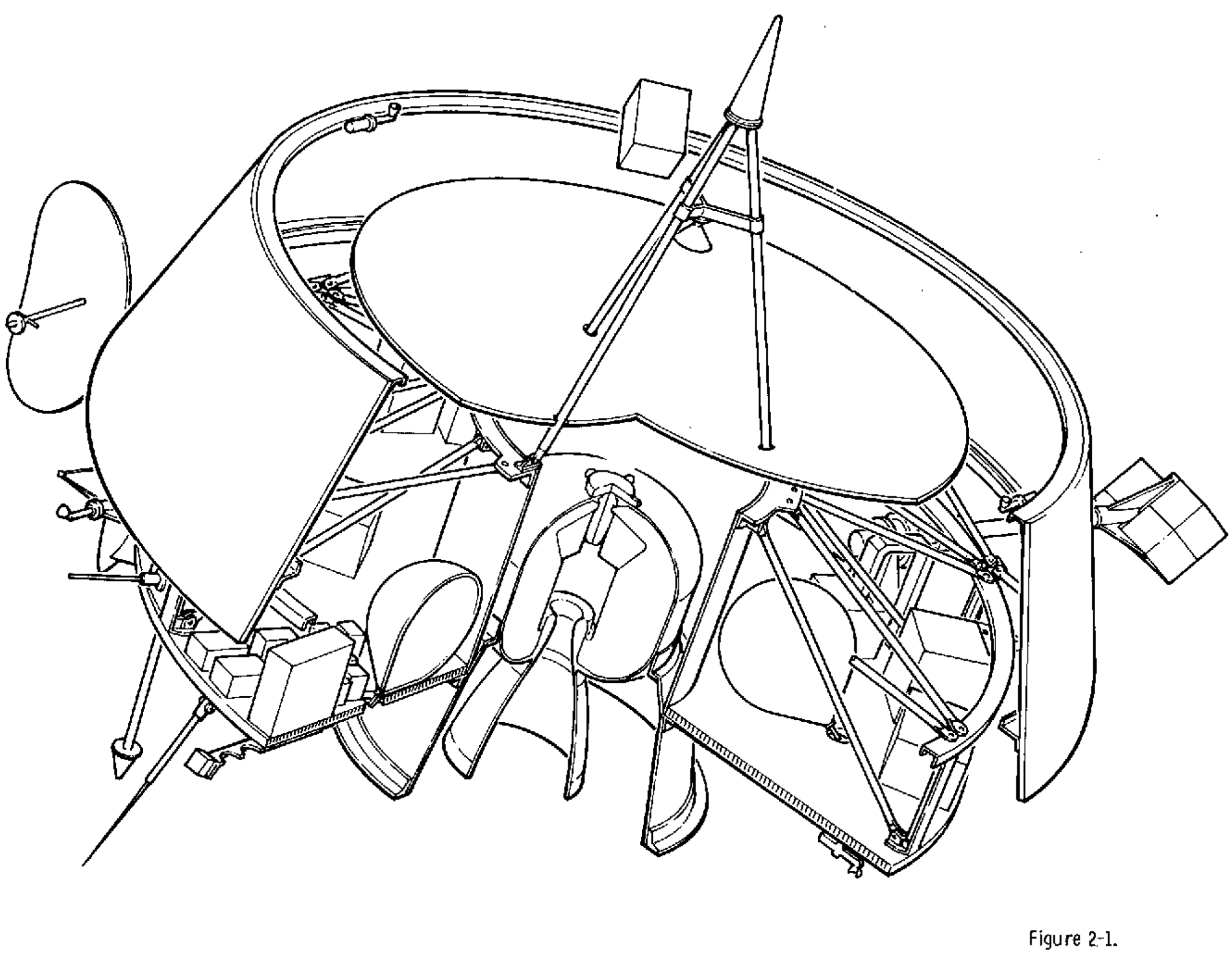

Figure 2-1.

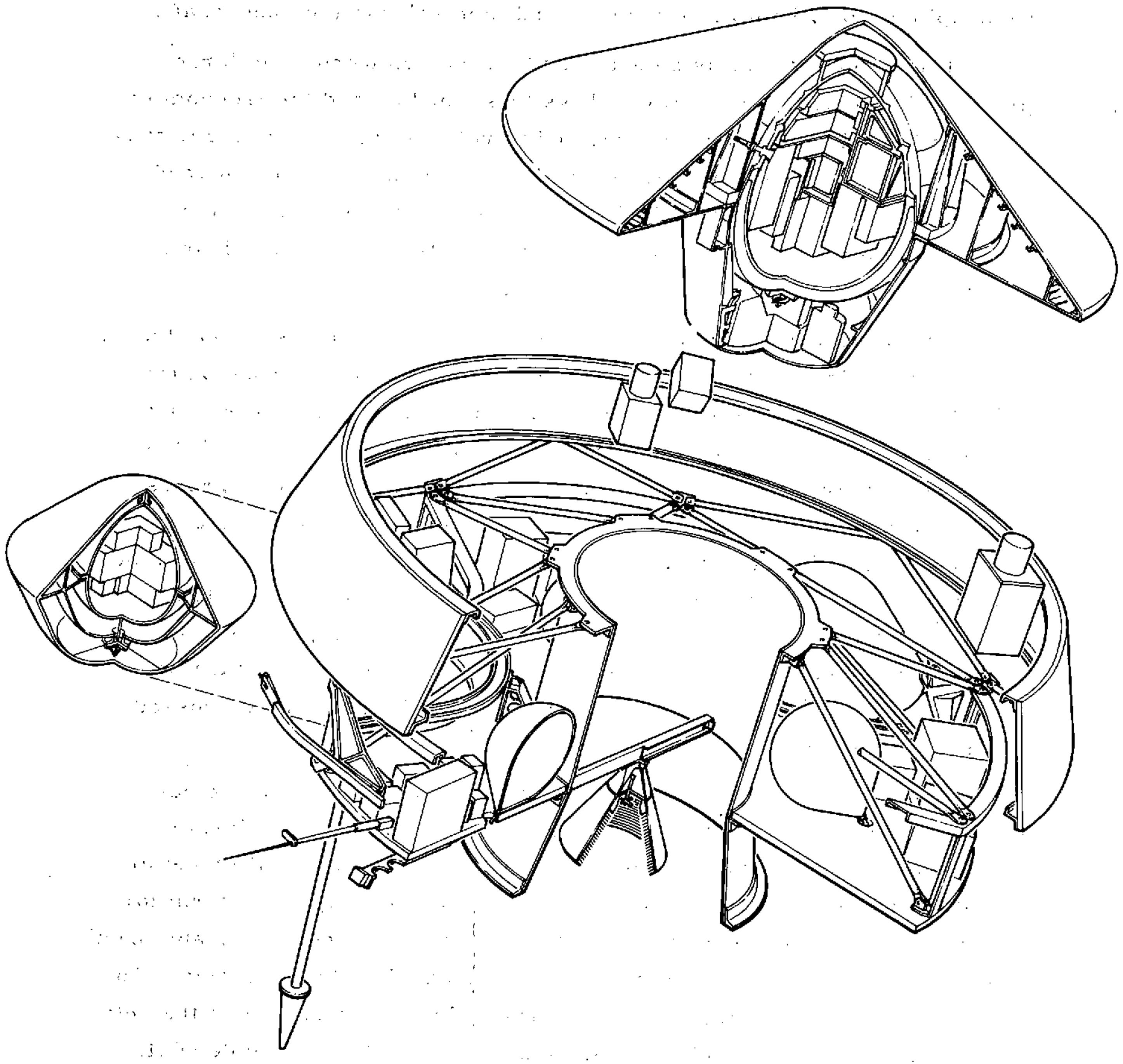

Figure 2-1. Preferred Spacecraft Configurations

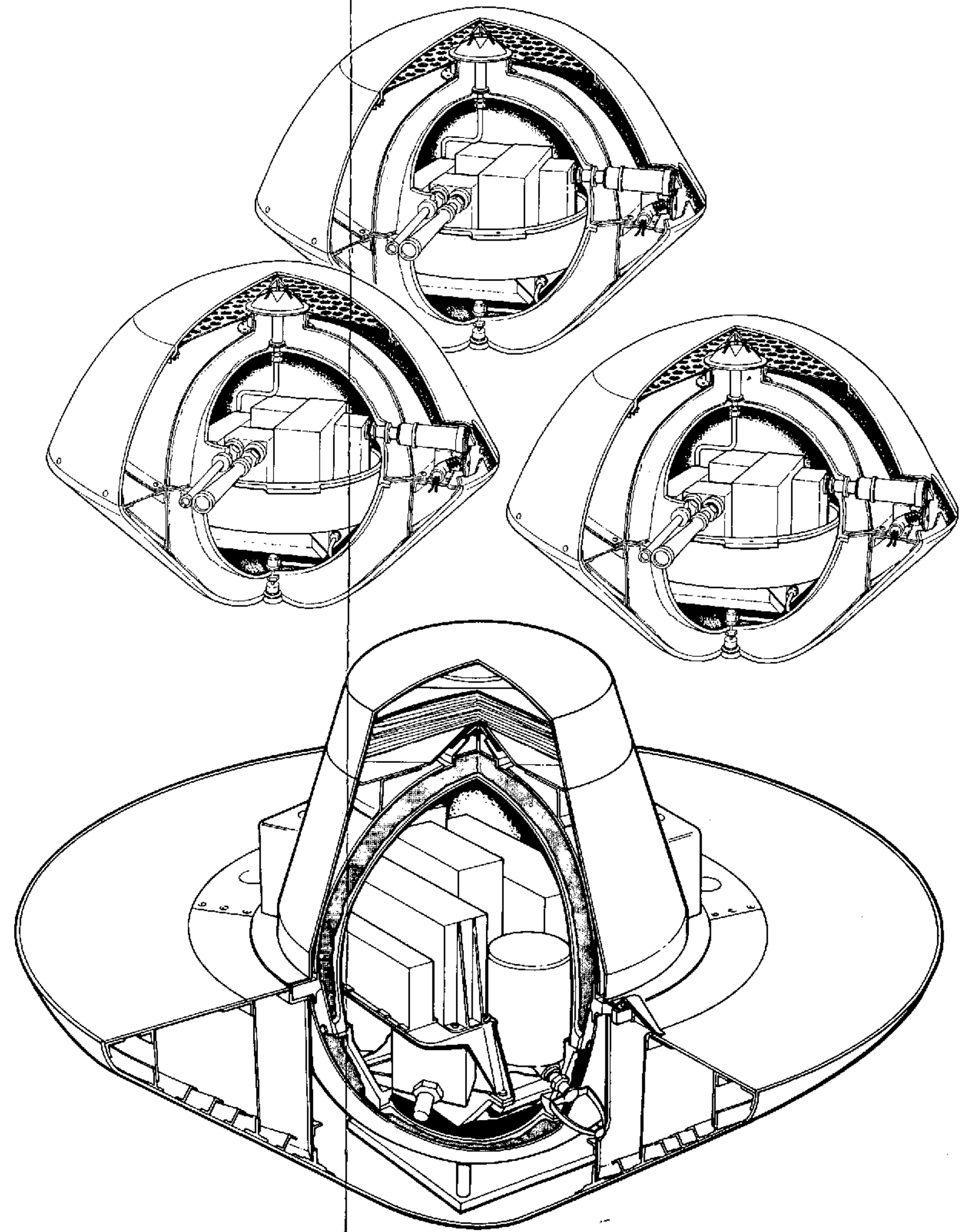

Figure 2-2. Preferred Probe Configurations

FOLDOUT FRAME 1

FOLDOUT FRAME 2

Figure 2-3 illustrates the multiprobe mission. The trajectory is 1978 Type I; it is assumed that the Centaur will provide a favored orientation, spin up to 0.5 rad/s (4.8 rpm), and then release the spacecraft.

The initial attitude is selected so that the sun warms the large probe. The conical solar array allows this freedom and the freedom to perform the midcourse corrections and to release the probes in any attitude without time-line constraints as long as the sun is in the forward hemisphere. The probe bus design allows sequential release of the probes, permitting the advantages of targeting freedom, arrival time control, and zero angle of attack at entry.

The targeting shown places the large probe over the subsolar trace, 0.436 radian (25 degrees) from the terminator; one small probe on the subsolar trace, 1.745 radians (100 degrees) from the large probe; and the other two small probes scattered in latitude to give a large [0.436 radian (45-degree)] latitude spread between the extreme small probes. This targeting is responsive to NASA/ARC desires verbally indicated for the Version IV science payload. It requires that the small probes be designed for a range of entry flight path angles from -0.436 to -1.047 radians (-25 to -60 degrees). The implications with respect to probe design are discussed in Section 4; other targeting options are also presented there. Cost tradeoffs related to these options will be discussed in our Phase C/D proposal.

The recommendation of the Science Steering Group that the bus enter near the entry point of the large probe imposes severe design requirements on the bus. It demands an increase in transmitter power to 150 watts, or a canted despun antenna, or a despun ram platform for some of the science instruments. This is because of the unfavorable earth look angle and ram angle geometry that accompanies this targeting. Consequently, the bus is targeted to a favorable location from which the entry ram vector, extended back, lies as near to the earth as possible while still guaranteeing that the bus does not skip out of the Venusian atmosphere before penetrating deeply enough to satisfy scientific measurement requirements. The targeting allows proper pointing of the ram experiments and at the same time modest antenna gain so that 1024 bits/second can be maintained with a 6-watt transmitter.

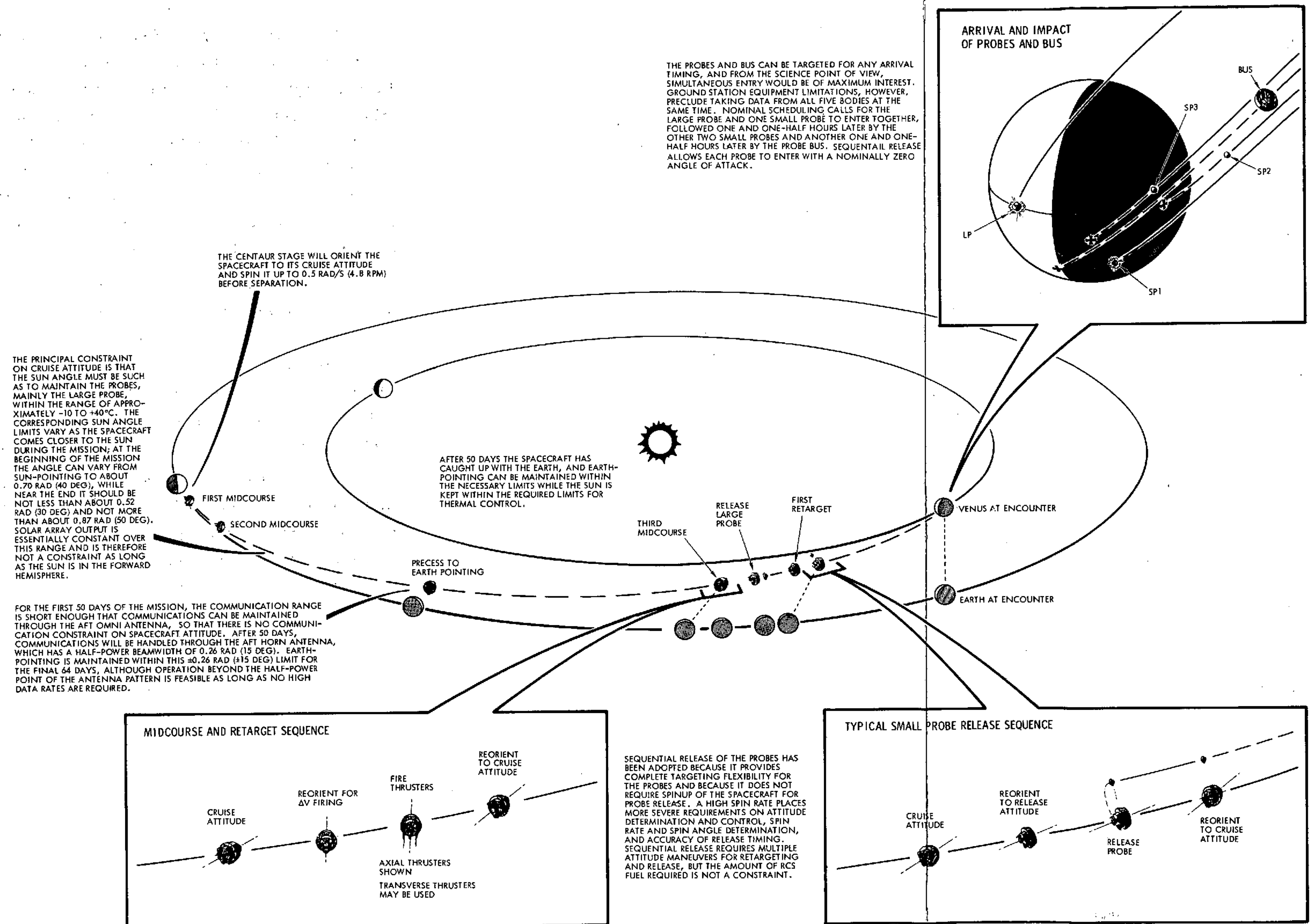

Figure 2-3. Probe Mission Profile

FOLDOUT FRAME 1

FOLDOUT FRAME 2

As shown in Figure 2-4, the orbiter is launched about a month before the probe spacecraft and arrives about 5 days earlier than the probes. Transit flight and midcourse corrections are similar to those for the probe mission except for differences arising from the use of a Type II trajectory. The main difference is that the nose of the spacecraft, rather than the tail, is pointing to the earth during the early part of the flight, and a spacecraft flip maneuver is required, as shown, at 108 days. Subsequent to this flip maneuver, normal communications are maintained using the aft, earth-pointing horn until the second flip maneuver 37 days after orbit insertion.

Insertion burn is made at a spin speed of 60 rpm and with earth occulted. However, all maneuvers to attain the insertion attitude can be done well in advance. The downlink via the omni antenna can be maintained for the orbit insertion and second flip maneuver, with subsequent long-range communications supported by the high-gain, earth-pointing antenna. Later maneuvers for periapsis trim can be in the earth-pointing attitude through the use of transverse thrusters in a pulsed mode.

The orbit shown was selected for its good latitude coverage but is inclined from a polar orbit, about 0.524 radian (30 degrees), to prevent periapsis from crossing the terminator (before 17 days) so that early periapsis passes are over sunlit portions. Orbit operations continue for at least a Venusian year.

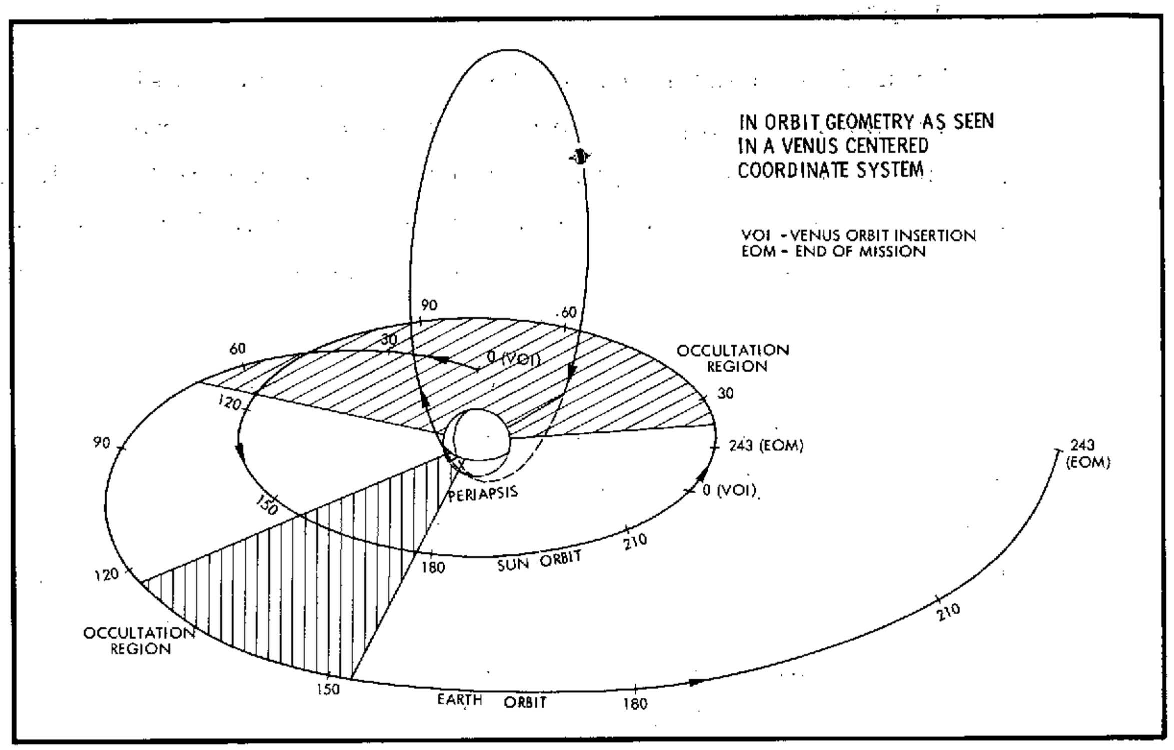

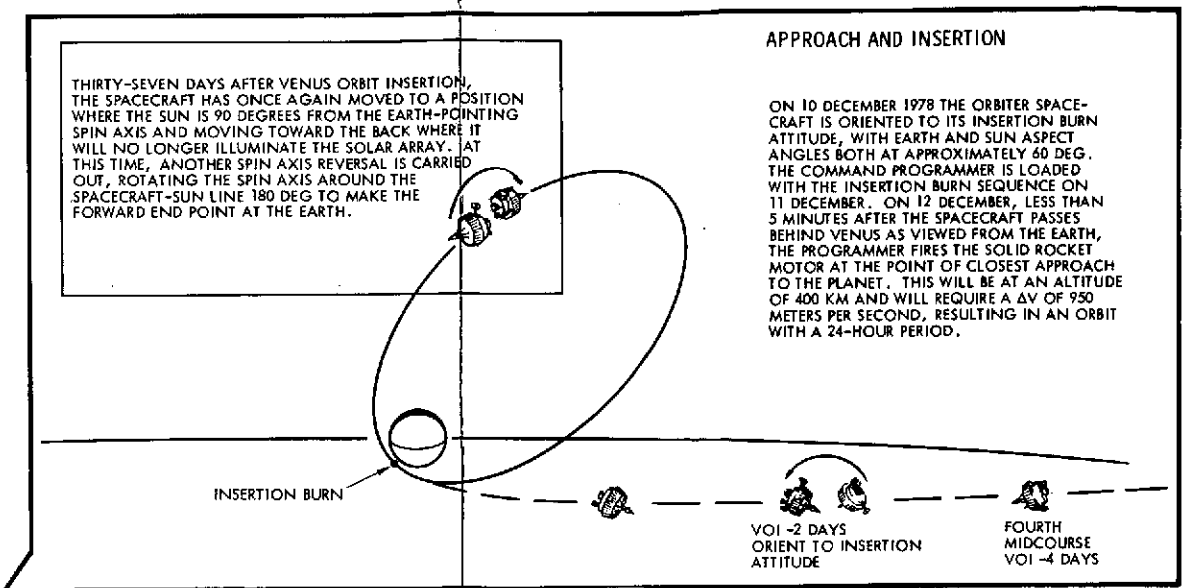

THIRTY-SEVEN DAYS AFTER VENUS ORBIT INSERTION, THE SPACECRAFT HAS ONCE AGAIN MOVED TO A POSITION WHERE THE SUN IS 90 DEGREES FROM THE EARTH-POINTING SPIN AXIS AND MOVING TOWARD THE BACK WHERE IT WILL NO LONGER ILLUMINATE THE SOLAR ARRAY. AT THIS TIME, ANOTHER SPIN AXIS REVERSAL IS CARRIED OUT, ROTATING THE SPIN AXIS AROUND THE SPACECRAFT-SUN LINE 180 DEG TO MAKE THE FORWARD END POINT AT THE EARTH.

APPROACH AND INSERTION

ON 10 DECEMBER 1978 THE ORBITER SPACECRAFT IS ORIENTED TO ITS INSERTION BURN ATTITUDE, WITH EARTH AND SUN ASPECT ANGLES BOTH AT APPROXIMATELY 60 DEG. THE COMMAND PROGRAMMER IS LOADED WITH THE INSERTION BURN SEQUENCE ON 11 DECEMBER. ON 12 DECEMBER, LESS THAN 5 MINUTES AFTER THE SPACECRAFT PASSES BEHIND VENUS AS VIEWED FROM THE EARTH, THE PROGRAMMER FIRES THE SOLID ROCKET MOTOR AT THE POINT OF CLOSEST APPROACH TO THE PLANET. THIS WILL BE AT AN ALTITUDE OF 400 KM AND WILL REQUIRE A ΔV OF 950 METERS PER SECOND, RESULTING IN AN ORBIT WITH A 24-HOUR PERIOD.

170 DAYS AFTER LAUNCH, THE SPACECRAFT HAS CAUGHT UP WITH THE EARTH AND LIES ON A LINE FROM EARTH TO SUN. THIS CONDITION IS KNOWN AS SYZYGY.

THE HORN ANTENNA HAS A 3-DB BEAMWIDTH OF ±12 DEGREES, ALLOWING A 12-DEG DRIFT EITHER SIDE OF EARTH POINTING BEFORE A CORRECTION IS NEEDED. DURING THIS PART OF THE MISSION, ATTITUDE CORRECTIONS ARE THEREFORE NEEDED ONLY EVERY FEW DAYS.

THE FORWARD-MOUNTED HIGH-GAIN ANTENNA IS NOW AGAIN POINTING AT THE EARTH, AND THE COMMUNICATION RANGE HAS INCREASED TO THE POINT WHERE IT IS NOW NECESSARY TO KEEP IT ACCURATELY POINTED IN ORDER TO ACHIEVE THE REQUIRED GAIN. POINTING ACCURACY REQUIREMENTS INCREASE WITH TIME AS THE DISTANCE BETWEEN THE EARTH AND VENUS INCREASES. VENUS IS AHEAD OF THE EARTH AT THE TIME OF VENUS ORBIT INSERTION AND CONTINUES TO GAIN ON THE EARTH UNTIL THE END OF MISSION.

ATTITUDE CORRECTIONS WILL BE REQUIRED MORE FREQUENTLY AS THE COMMUNICATION RANGE INCREASES AND OPERATION IN THE MAXIMUM-GAIN PORTION OF THE ANTENNA PATTERN BECOMES MORE CRITICAL. NEAR THE END OF MISSION, EARTH-POINTING WILL BE MAINTAINED TO WITH ±1 DEG AND WILL REQUIRE A CORRECTION ABOUT EVERY DAY AND A HALF.

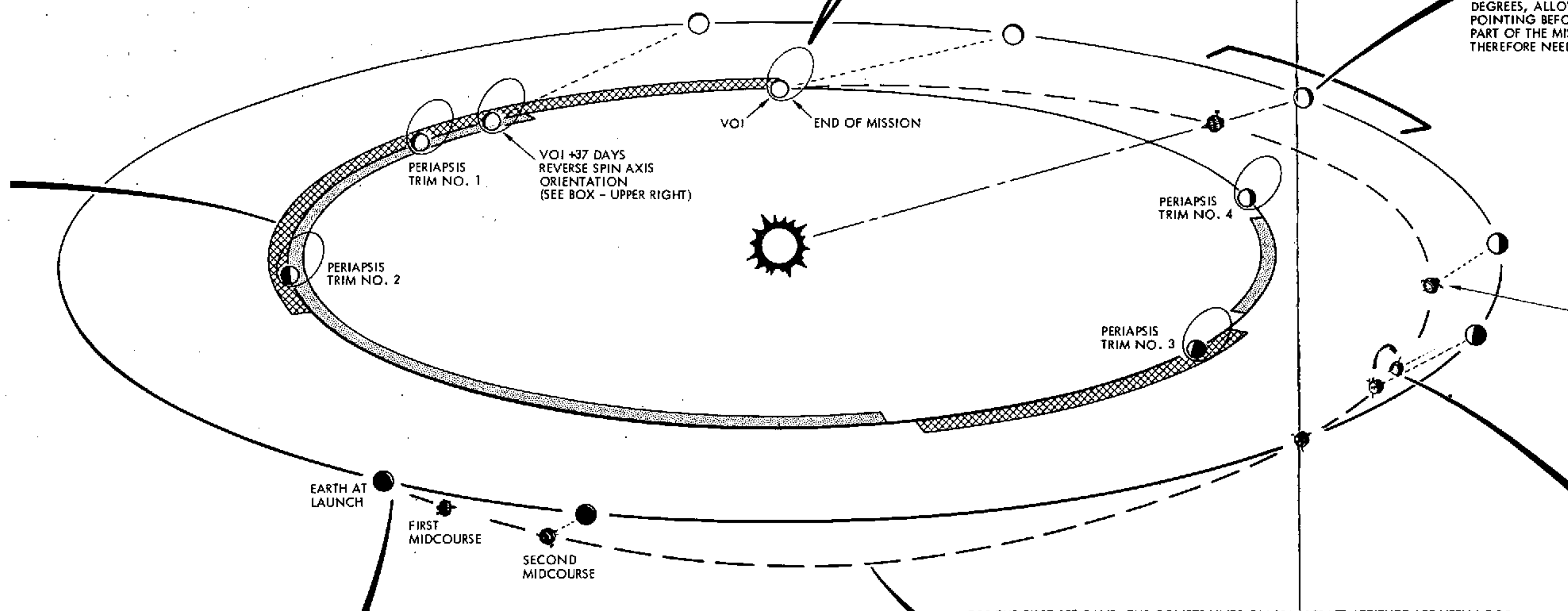

SUN OCCULTATION PERIOD

EARTH OCCULTATION PERIOD

THE SPACECRAFT IS BOOSTED OUT OF EARTH ORBIT IN A RETROGRADE DIRECTION TO CAUSE IT TO "FALL" TOWARD THE ORBIT OF VENUS. IT FOLLOWS A TRAJECTORY THAT IS OUTSIDE OF THE EARTH'S ORBIT FOR THE FIRST 78 DAYS, AND THE SPACECRAFT FOLLOWS BEHIND THE EARTH FOR MOST OF THE MISSION (IT CATCHES UP AFTER 170 DAYS).

FOR THE FIRST 108 DAYS, THE CONSTRAINTS ON SPACECRAFT ATTITUDE ARE VERY LOOSE. THE SUN CAN BE ANYWHERE IN THE FORWARD HEMISPHERE, AND THE COMMUNICATION RANGE IS SHORT ENOUGH THAT IT IS NOT NECESSARY TO KEEP THE EARTH DIRECTION ACCURATELY IN THE CENTER OF THE HIGH GAIN ANTENNA PATTERN. THE HIGH GAIN ANTENNA IS POINTED TOWARD THE EARTH, BUT ALLOWED TO DRIFT CONSIDERABLY AWAY FROM THE EARTH DIRECTION BEFORE A CORRECTION IS MADE. BY ALLOWING FOR THE DRIFT AND OFFSETTING SO THAT THE SPIN AXIS DRIFTS FROM ONE SIDE OF EARTH POINTING THROUGH EARTH POINTING TO THE OTHER SIDE OF EARTH POINTING, IT IS POSSIBLE TO MAKE ATTITUDE CORRECTIONS ONLY ABOUT ONCE A WEEK.

AFTER 108 DAYS THE SPACECRAFT HAS MOVED A QUARTER OF THE WAY AROUND THE SUN AND THE SUN ASPECT ANGLE IS 90 DEGREES WHEN THE SPIN AXIS IS POINTED AT THE EARTH. IF THE SPACECRAFT CONTINUED IN THE SAME ATTITUDE, THE SUN WOULD MOVE INTO THE AFT HEMISPHERE AND WOULD NOT ADEQUATELY ILLUMINATE THE SOLAR ARRAY. AT THIS POINT, THEREFORE, THE SPIN AXIS IS ROTATED 180 DEGREES ABOUT THE SPACECRAFT SUN LINE, SO THAT THE AFT END IS POINTING AT THE EARTH. COMMUNICATIONS ARE NOW HANDLED THROUGH THE AFT MOUNTED MEDIUM GAIN HORN ANTENNA.

Figure 2-4. Orbiter Mission Profile

FOLDOUT FRAME 1

FOLDOUT FRAME 2

2.1 DESIGN

Figure 2-5 illustrates what we see as the key design features of the probe bus. Perhaps the most significant is the conical solar array. It provides a freedom of spacecraft pointing which, in turn, leads to the possibility of some of the other features, in particular the ability to earth point and the consequent use of simple high-gain antennas. The latter is even more valuable for the orbiter mission.

For the probe mission, the benefit is twofold: 1) Midcourse correction and probe release can be performed in any functionally required attitude without constraining the time-line by battery capability. It also provides improved performance (for a given array size) over a cylindrical array in the probe bus entry attitude [solar aspect angle of 1.22 radians (70 degrees)]. 2) It allows solar heating of the large probe as appropriate during the transit trajectory, avoiding a 50-percent increase in array size that would be necessitated by electrical heaters.

Sequential probe release capability has been retained from the study proposal without weight or cost penalties. We believe that the indicated flexibility this provides is valuable.

The use of sun and RF aspect sensors for attitude reference eliminates the need for an expensive star mapper. Sequential release also contributes by reducing the accuracy requirements placed on the probe bus for attitude determination and release timing.

The requirements placed on the large and small probes by Venus entry and survival to the surface while accommodating an appropriate science payload are so constraining that the basic design concepts have remained unchanged from the original concepts developed several years ago.

EXPLODED VIEW OF PROBE BUS

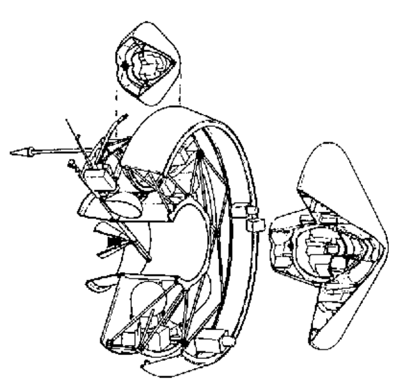

SEQUENTIAL SMALL PROBE RELEASE

- PROVIDES COMPLETE SMALL PROBE TARGETING FREEDOM, CONSTRAINED ONLY BY PROBE CAPABILITY
- ALLOWS SMALL PROBE ENTRY WITH NOMINALLY ZERO ANGLE OF ATTACK; IMPROVES ATMOSPHERE RECONSTRUCTION USING SINGLE AXIS ACCELEROMETER
- ALLOWS PROBE ARRIVAL SEPARATION SO NO MORE THAN TWO PROBES DESCEND AT THE SAME TIME, ALLOWING TWO RECEIVERS PER PROBE AT EACH DSN STATION
- ALLOWS RELEASE AT LOW SPIN SPEED [1.05 RAD/S (10 RPM)] RELIEVING ATTITUDE CONTROL AND RELEASE ANGLE REQUIREMENTS AND THEREBY ALLOWING THE USE OF MODERATE ACCURACY SOLAR AND RF ATTITUDE REFERENCES
- REQUIRES SMALL PROBES AND EXPENDABLES TO HAVE THE SAME CENTER OF GRAVITY STATION AS THE REMAINDER OF THE BUS (AFTER THE LARGE PROBE IS REMOVED)

SOLAR AND RF ATTITUDE REFERENCES

- AVOIDS THE EXPENSE (HARDWARE AND SOFTWARE) OF A STAR MAPPER, WHICH IS ASSOCIATED WITH TIGHTER ACCURACY REQUIREMENTS
- RF USED SUCCESSFULLY ON PIONEERS 10 AND 11 AND SOLAR ON INTELSAT III

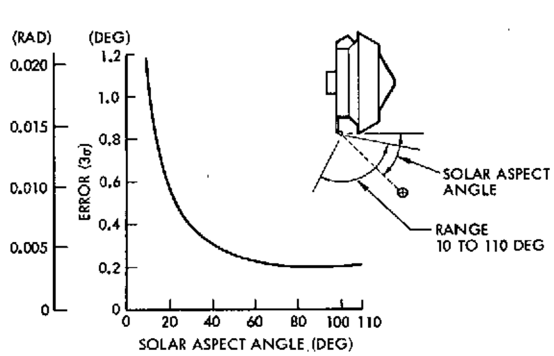

- SUN SENSOR PROVIDES ROLL REFERENCE AND SOLAR ANGLE. A SIMPLE MASK CHANGE OF INTELSAT III UNIT PROVIDES SUITABLE PERFORMANCE.

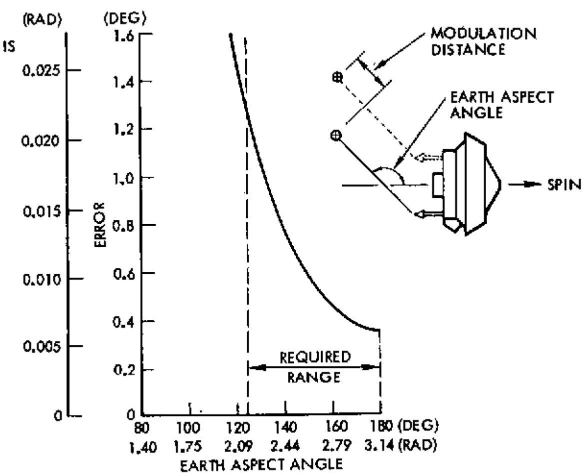

SPIN OF OFFEST OMNI (OR HORN) ANTENNA PROVIDES A DOPPLER MODULATION PROPORTIONAL TO THE SINE OF THE EARTH ASPECT ANGLE

CONICAL SOLAR ARRAY

PROVIDES POWER FOR 0<θ< 90° FOR 8% MORE ARRAY THAN A CYLINDRICAL ARRAY ⊥ TO ⊕

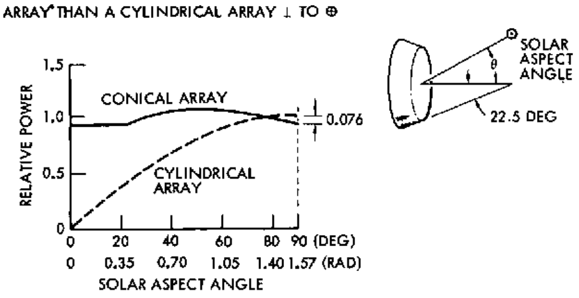

- ALLOWS FREEDOM TO STAY IN MANEUVER ATTITUDES INDEFINITELY WITHOUT TAPPING BATTERY
- ALLOWS SOLAR HEATING OF LARGE PROBE (EARLY IN MISSION), ELIMINATING THE NEED FOR AN ELECTRICAL HEATER WHICH WOULD INCREASE POWER REQUIREMENTS BY 50% OR ELSE REQUIRE A REMOVABLE INSULATION BLANKET OVER THE LARGE PROBE.
- AVOIDS ADDITIONAL FANBEAM ANTENNA ASSOCIATED WITH SPINNING PERPENDICULAR TO ECLIPTIC (AS IN PIONEERS 6 THROUGH 9)
- ENTAILS SLIGHTLY HIGHER (THAN CYLINDRICAL) ARRAY LAYUP AND WIRING COSTS ~$2.5K
- CONICAL ARRAYS FLIGHT PROVEN ON DSP SPACECRAFT

AXIAL HORN ANTENNA FOR ENTRY HIGH DATA RATE COMMUNICATIONS

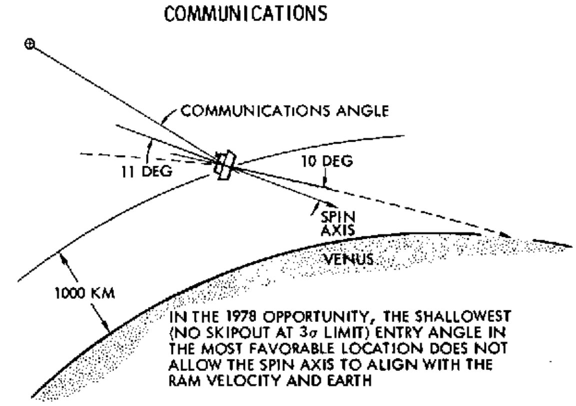

A COMPROMISE, MISALIGNING SPIN WITH RAM BY 0.175 RAD (10 DEG) AT 1000 KM [DECREASING TO 0.052 RAD (3 DEGREE) AT 130 KM] AND WITH A COMMUNICATIONS ANGLE OF 0.192 RAD (11 DEGREE) (NOMINAL), 0.209 RAD (12 DEGREE) (MAX), ALLOWS USE OF A HORN ANTENNA WHICH PROVIDES 1024 BITS/S WITH ONLY A 6-WATT TRANSMITTER. THE PIONEER 10 AND 11 MEDIUM GAIN HORN FORTUITOUSLY MEETS THIS REQUIREMENT.

Figure 2-5. Key Design Concepts: Probe Bus

The key concepts are shown in Figures 2-6 and 2-7. Changes are primarily associated with cost savings resulting from relieved weight and volume constraints arising from the selection of the Atlas/Centaur launch vehicle. Detailed, but significant, improvements in the design have also been incorporated as a result of our Phase B Study effort. The large and small probe savings directly attributable to the use of the Atlas/Centaur total $8 million, as is explained in Section 11.

The aeroshell configurations were developed on the basis of extensive test data on various configurations; they provide good entry stability and optimized heating for the desired drag characteristics. They also reflect a simplicity of design which will facilitate manufacture. The heatshield material, while not the lightest possible, offers significant test cost savings and ease of handling. The decelerator system for the large probe is conventional aircraft parachute technology, although the details of packaging and deployment, discussed in Section 7.5, appear to be a significant improvement over earlier concepts. The perforated stabilizing ring on the large probe descent capsule is simple, allows convenient mounting of the large probe in the bus, and at the same time offers the best performance of all stabilizing devices tested. The equipment ring concept for the large probe represents one of the detailed design improvements which reduce cost, particularly in integration and test.

The small probes also present challenging design problems. Their smaller weight and size preclude the use of a parachute or other techniques for separating an instrument package from the entry body. Thus the aeroshell with its hot heatshield is retained down to the surface. The key problem is to obtain uncontaminated exposure of the science instruments. Our solution is to contain the instrument windows or sampling inlets within the aeroshell throughout the entry heating and loading period, and then deploy or expose them through openings in the aeroshell. The covers over the openings are ejected and the instrument inlets deployed by highly reliable, flight proven mechanisms. Two examples are shown in Figure 2-7. The sampling inlets project far enough outside of the boundary layer to preclude contamination by heatshield outgassing products. All science instruments and supporting equipment are mounted on a central shelf, so that ease of assembly and accessibility for test and maintenance are essentially comparable to that offered by the large probe equipment ring.

ATLAS/CENTAUR PERFORMANCE CAPABILITY UTILIZED TO REDUCE COSTS

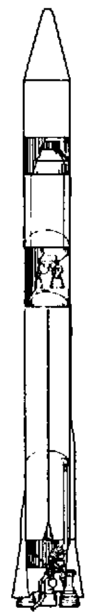

INCREASED SAFETY FACTORS AND DESIGN MARGINS INCORPORATED:

- ELIMINATES NEED FOR STRUCTURAL TEST MODEL
- ALLOWS USE OF HIGHER DENSITY HEAT SHIELD MATERIAL WHICH IS EASY TO FABRICATE AND WELL CHARACTERIZED, THEREBY REDUCING ENTRY SIMULATION TESTING
- ALLOWS THICKER INSULATION ON PRESSURE VESSEL, THUS REDUCING REQUIREMENTS FOR DESCENT SIMULATION TESTING

INCREASED WEIGHT AND VOLUME ALLOWS:

- GREATER UTILIZATION OF EXISTING SUBSYSTEM HARDWARE
- COMMONALITY OF SUBSYSTEM HARDWARE BETWEEN LARGE AND SMALL PROBES; E.G., IDENTICAL BATTERIES, ONE IN SMALL PROBE AND TWO IN LARGE PROBE
- COMMONALITY OF EQUIPMENT AMONG PROBES, BUS, AND ORBITER
- EASIER ACCESSIBILITY TO INSTRUMENTS AND SUBSYSTEMS, REDUCING INTEGRATION AND TEST COSTS
- GREATER FREEDOM TO ACCOMMODATE SCIENCE INSTRUMENT CHANGES OR GROWTH WITHOUT REDESIGN

AEROSHELL CONFIGURATION SELECTED FOR OPTIMUM ENTRY PERFORMANCE

- CONFIGURATION BASED ON EXTENSIVE AERODYNAMIC TEST DATA INCLUDING VIKING
- PROVIDES LARGE DRAG FOR HIGH ALTITUDE DECELERATION, RESULTING IN SUBSONIC SPEEDS ABOVE MAIN CLOUD LAYERS (70 KM)
- RUGGED HEAT SHIELD CAN WITHSTAND HIGH HEAT RATE, HIGH SHEAR ENVIRONMENT WITH LOW MASS LOSS. FLIGHT PROVEN ON HIGH SPEED MISSILES
- CONVENTIONAL, LOW COST ALUMINUM SKIN/ STRINGER AEROSHELL CONSTRUCTION WITHSTANDS ENTRY LOADS
- MINIMUM WEIGHT AND VOLUME AFTERBODY PROVIDES SIMPLEST INTERFACE WITH BUS, PERMITS COMMON CENTRAL CYLINDER IN BUS AND ORBITER

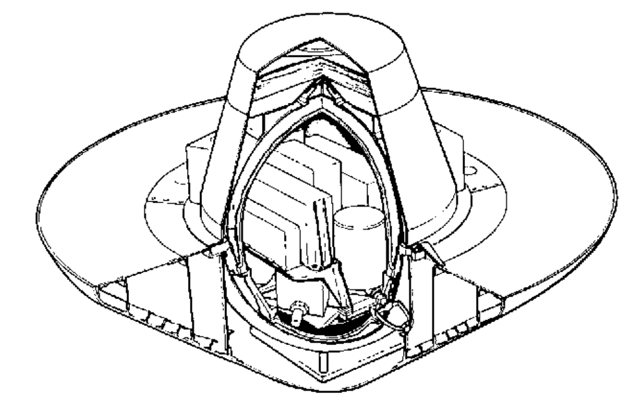

PARACHUTE EXTRACTS DESCENT CAPSULE FROM AEROSHELL AND PROVIDE LOW SPEED FOR UPPER ATMOSPHERE SCIENCE SAMPLING

- RELIABLE MECHANICAL SEPARATION HARDWARE UTILIZED: STANDARD COMMERCIAL ITEMS OR APPLICATIONS OF FLIGHT PROVEN DESIGNS
- RIBLESS GUIDE SURFACE PARACHUTE PROVIDES HIGH STABILITY AND APPROPRIATE DRAG
- NO NEW CHUTE DEVELOPMENT REQUIRED
- ZERO GLIDE CHARACTERISTICS IMPROVE WIND SPEED DETERMINATION

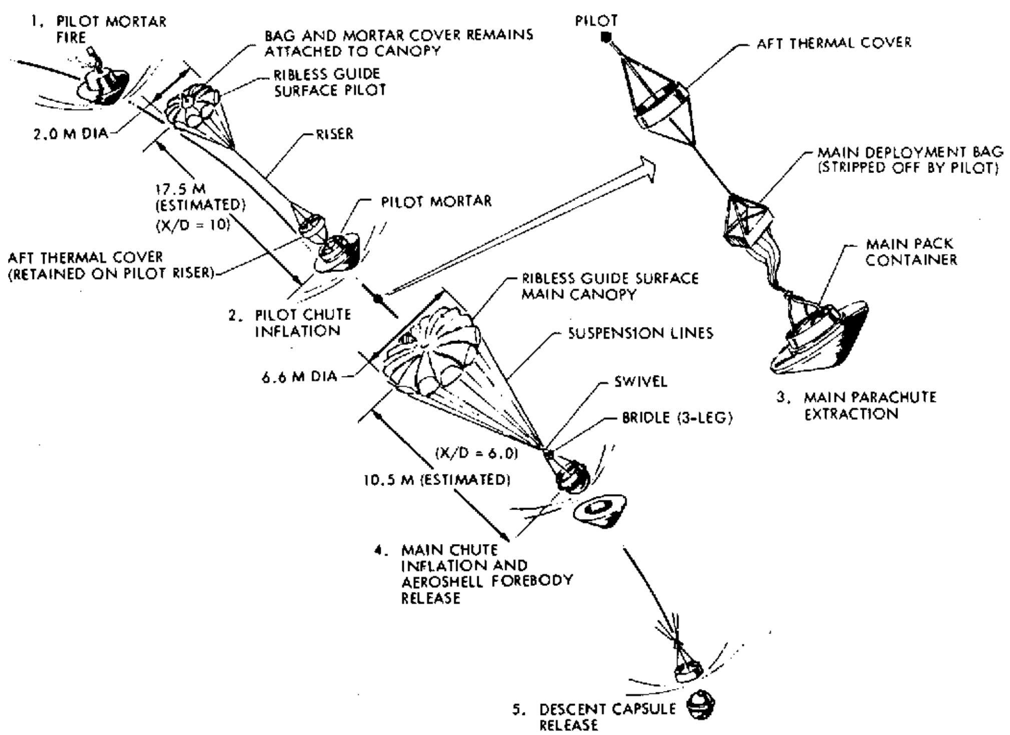

DESCENT CAPSULE EQUIPMENT RING ACCOMMODATES ALL SCIENCE INSTRUMENTS

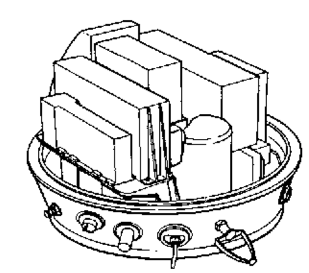

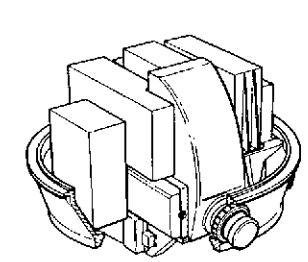

- INTEGRATED PRESSURE SHELL RING AND EQUIPMENT MOUNTING STRUCTURE SIMPLIFIES ASSEMBLY AND DISASSEMBLY OF PRESSURE VESSEL
- PERMITS MAINTAINING SCIENCE INSTRUMENT ALIGNMENT DURING ASSEMBLY AND TEST
- PROVIDES MAXIMUM ACCESS FOR EQUIPMENT AND INSTRUMENT INSTALLATION, CHECKOUT, AND MAINTENANCE
- CONCENTRATES ALL PRESSURE SHELL PENETRATIONS IN ONE BAND, PERMITTING GOOD CONTROL OF HEAT LEAKS
- AVOIDS BLIND CONNECTORS
- PROVIDES FAVORABLE LOCATION FOR SCIENCE SAMPLING: ALL PENETRATIONS ARE PROPERLY ORIENTED WITH RESPECT TO FLOW FIELD AND ARE PERPENDICULAR TO PRESSURE SHELL RING
- ALLOWS FLEXIBILITY IN ACCOMMODATING CHANGES IN SCIENCE INSTRUMENT LOCATION WITH MINIMUM IMPACT ON DESCENT CAPSULE DESIGN

Figure 2-6. Key Large Probe Design Concepts

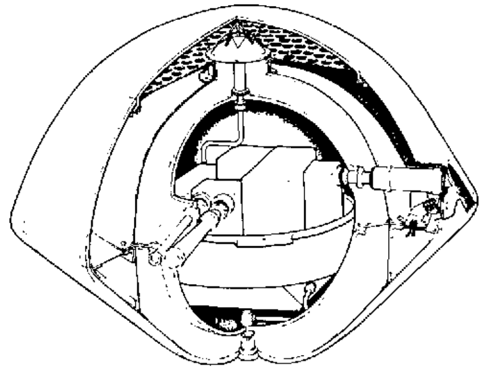

- UNIQUE AERODYNAMIC CONFIGURATION IS STABLE OVER ENTIRE SPEED RANGE FROM HYPERSONIC TO SUBSONIC
- INTEGRATED AEROSHELL PRESSURE VESSEL DESIGN UTILIZES LOAD CARRYING CAPABILITY OF MIN-K INSULATION, AVOIDS CONCENTRATED LOADS, AND REDUCES STRUCTURAL AND INSULATION FABRICATION AND INSTALLATION COSTS BY ELIMINATING FRAMES
- COMMONALITY OF DESIGN FEATURES AND HARDWARE WITH LARGE PROBE REDUCES DEVELOPMENT AND TEST REQUIREMENTS:
  - SAME HEAT SHIELD MATERIAL
  - SAME DESIGN SPHERICAL ALUMINUM PRESSURE VESSEL
  - SAME DESCENT THERMAL INSULATION
  - COMMON APPLICATION OF ELECTRICAL SUBSYSTEM HARDWARE
- SCIENCE INSTRUMENTS EXPOSED AFTER ENTRY HEATING BY FLIGHT PROVEN DEPLOYMENT MECHANISMS

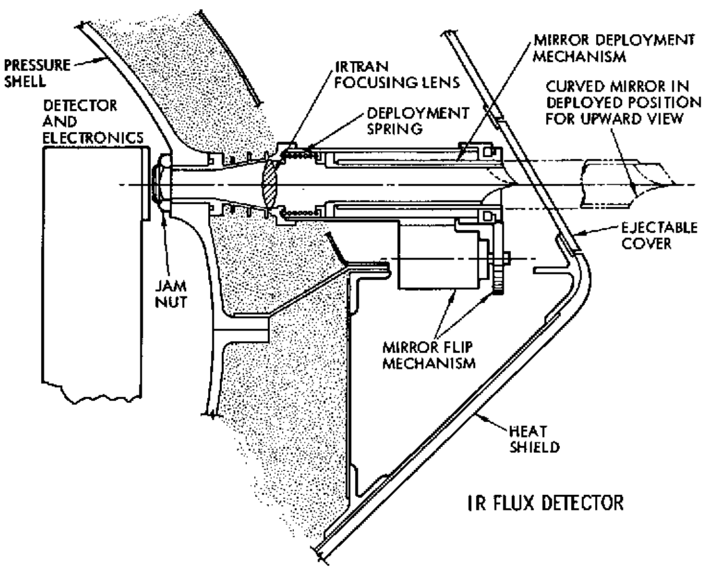

IR FLUX DETECTOR

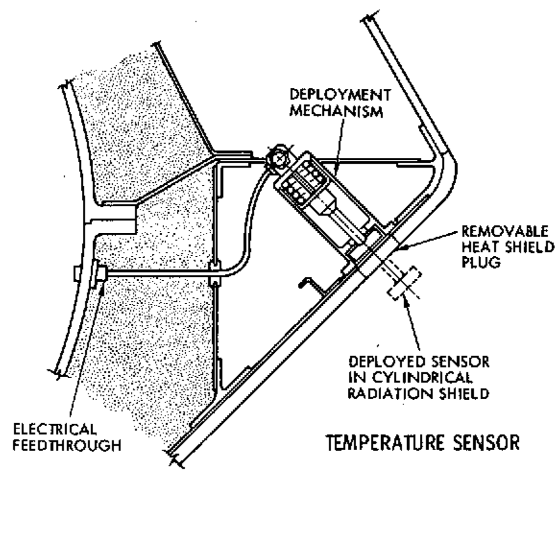

TEMPERATURE SENSOR

Figure 2-7. Key Small Probe Design Concepts

PRECEDING PAGE BLANK NOT FILMED

The earth-pointing, high-gain antenna is the dominant feature of the orbiter spacecraft (Figure 2-8). This configuration represents the least expensive way to satisfy the data rate requirements for the final (Version IV) science payload; it embodies direct equipment derivation from Pioneers 10 and 11. The main question, throughout the study, has been whether it appropriately satisfies the requirements of the scientific instruments. To meet this objective, a ram platform is needed, but once available, the platform improves the data gathering regime of the ram instruments, allowing measurements to be made not only at periapsis, but at any other altitude desired.

Discussions with the individual experimenters have indicated that the only objection to earth pointing is associated with programming and data reduction for a mission in which the geometry changes over the mission. However, there are concomitant advantages of greater latitude coverage for the body-fixed scanning instruments, simple low-cost accommodation of the X-band part of the dual frequency occultation experiment, and the freedom afforded by the ram platform.

Two additional RF attitude sensing techniques are required. The doppler shift technique illustrated is required for verification of the orbit insertion attitude, and the conical scan is required when the high-gain antenna is used.

EARTH POINTING HIGH-GAIN ANTENNA

A FORWARD-POINTING HIGH-GAIN ANTENNA, AS IN PIONEERS 10 AND 11, IS USED BECAUSE THE CONICAL SOLAR ARRAY ALLOWS EITHER THE NOSE OR TAIL OF THE SPACECRAFT TO POINT AT EARTH. ITS OPERATION WILL START AFTER THE FIRST 37 DAYS IN ORBIT, WHEN THE SPACECRAFT IS FLIPPED NOSE-TO-EARTH TO KEEP THE SUN IN THE FORWARD HEMISPHERE. IT PROVIDES HIGH GAIN DURING THE SUBSEQUENT PORTION OF THE MISSION AS COMMUNICATION RANGES BECOME LARGE.

ITS USE IS PROVEN, LEADS TO THE LOWEST SYSTEM COST, AND PROVIDES THE MOST RELIABLE WAY OF ACHIEVING THE DATA RATES DEMANDED BY THE VERSION IV SCIENCE PAYLOAD.

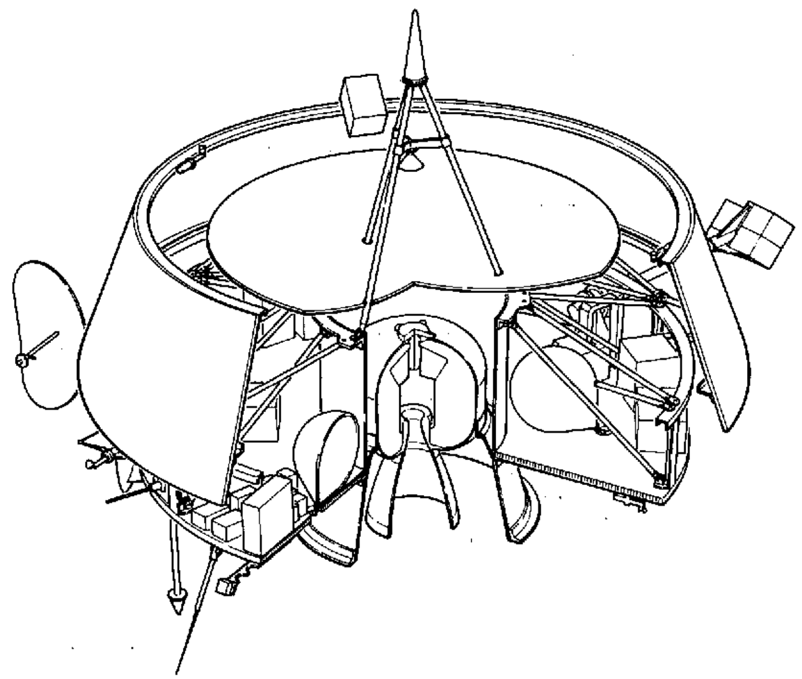

RAM PLATFORM

THE RAM EXPERIMENTS (NEUTRAL AND ION MASS SPECTROMETERS) REQUIRE A SINGLE GIMBALLED, DEPLOYABLE RAM PLATFORM TO ALLOW THEM TO POINT IN THE RAM DIRECTION, ONCE PER REVOLUTION, NEAR PERIAPSIS. THIS CAPABILITY IS NOT REQUIRED FOR CONFIGURATIONS SPINNING PERPENDICULAR TO THE ORBIT PLANE OF VENUS, AND REPRESENTS THE ONLY SIGNIFICANT PENALTY FOR AN EARTH-POINTING CONFIGURATION.

ONCE AVAILABLE, THE GIMBAL FREEDOM ALLOWS IMPROVED ALTITUDE COVERAGE, COMPENSATION FOR OFF POINTING FOR THE DUAL FREQUENCY OCCULTATION EXPERIMENT, AND THE POSSIBILITY OF A PROGRAMMED ANGLE DURING A PERIAPSIS PASS TO GIVE COMPLETE COVERAGE BELOW 4000 KM.

IT USES THE SAME GIMBAL REQUIRED (IN ANY CASE) FOR THE RADAR ALTIMETER AND HENCE ENTAILS NO ADDITIONAL DEVELOPMENT COST.

ADDITIONAL RF ATTITUDE SENSING

TWO RF SENSING TECHNIQUES ARE EMPLOYED FOR THE ORBITER IN ADDITION TO THE DOPPLER MODULATION TECHNIQUE USED FOR THE PROBE BUS:

1. DOPPLER SHIFT DUE TO A TRIAL ΔV (~1 METER/SECOND). KNOWING THE MAGNITUDE OF THE ΔV (WITH 3% ACCURACY) GIVES ASPECT ANGLE WITH THE ACCURACY SHOWN. THIS TECHNIQUE IS REQUIRED FOR ATTITUDE DETERMINATION IN THE VENUS ORBIT INSERTION ATTITUDE, BUT IT IS AVAILABLE FOR BOTH THE PROBE BUS AND ORBITER FOR ANY MIDCOURSE CORRECTION THAT DEMAND AN α IN THE VICINITY OF 1.57 RADIANS (90 DEGREES).

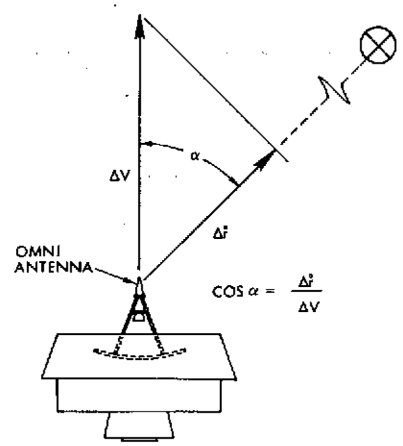

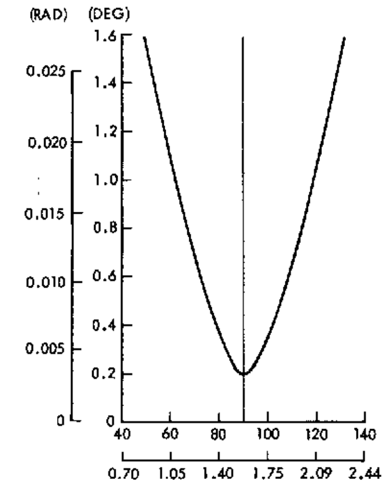

2. CONICAL SCAN WHEN USING THE HIGH-GAIN ANTENNA. EARTH ASPECT ANGLE INFORMATION IS TELEMETERED TO EARTH AND THE SYSTEM IS CAPABLE OF AUTOMATICALLY POINTING THE SPIN AXIS AT EARTH AS ON PIONEERS 10 AND 11. SYSTEM ACCURACY IS SHOWN AS A FUNCTION OF EARTH ASPECT ANGLE. THE GROUND SOFTWARE TO IMPLEMENT THIS FUNCTION EXISTS FOR PIONEERS 10 AND 11.

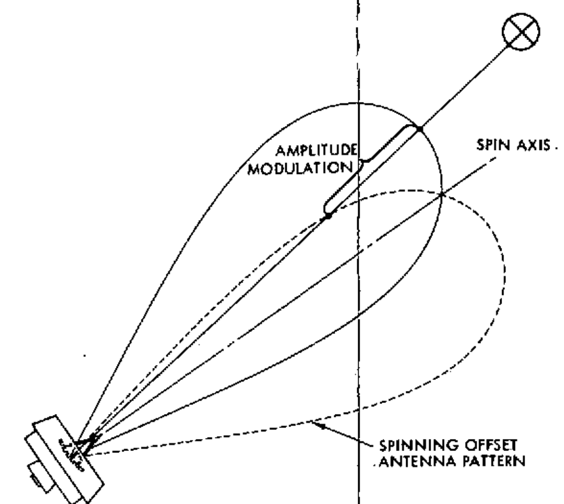

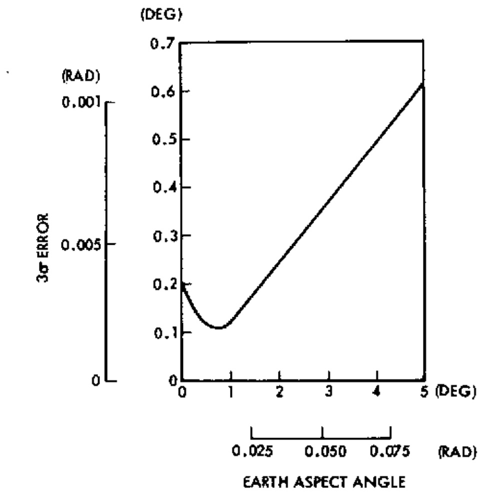

OTHER SCIENCE ACCOMMODATION

THE ONLY OTHER EXPERIMENTS SIGNIFICANTLY IMPACTED BY THE USE OF AN EARTH-POINTING CONFIGURATION ARE THE DUAL FREQUENCY OCCULTATION, THE UV SPECTROMETER, AND THE IR RADIOMETER:

1. DUAL FREQUENCY OCCULTATION

THIS IS EASILY ACCOMMODATED ON THE EARTH POINTED DURING THE FIRST 37 DAYS (BEFORE THE SPACECRAFT FLIP). AN X-BAND HORN PROVIDES A PATTERN SIMILAR TO THE AFT-FACING S-BAND HORN, AND THE SPACECRAFT IS PRE-POSITIONED AS SHOWN. WITH THE GAINS SELECTED AND A 200-MILLI-WATT X-BAND AND ~6 WATT S-BAND TRANSMITTER, THE EXPERIMENT SHOULD WORK WITH REFRACTION ANGLES UP TO 0.314 RADIAN (18 DEGREES FOR S-BAND) AND 0.175 RADIAN (10 DEGREES FOR X-BAND).

2. UV AND IR

THE UV AND IR EXPERIMENTS BENEFIT SIGNIFICANTLY FROM THE ORBIT-TO-ORBIT VARIATION IN THE ORIENTATION OF THE EARTH-POINTING CONFIGURATION NEAR PERIAPSIS. WITH THIS CONFIGURATION, THESE INSTRUMENTS CAN BE MOUNTED ON THE SPACECRAFT SO THAT THEIR VIEW DIRECTIONS TO THE SPIN AXIS ARE FIXED. THE VARIABLE GEOMETRY OF THE EARTH POINTER THEN PERMITS THE INSTRUMENTS TO OBSERVE THE ATMOSPHERE OF VENUS FROM LOW ALTITUDES OVER A DIFFERENT RANGE OF LATITUDES EACH ORBIT. IF THESE INSTRUMENTS REQUIRE NORMAL LIMIT SCANNING OF THE PLANET AT LOW ALTITUDES OVER A WIDE RANGE OF LATITUDES, IT CAN BE READILY ACCOMPLISHED WITH FIXED INSTRUMENTS CONTAINING FIXED SLIT APERTURES AS ILLUSTRATED.

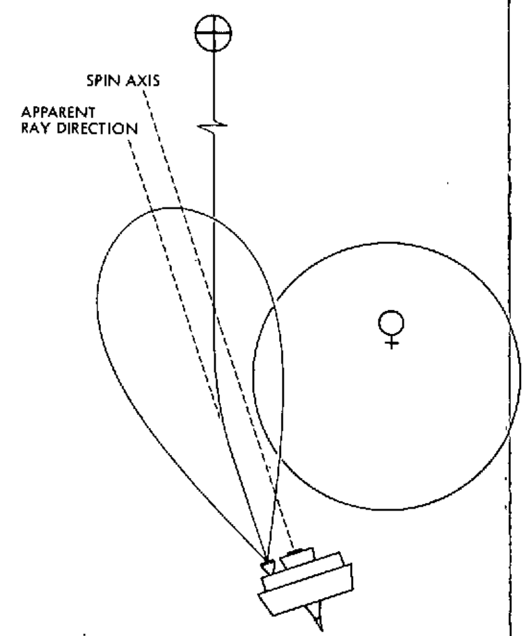

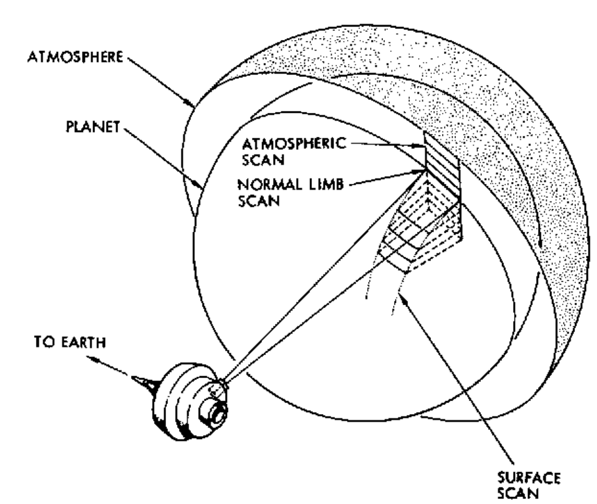

Figure 2-8. Key Design Concepts: Orbiter

FOLDOUT FRAME

FOLDOUT FRAME 2

Together Figures 2-9 and 2-10 summarize the characteristics of the probe bus and orbiter. Figure 2-9 shows the commonality of the block diagrams and presents design features that show the similarity in performance requirements. Figure 2-10 stresses the derivation of equipment from existing programs and the structural commonality between the bus and orbiter, even to common equipment locations.

The block diagram of Figure 2-9 demonstrates that the probe bus and orbiter are developed through additions of mission-peculiar elements to a basic bus.

Probe Bus	Orbiter
add large probe	add high-gain antenna
add small probes	add conscan processor
	add data storage
	add rocket motor
AgZn battery	NiCd battery
probe bus science instrument complement	orbiter science instrument complement (including X-band transmitter)

Figure 2-10 shows how the large probe and the deboost rocket can be mounted using the same basic central cylinder. The small probes are accommodated by the addition of a local support and release mechanism and cutouts in the equipment platform without change in the basic structure. The orbiter science instruments are in the space previously occupied by the small probes. The solar array support is identical; only the conical height of the array changes to support the much greater power requirement of the orbiter. The fixed-dish, high-gain antenna occupies the space previously reserved for the large probe.

SPACECRAFT DESIGN SUMMARY

	KEY FEATURES	PERFORMANCE
STRUCTURES AND MECHANISMS	EARTH POINTING PERMITS SAME BASIC DESIGN AND LAYOUT FOR PROBE BUS AND ORBITER DESIGN IS COMPATIBLE WITH EITHER SEQUENTIAL OR SIMULTANEOUS RELEASE OF PROBES PROBE STOWAGE AND CRUISE ATTITUDE PROVIDE PROBE THERMAL CONTROL WITHOUT HEATERS	WOBBLE DAMPING TIME CONSTANT: 40 MIN SPIN RATE: 4.8 RPM EXCEPT FOR 10 RPM FOR PROBE RELEASE AND 60 RPM FOR PROBE BUS ENTRY AND ORBITER ORBIT INSERTION
THERMAL CONTROL	PASSIVE SYSTEM USES PROVEN MATERIALS AND FABRICATION TECHNIQUES LOUVERS CONTROL EQUIPMENT COMPARTMENT TEMPERATURE SUN ASPECT ANGLE IS CONTROLLED TO ALLOW PASSIVE CONTROL OF LARGE PROBE TEMPERATURE	TEMPERATURE RANGES DURING CRUISE (PROBE): EQUIPMENT PLATFORM 4 TO 26°C SOLAR ARRAY -101 TO 63°C LARGE PROBE 6 TO 32°C TEMPERATURE RANGES DURING MISSION (ORBITER) EQUIPMENT PLATFORM 4 TO 24°C SOLAR ARRAY -148 TO 107°C RAM PLATFORM -30 TO 60°C
ELECTRICAL POWER	CONICAL SOLAR ARRAY PROVIDES NEARLY CONSTANT OUTPUT OVER $\pi/2$ RADIANS (90 DEGREES) OF SUN ASPECT ANGLE, PERMITTING WIDE FREEDOM OF ATTITUDE DURING CRUISE AND MANEUVERS ELECTRICAL POWER SYSTEM OPERATES IN FULLY AUTOMATIC MODE WITH BUILT IN FAILURE PROTECTION AND PROVISION FOR COMMAND OVERRIDE	PROBE BUS / ORBITER ARRAY OUTPUT: NEAR EARTH: 61 WATTS / 100 WATTS AT VENUS: 111 WATTS / 225 WATTS BUS VOLTAGE: 28 VOLTS ±2% / 28 VOLTS ±2% BATTERY TYPE: Ag Zn / Ni Cd BATTERY CAPACITY: 1.94×10^6 J / 1.24×10^6 J
ATTITUDE DETERMINATION AND CONTROL	DOPPLER MODULATION AND SHIFT TECHNIQUES PROVIDE ADEQUATE ATTITUDE DETERMINATION FOR PROBE BUS AND FOR ORBITER WHEN HIGH GAIN DISH IS NOT EARTH POINTING; NO SEPARATE ATTITUDE DETERMINATION EQUIPMENT NEEDED WHEN ORBITER HIGH GAIN DISH IS EARTH POINTING, CONSCAN TECHNIQUE PROVIDES ATTITUDE DETERMINATION USING EXISTING ON BOARD PROCESSOR AND GROUND SOFTWARE SUN SENSOR PROVIDES BOTH ROLL REFERENCE AND SUN ASPECT INFORMATION FOR USE IN ATTITUDE DETERMINATION	ATTITUDE DETERMINATION ACCURACY IS WITHIN 0.017 RADIAN (1 DEGREE) VALUE DEPENDS ON SPACECRAFT EARTH ASPECT AND TECHNIQUE BEING USED. MEETS ALL MISSION REQUIREMENTS
PROPULSION	MONOPELLANT HYDRAZINE REACTION CONTROL SYSTEM IS FLIGHT PROVEN BLOWDOWN PRESSURIZATION IS SIMPLE AND RELIABLE EIGHT THRUSTERS PROVIDE GOOD REDUNDANCY AND NO CONING ANGLE AMPLIFICATION TRANSVERSE THRUSTERS SIMPLIFY GROUND OPERATIONS ORBIT INSERTION MOTOR AND SAFE ARM DEVICE ARE FLIGHT PROVEN	SOLID ROCKET MOTOR: TOTAL IMPULSE 405 560 NEWTON SECONDS BURN TIME 23 SECOND MAXIMUM THRUST 2 155 NEWTONS LOADED MASS 166 KILOGRAMS REACTION CONTROL SYSTEM: EFFECTIVE IMPULSE 33 700 NEWTON SECONDS OPERATING PRESSURE 250 TO 120 N/CM^2 THRUST 4.5 NEWTONS
COMMUNICATIONS	FORWARD AND AFT OMNI ANTENNAS PROVIDE FULL COVERAGE DURING ALL MANEUVERS AND MISSION PHASES GAIN AND COVERAGE REQUIREMENTS ARE MET WITHOUT USE OF DESPUN ANTENNA OR REFLECTOR DESIGN MAKES USE OF RESIDUAL HARDWARE FROM PIONEERS 10 AND 11	PROBE BUS LINK PROVIDES 1024 BITS/SECOND AT ENTRY USING 64 METER DSN ORBITER LINK PROVIDES 32 BITS/SECOND AT MAXIMUM RANGE USING 26 METER DSN (1024 BITS/SECOND WITH 64 METER DSN)
DATA HANDLING	STORAGE IS PROVIDED FOR ORBITER DATA DURING EARTH OCCULTATION OR HIGH RATE DATA ACQUISITION PERIODS SIMULTANEOUSLY DATA CAN BE STORED FROM FOUR SOURCES AT DESIRED RATES AND TIMES DATA HANDLING SYSTEM PROVIDES SPIN SECTOR GENERATION FOR PRECESSION MANEUVERS, SMALL PROBE RELEASE, AND EXPERIMENTS NEEDING ACCURATE ROLL INDEX PULSE; PULSES CAN BE AVERAGED, STORED, REPEATED	DATA STORAGE: 1.23 MILLION BITS BIT RATES: 8 TO 1024 BITS/SECOND FRAME LENGTH: 768 BITS DATA CODING: CONVOLUTIONAL (RATE 1/2, K 32) A/D CONVERSION RESOLUTION: 10 BITS TELEMETRY MODULATION: PCM/PSK/PM
COMMAND	16 STORED COMMANDS WITH ASSOCIATED TIME DELAYS ARE PROVIDED; (NEEDED FOR ORBIT INSERTION FIRING DURING EARTH OCCULTATION AND SCIENCE OPERATING MODES IN OCCULTATION PERIODS)	COMMAND RATE: 1 BIT/SECOND WORD LENGTH: 22 BITS MODULATION: PCM/PSK/PM STORED COMMAND DELAY: TIME RESOLUTION 2 SECONDS MAXIMUM TIME DELAY 36 HOURS

PROBE BUS AND ORBITER BLOCK DIAGRAM

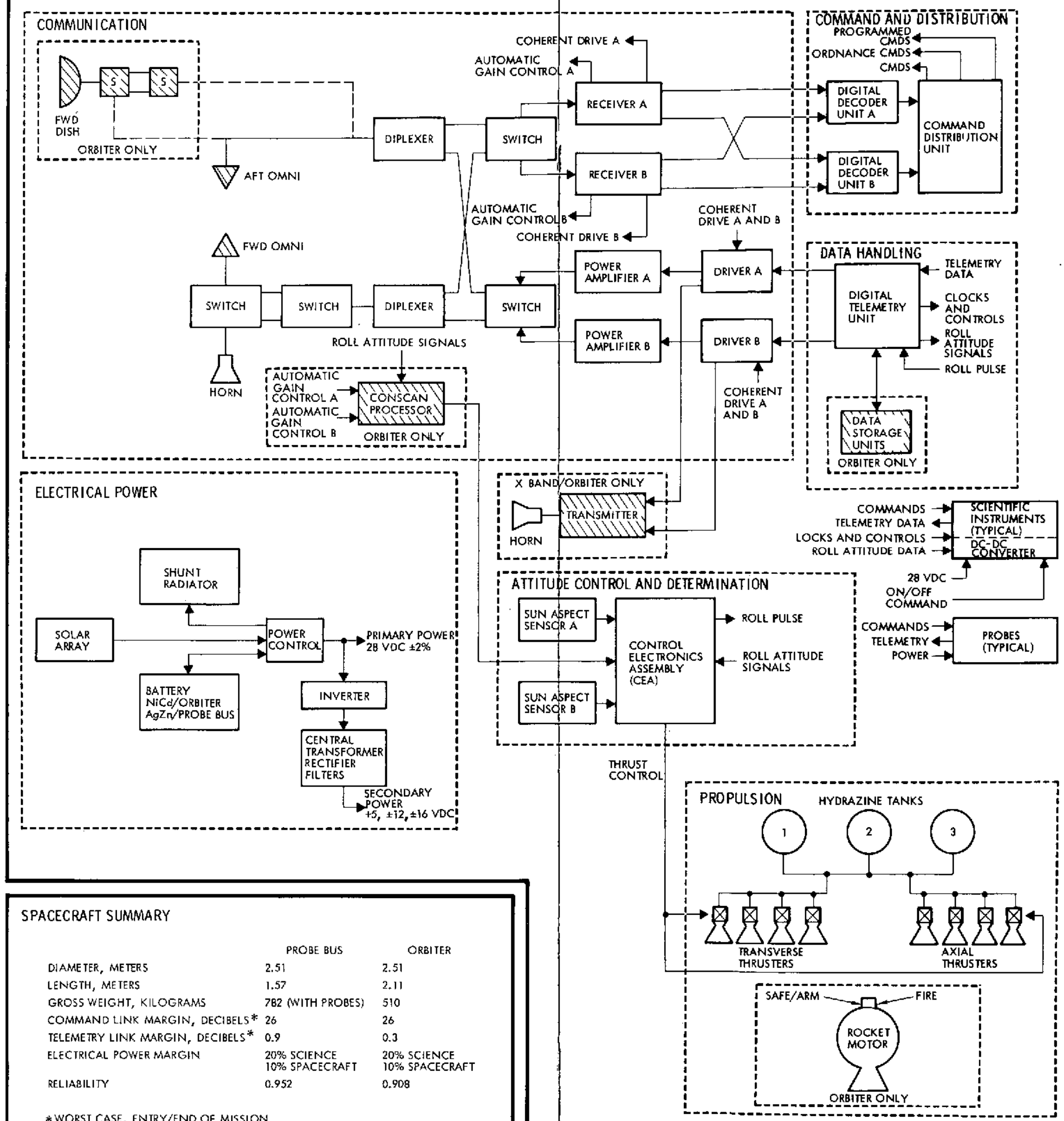

SPACECRAFT SUMMARY

	PROBE BUS	ORBITER
DIAMETER, METERS	2.51	2.51
LENGTH, METERS	1.57	2.11
GROSS WEIGHT, KILOGRAMS	782 (WITH PROBES)	510
COMMAND LINK MARGIN, DECIBELS*	26	26
TELEMETRY LINK MARGIN, DECIBELS*	0.9	0.3
ELECTRICAL POWER MARGIN	20% SCIENCE 10% SPACECRAFT	20% SCIENCE 10% SPACECRAFT
RELIABILITY	0.952	0.908

*WORST CASE, ENTRY/END OF MISSION

Figure 2-9. Probe Bus and Orbiter Design Summary

FOLDOUT FRAME

FOLDOUT FRAME 2

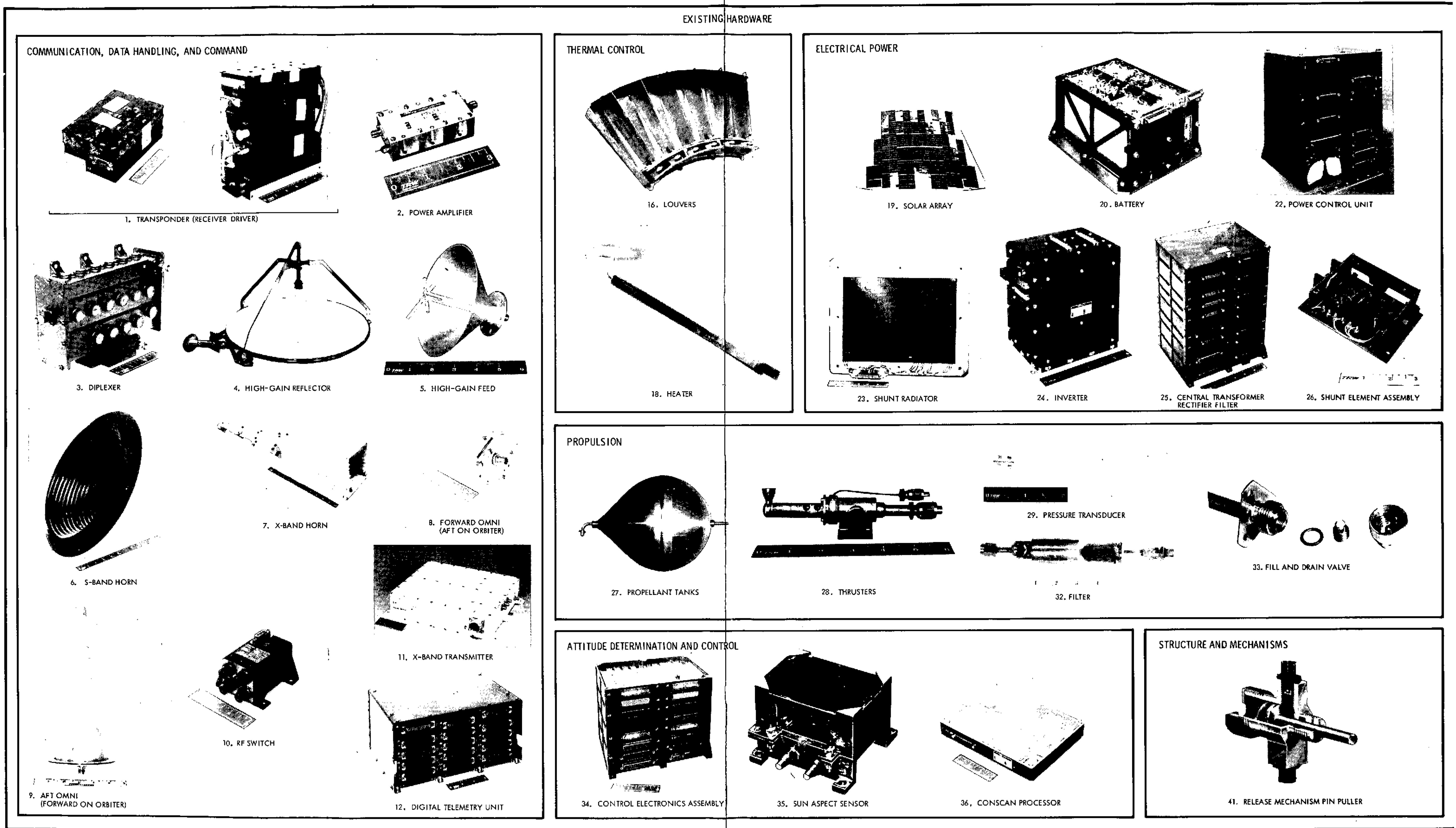
EXISTING HARDWARE
COMMUNICATION, DATA HANDLING, AND COMMAND
1. TRANSPONDER (RECEIVER DRIVER)
2. POWER AMPLIFIER
3. DIPLEXER
4. HIGH-GAIN REFLECTOR
5. HIGH-GAIN FEED
6. S-BAND HORN
7. X-BAND HORN
8. FORWARD OMNI (AFT ON ORBITER)
9. AFT OMNI (FORWARD ON ORBITER)
10. RF SWITCH
11. X-BAND TRANSMITTER
12. DIGITAL TELEMETRY UNIT
THERMAL CONTROL
16. LOUVERS
18. HEATER
ELECTRICAL POWER
19. SOLAR ARRAY
20. BATTERY
22. POWER CONTROL UNIT
23. SHUNT RADIATOR
24. INVERTER
25. CENTRAL TRANSFORMER RECTIFIER FILTER
26. SHUNT ELEMENT ASSEMBLY
PROPULSION
27. PROPELLANT TANKS
28. THRUSTERS
29. PRESSURE TRANSDUCER
32. FILTER
33. FILL AND DRAIN VALVE
ATTITUDE DETERMINATION AND CONTROL
34. CONTROL ELECTRONICS ASSEMBLY
35. SUN ASPECT SENSOR
36. CONSCAN PROCESSOR
STRUCTURE AND MECHANISMS
41. RELEASE MECHANISM PIN PULLER

SPACECRAFT SUBSYSTEMS AND COMPONENTS EQUIPMENT COMMONALITY AND DERIVATION

ITEM	BUS	ORBITER	DERIVATION	STATUS
COMMUNICATIONS				
1 TRANSPONDER (RECEIVER DRIVER)	X	X	PIONEERS 10 AND 11	1
2 POWER AMPLIFIER	X	X	COMMERCIAL APPLICATION	3
3 DIPLEXER	X	X	PIONEERS 10 AND 11	1
4 HIGH-GAIN REFLECTOR		X	DSCS II	1
5 HIGH-GAIN FEED		X	PIONEERS 10 AND 11	1
6 S-BAND HORN	X	X	PIONEERS 10 AND 11	1
7 X-BAND HORN		X	DSCS II	1
8 FORWARD OMNI (AFT ON ORBITER)	X	X	PIONEERS 10 AND 11	1
9 AFT OMNI (FORWARD ON ORBITER)	X	X	DEFENSE SUPPORT PROGRAM (DSP)	1
10 RF SWITCH	X	X	PIONEERS 10 AND 11	
11 X-BAND TRANSMITTER	X	X	PIONEERS 10 AND 11	
DATA HANDLING				
12 DIGITAL TELEMETRY UNIT	X	X	PIONEERS 10 AND 11	1
13 DATA STORAGE UNIT		X	NEW	4
COMMAND				
14 DIGITAL DECODER UNIT	X	X	PIONEERS 10 AND 11	1
15 COMMAND DISTRIBUTION UNIT	X	X	PIONEERS 10 AND 11	3
THERMAL CONTROL				
16 LOUVERS	X	X	HELIOS	2
17 INSULATION	X	X	PIONEERS 10 AND 11	2
18 HEATERS	X	X	PROGRAM 169	1
ELECTRICAL POWER				
19 SOLAR ARRAY	X	X	DSP	2
20 BATTERY		X	DSP, DSCS II	2
21 BATTERY	X		MMC (IR&D PROGRAM; PROBES USE SAME CELLS)	3
22 POWER CONTROL UNIT	X	X	PIONEERS 10 AND 11	2
23 SHUNT RADIATOR	X	X	PIONEERS 10 AND 11	1
24 INVERTER	X	X	PIONEERS 10 AND 11	2
25 CENTRAL TRANSFORMER RECTIFIER FILTER	X	X	PIONEERS 10 AND 11	2
26 SHUNT ELEMENT ASSEMBLY	X	X	VELA	
PROPULSION				
27 PROPELLANT TANKS	X	X	DSCS II	1
28 THRUSTERS	X	X	FLTSATCOM	
29 PRESSURE TRANSDUCER	X	X	PIONEERS 10 AND 11	1
30 TEMPERATURE TRANSDUCER	X	X	PIONEERS 10 AND 11	1
31 ROCKET MOTOR FOR INSERTION		X	VELA	1
32 FILTER	X	X	INTELSAT III	
33 FILL AND DRAIN VALVE	X	X	PIONEERS 10 AND 11	
ATTITUDE DETERMINATION AND CONTROL				
34 CONTROL ELECTRONICS ASSEMBLY	X	X	PIONEERS 10 AND 11	1
35 SUN ASPECT SENSOR	X	X	INTELSAT III	1
36 CONSCAN PROCESSOR		X	PIONEERS 10 AND 11	1
37 RAM PLATFORM DRIVE		X	FLTSATCOM	2
STRUCTURE AND MECHANISM				
38 STRUCTURE	X	X	NEW	3
39 NUTATION DAMPER	X	X	NEW	3
40 MAGNETOMETER BOOM		X	NEW	3
41 RELEASE MECHANISM	X		PIONEERS 10 AND 11 MINUTEMAN	1

STATUS:
1 EXISTING DESIGN, AS IS
2 MINOR MODIFICATIONS REQUIRED (NO REQUALIFICATION)
3 MODIFICATION OF EXISTING, REQUALIFICATION REQUIRED
4 NEW DESIGN, BASED ON PROVEN TECHNOLOGY

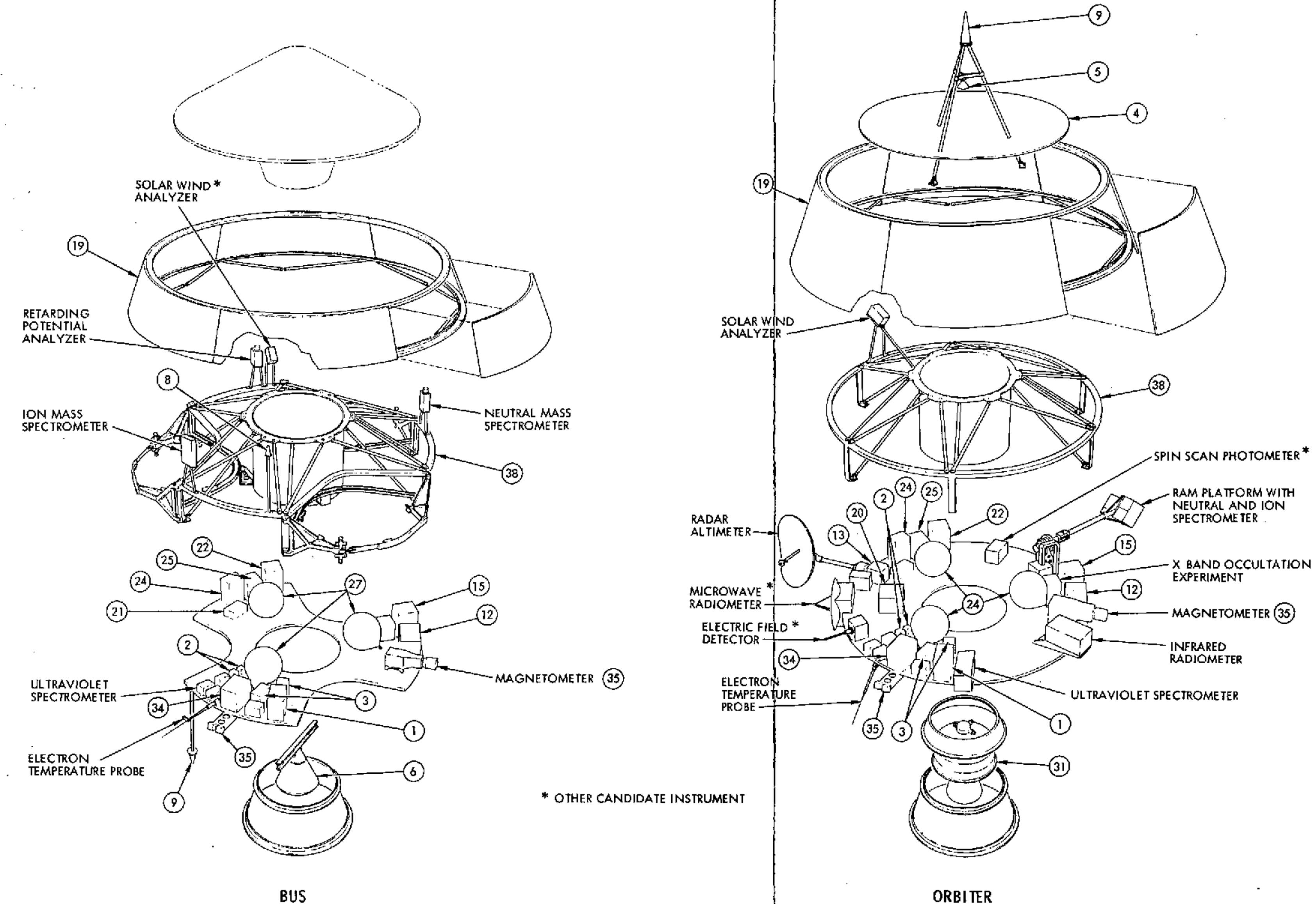

AS A MAJOR PART OF THE EFFORT TO DEVELOP A LOW COST DESIGN, EVERY EFFORT HAS BEEN MADE TO USE AS MANY COMMON COMPONENTS AS POSSIBLE IN BOTH PROBE BUS AND ORBITER, TO USE FLIGHT PROVEN COMPONENTS FROM PROGRAMS WHEREVER THEY CAN MEET THE MISSION REQUIREMENTS.

THE LIST AT THE LEFT SHOWS THAT NEARLY ALL OF THE SPACECRAFT SUBSYSTEM COMPONENTS ARE COMMON TO BOTH SPACECRAFT AND THAT NEARLY ALL ARE DERIVED FROM EARLIER SUCCESSFUL SPACECRAFT PROGRAMS. THE PRINCIPAL SOURCE OF FLIGHT PROVEN COMPONENTS HAS BEEN THE PIONEER 10 AND 11 PROGRAM, FOR WHICH THE REQUIREMENTS ARE IN MANY CASES QUITE SIMILAR TO THOSE OF THE PIONEER VENUS MISSION.

THE FIGURES ABOVE ILLUSTRATE HOW THE SAME BASIC DESIGN HAS BEEN USED EVEN IN THOSE CASES WHERE THE DETAILS MUST BE CHANGED TO SUIT THE DIFFERING REQUIREMENTS OF PROBE BUS AND ORBITER. THE EQUIPMENT PLATFORMS USE THE SAME STRUCTURAL MATERIALS AND TECHNIQUES FOR TRANSFERRING LOADS, AND SUBSYSTEM COMPONENTS ARE MOUNTED AT THE SAME LOCATIONS. ALTHOUGH THE ORBITER HAS A LARGER SOLAR ARRAY AREA, THE CONE ANGLE IS THE SAME AND THE FABRICATION TECHNIQUES ARE IDENTICAL FOR BOTH ARRAYS.

NOTE ALSO THAT THE RADAR ALTIMETER ANTENNA AND THE RAM PLATFORM USE THE SAME DRIVE MECHANISM, WHICH IS DERIVED DIRECTLY FROM THE FLTSATCOM PROGRAM AND INDIRECTLY FROM THE SOLAR ARRAY DRIVE ORIGINALLY DEVELOPED BY TRW FOR THE OGO SPACECRAFT. THIS MECHANISM HAS DEMONSTRATED SUCCESSFUL OPERATION IN SPACE FOR PERIODS FAR LONGER THAN THOSE REQUIRED FOR PIONEER VENUS.

Figure 2-10. Equipment Derivation and Commonality: Probe Bus and Orbiter

In the case of the probes, the environments associated with entry and descent into the Venusian atmosphere constrain our ability to apply hardware from other spacecraft programs. Nevertheless, as Figure 2-11 shows, a significant number of subsystem components can be built from existing designs with only minor modifications. Common use of identical components in both large and small probes has also been emphasized. Thus the 20-watt S-band power amplifier in the small probe is also used in parallel configuration in the large probe. The same one-and-two arrangement holds for the battery. The Viking-derived transponder in the large probe is built in modular form, and the receiver section is removed to provide the transmitter driver in the small probe.

Three items in the probes are common with the bus and orbiter. The standard probe battery cells are used in the bus. Identical diplexers are used in bus, orbiter, and large probe. The Pioneer 10 and 11 digital telemetry unit is used in the bus and orbiter; for the probes, it is modified only to remove redundant circuit boards or unneeded special features such as the spin-period sector generator.

The mechanical design features common design approaches for both large and small probes. Figure 2-11 shows the similarity in design of the aeroshell, heat shield, pressure vessel, and descent thermal insulation. Identical materials are used; the exceptions (aeroshell structure and radome) are associated with the requirement for the small probe to retain its aeroshell throughout terminal descent.

Significant probe system design and performance data are presented in Figure 2-12. The important design environments are listed there, together with the margins employed in developing the hardware designs. The margins have been made large to reduce cost in the development and qualification programs. (See Section 11.)

LARGE PROBE

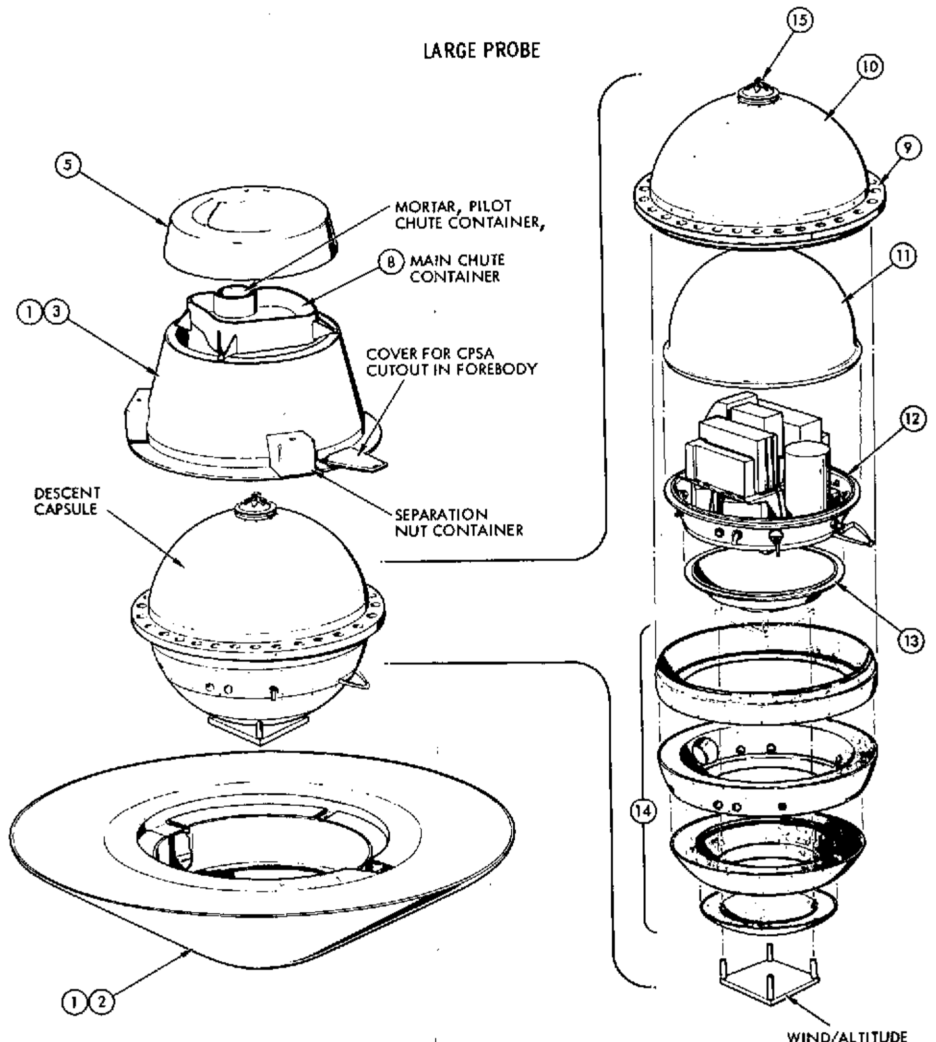

EQUIPMENT RING

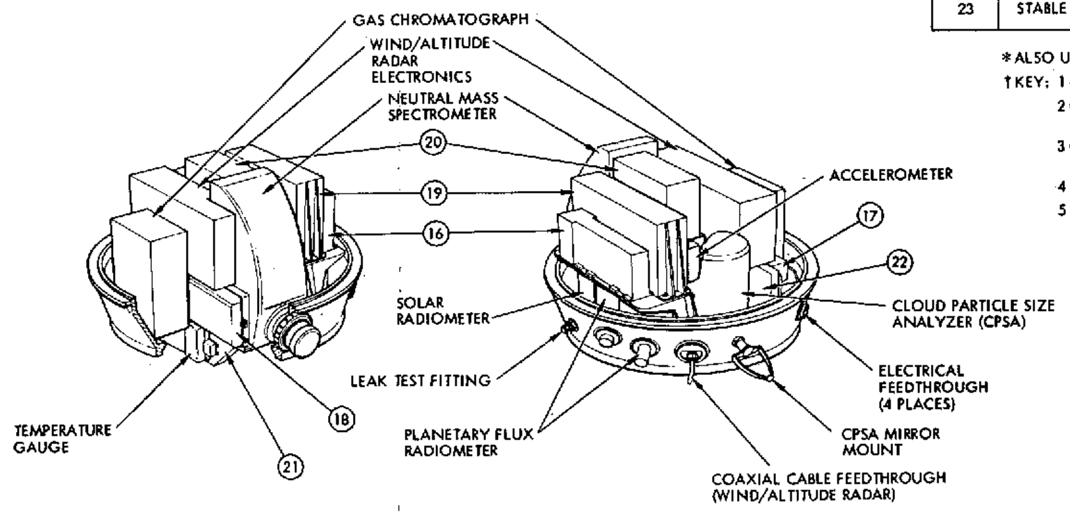

NO.	ITEM	LARGE PROBE	SMALL PROBE	DERIVATION/DESCRIPTION	STATUS†
1	AEROSHELL STRUCTURE	X		CONVENTIONAL DESIGN ALUMINUM MONOCOQUE STRUCTURE	4
			X	SAME AS LARGE PROBE WITH TITANIUM	4
2	AEROSHELL FOREBODY HEAT SHIELD	X	X	QUANTZ NITRILE PHENOLIC, FLIGHT PROVEN ON SPRINT INTERCEPTOR MISSILE	4
3	AEROSHELL AFTBODY HEAT SHIELD	X	X	ELASTOMERIC SILICONE ESA 3560 FILLED HONEYCOMB, FLIGHT PROVEN ON USAF PRIME AND NASA ARC PAET REENTRY VEHICLE. ALSO QUALIFIED FOR USE ON VIKING	4
4	SEPARATION NUTS AND INITIATORS	X		VIKING LANDER	2
5	RADOME	X		ESA 3560: MATERIAL IS RF TRANSPARENT, ALSO REMOVED BEFORE DATA TRANSMISSION BEGINS	4
			X	TFE TEFLON: FLIGHT PROVEN ON NUMEROUS ENTRY SYSTEMS	4
6	MORTAR	X		STANDARD USAF DESIGN FOR CHUTE EXTRACTION, VIKING STANDARD INITIATORS	3
7	PILOT CHUTE	X		NYLON RIBLESS GUIDE SURFACE CANOPY, EXTENSIVELY USED BY USAF AS PILOT CHUTE	3
8	MAIN CHUTE	X		SAME AS PILOT CHUTE	3
9	STABILIZING RING	X		TITANIUM RING, STANDARD DESIGN AND MACHINING PRACTICES	4
10	INSULATION COVER	X	X	TITANIUM SHELL, STANDARD DESIGN AND FABRICATION TECHNIQUES	4
11	UPPER PRESSURE SHELL CLOSURE	X	X	HEMISPHERICAL ALUMINUM MONOCOQUE SHELL, MACHINED FROM FORGING	4
12	EQUIPMENT RING	X		CONICAL FRUSTUM, MACHINED ALUMINUM FORGING	4
			X	PAN SHAPED ALUMINUM STRUCTURE	4
13	LOWER PRESSURE SHELL CLOSURE	X	X	SAME AS UPPER CLOSURE	4
14	THERMAL INSULATION	X	X	MIN K TE 1400, PERFORMANCE ESTABLISHED AND FABRICATION TECHNIQUE DEMONSTRATED BY MMC IR&D	4
15	COMMUNICATIONS ANTENNA	X	X	VIKING LANDER	3
16	TRANSPONDER	X		VIKING LANDER	3
			X	SMALL PROBE USES ONLY TRANSMITTER DRIVER PORTION OF TRANSPONDER	3
17	S BAND POWER AMPLIFIER	X	X	COMMERCIAL APPLICATION, 2 ON LARGE PROBE, 1 ON SMALL PROBE	3
18	DIPLEXER*	X		PIONEERS 10 AND 11	3
19	DIGITAL TELEMETRY UNIT*	X	X	PIONEERS 10 AND 11	3
20	POWER CONTROL UNIT	X	X	PIONEER 10 AND 11 CIRCUITS	3
21	BATTERY*	X	X	MMC IR&D DEVELOPMENT, 2 ON LARGE PROBE, 1 ON SMALL PROBE	3
22	PHASE CHANGE THERMAL CONTROL DEVICE	X	X	DEVELOPED UNDER NASA MSFC CONTRACT AND MMC IR&D	3
23	STABLE OSCILLATOR		X	NEW	3

*ALSO USED ON PROBE BUS AND/OR ORBITER

†KEY: 1 = EXISTING DESIGN, USED AS IS
2 = MINOR MODIFICATION FROM EXISTING DESIGN, NO REQUALIFICATION
3 = MINOR MODIFICATION FROM EXISTING DESIGN, REQUALIFICATION REQUIRED
4 = NEW DESIGN, PROVEN TECHNOLOGY
5 = NEW DESIGN, ADVANCED TECHNOLOGY

AN EFFORT HAS BEEN MADE TO REDUCE COSTS BY USING IDENTICAL COMPONENTS, MATERIALS, AND DESIGN APPROACHES FOR BOTH LARGE AND SMALL PROBES. DEVELOPED HARDWARE HAS ALSO BEEN ADOPTED TO THE FULLEST EXTENT, RECOGNIZING THAT MINOR MODIFICATIONS MAY HAVE TO BE MADE TO ENABLE THE UNIT TO WITHSTAND THE VENUS ENTRY AND DESCENT ENVIRONMENT. IT IS FOR THIS REASON THAT ALMOST ALL OF THE EQUIPMENT LISTED ABOVE IS EITHER NEW OR MUST BE REQUALIFIED, IF EXISTING.

THE FIGURES ILLUSTRATE SOME OF THE DESIGN COMMONALITIES BETWEEN LARGE AND SMALL PROBES: SPHERICAL PRESSURE VESSEL, EXTERNAL THERMAL INSULATION LAID UP IN SEGMENTS, CENTRAL RING TO MOUNT ALL SCIENCE INSTRUMENTS AND SUBSYSTEM EQUIPMENT. ELECTRICAL/ELECTRONIC COMPONENTS USED IN BOTH PROBES ARE IDENTICAL.

SMALL PROBE

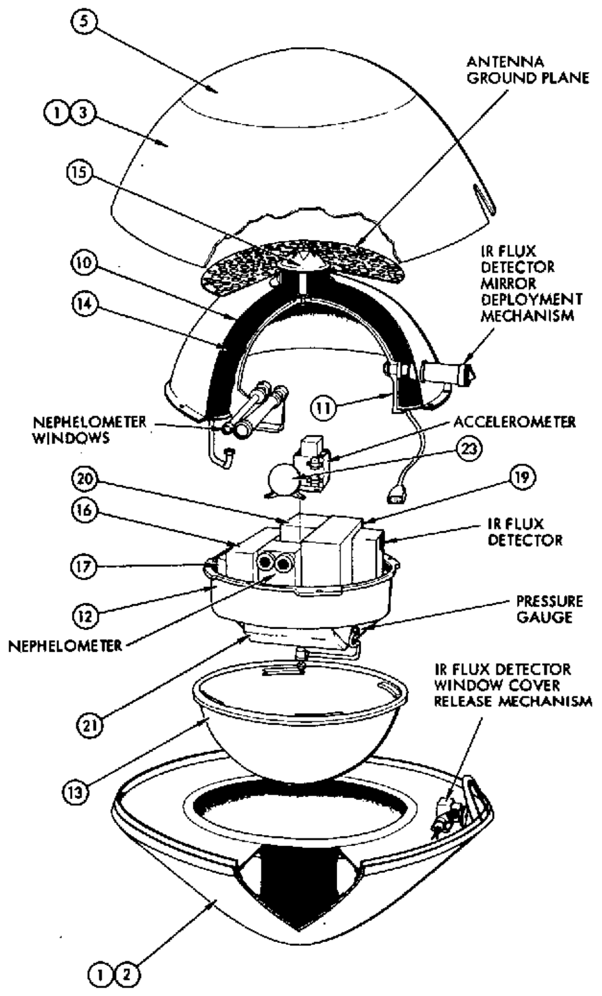

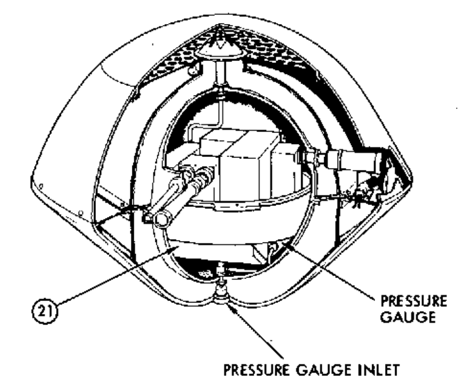

Figure 2-11. Equipment Derivation and Commonality - Probes

FOLDOUT FRAME 1

FOLDOUT FRAME 2

A MISSION SUCCESS

	SUCCESS PROBABILITY
LARGE PROBE	0.945
SMALL PROBE	0.964
LARGE PROBE AND ONE SMALL PROBE	0.911
LARGE PROBE AND TWO SMALL PROBES	0.878
LARGE PROBE AND THREE SMALL PROBES	0.847

B SUMMARY WEIGHT STATEMENT

		KG
LARGE PROBE (INCLUDING 16.5% CONTINGENCY)		307.1
SMALL PROBE (INCLUDING 16.5% CONTINGENCY)	81.5 x 3 =	244.5
TOTAL PROBE WEIGHT		551.6

C PROBE ENVIRONMENTAL DESIGN AND VERIFICATION REQUIREMENTS

PROBE ENVIRONMENTS	FLIGHT LEVELS: SMALL PROBE	FLIGHT LEVELS: LARGE PROBE	DESIGN LIMITS: STRUCTURE (TIMES FLIGHT LEVEL)	DESIGN LIMITS: PAYLOAD EQUIPMENT (TIMES FLIGHT LEVEL)
DECELERATION				
AXIAL (a)	488G	358G	1.56	1.5
LATERAL (a)	8.5G	2G	1.56	1.5
ACCELERATION				
AXIAL (b)	20G		1.56	1.5
LATERAL (b)	12G		1.56	1.5
SPIN RATE				
LAUNCH (b)	90 RPM		1.56	1.5
PROBE CRUISE (b)	10 RPM		1.56	1.5
TEMPERATURE				
EXTERIOR TO PRESSURE VESSEL				
AFTBODY (a)	209.8 TO 755.4°K (-82 TO 900°F)	177.6 TO 422.0 °K (-140 TO 300°F)	1.0	N/A
FOREBODY (a)	224.3 TO 755°K (-56 TO 900°K)	265.4 TO 541.5°K (18 TO 515°F)	1.0	N/A
PRESSURE SHELL (a)	275.9 TO 403.7°K (37 TO 267°F)	267.0 TO 369.8°K (21 TO 206°F)	1.0	N/A
PRESSURE SHELL EQUIPMENT (a)	255.4 TO 338.7°K (0 TO 150°F)	255.4 TO 338.7°K (0 TO 150°F)		219.3 TO 348.7°K (-65 TO 168°F) PLATE TESTS
PRESSURE				
LAUNCH - PROBE (b)	1.01 NEWTONS/METER^2 (760 X 10^{-5} TORR)		0.001 NEWTONS/METER^2 (10^{-5} TORR)	0.10 MEGANEWTONS/METER^2 TO 0.05 MEGANEWTONS/METER^2 (1 TO 0.5 ATMOSPHERES)
CRUISE - PROBE (b)	1.33 X 10^{-12} NEWTONS/METER^2 (10^{-14} TORR)		0.001 NEWTONS/METER^2 (10^{-5} TORR)	0.10 MEGANEWTONS/METER^2 TO 0.05 MEGANEWTONS/METER^2 (1 TO 0.5 ATMOSPHERES)
ENTRY - DESCENT CAPSULE (b)				
EXTERNAL	0.01 MEGANEWTONS/METER^2 TO 9.42 MEGANEWTONS/METER^2 (0.1 TO 93 ATMOSPHERES)		11.75 MEGANEWTONS/METER^2 (116 ATMOSPHERES)	0.10 MEGANEWTONS/METER^2 TO 0.05 MEGANEWTONS/METER^2 (1 TO 0.5 ATMOSPHERES)
INTERNAL	0.10 MEGANEWTONS/METER^2 (1 ATMOSPHERE)		0.61 MEGANEWTONS/METER^2 (6 ATMOSPHERES)	0.10 MEGANEWTONS/METER^2 (1 ATMOSPHERE)
VIBRATION				
SINE (b)	AXIAL 1.5G; 5 TO 15 HZ 4.5G; 15 TO 21 HZ 1.5G; 21 TO 100 HZ LATERAL 1.6G; 5 TO 14 HZ 1.0G; 14 TO 100 HZ		AXIAL 7.2G; 5 TO 15 HZ 19.6G; 15 TO 21 HZ 7.2G; 21 TO 100 HZ LATERAL 7.2G; 5 TO 14 HZ 4.68G; 14 TO 180 HZ 4 MIN/AXIS DURATION	AXIAL 7.5G; 5 TO 15 HZ 22.5G; 15 TO 21 HZ 11.3G; 21 TO 35 HZ 7.5G; 35 TO 50 HZ 4.5G; 50 TO 100 HZ LATERAL 7.5G; 5 TO 30 HZ 4.5G; 30 TO 100 HZ 1 MIN/AXIS DURATION
RANDOM (a)	6.1G RMS - 20 TO 300 HZ +3 DB/OCTAVE 300 TO 2000 HZ; 0.02 PSD		LP 9.3G RMS 20 TO 150 HZ, TO DB/OCTAVE 150 TO 2000 HZ; 0.045 PSD SP 19.6G RMS 20 TO 60 HZ; 0.11 PSD 60 TO 100 HZ; -3 DB/OCTAVE 300 TO 1200 HZ; 0.25 PSD 4 MIN/AXIS DURATION	29.4G RMS - 20 TO 60 HZ; 0.11 PSD 60 TO 300 HZ; -3 DB/OCTAVE 300 TO 1200 HZ; 0.56 PSD 1 MIN/AXIS DURATION
SHOCK (a)	5200G AT 2000 HZ		THREE ACTUAL SUCCESSIVE SHOCKS	THREE ACTUAL SUCCESSIVE SHOCKS
ACOUSTICS				
LAUNCH (b)	142-DB OVERALL LEVEL		146-DB OVERALL LEVEL	146-DB OVERALL LEVEL
ENTRY (a)	149-DB OVERALL LEVEL	141-DB OVERALL LEVEL	150-DB OVERALL LEVEL	145-DB OVERALL LEVEL

NOTE: THE DESIGN LIMITS, ULTIMATE FACTORS OF SAFETY, AND MARGINS WERE ESTABLISHED BASED ON PROBE MISSION THROUGH VENUS SURFACE IMPACT TO ASSURE ACCOMPLISHMENT OF SCIENTIFIC OBJECTIVES, WHICH ARE SATISFIED PRIOR TO SURFACE IMPACT.

(a) OPERATING CONDITION
(b) NONOPERATING CONDITION

D LARGE PROBE FUNCTIONAL BLOCK DIAGRAM

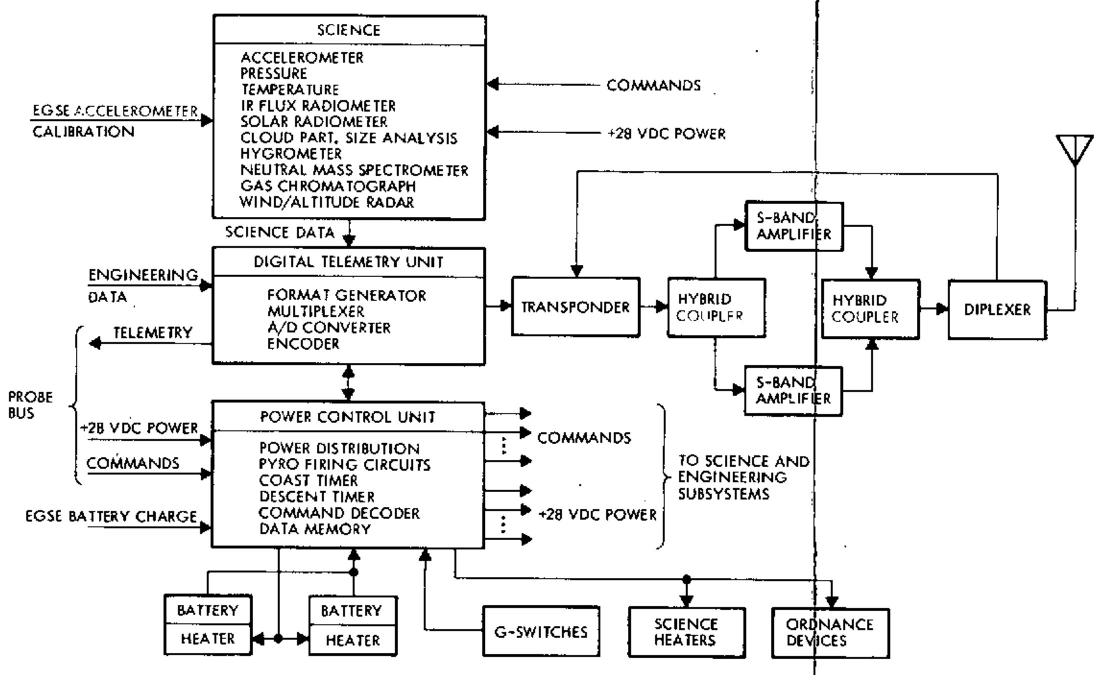

E SMALL PROBE FUNCTIONAL BLOCK DIAGRAM

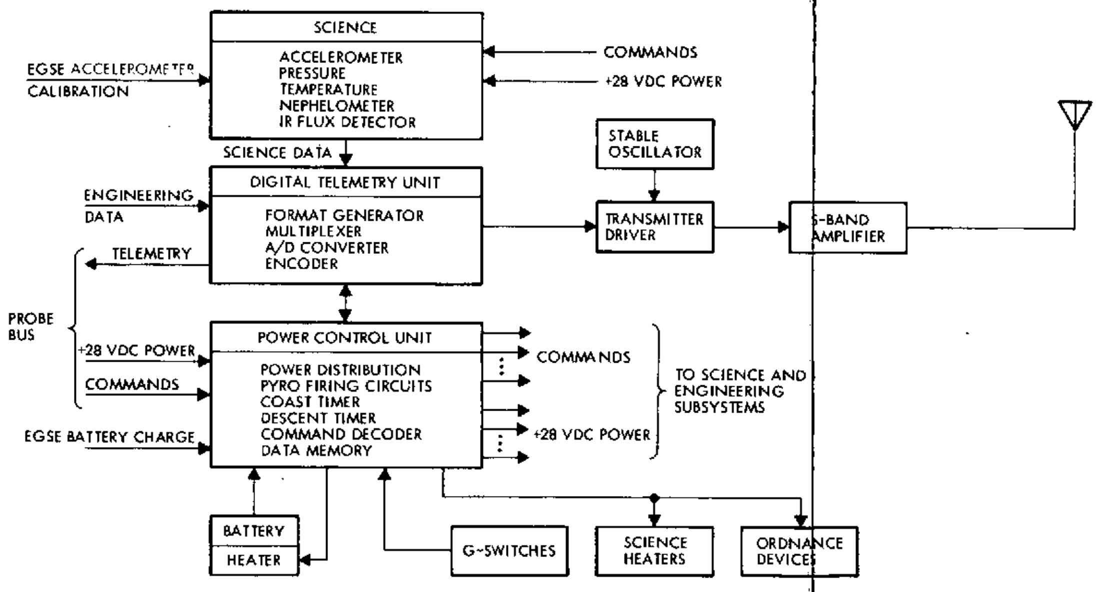

F LARGE PROBE OPERATIONAL PROFILE

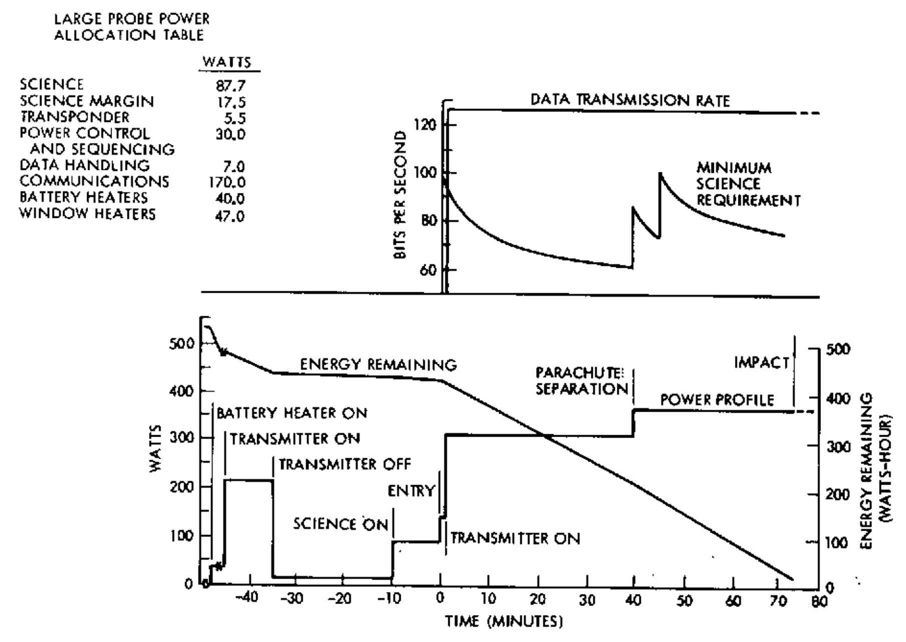

G SMALL PROBE OPERATIONAL PROFILE

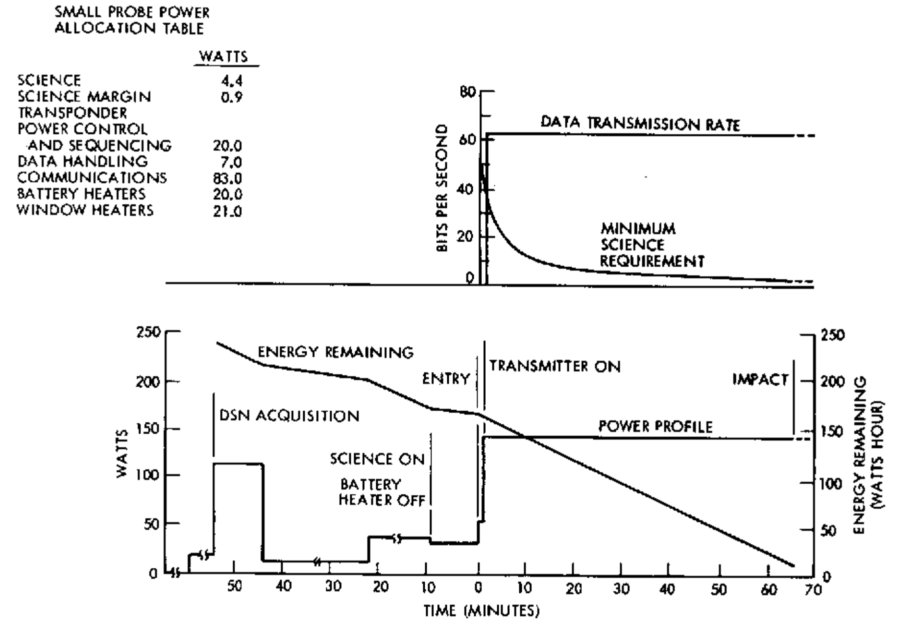

Figure 2-12. Large and Small Probe Design Summary

FOLDOUT FRAME 1

FOLDOUT FRAME 2

FOLDOUT FRAME 3

2.2 MAJOR TRADEOFFS: PROBE BUS AND ORBITER

Many of the key probe bus and orbiter trades — conical solar array, sequential probe release, earth pointing and solar and RF attitude sensing — have already been covered in this summary. A different view of these trades is obtained by looking at the historical sequence that led to the final recommended design. This view illustrates how sensitive the optimum low cost response is to the ground rules and detailed science instrument requirements. This historical view is shown in Figure 2-13 for both the Thor/Delta and Atlas/Centaur launched versions. In all cases, the conical solar array was recommended because of the operational freedom it allowed, and because it permitted solar heating of the large probe early in the mission, thereby removing a large heater power requirement. Thus, the design concept for the probe bus has remained unchanged throughout the study although the design of the probes themselves evolved.

The evolution of the orbiter configuration is also shown. The initial concept, presented at the December informal review, was an earth-pointing configuration based on our proposal for this study. The response was lukewarm, primarily because of the preference of the Science Steering Group* for a spin axis orientation perpendicular to the ecliptic and a strong bias by the potential ESRO participators for a configuration which used the HELIOS despun reflector antenna.

As a consequence, a configuration using such an antenna was investigated in detail and presented at the midterm. This configuration, however, was at least $1 million more expensive than the earth pointer. As a result, an alternative was also presented which preserved the orientation but was lower cost. This alternative used the Pioneer 6 to 9 fanbeam antenna and a 20-watt transmitter (as compared to 6 watts for the earth pointer) which would be suitable with the 26-meter DSN stations if they used a receiver with a 3-Hz loop bandwidth. It also relied on

*"Pioneer Venus Report of a Study by the Science Steering Group," Ames Research Center, National Aeronautics and Space Administration, Moffett Field, Calif., June 1972, p. 37.

memory for high data rate periods at periapsis, required in the early part of the mission when this data is gathered during earth occultation.

Subsequently, NASA/ARC determined that the 3-Hz loop capability had not been maintained at these stations and, as a result, we investigated the same configuration with a 12-watt transmitter to be used exclusively with the 64-meter DSN net. The data rate capability was such that nominally only one station contact was required per day. This is the lowest-cost option considered in the study, although only slightly cheaper than the earth pointer.

The requirement was then established that normal operations be performed relying only on the 26-meter DSN net. To meet this requirement, the final perpendicular configuration was investigated, making use of a nominal 36-watt (31-watt minimum) fanbeam. As is apparent, a significantly larger solar array is required with correspondingly increased power system cost, but the configuration is still considerably less expensive than the despun reflector version.

All of these perpendicular configurations rely on an additional fanscan receive antenna that uses the identical conscan processor of Pioneers 10 and 11. Earlier investigations of the pattern search techniques of Pioneers 6 to 9, in which the spacecraft is precessed so that the earth passes through various parts of the antenna pattern, were dropped because of the operational load involved.

Meanwhile, further contacts with the potential experimenters indicated that early opposition to earth-pointing configuration was not sustained. When detailed discussions were held, no objections were found other than the fact that the timing of events changes during the mission, increasing the complexity of control and data reduction.

In fact, a corollary advantage of earth pointing is that it increases latitude coverage for body-fixed instruments. Moreover, the ram platform permits normal operation of the neutral and ion mass spectrometers at any altitude above periapsis that is desired.

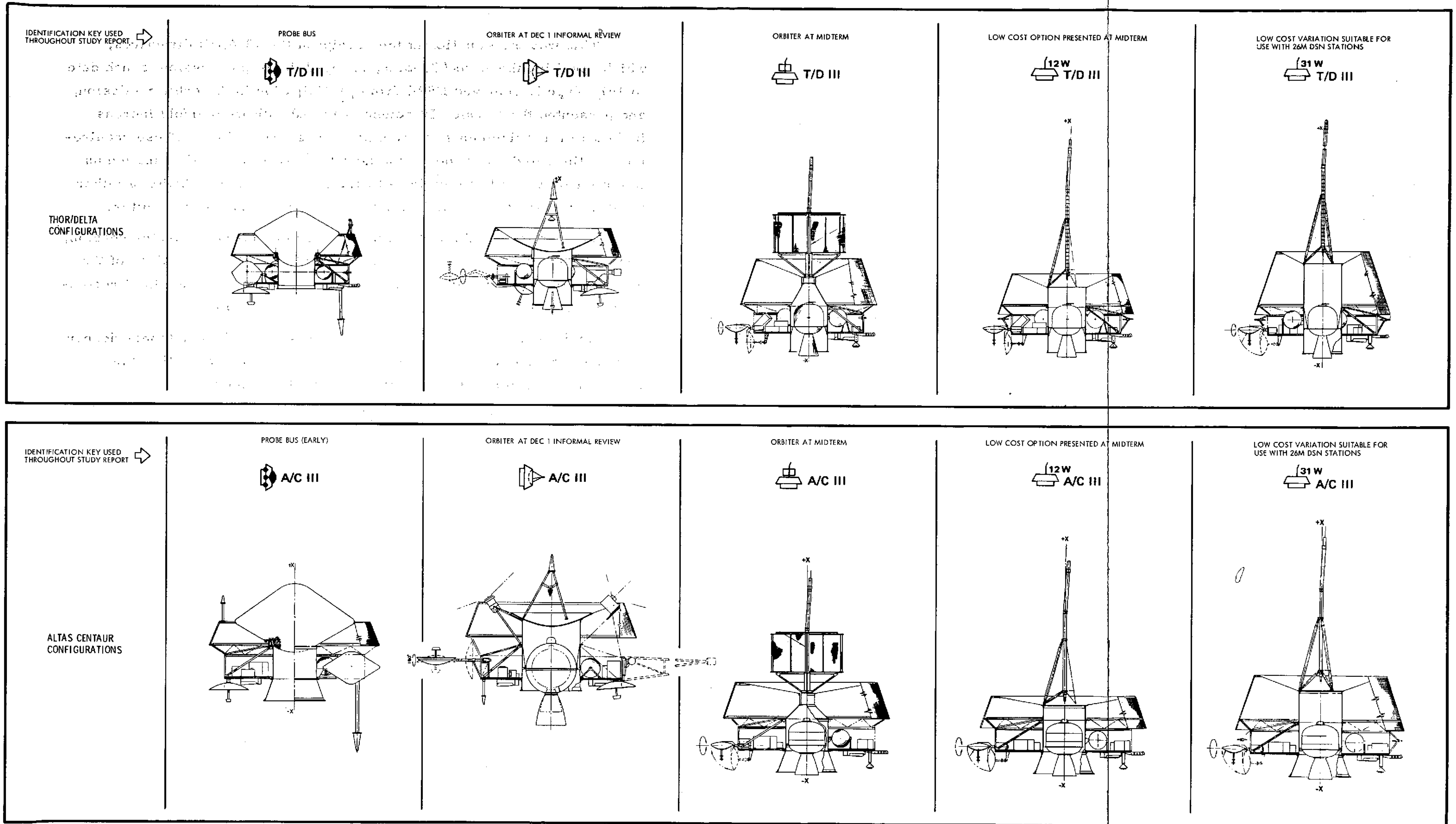

Figure 2-13. Configuration Options: Probe Bus and Orbiter

FOLDOUT FRAME

FOLDOUT FRAME

This was the situation at the receipt of the 13 April directives, which specified the Atlas/Centaur, changed the probe mission launch date to 1978 Type I, removed ESRO from participation in the orbiter mission, and presented the Version IV science payload with its fourfold increase in data rate requirements for both probe bus and orbiter. These requirements eliminated the fanbeam configurations from contention and led us to the single probe bus highlighted earlier and to the possibility of either the despun reflector or earth-pointing configurations for the orbiter.

The removal of the ESRO pressure for the despun reflector version, combined with the experimenter contacts indicating the suitability of the earth pointer for scientific purposes, allowed us to make our final recommendation based on the cost advantage of the earth pointer.

Additional alternatives covered in the study include antennas despun both mechanically and electrically and despun platforms. All of the alternatives are discussed in detail later in this report.

2.3 MAJOR TRADEOFFS: LARGE AND SMALL PROBES

As shown in Figure 2-14, our study began with the configurations of the large and small probes resulting from 3 years of pre-Phase B study. Continuing tradeoff analyses of the external configuration, in association with the other probe studies summarized on Figure 2-14, led to the configurations presented at the midterm review. The Thor/Delta probes were configured distinctly for aerodynamic, performance, and packaging reasons. At that time common shapes for the large and small probes were adopted for the Atlas/Centaur, using the PAET forebody.

With the definition of the Version IV payload and the decision to use the Atlas/Centaur, these probe designs for the Atlas/Centaur were given further study. The adoption of a larger parachute and the perforated ring concept over the vented flare of the midterm configuration introduced the possibility of a tailored afterbody, which improved aeroshell staging and mounting of the large probe on the bus. Since this afterbody geometry was not appropriate to the small probe, we decided to abandon the advantages of geometric commonality between the two probes. We therefore reverted to the midterm configuration of the small probe for Thor/Delta launch since it permitted packaging that moved the c. g. further forward, improving entry and descent stability.

Early in the study, our examination of the relative merits of a staged or unstaged large probe led us to select a staged configuration. In the unstaged version, the aeroshell is retained. In the staged version, the aeroshell is jettisoned and a capsule containing the science instruments is lowered to the surface. The instruments are exposed to the atmosphere as soon as the shell is jettisoned. The unstaged version ejects a nose cap or instrument covers. In that version, data handling is more complex and the scientific data can be contaminated by the presence of the hot heat shield and by converging channelized flow within the areoshell.

Once we had selected extraction and descent by parachute and had determined the characteristics of the parachute, extensive low-speed spin tunnel tests were performed on terminal descent configurations of the large and small probes. Drag rings, fins, and vented flares were tested on the large probe spherical descent capsule. Various forebody and afterbody configurations of the small probe were also tested. The midterm configurations evolved from these tests. Additional tests showed that an equatorial drag ring, with canted perforations to induce spin, improved the limit cycle behavior of the descent capsule. This combined with other advantages reviewed on Figure 2-14, led to the selection of the performated drag ring as the preferred stabilizing device. The preferred small probe configuration, which is similar to the Thor/Delta configuration at midterm, has better low-speed performance than the midterm Atlas/ Centaur small probe, further justifying the decision to forego identical aeroshell configurations for large and small probes.

The wind-altitude radar antenna, mounted at the forward stagnation point of the pressure vessel, caused the descent capsule to trim at small angles of attack. Ballast, drag ring modifications, and additional wind tunnel testing may be required to remove this difficulty. Alternatively, contouring the antenna to fit flush with the descent capsule, if feasible, would be a solution.

A. ENTRY CONFIGURATION

PHASE B STUDY PROPOSAL CONFIGURATIONS

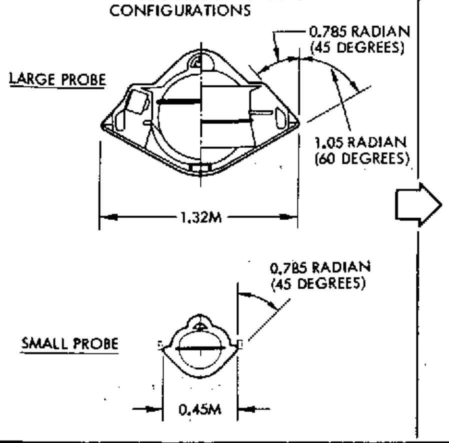

MAJOR STUDIES

- FORBODY AND AFTERBODY SHAPE: BLUNTED LARGE ANGLE CONE FOREBODIES (70, 60, 55 AND 45 DEGREE HALF ANGLE) AND SPHERE CONE, HEMISPHERE, AND TAILORED AFTER BODIES
- EXISTING VERSUS NEW CONFIGURATIONS: VIKING, PAET, AND APOLLO SHAPES WITH COST SAVINGS POSSIBLE FROM AVAILABILITY OF WIND TUNNEL A MAJOR FACTOR
- IDENTICAL VERSUS DISTINCT LARGE AND SMALL PROBE SHAPES WITH COST SAVINGS POSSIBLE FROM REDUCED DESIGN AND TEST REQUIRE MENTS

VARIOUS OPTIONS OF THE MAJOR SYSTEM VARIABLES WERE STUDIED: ENTRY GEOMETRY, DESCENT CONFIGURATION, DECELERATION STAGING TECHNIQUE AND PACKAGING, PRESSURE VESSEL SIZE.

MIDTERM CONFIGURATIONS

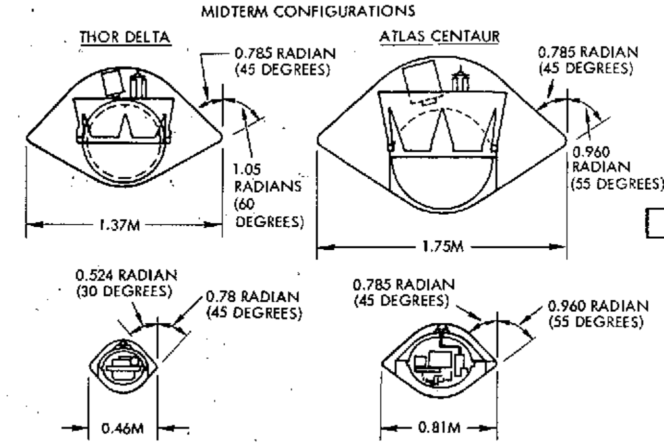

MAJOR STUDIES

- SLOWER DESCENT VERSUS COMPLEXITY OF DATA SYSTEM AND MEMORY: LARGER PARACHUTE ADOPTION
- PARACHUTE AND ANTENNA PACKAGING
- DESCENT CAPSULE STABILIZATION TECHNIQUE: PERFORATED RING CONCEPT SUGGESTED BY NASA/ARC ADOPTED

TAILORED AFTERBODY FOR LARGE PROBE PERMITTED GREATER ADVANTAGES THAN GEOMETRIC COMMONALITY BETWEEN LARGE AND SMALL PROBE

FINAL PREFERRED CONFIGURATIONS

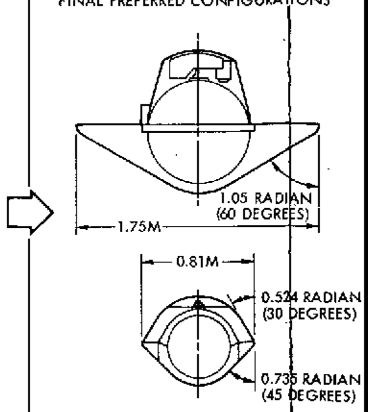

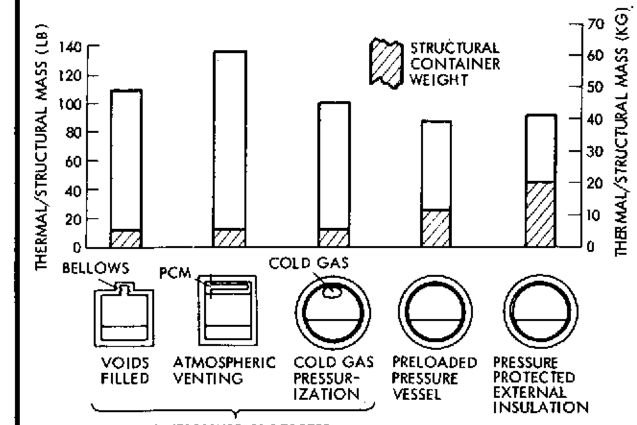

PRESSURE PROTECTED VERSUS NONPRESSURE PROTECTED. THE SKETCH ABOVE SHOWS THE APPROACHES CONSIDERED. ALTHOUGH THE PRESSURE PROTECTED DESIGN ENTAILS A RELATIVELY HEAVY STRUCTURE, IT ALSO REQUIRES THE LEAST WEIGHT OF INSULATION AND PHASE CHANGE MATERIAL. THE PRE-LOADED PRESSURE VESSEL IS SLIGHTLY LIGHTER, BUT INVOLVES HIGHER COST AND RISK TO QUALIFY INSTRUMENTS TO THE HIGH PRESSURE LEVELS. THE PRESSURE-PROTECTED APPROACH IS PREFERRED

B. STAGING TECHNIQUE

STAGED VERSUS UNSTAGED LARGE PROBE

- DESCENT VELOCITY OF UNSTAGED CONFIGURATIONS NECESSITATES MUCH HIGHER DATA SAMPLING RATE AND LARGER MEMORY
- HOT HEAT SHIELD MIGHT CONTAMINATE SCIENTIFIC DATA

STAGED APPROACH SELECTED

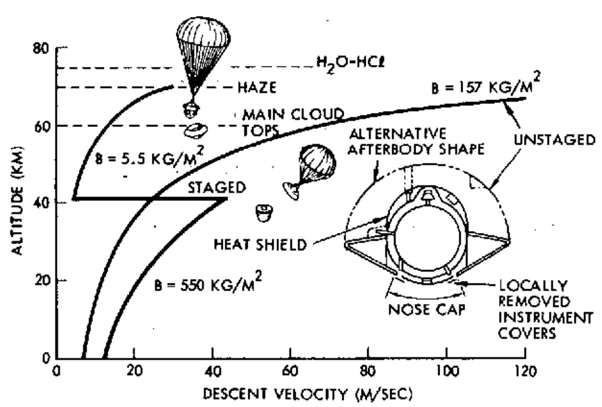

MECHANICAL VERSUS PARACHUTE STAGING. THE MECHANICALLY STAGED CONCEPT SHOWN BELOW WAS TRADED AGAINST PARACHUTE EXTRACTIONS OF THE DESCENT CAPSULE SHOWN AT RIGHT. AFTER DECELERATION TO SUBSONIC SPEEDS, THE FOREBODY IS SPLIT INTO SEGMENTS THAT ARE DEPLOYED; THE DESCENT CAPSULE IS RELEASED AND FALLS FREE. THIS APPROACH WAS DISCARDED BECAUSE:

- MORE COMPLEX AND THEREFORE LESS RELIABLE
- NO SIGNIFICANT COST SAVING
- LESS FLEXIBILITY IN TAILORING DESCENT PROFILE FOR OPTIMUM SCIENCE SAMPLING

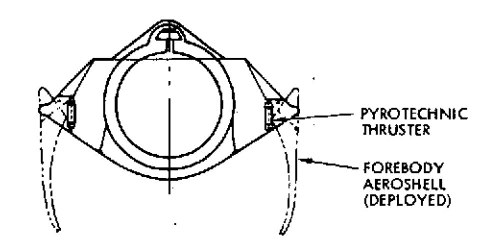

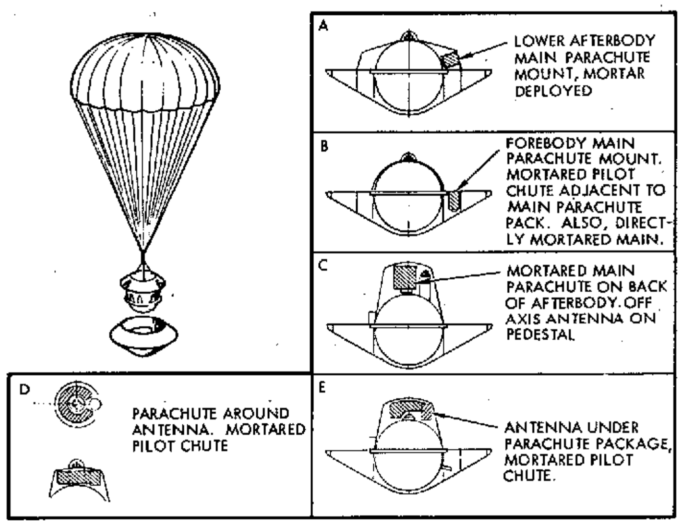

PARACHUTE

- SINGLE VERSUS MULTISTAGE – SUPERSONIC-TRANSONIC DROGUE FOLLOWED BY A SUBSONIC MAIN CHUTE WAS DISCARDED IN FAVOR OF A SINGLE STAGE SUBSONIC MAIN. REASONS: MORE COSTLY DEVELOPMENT PROGRAM; CHUTE STABILIZATION OF AEROSHELL NOT NEEDED AT TRANSONIC SPEEDS; DESCENT CAPSULE STAGING ABOVE 70 KM NOT REQUIRED DESCENT
- LOCATION AND DEPLOYMENT METHOD – ON AXIS LOCATION IS DESIRABLE BUT CONFLICTS WITH ANTENNA LOCATION REQUIREMENTS (CONFIGURATIONS C ABOVE. OFF AXIS LOCATIONS (A, B, AND D) REQUIRED MASS BALANCE AND CAUSE OSCILLATIONS ON DEPLOYMENT. SMALL DIFFERENCES BETWEEN DIRECT MORTARING AND PILOT EXTRACTION OF MAIN CHUTE IN TERMS OF PERFORMANCE AND RELIABILITY. POTENTIAL COST IMPACT IF MAIN CHUTE SIZE CHANGES: NEW MORTAR DEVELOPMENT REQUIRED WHERAS PILOT CHUTE UNAFFECTED. CONFIGURATION E IS PREFERRED DESIGN.
- CANOPY CONFIGURATION MATERIAL – FACTORS CANOPY SELECTION: DRAG/WEIGHT EFFICIENCY, STABILITY, GLIDE CHARACTERISTICS, OPENING LOADS, MANUFACTURING COMPLEXITY, COST, AND USE HISTORY. RIBLESS GUIDE SURFACE CANOPY SELECTED FOR PERFORMANCE AND LOW GLIDE CHARACTERISTIC. NYLON WAS SELECTED FROM AMONG THE TEXTILE SYNTHETICS BECAUSE OF ITS ABILITY TO MEET TEMPERATURE ENVIRONMENT AND ITS AVAILABILITY UNDER MIL SPECS.
- EXISTING CHUTES VERSUS NEW DESIGN NO EXISTING CHUTE WAS FOUND TO MEET THE DRAG AND LOW GLIDE REQUIREMENTS. PREFERRED DESIGN IS WELL PROVEN IN OTHER APPLICATIONS: DEVELOPMENT RISK IS LOW.

C. TERMINAL DESCENT STABILITY

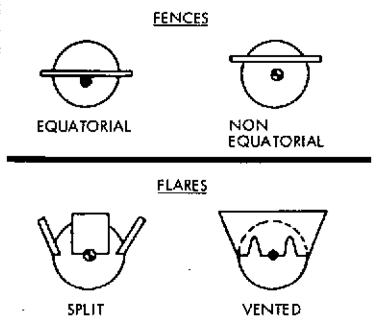

- LOW SPEED SPIN TUNNEL TESTS CONDUCTED COVERING DRAG RINGS, FINS, AND VENTED FLARES ON LARGE PROBE SPHERICAL CAPSULE.
- TESTS ON FOREBODY AND AFTERBODY CONFIGURATIONS OF SMALL PROBE

EQUATORIAL DRAG RING WITH CANTED PERFORATIONS TO REDUCE SPIN IMPROVES LIMIT CYCLE BEHAVIOR OF THE DESCENT CAPSULE AND IS THE PREFERRED STABILIZING DEVICE

FINAL

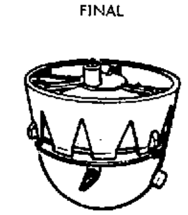

MIDTERM

D. PRESSURE VESSEL

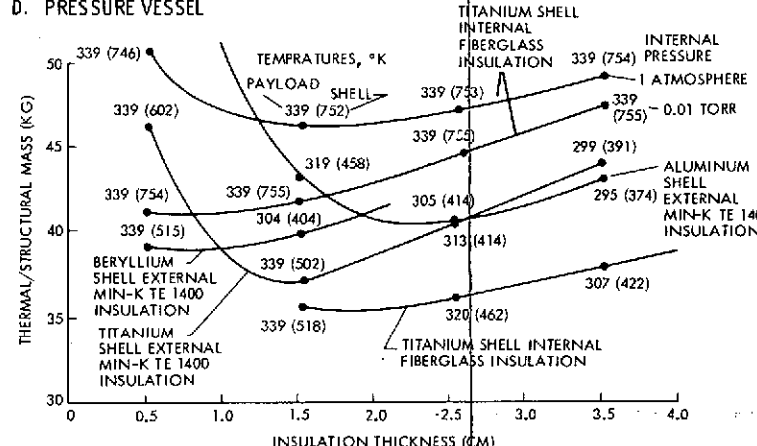

SHELL AND INSULATION MATERIAL. THE MATERIAL COMBINATIONS EXAMINED ARE IDENTIFIED ABOVE. THE TEMPERATURES AT THE END OF DESCENT ARE IDENTIFIED. PERFORMANCE, WEIGHTS, COST, AND RISK CONSIDERATIONS LED TO AN ALUMINUM PRESSURE VESSEL WITH EXTERNAL MIN K INSULATION AS THE PREFERRED DESIGN FOR BOTH LARGE AND SMALL PROBES.

		ADVANTAGES	DISADVANTAGES	RATIONAL FOR SELECTION OR REJECTION
1 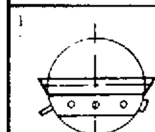	THREE PIECE, NARROW EQUIPMENT RING BELOW LOAD CONE.	1. EASY ACCESS TO CRITICAL COMPONENTS. 2. EQUIPMENT RING CAN BE REMOVED WITHOUT DIS TURBING AEROSHELL AFTERBODY. 3. NARROW RING GIVES GREATEST ACCESS ON BENCH.	1. SHORT LOAD CONE PROVIDES SHORT HEAT AND SHOCK PATH. 2. MULTIPIECE INSULATION DISASSEMBLY REQUIRED TO GAIN ACCESS.	EASIEST TOTAL ACCESSABILITY.
2 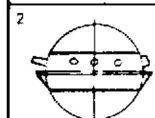	THREE PIECE, WIDE EQUIPMENT RING CENTERED. LOAD CONE BELOW PENETRATIONS.	1. EASY ACESS TO CRITICAL COMPONENTS. 2. INSULATION ON EQUIPMENT RING DOES NOT HAVE TO BE DISTRUBED FOR DISASSEMBLY.	1. COMPLETE PROBE DISASSEMBLY REQUIRED TO GAIN COMPLETE ACCESS. 2. EITHER SHORT LOAD CONE OR SENSORS PENETRATE CONE	NEED FOR AEROSHELL DISASSEMBLY TO REMOVE EQUIPMENT RING.
3 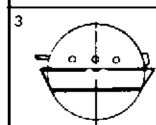	TWO PIECE, UNSYM METRICAL. LOAD CONE BELOW PENETRATIONS.	1. ONLY ONE JOINT TO SEAL.	1. COMPLETE PROBE DISASSEMBLY REQUIRED TO GAIN COMPLETE ACCESS. 2. SCIENCE ALIGNMENT AND CONNECTIONS BY TRAIL AND ERROR AND SPECIAL TOOLS.	SAME AS CONFIGURATION 2 PLUS SHORT LOAD CONE.
4 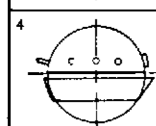	TWO PIECE, SYM METRICAL. LOAD CONE BELOW PENETRATIONS.	1. ONLY ONE JOINT TO SEAL. 2. ONE FORGING DESIGN.	1. SAME AS CONFIGURATION 3 PLUS SHORT LOAD CONE OR SENSORS PENETRATE CONE.	SAME AS CONFIGURATION 3 PLUS SHORT LOAD CONE.

PRESSURE SHELL ASSEMBLY. THE TABLE ABOVE IDENTIFIES THE OPTIONS CONSIDERED. THE THREE SEGMENT DESIGN WITH THE EQUIPMENT RING BELOW THE EQUATOR IS THE PREFERRED LARGE PROBE DESIGN. THE UPPER AND LOWER SPHERICAL SEGMENTS HAVE NO PENETRATIONS. A SIMILAR TRADEOFF STUDY FOR THE SMALL PROBE LED TO TWO SEGMENT PRESSURE VESSEL DESIGN WITH A REMOVABLE EQUIPMENT SHELF.

Figure 2-14. Major Tradeoffs - Large and Small Probes

FOLDOUT FRAME 1

FOLDOUT FRAME 2

2.4 ATLAS/CENTAUR VERSUS THOR/DELTA

Spacecraft hardware costs are strongly influenced by:

- Use of existing designs to reduce the design and development cost
- Commonality of design between elements of the system to reduce parallel effort and realize efficiencies in design, manufacture, and testing
- Generous margins in critical parameters (such as weight, volume, and power) to simplify new designs and to provide greater flexibility in application of existing designs.

Thus the launch vehicle tradeoff studies focused on the degree to which relaxation of weight and volume constraints (consistent with Atlas/Centaur capability) could reduce overall program cost in view of these factors. The effects of weight and volume relief on costs were examined in depth for major elements of the spacecraft systems, the probes, and the probe bus/orbiter. The benefits are much greater for the probes than for the bus/orbiter, and strongly influenced the recommended mission system. The qualitative results are summarized in Figure 2-15.

DESIGN UTILIZATION AND COMMONALITY

ATLAS/CENTAUR CAPABILITY PERMITS SUBSTANTIAL DECREASE IN REQUIREMENT FOR NEW PROBE EQUIPMENT DESIGNS AND INCREASES IN COMMONALITY BETWEEN SMALL AND LARGE PROBES. EFFECTS ON THE BUS/ORBITER ARE SMALL.

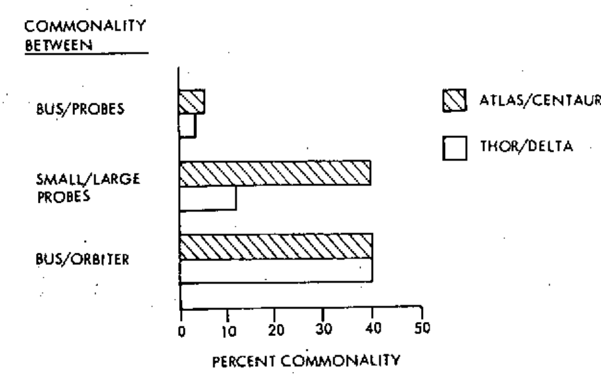

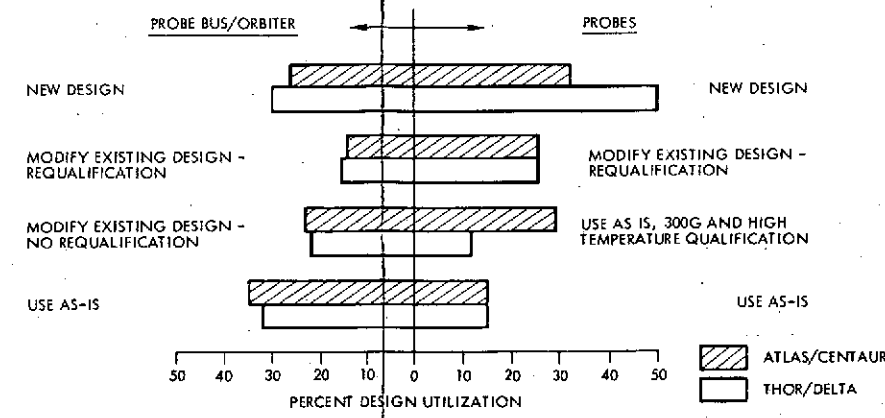

WEIGHT OPTIMIZATION

FOR COST/WEIGHT TRADEOFFS, THE PROBE AND PROBE BUS DESIGN ANALYSES EXPLORED THE RANGE OF POTENTIAL COST SAVINGS, UP TO THE FULL AMOUNT OF INCREASED CAPABILITY AVAILABLE: 386 KG (851 LB). THESE ANALYSES, SUMMARIZED IN THE GRAPHS BELOW, SUBSTANTIATED THAT THE PROBES SHOW SIGNIFICANTLY MORE COST SAVINGS POTENTIAL THAN THE BUS/ORBITER. AS DETAILED IN SECTION 11.3, AN OPTIMUM PAIR OF PROBE/BUS CONFIGURATIONS DOES EXIST.

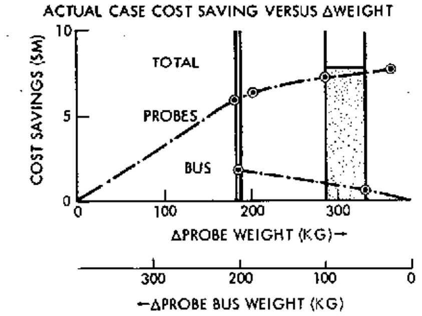

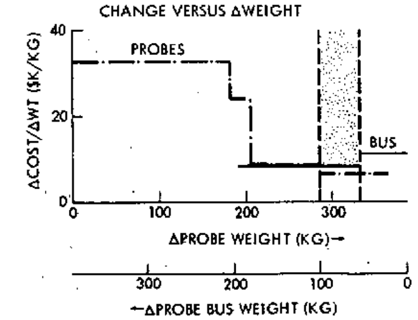

WEIGHT/VOLUME EFFECT COST SUMMARY

REMOVAL OF WEIGHT AND VOLUME RESTRAINTS PERMITS LARGE COST SAVINGS FOR PROBES. A MAJOR REASON FOR THIS RELATIVELY SMALL BUS/ORBITER IMPACT IS THE EXISTING DESIGN UTILIZATION IN THE BASELINE CONFIGURATION

	APPROXIMATE SAVINGS ($M)	
	BUS/ ORBITER	PROBES
GREATER UTILIZATION OF EXISTING DESIGNS	0.3	1.5
IMPROVED COMMONALITY	---	3.6
SIMPLIFICATION OF NEW DESIGNS	0.5	1.4
OTHER FACTORS THAT LOWER COST	0.3	1.5
TOTALS	1.1	8.0

LAUNCH VEHICLE COST TRADEOFF SUMMARY

INCLUSION OF THE LAUNCH VEHICLE AND OTHER RELATED COSTS, SUMMARIZED IN THIS TABLE, SHOWS THAT USING DIFFERENT LAUNCH VEHICLES FOR THE PROBE AND ORBITER MISSIONS IS COST EFFECTIVE AND GREATLY REDUCES THE RISK INHERENT IN THE DEMANDING MULTIPROBE MISSION. WITHIN THE STUDY GUIDELINE AND OUR UNDERSTANDING OF RELATED COSTS, THIS WAS THE MISSION SYSTEM RECOMMENDED AT MIDTERM.

	ALL THOR/DELTA	ALL ATLAS/CENTAUR	ATLAS/CENTAUR PROBE THOR/DELTA ORBITER
SPACECRAFT			
PROBE BUS	BASELINE	- 0.6	- 0.6
PROBES	↓	- 8.0	- 8.0
ORBITER		- 0.5	+ 1.0
SUBTOTAL		- 9.1	- 7.6
LAUNCH VEHICLE		+18.0	+ 9.0
TOTAL HARDWARE COST		+ 8.9	+ 1.4
RELATED COSTS			
GROUND DATA HANDLING		- 0.5	- 0.5
SCIENCE DEVELOPMENT		- 2.4*	- 2.4*
INTANGIBLE		- 2.0	- 1.5
SUBTOTAL		- 4.9	- 4.4
TOTAL COST DIFFERENCE		+ 4.0	- 3.0

*BASED ON ASSESSMENT OF PROBE SCIENCE ONLY

Figure 2-15. Thor/Delta and Atlas/Centaur Tradeoffs

FOLDOUT FRAME 1

FOLDOUT FRAME 2

2.5 NASA/ESRO ORBITER INTERFACE

The technical cost tradeoff to determine the most effective method of performing the orbiter mission as a cooperative venture with the European Space Research Organization (ESRO) was based on variations of NASA planning which assumed that the bus portion of the spacecraft would be provided to ESRO for integration of orbiter mission-peculiar subsystems and scientific instruments, and that ESRO would perform the system test program for this mission and deliver the spacecraft for NASA launch and flight mission operations control.

The results are based on work through midterm, as directed by ASD:244-9/32-042, 13 April 1973; they do not reflect the subsequent shift to Atlas/Centaur, the addition of the X-band occultation experiment, or the delay of the probe mission from 1977 to 1978.

The technical versus cost factors analyzed during the study were based on the following criteria:

- Maximum use of probe mission hardware and design
- Assignment of hardware to the original NASA contractor to sustain the experience developed on the probe mission
- Use of the probe mission design, manufacturing, and test planning and control documentation.

To fulfill these criteria, probe and orbiter commonality has to be maximized. This line of analysis points to orbiter mission-peculiar hardware and other program factors as the logical assignment for ESRO participation.

It was determined that the anticipated ESRO deboost propulsion system is adequate for the Atlas/Centaur orbiter mission and that the anticipated use of the Helios despun reflector antenna is suitable, except that the incorporation of an X-band link is difficult. Figure 2-16 illustrates the key orbiter mission-peculiar equipment incorporated into a configuration compatible with the probe bus.

Table 2-1 expands on the mission-peculiar items. The main question was the extent of ESRO participation, and options can best be presented in terms of integration and test activities. Three NASA/ESRO participation options are shown in Figure 2-17.

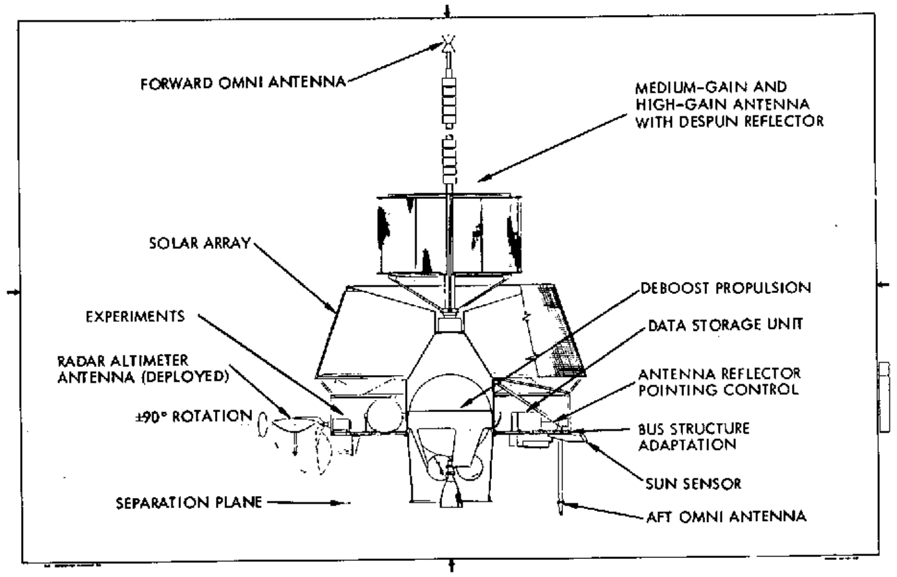

Figure 2-16. ESRO Hardware Participation

Table 2-1. ESRO Participation Definition

ORBITER MISSION-PECULIAR ITEMS	FURTHER WORK REQUIRED
1. EXPERIMENTS	INTERFACE DEFINITION AND CONTROL
2. SCIENCE DATA REDUCTION AND ANALYSIS	MISSION REQUIREMENTS INPUTS DEFINITION
3. DEBOOST PROPULSION	DEFINITION FOR DESIGN INTEGRATION
4. HIGH-GAIN ANTENNA	DEFINITION FOR DESIGN INTEGRATION
5. ADAPTATION OF PROBE BUS STRUCTURE	DEVELOPMENT STATUS AND APPLICATION
6. INTEGRATION AND TEST	THREE OPTIONS DISCUSSED (SEE FOLLOWING TEXT AND CHARTS)

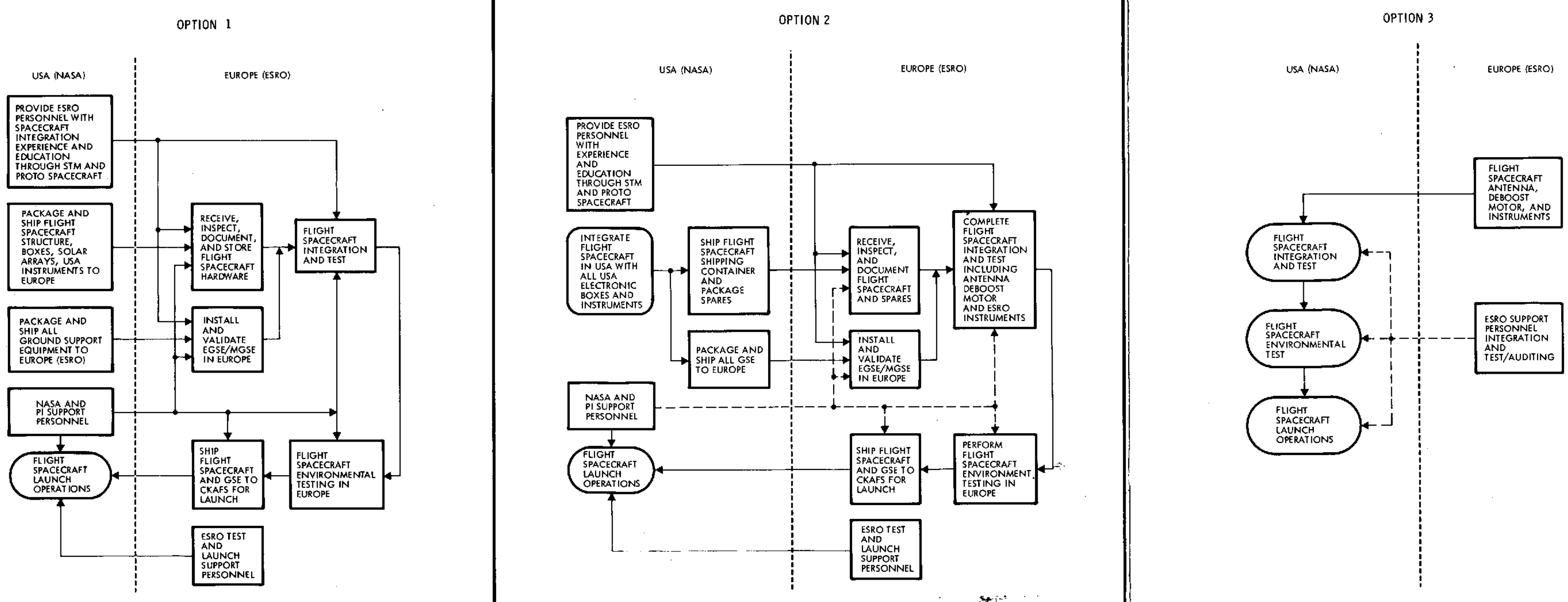

Figure 2-17. NASA/ESRO Participation Options

FOLDOUT FRAME 1

FOLDOUT FRAME 2

Key parts of each option are summarized in Table 2-2. The second option is recommended on the basis of the lowest total cost to NASA. However, this option also presents the most difficult management interface between NASA and ESRO because of the split in spacecraft operations between Europe and the United States.

Table 2-2. NASA/ESRO Integration and Test Operations

OPTION 1	OPTION 2	OPTION 3
INDIVIDUAL FLIGHT SPACECRAFT ELECTRICAL BLACK BOXES, APPENDAGES, THERMAL CONTROL, AND PROPULSION SHIPPED TO ESRO STRUCTURE SHIPPED TO EUROPE OR MANUFACTURED IN EUROPE USA SCIENTIFIC INSTRUMENTS SHIPPED TO ESRO ALL INTEGRATION AND ENVIRONMENTAL TEST PERFORMED IN EUROPE	INTEGRATE FLIGHT SPACECRAFT ELECTRICAL BLACK BOXES, APPENDAGES, PARTIAL THERMAL CONTROL, AND PROPULSION IN USA INTEGRATE USA SCIENTIFIC INSTRUMENTS IN USA SHIP FLIGHT SPACECRAFT TO ESRO FOR FINAL INTEGRATION OF ANTENNA, DEBOOST PROPULSION, AND EUROPEAN INSTRUMENTS PERFORM ALL FLIGHT SPACECRAFT ENVIRONMENTAL TESTS AT ESTEC FACILITIES	INTEGRATE FLIGHT SPACECRAFT IN USA WITH ESRO SUPPORT SHIP EUROPEAN SCIENTIFIC INSTRUMENTS, ANTENNA, STRUCTURE, AND DEBOOST PROPULSION TO USA FOR FLIGHT SPACECRAFT INTEGRATION AND TEST FINAL INTEGRATION AND ENVIRONMENTAL TEST COMPLETED IN USA WITH ESRO SUPPORT
MAXIMUM OVERLAP OF ORBITER AND PROBE SCHEDULE TO MEET ORBITER LAUNCH DATE	MINIMUM SCHEDULE OVERLAP	NO SCHEDULE OVERLAP
NO USE OF APPLICABLE PROBE MISSION GSE	USE OF APPLICABLE EGSE FROM PROBE MISSION	USE OF ALL APPLICABLE PROBE MISSION GSE
PROGRAM COST HIGHER THAN OPTION 2	LOWEST PROGRAM COST TO NASA	HIGHEST PROGRAM COSTS TO NASA
EASIER INTERFACE BETWEEN NASA AND ESRO THAN OPTION 2	HARDEST INTERFACE BETWEEN NASA AND ESRO	EASIEST INTERFACE BETWEEN NASA AND ESRO

PRECEDING PAGE BLANK NOT FILMED

2.6 DEVELOPMENT COSTS

System development is a significant area for minimizing program costs, particularly system tests. A key cost reduction technique in the test sequence is to use a single spacecraft for early qualification and thermal-vacuum tests and for acceptance-level vibration and shock tests. As shown in Figure 2-18, these are followed by an acceptance-level acoustic test and final-acceptance space simulation tests. This proto/flight concept minimizes the length of the test cycle, the number of test items, and manpower needs.

This proto/flight concept exposes the spacecraft system to acceptance-level vibration, shocks, and acoustics rather than qualification levels. The supporting rationale is:

- All bus/orbiter subsystems and probes designs will have been qualified at the unit level
- All bus/orbiter subsystem and probe units will have been acceptance tested
- The only remaining unit not tested to qualification levels is the harness and the thermal blankets. However, acceptance level mechanical environments are sufficient to verify the integrity of the harness and insulation installation.

The proto/flight concept provides for two thermal-vacuum tests. The first uses the updated thermal design (based on results of the thermal model test) and flight hardware. This test provides a final evaluation of the thermal design and also an opportunity to evaluate the performance of the other subystems and science. The second test verifies the final thermal design and the spacecraft/science system.

The extensive use of existing equipment and designs also of course saves costs in time, equipment, and documentation for system tests. Commonality of equipment permits the multiple use of test and flight models.

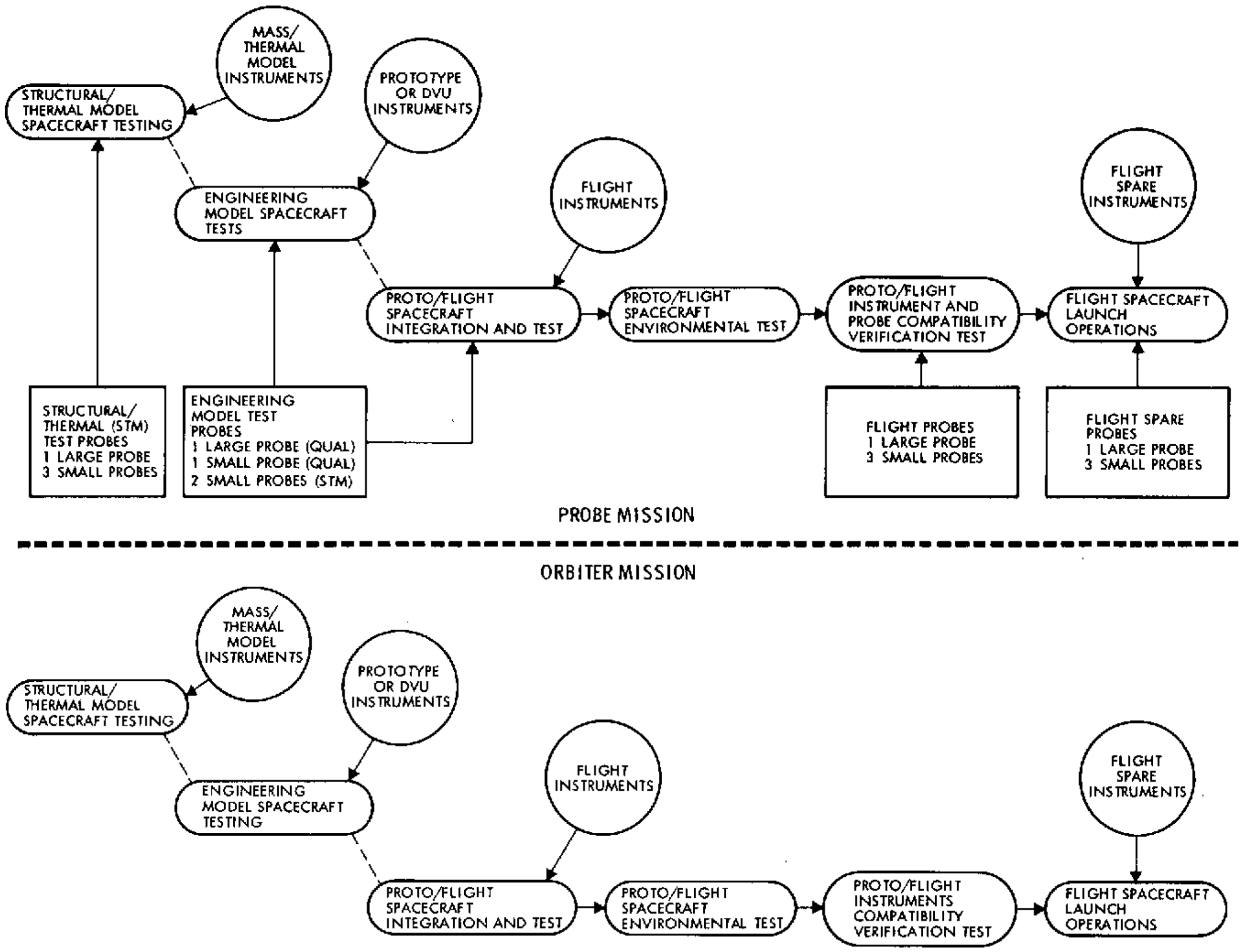

Figure 2-18. Preferred Prototype/Flight Integration Test and Launch Flow Diagrams

3. SCIENCE ANALYSIS AND EVALUATION

3.1 PROBE SCIENCE, ATLAS/CENTAUR

3.1.1 Science Requirements and Impact on Mission and System Design

3.1.1.1 Science Objectives and Guidelines

This section summarizes the basic scientific objectives and guidelines used to establish mission and system design requirements for the study. The general scientific objectives for the Pioneer Venus probe mission are given in Table 3-1 with an indication of their relation to the probe types. Note that all probes contribute to all objectives.

Table 3-1. Scientific Objectives for Pioneer Venus Probe Missions

Objectives	Large Probe	Small Probe
Nature and Composition of the Clouds	X	X
Composition and Structure of the Atmosphere from Surface to High Altitudes	X	X
General Circulation Pattern of the Atmosphere	X	X

The large probe will obtain a comprehensive set of measurements relating to the atmosphere structure and composition, the cloud properties, the local winds, and the solar and thermal radiation fluxes and their interactions from high altitudes to the surface. The primary emphasis is on the planetary energy balance and the clouds.

The three small probes, targeted to widely separated points on the planet, are intended to obtain basic measurements relating to variations in the atmosphere cloud structures and winds. The primary emphasis is on information concerning the general circulation on Venus.

The contractually specified science payloads cover the range of generic measurement types recommended by the Science Steering Group (SSG) to accomplish the basic objectives. Tables 3-2 and 3-3 summarize the specific objectives for each of the experiments in the Version IV science payloads along with the relative priorities assigned by the SSG. The nominal payloads were used to establish the baseline mission and system design requirements, while the impact of incorporating each of the "other candidate instruments" into the baseline design was assessed separately.

Table 3-2. Large Probe Experiments (Version IV)

NOMINAL PAYLOAD (a)		
EXPERIMENT	OBJECTIVES/MEASUREMENTS	PRIORITY
TEMPERATURE	ATMOSPHERIC STRUCTURE, ANCILLARY FOR OTHER MEASUREMENTS	A
PRESSURE		A
ACCELEROMETERS	UPPER & LOWER ATMOSPHERE STRUCTURE, TURBULENCE, SEISMIC NOISE (POST-IMPACT)	A
NEUTRAL MASS SPECTROMETER	COMPOSITION OF ATMOSPHERE, CONDENSIBLES	A
GAS CHROMATOGRAPH		
CLOUD PARTICLE SIZE ANALYZER	AEROSOL SIZE, NUMBER DISTRIBUTIONS	A
SOLAR RADIOMETER	SOLAR FLUX PROFILE, ENERGY BALANCE	A
IR FLUX RADIOMETER	THERMAL FLUX PROFILE, ENERGY BALANCE CLOUD LAYERING	A
TRANSPONDER (b)	WINDS FROM DOPPLER, DLBI TRACKING	A
WIND-ALTITUDE RADAR	ALTITUDE, WINDS BELOW 40 KM	-
NEPHELOMETER	CLOUD LAYERING	B
HYGROMETER	WATER VAPOR CONCENTRATION	B
OTHER CANDIDATE INSTRUMENTS (c)		
X-RAY FLUORESCENCE	CLOUD PARTICLE COMPOSITION	-
AUREOLE/EXTINCTION DETECTOR	CLOUD PROPERTIES, SOLAR ATTENUATION THROUGH CLOUD TOPS	A
SHOCK LAYER RADIOMETER	ATMOSPHERE COMPOSITION (DURING ENTRY ONLY)	C
ATTENUATED TOTAL REFLECTION SPECTROMETER	COMPOSITION OF CONDENSIBLES, CLOUD PARTICLES	-

(a) CONTRACTUAL PAYLOAD FOR ESTABLISHING BASELINE MISSION AND SYSTEM DESIGN REQUIREMENTS.

(b) NOT LISTED AS A VERSION IV SCIENCE INSTRUMENT, BUT DLBI EXPERIMENT MAY REQUIRE IT.

(c) IMPACT OF EACH INSTRUMENT ON BASELINE SYSTEM DESIGN TO BE ASSESSED AS SEPARATE TASKS.

Table 3-3. Small Probe Experiments (Version IV)

NOMINAL PAYLOAD		
EXPERIMENT	OBJECTIVES/MEASUREMENTS	PRIORITY
TEMPERATURE	ATMOSPHERIC STRUCTURE, HORIZONTAL VARIATIONS	A-1
PRESSURE		
NEPHELOMETER	CLOUD LAYERING, HORIZONTAL VARIATIONS	A-2
STABLE OSCILLATOR	WINDS FROM DOPPLER, DLBI TRACKING	A-3
ACCELEROMETER	ATMOSPHERIC STRUCTURE DURING ENTRY AND DESCENT; TURBULENCE; SEISMIC NOISE (POST-IMPACT)	A-4
IR FLUX RADIOMETER	THERMAL (IR) FLUX PROFILES, HORIZONTAL VARIATIONS	---
OTHER CANDIDATE INSTRUMENTS		
RF ALTIMETER	ALTITUDE FOR ATMOSPHERIC RECONSTRUCTION	---
MAGNETOMETER	PLANETARY MAGNETIC FIELD, VARIATIONS	A-4

The altitude regions of interest for the probe mission are illustrated in Figure 3-1 along with the salient features of the atmospheric structure and winds as inferred from Mariner and Venera measurements. The composition and locations of postulated cloud layers, as given in NASA SP-8011 are also indicated; frozen sulfuric acid particles have recently been added to the list of candidate cloud materials. Venera 8 measurements of solar flux at ~5.5 degrees from the morning terminator indicate a significant change in the optical density between 40 and 35 km suggesting that the bulk of the cloud cover lies above 35 to 40 km, as shown in the figure. While the Venera probes have provided some basic measurements of the general structure of the lower atmosphere, there are many first order questions that will remain unanswered until science payloads of the type recommended by the SSG are sent to probe the lower atmosphere.

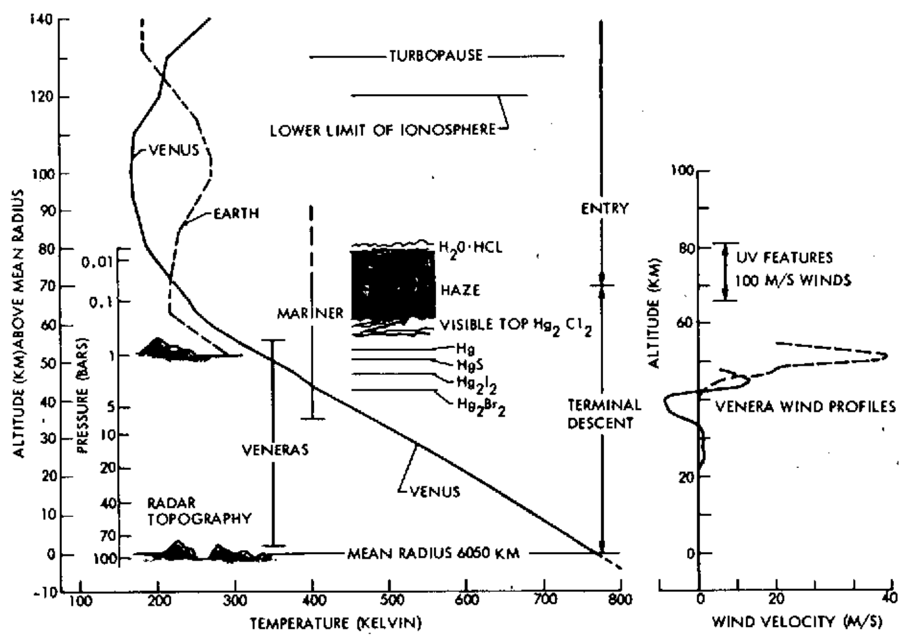

Figure 3-1. Venus Atmosphere Structure

The primary objective of the Pioneer Venus Probe Mission is to explore in detail the atmosphere from pressure levels of a few tens of millibars (above the clouds) down through the lowest scale height of the atmosphere to the solid surface. There is no requirement to survive on the surface, but the possibility that the probes may survive low velocity (~10 to 15 m/s) surface impact led the SSG to recommend that the accelerometers be designed to function as seismometers if the probes survive impact. The SSG emphasizes that this is not a design requirement for surface survival or that the probes be designed for pressures and/or temperatures greater than the mean values given by NASA SP-8011 (Reference 1) (767°K, 94.9 bars at 6050 km radius). The SSG also points out that a probe giving results to 90 atmospheres would be a complete success even in the absence of surface impact.

All descent instruments on both large and small probes should be deployed and obtaining measurements through the haze layer above the main cloud tops. According to NASA SP-8011, the main cloud top is between 60 and 63 km and the haze extends up to the thin cloud layer between 77 and 81 km. Earth-based and other remote sensing observations in the UV, visible, and IR are restricted to this region above 200 mb (<62 km) or higher; the Venera probes have never obtained *in situ* measurements above about 500 to 600 mb (56 to 57 km). The RF occultation data from Mariner V provided information on the atmospheric structure below 90 km, but is unreliable in its detail above 70 km. The 100 to 150 m/s winds observed from earth very likely occur near or slightly below the top of the haze layer. The composition of this region (with respect to minor constituents) may be quite different from that below the main cloud top due to condensation processes and chemical and/or photochemical reactions.

Thus, all objectives in Table 3-1 require *in situ* measurements through the haze layer from as high above the main cloud top as possible. The entry accelerometer measurements on all probes will obtain the atmospheric structure during the entry phase down through the 30 to 50 mb levels where subsonic velocities are reached. While direct *in situ* measurements at subsonic velocities are not possible through the thin cloud at 77 to 81 km, subsonic deployment between 30 to 50 mb will permit observation of the sun through the thin cloud and haze above the probe, and hence obtain some of its physical properties (e.g., particle size distribution, homogeneity), provided that a sufficient number of measurements are obtained before descending through the main cloud top. A mass spectrometer or gas chromatograph sample obtained before reaching the main cloud should allow inference of the thin upper cloud composition since the material will probably be present in gaseous form throughout the haze layer.

Since H_2O will be present only as a vapor above its boiling point, and since the vapor should be uniformly mixed at higher temperatures down to the surface, hygrometer measurements need not be continued all the way to the surface. The measurements should be made at least down to a temperature above the boiling point of water. This occurs at about $406^{\circ}K$ in the SP-8011 nominal model atmosphere or at $\sim$43 km and 3 atm pressure. The condensation point depends upon the amount of water present and will occur at higher altitudes (above 60 km for less than 1% H_2O). Liquid water will evaporate at lower temperatures $\left(T < 406^{\circ}K\right)$ but droplets (precipitation) could exist down to $\sim$43 km, at which point they will spontaneously evaporate (i.e., boil). Thus, the mixing ratio of water could be variable above $\sim$43 km and hygrometer measurements should be made down to at least that altitude to obtain the true mixing ratio. However, the Venera data indicate that the H_2O mixing ratio decreases with decreasing altitude from $\sim$1.1 percent at 55 km to $\sim 10^{-4}$ percent at 30 km, implying that hygrometer measurements should be made at lower altitudes.

The main objective of the small probes is to obtain information for constructing general circulation models by observing the wind, cloud, and pressure/temperature profiles at widely separated points on the planet. There are two major altitude regions of importance to the general circulation: the region above 100 mb characterized by 100 to 150 m/s winds ("the 4-day wind"), and the region below the cloud tops characterized by high velocities ($\sim$50 m/s) at high altitudes (40 to 60 km) and low velocities ($\sim$1 m/s) in the lowest scale height. An understanding of the driving mechanism for 4-day wind requires a knowledge of the horizontal temperature gradients in the 10 to 100 mb region and the vertical and latitudinal distribution of the wind. In situ temperature and pressure measurements near the 50 mb level in conjunction with the entry accelerometer measurements are required to give a reasonably accurate temperature profile through the 10 to 50 mb region. It would be desirable to obtain direct pressure and temperature measurements at higher altitudes, but this requires supersonic deployment ($M > 1.5$) of the instruments.

The wind parameters specified in NASA SP-8011 are:

Mean horizontal velocities at cloud altitudes (60 to 70 km or higher)	100 m/s
Mean horizontal velocities at lower altitudes	30 m/s near 50 km
	2 m/s or less below 30 km
Maximum wind shear	0.05 m/s/m
Mean vertical wind velocity	1 m/s

These values are generally consistent with the Venera measurements (Figure 3-1) and recent theoretical models. The Venera wind profiles then give an indication of the magnitude of the winds to be expected and measured at various altitudes. Whatever technique is to be used for obtaining the wind profiles (DLBI, Doppler, accelerometers, or some combination), it should be capable of measuring winds with accuracies of 1 m/s at all altitudes above ~40 km and 0.1 m/s below ~40 km to be of significant value to circulation theories.

It should be stressed that the above scientific desiderata were used only as general guidelines for establishing mission goals; the detailed science requirements of the Version IV payloads are given in Sections 3.1.1.3 and 3.1.1.4.

3.1.1.2 Probe Targeting Guidelines and Tradeoffs

The probe targeting strategies recommended by the SSG (Reference 2) are summarized in Table 3-4. Figure 3-2 illustrates the desired coverage in a subsolar/orbit plane coordinate system. Also shown in the figure is the 70-degree communications boundary beyond which atmospheric attenuation near the surface becomes severe. The 70-degree limit would permit achieving the maximum 0 to ±60 degree latitude spread desired for the small probes, but should be considered as a design goal rather than a requirement. The SSG recommends targeting to obtain

Table 3-4. Recommended SSG Probe Targeting Strategies

Large Probe	
Lightside entry	
Near equator (0° ± 15°)	
Within 70° of subsolar	
Small Probes	
Latitude spread:	0° to ± 30° minimum
	0° to ± 60° maximum
Longitude spread:	90° minimum
	120° maximum
All Probes	
Desirable for all probes to reach surface prior to Bus entry for DLBI tracking.	

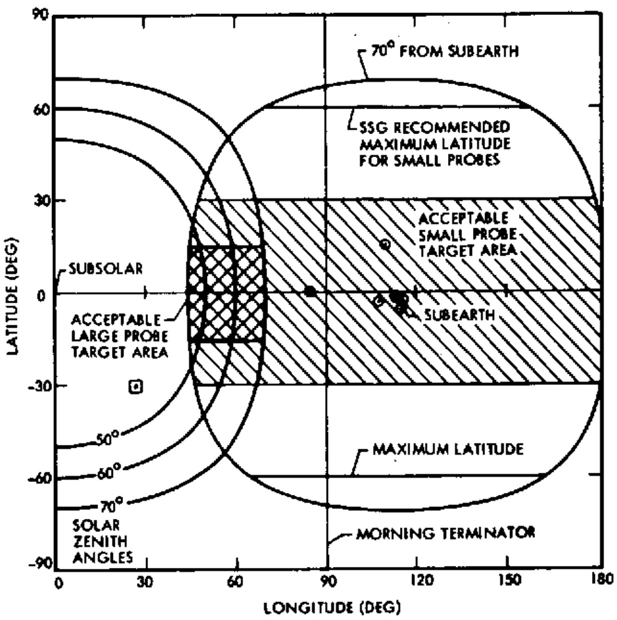

NOTE: 70° COMMUNICATIONS LIMIT FROM SUBEARTH (⊕) SHOWN FOR DECEMBER 18, 1978 ENCOUNTER. VENERA PROBE ENTRY SITES (⊙). LATITUDES MEASURED FROM VENUS ORBIT PLANE, POSITIVE IN DIRECTION OF CELESTIAL NORTH.

Figure 3-2. SSG Recommended Probe Target Areas

the greatest possible latitude spread independent of hemisphere; placing all four probes in one hemisphere (north or south) is acceptable. Note that there is no requirement to target the small probes to the sunlit side; light and dark side entries at some distance from the terminator are equally valuable. However, achieving the maximum latitude spread is considered more desirable than achieving the maximum longitude spread. The large probe requires a light-side entry within 70 degrees or less of the subsolar point to obtain useful solar flux measurements; the closer the subsolar point, the better. The "region of the equator" is taken to be within ± 15 degrees of the orbit plan for purposes of establishing targeting requirements since the Venus orbit plane and equatorial plane are within a few degrees of each other. The orbit plane is used as the zero latitude in this report unless otherwise noted.

Two major mission parameters affected by the science targeting requirements are the probe entry flight path angle (γ) and the probe-earth communications angle (θ) illustrated in Figure 3-3. The entry flight path angle is the dominant parameter in determining the entry heating and deceleration loads, while the communications angle sizes the communications subsystem for a given bit rate. The entry flight path angle also determines the altitude at which subsonic velocities are first achieved; shallow entry angles permit instrument deployment at higher altitudes than do steep entry angles. Thus, the target site selection must consider altitude coverage requirements as well as latitude/longitude coverage requirements and mission constraints.

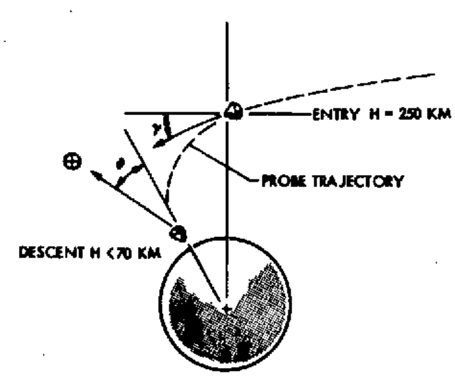

Figure 3-3. Definition of Probe Entry Angle (γ) and Probe-Earth Communications Angle (θ)

Figure 3-4 shows contours of constant entry flight path angle and communications angle in subsolar/orbit plane coordinates for the 1978 opportunity. The desire to target the large probe within 70 degrees of subsolar near the equator (±15 degrees) implies entry flight path angles between -30 and -40 degrees and communications angles greater than 45 degrees from subearth. A nominal large probe target on the equator at 65 degrees longitude results in a flight path angle of -35 degrees and a communications angle of about 50 degrees. This represents a reasonable balance between science achievement and system design cost as discussed in Section 4.0. As the probe target moves toward the subsolar point, the entry angles became shallower (total heating increases) and the communications angle increases (required transmitter power increases and/or probability of data dropout increases). An entry angle of -35 degrees (±3 degrees) results in subsonic velocities and chute deployment well above the cloud top.

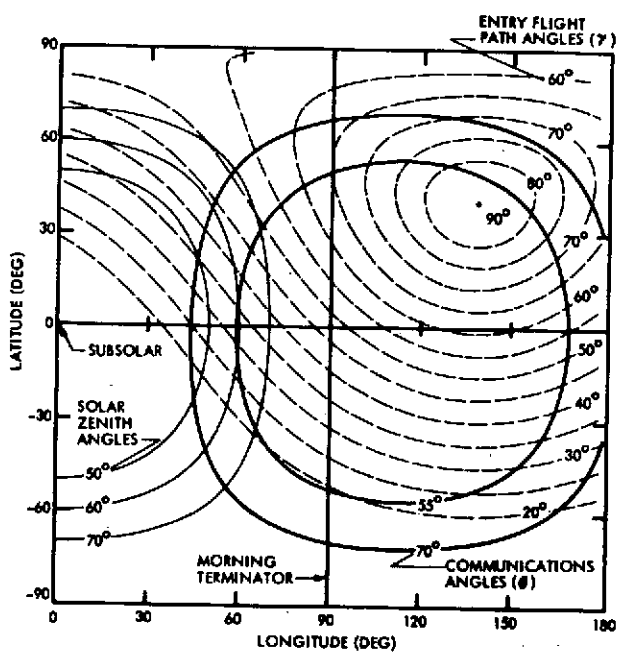

Figure 3-4. Contours of Constant Entry Flight Path Angle (γ) and Communications Angles (θ) for 1978 Probe Mission

Small probe targets near ±60 degrees latitude require communications angles of about 60 degrees, steep (~-75 degrees) entry angles in the Northern hemisphere and shallow (~-20 degrees) entry angles in the Southern hemisphere. Equatorial targets separated from the nominal large probe site by

90 and 120 degrees in longitude require communications angles of $\sim$40 and $\sim$70 degrees respectively, and entry angles of -50 to -60 degrees. A 90-degree longitude separation from the large probe site can also be achieved with a shallow ($\sim$-30 degree) entry angle and $\sim$55-degree communication angle in the Southern hemisphere; a 120-degree longitude separation with a shallow entry angle requires communications angles greater than 70 degrees.

The conservative 55-degree communications limit selected for the baseline design assures a reliable communications link from the small probes near the surface and allows targeting a small probe as far as 100 degrees in longitude from the large probe site. The maximum achievable latitudes within this limit are +54°N with $\gamma = -75$ degrees and -56°S with $\gamma = -20$ degrees. Requiring the small probes to survive over this range of entry angles results in a significant weight penalty as discussed in Section 4.2.3. It also requires instrument deployment at Mach numbers greater than three and dynamic pressures greater than 14 300 N/m^2 for at least one probe. Restricting the flight path angle range slightly (-25 to -60 degrees) alleviates these difficulties and results in a lower cost test program while still achieving more than the minimum desired planet coverage. The -25 to -60 degree flight path angle range and the 55-degree communications limit permits targeting to latitudes between +44°N and -52°S and longitudes up to $\sim$100 degrees from the large probe site (65 to 165 degrees).

Expanding the communications limit to 70 degrees from subearth would increase the achievable longitude separation along the equator to $\sim$140 degrees (44 to 184 degrees) and permit targeting to 64°N within the -25 to -60 degree entry angle corridor. Greater latitude coverage in the Southern hemisphere would require very shallow entry angles ($\sim$-10 to -20 degrees). Increasing the communications angle to 70 degrees would require either a wider beam antenna and increased transmitter power or acceptance of increased probability of sporadic data loss due to possible probe pitching near the surface.

The discussions above have not considered probe targeting dispersions due to trajectory uncertainties and probe release errors. Probes designed to survive entry over the flight path angle range -25 to -60 degrees must be nominally targeted to angles slightly steeper and shallower than -25 and -60 degrees, respectively. Typically, the small probe flight path angle dispersions are ± 4.5 degrees at $\gamma = -30$ degrees and ± 3.5 degrees at $\gamma = -55$ degrees. Thus, the nominal entry angle corridor for the small probes is from -29 to -56 degrees, resulting in a nominal latitude spread capability of $+40^{\circ}$N to -45°S and a nominal longitude spread capability of 100 degrees (65 to 165 degrees) within the 55-degree communications limit. The large probe dispersions are about ± 3 degrees at $\gamma = -35$ degrees. More detailed discussions of the probe targeting tradeoffs are given in Section 4.2.2.

3.1.1.3 Entry Measurement Requirement and Tradeoffs

This section discusses the science requirements and tradeoffs for measurements to be made during the high-speed probe entry phase; the low-speed descent phase requirements are treated in the following section. The entry phase, as defined in this report, covers the altitude region between 250 km and ~70 km. This region includes the turbopause, most of the ionosphere, and a thin cloud or haze layer above the main cloud tops. The Version IV (Reference 3) science payload includes accelerometers as the only instruments required to obtain measurements during the entry phase; a shock layer radiometer was also included in a previous version and is discussed in Section 3.3 for the Thor/Delta configuration.

Entry accelerometer data are required from an acceleration level of 4×10^{-4} g through blackout (0.5 g to 0.5 g + 10 seconds) and from end of blackout until parachute deployment (large probe) or instrument deployment (small probes) at the rates shown in Table 3-5. These rates were taken from the Version III science preliminary instrument descriptions because the Version IV science descriptions provided sampling requirements only for the descent phase.

Data storage is required only for the RF blackout period, but since the high Doppler rates before, during, and after blackout also preclude DSN signal acquisition, all entry data must be stored for transmission during descent. Since the total entry period is very short (~30 seconds) this does not result in a significant increase in memory size or complexity over that required for just the blackout period (Section 7.7). The baseline design

C2

Table 3-5. Entry Accelerometer Sampling Requirements

WORDS/S (b) & (BPS) LARGE PROBE, THREE-AXIS SYSTEM						SMALL PROBE, SINGLE AXIS	
ENTRY PHASE	PRIMARY AXIAL	BACKUP AXIAL	LATERAL X-AXIS	LATERAL Y-AXIS	TURBULENCE (INTEGRATED)	AXIAL ACCELEROMETER	TURBULENCE (INTEGRATED)
4×10^{-4} G TO 0.5 G	8 (80)	—	—	—	—	1 (10)	—
BLACKOUT (c) 0.5 G TO 0.5 G + 10^S	2.5 (25)	2.5 (25)	2.5 (25)	2.5 (25)	—	1 (10)	—
POST-BLACKOUT 0.5 G + 10^S TO ~70 KM	1 (10)	1 (10)	1 (10)	1 (10)	1/7 (1)	1/20 (0.5)	1/14 (0.5)

(a) ACCELEROMETER TEMPERATURE OUTPUT ALSO REQUIRED AT RATE OF ONE 7-BIT WORD EVERY 140 SECONDS.
(b) ALL 10-BIT WORDS EXCEPT 7-BIT TURBULENCE MEASUREMENT.
(c) MINIMUM DATA STORAGE REQUIRED DURING RF BLACKOUT PERIOD. 1000 BITS FOR LARGE PROBE; 250 BITS FOR SMALL PROBES.

incorporates common 5120-bit memory units (with 2560-bit blocks used for the bus and orbiter) for both large and small probes since this is more cost-effective than designing and qualifying separate 1000-bit and 250-bit units. The baseline design also incorporates a modified Pioneer 10 and 11 data telemetry unit with binary sampling rate capability (e.g., 16, 32, 64, 128, 256, etc., bps). The large probe sampling requirements (40, 80, 100 bps) can be accommodated with the 64 and 128 bps rates while the small probe requirements (10 bps) can be met with the 16 bps rate leaving sufficient margin for engineering data and/or an increase in accelerometer sampling rates.

Figures 3-5 and 3-6 show the altitude-time profiles during entry for the large and small probes. Since the times of various entry events relative to separation from the bus cannot be accurately predicted ($\sim\pm 2$ minutes), a g-switch signal was selected to obtain the necessary measurement profile. The accelerometer output could be used to control the data storage sequence, but since redundant 50-g switches are used to start a timer for the parachute deployment and descent sequences, the 50-g level was selected as a reference for the entry data sequence also.

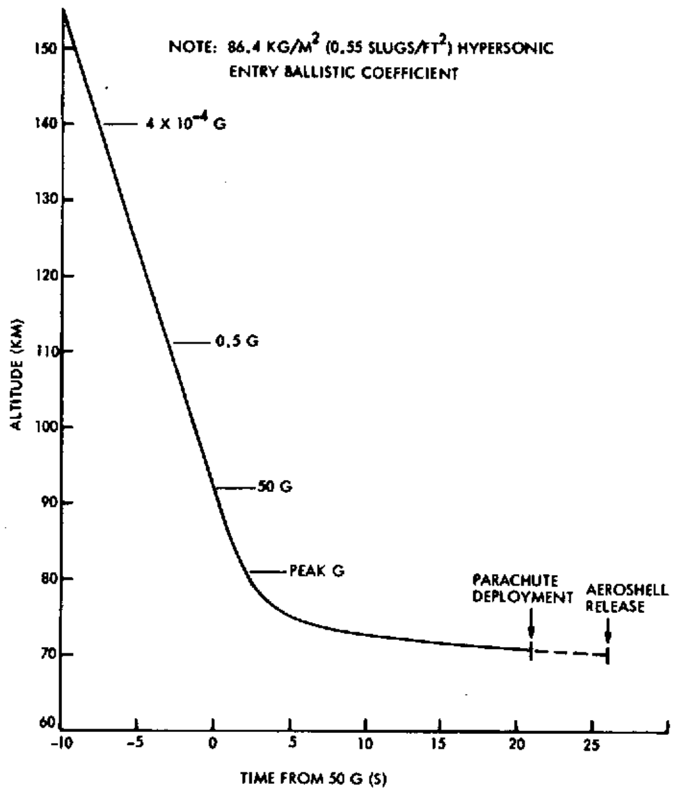

Figure 3-5. Large Probe Altitude Profile versus Time from 50 g Acceleration Level for $\gamma_E = -35^0$

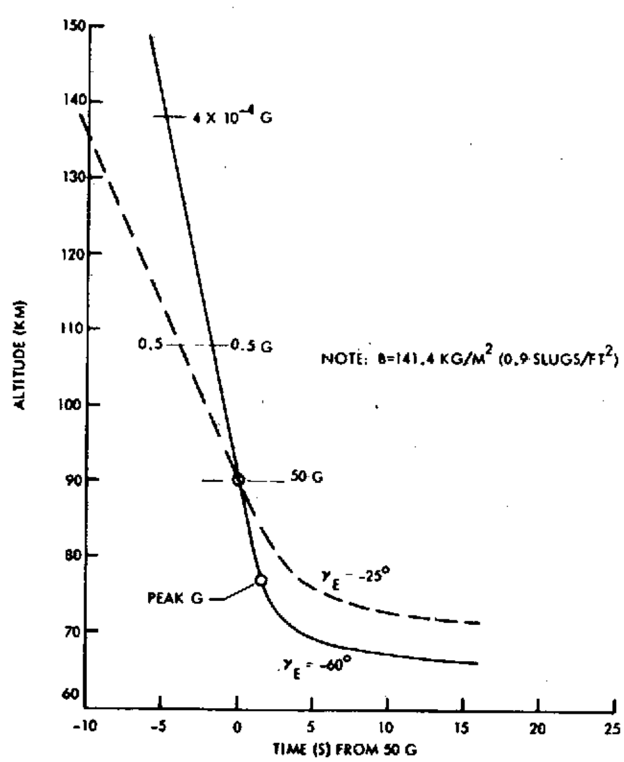

Figure 3-6. Small Probe Altitude Profiles versus Time from 50 g Acceleration Level for $\gamma_E = -25^0$ (– –) and $\gamma_E = -60^0$ (——)

To obtain data during the period from 4×10^{-4} g to 50 g, axial accelerometer sampling is initiated at 10 minutes prior to the expected time of entry when probe power is turned on. The large probe axial accelerometer data (and engineering data) are cycled into one 2560-bit memory block at 128 bps so that the most recent 20 seconds of data are always in storage. The signal from the 50-g switch then triggers sampling and storage of data from all four axes into a second 2560-bit block at 128 bps (including engineering data). At 50 g + 6 seconds (post-blackout) the storage rate is reduced to 64 bps until 50 g + 26 seconds when the aeroshell is released and the descent measurements are begun. A 50-g switch was selected rather than a 0.5-g switch because the 0.5-g switch must be armed after probe-bus separation to prevent switching during launch, retargeting maneuvers, or probe separation. The 50-g switches, with an appropriate time constant, can be armed prior to launch, thus obviating the need for a complex arm-disarm sequence. Since the axial deceleration is still almost linear with time up to ~50 g (Figure 3-7) and lateral accelerations are just becoming important, the switch from single-axis to four-axis sampling at 50 g rather than 3 seconds earlier at 0.5 g should not compromise the atmospheric reconstruction process.

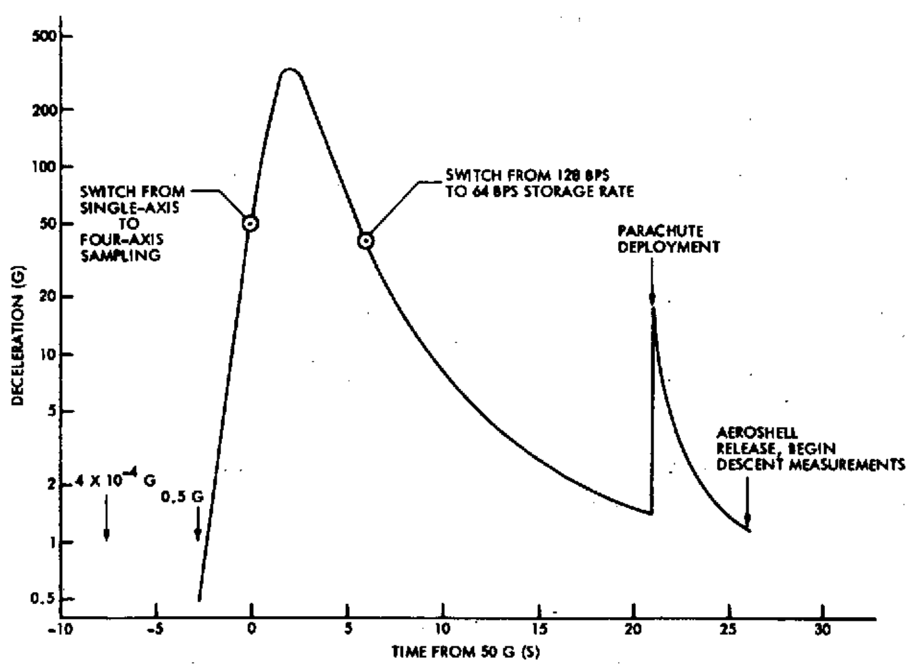

Figure 3-7. Baseline Large Probe Axial Acceleration Profile During Entry

Other entry data sampling schemes that could be implemented with the 5120-bit entry memory unit include:

1) Use of the output of the axial accelerometer or a dedicated 0.5 g switch to change to the four-axis sampling mode at 0.5 g with the 50-g switches used as backup (in addition to their primary function).

2) Store data at 128 bps during the entire entry period. This fills up the second 2560-bit block at 50 g + 20 seconds and requires storing the remaining 6 seconds of data over the first 6 seconds of data in the first 2560-bit block. This has the advantage of using only one clock rate (128 bps) for both entry and descent.

3) Combine 1) and 2) above.

Sampling and storage of the single-axis small probe data are also initiated at 10 minutes prior to entry, but data are cycled through one memory block at 64 bps until 50 g + 16 seconds when the descent instruments are deployed. Thus, the most recent 40 seconds of entry data (2560 bits) is retained for transmission during descent. The second 2560-bit memory block could be used to store the first 40 seconds of the descent data while the Doppler rates are still high.

3.1.1.4 Descent Measurement Requirements and Trades

The terminal descent data sampling requirements given for the Version IV science payloads are reproduced (Reference 3) below and in Tables 3-6 and 3-7. This section discusses their impact on the probe descent trajectories and data profiles.

"The experiment data sampling requirements shown in Table 3-6 for the large probe are based on the following assumptions:

1) The altitude interval from 66 to 44 km above the surface is selected as the reference measurement regime. The minimum acceptable number of measurements, per unit distance (minimum sampling interval), is specified for each instrument for this altitude interval.

2) The number of measurements sampled above 66 km shall be dictated by the sampling rate selected to satisfy the requirements for the reference altitude interval, per (1) above.

3) It is recognized that subsequent to parachute jettison, probe velocity will, for a time, exceed that which permits sampling equal to that specified for the reference altitude interval. The minimum measurement rate for the altitude interval from 44 to 29 km shall not be less than 40% of the reference rate.

Table 3-6. Large Probe Terminal Descent (Nominal) Experiment Data Sampling Requirements

INSTRUMENT	MEASUREMENT DESCRIPTION	MEASUREMENT SIZE (BITS)	MINIMUM SAMPLING INTERVAL ALTITUDE (M)	MINIMUM SAMPLING INTERVAL TIME (S)
TEMPERATURE	ATM TEMP	10	200	NA
	THERMISTOR	7	NA	140
PRESSURE	ATM PRESSURE	10	200	NA
	THERMISTOR	7	NA	140
ACCELERATION (a)	TURBULENCE	7	100	NA
	AXIAL	10	NA	20
	AXIAL B U	10	NA	20
	LATERAL	10	NA	40
	LATERAL	10	NA	40
	THERMISTOR	7	NA	140
HYGROMETER	HUMIDITY	10	500 (b)	NA
	RANGE	1	500 (b)	NA
	HOUSEKEEPING	10	1 PER EVERY 10 HUMIDITY MEASUREMENTS	NA
PARTICLE SIZE SPECTROMETER	SCIENCE AND HOUSEKEEPING	240	200	NA
SOLAR RADIOMETER	SCIENCE AND HOUSEKEEPING	240 (c) 72 (d)	750	NA
IR FLUX	SCIENCE AND HOUSEKEEPING	100	750	NA
WIND-ALTITUDE RADAR	SCIENCE	37 (d)	NA	20
	VOLTAGE	7	NA	60
	TEMPERATURE	7	NA	60

(a) A TOTAL OF 1000 BITS OF DATA RECORDED DURING ENTRY ARE TO BE READ OUT DURING THE PROBE DESCENT.
(b) NO MEASUREMENTS REQUIRED BELOW 44 KM
(c) 66 KM TO 44 KM
(d) 44 KM TO THE SURFACE

Table 3-7. Small Probe Terminal Descent (Nominal) Experiment Data Sampling Requirement

INSTRUMENT	MEASUREMENT DESCRIPTION	MEASUREMENT SIZE (BITS)	MINIMUM SAMPLING INTERVAL ALTITUDE (M)	MINIMUM SAMPLING INTERVAL TIME (S)
TEMPERATURE	ATM TEMP	10	200	NA
	THERMISTOR	7	NA	140
PRESSURE	ATM PRESS	10	200	NA
	THERMISTOR	7	NA	140
ACCELEROMETER (a)	TURBULENCE	7	100	NA
	AXIAL	10	NA	20
	THERMISTOR	7	NA	140
NEPHELOMETER	SCIENCE	43	200	NA
	CALIBRATION	10	NA	900
FLUX RADIOMETER	NET FLUX	8	NA	30
	DETECTOR TEMP	8	NA	60
	WINDOW TEMP	8	NA	60

(a) A TOTAL OF 250 BITS OF DATA RECORDED DURING ENTRY ARE TO BE READ OUT DURING THE PROBE DESCENT.

4) From 29 km to the surface, the minimum measurement rate shall equal that of the reference altitude interval.

5) Certain measurements are to be sampled on a time interval basis which is not dependent on the altitude interval traveled.

6) Several instruments have special sampling requirements not satisfied by the aforementioned assumptions. These are:

   (a) Mass Spectrometer - A minimum of 80,000 bits of data will be generated between 66 km and 44 km. This data is to be sampled at a constant rate. Data read out above 66 km shall be sampled at this same rate. The number of bits per complete measurement will vary. However, all formatting is done within the instrument.

   From 44 km to the surface a minimum of 88,000 bits are generated. This data is to be sampled at a constant rate.

   (b) Gas Chromatograph - This instrument will make one (1) measurement every twenty (20) minutes regardless of altitude interval. During the first 10 minutes, the instrument will generate and store 13,200 bits in a buffer memory. No data is to be read out by the probe during this period. During the last 10 minutes the instrument is not in a measurement taking mode. It is required that the 13,200 bits be read out by the spacecraft during this time."

"The experiment data sampling requirements shown in Table 3-7 for the Small Probes are based on the following assumptions:

1) The altitude interval from 66 km to the surface is selected as the reference measurement regime. The minimum acceptable number of measurements, per unit distance (minimum sampling interval), is specified for each instrument for the altitude interval.

2) The number of measurements sampled above 66 km shall be dictated by the sampling rate selected to satisfy the requirements for the reference altitude interval, per (1) above.

3) Certain measurements are to be sampled on a time interval basis which is not dependent on the altitude interval traveled."

The altitude at which a probe can first obtain subsonic measurements depends on the entry flight path angle and entry ballistic coefficient $\left(B = m/C_D A \right)$. Given these, the instrument deployment can be accurately timed from some reference event (50 g increasing) to occur at a desired altitude or Mach number or dynamic pressure. For the baseline large probe, targeted to $\gamma_E = -35 \pm 3$ degrees with a hypersonic ballistic coefficient of 86.4 kg/m^2 $\left(0.55 \ slugs/ft^2 \right)$, aeroshell release and instrument deployment is timed to occur at a subsonic velocity near 70 km as desired by the science objectives.

Instrument deployment for each small probe could also be timed to occur at a subsonic velocity but at altitudes depending on the entry flight path angle. Figure 3-8 shows the small probe altitude at various times after 50 g increasing as a function of entry flight path angle; the altitudes at which various Mach numbers occur are also shown. To deploy all probes at either a given altitude or a given Mach number, each probe must be timed differently. For example, probes entering at γ = -25 and -60 degrees reach M = 1 at 21 and 11 seconds after 50 g, respectively. Since this requires different times and sequencers for each probe, it is undesirable from the standpoint of both cost and data handling. The baseline design therefore incorporates identical timers for all small probes. A deployment time of 16 seconds after 50 g was selected since this gives deployment at or above the reference altitude (66 km) for γ = -60 degrees while keeping the Mach number at deployment below M = 1.5 for γ = -25 degrees. Figure 3-9 plots the minimum and maximum entry angles that can be achieved for various deployment conditions while satisfying the requirement to obtain measurements at or above 66 km. As can be seen, all small probes can begin descent measurements above 66 km over a wide range of entry angles while keeping the Mach numbers at deployment less than 1.5 to 2.

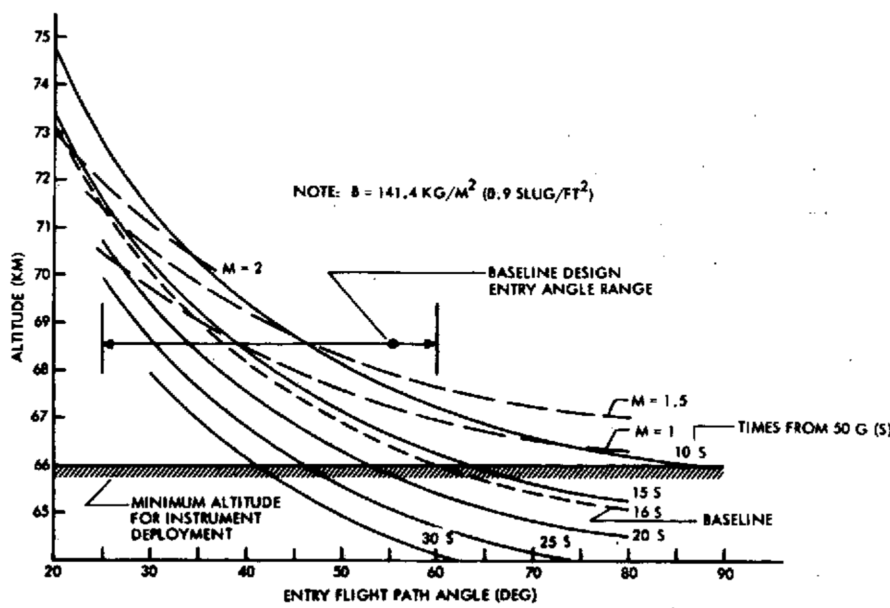

Figure 3-8. Small Probe Altitude versus Entry Flight Path Angle and Time from 50 g Increasing

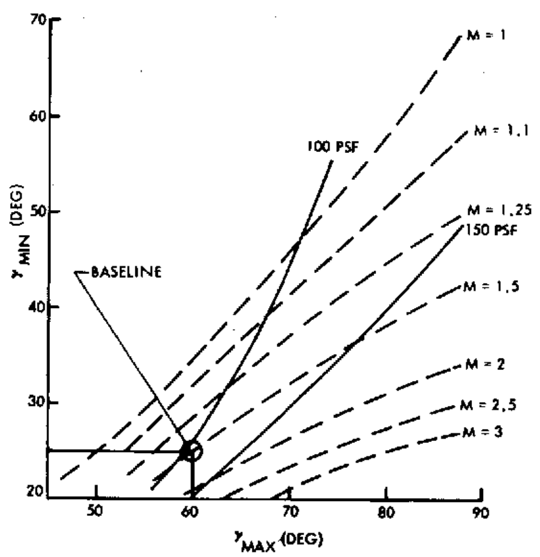

Figure 3-9. Small Probe Entry Angle Range and Deployment Conditions at Fixed Times after 50 g, Above 66 km

Figure 3-10A shows the total science data rate required to obtain the minimum altitude sampling intervals as a function of altitude for the baseline small probe with B = 198 kg/m^2 (1.26 slugs/ft^2). The maximum data rate required (at 66 km) is also shown to be a relatively insensitive function of probe ballistic coefficient. As can be seen, a binary data transmission rate of 65 bps meets the requirements at 66 km and was selected for the baseline design. One alternative, discussed in Section 7, would be to reduce the bit rate in binary or nonbinary steps to follow the minimum requirements curve as the probe descends. This would result in a more complex data handling subsystem than the fixed-rate baseline design, but would provide more power per bit near the surface. The baseline design, however, provides a sufficient margin and is preferred because of its simplicity. Figure 3-10B shows the altitude intervals actually obtained with the baseline design probe data format.

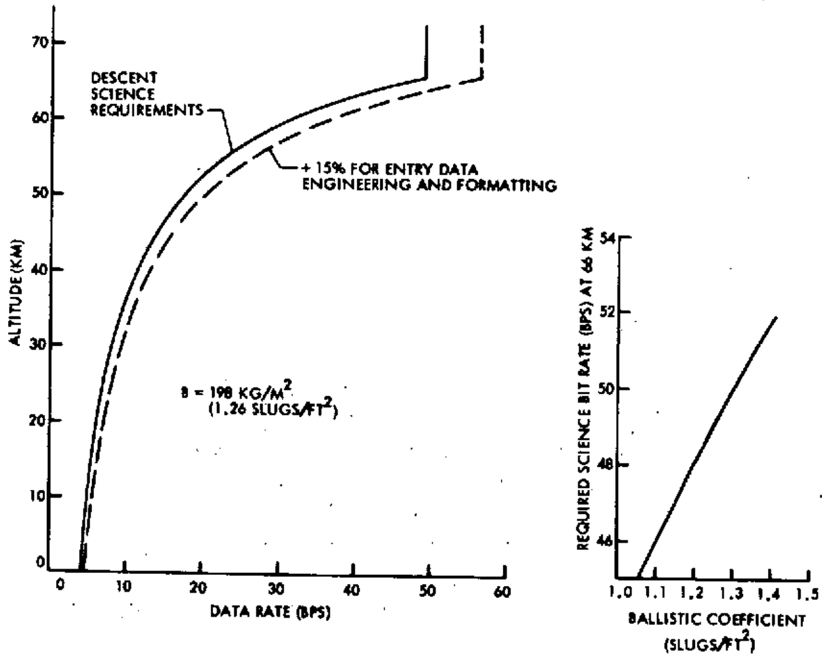

Figure 3-10A. Small Probe Version IV Science Data Requirements

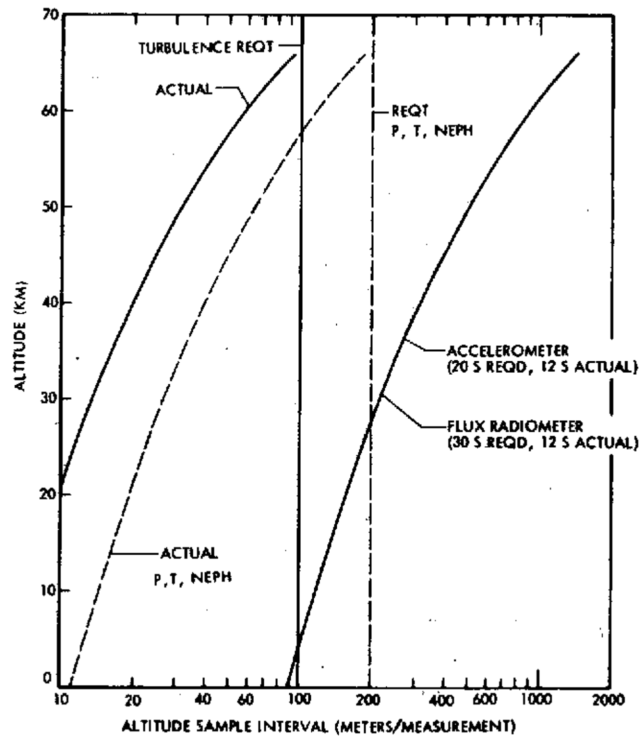

Figure 3-10B. Baseline Small Probe Altitude Sampling Interval Profile Compared to Requirements

The large probe data rate requirements are strong functions of both parachute and descent capsule ballistic coefficient as illustrated in Figure 3-11. The curves show the total science data rates required at the 66 and 29 km reference altitudes assuming a constant 11 bps rate for the gas chromatograph. The data rate required at 29 km is a function of the parachute and descent capsule ballistic coefficients and the chute release altitude as shown by the two curves at the right in Figure 3-11. This results from the requirement to transmit 88 000 bits from the mass spectrometer below 44 km at a constant rate. The data rate requirements at 29 km are shown parametrically in Figure 3-12 for a chute release altitude of 43 km. The unshaded region represents the data rate-ballistic coefficient combinations that result in descent times below 66 km longer than the 70 minutes required by an 11 bps gas chromatograph readout. Figure 3-13 shows the ballistic coefficient combinations that result in 60 to 70 minute descent times below 66 km with chute release at 43 km.

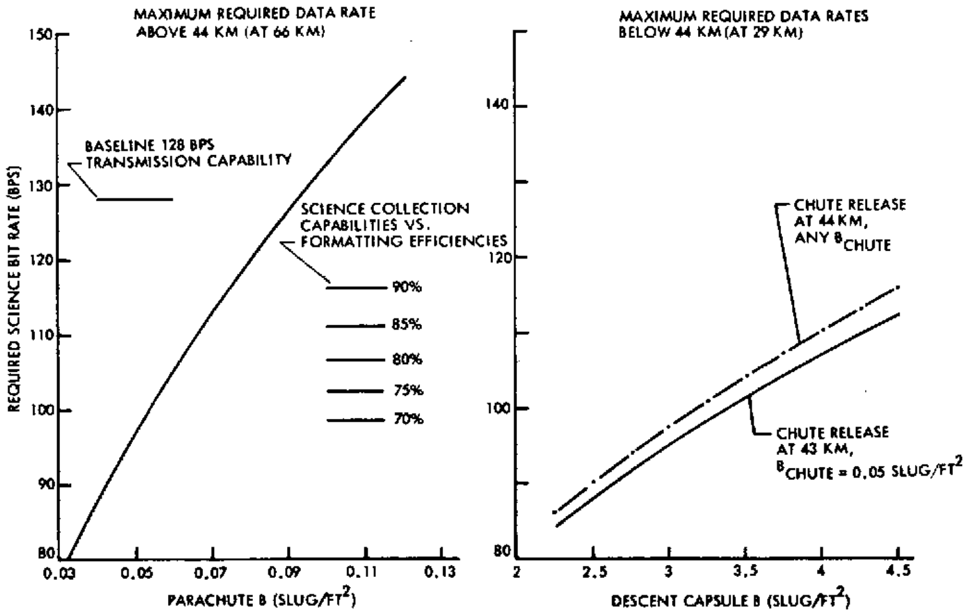

Figure 3-11. Large Probe Science Data Rate Requirements versus Ballistic Coefficients

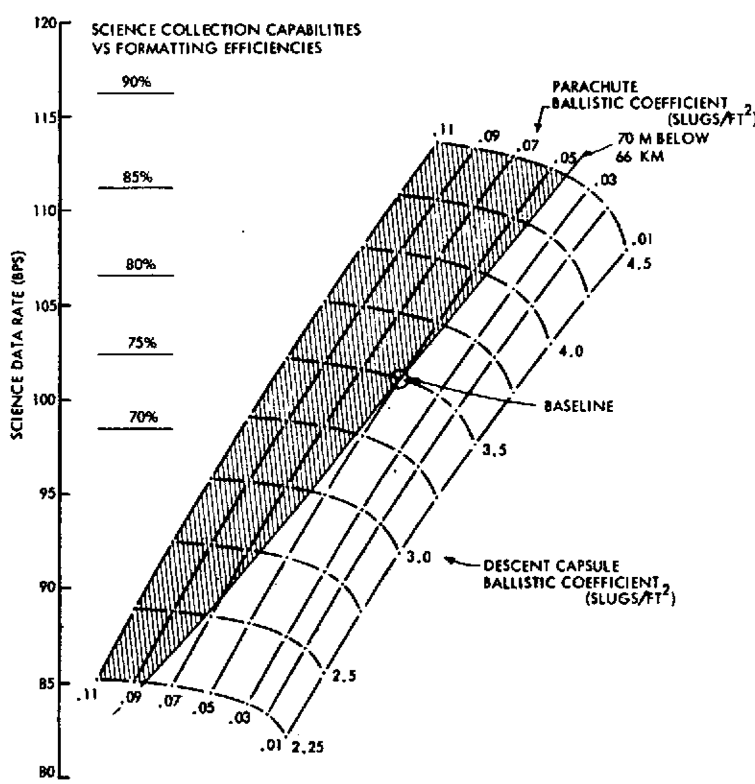

Figure 3-12. Maximum Required Science Data Rates Below 44 km
(at 29 km) Chute Release at 43 km

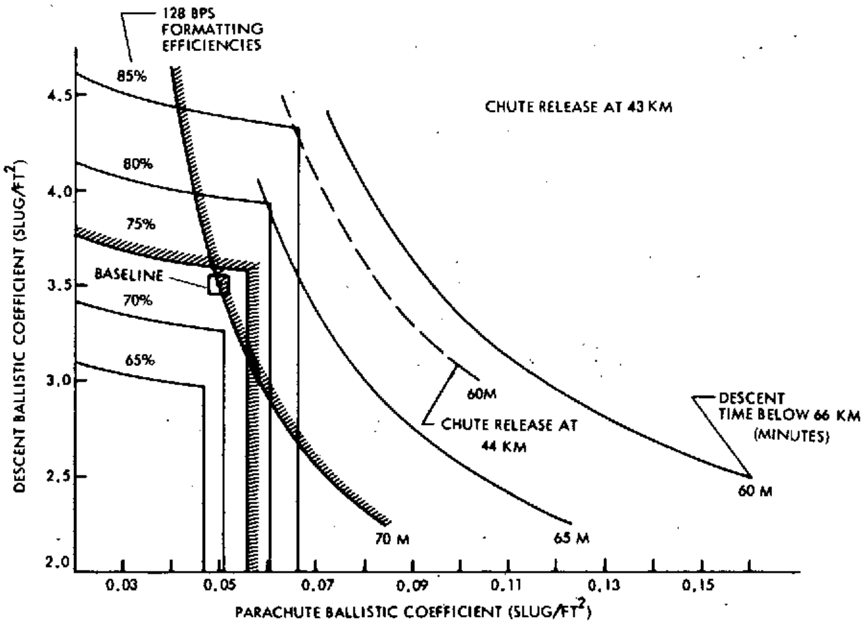

Figure 3-13. Large Probe Ballistic Coefficient Combinations for Various Descent Times Below 66 km and Formatting Efficiencies

The gas chromatograph requirement to obtain one measurement every 20 minutes below 66 km could be implemented with either a 60 or 70 minute descent time depending how the data are read out. Figure 3-14 illustrates 60- and 70-minute descent profiles that meet all data sampling requirements with a 128 bps transmission rate. Readouts of the gas chromatograph buffer are made at 22 bps during the 10 minutes following each analysis for the 60-minute descent or at 11 bps during 20 minutes after each analysis for the 70-minute descent. The 60-minute profile obtains the last sample at a lower altitude than does the 70-minute descent but requires switching of sampling rates for all instruments every 10 minutes to accommodate the 22 bps bursts. The 70-minute profile was selected for the baseline design since it requires a simpler data handling subsystem. The weight savings (battery, parachute) associated with the 60-minute descent are very slight since both profiles are the same through the hot lower atmosphere and the thermal control weight remains the same (see Section 4.2.4).

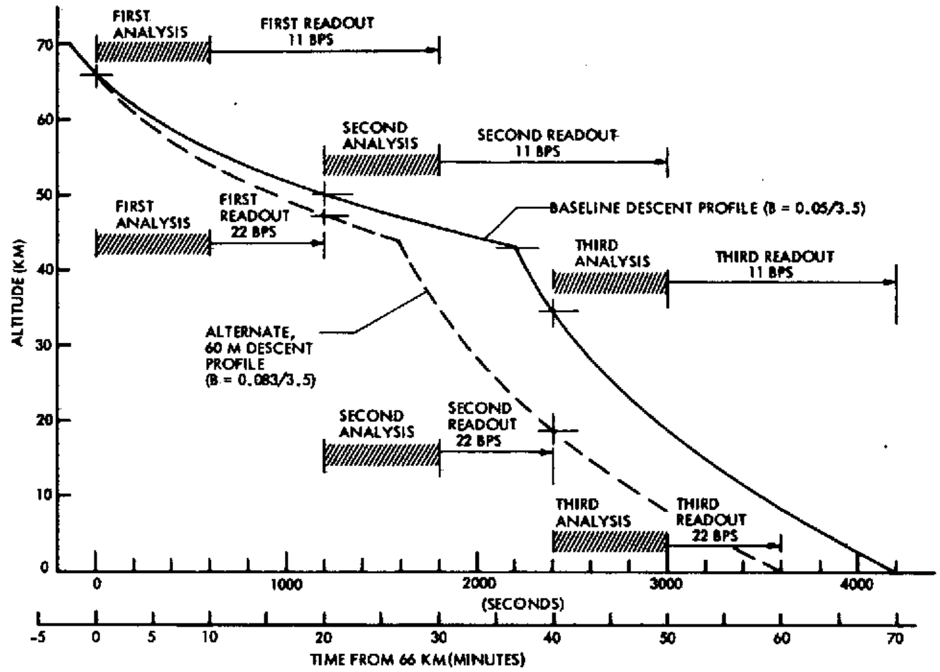

Figure 3-14. Large Probe Descent Profiles Showing Alternative Gas Chromatograph Readout Schemes

Figures 3-11 through 3-13 also show the science data collection capabilities versus formatting efficiency for a 128-bps transmission capability. An efficiency of 75 percent was assumed as a design goal to allow for engineering data, frame synch and ID and nonstandard science word lengths. As shown in Figure 3-13, any combination of ballistic coefficients below and to the left of the shaded boundaries (70 minute minimum descent time bound and the 75 percent efficiency bounds) will meet or exceed the data sampling requirements. The 0.05/3.5 combination was chosen for the baseline design. The total science data rate requirements versus altitude for the baseline are shown in Figure 3-15A. The dashed curve between 29 and 43 km shows the total rate needed to obtain the altitude sampling intervals specified for the reference measurement regime (66 to 44 km); the solid curve between 29 and 43 km shows the minimum acceptable rate corresponding to 40 percent of the reference rate. Figure 3-15B shows the altitude intervals obtained for the baseline design data format and 128 bps transmission capability.

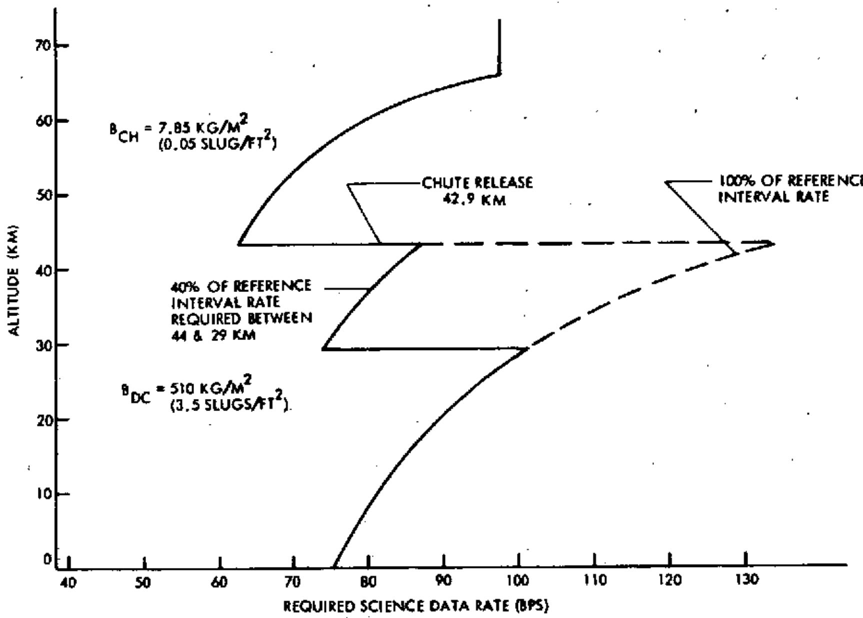

Figure 3-15A. Large Probe Science Data Collection Rates Required to Meet Sampling Interval Requirements

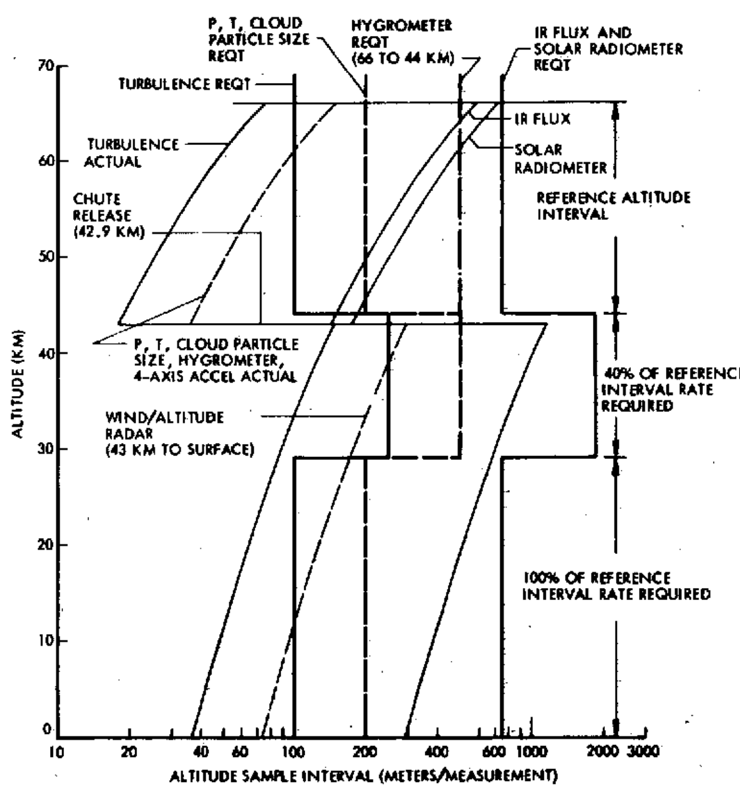

Figure 3-15B. Baseline Large Probe Altitude Sampling Interval Profile Compared to Requirements

3.1.2 Instrument Accommodation Studies

The concepts we have chosen for accommodating the nominal payloads for both large and small probes launched with the Atlas/Centaur are discussed in this section. The instruments considered here are those in the payloads of the Version IV Science Definition, 13 April 1973. This section also includes accommodation concepts for "Other Candidate Instruments."

The key design concept involved in the instrument accommodation on the large probe is the equipment ring assembly which holds all the experiments and probe subsystems. All of the optical, electrical, and gas penetrations are made through the pressure shell part of this ring assembly, thereby making it possible to integrate and test the fully instrumented probe before assembling the top and bottom pressure shell covers. This concept makes it somewhat easier to adapt to possible early modifications and changes in experiments. It also facilitates system level assembly and testing, thereby reducing costs in those areas.

Our standardized approach to window and electrical penetrations serves as a cost reduction factor by using the same developmental work to deal with the windows and feed-throughs for all the experiments. Our developmental work in this area has resulted in a lightweight window concept which has been designed and successfully tested in a descent through a simulated Venus environment. This design incorporates thermal isolation and window heating for minimizing thermal leakage into the probe and eliminating window contamination by atmospheric condensates and particulates.

The deployment mechanisms used for the temperature gauge and IR-flux detector mirror on the small probe are essentially the same as those proven for use with the temperature gauges on PAET and Viking.

The following sections describe in detail our instrument accommodation concepts for both large and small Atlas/Centaur probes. The capability of our designs to accept other candidate instruments is next discussed. Potential problems and areas where payload conflicts may occur are then discussed. This section finally identifies engineering experiments, which can be incorporated to improve probe designs for future missions.

3.1.2.1 Large Probe Instrument Accommodation Concepts

Structural and Mechanical

The basic mechanical accommodation feature for instruments in the large probe is the equipment ring assembly shown in Figure 3-16. It consists of equipment support beams that serves as a mounting platform for all the instruments (with some exceptions) and a slice of the lower hemisphere of the pressure shell. The instruments that require a penetration of the pressure shell make that penetration (window, electrical, gas inlet, etc.) through the pressure shell ring. The internal parts of the instruments are mounted on the instrument platform part of the assembly.

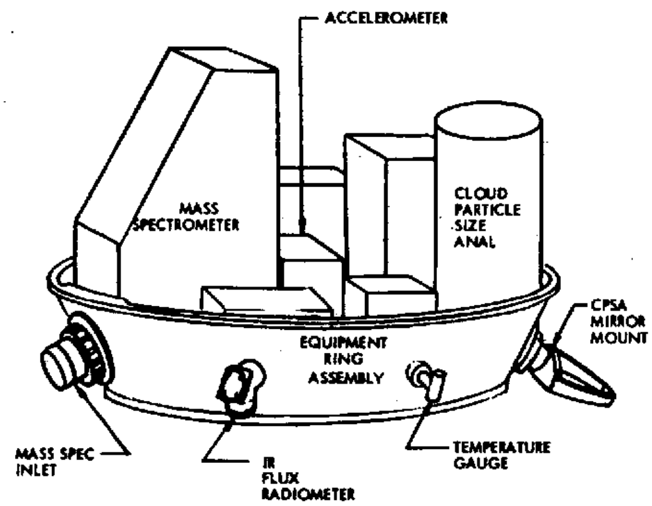

Figure 3-16. Equipment Ring Assembly Concept

Some of the optical parts of instruments are mounted on this instrument platform and their windows are mounted directly on the pressure shell. Alignment concerns between the parts are minimized because the equipment ring assembly is final machined after the equipment support beams are installed.

The instrument mounting surfaces will be held to alignment tolerances of $\pm$ 1/2 degree with respect to the probe coordinate system. The mounting points for the instruments have out-of-plane tolerance not exceeding 0.0127 cm (0.005 in.).

Any instrument requiring a penetration of the pressure shell is mounted with a threaded fitting and compression nut assembly similar to that shown in Figure 3-17 for a window mounting. The gasket (a metal O-ring) is mounted in a groove in the shoulder of the fitting and seals against a flat surface machined into the pressure shell around the hole. In this way penetration hardware can be mounted and demounted with minimum risk of damage to the pressure shell, such as stripping threads, breaking a fitting, etc. All the window assemblies are constructed with sealed double windows consisting of an external and an internal window (or lens).

Some instruments require special optical considerations beyond a simple aperture in the probe. Two of these are the solar radiometer and planetary flux radiometer. These instruments have special field of view and transmission considerations that require optical design in the penetration window assembly. We have made some preliminary designs of these windows using the NASA instrument descriptions supplemented by discussions with candidate principal investigators (PI's).

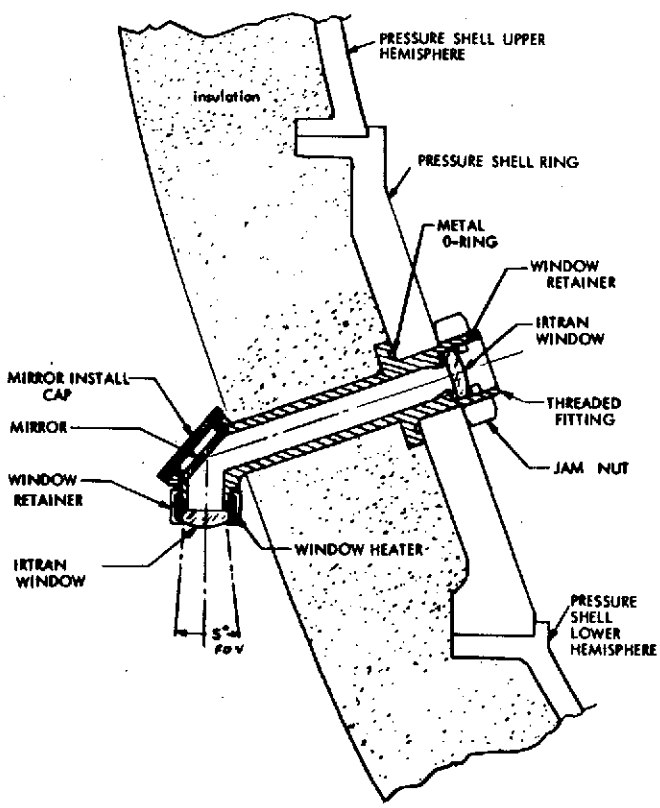

Figure 3-17. Planetary Flux Radiometer Window

The planetary flux radiometer accommodation is shown in Figure 3-17 with an elbow telescope configuration to achieve the 5-degree down-looking field of view from the equipment ring assembly. The right angle bend is achieved with a gold coated front surface mirror. The 10-mm clear aperture Irtran lens has a 53-mm focal length, which sets the prime focus at the pressure vessel so that a 4.6-mm aperture stop provides the 5-degree full cone angle field of view. This small aperture stop allows for a reduced window assembly size at the probe wall, while reducing the thermal leak. To transmit at long wavelengths (10 percent transmittance at 29 μm with 6 mm thickness), Irtran 6 is preferable. Since the lens also serves as a pressure window, it must be thick enough to withstand rupture at Venus surface temperature and pressure. This material has not been tested at high pressure and temperature, but a 6 mm thickness appears adequate, based on a safety factor of 4.5 with the modulus of rupture measured at 373°K. If tests show unacceptable strength or chemical activity at high temperatures, then IRTRAN 4 or IRTRAN 2 will be required. Our tests of IRTRAN 2 have demonstrated its suitability. A 5.7-mm-thick IRTRAN 2 window was assembled with a clamped metal O-ring as discussed in Appendix 3A. The aperture was 12.2 mm and it survived without leaking while exposed to a pressure differential of 9.3 MN/m^2 and temperature of 728°K.

This window concept was reviewed with members of the candidate PI's team recently. The concept appeared to them to be satisfactory. There was some discussion of eliminating the special plug to install the mirror, and installing the mirror through the objective end of the tube. This would simplify the design and eliminate a potential leakage point. This thought will be pursued in subsequent detailed design.

The experimenters (messrs Miller and Giver) also expressed interest in the choice of probe fill gas. Dry nitrogen was chosen because of its ready availability, and leakage and dielectric strength characteristics. If it is shown that its activity in the infrared would interfere with the radiometer, we could use argon following a check of its leakage and dielectric strength characteristics.

The solar radiometer accommodation requires compressing two wide and divergent fields of view into a reasonable size thermal penetration. The basic problem is to satisfy the requirements implied by the configuration shown in Figure 3-18 while reducing considerably the thermal leak, which this would cause. An approach that could achieve this is shown in Figure 3-19 where the upward and downward fields of view are obtained by two separate wide angle telescopes, which direct the light alternately onto the same detector array. Each telescope has a 0.44 rad (25 degree) half cone angle field of view with center lines pointing $\pi/6$ rad (30 degree) above and below the horizontal. Each telescope consists of three lenses. The first is a strongly negative lens with -8 mm focal length and a clear aperture of 4 mm. The second and third lenses are identical positive lenses with +8 mm focal length and 10-mm clear aperture. The two holes required in the pressure vessel and in the insulation are about 16 mm in diameter. A relay mirror system combined with the tuning fork chopper is then used inside the probe to transfer the "images" from the telescope onto the detector.

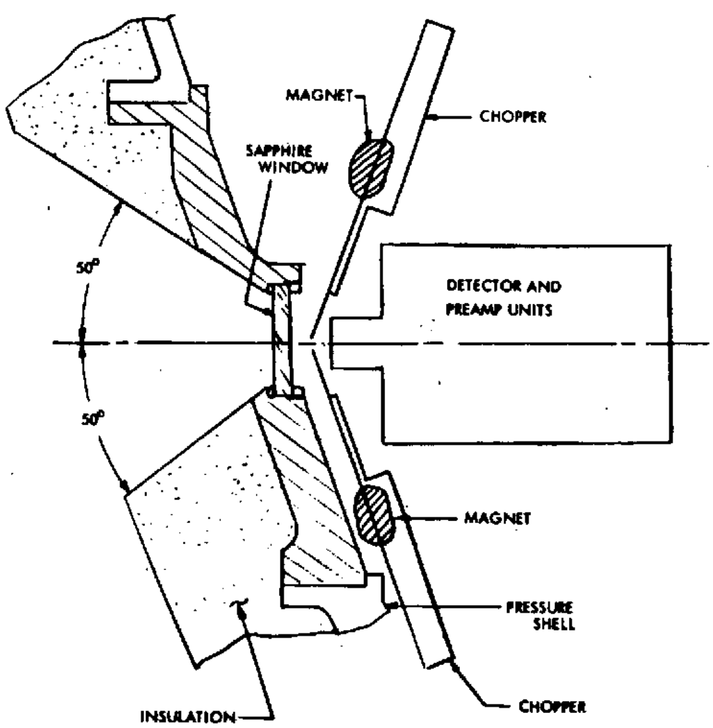

Figure 3-18. Single Window Solar Radiometer Configuration

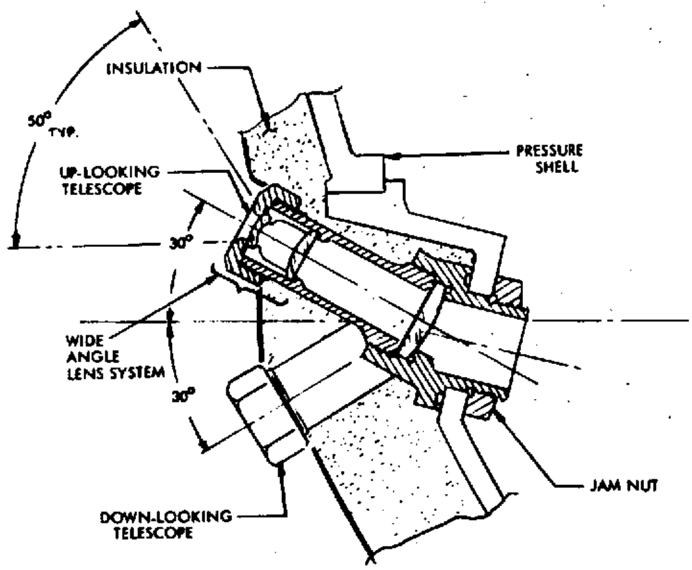

Figure 3-19. Two Telescope Solar Radiometer

An approach that compresses the wide fields of view into a single probe penetration is shown in Figure 3-20 as our preferred accommodation for the solar radiometer. This configuration uses a standard fisheye lens system (designed with sapphire lenses) followed by a dual sapphire light pipe assembly. The effect of the lens system is to image the wide field of view onto the light pipe surfaces with a beam divergence considerably smaller than the observed field of view. With this arrangement, the upward and downward images are separated by the two light pipes and guided into the instrument package where the chopper mirror system alternately directs the two light beams onto the detector system. The preferred configuration incorporates the best features of two earlier configurations discussed recently with members of the candidate PI's team.

The cloud particle size analyzer (CPSA) requires special alignment consideration due to the high spatial resolution imaging characteristic of the instrument. The mounting method illustrated in Figure 3-21 provides a single mounting point for the entire optical assembly. The equipment assembly feed-through is an integral part of the internal optical assembly. It is mounted to the hole in the pressure shell ring with the jam nut on the outside. The 12.5 cm length of the external mirror mount resulted from a tradeoff between clearance during aeroshell separation and a requirement

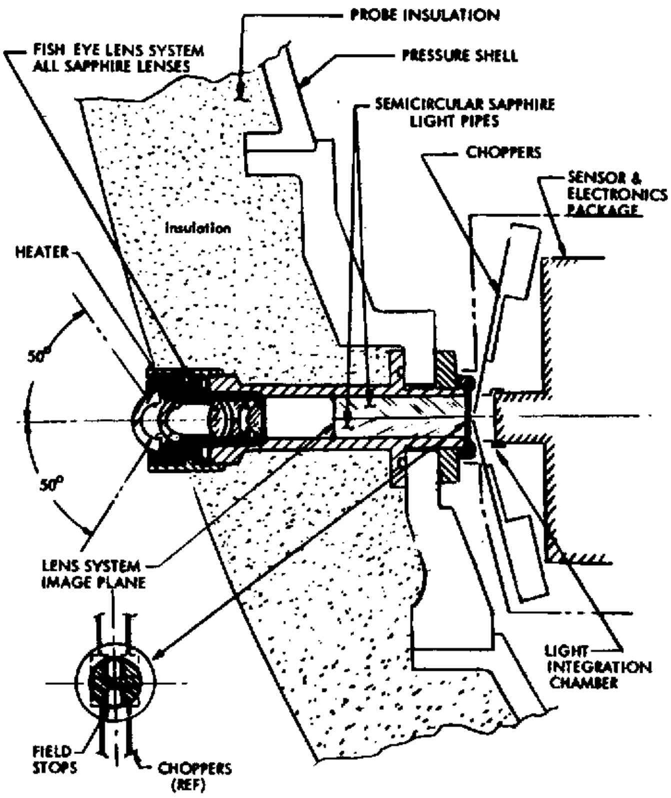

Figure 3-20. Solar Radiometer

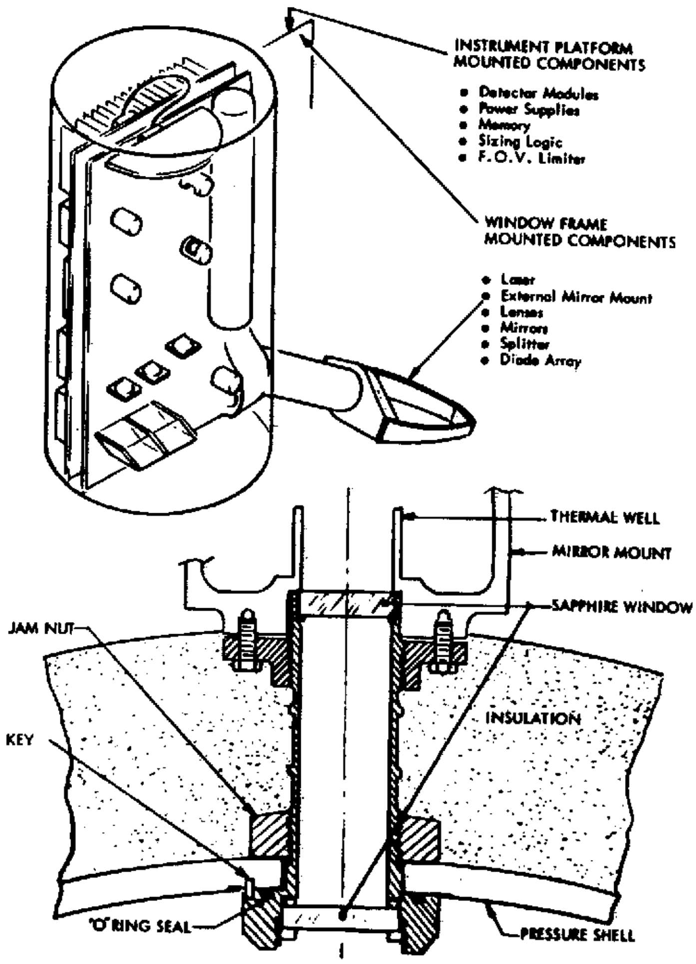

Figure 3-21. Cloud Particle Size Analyzer

to project the focal point of the laser beam beyond the probe boundary layer. To minimize distortion of the optical assembly during entry, the assembly is arranged with its long axis along the deceleration axis.

As presently conceived, the entire window assembly would be supplied by the probe contractor to NASA to be sent to the PI or instrument contractor. The inner end of the window will then permanently be joined to the instrument laser and optics housing, the mirror mount fabricated and attached to the mirror mount flange, and the complete instrument aligned using adjustments available in the internal optics housing. In this procedure, a simulated section of the pressure vessel will be used to allow the tension effect on the window of the jam nut to be incorporated into the alignment. An index will be made of the mirror mount to window position at this point. Prior to installation, the mirror mount flange with the mirror mount attached, will be unscrewed from the window and the jam nut removed, allowing the instrument to be installed onto and through the probe structural shell segment. After this the jam nut and complete mirror mount can be screwed back into place. The concept of structurally tying the external mirror to the internal optics through the window assembly and floating the internal optics from the instrument case, has been reviewed with the candidate PI who considered it acceptable.

The mass spectrometer mechanical accommodation for the quadrupole instrument with multiple inlet is shown in Figure 3-22. It involves primarily a large access hole through the pressure shell ring and insulation to mount the multiple inlet so that it projects into the free stream flow. The required hole is 7.6 cm, although in a recent discussion the candidate PI,

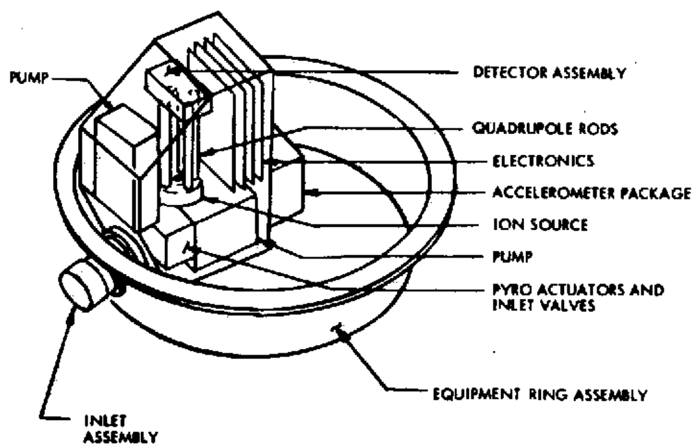

Figure 3-22. Mass Spectrometer Accommodation

Nelson Spencer, indicated a 5.1 cm opening may be adequate. The inlet system is an integral part of the instrument package and is mounted by inserting the inlet assembly through the hole from the inside of the pressure shell ring as with the cloud particle size analyzer. Since the spacing among the quadrupole rods is a critical dimension, they are placed parallel to the deceleration axis to minimize permanent distortion of this dimension during entry. The package is attached both to the pressure shell and the instrument platform parts of the ring assembly so that the deceleration loads do not produce a torque at the inlet attachment point. The quadrupole analysis is somewhat sensitive to magnetic fields. Therefore the placement of the rods in the package is designed to maximize their distance from the accelerometer, which generates magnetic fields of the order of several μT at 1 cm and about 50 nT at 16 cm.

The accommodation for the alternative magnetic sector instrument with single inlet is similar except for the size of the inlet penetration, which is much smaller (~10 mm). The critical dimensions with a magnetic sector requires placement of the analysis path of the ions in the plane normal to the deceleration axis.

The wind altitude radar accommodation requires some unique considerations. The characteristic feature of the external part of this experiment is its large planar antenna. As described by Mr. Lester Goldfischer of the radar study contractor, the antenna consists of an assembly of slotted titanium waveguides fed by two rigid coaxial feeds. Concern over the aerodynamic effects of the flat antenna led to several accommodation concepts. These included using a curved rather than a flat antenna or covering the flat antenna with a thin radome. Both concepts would introduce serious compromises in instrument performance with power loss in the curved antenna and reflection problems from the radome. Therefore, aerodynamic tests were performed in the Langley vertical wind tunnel to compare an exposed flat antenna configuration (Section 7.1) with a radome covered configuration. The results indicated greater stability for the exposed flat antenna than for the flat antenna covered with a faired radome, although both shapes were poorer than the basic sphere without the antenna.

As shown in Figure 3-23, the two rigid coaxial pressure rated waveguides are routed inside the insulation to feed-throughs in the equipment

Figure 3-23.
Wind Altitude Radar Antenna and Pressure Inlet

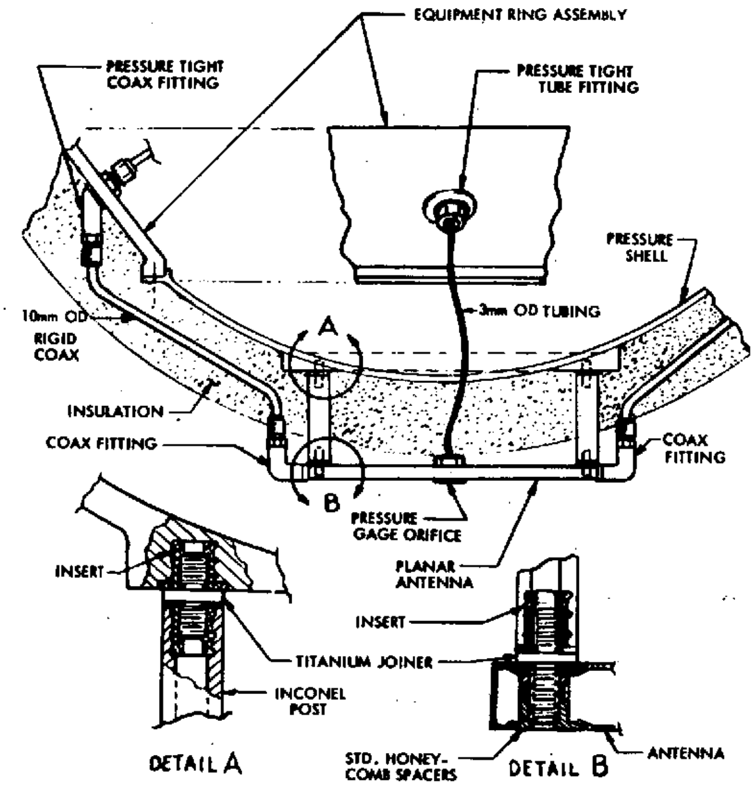

ring assembly. The antenna corners are mounted with standoff posts (for thermal insulation and mechanical support) to a boss on the bottom of the pressure shell. An alternative attachment being considered has the antenna attached directly to a double thickness (1.0 mm) section of the titanium insulation cover.

The pressure gauge requires an inlet near the stagnation point. To accommodate it in the equipment ring assembly, the feed-through is located there with an extension tube to the stagnation point, as shown in Figure 3-23. The diameter-to-length ratio of the tube is great enough to maintain a pressure response time of about 0.6 s. The entrance end of the tube is mounted in a slot existing in the center of the wind altitude radar antenna so that it can project directly to the stagnation point.

The temperature gauge located in the equipment ring assembly is at an ideal location for maximum mass flow. It projects far enough beyond the insulation, as shown in Figure 3-16, to be beyond the boundary layer. Its cylindrical radiation shield is parallel to the flow velocity.

The accelerometer is the only instrument not requiring access to the outside. The sensor and electronics are mounted as shown in Figure 3-16 where its position is dictated by the requirement that the primary axial sensor be located precisely at the center of mass of the probe with its sensitive axis along the spin axis. The approximate location for the instrument (within about 3 mm) will be determined from calculations of the inertial axis and center of mass. The final positioning will be determined by dynamic and static balance tests on the probe. Then the accelerometer will be moved accordingly by shimming, sliding in the bolt hole tolerances, and final pinning. A calibration connector will be provided through the pressure vessel and aeroshell for electrical torque simulation of the proof mass as required.

The hygrometer mounting location is rather flexible as long as the inlet orifice is pointed into the flow stream direction. An accommodation which satisfies this requirement and is well suited to the probe configuration is illustrated in Figure 3-24 where the orifice is just aft of the mirror mount of the cloud particle size analyzer. This location allows for placement of the hygrometer orifice in the flow stream without adding another cutout in the structural support for the aeroshell. The exhaust tube is then in a position to allow full venting of the flow-through gas.

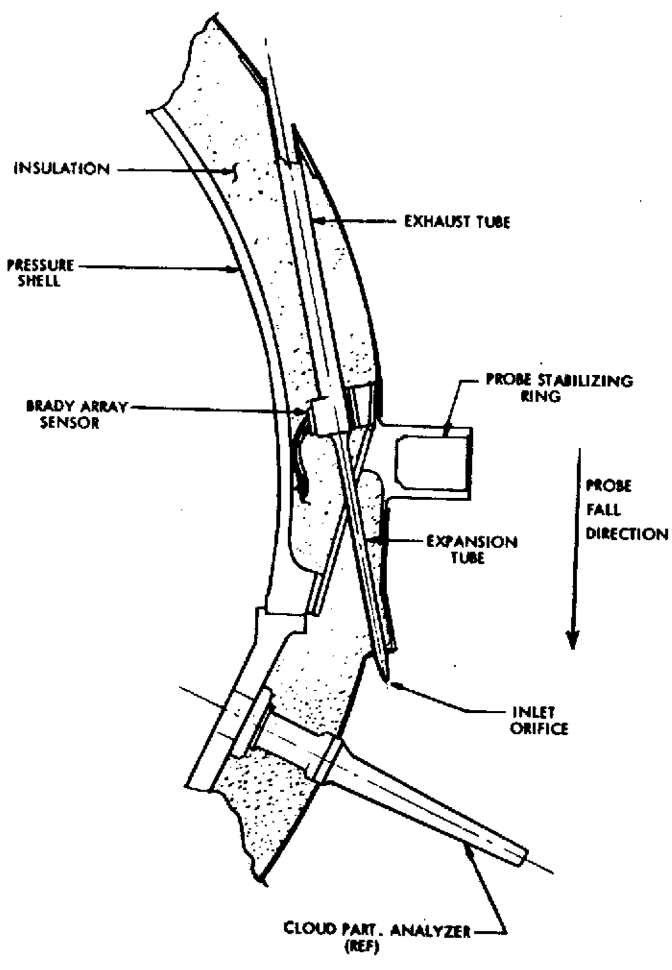

Figure 3-24. Hygrometer Mounting

The inlet requirements for the gas chromatograph are somewhat similar to those for the hygrometer in that gas from the free stream is to flow through the inlet system and be vented back to the atmosphere. However, in this case the gas must enter the interior of the probe for sensing rather than being sensed externally as with the hygrometer. A standard type of pitot tube whose entrance orifice is directed along the flow stream is the preferred method of providing this inlet. Thus, a feed-through assembly, as shown in Figure 3-25, provides such flow-through with gas entering the center tube and flowing to the sample loop in the instrument and out through the vent holes. The flow is forced by the difference between dynamic pressure at inlet and static pressure at the vent holes. This effect is enhanced by Bernoulli pressure reduction at the vent holes located on the sides of the outer tube.

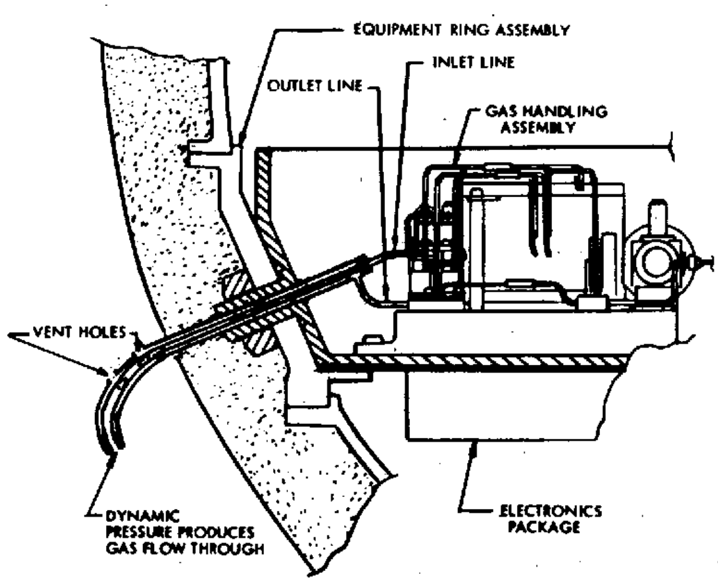

Figure 3-25. Gas Chromatograph Inlet Configuration

Thermal

To minimize heat leakage into the probe, it is preferred that instruments not be mounted physically to the pressure vessel, but be mounted in contact with the internal instrument platform. Some instruments have elements that need to be tied structurally to the pressure vessel surface. The thermal characteristics of the mechanical attachment are designed to promote heat transfer between the instruments and the instrument platform.

Assuming such heat transfer properties, the instrument platform temperatures will reach the values shown in Table 3-8 at the indicated times during the large probe descent. The temperatures of the equipment ring assembly are also shown to identify the thermal environment for those parts of the experiments that must be mounted directly on the pressure shell ring.

Table 3-8. Temperatures of Instrument Platform and Pressure Shell Ring

EVENT	TIME (S)	PLATFORM (°K)	RING (°K)
AEROSHELL SEPARATION	0	305	305
CHUTE RELEASE	2340	312	310
	3385	315	324
SURFACE IMPACT	4430	322	370

Thermal control is provided by the aeroshell heat shield and by thermal insulation, coatings, and science window heaters on the descent capsule to maintain an environment assuring that all probe components are within their temperature limits for all mission phases. The large probe temperature limits for components interior and exterior to the pressure vessel as a function of the mission phase are given in Table 3-9.

Table 3-9. Temperature Limits of Large Probe Components

MISSION PHASE	INTERIOR TO PRESSURE VESSEL (°K)	EXTERIOR TO PRESSURE VESSEL (°K)
PRELAUNCH (OPERATING)	256 TO 305	256 TO 325
PRELAUNCH (NONOPERATING)	256 TO 302	227 TO 344
LAUNCH AND CRUISE (NON-OPERATING)	256 TO 302	227 TO 344
CRUISE (OPERATING)	256 TO 305	256 TO 325
DESCENT (OPERATING)	305 TO 322	256 TO *

*EACH EXTERIOR COMPONENT MUST BE DESIGNED WITH UPPER TEMPERATURE LIMIT CONSISTENT WITH MAXIMUM ATMOSPHERIC TEMPERATURE FOR WHICH IT IS INTENDED TO OPERATE

The various windows and optical feed-throughs illustrated in Figures 3-17, 3-18, and 3-20 have thermal considerations as an essential part of their designs. The thin-walled rib-reinforced stainless window supports have low thermal conductance. The optical design to produce minimum diameter penetrations helps to reduce the heat leak. The double-window construction isolates the region between the window, minimizing convective heat leaks to the probe interiors.

Exterior windows (or lenses) will be provided with heaters to keep them above ambient temperature to prevent condensation. The need to minimize heat leakage from the exterior window to the probe interior is particularly important when this window heating is considered (both from the standpoint of conserving heater power and reducing the probe interior heating). The design considerations in window heating for four different types of heaters are discussed in Section 3.1.2.5.

An alternative concept to heating the windows would be to use tandem outer window elements as discussed in Section 3.1.2.1. The outermost element would be removed, say at the midpoint of the descent trajectory, ensuring a clean surface at two points in the terminal descent.

Electrical and Power

The large probe electrical power subsystem is discussed in Section 7.9. Each scientific instrument receives 28 volts ± 10 percent electrical power through an individual, fused branch circuit as listed in Table 3-10.

Table 3-10. Large Probe Instrument Load Characteristics

INSTRUMENT	FUSE RATING (AMPS)	AVERAGE CURRENT (AMPS)	PEAK CURRENT (AMPS)
TEMPERATURE GAUGE	1/16	0.018	
PRESSURE GAUGE	1/16	0.008	
ACCELEROMETER	3/8	0.082	0.2
MASS SPECTROMETER	2	0.430	0.86
SOLAR RADIOMETER	3/8	0.143	
CLOUD PARTICLE SIZE ANALYZER	2	0.715	
IR FLUX RADIOMETER	3/8	0.107	
GAS CHROMATOGRAPH	1	0.214	
HYGROMETER	1/16	0.009	
WIND ALTITUDE RADAR	5	1.43	
NOTE: FUSE TYPE IS LITTLEFUSE 256 SERIES, PICOFUSE			

The branch circuit will be energized/de-energized by probe sequencer control. The power allotted to the instrument is measured at the spacecraft/instrument interface connector. All power conditioning will be synchronized by the probe supply.

Except for the transient voltage excursions specified below, the peak-to-peak amplitude of any voltage excursion, periodic or aperiodic, will not exceed 1.0 volt at any frequency between 30 Hz and 10.0 kHz decreasing at 6 dB/octave to 0.5 volts at 20.0 kHz and remaining at 0.5 volts through 100 MHz. Instruments should be designed to accommodate, without performance degradation, voltage transients up to +42 VDC or down to +18 VDC for durations of 10 microseconds or voltages down to +20 VDC for durations of 500 milliseconds on the nominal +28 VDC bus. The instruments should be designed so that no damage, long-term degradation, or modes where proper performance is not automatically resumed when the transient is removed, will occur when 10 microseconds voltage transients up to +56 VDC or down to 0 VDC are seen on the nominal +28 VDC bus.

Based upon the large number of different instrument voltages presently specified and upon concerns to minimize power distribution costs and RF interference (see Section 3.1.2.1, Electromagnetic Interference Considerations) we prefer power conditioning to be performed by the individual instruments. The individual converters will be operated synchronously by a centrally supplied oscillator drive signal at a frequency that is not fundamental to any instruments or other probe subsystems. If the variety of user voltages were to decrease substantially, then centralized power conditioning may become the better approach for the program.

Pressure vessel electrical feed-throughs will be provided in the equipment ring assembly for the temperature sensor, wind altitude radar, hygrometer, and for the accelerometer calibration connector. These feed-throughs are shown in Figure 3-26. The connector provided on the spacecraft harness for connection to the various science instruments will be female (straight or coaxial insert) pin connectors selected from the Cannon nonmagnetic series (NMC-A-106 suffix).

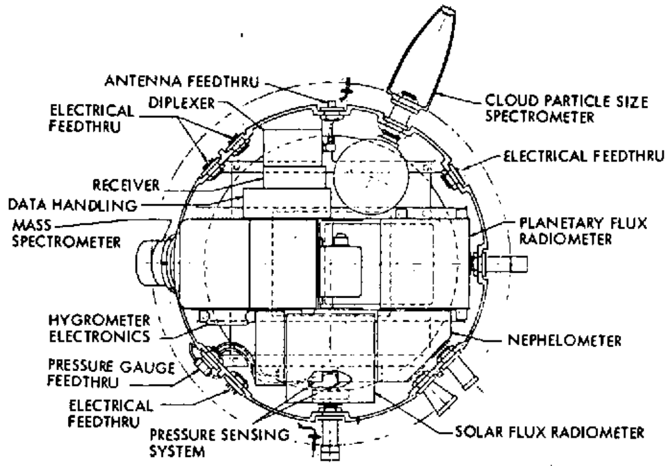

Figure 3-26. Plan View of Equipment Ring Assembly Showing Instrument Electrical Feedthroughs

Data Handling and Command (DHC)

The large probe DHC will accept information in digital, analog, or state form, convert the analog information to digital form, and arrange all information in an appropriate format for time-multiplexed transmission to earth or storage on board the probe. The probe will also supply the instruments with various timing and operational status signals and functiona commands. A telemetry word in all formats will consist of 7 or 10 bits. Probe generated words will be transmitted with the most significant bit first. See Section 7.7 for detailed discussion of the DHC.

Additional Accommodation Considerations

This section discusses a number of supplementary considerations ensuing from recent conversations with the scientific community. These include: the use of argon as the large probe fill gas; configuration of windows for the infrared and solar radiometers and the cloud particle size analyzer; the size of the mass spectrometer inlet; and the feed and positioning of the wind-altitude radar antenna. Additional items arising from these conversations are discussed below with regard to their potential impact.

Solar Radiometer. One of the experimenters, Dr. James Pollack, strongly desires a view of the sun above the clouds to provide a reference for the instrument. Since the instruments' view is obstructed by the aeroshell, the impact of this request could be to deploy the aeroshell or a hatch earlier than now scheduled so that the instrument can see the sun at a higher altitude (above the haze and uppermost cloud layer). Another approach would be to provide a window or light pipe to the instrument. Removing the aeroshell earlier requires deployment while the probe is still supersonic and therefore has significant impact on the design of the aeroshell, the parachute, and various mechanisms. Because of the probe shape and the location of the sun, deploying a hatch in the aeroshell would require removing a large section at the maximum diameter while the probe is still supersonic. The use of a light pipe to direct sunlight to the instrument as shown on Figure 3-27 appears to offer the best solution with minimum impact. The measurement would be obtained prior to entry, well above the atmosphere. A preentry solar calibration is also desired for the version of the solar radiometer proposed by the University of Arizona. Although they indicated this could be done through a slit in the aeroshell, the concept shown on Figure 3-27 could also suffice for their instrument. The proposer has also assumed that his analog outputs would be digitized by the probe. This could be done with no impact on the probe subsystems.

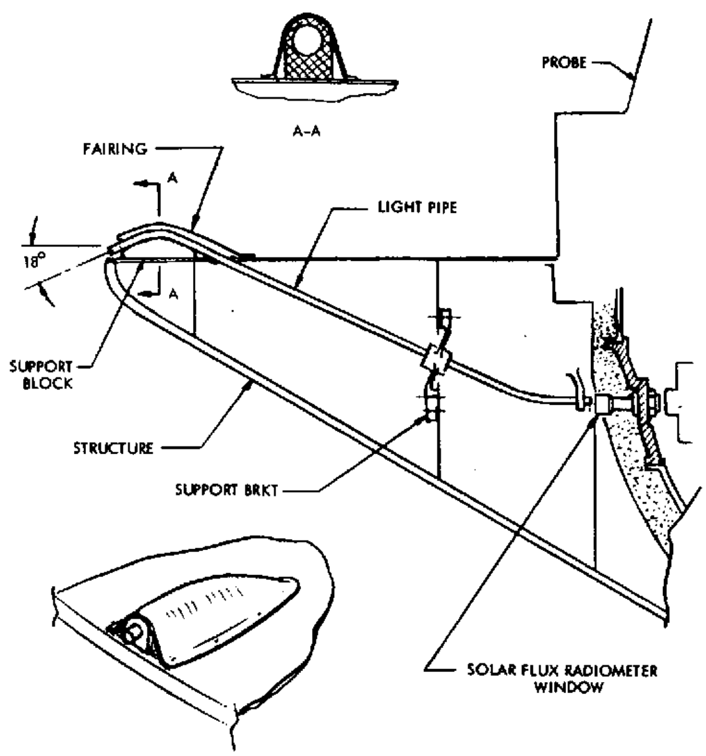

Figure 3-27. Light Pipe to Solar Radiometer

Wind-Altitude Radar. The NASA contractor for this instrument is assuming that the probe will provide a spin rate signal to his instrument during descent for use in operating and processing data for the radar. Since the instrument operates from 40 km to the surface, it does not appear practical to use the sun as a visible source. The techniques discussed in Appendix 3B (for planet reference for the magnetometer), namely, using either the sun as a source in X-band or the DSN S-band uplink, could be used here with the addition of on-board logic to read the signal and to provide the reference signal to the wind-altitude radar. Since the location of the RF source is known, the signal can also be used for a reference of the planet coordinates in interpreting the wind data. The reader is referred to Section 4 of Appendix 3B for a discussion of the impact of using RF techniques. The use of an angular accelerometer would also provide a spin rate signal to the radar with much less impact on the probe. However, this would not provide the planet reference needed to interpret the wind direction data.

Gas Chromatograph. The experimenter Dr. Oyama, has assumed that the probe would take his analog output and digitize and store it. Version IV of the instrument payload received from NASA shows a digital output for this instrument and has no requirement for the probe to provide the 13 200-bit storage. There would be no impact in having the probe perform the A/D conversion, however, adding a 13 200-bit memory would require another board to be added to the PCU, which in our present design now contains the entry data memory.

Planetary Flux Radiometer. The experimenter, Mr. Jacob Miller, believed the probe to be power limited when he chose the starting time for the IR cavity heater at 2 to 4 days prior to entry. An alternative would be to use a higher power heater and turn it on shortly before entry. One hour at 5 watts would be preferable to us because the heater could be activated coincidentally with a number of other events prior to entry, instead of requiring a special signal from the coast timer.

3.1.2.2 Other Candidate Instrument Accommodation

In addition to the ten instruments whose accommodation is described above, four other candidate experiments have been identified. The accommodation concepts for these instruments are discussed in this section.

The X-ray fluorescence experiment requires mounting two proportional counter sensor tubes outside of the pressure vessel. The only feed-through requirement is a dual high voltage coaxial electrical connector which provides the 3 kV activation for the sensors and also the signal from the sensors. This arrangement is shown in Figure 3-28 with the penetration as before in the equipment ring assembly. The only constraint on the position is to allow the clear field of view into the atmosphere as shown. Both high voltage conductors are placed in the same coaxial connector and the mounting is with the jam nut on the inside. Then a high voltage cable from the electronics package is attached to this feed-through with a dual high voltage connector. The instrument does its own power conversion to provide the 3 kV for the sensors. The basic data accumulation mode involves internal storage of randomly gathered pulses from the detectors, which are read out periodically as a stream of binary data on command from the data handling system.

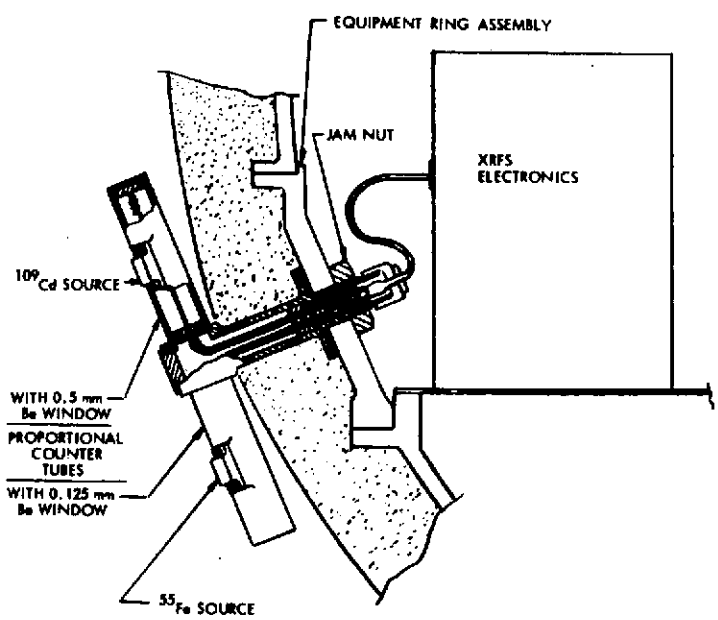

Figure 3-28. X-Ray Fluorescence Experiment

The attenuated total reflectance spectrometer can also be conveniently mounted in the equipment ring assembly with its total internal reflectance diamond window exposed to the condensates in the Venus atmosphere as shown in Figure 3-29. This concept has been reviewed with Dr. Boris Ragent who proposed the experiment. The design is based on

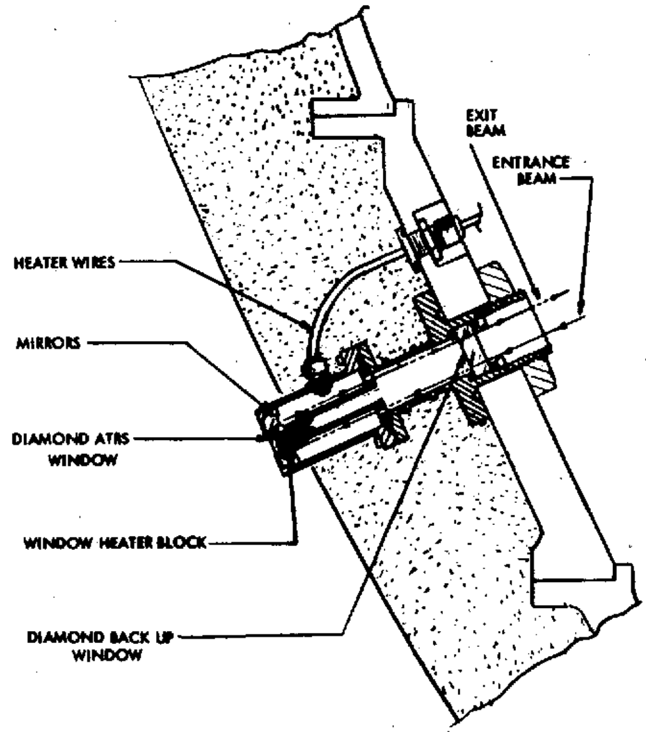

Figure 3-29. Attenuated Total Reflectance Spectrometer Window Assembly

controlling the diamond window temperature over a range of $\pm 40^{\circ}K$ relative to the local Venus atmosphere to provide the consensation and evaporation cycles necessary for the measurement. It also allows contact with the diamond window over only a small portion of its surface area to allow for multiple total internal reflections. The inner tube of the window assembly supports the heater block to which the heater coil and inner mirrors are attached. Mirrors and high temperature insulation have been suitably tested for this application. Sealing to the diamond window is similar to techniques we have used for IRTRAN 2 tests. The concept uses the spring force of a thin elastic metal ring with a center hole and the atmospheric pressure to press the specially plated sealing surface onto the diamond window. An electrical feed-through in the outer section of the assembly routes the electrical connections around the backup diamond window and into the probe through an electrical feed-through in the equipment ring frame.

The aureole detector accommodation for the Atlas/Centaur configuration is somewhat similar to that shown for the Thor/Delta configuration in Section 3.2.2.2. The basic concept of mounting the entire instrument exterior to the pressure shell and insulation is maintained, but the configuration details are different. In this configuration, shown in Figure 3-30, the entire instrument including collimators and electronics is attached to the aft cover and is jettisoned with it at parachute jettison (42.9 km) since the prime objectives of the experiment are served before this. Thus, the cable severs the power and data connection cable leading to the probe interior. The data format would be changed as discussed in Section 3.2.2.2 to accommodate the aureole before jettison and fill the slot with other data afterward.

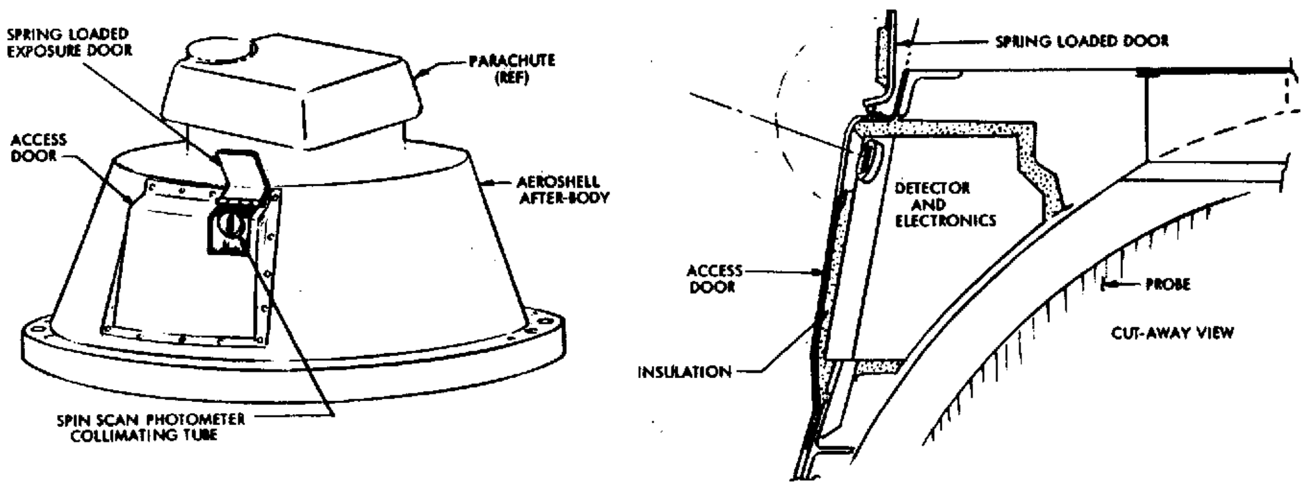

Figure 3-30. Aureole Detector Accommodation

The shock layer radiometer arrangement shown for the Thor/Delta configuration in Section 3.2.2.2 is mounted directly behind the aeroshell and outside the probe insulation. This arrangement is directly applicable to the Atlas/Centaur configuration even with the wind altitude radar antenna as shown in Figure 3-31 since there is enough room to put it in without any configuration modification except the heat shield modification discussed in Section 3.2.2.2. With this arrangement it is not necessary to view through a hole in the radar antenna since the entire experiment is forward of the antenna.

The probability of having excess capability (weight, descent capsule volume, power, and data handling), given certain assumptions on the growth probabilities of the nominal science instruments and subsystem weights, has been evaluated. Results indicate that sufficient excess weight and power may be available at the end of the procurement phase of hardware

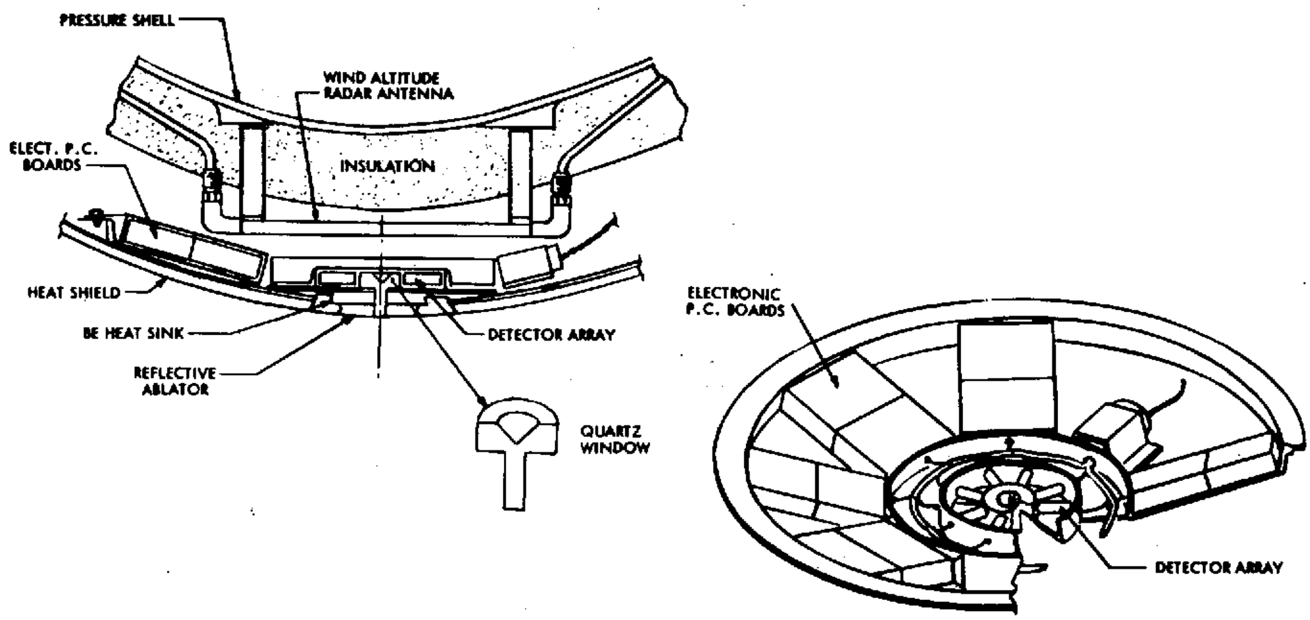

Figure 3-31. Shock Layer Radiometer Accommodation

development to accommodate all four large probe "other candidate instruments." Statistical results for descent capsule excess volume indicate that one or two additional instruments could probably be accommodated.

The current data handling subsystem design could provide an additional science data rate of 10 bps. This data rate would accommodate the X-ray fluorescence and shock layer radiometer experiments. Significant increases in science data rate, say the equivalent of 36 bps for the ATR spectrometer or 23 bps for the aureole detector, cannot be reasonably provided by decreasing ballistic coefficients because of associated increases in battery energy and thermal control requirements.

Figure 3-32 shows the total descent time, additional battery energy (assuming no additional science load), and thermal/structural weight increase associated with additional science data capability derived from ballistic coefficient reductions. An increase of 40 bps would increase the battery energy requirement by almost 50 percent and increase thermal control/structural weight by 20.5 kg (45 lb).

The second method to accommodate additional science data—addition of nonbinary data acquisition and increased memory—would provide an additional 43 bps for the existing descent trajectory. Only 5 kbits of additional memory would be required, but this option does require modification of the memory and programmer PC boards as well as replacement of the ROM's. The science

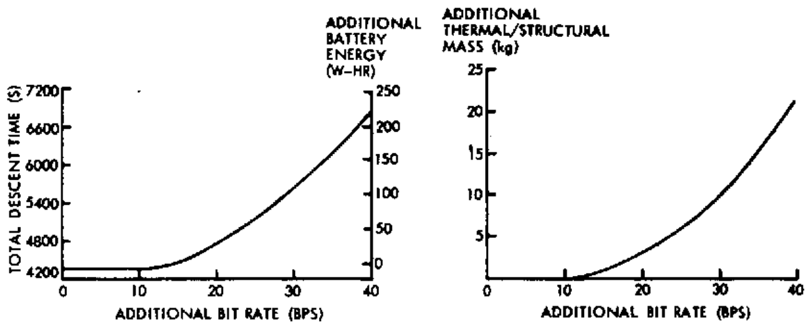

Figure 3-32. Battery and Thermal Control Weight Increases for Additional Science Data

data transmission rate could be increased 50 bps by changing the descent capsule ballistic coefficient to 471 kg/m^2 (3.0 $slugs/ft^2$) while no change in parachute size would be required.

3.1.2.3. Small Probe Instrument Accommodation Concepts

Structural and Mechanical

An important feature of the small probe experiments accommodation is commonality between large and small probe systems. Thus the electronics units for the temperature and pressure gauges are identical in the two systems. In this same spirit of commonality the DHC from Pioneer 10 and 11 is used for both large and small probes.

The other important aspect of the small probe accommodation results from retention of the aeroshell for the entire descent. Therefore, deployment mechanisms are necessary to expose sensors to the environment outside of the aeroshell base cover after entry for the temperature gauge, pressure gauge, IR flux detector, and nephelometer. The last two instruments require windows. It may be desirable to make the entire instrument and window an integral unit. The probe contractor would design and perhaps also fabricate the window assembly or the entire instrument housing, which would include the window assembly.

The temperature sensor, as discussed above for the large probe, is required to project beyond the boundary layer at the position of maximum mass flow and to have its cylindrical radiation shield aligned parallel to the flow field. However, since the aeroshell stays with the probe, a spring-loaded deployment mechanism (shown in Figure 3-33), is included in the accommodation. This mechanism, which is essentially the same as that used on PAET and Viking, pushes out a plug in the aeroshell at the time of

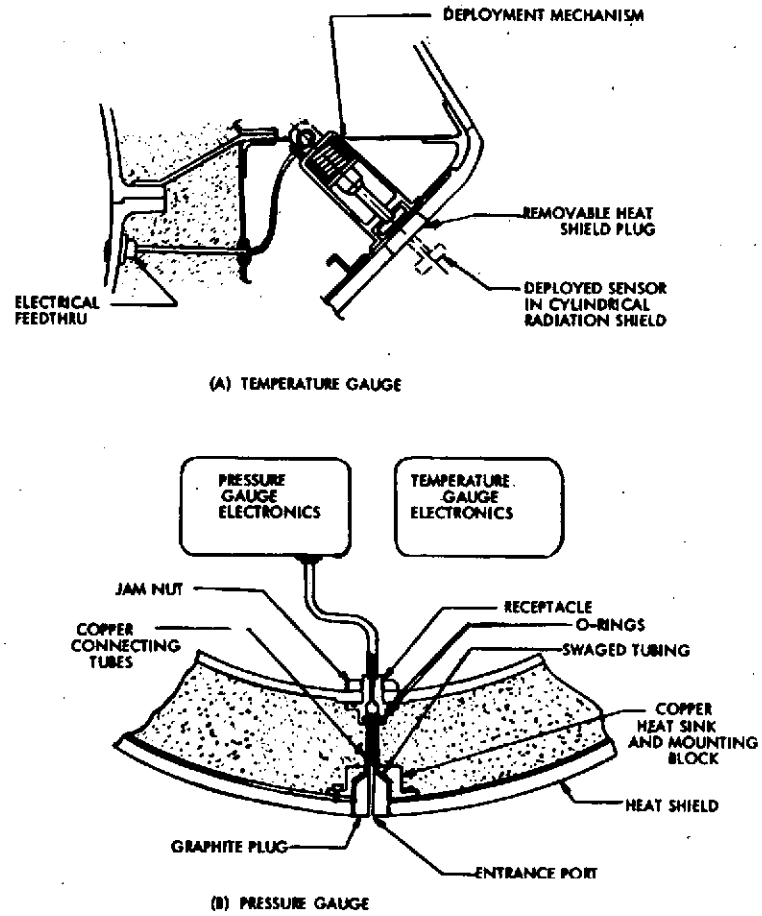

Figure 3-33. Small Probe Temperature and Pressure Gauge Mechanisms

deployment and places the sensor at the desired position and orientation in the airstream. This plug is fabricated with quartz nitrile phenolic, the heat shield material.

The pressure gauge opening, as with the large probe gauge, must be located near the stagnation point. The pressure port feed through shown in Figure 3-33 is designed to withstand the entry environment and yet provide gauge access to the stagnation point pressure. This design consists of a graphite pressure port tube backed up by a copper heat sink to accommodate the energy soaked into the graphite. It is assembled by threading the graphite plug into the copper heat sink and mounting block, thereby sealing the swaged end of the copper connecting tube. This assembly is bolted onto the aeroshell, causing the graphite plug to project through a hole in the heat shield with their exterior surfaces flush. Then as the probe is assembled to the heat shield, the straight end of the connecting tube inserts into the receptacle, thereby effecting a seal with the captive O-ring. This design has been tested in the NASA/Ames Plasma Arc Heat Transfer tunnel with 32 MW/m^2 heating for 2 seconds duration at 0.4 MN/m^2 stagnation pressure. The resulting oblation was very uniform across the heat shield-graphite boundary.

The nephelometer uses two windows with overlapping fields of view, one for the outgoing beam and another one for observing the cloud scattered light. Two separate windows are necessary to prevent scattered source light within the window material from being detected by the experiment. The two-window arrangement has been conceived in two proposed configurations; the first uses two concentric windows requiring a single penetration, while the other uses two separate penetrations with the pointing arranged to provide overlapping fields of view at a distance of about 15 cm beyond the aeroshell edge. Both methods use a GaAs light source that emits near IR light at $0.9 \pm 0.02\ \mu m$. A piece of the base cover is removed in both cases by a pyrotechnic actuator to allow a clear field of view as illustrated in Figure 3-34 for the two-penetration configuration.

The two-penetration configuration makes use of the conical shaped window with a brazed sapphire lens as the outer window which is described in Section 3.1.2.1. This window type, which was discussed with Dr. Boris Ragent, is useful for minimizing the thermal leak in narrow field of view optical experiments. The prime focus of the lens is at the probe pressure shell. Thus the aperture, d, at the pressure vessel can be reduced to $d = \alpha F$ where α is the angular field of view and F is the focal length.

The accommodation concept, illustrated in Figure 3-34, has a source window diameter of 11.5 mm and a viewing lens diameter of 19 mm. The viewing lens focal length is 50 mm resulting in a window aperture at the pressure shell of 9.3 mm diameter to provide a 0.18 rad (10 degree) full cone angle field of view.

The angular placement of the two windows was determined to meet the requirement that the region of overlap between the source and viewing fields of view be centered beyond the probe boundary layer and wake. This distance is estimated to be 15 cm beyond the exterior of the insulation. The smallest practical separation between centers of the two window assemblies at the pressure shell is 5.1 cm, which results in an angle of 0.28 rad (16 degree) between the source and viewing windows.

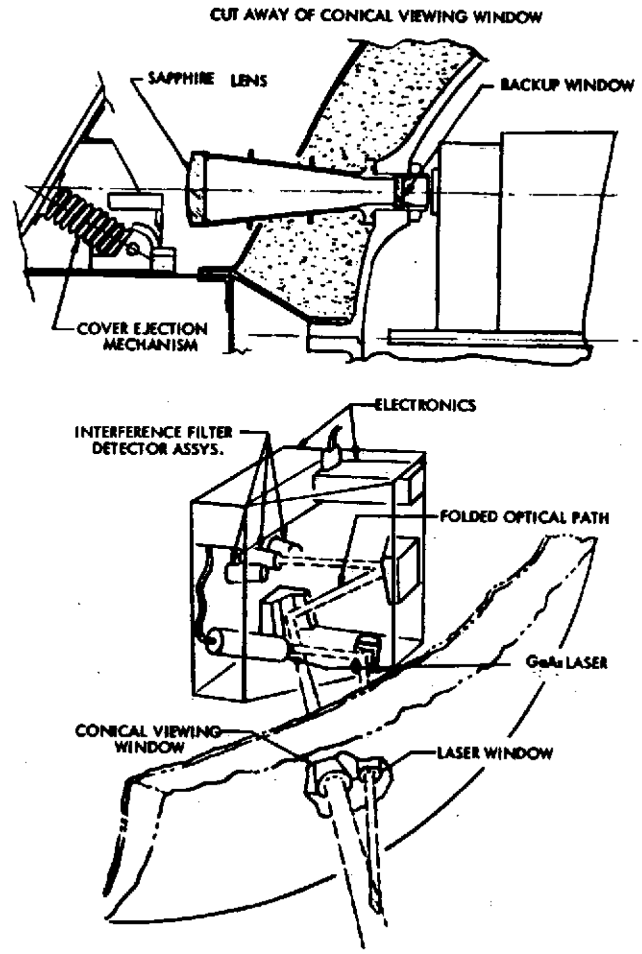

Figure 3-34. Dual Penetration Nephelometer Configuration

The concentric window concept has as an essential feature an emitted beam of polarized light whose backscattering within a 5-degree full cone angle field of view provides information on cloud particle size and shape. The proposed concept uses a GaAs light source located at the focal point of a spherical mirror which directs the light through a Glan-Thompson polarizing prism. This prism is made of two pieces of calcite cemented together with birefringent optical axes normal to each other. Designing such a prism for high temperature operation would present some problems due to the optical contact cement and the different coefficients of expansion along the two directions in the calcite.

Figure 3-35 shows a configuration that provides thermal conduction from the probe pressure vessel directly to the source-polarizer assembly and thermal isolation from the exterior high temperature in order to keep it down to the 370°K maximum temperature of the pressure vessel wall. We have also suggested an alternative concept to Dr. Bob Samuelson using a large optical cavity gallium arsenide laser to avoid entirely the use of the Glan-Thompson prism. These RCA lasers, qualified for military specifications, produce polarized light from a very small source. Thus with the proper optics, a 5 degree divergent field of view can easily be achieved. A 1.75-mm focal length and 4.2-mm aperture lens would accomplish the proper convergence of the 50-degree half angle, 98 percent polarized light from the 0.15-mm-wide source. This laser-lens assembly is placed near the pressure vessel penetration where the temperature is not too high. An exit window 13 mm in diameter and 100 mm away (at the exterior of the insulation) is adequate to allow full transmission of the 5 degree divergent light. The return light from the cloud particles is received through the outer part of the annular window.

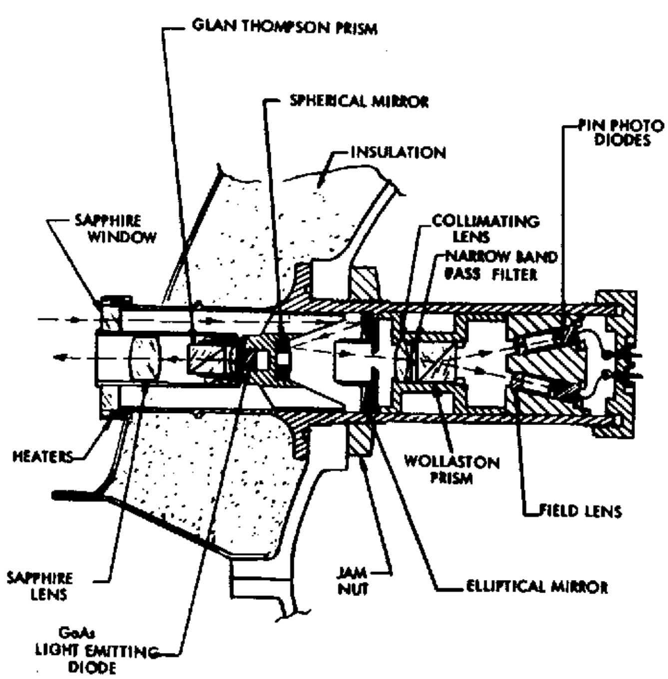

Figure 3-35. Concentric Window Nephelometer

The single-axis accelerometer requires placement at the probe center of mass with its axis aligned parallel to the probe spin axis. The mounting technique described above for the large probe is similar for the small probe with the rough placement determined from the calculated center of mass and the final placement determined from the dynamic and static balance tests.

The IR flux detector on the small probe, as conceived by Dr. Verner Suomi, is either a net flux radiometer or a flipped mirror radiometer. The net flux sensor consists of a differential thermopile detector projecting out beyond the edge of the aeroshell so that the bottom sees the upward flux and the top sees the downward flux. The flipped mirror radiometer, preferred by Dr. Suomi, has a curved mirror, projecting beyond the aeroshell edge. The mirror is viewed by a sensor inside the probe from behind a window in the pressure vessel, as shown in Figure 3-36. Although the mirror views a wide field from horizon to zenith in the upward position and from horizon to nadir in the downward position, it compresses this view into a narrow angle at the window. Therefore, the conical shaped window assembly discussed above for the nephelometer is applicable in this case, except that IRTRAN windows rather than sapphire would be required to achieve the desired spectral response out to about 24 μm. To reach this spectral response, the yet untested IRTRAN 4 or 6 is required. If these are adequate as pressure windows at the high Venus temperature, then this configuration appears preferable; but if they are not, then the net flux radiometer configuration could be used because the sensor stays at Venus ambient pressure. The net flux radiometer is not the preferred concept because convective heat exchange differences between top and bottom introduce errors and the operation of the sensor at high temperature increases the noise.

The mechanism for deploying the mirror beyond the aft cover is a spring-loaded system similar to the temperature gauge deployment mechanism. Its plug in the aft cover is ejected by the same motion. This deployment mechanism, as well as the flipping mechanism, are stored outside the probe insulation but inside the aft cover-aeroshell.

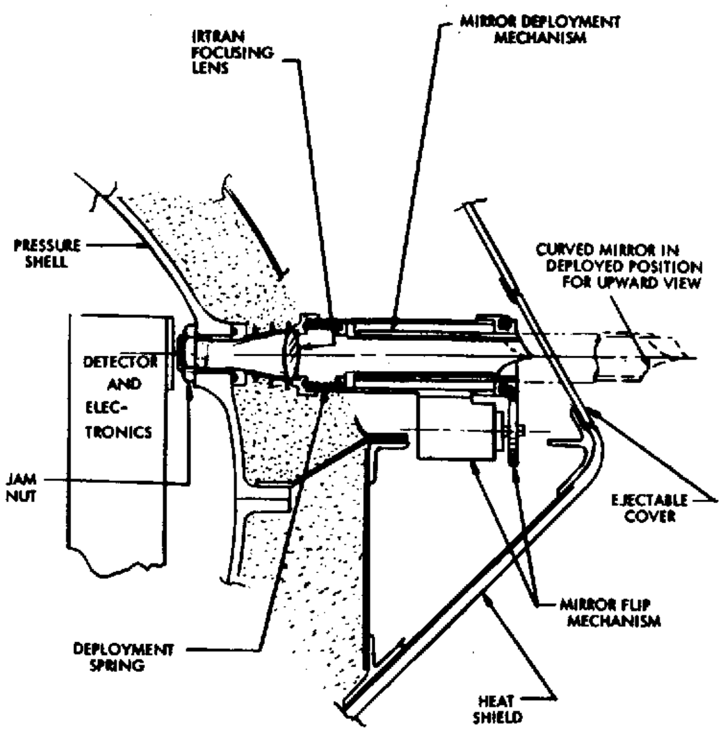

Figure 3-36. Small Probe IR Flux Detector

Dr. Suomi envisions the possibility of making changes in the reflective surface of the curved mirror and in the windows to change the spectral range of the instrument to include the solar spectrum for a small probe targeted to the sunlit side of Venus. This position, however, deviates from the presently accepted concept of identical units for all small probe subsystems. Furthermore, our small probe targeting strategy has one option that gives the greatest latitude spread where all three probes are on the dark side. Therefore this concept of spectral modification will have to be examined critically with respect to these two considerations.

To achieve the objectives of the experiment the data needs to be integrated over one or more complete probe rotations. Thus a probe spin is required, but its rate is not at all critical. About 400 measurements achieved during the entire descent would be adequate. This implies an average rotation rate of about 0.6 rad/s (6 rpm).

The principal accommodation required for the probes' stable oscillator is its thermal control. The method used here is essentially that discussed in a report from the Thermal System Design Project at the Johns Hopkins Applied Physics Laboratory (transmittal letter ASD: 244-9/32-032). The sphere shown in Figure 3-37 is a container with a shell of phase change material. Our analysis shows that when the power dissipated by the oscillator is included, the temperature of the oscillator will remain constant to within $3^{o}K$.

Thermal

To minimize heat leakage into the probe, only the penetration part of the science instruments are attached to the pressure vessel and the electronic circuits are mounted on the electronics shelf, wherever possible. However, the nephelometer and IR flux detector may have the pressure vessel penetration integral with the instrument case. The average temperature of the interior assembly at the time of planet surface impact will be $322^{o}K$ and the average pressure shell temperature will reach $405^{o}K$. Temperatures at other times in the descent are shown in Table 3-11.

Table 3-11. Average Temperatures During Small Probe Descent

TIME (S)	PRESSURE SHELL (°K)	INSTRUMENT SHELF (°K)
0	305	305
1116	310	310
2775	351	311
3890	405	322

Thermal control of the descent capsule is provided by thermal insulation, coatings, phase change material window heaters for the nephelometer and IR flux detector, and a heater for the IR detector mirror. The aeroshell heat shield provides thermal control during the entry heating period to maintain an environment assuring that all probe components are within their temperature limits.

The small probe temperature limits interior and exterior to the pressure vessel as a function of the mission phase are given in Table 3-12 under both operating and nonoperating conditions.

Table 3-12. Temperature Limits of Small Probe Components

MISSION PHASE	INTERIOR TO PRESSURE VESSEL (°K)	EXTERIOR TO PRESSURE VESSEL (°K)
PRELAUNCH (OPERATING)	256 TO 305	200 TO 366
PRELAUNCH (NONOPERATING)	256 TO 302	200 TO 366
LAUNCH AND CRUISE (NON-OPERATING)	256 TO 302	200 TO 366
CRUISE (OPERATING)	256 TO 305	200 TO 366
DESCENT (OPERATING)	266 TO 322	200 TO *

*EACH EXTERIOR COMPONENT MUST BE DESIGNED WITH UPPER TEMPERATURE LIMIT CONSISTENT WITH MAXIMUM ATMOSPHERIC TEMPERATURE FOR WHICH IT IS INTENDED TO OPERATE

Electrical and Power

The small probe electrical power subsystem is discussed in Section 7.8. Each instrument receives electrical power through an individual fused branch circuit as listed in Table 3-13. All power conversion is synchronized by a probe-generated oscillator drive signal. The branch circuit is energized/de-energized by probe sequencer control. The power allotted to the instrument is measured at the spacecraft/instrument interface.

Table 3-13. Small Probe Instrument Load Characteristics

	FUSE RATING (AMPS)	AVERAGE CURRENT (AMPS)	PEAK CURRENT (AMPS)
TEMPERATURE GAUGE	1/16	0.02	
PRESSURE GAUGE	1/16	0.02	
ACCELEROMETER	1/4	0.036	0.16
IR FLUX DETECTOR	3/4	0.071	0.28
STABLE OSCILLATOR	1/16	0.009	
NEPHELOMETER	1/4	0.071	

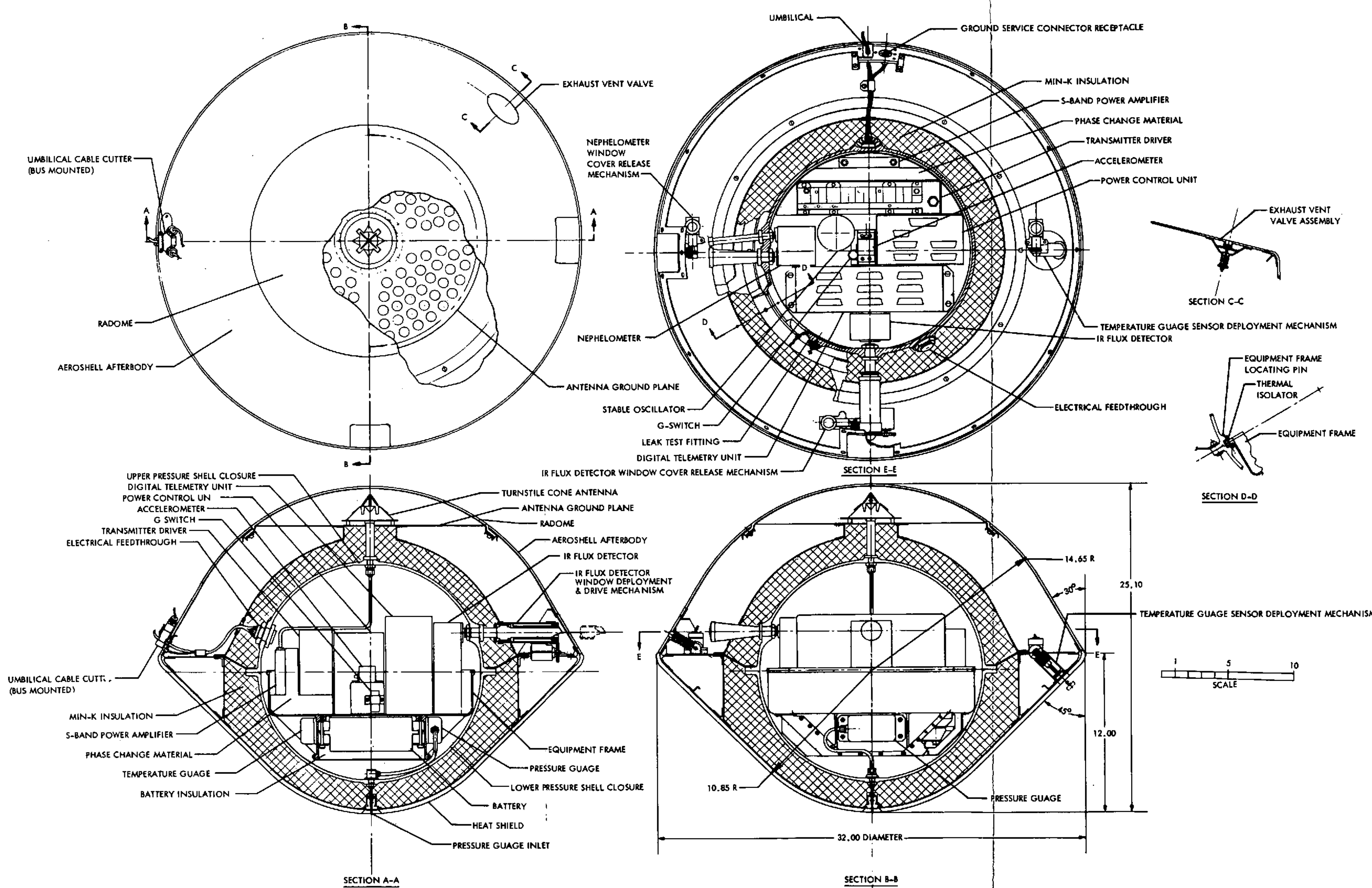

Figure 3-37. General Arrangement of Small Probe

FOLDOUT FRAME 1

FOLDOUT FRAME 2

Transient voltage and peak-to-peak voltage excursions for the small probe are the same as those defined for the large probe above.

Pressure Vessel electrical feed-throughs will be provided for the temperature sensor, accelerometer calibration connector, window heaters, deployment mechanisms, and mirror flipping mechanism.

Data Handling and Command

The small probe DHC will accept information in digital, analog, or state form, convert the analog information to digital form, and arrange all information in an appropriate format for time-multiplexed transmission to earth or storage on board the probe. The probe will also supply the instruments with various timing and operational status signals and functional commands. A telemetry word in all formats will consist of 7 or 10 bits. Probe generated words will be transmitted with the most significant bit first. See Section 7.7 for detailed discussion of the DHC.

3.1.2.4 Other Candidate Instrument Accommodation

In addition to the instruments identified for the nominal payload two others have been cited as alternative candidates. These are the magnetometer and RF altimeter.

The magnetometer accommodation is discussed at length in Section 3.2.2.2 for the Thor/Delta configuration. The same considerations hold for the Atlas/Centaur configuration except that as a result of the increased size of the small probes, the magnetometer is removed further from the remanent field sources while still inside the aeroshell. This increased distance more than compensates for increases in stray fields. These resulted from changing the integrated electronics to discrete modules and using Pioneer 10-type components and magnetic cleanliness technique. With the magnetometer inside the aeroshell the total remanent field at the sensor is 60 to 75 nT. Even if the sensor is located inside the probe the total remanent field is only 300 to 350 nT.

The RF altimeter accommodation favored at first by Drs. Suomi and Nadev Levanon involved using an antenna mounted inside the heat shield, either a ring or a slotted array. However, we studied the RF attenuation effects of heat shield material (quartz nitrile phenolic) which had been charred by exposure to an environment simulating the Venus entry convective heating (but without the radiative heating). The results indicated a one-way attenuation of the order of 16 dB for the S-band and C-band ranges (2.6 to 6.0 GHz). After receiving these results, Suomi and Levanon decided on a much simpler alternative approach. It consists of a dual dipole whip antenna stowed in a wrapped configuration around the periphery of the afterbody, as shown in Figure 3-38. After entry the two pyro release devices let the ends of the antenna spring out, resulting in the deployed configuration shown. No other mechanism is required for deployment.

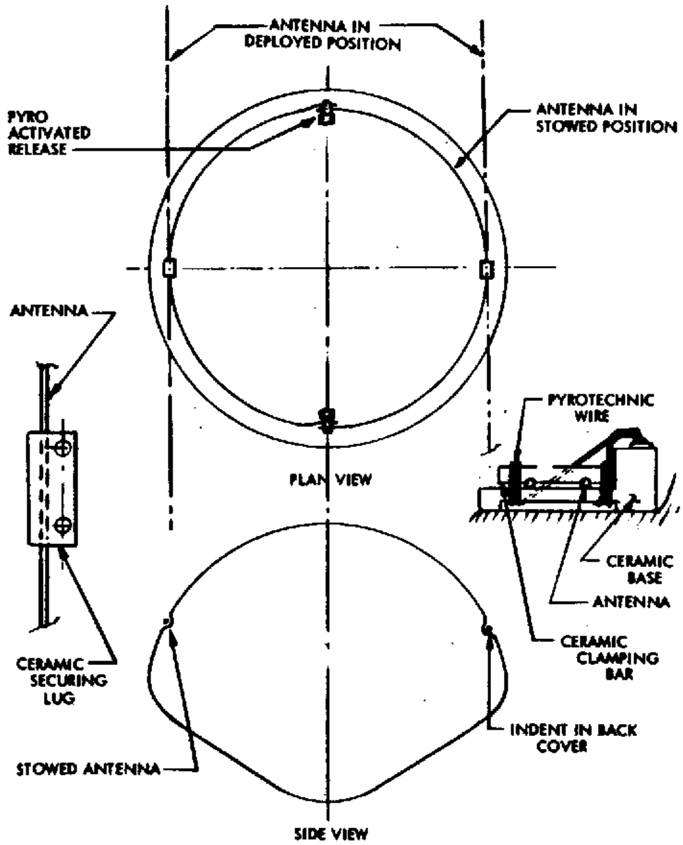

Figure 3-38. RF Altimeter Antenna

3.1.2.5 Instrument Accommodation Studies

Existing Instrument Studies

Since the relaxed weight, volume, and power constraints on the Atlas/Centaur configuration are to be used to reduce costs, an obvious approach is to use instruments already developed for other missions. Evidently the majority of instruments developed for space missions are not applicable to the descent probe since they do not represent atmospheric-type experiments. Earth meteorological instrumentation would seem the most likely candidates. However, upon examining the available instruments it became evident that these are generally not applicable as they were not designed for: (1) the reliability required for a planetary mission; (2) the environments of launch, space cruise, planetary entry, and the Venus descent environment; and (3) measurements of the ranges and compositions expected in the Venus atmosphere. Therefore, on close examination of available instruments, we conclude that none are directly applicable to Pioneer Venus descent probes without extensive modification. In pursuing this search we have used the services of Professor Patrick Squires of the University of Nevada Desert Research Institute as a consultant. We have also contacted Dr. Richard Kirschner (APL), Commander Ronald Oberle (ONR), Dr. George Paulikas (Aerospace Corp), and Captain Neil Anderson (SAMSO), all of whom were referred to us about this subject by Hap Hazard (NASA). Numerous attempts to contact Dr. Al McIntyre (AFCRL) about existing instruments were unsuccessful.

Window Studies

The nominal Pioneer Venus large probe payload requires approximately ten optical windows. The number depends both on experiment selection and instrument design. These windows with their associated heat leaks, field of view problems, surface heating requirements, failure impact on the mission, and specific optical requirements represent an important probe engineering task. Extensive studies of opto-mechanical design and heating methodology have been performed.

The window configurations studied and tested have evolved over a 2-year period. Variants of brazed and clamped window concepts are shown in Figure 3-39. These are combined to form the double window configurations of Figures 3-17 and 3-19. The rationale behind the double-window concept is based on reliability considerations (a window failure results in a catastrophic probe failure) and thermal considerations (convective heat transfer is minimized by the intrawindow dead space). The outer window is brazed to the rib stiffened Inconel 718 window wall and the inner window is clamped. This configuration has been tested repeatedly under more severe conditions than are anticipated in the Venus atmosphere. Appendix 3A contains detail of the design, fabrication, and test considerations for these windows.

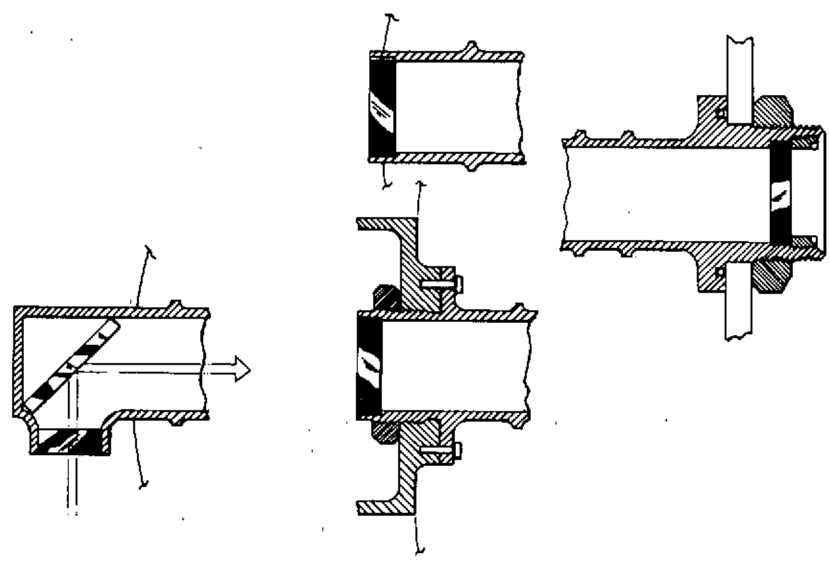

Figure 3-39. Window Configuration Concepts

The heat transfer situation leading to the choice of a sealed double window is shown for a conical version of the window in Figure 3-40. The figure summarizes the analysis of the heat transferred from the atmosphere to the interior of the descent probe. By evacuating the space between windows, convective heat transfer is eliminated. Conduction through window support structure dominates radiative transfer and is a pacing consideration in determining the structural configuration.

Inconel 718 has been selected as a support material on a basis of high strength and low thermal conductivity at elevated temperatures. Sapphire, a suitable window material for many experiments, can be bonded to Inconel 718. Depending upon experiment selection, it may be important that Inconel 718 is not magnetic.

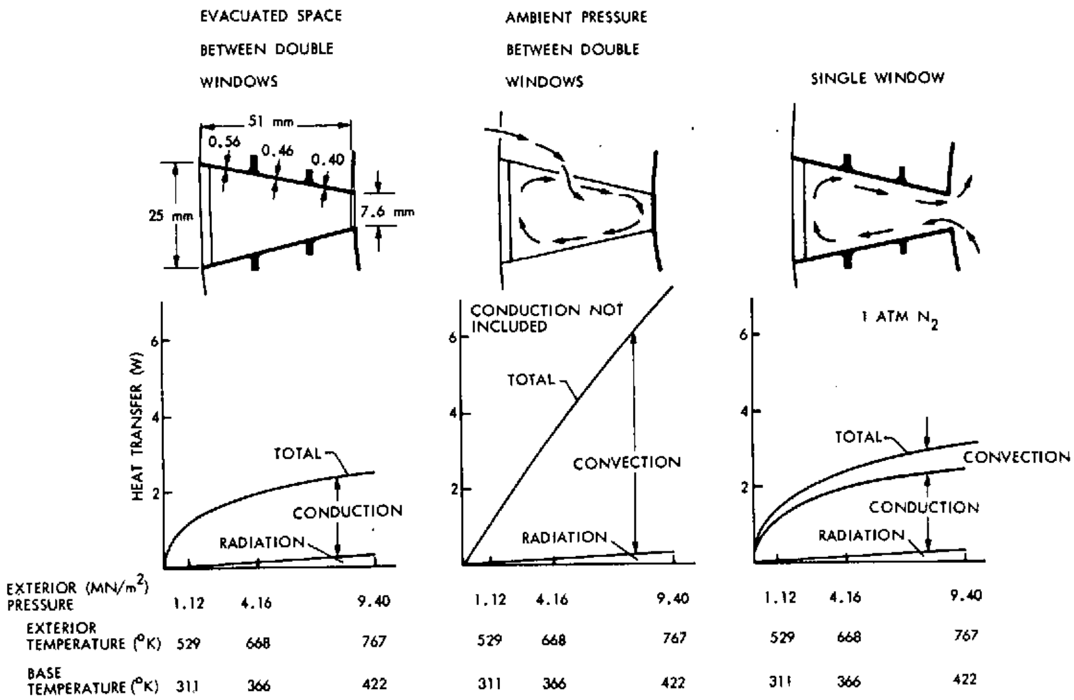

Figure 3-40. Heat Transfer Tradeoffs of Venus Probe Windows

Some important variants to the basic window include:

1) Infrared Windows--Because of the long wavelength limitation of a sapphire window, IRTRAN is the nominal window material for infrared experiments. IRTRAN cannot be brazed to Inconel 718, and hence infrared windows are of a clamped design.

2) Special Fields of View--Instruments such as the solar and planetary flux radiometers require fields of view that dictate windows with internal optical systems. Instruments with narrow fields of view permit use of a conical window configuration (Figure 3-41) that has structural and thermal advantages over a cylindrical window with the same aperture. The solar radiometer may require wide fields of view in opposing directions and coupled to a single detector. For this purpose, viewing ports with diffusers and light pipes have been considered.

3) Antireflective Coatings--Instruments, such as the cloud particle size analyzer, which are subject to interference effects will require antireflective coated windows.

4) Alignment Requirements--An instrument, e.g., the cloud particle size analyzer, which has both internal and external optical components and close alignment tolerances, requires a common mechanical reference such as the window support structure.

5) Special Requirements--Certain growth instruments, the attenuated total reflectance spectrometer is an example, require windows that are a totally unique optical design.

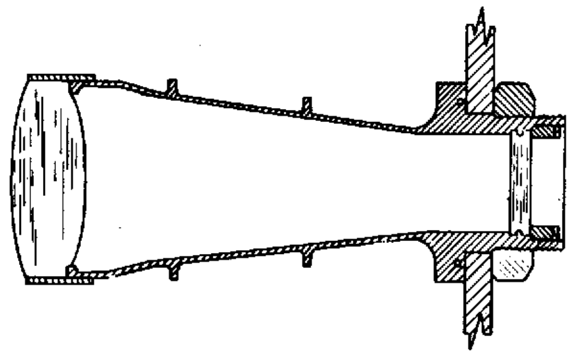

Figure 3-41. Conical Window Configuration

Among the window designs that have been tested for structural survival at high temperatures and pressures (in addition to the cylindrical double sapphire window, brazed outer, clamped inner) are cylindrical brazed sapphire windows, clamped IRTRAN windows and conical walled, clamped sapphire windows. Designs for windows for a wide field of view solar radiometer and a narrow field of view, down-looking planetray flux radiometer are discussed in Section 3.1.2.1.

During the descent through the Venus atmosphere, probe surfaces, unless separately heated, will lag the atmosphere in temperature. This could lead to the fogging of windows by condensation or thermal precipitation. For this reason probe windows will be heated. This can be accomplished by Joule (resistive), thermoelectric, or chemical heaters. A tradeoff between these methods is summarized in Table 3-14. Primarily because of its state of development, Joule heating is the baseline approach. For a 0.025-meter (1 in.) diameter window the associated mass penalty for heating throughout the descent is approximately 0.3 kg. This is based on an average power requirement of 15 watts.

Table 3-14. Heater Tradeoff for Window Heated 10°K Over Atmospheric Temperature, 0.025 m (1 in.) Window Diameter

		JOULE HEATER	THERMOELECTRIC HEATER (COEFFICIENT OF PERFORMANCE OF 3.0)	CHEMICAL HEATER (LiOH)
POWER (WATT)	BATTERY	15	5	
	ATMOSPHERE		10	
	CHEMICAL			15
MASS (KG)	BATTERY	0.31	0.10	
	HARDWARE (FINS, CONTAINERS,---)		0.03	0.09
	HEATER ELEMENT	0.01	0.02	0.02
	TOTAL	0.32	0.15	0.11
STATUS		STATE OF THE ART	DEVELOPMENT OF HIGH TEMPERATURE DEVICE REQUIRED	DEVELOPMENT OF REACTION CONTROL REQUIRED

Tests have been performed with a 0.025-meter window heated with a constant 15 watt Joule heater and subjected to a simulated Venus descent. The temperature of the window base was maintained at temperatures representative of the temperature of the probe pressure shell during descent. Test results are summarized in Figure 3-42. A large difference between gas and window temperatures is observed initially when gas pressure is low. This difference decreases and, indeed, goes negative at a simulated altitude of roughly 11 km. Comparing the results for the 15 watt heater with those for no heater, it appears that a continuous 20 watt would provide the desired positive difference throughout descent. A positive temperature difference could also be obtained by either an increased power at low altitudes or a higher window base temperature that would reduce conductive losses.

One can scale power requirements for a 0.025-meter window to other window sizes by considering the change in thermal conductance of a cylinder when its diameter changes and the wall thickness is adjusted to maintain the same critical pressure for structural failure. This leads to a 1.6 power dependence of thermal conductance on window diameter as shown in Figure 3-43.

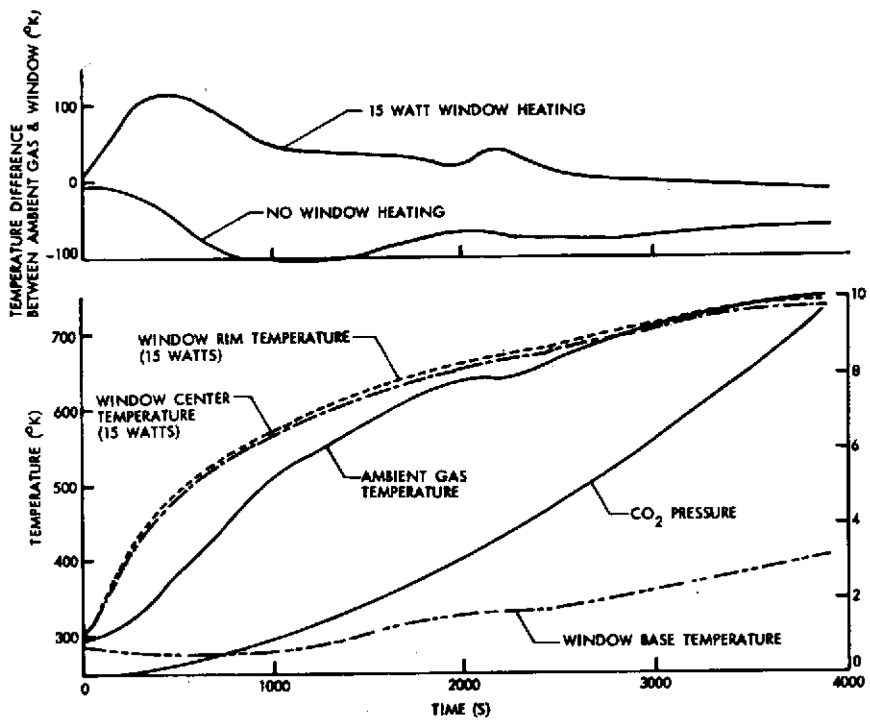

Figure 3-42. Thermal Test of Window Heating During Simulated Venus Descent

A conical window requires less power to heat than a cylindrical window with the same diameter of exterior window because of the decreased thermal conductance of the narrow interior end of the conical section.

Figure 3-43 illustrates the Joule heating approach, Figure 3-44 the thermoelectric heating approach, and Figure 3-45 the chemical heating approach. The thermoelectric heater shows some promise if lead telluride thermoelectric junctions can be manufactured with high-temperature electrical connections. Discussions with Borg-Warner have indicated that a coefficient of performance of about five can be achieved with these junctions with the temperature differences required for this application at ambient temperatures in the range of Venus temperatures. The chemical heater appears attractive but experimental verification of existing concepts is required. A preliminary test of a heater using LiOH, reacting with atmospheric CO_2, showed a very rapid initial energy release and then no further output. The total heat output was markedly less than that expected from the reaction had it gone to completion for all the LiOH used. If the reaction can be controlled (e.g., by controlling CO_2 flow to the LiOH) it would appear that a chemical heater would incur only about one third the weight penalty associated with the corresponding resistive (Joule) heater, but a significant development would be required.

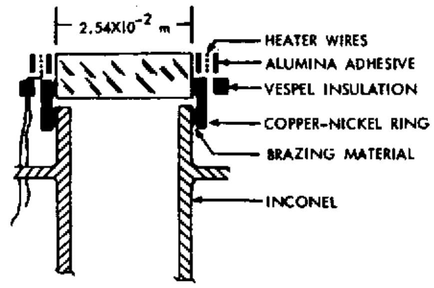

Figure 3-43. Window Joule Heating Approach

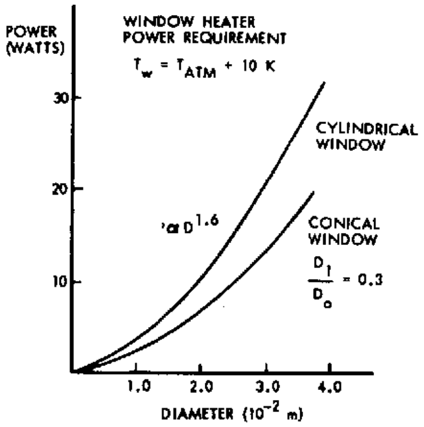

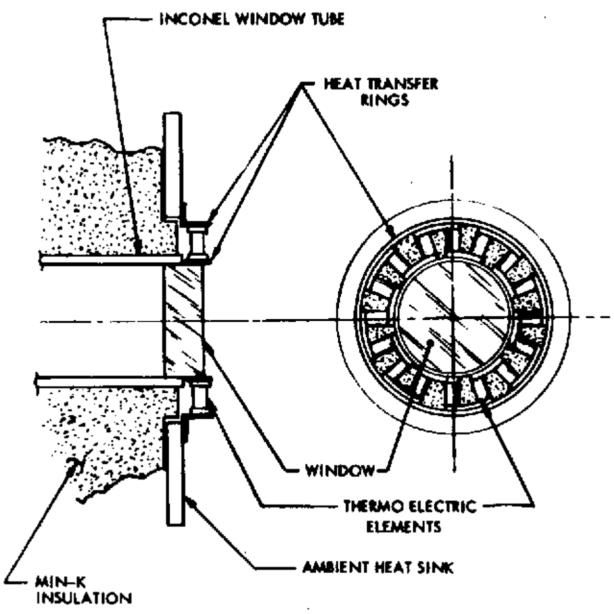

Figure 3-44. Thermoelectric Heater Concept

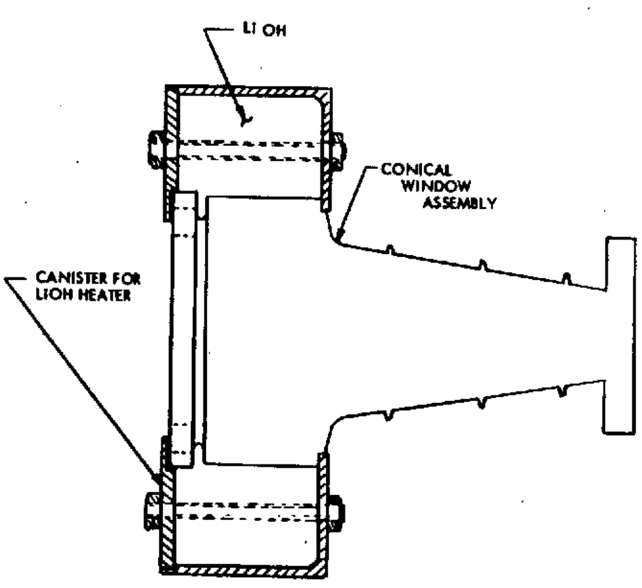

Figure 3-45. Chemical Window Heater

An alternative concept for obtaining a clean window surface has been investigated. The approach is to jettison the initial exterior window at some time during descent, baring a fresh surface at least temporarily clear of accumulated material. Two separate methods of mechanizing the removable window technique are shown in Figures 3-46 and 3-47. The approach shown in Figure 3-46 uses a pyrotechnic wire as a retaining shear ring. The approach shown in Figure 3-47 uses retaining wedges held in place by pyrotechnic blocks. When the pyrotechnics are fired, they convert to gas and fill the expansion chamber, allowing the spring to eject the outer window. Release by solenoid-actuated mechanism was also considered but was excessively bulky. Power to fire the pyrotechnic devices could come through the same line used to supply the window heater power. An alternative passive approach would replace the pyrotechnic blocks on Figure 3-47 with a low melting point metal. Melting of the metal blocks would allow the lens retainer wedges to retract under their spring tension and the lens to be rejected under its spring compression. Molten metal would be retained in the expansion chambers as shown.

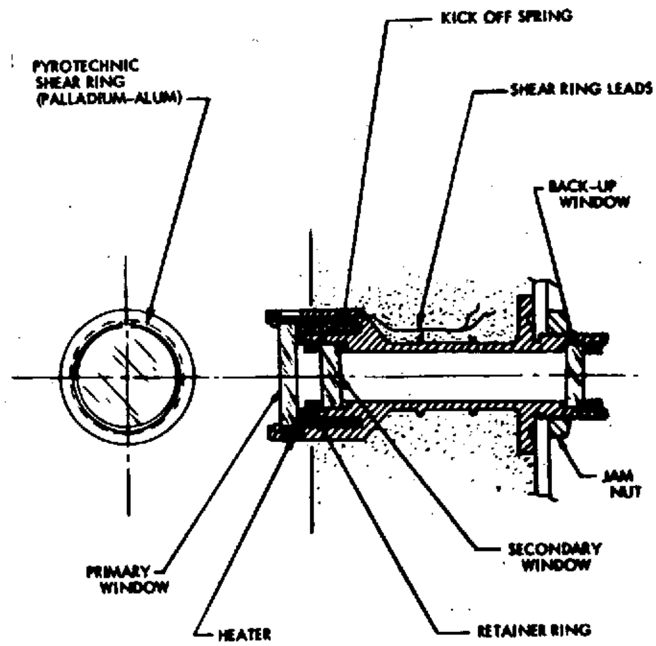

Figure 3-46. Removable Window (Pyrotechnic Shear Ring)

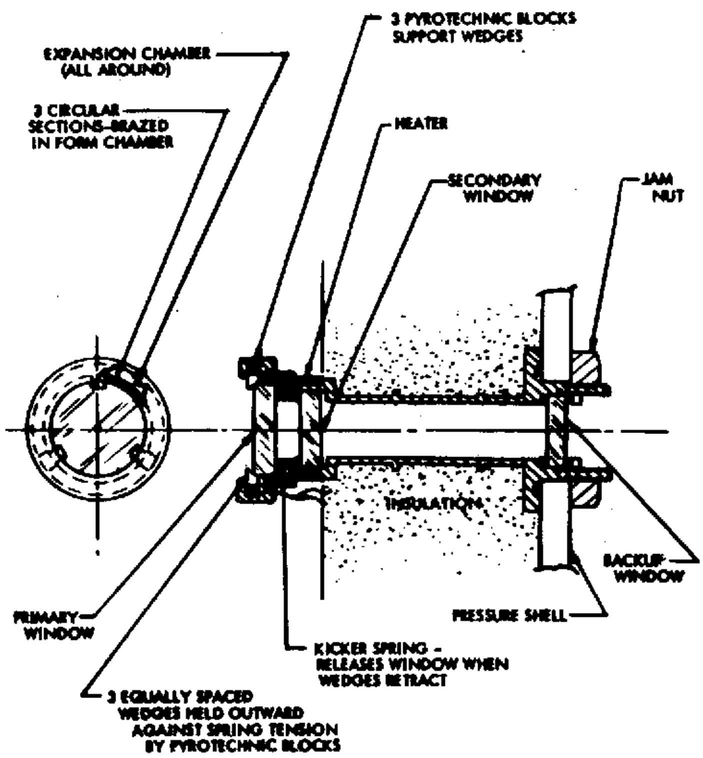

Figure 3-47. Removable Window (Phase Change Release)

Mass Spectrometer Inlet Studies

The inlet system for the mass spectrometer experiment has some special requirements that have significant impact on the large probe. Ideally the inlet system should: reduce the atmospheric pressure to levels compatible with the operation of an ion source; do so without disturbing the relative abundance of the gas constituents; be unaffected by atmospheric particles and condensables; and have a short response time. The corresponding system requires pressure shell penetrations, special thermal control, sequencing operations, and a general size and mass that are major experiment integration considerations. Two separate studies were performed that bear on the mass spectrometer inlet. The first, an internal research task, consisted of the conceptual design and analysis, fabrication, and testing of an inlet system suitable for the sampling of dense planetary atmospheres. The second, a contract study, consisted of a survey of sorption pumps, a study of their potential application to the Pioneer Venus mission, and testing of one particularly promising type of sorption pump. The remainder of this section is a summary of the significant results of the two studies.

In the inlet system study* three generic types of inlet system were considered:

1) Direct flow systems, in which gas flow to the ion source is controlled by in-line leaks and volumes, and all gas that enters the system ultimately passes through the ion source.

2) Diverted flow systems, in which a portion of the gas entering the system is diverted into a ballast volume or pumped without passing through the ion source.

3) Multiple inlet systems, in which the increasing atmospheric pressure is accommodated by switching from one inlet to another with a lower conductance.

In general, direct flow systems** suffer from a conflict between high-altitude sensitivity requirements and low-altitude pumping requirements.

*W. Fraser and L. Bergquist, "Mass Spectrometer Inlet System for a Venus Probe Mission," P72-44487-194, Martin Marietta Corporation, Denver, Colorado.

**An example of such a system was described in: R. P. Shirsov, "Mass Spectroscopic Study of the Composition of Dense Planetary Atmospheres," Kosmicheskia Isselepox, YA 6, 1, USSR (1968).

A flow conductance that admits sufficient gas for analysis at high altitude admits so much gas at lower altitudes that a large pump is required to maintain the ion source pressure. In-line variable leaks could, in principle, alleviate this problem but, operating in a closing mode, they are subject to blocking open and causing the mass spectrometer to be swamped. Response time and dynamic range difficulties are the principal drawbacks of direct systems.

Multiple inlet systems require complex mechanization that should be avoided if possible. On the other hand, they can be designed to minimize response time, composition alteration, and blockage difficulties.

Diverted flow systems appear to meet the experiment requirements. While the basis for selection must be recognized as subjective, the system described below was chosen for laboratory modeling and testing.

Shown in Figure 3-48, the inlet system built and tested in this study uses a variable leak into a ballast volume or pump to control flow onto the ion source.

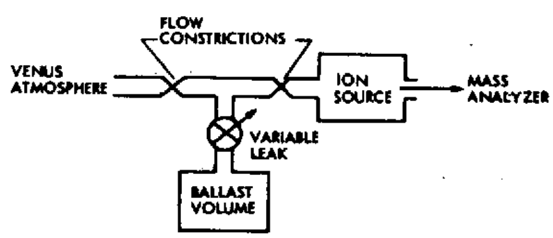

Figure 3-48. Ballast Volume Inlet System

The major portion of the gas entering the system is diverted into the ballast volume. The variable leak into the ballast volume is controlled by requiring a constant ion source current. By maintaining a constant flow to the ion source in this manner, the dynamic range of the mass spectrometer is not diminished by the range of pressures in the planetary atmosphere. Two models of this system have been built and tested. These models used sintered platinum leaks as the flow constrictions. The choice of these leaks, while not essential to the operation of the system, was intended to reduce chemical reactions in the flow constriction. Because of their large surface area it is possible that porous plug leaks, however inert the material from which they are made, seriously diminish the relative abundance of active gases. The tests of this system have established that an inlet which accommodates the full range of Venus atmospheric pressures and provide a gas sample that changes in a short time relative to the nominal Pioneer Venus mass spectrometer sampling interval can be built to occupy a volume of 1 liter or less. A variant on this inlet approach (Figure 3-49) has been proposed for the Pioneer Venus mission by Hoffman of the University of Texas.

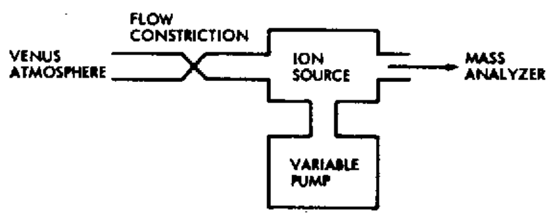

Figure 3-49. Proposed Pioneer Venus Mass Spectrometer Inlet

A preliminary version of this inlet system has performed satisfactorily in simulated large probe descents in a Martin Marietta Venus Atmospheric Simulation Chamber (J. H. Hoffman and M. A. Kolpin, "Venus Atmosphere Mass Spectrometer Inlet System Test," submitted to the Journal of Geophysical Research, April 1973).

The sorption pump study survey was conducted to determine the current availability of pumping materials with applicability to the Pioneer Venus mass spectrometer mission. Three applications were considered.

1) Reduction of atmospheric pressure to levels compatible with the operation of an ion source.

2) Enhancement of the noble gas content in an atmospheric gas sample.

3) Vacuum maintenance during cruise phase.

Atmospheric pressure reduction can be accomplished with a sorption pump under restricted conditions. Since the pumping rate of such pumps is, in general, strongly dependent on the pumped gas species, care must be taken to avoid drastic composition changes in the sampled gas. Such a pump could be used to reduce the required volume in the ballast volume system discussed previously. Since flow through the variable leak is always viscous composition, alteration would be minimal in this case.

Some sorption pumping materials do not pump noble gases and are thus useful in preparing an enriched sample for noble gas analysis. The Venus atmospheric abundance of noble gases is sufficiently low that a specific analysis of the relative abundance of noble gases requires some pre-analysis processing that produces a sample enriched in the noble gases. Otherwise the dynamic range of the instrument would be used up in accommodating the more abundant chemically active species and only the most abundant noble gases would be detectable.

During the period of time after the mass spectrometer is delivered by the experimenter for integration into the probe, until the probe enters the Venus atmosphere, the instrument will be subjected to a differential pressure of roughly one atmosphere. Prior to assembly of the probe this is due to the earth's atmosphere. Later it is due to the internal pressurization of the large probe. Either a small leak or a low outgassing rate in the instrument could produce a high enough pressure in the instrument at time of entry that an ion pump would not start. Simple calculation shows that a leak of 10^{-17} m^3/sec or an outgassing rate of 10^{-12} Nm/sec would cause the internal pressure in the mass spectrometer to be of the order of 10^{-2} N/m^2. At this pressure it is questionable that an ion pump will start. Certain reduction of either the leak rate or outgassing rate below these levels may not be possible. To assure adequately low pressure in the mass spectrometer at entry, the ion pump could be run periodically during cruise. Alternatively, if a suitable sorption pumping material exists, a small amount of it could be included within the instrument.

In the survey, yet to be reported, a number of potentially useful pumping materials were identified. All of these were of a chemisorption type. Physisorption materials, such as the zeolites, graphite, and silicagel, have relatively low pumping speed per unit mass values, and many of them have high ultimate pressures. The most promising chemisorption materials were SAES ST-101, SAES ST-171, and ceralloy. Operated at 700°K, these materials have pumping speeds of the order of 0.5 m^3/sec-kg and capacities of the order of 50 Nm/kg. These speeds and capacities vary with operating pressure and with the gas pumped. For noble gases their pumping speed is effectively zero. At lower temperatures (300°K), the SAES ST-171 material retains a significant fraction of its pumping capability, making it an attractive candidate for long-term vacuum maintenance. ST-101 is a zirconium aluminum mixture. ST-171 is a zirconium graphite mixture. Ceralloy is made of thorium, aluminum, and rare earths by the Ronson Corporation. Other materials such as Oremet Zr-Ti, titanium, and pure zirconium all either weigh more for a given pumping capability than ST-101, ST-171, or ceralloy, or require considerable operating power.

Tests have been run on ST-101 under conditions pertinent to a Pioneer Venus noble gas analysis experiment. In this experiment a valve is opened into a processing volume containing, in this case, an ST-101 pump (Figure 3-50). After a measured amount of atmospheric gas has been admitted, the valve is closed and the pump removes most of the active gases leaving the noble gases. Then an outlet valve is opened and the noble gas enriched sample is leaked into the ion source of the mass spectrometer.

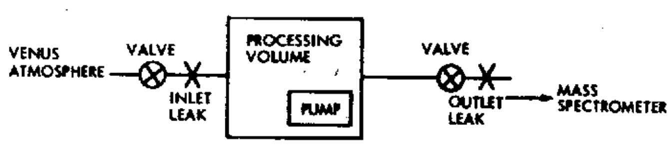

Figure 3-50. Schematic of Noble Gas Enriching Inlet

Detailed parameters for the system depend upon the stability requirement for the enriched gas source, the maximum ion source pressure, the pumping speed of the mass spectrometer system, the desired degree of enrichment, and the analysis time. Using nominal values for these parameters:

Source Stability	10%
Ion Source Pressure	10^{-4} N/m^2
Mass Spectrometer Pumping Speed	10^{-3} m^3/sec
Enrichment	10^4 (making the active gas-to-noble gas ratio approximately 1)
Analysis Time	10^2 sec

Together with measured performance characteristics of ST-101, a preliminary design has been produced for a pump and processing volume for this experiment. The combination, not including valving, has a mass of 1.3 kg. This design assumes that the noble gas measurement is made at low altitude where the pump, located outside the descent probe, can be heated by the atmosphere. A thermal analysis of the externally located package indicates that heating the pump with the atmosphere is a practical consideration.

The efficiency of using chemisorption materials for purposes of pressure reduction in the mass spectrometer inlet lies in the fact that they can operate without use of in-flight power.

The results of the mass spectrometer studies can be summarized as follows:

1) A mass spectrometer inlet system suitable for the Pioneer Venus experiment built to occupy less than 10^{-3} m^3 has been experimentally verified.

2) The use of a chemisorption pump in a noble gas experiment has been investigated analytically and experimentally and a preliminary pump for this purpose designed.

3) The possibility of unpowered vacuum maintenance prior to atmospheric entry with 10^{-3} to 10^{-2} kg of chemisorbant has been identified.

4) The use of chemisorbants for purposes of atmospheric pressure reduction has been found marginally attractive and decisions relative to its use dependent on details of the experiment design.

3.1.2.6 Payload Conflicts and Problem Areas

Electromagnetic Interference Considerations

A potential source of electromagnetic interference identified by NASA/ARC is the operation of the mass spectrometer ion pump. This, in addition to on-board permanent magnetic fields, could affect the small probe magnetometer and large probe accelerometers and mass spectrometer. These devices use a high voltage DC field and an intense magnetic field to accelerate the ions. Penning discharges are associated with ion impact and burial at the pump cathode. These are high frequency discharges and have been noted in at least one case on an FM radio operating in a laboratory near an operating ion pump. The cloud particle size analyzer counts particles with frequency response up to 100 MHz so that RF interference at these frequencies could be misinterpreted as cloud particles. We have discussed this subject with a number of mass spectrometer experimenters and found no evidence of any RF interference problems from mass spectrometers flown in space programs.

Any leakage of RF from the ion pump can be avoided by shielding and filtering the high voltage line to the pump and adding a thin foil or mesh shielding around the pump. (The pump housing may already provide this shielding.) A corollary interference consideration was identified in our examination of the RF interference. The ion pumping process liberates photons that require optical baffling to prevent them from being "seen" by any of the photon-sensitive analyzer detectors. Good practices normal in the design of the mass spectrometer should provide both the RF and optical shielding. Nevertheless, we recommend that the Science Instrument Interface Documents require shielding of the pump and high voltage leads specifically and adherence to MIL-STD 461 or equivalent.

DC-DC power conversion on board is a concern as a source of RF in the very low frequency range. This is identical to the drive frequency of the flux gate magnetometer core and also would introduce noise where a Sferics detector may be operating. Solutions to the potential problem extend from locating all power conversion centrally, operating with a well-shielded oscillator (at a frequency not fundamental to any other probe subsystem or instruments), to letting each user perform his own power conditioning. A compromise approach was used on PAET, where individual converters were operated synchronously by a centrally supplied AC oscillator drive signal.

Our design uses the same approach. The nominal frequency is 16.3 kHz, which appears compatible with the instruments. This frequency choice will be re-evaluated as more information is obtained on user requirements and RF interference sensitivities.

Effect of Probe Charge on Trajectories of Neutral Particles

The Pioneer Venus large probe might acquire an appreciable electrostatic charge while falling through the various known or suspected cloud layers in the Venus atmosphere. Therefore, we investigated how much the resulting electrostatic field can affect the dynamics of neutral or moderately charged aerosol particles in the vicinity of the probe to be sure that these effects cannot cause an appreciable redistribution of the aerosol concentration around the probe. This redistribution would introduce errors into experiments concerning the number density, size distribution, and composition of the atmospheric aerosols.

We distinguished between uncharged particles that will be attracted into the nonuniform field of the probe regardless of its polarity, and charged particles that will either be attracted or repelled, depending on whether their charge has the opposite or the same polarity as the probe.

We consider here only the uncharged particles. Our conservative estimate shows that the particles will not be appreciably affected by the probe charge, unless its surface potential exceeds around 10^6 volts. Charged particles will be considered in a subsequent section.

We assume, for the following analysis, that the probe is a conducting sphere of diameter, D, and that it has somehow acquired a positive or negative electric charge which gives its surface a potential, V. The electric field around the probe is then

$$E(r) = \text{grad}\ \frac{VD}{2r} = -\ \frac{VD}{2r^2}$$

In this nonuniform field, a small sphere of diameter, d, and dielectric constant, ϵ, experiences then a force

$$F = \frac{d^3}{16}\ \frac{\epsilon - 1}{\epsilon - 2}\ \text{grad}\ E^2$$

An upper bound on this force is obtained by considering the field at the probe surface and a particle with a large dielectric constant.

$$F \leqq 2\ \frac{d^3}{D^3}\ V^2$$

To use this to estimate possible displacements of aerosol particles from their normal trajectories, consider a particle with a density, ρ. Its mass is given by

$$m = \frac{\pi}{6} d^3 \rho$$

and its acceleration by the force, F, is bounded by

$$a < \frac{12}{\pi} \frac{V^2}{D^3 \rho}$$

which is independent of the particle size as it has to be in our case where the induced dipole moment of the particle is simply proportional to its volume.

This acceleration acts on the particles (in general by far less than with this magnitude) for a time of the order of

$$t \sim \frac{D}{U}$$

which it takes the probe to fall a distance equal to its diameter, D. U is the probe descent speed.

That is, it can at most lead to a displacement

$$\delta < \frac{a}{2} t^2 = \frac{6 V^2}{\pi D \rho U^2}$$

of particles from their normal trajectories through the flow field around the probe. Actually much smaller displacements are expected since this estimate disregards the substantial aerodynamic drag of small particles moving through a viscous gas. In this expression δ is in centimeters if D is in centimeters, ρ in gram/cm^3, U in cm/sec, and V is in stat volts. Converting to SI units, with V in volts, the displacement is given, in meters, by

$$\delta \lesssim 10^{-15} V^2$$

Displacements of 10^{-3} meter might be of marginal concern. These will not occur with a probe potential of less than 10^6 volts. This corresponds to an electric field of about 3×10^5 volt/meter at the probe surface. Such a field can readily be discharged in the rather unlikely event that charge sufficient to produce it could be accumulated on the slowly falling Pioneer Venus probe.

The dielectric strength of the Venus atmosphere should be less than 8×10^7 volt/meter, a value approached by CO_2 at Venus surface conditions. The potentially troublesome probe field of 3×10^5 volt/meter could be discharged by a corona device with a radius of approximately 1×10^{-3} meter. The presence of probe proturberances with radii of curvature of the order of a millimeter would satisfactorily limit the probe potential without use of specific discharge devices.

Effect of Probe Charge on Trajectories of Charged Particles

The preceding section showed that the attraction of neutral dielectric aerosol particles into the nonuniform electrical field around the charged Pioneer Venus probe is too weak to cause any appreciable errors in the mission experiments concerning the number density, the size distribution, and the chemical composition of the atmospheric aerosols, unless the charge of the probe is so large that its surface potential becomes several million volts.

Here we consider the case of charged aerosol particles that are strongly affected by the field of the probe. We will show that this also will not lead to unacceptable errors in the experiments, if the probe potential is restricted to some reasonable value by a simple corona discharge device. Indeed, adequate discharge capability will probably be provided by sharp edges and corners already present in probe design.

For the following analysis, we assume that the roughly spherical probe is a perfect sphere with a diameter $D = 0.7$ meter, and that it is charged to a surface potential, V.

We also assume that the aerosol particles are small spheres with a diameter, d, that may range from about 10^{-6} meter to about 2.5×10^{-4} meters.

We do not now have any good idea about the nature of the aerosol or cloud particles in the Venus atmosphere. We assume that the smaller particles, up to about 30 microns, can be of a very high density material, such as solid mercury halides with densities between 6 and 7×10^3 kg/m^3 or even liquid mercury metal with twice this density. They may, however, also consist of low density material, with a density between 1.0 and 1.5×10^3 kg/m^3.

We assume also that these small particles have grown to their size by condensation around some nucleus, and that they carry an electrical charge, q, which they obtained by atmospheric ions attaching themselves to their surface.

With respect to the larger particles, with diameters between about 0.3 and 2.5×10^{-4} m, we assume that they are mostly liquid droplets of density, $\rho \approx 1.3 \times 10^3$ kg/m^3, and that they have been formed by coagulation of smaller "fog droplets." This implies that their charge is the sum of the charges of the particles from which they were formed, up to a certain limit, and not counting losses by any discharge mechanisms, or that their charge is roughly proportional to their volume.

Our assumptions include the following considerations:

1) The assumption of spherical aerosols excludes the consideration of snowflake-like solid particles that may well exist somewhere in the Venus clouds and could carry an appreciable electrical charge. These particles would have a very great aerodynamic drag so that their motion in the flow field is affected very little by the additional electrical force acting on them.

2) The assumption of the basic charging process by ion attachment to the particle surface excludes the more violent charge separation process that can occur by the disintegration of large raindrops in the strong turbulence of thunderstorm clouds. It may, however, be argued that thunderstorms, should they occur in the Venus atmosphere at all, are very probably rare and too localized to be of concern for our purpose.

3) There is no reliable way to predict the polarity of the charge on either the probe or the aerosol particles, since this would require a very detailed knowledge of the composition of the aerosols, and the nature and "mobility" of the atmospheric ions. We therefore have no choice but to disregard the polarities of these charges. This is not a serious problem becuase we can still get a good estimate of the magnitude of the "electrical displacement error"

for our aerosol particles from their "normal" trajectories through the flow field, although we would not know whether the error is positive or negative.

The electric field near the surface of the probe is given by

$$E = -\frac{2V}{D}$$

and the force on a particle with a charge q in this region is given by

$$F = qE$$

To estimate the effect of this force on aerosols we need to estimate the charge that will reside on the particle. For small particles this is done by recognizing that the energy required to overcome the potential of previously attached charges and the energy to attach one more electronic charge must be supplied by the thermal activity of the gas. The potential of the charges on the particle is given by

$$\phi = \frac{q}{2\pi\epsilon_o d}$$

If one considers an ion with an order of magnitude more energy than the average for the temperature of the gas one has an available energy of 15 KT, where K = the Boltzmann constant and T = temperature. The number of ions with more energy than this is negligible and 15 KT can be considered a conservatively high estimate of available ionic thermal energy. For deposition of an additional charge, e, we require

$$15\,KT > \phi e$$

we thus have a practical bound on the charge on an aerosol particle due to ionic bombardment.

$$q < \frac{15\,KT \times 2\pi\epsilon_o d}{e}$$

with

$K = 1.38 \times 10^{-23}$ watt sec $(^oK)^{-1}$
$\epsilon_o = 8.85 \times 10^{-12}$ coul $(\text{volts})^{-1}$ $(\text{meter})^{-1}$
$e = 1.60 \times 10^{-19}$ coul (one electronic charge)

and

$T = 750^oK$ (Venus atmosphere maximum)

This becomes

$q < 5.4 \times 10^{-11} d$, for small aerosols with q in coulombs, d in meters.

For larger particles we estimate the charge from measurements on earth raindrops (H. Neuberger, Introduction to Physics Meteorology, Pennsylvania State University, 1957)

$q < 1.7 \times 10^{-3} d^3$ for large aerosols

The maximum charge estimate for small aerosols is larger than the estimate for large aerosols up to a diameter of roughly 1.8×10^{-4} meter.

One now can estimate the velocity, v, of the particles relative to the local flow by setting the electric force equal to the aerodynamic drag

$qE = 3\pi\mu dv$

Where μ is the viscosity of the Venus atmosphere. The maximum effect occurs for the largest particles, 2.5×10^{-4} meter, and at the altitude 70 km, where the viscosity is minimum, 1.1×10^{-5} kg/(m sec). One obtains

$v < 9.7 \times 10^{-7} E$ meter/second

if the surface field of the probe were 3×10^5 volt/meter, the value discussed in the previous section, the displacement of a particle during the approximately 0.1 second required to pass by the probe would be bounded by 0.03 meter. This is a very conservative bound. Furthermore the surface field should be restrictable to 3×10^5 volt/meter without special discharge devices.

Requirements for Electrostatic Discharge of the Large Probe

We have shown in the preceding sections that a large (3×10^5 volt/meter) electric field due to accumulated charge could distort the distribution of particles in the flow past the Pioneer Venus probe. The need for coronal discharge devices on the probe must be considered. Avoiding the question of identifying the charging mechanism, we consider here the requirements for a device that would maintain the probe field at a value less than 3×10^5 volt/meter. The required radius of curvature of the discharge device is estimated by assuming the probe and discharge device to be electrically connected spheres, as shown in the following sketch.

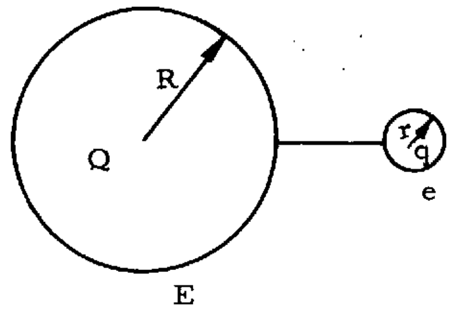

The two spheres form an equipotential.

$$\frac{Q}{4\pi\epsilon R} = \frac{q}{4\pi\epsilon r} \quad \text{i. e,} \quad \frac{Q}{q} = \frac{R}{r}$$

so the electric fields, E and e, at the surfaces of the spheres are related as follows:

$$e = \frac{q}{4\pi\epsilon r^2} = E \cdot \frac{R}{r}$$

when e is restricted to values less than E_B, the breakdown field of the gas in which the spheres are located, and E is restricted by

$$E = \frac{r}{R}\, e \leqq \frac{r}{R}\, E_B$$

If the field, E, about the large sphere is to be restricted to values less than a critical value, E_o, this provides an expression for the radius of the discharging electrode in terms of that of the large sphere.

$$r \leqq R\, \frac{E_o}{E_B}$$

The breakdown field in the Venus atmosphere can be estimated by scaling the dielectric strength, E_{Bo}, of CO_2 at STP linearly in pressure and the reciprocal of temperature.

$$E_B \approx E_{Bo}\, \frac{P}{Po}\, \frac{To}{T}$$

This scaling procedure is based on the assumption that a spark occurs when the average energy, ϵ, attained by an ion between collisions is sufficient to cause ionization of another molecule.

$$\epsilon \cong q E_B S \quad \epsilon_{ion}$$

or

$$E_B = \frac{\epsilon_{ion}}{qS}$$

where

q is the electronic charge and S is the mean free path of an ion

Since S is proportional to the temperature/pressure ratio, the required breakdown field is proportional to the pressure/temperature ratio. Using

$E_{Bo} = 2 \times 10^6$ Volt/meter (dry CO_2 at STP)

$\left.\begin{array}{l} P/Po = 100 \\ T/To = 2.5 \end{array}\right\}$ Venus surface conditions, under which discharge is most strongly inhibited

and

$R \quad = 0.4$ meter,

one obtains as the radius of a discharge device which would maintain the large probe surface field at $\leqq 3 \times 10^5$ Volt/meter

$r \leqq 1.5 \times 10^{-3}$ meter (0.060 inch).

Points and edges with this magnitude of radius of curvature will prevent excessive probe fields without special "lightning rod" devices. The aerodynamic "fence" around the large probe could easily be manufactured with much sharper edges than this, and thus provide control of accumulated probe charge.

<u>Distortion of Natural Electric Fields in the Venus Atmosphere by the Large Pioneer Venus Probe</u>

While violent electrical phenomena similar to our thunderstorms are probably very rare, if not entirely absent in the Venus atmosphere, it is quite likely that there will be some natural electric fields in the clouds of the planet.

While falling through the clouds, the large probe will then distort these fields somewhat in its vicinity, since it behaves roughly like a conducting sphere in a uniform electrical field.

Assuming the undisturbed field to be in a Z-direction (which would not have to be vertical), and assuming its field strength as E volt m^{-1}, the field around a conducting sphere of radius R has the potential

$$U = E Z \left[1 - \frac{R^3}{\sqrt{r^2 + Z^2}^{\,3}} \right] \tag{1}$$

where r is the radial distance from the original field line through the center of the sphere. (This line remains unchanged.) As it should be, U is constant, and equal to zero in our normalization, in the plane Z = 0 through the center of the sphere, and also its surface $r^2 + Z^2 = R^2$.

The field strength grad U then has the components

$$\frac{\partial U}{\partial r} = 3 E R^3 \frac{Z r}{\sqrt{r^2 + Z^2}^{\,5}} \tag{2}$$

$$\frac{\partial U}{\partial Z} = E \left[1 - R^3 \frac{r^2 - 2 Z^2}{\sqrt{r^2 + Z^2}^{\,5}} \right] \tag{3}$$

We find therefore that the distorted field has a maximum strength

$$\left| \text{grad } U \right|_{MAX} = 3 E \tag{4}$$

at the two "poles" Z = R, r = 0 of the sphere, and that it vanishes at its "equator" Z = 0, r = R.

It is clear that any experiment which is insensitive to the free field magnitude E is unlikely to be sensitive to the maximum enhanced magnitude 3E. Only an electric field measurement is likely to be affected. It is concluded that probe distortion of ambient fields will not affect experiments other than measurements of the fields themselves.

As far as a possible electric field experiment is concerned, the field distortions can be accommodated if the probe were actually a perfectly conducting sphere. Equations (2) and (3) could be used to obtain the free field vector from a measured field vector. Since a real probe will deviate from this idealization, it would either be necessary to determine empirically the transformation from measured field components to imposed field components or to locate the sensors far enough from the probe that the distortions are unimportant. Hence, for an electromagnetic field measuring experiment, there is a tradeoff between an extensive field mapping test program, in which the test item is the assembly probe, and deployment of the sensors some distance from the probe. From Equations (2) and (3) it is clear that field distortions drop off as the ratio $(R/r)^3$. At the probe surface the distortions are of the same order of magnitude as the imposed field. For each additional probe radius the sensor is removed from the probe, and the distortions are reduced by a factor of 8. For a 10% determination of the field it is sufficient to remove the sensor somewhat more than one probe radius from the probe surface.

Thermal Precipitation

During its descent through the lower Venus atmosphere, from the cloud top level down to the surface of the planet, the surface of the Pioneer Venus probe is generally somewhat (of the order of 10 to 100°K) cooler than the surrounding atmosphere. This can lead to a thermal precipitation of small liquid or solid aerosol particles, such as cloud material or atmospheric dust, on the surface of the probe, and on observation windows and the inlet of the mass spectrometer. This process has been noted on a number of occasions on the underside of horizontal windows in our Venus simulation chamber tests of the cloud particle size analyzer. In those tests the windows became coated with the dust used to check out the instrument's performance. To evaluate this effect, we performed an order-of-magnitude analysis of the basic mechanism of thermal precipitation from a hot environment to a cooler surface.

In the following analysis, we will calculate the rate at which atmospheric aerosols are deposited on a unit area of probe surface as the probe descends through the Venus atmosphere. The particles in question are considered to be small enough that their motion relative to the flow is governed by an equilibrium between aerodynamic forces and forces due to the thermal gradient, with inertial effects being negligible. Since the pertinent Reynold's numbers will always be small, the aerodynamic forces can be obtained from Stoke's Law. The forces due to the thermal gradient are taken from the Epstein equation (R. D. Cadle: Particle Size, Theory and Industrial Applications, Reinhold Publishing Corp, New York, 1965).

The equation of motion for a particle of mass, M, moving under the influence of an aerodynamic force, $\underline{F}_D$, and a force, $\underline{F}_T$, due to a thermal gradient, ∇T, is

$$m\ddot{\underline{r}} = \underline{F}_D + \underline{F}_T \tag{5}$$

$\underline{r}$ is the coordinate vector of the particle. For aerosol particles with small masses, the inertial term can be neglected and the equation of motion is

$$\underline{F}_D = -\underline{F}_T \tag{6}$$

From Stoke's Law the aerodynamic force can be written

$$\underline{F}_D = -3\pi\mu d\,(\dot{\underline{r}} - v) \tag{7}$$

where

μ = is the viscosity of the gas

d = is the diameter of the particle

v = is the gas velocity

The Epstein equation for the force due to a thermal gradient is

$$\underline{F}_T = \frac{9\pi}{2}\, d \left(\frac{K_a}{2K_a + K_i}\right) \frac{\mu^2}{\rho T} \underline{\nabla} T, \tag{8}$$

where

K_a is the thermal conductivity of the gas

K_i is the thermal conductivity of the particle

ρ is the mass density of the gas

and

T is the gas temperature.

Thus the equation of motion becomes

$$\dot{r} - v = -\frac{3}{2}\left(\frac{K_a}{2K_a + K_i}\right)\frac{\mu}{\rho T}\nabla T \tag{9}$$

Choosing a coordinate system in which the X direction is the direction of the gas flow and the Z direction is normal to the probe surface (and hence in the direction of the temperature gradient) we have

$$\dot{X} = \frac{dx}{dt} = v \tag{10}$$

$$\dot{Z} = \frac{dz}{dt} = -\frac{3}{2}\left(\frac{K_a}{2K_a + K_i}\right)\frac{\mu}{\rho T}\frac{\partial T}{\partial Z} \tag{11}$$

The equation of the trajectory of the particle is obtained from these equations by division

$$\frac{dz}{dx} = -\frac{3}{2}\left(\frac{K_a}{2K_a + K_i}\right)\frac{\mu}{\rho T v}\frac{\partial T}{\partial Z} \tag{12}$$

To use this equation one needs to describe the velocity distribution, $v(Z)$, through the boundary layer and the temperature gradient. To obtain the velocity distribution we assume simple shear flow, or a linear velocity distribution, joining the constant exterior flow of velocity v_o, at a distance δ from the surface. The slope of the velocity distribution is fixed by the surface friction.

$$\frac{1}{2}\rho v_o^2 C_f = \mu\frac{\partial v}{\partial Z} = \mu\frac{v_o}{\delta} \tag{13}$$

where

C_f is the surface friction coefficient.

This gives a velocity profile within the boundary layer of

$$v(Z) = \frac{\rho v_o^2 C_f}{2\mu} Z, \quad 0 \leq Z \leq \delta \tag{14}$$

And a boundary layer thickness of

$$\delta = \frac{2\mu}{\rho v_o C_f} \tag{15}$$

We assume a linear thermal boundary layer of the same thickness of the velocity boundary layer, hence for a probe temperature, T_o,

$$\frac{\partial T}{\partial Z} = \frac{T - T_o}{\delta} \quad \rho v_o C_f \cdot \frac{T - T_o}{2\mu} \tag{16}$$

We can now write the trajectory in the readily integrable form

$$\frac{dz}{dx} = -\frac{3}{2}\left(\frac{K_a}{2K_a + K_i}\right) \frac{\mu(T - T_o)}{\rho T Z v_o} \tag{17}$$

Integrating this equation, one has an expression for the trajectory of a particle which passes through the point $X = 0$, $Z = Z_o$ in the thermal boundary layer.

$$Z^2 = Z_o^2 - 3\left(\frac{K_a}{2K_a + K_i}\right) \frac{\mu(T - T_o)}{\rho v_o T} \; X \tag{18}$$

Hence the aerosols passing through an elemental area normal to the average flow in the boundary layer and extending a distance Z_o from the probe surface will strike the probe surface in an area X_o in length, with X_o given by

$$X_o = \frac{1}{3}\left(\frac{2K_a + K_i}{K_a}\right) \frac{\rho v_o T}{\mu(T - T_o)} \; Z_o^2 \quad \text{(See sketch below)} \tag{19}$$

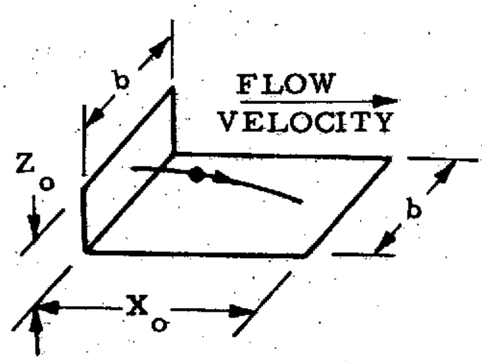

One can think of the rate of aerosol deposit on a probe surface area, b wide and X_o long, in terms of the volume of gas flowing through an area, b wide and Z_o high, normal to both the flow and the probe surface. The volume of gas, Q, flowing through this area per unit time is given by

$$Q = \int_o^{Z_o} b\, v(Z)\, dz \tag{20}$$

$$= \frac{b\rho v_o^2 C_f Z_o^2}{4\mu} \tag{21}$$

Substituting from Equation (19) for a cloud with a concentration, η, of particle mass per unit volume one has as the Rate of Deposit of Aerosol Mass per unit probe surface area.

$$\frac{\eta Q}{bx_o} = \frac{3\eta v_o C_f (T - T_o)}{4T} \left(\frac{K_a}{2K_a + K_i}\right) \tag{22}$$

where, to review

$\frac{\eta Q}{bx_o}$ = Rate of aerosol mass deposit in $\left[\frac{\text{mass}}{\text{surface area}}\right]$/ unit time

η = cloud aerosol mass density $\left[\frac{\text{mass}}{\text{volume}}\right]$

v_o = gas flow speed outside the boundary layer

C_f = surface friction coefficient

T = gas temperature outside the boundary layer

T_o = probe surface temperature

K_a = gas thermal conductivity

K_i = particle thermal conductivity

A few comments are in order about this analysis:

1) The Epstein equation is in reasonably good agreement with experimental evidence for poor thermal conductions but under-estimates the effect for good conductors such as mercury droplets.

2) As is indicated by the independence of the deposition rate on particle size and mass density, the analysis applies to particles small enough that inertial effects are negligible and large enough that their diameters are much larger than the mean free path for a gas molecule in the surrounding atmosphere. For particles of moderate density this means the analysis is applicable for particle diameters from a few tenths of a micron to a few tens of microns.

The impact of the deposition rate, Equation (22) can be seen by considering the following extreme example:

1)	The mass density of atmospheric aerosols	$1 \frac{kg}{m^3}$
2)	descent speed	10^2 m/s
3)	friction coefficient	4×10^{-3}
4)	$\frac{T - T_o}{T}$	0.2
5)	$\frac{K_a}{2K_a + K_i}$ (for a thermal insulator)	0.5

The resulting deposition rate is 3×10^{-2} kg/m^2 second for a very dense, nonconducting cloud, a high descent rate, and a large temperature difference, all tending to increase the deposition rate. This deposition rate is high enough that, even in the absence of condensible compounds, an undeated window could become totally obscured by thermal precipitation of particulates.

3.1.2.7 Engineering Experiments to Improve Probe Design

One of the study tasks was to identify engineering experiments to be made on the descent probe that would yield data for use in the design of probes for subsequent missions. The task did not include the diagnostic measurements of operating state temperatures, voltage, and current that are usually made on spacecraft to provide housekeeping data. These measurements can yield insight to understanding anomalous performance. With this information, the design of subsequent spacecraft can be modified to eliminate anomalous performance.

The first step in identifying specific engineering experiments was to consider those subsystems that may have been "overdesigned" because of uncertainties in the operating environments in the Venus atmosphere. We evaluated specific experiments that could be performed to determine the extent of this "overdesign" margin so that it could be reduced or eliminated in the future.

The detailed task output is presented in Section 3.2.2.5 because the quantitative estimates of subsystem uncertainty penalties are applicable to the Thor/Delta configuration. Qualitatively, the results of the task are applicable to both Atlas/Centaur and Thor/Delta. Furthermore, the potential improvements in future design are greater on Atlas/Centaur because additional weight has been used to "beef up" design in a number of subsystems. This added weight could be trimmed from future missions.

In approaching the task we considered four categories:

1) On-board housekeeping/diagnostic measurements, which with added analysis of the measurements could yield engineering design data.

2) On-board science experiments, which with added analysis of their data could yield engineering design data.

3) On-board science experiments, which could yield engineering design data if modifications were made to the instrument or the data output.

4) Adding new experiments solely to provide engineering design data.

In the first category we have identified using temperature gauges implanted in the external insulation. These, together with pressure shell temperature measurements and temperature measurements inside the probe, will provide the basis for evaluating the descent capsule's thermal protection subsystems versus time. Temperature gauges in the backface of the aeroshell forebody and afterbody will indicate whether the heat shield for future missions should be redesigned. Supplementing these with data from the on-board science experiments (Category 2) for atmospheric temperature, pressure, density, and composition will enable the performance of the thermal protection system to be related to pertinent atmospheric parameters. Design of thermal protection systems for future missions to other planets having different atmospheric or entry environments can be extrapolated. This requires no additional data output or modifications to the existing science instruments.

Temperature measurements of the outer and inner surfaces of the science instrument windows will be made. Analyses of these data (Category 1) plus concurrent data on the ambient environment (Category 2, temperature pressure, density, composition, humidity) will yield information for the design of windows and heaters for subsequent missions.

Our study identified only one experiment in Category 3 and none in Category 4.

The X-ray fluorescence experiment for the large probe (not presently on the nominal payload) could be augmented with radioactive sources implanted in the heat shield of the aeroshell. As the heat shield surface recedes during entry, the detected flux of backscattered X-rays would decrease proportionately. These data would give a measure of heat shield performance that could be used in future designs. Some modifications to the data handling system logic and memory size would be required to operate the instrument during entry in a fast mode and store the data for later transmission. Since the instrument is not presently in the nominal payload, these modifications have not been factored into the data handling system design. They are, however, rather insignificant.

SECTION 3.1 REFERENCES

1. "NASA Space Vehicle Design Criteria (Environment), Models of the Venus Atmosphere (1972)" NASA SP-8011 (September 1972).
2. Pioneer Venus Report of a Study by the Science Steering Group, Ames Research Center/NASA (June 1972).
3. ARC Letter ASD: 244-9/32-042 (April 13, 1973), J. J. Hunt to W. H. Simmons (Version IV science payloads enclosed).

3.2 PROBE SCIENCE, THOR/DELTA

3.2.1 Science Requirements and Impact on Mission and System Design

This section summarizes the science requirements and tradeoffs involved in the early Thor/Delta mission/system studies. These studies considered the Versions I through III science payloads and the 1977 opportunity. The Version III experiment complements are summarized in Tables 3-15 and 3-16. Version III of the large probe nominal payload includes a shock layer radiometer and an aureole extinction detector, which are considered as candidate instruments for the Version IV payloads; the wind/altitude radar and gas chromatograph included in the nominal payload for the Version IV science, were treated as candidate instruments for Version III. The Version III small probe payloads also include the same instrument types as Version IV, but the magnetometer was considered as a nominal instrument in Version III while the IR flux detector was a candidate instrument. As discussed below, both the magnetometer and shock layer radiometer can be accommodated in the Thor/Delta baseline configurations.

Table 3-15. Small Probe Experiments (Version III)

INSTRUMENT	OBJECTIVES/MEASUREMENTS	PRIORITY
	NOMINAL PAYLOAD	
TEMPERATURE	ATMOSPHERIC STRUCTURE, HORIZONTAL VARIATIONS	A-1
PRESSURE		A-1
NEPHELOMETER	CLOUD LAYERING, HORIZONTAL VARIATIONS	A-2
STABLE OSCILLATOR	WINDS FROM DOPPLER, DLBI TRACKING;VARIATIONS	A-3
ACCELEROMETER	ATMOSPHERIC STRUCTURE DURING ENTRY AND DESCENT	A-4
MAGNETOMETER	PLANETARY MAGNETIC FIELD, VARIATIONS	A-4
	OTHER CANDIDATE INSTRUMENTS	
RADAR ALTIMETER	ALTITUDE FOR ATMOSPHERIC RECONSTRUCTION	---
NET FLUX RADIOMETER	THERMAL (IR) FLUX PROFILES, HORIZONTAL VARIATIONS	---

3.2.1.1 Probe Targeting Guidelines and Mission Trades, 1977

The science objectives and probe targeting guidelines discussed in Section 3.1 also apply to the 1977 Thor/Delta mission. The targeting geometry for 1977, illustrated in Figure 3-51, is almost a mirror image of the 1978 geometry with respect to the Venus orbit plane. Approximately the same latitude/longitude spreads can be achieved for the same range of entry angles as for 1978 but the Northern rather than the Southern hemisphere is accessible with shallow entry angles in 1977. Table 3-17 and Figure 3-52

Table 3-16. Large Probe Experiments (Version III)

INSTRUMENT	OBJECTIVES/MEASUREMENTS	PRIORITY
	NOMINAL PAYLOAD (A)	
TEMPERATURE	ATMOSPHERIC STRUCTURE, ANCILLARY FOR OTHER MEASUREMENTS	A
PRESSURE		A
ACCELEROMETERS	UPPER & LOWER ATMOSPHERE STRUCTURE, TURBULENCE, SEISMIC NOISE (POST-IMPACT)	A
MASS SPECTROMETER	COMPOSITION OF ATMOSPHERE, CONDENSIBLES	A
CLOUD PARTICLE SIZE SPECTROMETER	AEROSOL SIZE, NUMBER DISTRIBUTIONS	A
SOLAR FLUX RADIOMETER	SOLAR FLUX PROFILE, ENERGY BALANCE	A
PLANETARY FLUX RADIOMETER (IR)	THERMAL FLIX PROFILE, ENERGY BALANCE CLOUD LAYERING	A
AUREOLE/EXTINCTION DETECTOR	CLOUD PROPERTIES, SOLAR ATTENUATION THROUGH CLOUD TOPS	A
TRANSPONDER	WINDS FROM DOPPLER, DLBI TRACKING	A
NEPHELOMETER	CLOUD LAYERING	B
HYGROMETER	WATER VAPOR CONCENTRATION	B
SHOCK LAYER RADIOMETER	ATMOSPHERE COMPOSITION (DURING ENTRY ONLY)	C
	OTHER CANDIDATE INSTRUMENTS (B)	
WIND DRIFT RADAR	WIND VELOCITY AND ALTITUDE	-
FLUORESCENCE SPECTROMETER	CLOUD PARTICLE COMPOSITION (X-RAY OR ALPHA SCATTER)	-
FR/SFERICS DETECTORS	RF BACKGROUND NOISE, OCCURRENCE OF LIGHTNING, ATMOSPHERIC CONDUCTIVITY	-
ATTENUATED TOTAL REFLECTION SPECTROMETER	COMPOSITION OF CONDENSIBLES OR DUST PARTICLES	-
GAS CHROMATOGRAPH	ATMOSPHERIC COMPOSITION	-

(A) CONTRACTUAL PAYLOAD FOR ESTABLISHING BASELINE MISSION AND SYSTEM DESIGN REQUIREMENTS

(B) IMPACT OF EACH INSTRUMENT ON BASELINE SYSTEM DESIGN TO BE ASSESSED AS SEPARATE TASKS

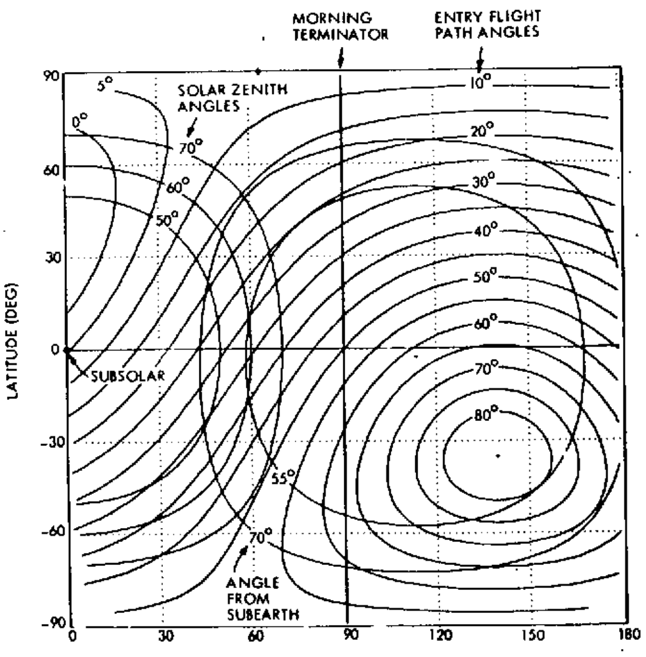

Figure 3-51. 1977 Probe Mission Targeting Geometry

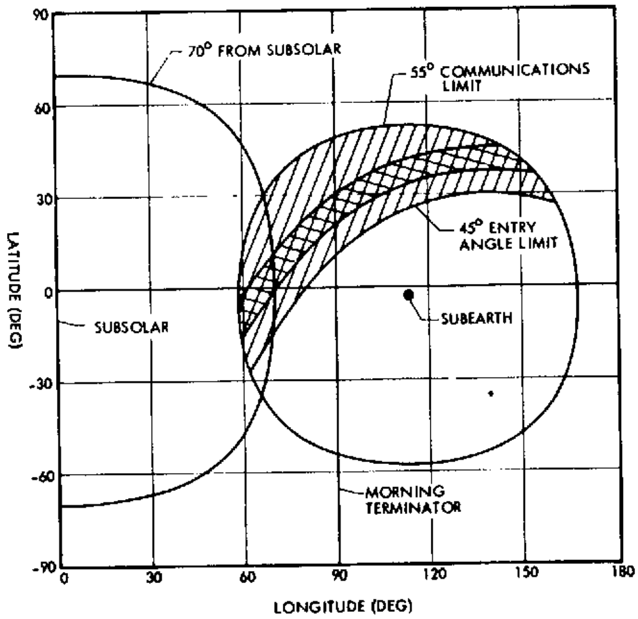

Figure 3-52. 1977 Baseline Probe Mission Targeting Capability

Table 3-17. Baseline Mission Targeting Capability

LARGE PROBE		
LATITUDE	0° ± 10°	(-10° TO + 40°) (A)
LONGITUDE	65° ± 5°	(60° TO 155°) (A)
SOLAR ZENITH ANGLE	65° ± 5°	(60° TO 150°) (A)
ENTRY ANGLE OF ATTACK	0° ± 3°	
SMALL PROBES		
LATITUDE	-20° TO + 49°	
LONGITUDE	60° TO 160°	
SOLAR ZENITH ANGLES	60° TO 155°	
ENTRY ANGLE OF ATTACK	0° ± 3°	

(A) VALUES IN ( ) INDICATE RANGE OF CAPABILITY WITHIN 55 DEGREE COMMUNICATIONS LIMIT; NOMINAL RANGE IS FOR LIGHT SIDE TARGET WITHIN 70 DEGREES OF SUBSOLAR

summarize the baseline Thor/Delta 1977 mission targeting capabilities. The small probe entry flight path angle range (-25 to -45 degrees) was selected to permit descent instrument deployment as high as possible consistent with achieving the desired latitude/longitude spread within the 55 degree communications limit. Since weight considerations are critical for the Thor/Delta configurations, the choice of -45 degree limit was also affected by the desire to minimize entry deceleration loads and structural weight.

The shaded portion of Figure 3-52 shows the area of the planet within which the baseline design small probes can reliably survive entry and transmit their data to earth during the 1977 opportunity. The cross-hatched area represents the baseline large probe capability. The baseline large probe target area is, however, restricted to that portion within 70 degrees of subsolar in keeping with the solar flux measurement requirements.

The baseline 55 degree communications limit permits nominal targeting of the small probes as far apart as 49 degrees in latitude and 95 degrees in longitude within the North (celestial) hemisphere, thus exceeding the SSG minimum latitude/longitude separation requirements. The maximum recommended small probe latitude/longitude spreads (60 and 120 degrees) can be achieved within the -25 to -45 degree baseline entry angle corridor if the communications angle capability is increased to 65 degrees, or if some loss of data near the surface due to possible probe pitching is acceptable. The former requires an increased transmitter power, a wider beam antenna, and hence, an increased weight allocation.

Expanding the small probe entry angle corridor to include angles as steep as 80 degrees within the 55 degree communications limit would increase the achievable longitude spread by about 10 degrees and allow targeting to 55 degrees South, but would require designing and testing to higher entry loads (g max 500) and peak heating rates. It also results in lower altitudes where subsonic velocities are first achieved (100 mb) as discussed below.

The choice of a sequential release sequence as baseline for the small probes provides a nominal zero angle-of-attack at entry, thereby simplifying the interpretation of the single axis accelerometer data in terms of the atmospheric structure. The large probe also has a nominal zero angle of attack at entry as required for the shock layer radiometer measurements.

3.2.1.2 Entry Measurement Requirements and Trades, Thor/Delta

In addition to a four-axis accelerometer system, the Version III nominal large probe payload included a shock layer radiometer (SLR) for obtaining measurements of the stagnation point radiation intensity during entry. The SLR requires a near-zero angle of attack, data storage (2100 bits), and a method of initiating data storage for the few seconds just prior to peak radiation intensity. Figure 3-53 illustrates the large probe entry data collection and storage requirements as a function of time.

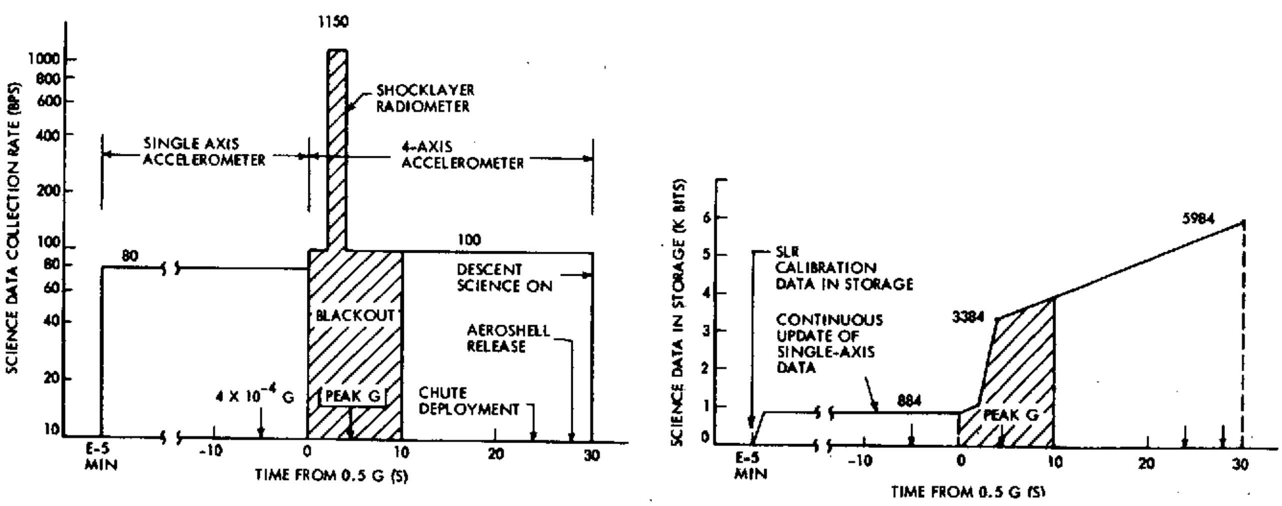

Figure 3-53. Large Probe Entry Science Data Requirements

Since the high Doppler rates and timing uncertainties during the pre-entry through post-blackout phase preclude DSN signal lockup all data during that period must be stored for transmission during descent. Neither the 4×10^{-4} g level, nor the peak deceleration, can be accurately predicted as functions of time from probe separation from the bus (13 to 25 days prior to entry). Since the sampling rate of the large probe accelerometer must be changed upon sensing the 0.5 g level, that event is used as a reference for obtaining the required data. The onset of sensible radiation occurs within a few seconds after 0.5 g while the 4×10^{-4} g level occurs about 5 seconds prior to 0.5 g. Sampling of the SLR can be initiated at a fixed time (0 to 4 seconds) after a g switch senses 0.5 g. The g switch signal can be used as a reference for timing all other entry and descent events. Since the 4×10^{-4} g level occurs prior to the 0.5 g level, accelerometer sampling must be initiated by the coast timer at a time well before that level is expected to occur. Initiation of sampling at 5 minutes prior to the expected time of entry would account for all timing uncertainties. Rather than transmit or store the accelerometer output during this entire period, the output is read into storage so that the most recent 10 seconds of data are retained in storage and continuously updated until the 0.5 g level is sensed. At that point the 10 seconds of single axis data are locked in storage and the accelerometer sampling and storage is changed to the four-axis mode. The post-blackout accelerometer sampling requirement is 40 bps, but the baseline design provides 100 bps to avoid an extra format for the 20-second period between end of blackout and initiation of the descent science.

Small probe accelerometer sampling is initiated and the data stored in the same manner as for the large probe. The small probes obtain and store only accelerometer measurements during entry, but magnetometer data are obtained and stored during the period just after probe separation from the bus. These data are transmitted during a 10-minute period at E-1 hour and again during descent. For the large probe, the accelerometers are sampled more rapidly than required during the post-blackout, pre-descent phase to avoid an extra format. Figure 3-54 illustrates the small probe entry data collection and storage requirements.

The baseline large and small probe entry measurement profiles are shown in Figures 3-55 and 3-56 as function of time from the 0.5 g acceleration level. Figures 3-57 and 3-58 show the number of measurements obtained per pressure scale height as a function of altitude during entry. At least one measurement per scale height is required for an accurate definition of the density or pressure profile, while two to four measurements per scale height are needed to extract details of the temperature structure. As can be seen

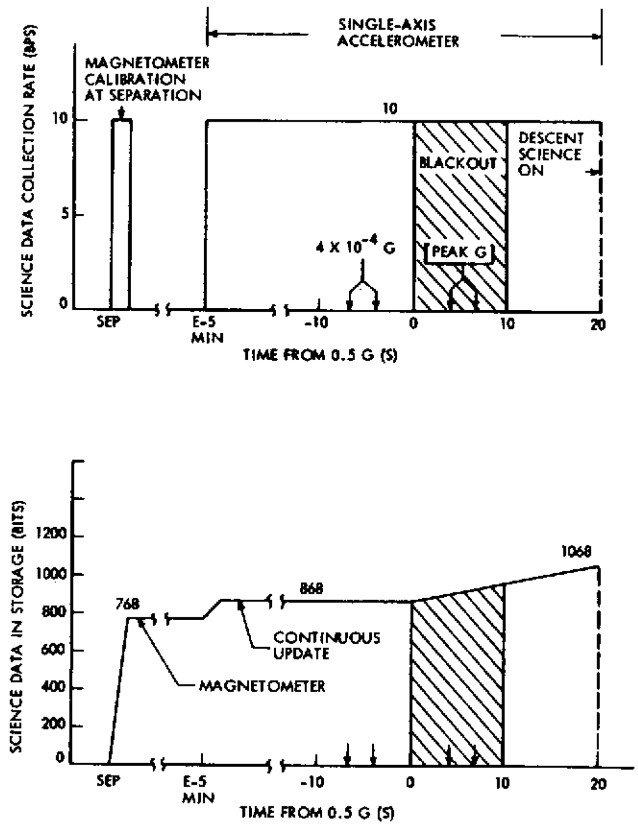

Figure 3-54. Small Probe Entry Science Data Requirements

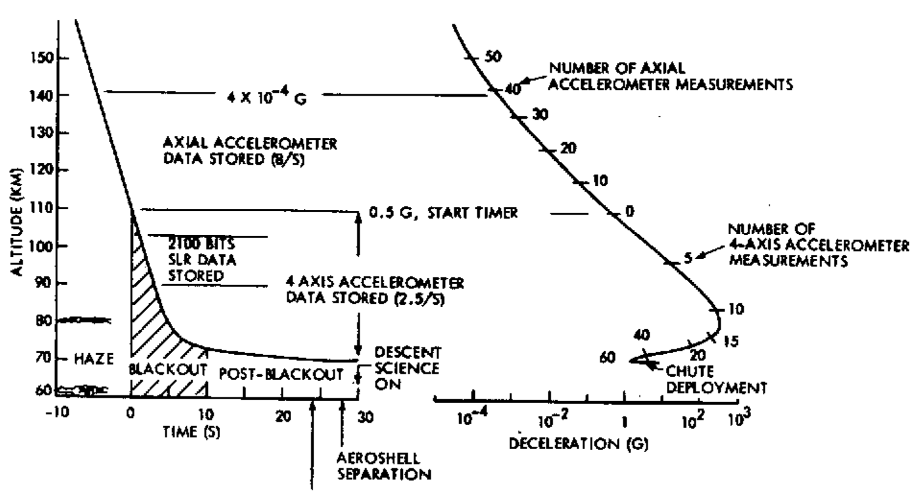

Figure 3-55. Baseline Large Probe Entry Measurement Profile

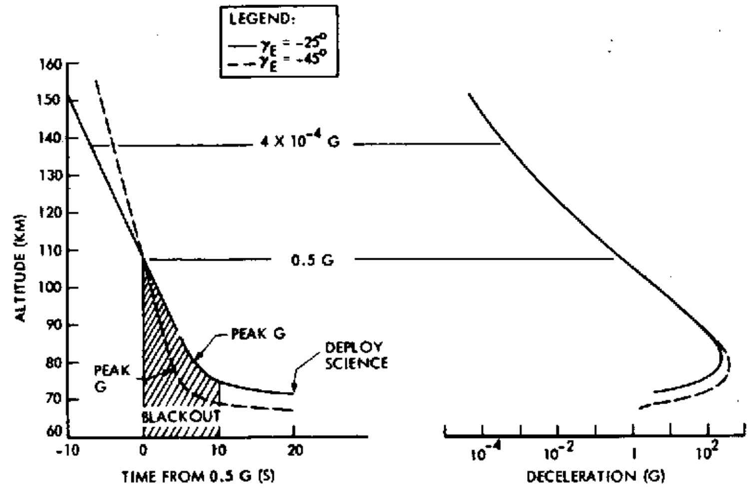

Figure 3-56. Baseline Small Probe Entry Accelerometer Measurement Profiles

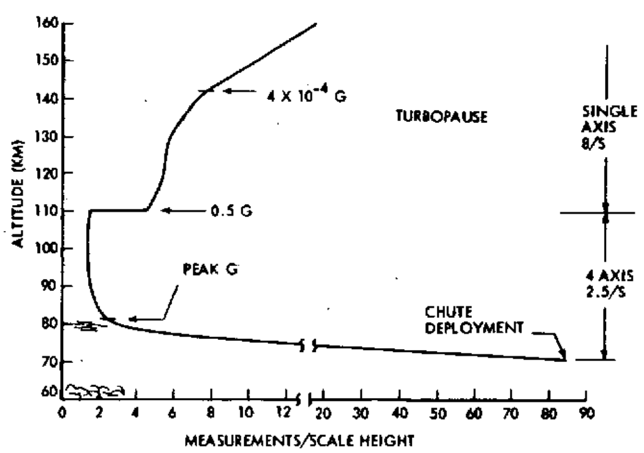

Figure 3-57. Number of Accelerometer Measurements per Pressure Scale Height During Entry for Baseline Thor/Delta Large Probe $\left[\gamma_E = -37.5^0,\ B_H = 70.7\ \text{kg/m}^2\ (0.45\ \text{slugs/ft}^2)\right]$

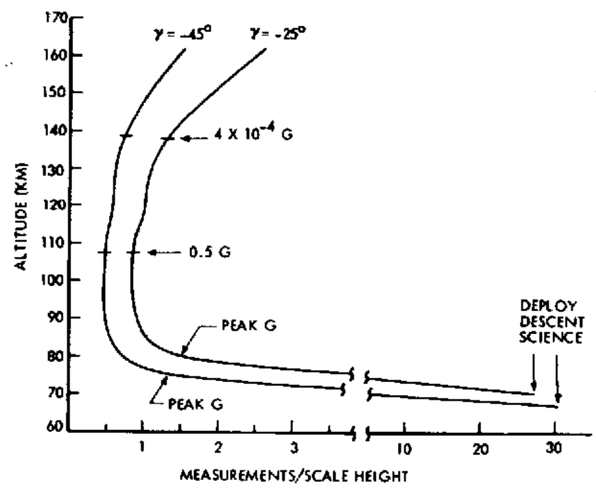

Figure 3-58. Number of Single Axis Accelerometer Measurements per Pressure Scale Height During Entry for Baseline Thor/Delta Small Probes $\left[B_H = 141.4\ \text{kg/m}^2\ (0.9\ \text{slugs/ft}^2)\right]$

from the figures, the large probe obtains about two measurements per scale height through peak deceleration while the small probes obtain between one and two per scale height near peak deceleration. While these are adequate for determining the general temperature structure, it may be desirable to increase the sampling rates to about five per second through the peaks to obtain the details of the temperature structure between 70 and 90 km. For the small probes, this would require an increase in memory allocation from 200 bits to 1000 bits. Since the baseline small probe storage capacity is

7680 bits and is read out approximately 1.5 times during descent, the additional entry data could easily be accommodated. For the large probe, the increased entry data rate could be accommodated by adding one 2560 bit C-MOS memory cell.

3.2.1.3 Descent Measurement Requirements and Trades, Thor/Delta

The desire to obtain subsonic, in situ measurements near or above 70 km (~50 mb) primarily impacts the selection of entry flight path angle corridors, entry ballistic coefficients, and, for the large probe, the selection of a subsonic decelerator configuration (subsonic chute vs supersonic chute). A subsonic chute was chosen for the baseline because deployment can be affected at subsonic velocities above 70 km. Achieving subsonic velocities at higher altitudes (e.g., ~75 km) requires supersonic chute deployment, much lower entry ballistic coefficients, shallower flight path angles, or a combination of all three. These are all impractical from the standpoint of both weight and cost for the Thor/Delta mission. Figures 3-59 and 3-60 illustrate the effect of entry angle and entry ballistic coefficient uncertainty on the altitudes of chute deployment for the large probe and instrument deployment for the small probes. Note that one of the small probes could start as low as 67 km for the steepest flight path angle of -45 degrees, but this is still well above the visible cloud tops at 63km.

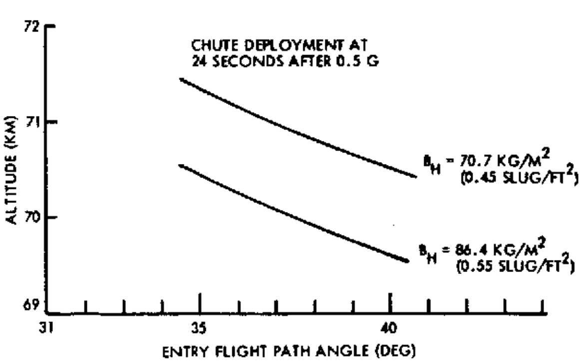

Figure 3-59. Altitude of Chute Deployment for Large Probe vs Entry Angle and Ballistic Coefficient
Nominal B_H - 78.5 ± 7.85 kg/m^2 [0.50 (±0.05) slug/ft^2]

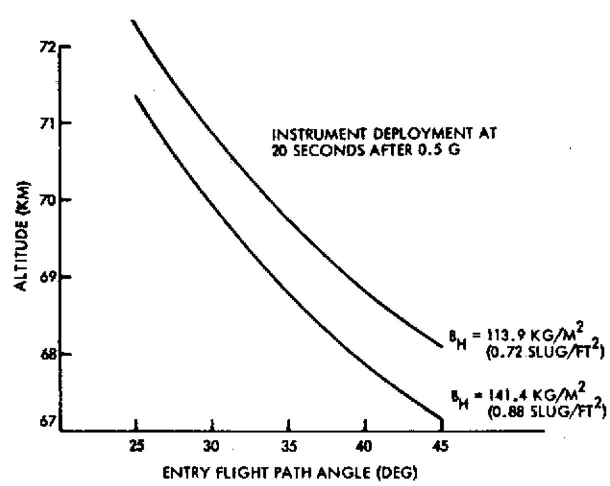

Figure 3-60. Altitude of Descent Instrument Deployment for Small Probes vs Entry Angle and Ballistic Coefficient
Nominal B_H - 125.7 (± 12.6) kg/m^2 [0.80 (± 0.08) slug/ft^2]

The atmospheric reconstruction process requires a knowledge of the ambient pressures and temperatures. The measured values are affected by the angle of attack, velocity, and flow compressibility and must be converted to ambient values by an iterative process. Figures 3-61 and 3-62 illustrate the differences between measured and ambient pressures and temperatures for the baseline large and small probes assuming zero angle of attack and isentropic flow. As can be seen, the differences are small for the large probe, but are substantial for the small probes during the initial high-velocity period above the cloud top.

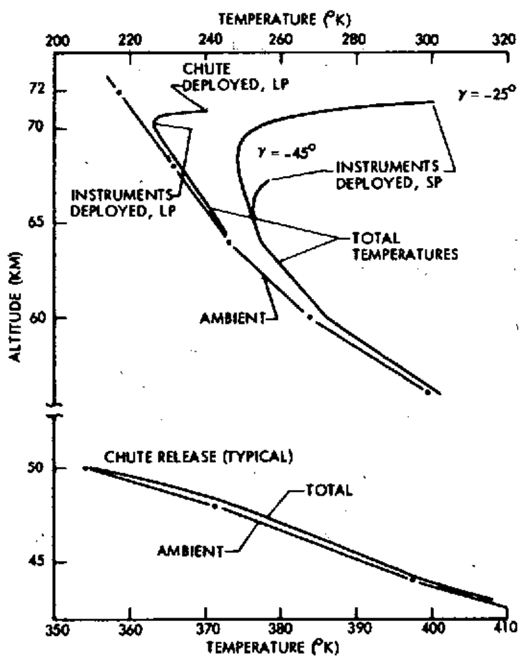

Figure 3-61. Total (Measured) Temperatures Compared to Ambient Temperature During High-Velocity Periods of Descent

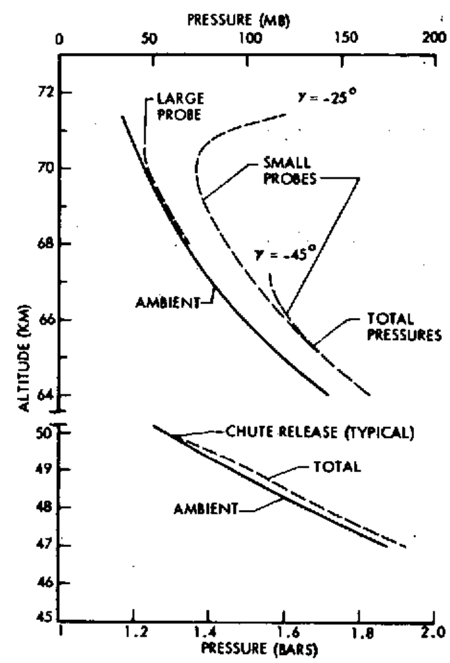

Figure 3-62. Stagnation (Measured) Pressures Compared to Ambient Pressure During High Velocity Periods of Descent

The descent experiment data sampling requirements for the Version III payloads were specified in terms of minimum data rates (bps) for each instrument. The descent science data rate requirements for the nominal payloads are summarized in Figures 3-63 and 3-64. The Thor/Delta baseline large probe data transmission capability at 55 degrees from subearth is only 102.4 bps using the sum of the adverse tolerances (Section 7.6). This leaves about 88 to 95 bps available for science.

Note that two large probe instruments, the mass spectrometer and the cloud particle size analyzer (CPSA), account for 81.3 percent of the 128 bps total requirement (31.3 percent for mass spectrometer, 50 percent for CPSA). Removal of the category B instruments will not alleviate the problem. The baseline solution to the bit rate problem is to reduce the CPSA bit rate to 24 bps as shown in Figure 3-65. An alternative solution is to increase the

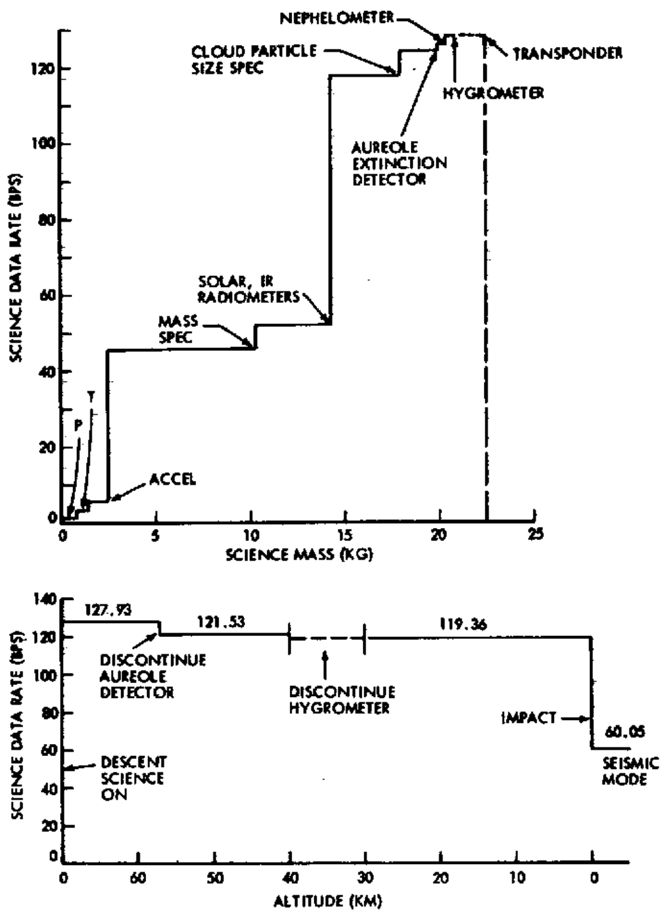

Figure 3-63. Large Probe Descent Science Data Rate Requirements

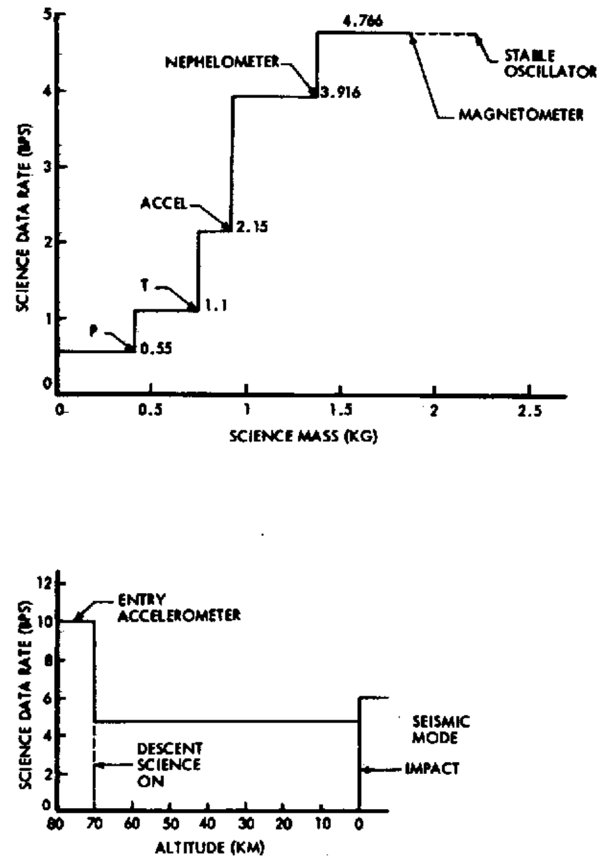

Figure 3-64. Small Probe Descent Science Data Rate Requirements

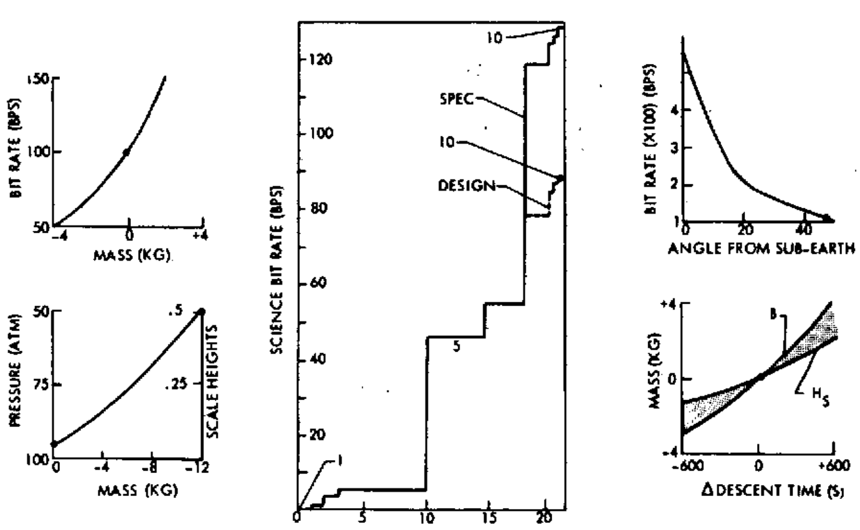

Figure 3-65. Thor/Delta Bit Rate and Mass Trades

science bit rate capability. This can be done in two ways. This first is to move the large probe entry site closer to subearth, thus increasing the bit rate simply by increased antenna gain. This will, however, not be in compliance with the SSG's desire to enter within 70 degrees of the subsolar point. The second alternative is to increase the transmitter power to make up the required bit rate, requiring additional weight as shown in Figure 3-65.

Alternative mission designs, not affecting the large probe systems design, are available to make up the needed weight. The first is simply not to design the large probe to survive to the surface, but to some altitude near the surface. The second is to decrease the descent time to the surface by varying the ballistic coefficient (B) or the height of staging (H_S), and thirdly, by a combination of these alternatives. Figure 3-66 illustrates the sensitivity of descent time to chute release altitude and descent capsule ballistic coefficient.

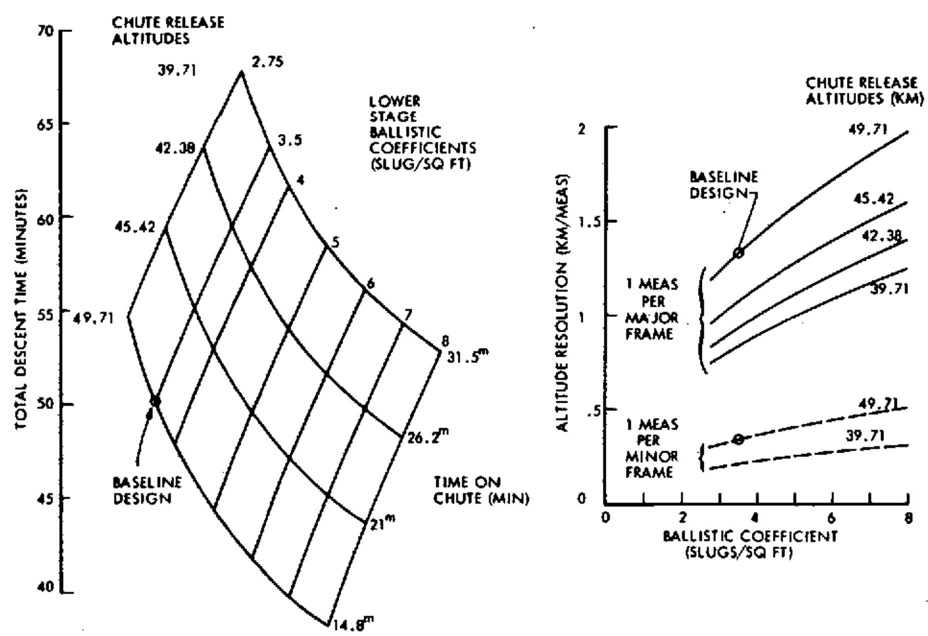

Figure 3-66. Descent Time Sensitivity to Chute Release Altitude and Lower Stage Ballistic Coefficient for 0.12 slug/sq ft Upper Stage

In addition to the alternatives addressed in Figure 3-65, three other options should be mentioned. The first two involve a decrease in the communication link margins. In the first case, the required increase in data rate can be obtained by RSS'ing the adverse tolerances, as opposed to summing them. Secondly, the adverse tolerance due to wind gusts could be reduced, increasing the probability of real-time data dropout. The third alternative is to vary the sampling rates of the instruments to provide a more uniform and effective measurement schedule during the descent. This can be done by storing part of the data at the higher altitudes and taking advantage of memory storage. The sample rates of the instruments could then be reduced at the lower altitudes, still preserving a uniform and effective measurement schedule. The stored data could be completely transmitted during this time well before impact.

The distribution of altitude resolutions obtained by each of the instruments during descent are summarized in Figures 3-67 and 3-68. The solid curves show the number of kilometers between measurements as a function of altitude; the dashed curve shows the density scale height profile. The small probes obtain atmospheric structure measurements at intervals ranging from about 2000 meters (2.5 per scale height) at high altitudes down to 150 meters (133 per scale height) near the surface. The resolution rapidly improves at high altitudes giving one measurement per kilometer (7 per scale height) as the probe descends through the visible cloud top. The large probe obtains much finer resolution (100 to 500 meters) due to its slower descent on the parachute. A total of 54 atmospheric and cloud structure measurements and two 16 000-bit mass spectrometer samples are obtained by the time the large probe reaches 55 km where the Venera probes first obtained

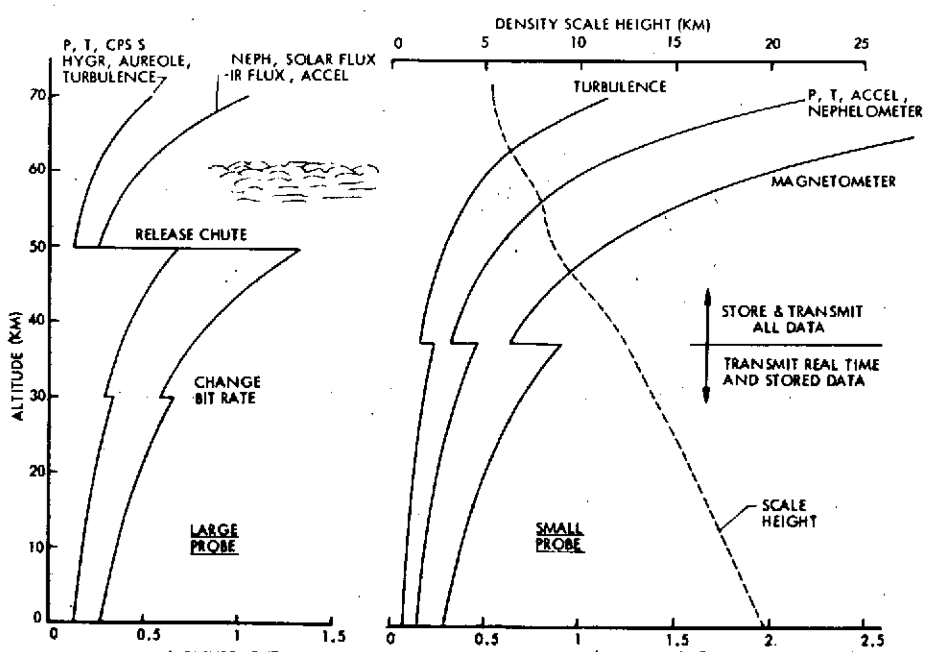

Figure 3-67. Large and Small Probe Baseline Altitude Resolutions During Descent

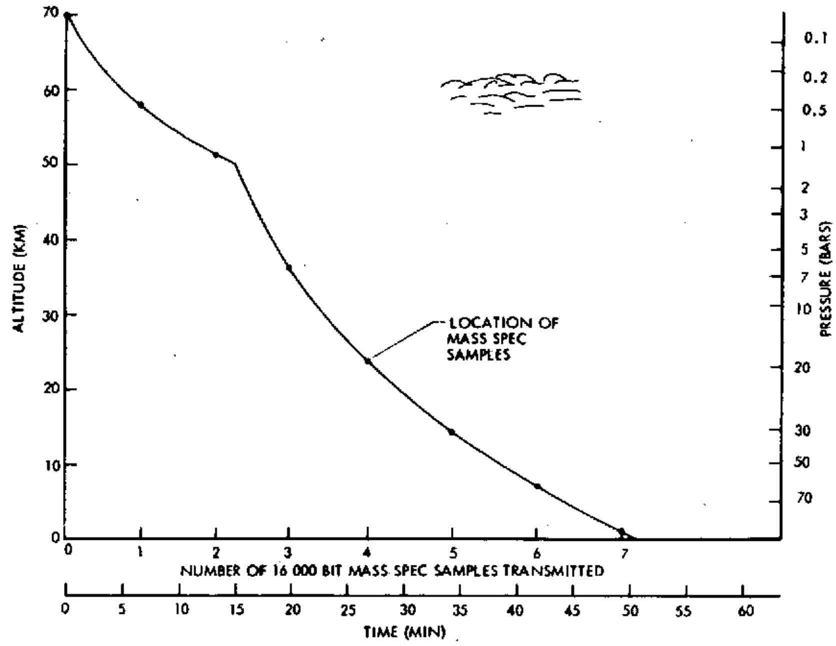

Figure 3-68. Mass Spectrometer Altitude Resolution

measurements. A total of seven mass spectrometer measurements are obtained and transmitted during descent with the last sample being taken at 7 km above the nominal surface.

The cloud particle size spectrometer is the instrument most affected by the probe descent velocities, as illustrated in Figure 3-69. The curves show the size of the minimum detectable particles as a function of altitude for various probe ballistic coefficients and a 10 MHz response for the detector modules. The inset at the right shows a typical 30-channel size spectrum for the instrument. As can be seen, 90 percent (larger than 6 μm) of the desired spectrum can be observed at all altitudes with the baseline descent profile (solid curve). Only the two smallest sizes (0 to 2 μm and 2 to 4 μm) are not detected above the visible cloud top, but this region can be investigated remotely from earth and orbiting spacecraft. The observable spectrum can be extended to pick up the 2 to 4μm size range near 70 km by either decreasing the chute ballistic coefficient by a factor of 10 or by increasing the frequency response to 30 MHz. A factor of 10 decrease in the chute ballistic coefficient would result in a 2.8-hour descent time for the same chute release altitude or require chute release at 60 km to keep the same descent time.

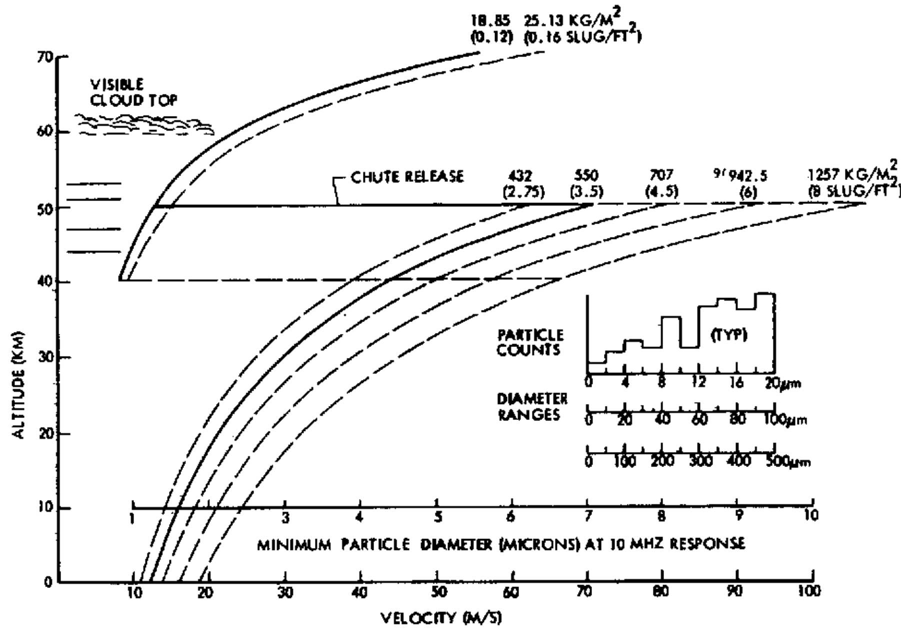

Figure 3-69. Cloud Particle Size Analyzer Measurement Sensitivity to Large Probe Ballistic Coefficients and Chute Release Altitudes

Several other descent options are also illustrated in Figure 3-69. In view of the Venera 8 reports implying clouds down to $\sim$40 km and the previous indications of a wind reversal layer near the same level, it would appear desirable to remain on the chute to 40 km. Figure 3-66 shows the total descent times for various combinations of chute release altitudes and lower stage ballistic coefficients. For the same total descent time as the baseline (50 minutes), releasing the chute at 42.38 km requires a lower stage ballistic coefficient of 1100 kg/m^2 (7 slugs/ft^2) or, remaining on the chute down to 39.71 km and using a lower stage ballistic coefficient of 942.5 kg/m^2 (6 slugs/ft^2) results in a total descent time of 56 minutes. The additional battery weight required for the slightly longer descent time would be offset by a smaller thermal protection weight since the probe descends more rapidly through the hot lower atmosphere. Figure 3-69 shows that chute release at 40 km to a lower stage ballistic coefficient of 942.5 kg/m^2 (6 slugs/ft^2) gives a more balanced velocity profile in that the maximum velocities (at chute deployment and after chute release) are about the same.

Figure 3-70 illustrates the performance of the DLBI (Doubly-Differenced Long Baseline Interferometry) technique for determining the winds from probe tracking during descent. The figure on the right plots the magnitudes of the semimajor and semiminor axes of the uncertainty ellipses for the horizontal velocity (at the surface) for different levels of phase uncertainties of the DLBI

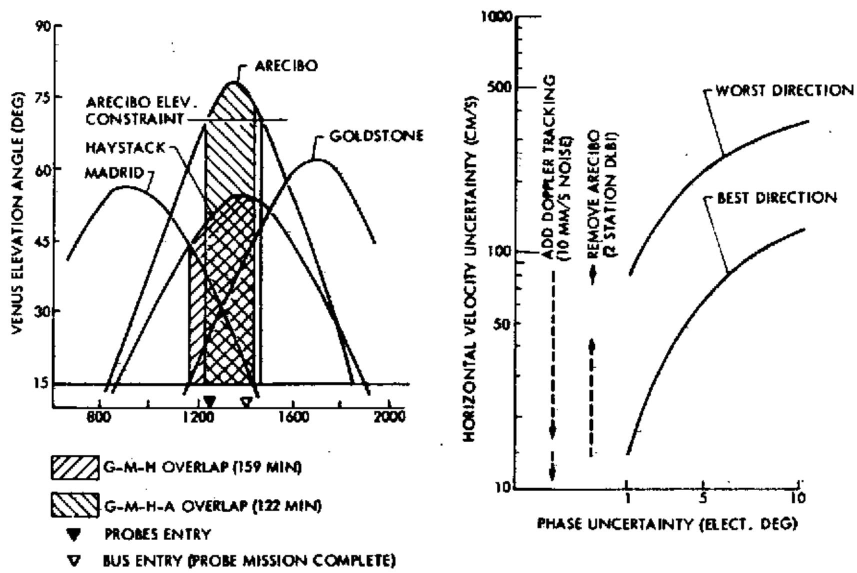

Figure 3-70. Wind Velocity Determination with DLBI Technique, 1977 Mission

measurement. Thus the horizontal velocity may be determined to 14 and 81 cm/s (1σ) in the best and worst directions, respectively, for a phase uncertainty of one electrical degree. If Arecibo is eliminated and DLBI measurements are processed from only two stations, the uncertainty in the best dirction is increased to 46 cm/s while the worst direction error is only slightly increased. If Doppler tracking is added, the results are much improved. The best direction error is decreased to 0.6 cm/s and the worst direction uncertainty to 15 cm/s. The Doppler noise of 10 mm/s corresponds to an order of magnitude degradation over interplanetary tracking because of Venus atmospheric effects. Our analyses have indicated that the measurement noise is the dominant factor in the effectiveness of DLBI; descent speed, ballistic coefficient uncertainty, and probe-bus geometry are second order effects.

The left side of Figure 3-70 illustrates the tracking station coverage on the 1977 probe mission arrival date. Madrid Haystack, and Goldstone have an overlap period of 159 minutes with Venus at least 15 degrees above the horizon for each station. If Arecibo is added to the combination its rather stringent requirement of elevation angles greater than 70 degrees produces a four-station coverage overlap time of 122 minutes. The 1977 Thor/Delta mission sequence has nearly simultaneous (± 2 minutes) entry times for the large and small probes with bus entry delayed to occur 90 minutes later, following the conclusion of the probes' descent (to accommodate differencing of the probes' atmospheric trajectories with the better known ballistic trajectory of the bus). Thus, the entire mission may be viewed by the four stations simultaneously and the DLBI experiment may be accomplished with a comfortable margin. A more detailed discussion of the DLBI experiment for both the 1977 and 1978 missions is given in Section 4.2.4.4.

3.2.2 Science Instrument Accommodation Studies

Our design concepts for accommodating the science instruments on the probes launched with the Thor/Delta are discussed in this section. The science complement used was given by NASA as Science Definition Report, Version I on 22 September 1972, augmented by Preliminary Experiment Interface Descriptions, 19 December 1972. We have also considered "other candidate instruments" listed in the Version I science and other candidate instruments and alternative nominal instruments, as described to us on 14 February 1973 in a briefing at NASA/ARC.

3.2.2.1 Large Probe Instrument Accommodation Concepts

Structural and Mechanical

The basic accommodation feature for instruments in the large probe is the equipment ring assembly shown in Figure 3-71. It consists of equipment

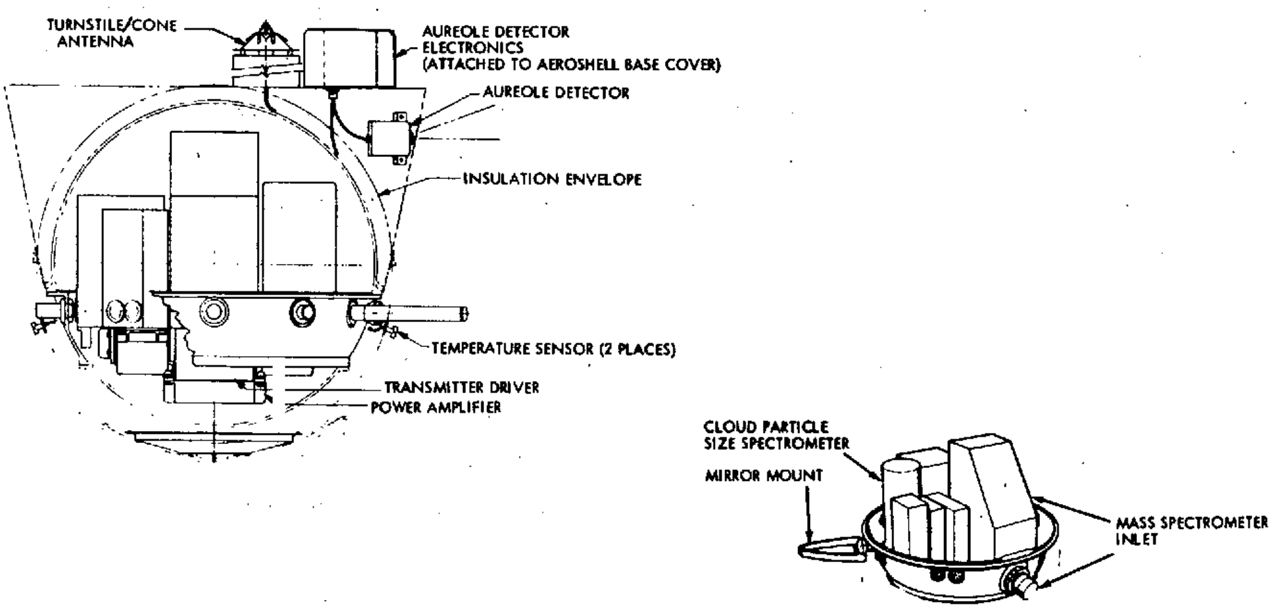

Figure 3-71. Equipment Ring Assembly Concept

support beams that serve as a mounting platform for all the instruments (with some exceptions) and as a slice of the lower hemisphere of the pressure shell. The instruments that require a penetration of the pressure shell make that penetration (window, electrical, gas inlet, etc.) through the pressure shell ring. In some instances, this was not practical and those exceptions are accommodated separately. The internal parts of the instruments are mounted on the instrument platform part of the assembly.

Some of the optical parts of the experiment are mounted on the instrument platform of the frame and the window is mounted directly to the pressure shell. Alighment problems between the parts are minimized because the equipment ring assembly is final machined after the equipment support beams are installed.

The instrument mounting surfaces will be held to alignment tolerances of $\pm$ 0.00873 rad ($\pm$ 1/2 degree) with respect to the probe coordinate system. The mounting points for the instruments have out-of-plane tolerance not exceeding 0.0127 cm (0.005 in.).

Any instrument parts requiring a penetration of the pressure shell are mounted with a threaded fitting and compression nut assembly similar to that shown in Figure 3-72 for a window mounting. The gasket (a metal O-ring) is mounted in a groove in the shoulder of the fitting and seals against a flat surface machined into the pressure shell around the hole. This way penetration hardware can be mounted and demounted with minimum risk of damage to the pressure shell, such as stripping threads, breaking a fitting, etc. All the window assemblies are constructed with sealed double windows--an external and an internal window (or lens).

Two instruments that require some special optical considerations in the probe penetration are the solar radiometer and planetary flux radiometer. These instruments have special field-of-view considerations which require some optical design in the penetration window assembly.

The planetary flux radiometer accommodation is shown in Figure 3-72(a) with an elbow telescope configuration to achieve the 5-degree down-looking field of view from the equipment mounting assembly. The right angle bend is achieved with a gold-coated front surface mirror. The 10-mm clear aperture IRTRAN lens has a 53-mm focal length, which sets the

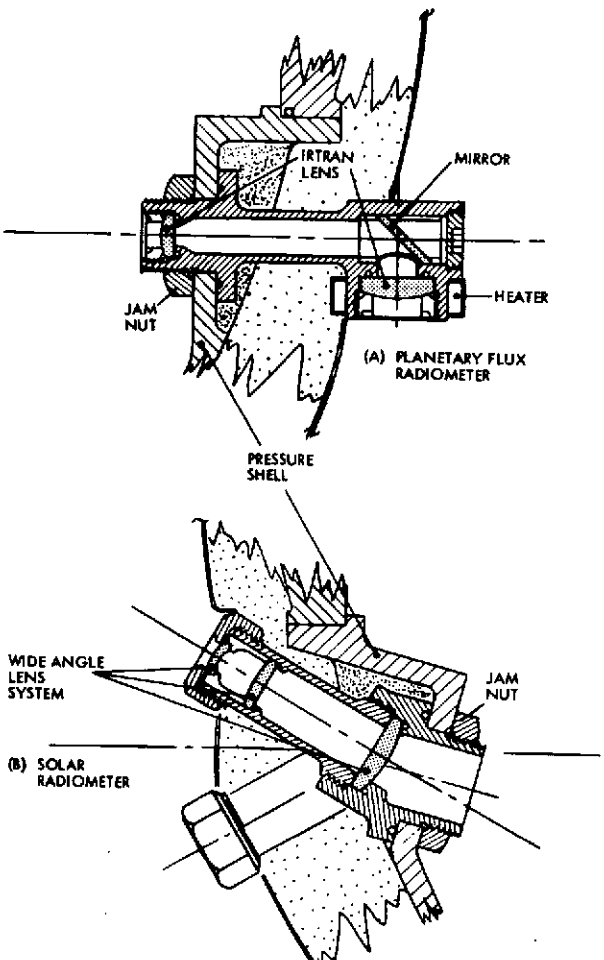

Figure 3-72. Optical Designs for Probe Penetrations

prime focus at the pressure vessel so that a 4.6-mm aperture stop provides the 5-degree full cone angle field of view. This small aperture stop allows for a reduced window assembly size at the probe wall while reducing the thermal leak. To achieve transmission at long wavelengths (10 percent transmittance at 29 μm with 6-mm thickness) IRTRAN 6 is preferable. Since the lens also serves as a pressure window, it must be thick enough to withstand rupture at Venus surface temperature and pressure. IRTRAN 6 has not been tested at high pressure and temperature, but a 6-mm thickness appears adequate based on a safety factor of 4.5 with the modulus of rupture measured at 373°K. If tests show unacceptable strength at high temperatures, then perhaps IRTRAN 4 or even IRTRAN 2 will be required. Our tests of IRTRAN 2 have demonstrated its suitability.

The solar radiometer accommodation is shown in Figure 3-72(b) with a dual sapphire wide angle lens system. The principal problem in this accommodation is compressing these two wide and divergent fields of view into a reasonable thermal penetration.

The window assembly consists of two wide angle telescopes with centerlines pointing 30 degrees above and below the horizontal, each with a half cone angle field of view of 30 degrees. Each telescope consists of three lenses. The first is a strongly negative lens with - 8 mm focal length and a clear aperture of 4 mm. The second and third lenses are identical positive lenses with + 8 mm focal length and 10 mm clear aperture. The two holes required in the pressure vessel and in the insulation are about 16 mm in diameter. A relay mirror system combined with the tuning fork chopper is then used inside the probe to transfer the "images" from the telescope onto the detector.

We recognize that the final solar radiometer chosen could well be one requiring a different accommodation from the one described here. This is discussed further in Section 3.2.2.3, Other Candidate Instrument Accommodations.

The nephelometer uses two windows with overlapping fields of view, a small window for the outgoing laser beam and a larger one for observing the cloud scattered laser light. Two separate windows are necessary to prevent laser scattered light within the window material from being detected by the experiment. The accommodation concept is illustrated in Figure 3-73. The laser window diameter is 11.5 mm and the viewing window diameter is 19 mm. The viewing window is designed as a lens with it prime focus at the pressure shell. Its focal length is 50 mm, resulting in a window aperture at the pressure shell of 9.3 mm diameter to provide a 0.18 rad (10 degree) full cone angle field of view.

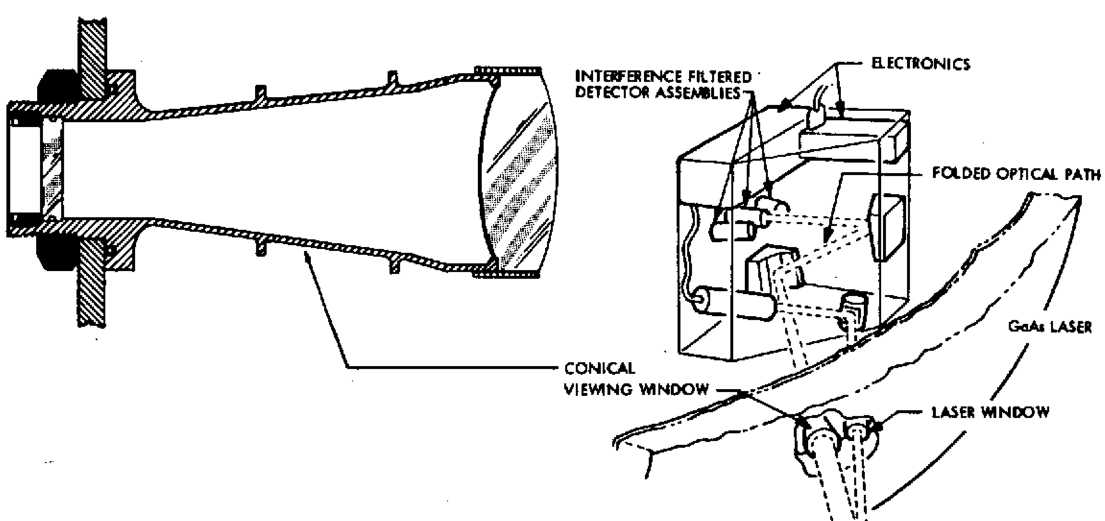

Figure 3-73. Nephelometer Accommodation

The angular placement of the two windows was determined to meet the requirement that the region of overlap between the source and viewing fields of view be centered beyond the probe boundary layer and wake. This distance is estimated to be 15 cm beyond the exterior of the insulation. The smallest practical separation between centers of the two window assemblies at the pressure shell is 5.1 cm, which results in an angle of 0.28 rad (16 degrees) between the source and viewing windows.

The cloud particle size spectrometer requires special alignment considerations due to the high spatial resolution imaging characteristic of the instrument. The mounting method illustrated in Figure 3-74 provides a single mounting point for the entire optical assembly. The pressure shell feed-through is an integral part of the internal optical assembly. It is mounted to the hole in the pressure shell with the jam nut on the outside. To minimize the distortion loading on the optical assembly during entry, the assembly is arranged with its long axis along the deceleration axis. The 12.5 cm length of the external mirror mount resulted from a tradeoff between clearance during aeroshell separation and a requirement to project it beyond the probe boundary layer and wake.

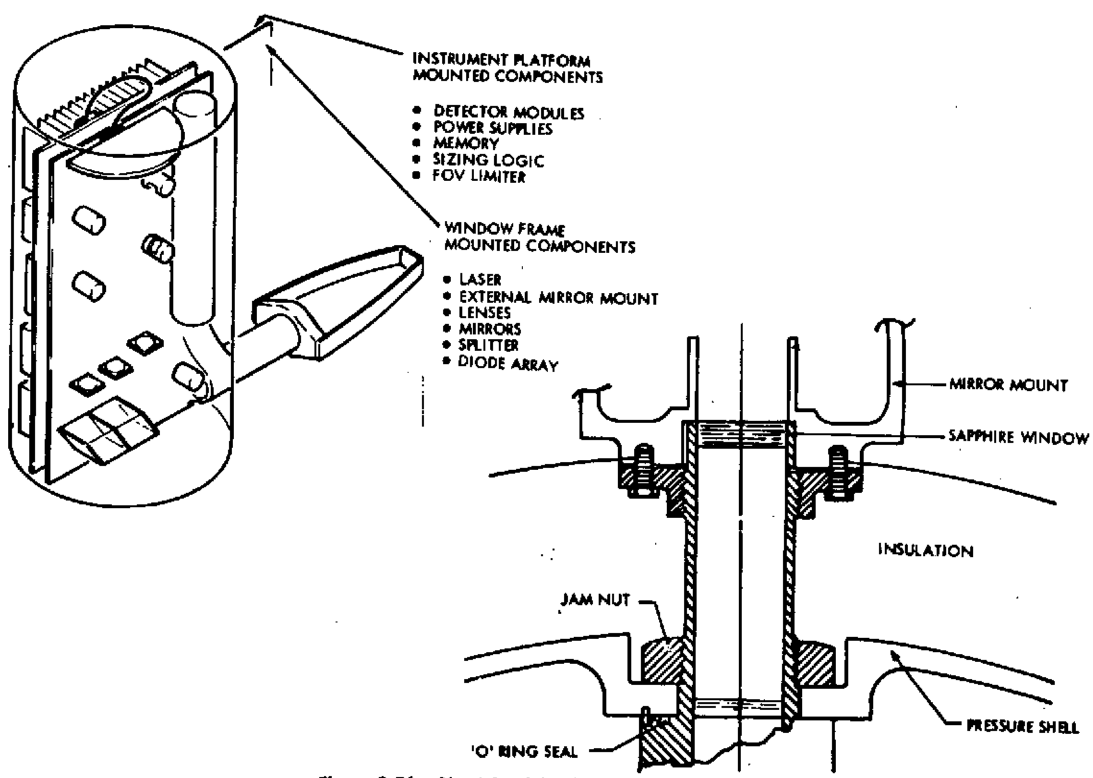

Figure 3-74. Cloud Particle Size Spectrometer

The aureole extinction detector uses a pair of externally mounted collimators pointing 20 degrees above the horizon (the solar elevation) as shown in Figure 3-75. The principal objectives of the aureole detector involve measurements relating to the sun as a discrete source, but below 50 to 55 km the sun is totally diffused by the clouds. Therefore, the

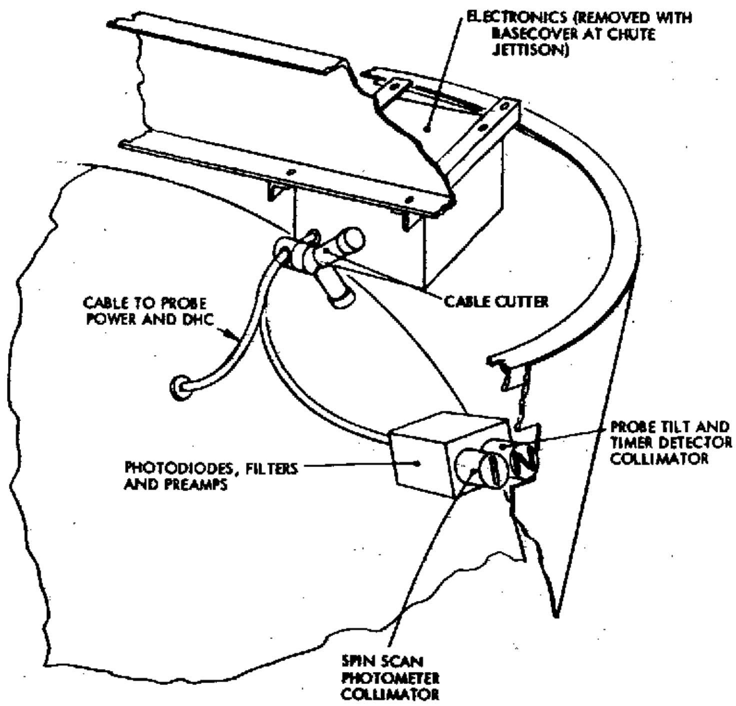

Figure 3-75. Aureole Extinction Detector Accommodation

aureole experiment ends with the parachute jettisoning (49.72 km). This allows the entire instrument (collimators, optics, detectors, and electronics) to be placed outside the pressure vessel since the temperature and pressure do not exceed 354°K and 0.129 MN/m^2 before parachute jettison. The experiment electronics package is attached to the aft part of the afterbody and is also jettisoned with the parachute.

The mass spectrometer mechanical accommodation involves providing a large access hole through the pressure shell and insulation to mount the complex multiple inlet system. This requires a hole 7.6 cm in diameter. The mounting is again on the equipment ring assembly and is illustrated in Figure 3-76(a). The instrument is mounted with its long axis along the deceleration axis and with particular attention to the quadrupole rods. Attachment is to the pressure shell and the instrument platform so that the deceleration loads do not produce a torque at the inlet attachment point. The probe supplies two-stage heater power to the inlet and ordnance control logic and firing power for the sequentially operated inlet tubes.

The pressure gauge is required to have its inlets near the stagnation point. To accommodate it in the equipment ring assembly, the feed-through is located there with two extension tubes going to two locations π

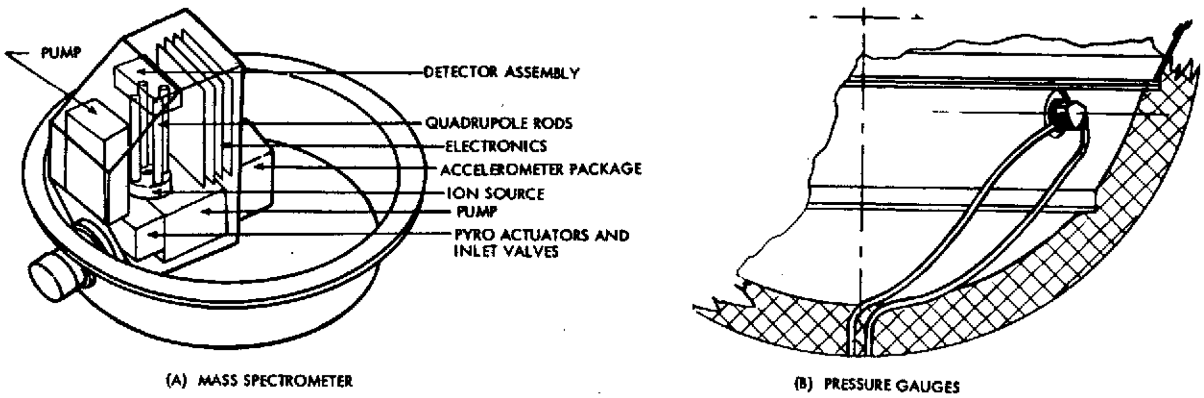

Figure 3-76. Mass Spectrometer and Pressure Gauges Accommodation

radians apart near the stagnation point, as shown in Figure 3-76(b). The diameter-to-length ratio of the tube is great enough to maintain a pressure response time of about 3 ms.

The temperature gauges are required to be located on either side of the probe with their cylindrical radiation shields parallel to the flow velocity, beyond the boundary layer, and at the position of maximum mass flow. Sensor protrusions, as shown in Figure 3-71, are suited ideally for satisfying these requirements on the equipment ring assembly.

The accelerometer is the only instrument that requires no sensor access to the outside. The sensor and electronics are mounted as shown in Figure 3-77 near the center of mass of the probe. The primary axial sensor is precisely at the center of mass with its sensitive axis along the spin axis. The approximate location for the instrument will be determined from calculations of the inertial axis and center of mass and verified on the test models.

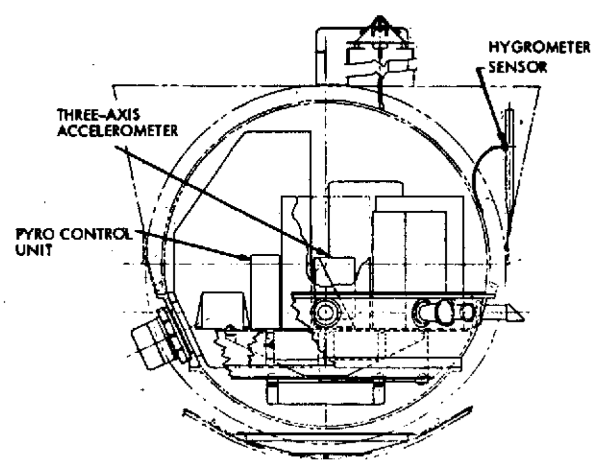

Figure 3-77. Accelerometer Sensor and Electronics Locations

The shock layer radiometer has a unique accommodation feature because it only operates during entry deceleration. Therefore, it can be mounted entirely outside of the pressure vessel and insulation as shown in Figure 3-78. This compact arrangement allows the entire instrument to be

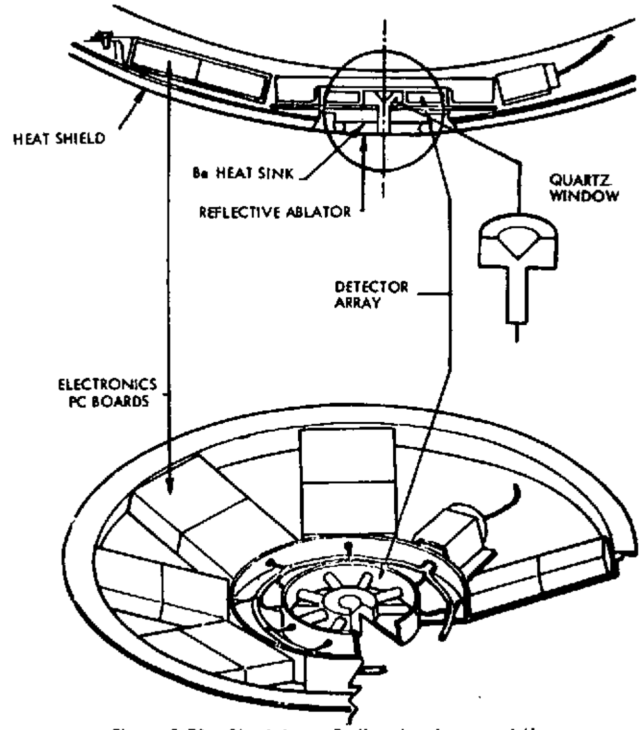

Figure 3-78. Shock Layer Radiometer Accommodation

packaged behind the aeroshell and heat shield with a special four-element heat shield section for the window. This section was specially designed to provide a mounting for the quartz viewing window to prevent the field of view from being contaminated by ablation products. These products would give erroneous upper atmospheric composition. The ceramic quartz reflective ablator produces no ablation products. It is backed up with a beryllium heat sink with enough heat capacity and thermal conductivity to absorb the heat pulse from the ablator. The ablator is held in place with a beryllium heat sink with enough heat capacity and thermal conductivity to absorb the heat pulse from the ablator. The ablator is held in place with a machined carbon ring mounted into the heat shield with the beryllium by a phenolic tape wrapping. This design is discussed in Section 7.2.

The quartz window behaves like a right-angle prism directing shock front excitation light into the radial array of 10-pin photodiode detectors. The outputs are fed into the electronics PC boards laid in a tray surrounding the detectors. The electrical interface between this tray-mounted instrument and the probe power and data handling subsystems is through a cable cutter assembly that activates on aeroshell separation.

Inflight calibration of the shock layer radiometer can be provided without the use of a power-consuming lamp, i.e., β-light source used to illuminate exit signs on commercial aircraft. This would consist of a phosphor mixture with wavelengths of the radiometer channels excited by a Tritium or Krypton 85 source. This illuminator would be mounted on the inner surface of a protective cap, which is removed before entry. The light intensity at the quartz window required in each filter transmission band would be in the range of 10^{-1} to 10^{5} watts/(m^2 ster). This represents the sensitivity range of the detector and optics.

Thermal

To minimize heat leakage into the probe, instruments should not be mounted physically to the pressure vessel, but mounted in contact with the internal instrument platform. Some instruments will have elements that must be tied structurally to the external and internal pressure vessel surfaces.

The thermal characteristics of the mechanical attachment are designed to promote heat transfer between the instruments and the instrument platform. Assuming such heat transfer properties, the instrument platform temperatures will reach the values shown in Table 3-18 at the indicated times during the large probe descent. The temperatures of the equipment ring assembly are also shown to identify the thermal environment for those parts of the experiments that must be mounted directly on the pressure shell ring.

Table 3-18. Temperatures of Instrument Platform and Pressure Shield Ring

EVENT	TIME (HR)	PLATFORM (°K)	RING (°K)
AEROSHELL SEPARATION	0	270	270
CHUTE RELEASE	0.400	276	290
	0.600	282	339
SURFACE IMPACT	0.825	300	415

Thermal control is provided by thermal insulation, coatings, and science window heaters on the descent capsule and the aeroshell heat shield to maintain an environment assuring that all probe components are within their temperature limits for all mission phases.

The large probe temperature limits, interior and exterior to the pressure vessel as a function of the mission phase, are given in Table 3-19.

Table 3-19. Large Probe Temperature Limits

MISSION PHASE	INTERIOR TO PRESSURE VESSEL (°K)	EXTERIOR TO PRESSURE VESSEL (°K)
PRELAUNCH (OPERATING)	256 TO 305	256 TO 325
PRELAUNCH (NONOPERATING)	256 TO 302	227 TO 344
LAUNCH AND CRUISE (NON-OPERATING)	256 TO 302	227 TO 344
CRUISE (OPERATING)	256 TO 305	256 TO 325
DESCENT (OPERATING)	266 TO 339	256 TO *

* EACH EXTERIOR COMPONENT MUST BE DESIGNED WITH UPPER TEMPERATURE LIMIT CONSISTENT WITH MAXIMUM ATMOSPHERIC TEMPERATURE FOR WHICH IT IS INTENDED TO OPERATE.

The various windows and optical feed-throughs illustrated in Figures 3-72, 3-73, and 3-74 have thermal considerations as an essential part of their designs. The thin-walled rib reinforced stainless window supports have low thermal conductance. The optical design to produce minimum diameter penetrations help reduce the heat leak. The double window construction minimizes convective heat leaks to the probe interior.

All exterior windows (or lenses) will be provided with heaters to keep them above ambient temperature to prevent condensation. The need to minimize heat leakage from the exterior window to the probe interior is particularly important when this window heating is considered (both from the standpoint of conserving heater power and reducing the probe interior heating). The design considerations in window heating for four different types of heaters are discussed in Section 3.1.2.1.

Electrical and Power

Each scientific instrument will receive electrical power through an individual, fused, branch circuit as listed in Table 3-20. The branch circuit will be energized/de-energized by probe sequencer control. The power allotted to the instrument is measured at the spacecraft/instrument interface connector. All power conditioning will be synchronized by the probe supply.

Table 3-20. Large Probe Instrument Load Characteristics

INSTRUMENT	FUSE RATING (AMPS)	VOLTAGE (VOLTS)	AVERAGE CURRENT (AMPS)	PEAK CURRENT (AMPS)
TEMPERATURE GAUGE	1/8	28 ± 10%	0.036	
PRESSURE GAUGE	1/8	28 ± 10%	0.036	
ACCELEROMETERS	3/8	28 ± 10%	0.082	0.2 AMP AT 400 G FOR 10 SECONDS
NEPHELOMETER	1/4	28 ± 10%	0.071	
NEUTRAL MASS SPECTROMETER	2	28 ± 10%	0.86 (MAX.)	
CLOUD PARTICLE SIZE SPECTROMETER	2	28 ± 10%	0.72	
SOLAR FLUX RADIOMETER	3/8	28 ± 10%	0.16	
PLANETARY FLUX DETECTOR	3/8	28 ± 10%	0.16	
AUREOLE/EXTINCTION DETECTOR	1/4	28 ± 10%	0.071	
SHOCK LAYER RADIOMETER	1/8	28 ± 10%	0.036	
HYGROMETER	1/16	28 ± 10%	0.011	

NOTE: FUSE TYPE IS LITTLEFUSE 256 SERIES, PICOFUSE

Except for the transient voltage excursions specified below, the peak-to-peak amplitude of any voltage excursion, periodic or aperiodic, will not exceed 1.0 volt at any frequency between 30 Hz and 10.0 kHz decreasing at 6 dB/octave to 0.5 volts at 20.0 kHz and remaining at 0.5 volts through 100 MHz. Instruments should be designed to accommodate, without performance degradation, voltage transients up to +42 VDC or down to +18 VDC for durations of 10 microseconds or voltages down to +20 VDC for durations of 500 milliseconds on the nominal +28 VDC bus. The instruments should be designed so that no damage, long-term degradation, or modes, where proper performance is not automatically resumed when the transient is removed, should occur when 10 microsecond voltage transients up to +56 VDC or down to 0 VDC are seen on the nominal +28 VDC bus.

Pressure vessel electrical feed-throughs will be provided for the temperature sensor, aureole/extinction detector, shock layer radiometer, hygrometer, and the accelerometer calibration connector. These feed-throughs are shown in Figure 3-79. The connector provided on the spacecraft harness for connection to the various science instruments will be female (straight or coaxial insert) pin connectors selected from the Cannon nonmagnetic series (NMC-A-106 suffix).

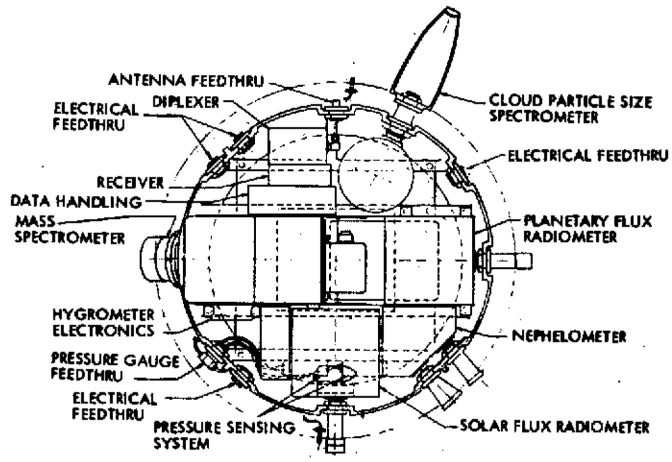

Figure 3-79. Plan View of Equipment Ring Assembly Showing Instrument Electrical Feedthroughs

<u>Data Handling and Command</u>

The large probe DHC will accept information in digital, analog, or bilevel form, convert the analog information to digital form, and arrange all information in an appropriate format for time multiplexed transmission to earth or storage on board the probe. The probe will also supply the instruments with various timing and operational status signals and functional commands. A telemetry word in all formats will consist of 8 or 10 bits. Probe-generated words will be transmitted with the most significant bit first. See Section 7.7 for detailed discussion of the DHC.

3.2.2.2 Small Probe Instrument Accommodation Concepts

<u>Structural and Mechanical</u>

An important accommodation feature for the small probe experiments is an integral packaging configuration. This was motivated by the intent to reduce stray magnetic fields and by the required high packing density. This configuration, illustrated in Figure 3-80, is characterized by locating the electronics for all the instruments (except the nephelometer) with the data handling system in a single box. The other units in the small probe are all

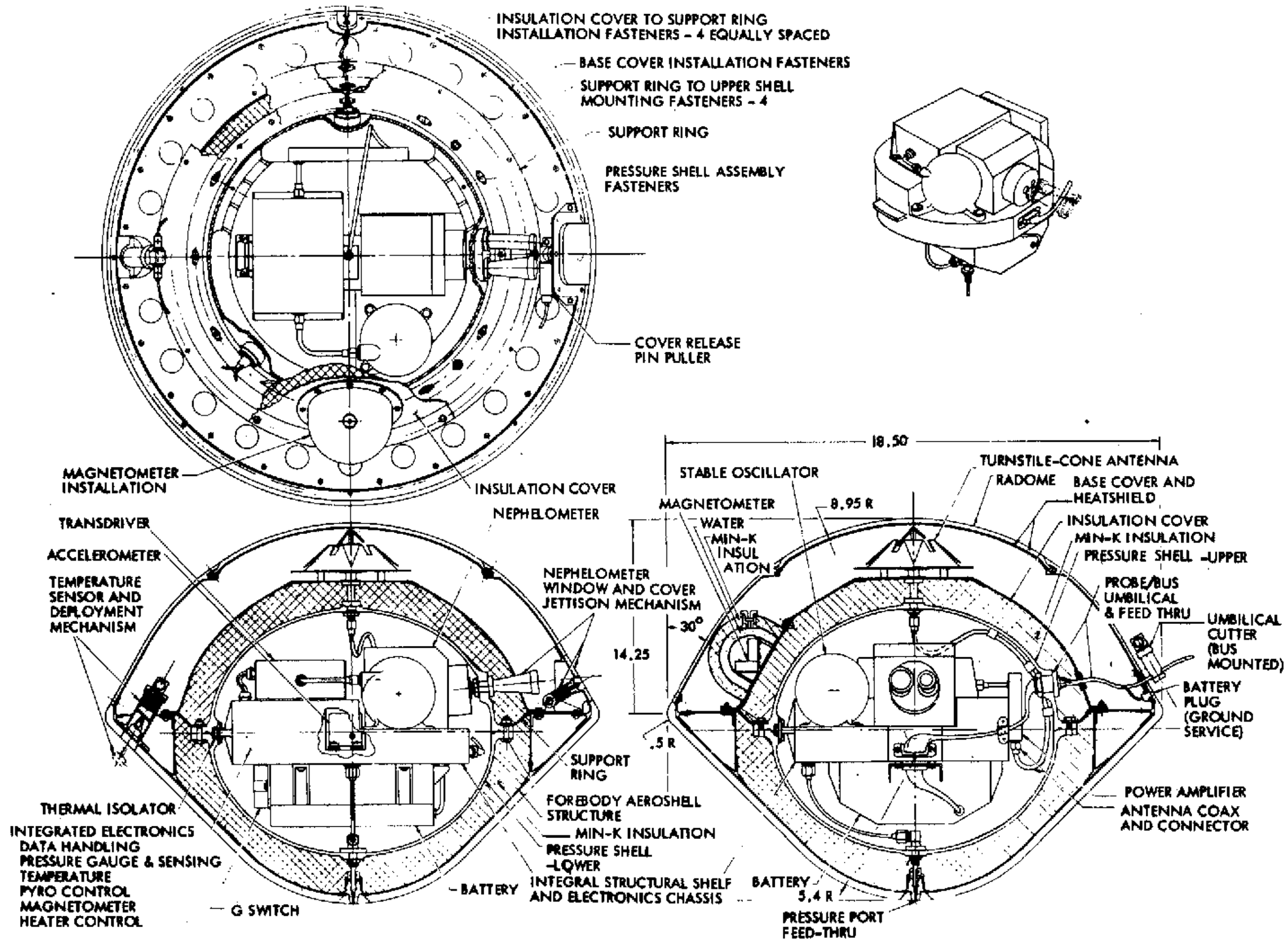

Figure 3-80. Small Probe Configuration for Thor/Delta Launch Vehicle

mounted directly onto this box, which serves as an equipment shelf. On the large probe the shelf was extended to provide a section of the pressure vessel wall. This facilitates installation of the large number of instruments that use windows or inlets through the pressure vessel, including the mass spectrometer and cloud particle size analyzer, where the penetration is an integral part of the instrument structure. On the small probe only, the nephelometer uses a window and is not an integral part of the instrument. Therefore, the equipment shelf does not extend through the pressure vessel, a simpler arrangement.

Another important characteristic of the small probe instrument accommodation results from retention of the aeroshell for the entire descent. Therefore, such sensors as the pressure and temperature gauges, and nephelometer require methods of exposing them to the environment after entry.

The temperature sensor, discussed earlier in Section 3.1.2.1 for the large probe, is required to project beyond the boundary layer at the position of maximum mass flow and to have its cylindrical radiation shield aligned parallel to the flow field. However, since the aeroshell stays with the probe, a spring-loaded deployment mechanism (shown in Figure 3-80) is included in the accommodation. This mechanism, which is essentially the same as that used on PAET and Viking, pushes out a plug in the aeroshell at the time of deployment and places the sensor at the desired position and orientation in the airstream.

The pressure gauge opening, as with the large probe gauge, must be located near the stagnation point. The pressure port feed-through shown in Figure 3-80 is specially designed to withstand the entry environment and yet provide gauge access to the stagnation point pressure. This design is discussed in Section 7.2.

The two nephelometer windows, for the laser source and for the cloud-reflected light, are mounted exactly the same as on the large probe to provide intersecting fields of view beyond the boundary layer and wake. The pressure shell penetrations are also similar to those on the large probe with threaded fitting and jam nut through a penetration in the upper section of the shell. Following probe entry, a section of the afterbody is removed by the window cover jettison mechanism, providing a dear field of view for the instrument.

The single-axis accelerometer requires placement at the probe center of mass with its axis aligned parallel to the probe spin axis. To fit at the center of mass it is nested in the center of the integrated electronics module. The mounting technique involves the same type of adjustment procedure as discussed for the large probe.

The principal accommodation required for the probes' stable oscillator is its thermal control. The method used here is essentially that discussed in a report from the Thermal System Design Project at the Johns Hopkins Applied Physics Laboratory. (Transmittal letter ASD: 244-9/32-032, "A Preliminary Study Report for the Thermal Control Design of a Venus Descent Probe Transmitter Oscillator," Internal Report 545-72-074, July 12, 1972). The sphere shown in Figure 3-80 is a container with a shell of phase change material. Our analysis shows that when the power dissipated by the oscillator is included, the temperature of the oscillator will remain constant to within 3 K degrees.

The magnetometer accommodation is most challenging because of the need for low background magnetic fields. The integrated electronics approach discussed above is oriented to meet this requirement by reducing the stray fields generated by interconnecting wires and increasing the separation between the sensor and field producing assemblies. Several "good housekeeping" techniques, such as using hybrid electronics and side brazed and bottom brazed dual in line packages (DIPS), can also be employed to reduce the remanent fields at the sensor. The traditional approach of putting the sensor on a boom to remove it from spacecraft fields is difficult in this case due to probe aerodynamics requirements and the severe environments. The tradeoffs between magnetic cleanliness programs and a thermally protected external sensor mounting are discussed in Section 3.2.2.4. The accommodation method chosen is shown in Figure 3-80 with the sensor mounted outside the pressure vessel, but inside the aeroshell afterbody. Its thermal protection is provided by the water jacket heat sink surrounded with Min-K insulation. This location provides the maximum separation from the probe remanent fields without the use of a deployment mechanism.

Thermal

To minimize heat leakage into the probe, only the penetration part of the science instruments is attached to the pressure vessel and the electronic circuits are contained in the integrated electronics assembly. The average temperature of the interior assembly at the time of planet surface impact will be 331°K and the average pressure shell temperature will reach 551°K.

Thermal control of the descent capsule is provided by thermal insulation, coatings, phase change material, and a nephelometer window heater. The aeroshell heat shield provides thermal control during the entry heating period to maintain an environment assuring that all probe components are within temperature limits.

The small probe temperature limits, interior and exterior to the pressure vessel as a function of the mission phase, are given in Table 3-21 under both operating and nonoperating conditions.

Table 3-21. Small Probe Temperature Limits

MISSION PHASE	INTERIOR TO PRESSURE VESSEL (°K)	EXTERIOR TO PRESSURE VESSEL (°K)
PRELAUNCH (OPERATING)	256 TO 305	200 TO 366
PRELAUNCH (NONOPERATING)	256 TO 302	200 TO 366
LAUNCH AND CRUISE (NONOPERATING)	256 TO 302	200 TO 366
CRUISE (OPERATING)	256 TO 305	200 TO 366
DESCENT (OPERATING)	266 TO 339	200 TO *

* EACH EXTERIOR COMPONENT MUST BE DESIGNED WITH UPPER TEMPERATURE LIMIT CONSISTENT WITH MAXIMUM ATMOSPHERIC TEMPERATURE FOR WHICH IT IS INTENDED TO OPERATE.

Electrical and Power

The small probe electrical power subsystem is discussed in Section 7.8. Each instrument will receive electrical power through an individual fused, branch circuit as described in Table 3-22. All power conversion will be synchronized by a probe-generated oscillator drive signal. The branch circuit will be energized/deenergized by probe sequencer control. The power allotted to the instrument is measured at the spacecraft/instrument interface. Transient voltage and peak-to-peak voltage excursions for the small probe are the same as those defined for the large probe. Pressure vessel electrical feed throughs will be provided for the temperature sensor, magnetometer, and the accelerometer calibration connector.

Table 3-22. Small Probe Instrument Load Characteristics

INSTRUMENT	FUSE RATING (AMPS)	VOLTAGE (VOLTS)	AVERAGE CURRENT (AMPS)	PEAK CURRENT (AMPS)
ACCELEROMETER	1/4	+28 VDC ± 10%	0.036	0.16 AT 400 G PEAK, DURATION 10 SECOND
PRESSURE	1/16	+28 VDC ± 10%	0.02	
TEMPERATURE	1/16	+28 VDC ± 10%	0.02	
MAGNETOMETER	1/16	+28 VDC ± 10%	0.036	
NEPHELOMETER	1/4	+28 VDC ± 10%	0.071	

Data Handling and Command

The small probe DHC will accept information in digital, analog, or bilevel form, convert the analog information to digital form, and arrange all information in an appropriate format for time multiplexed transmission to earth or storage on board the probe. The probe will also supply the instruments with various timing and operational status signals and functional commands. A telemetry word in all formats will consist of 7 or 10 bits. Probe-generated words will be transmitted with the most significant bit first. See Section 7.7 for detailed discussion of the DHC.

3.2.2.3 Other Candidate Instrument Accommodations

The accommodation discussions in the previous sections were based on the nominal payload list of instruments. In addition to this list, there are alternative experiments, some of which could conceivably be in the final list of experiments to fly on the Pioneer Venus probes. The large probe list includes X-ray fluorescence, gas chromatograph, attenuated total reflectance spectrometer, wind drift/altitude radar, atmospheric electrical phenomena detectors, and electrostatic probe. Other candidates for the small probe include a radar altimeter and net flux radiometer. In addition, instrument configurations other than the ones illustrated for the nominal payload might be significantly different, and some instruments on the nominal payload may not be on the final list.

One example of accommodating a different instrument configuration is a possible solar radiometer configuration. This configuration has four solar flux sensors, two of which require a 2π ster upward field of view and two that need a similar field of view downward. Instead of trying to install these on the equipment ring assembly, it is preferable to mount the four sensor assemblies separately directly onto pressure shell penetrations in the upper and lower parts of the pressure shell. Figure 3-81 illustrates the mounting for one of these sensors. The light guide and pressure tube end of the module with detectors, filters, and preamp is inserted through the pressure shell from the inside and attached with a jam nut on the outside. The diffuser head is then screwed onto the end of this assembly from the outside to produce a seal at the metal O-ring. Before final assembly, the flexible electrical connector and fiber optic calibration light guide are attached. Identical assemblies are used for the other three sensors, but with slightly different diffuser heads.

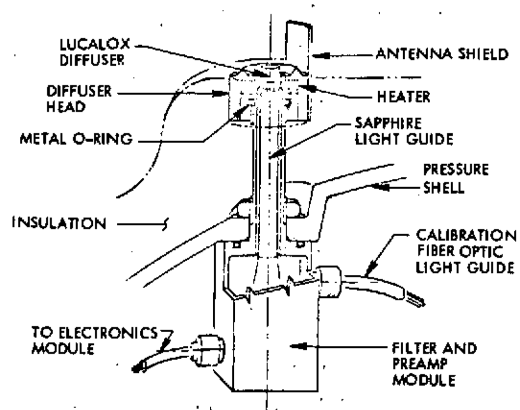

Figure 3-81. Upper Hemisphere Cos θ Response Flux Detection for Solar Radiometer

An example of accommodation for an experiment not on the nominal payload is illustrated in Figure 3-82 for the attenuated total reflectance spectrometer. In this arrangement, collimated IR light is directed by mirrors to enter the diamond window for total reflectance at its exposed surface. The light experiences a total of seven internal reflections from the front and back surfaces of the diamond with four of these occurring at the front (exposed) surface where the Venus atmosphere constituents can introduce their characteristic absorption spectra.

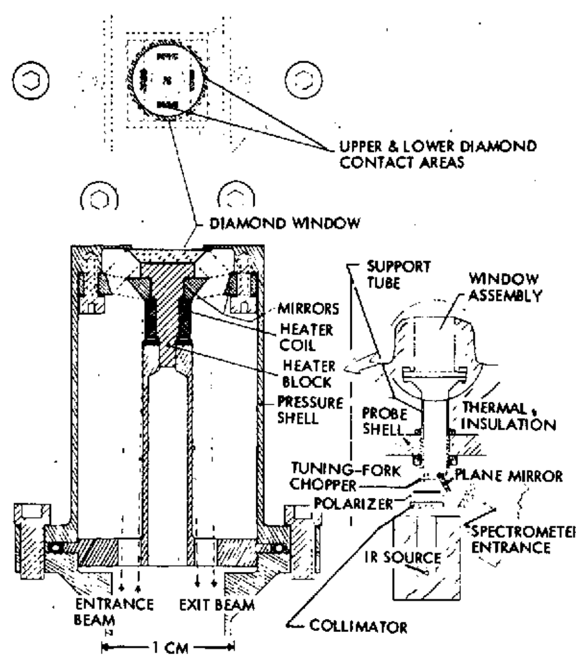

Figure 3-82. Attenuated Total Reflectance Spectrometer Window Assembly Design Concept and Optical Configuration

We have considered the accommodation of not only the "other candidate instruments" listed in the Science Definition Report, but also those additional and alternative instruments proposed to NASA last December. With the exception of two alternative solar radiometer configurations, we could accommodate any of these instruments on a replacement basis (weight and power) for any instrument now in the nominal payload. The two alternative solar radiometers, which utilize four wide field windows in pairs near the top and bottom of the probe, would require a departure from our concept of attaching instruments and windows to the equipment ring assembly and would somewhat complicate probe assembly and disassembly. Accommodating one of these would be particularly complex because of the use of light pipes to connect the four sensor packages to a single calibration source, as shown on Figure 3-81.

Although there is space available inside and outside the large probe pressure vessel for quite a few other candidate instruments (i.e., gas chromatograph, attenuated total reflectance spectrometer, wind/altitude radar, atmospheric electrical phenomena detectors, electrostatic probe, and X-ray fluorescence spectrometer) there is no weight or power margin available to them on the Thor/Delta large probe.

As designed, the small probe accommodates all the nominal instruments listed in the Science Definition Report. An RF altimeter and net flux radiometer are the only other proposed candidates. Although there is enough space available to add the proposed net flux radiometer (71 cm^3), there is no weight margin available on the Thor/Delta small probe for the instrument with the complex boom/window deployment mechanism it requires. The volume requirements for the RF altimeter could just be met if the instrument were divided into three or four segments. Furthermore, if a loop antenna for this instrument embedded in the aeroshell can not survive the entry temperature or transmit through the carbonized ablator, then a considerable weight penalty may be imposed for one alternative concept that requires the removal of a cap after entry and the deployment of a small yagi antenna. A second alternative concept using two whip dipoles (lashed around the probe base cover and released after entry) would impose a smaller weight penalty. We also considered the impact of alternative candidates proposed for the nephelometer. A proposed aft-looking nephelometer with a series of external reflecting targets would impose a significant penalty in heating and deploying the external targets.

3.2.2.4 Payload Conflicts and Problem Areas

Descent Capsule Roll Rate

The roll rates required by the aureole/extinction detector appears to conflict with roll rates which are preferable for the solar radiometer. A requirement to make 10 measurements/km is identified for the aureole experiment. Since the basic purpose of the aureole detector is to measure the halo about the sun, a measurement would be required on each probe revolution, i.e., each time the field of view crosses the sun. Therefore, the requirement is interpreted as 10 rev/km = 20π rad/km. This corresponds to roll rates of 4.4 rad/sec to 0.79 rad/sec over the velocity profile of the descent capsule, which ranges from 70 to 12.5 m/sec. On the other hand, a roll rate requirement of 0.52 to 0.10 rad/sec is identified for the solar radiometer. Thus, it is not possible to simultaneously satisfy both instruments. We examined three compromise arrangements to resolve this discrepancy:

1) Define the altitude region before parachute jettison (above 49.75 km) as top priority for the aureole experiment and the region below this as top priority for the solar radiometer by installing two sets of roll fins on the probe. One set on the afterbody would control the roll rate at 20π rad/km for the aureole experiment while on the parachute. The other set on the probe sphere would be shielded by the afterbody while on the chute, but would be exposed to the airflow after parachute jettison (the afterbody is jettisoned with the chute). This approach satisfies the stated requirements within the limitations of the priority region definitions for the two experiments.

2) Establish an average roll rate with a single set of roll fins that compromises the two nonoverlapping ranges. Such a roll rate could be 6π rad/km, resulting in a range from 0.25 to 1.06 rad/sec after parachute jettison. This approach does a poor job of satisfying each requirement.

3) Use a single set of roll fins to satisfy the aureole requirement and use a programmed sampling rate for the solar radiometer to satisfy the intent of the requirement more adequately than the requirement itself. The solar radiometer roll rate requirement is based on the experimenter's desire to obtain azimuthal distributions of sunlight about complete 2π radian scans. The preferred azimuthal resolution is $\pi/3$ radians (60 degrees). Therefore, an ideal measurement would be obtained by adjusting the sampling

rate to obtain six measurements per revolution and limiting the number of data-taking revolutions in keeping with the data allocation for the instrument. It is not practical to continually adjust the sampling rate to give a $\pi/3$ radian scan with the continually varying probe roll rate. It is preferable to use three discrete sampling rates to be selected sequentially during descent. In this way, the azimuthal resolution is maintained at $\pi/3 \pm 23$ percent.

Of the three approaches described above, the order of preference is three, one, two. The second approach is essentially unacceptable. It falls short of satisfying the objectives for either experiment because the stated required roll rates of 0.52 to 0.1 rad/sec are too large for the $\pi/3$ resolution. Based on the specified 25 seconds per measurement, the resolution at the specified roll rates becomes 2.6 to 13.1 radians per measurement, all of which are considerably larger than $\pi/3 \sim 1$.

The use of dual roll rates appears attractive; however, the specified roll rate requirement for the solar radiometer is not satisfactory for the solar radiometer objectives. The assumption that the solar radiometer objectives should be completely subjugated to the aureole objectives at altitudes above 49.75 km is not necessarily a good one.

The use of a single set of roll fins with programmed sampling of the radiometer is the most satisfactory solution since it can satisfy the objectives of both experiments. Because of limitations in data capacity, measurements must be limited to 5/kilometer rather than 10; and therefore, the roll rate can be set for 10π rad/km rather than 20π. The programmed sampling rate is set at three discrete values of 1.4, 0.7, and 0.48 measurements per second, where a measurement for this experiment is defined as one 100 bit word. Thus, for example, the first two sets of six measurements are taken at 1.4 per second, the next two at 0.7 per second, and the next four at 0.48 per second. The time interval between 600-bit sets is 118 seconds (1.97 minutes) until the probe reaches 30 km when the interval is increased to 135 seconds (2.25 minutes). These sampling rates with corresponding roll rates, descent velocities, altitudes, and times are shown in Table 3-23. The last column in the table shows δ, the percentage deviation of resolution from $\pi/3$.

Small Probe Magnetic Cleanliness

The instrument with the major impact upon the probe systems is the small probe magnetometer. In our study, we evaluated technical approaches

Table 3-23. Measurement Rates for Solar Radiometer

H(KM)	T(MIN)	V(M/S)	ω(RAD/S)	N(MEAS/S)	δ (%)
70	0	56.0	1.76		-20
64.7	1.97	35.3	1.11	1.4	23
61.3	3.94	27.2	0.86		-17
58.4	5.91	22.1	0.69	0.7	5
55.8	7.88	18.5	0.58		-16
53.5	9.85	16.0	0.50		0
51.7	11.82	14.6	0.46	0.48	11
50.1	13.79	14.0	0.44		13
PARACHUTE JETTISON					
45.4	15.76	56.5	1.77		-21
40.0	17.73	44.0	1.38	1.4	6
35.2	19.70	36.1	1.13		23
31.1	21.67	31.1	0.98		-17
DATA RATE CHANGE					
27.0	23.92	26.8	0.84		0
23.8	26.17	23.5	0.74		12
20.5	28.42	22.0	0.69	0.7	17
18.0	30.67	20.5	0.64		23
15.3	32.92	19.0	0.60		-19
13.0	35.17	17.6	0.55		-10
10.5	37.42	16.6	0.52		- 3
8.7	39.67	15.5	0.49		3
6.6	41.92	14.8	0.47	0.48	7
5.0	44.17	14.0	0.44		13
3.2	46.42	13.4	0.42		16
1.5	48.67	12.9	0.41		20

to accommodate this sensor at different levels of magnetic cleanliness. We also examined approaches to meet the experiments supporting requirements of controlled probe roll and planet reference. Finally, we evaluated the cost impact of accommodating the sensor and its supporting requirements. The results of these studies are summarized here and detailed in Appendix 3B.

From a matrix of magnetic control levels and candidate sensor locations examined, we selected a location inside the aeroshell but on the outside of the pressure vessel insulation. This choice is a compromise between experiment performance and the cost and weight factors to accommodate the sensor.

The sensor would see a background from the probe of approximately 300 nT. This is considerably greater than the 100 nT indicated in the SSG report but (in the light of subsequent numbers furnished to NASA/ARC by the co-investigators) is probably adequate. Implicit with this would be a comprehensive magnetic cleanliness program for the system contractor (and for the GFE instruments) and the development of a semi-active thermally protected (to 583^{o}K) enclosure for the sensor. A program to develop a sensor to operate to 583^{o}K is also required. The selected approach is feasible from technological and schedule viewpoints, but the cost and weight factors may be impractical for Pioneer Venus. We have not included the experiment support items of planet reference and roll control. These have significant additional cost and weight impact (as discussed in Appendix) 3B) and according to at least one of the investigators are not firm requirements.

Another facet of accommodating the magnetometer arose with the disclosure of a significant leakage field from the permanent magnet in the force rebalancing type of accelerometer being considered for Pioneer Venus. Although the specific model accelerometer for the small probe does not yet exist, measurements made by the manufacturer of similar models (Bell Models VII and IX) indicate values as high as 7×10^{-4} Tesla (7 Gauss) at the sensor case. The test conditions described to us by the manufacturer had some shortcomings. The implications were significant to warrant conducting our own measurements. Three Bell Model VII sensors were obtained for this purpose and were surveyed in our Magnetics Laboratory. The results of our measurements were no greater than 4800 nT at 2 cm from the bare sensor case, but as high as 10 800 nT (in one axis and 11 800 nT in another) at 2 cm from the case of a sensor with an attached cable. Undoubtedly, the cable contributed some part of this field, but how much was not determined, because we did not remove the cable from the borrowed sensor ($\sim$50 percent variation was noted in the values from the two bare sensors). Extrapolating these data to the Model XI is difficult due to the nonlinear behavior of magnetic fields. However, the Model XI may have less inherent shielding in its structure. Therefore, the field strength may be as great or greater than the Model IX (which is greater than the Model VII). The smaller size of the new sensor may offset this somewhat in the field seen at the magnetometer sensor.

As a result of this study, we recommend including magnetic compensation of the small probe accelerometer. Compensation was chosen over shielding because the "soft" shield material properties may change with temperature during probe descent.

The accelerometer field has implications for the large probe if a quadruple mass spectrometer is chosen for Pioneer Venus. The leakage field from three Model IX accelerometers could impose upon the spectrometer's analyzing field and degrade that instrument's resolution. We recommend shielding the accelerometers because it is simpler to accomplish than compensation, and the variation with temperature of the shield properties would not be significant in this application.

Another source of probe magnetic field is from the ion pumps used on various mass spectrometers and the analyzing field on magnetic sector mass spectrometers. Since the mass spectrometer is on the large probe, and the magnetometer is on the small probe, these fields will not affect the magnetometer. However, it is possible that a large leakage field from the mass spectrometer could affect the accelerometer in the same manner that the accelerometer field could degrade the mass spectrometer. At worst, this would impose a constant offsetting force to the accelerometer sensing mass. It appears that no interference existed between these two instruments on PAET, and none exists in the Viking Lander. Nevertheless, a specific evaluation for Pioneer Venus should be made when the specific instruments are selected.

3.2.2.5 Engineering Experiments to Improve Future Probe Design

We considered the following questions related to probe design:

1) What are the existing uncertainties that may result in overdesign of a specific subsystem?

2) What are the resulting penalties in any overdesign in terms of weight, data handling capacity, power, thermal control, etc?

3) How may the uncertainties and their associated penalties for subsequent probe missions be reduced by measurements on the present probe?

For convenience, each subsystem was considered separately, listing the major environmental factors associated with some uncertainty. A qualitative estimate of that degree of uncertainty was made so that the relative significance of the various items may be evaluated. In the thermal control, heat shield, communications, pressure vessel, and power subsystems engineering data would aid in reducing these uncertainties.

Thermal Control Subsystem

The properties of the surface coatings, principally absorptivity, currently have a large uncertainty. Testing will probably not provide enough information to significantly reduce the uncertainty. Measurement of the backface temperature of the aeroshell prior to entry would be useful in evaluating the performance of the surface coatings and determining whether any changes should be made for future missions.

As noted in Table 3-24, insulation performance unknowns are a significant contributor. Some weight penalty may be associated with the uncertainty in insulation performance. Again, tests will be performed to provide information; however, the cost per test is significant. Additionally, coupon tests do not accurately represent the actual probe in terms of penetrations, thermal joints, geometry, etc. Engineering data obtained from measurements on-board the probe (i.e., implanted thermocouples) would provide information to aid in understanding the behavior of the probe insulation materials. These measurements will provide information relative to basic insulation performance and will allow an estimate of the exterior film coefficients. For the large probe, knowledge of film coefficient values could be used to obtain a backup estimate of the probe descent velocity. Additionally, such information would aid in design of any follow-on planetary probe missions. Engineering measurements planned for Pioneer Venus will obtain the necessary data. Specifically, these measurements include temperature of the aeroshell forebody and afterbody, probe interior pressure, temperature of the equipment platform, exterior insulation temperature, and exterior pressure shell temperature.

Thermal coupling uncertainties are primarily concerned with heat transfer from the pressure shell to the internal equipment. This occurs along conduction, convection, and radiation paths. The uncertainties connected with conduction and radiation lend themselves to resolution via ground testing. However, the tests conducted prior to or during the development phase will not significantly lessen the convection problem due to the

Table 3-24. Thermal Control Subsystem Uncertainties

ELEMENT WITH UNCERTAINTY	RELATIVE DEGREE OF UNCERTAINTY IN MEASUREMENT (%)
SURFACE COATINGS	~11
ABSORPTIVITY EMISSIVITY	
INSULATION PERFORMANCE	~10
THERMAL COUPLING	~10

different "earth-test" environments as opposed to actual flight environments, i.e., gravity, acceleration, and probe rotation effects. Measurement of pressure vessel and payload internal temperatures obtained during descent will allow for a real evaluation of convection under actual Venus descent conditions. This would then provide a better value for including the effects of convection in the design of subsequent probes.

Heat Shield

Table 3-25 lists the uncertainties and the corresponding margin in heat shield thickness each implies. It should be noted that the uncertainty levels are those expected at the time of final design. Present uncertainties are significantly greater, but should be reduced through testing.

Table 3-25. Heat Shield Uncertainties

ELEMENT WITH UNCERTAINTY	THICKNESS MARGIN REQUIRED (%)
MATERIAL PERFORMANCE	12.8
HEATING RATE	
CONVECTIVE RADIANT	~3.6
ENTRY ENVIRONMENTS	~1.3
COMPOSITION SCALE HEIGHT	
MANUFACTURING TOLERANCES	~6.7

The heat shield design thickness is currently baselined with an approximate 20 percent margin or overdesign due to the above uncertainties. This margin is based on a statistical combination of all associated uncertainties.

Material performance is one of the most significant contributors to the overall uncertainties. Some additional reduction in the material property uncertainties can be achieved by more extensive tests (prior to flight) than presently planned. These tests are not expected to do much in the way of reducing heating rate uncertainties. Costs to obtain more definitive knowledge of material properties are high, and present design philosophy is to minimize the cost by allowing some weight increase. Engineering measurements made on the probe, however, could significantly reduce some uncertainties for follow-on missions through post-flight analysis of the recorded data.

The necessary measurements are determination of the aeroshell forebody and afterbody temperatures, pressure shell exterior temperatures and exterior insulation temperatures. Both material properties and heating rate overdesign uncertainties could be reduced for subsequent probes using these specified measurements.

Concerning the entry environment, there exists an uncertainty associated with the Venus atmospheric composition and scale height. There could be a variation of 80 to 100 percent in the amount of CO_2 present; this results in dispersions in the entry heating. The current official model gives 97.3 percent CO_2. Better definition of atmospheric composition, as will be obtained by the large probe shock layer radiometer and mass spectrometer, could aid in reduction of the associated uncertainties. The pressure and temperature models currently being used for the lower atmosphere have no effect in terms of increasing the entry environmental uncertainty parameters; however, there is an uncertainty in the scale height at 80 km altitude of approximately $\pm$ 8 percent.

The manufacturing tolerances and their associated uncertainties are self-explanatory and may not be reduced except through more stringent control of hardware machining and build tolerances.

To reduce the heat shield design uncertainty by measuring the mass loss by ablation during entry, an X-ray fluorescence experiment, such as the one proposed by the MIT-Martin Marietta team for heavy element detection, could conveniently be adapted. The X-ray fluorescence experiment has a ^{109}Cd radioisotope source that emits 22.2 keV X-rays outward from the surface of the probe exterior. In its normal operation in the

Venus atmosphere these X-rays stimulate the emission of fluorescent X-rays from the various minority constituent elements in the Venus atmosphere. These fluorescent X-rays, whose energies are characteristic of the particular elements emitting them, are detected by a proportional counter that identifies the X-rays according to their energies. Thus, it effectively measures quantitatively the amount of each element present. This can be adapted to measuring the rate of surface recession and of mass loss in the entry heat shield as follows.

A beryllium encapsulated ^{109}Cd source could be added to the heat shield about 0.4 mm below the surface (which is the approximate expected depth of total surface erosion). The 22.2 keV X-rays from this source would penetrate the heat shield and be detected by the experiment proportional counter. As presently conceived, the heat shield is 0.46 cm thick with a density of 1.12 gm/cm^3, and composed of 74.5 percent carbon, 13.2 percent silicon, 9.1 percent oxygen, and 3.2 percent hydrogen. The effective transmission of the 22.2 keV X-rays in the full thickness of this heat shield is 48 percent. The aluminum aeroshell would decrease this transmission to 17.8 percent. However, one could replace a section of the aluminum with beryllium with a thickness sufficient to have the same heat capacity as the aluminum. Such a beryllium thickness would reduce the transmission only very slightly to 46.5 percent. As the mass of the heat shield is reduced by evaporation and combustion (calculated loss of 12.2 percent) the transmission will increase from 46.5 percent to about 51.9 percent, or an increase in counting rate of 11.6 percent. The estimated counting rate with a 50 millicurie source (which is rather a weak one) would be 5.9×10^5 per second so that counts could be integrated for 0.1-second intervals over the 4-second interval of the burning pulse to yield 0.5 percent accuracy in the counts. This is very adequate to monitor the estimated 11.6 percent increase in counting rate. The backscatter counts from the source on the experiment would contribute only about 0.5 percent to the counting rate.

The rate of recession of the surface can be monitored with an imbedded molybdenum compound near the surface. The molybdenum becomes a secondary source yielding fluorescent X-rays at 17.5 keV. As the surface wears away the Mb compound would also disappear and would be observable as a decrease in the 17.5 keV X-ray count rate.

Communications Subsystem

Table 3-26 lists the communications subsystem uncertainties.

These uncertainties result in an overall margin of approximately 3 to 4 dB in the transmitter/communications system to account for tolerances. Some of the listed uncertainties may, of course, lessen and some may even disappear as the design firms up. However, no significant changes are anticipated.

Table 3-26. Communications Subsystem Uncertainties

ELEMENT WITH UNCERTAINTY	RELATIVE DEGREE OF UNCERTAINTY (%)			
	LARGE PROBE		SMALL PROBE	
	30 KM ALTITUDE	NEAR SURFACE	30 KM ALTITUDE	NEAR SURFACE
OUTPUT VARIATIONS PROBE TEMPERATURE BASIC DESIGN OF TRANSMITTER AGING PROPERTIES ANTENNA PATTERN RIPPLE DAMAGE DURING ENTRY VOLTAGE CHANGES	26	26	26	26
ATMOSPHERIC ABSORPTION MULTIPATH (TURBULENCE AND FADING RATES) DEFOCUSING LOSSES PLANET REFLECTED SIGNAL MULTIPATH	10	10	10	10
TARGETING ANTENNA GAIN (PRIMARY CONTRIBUTOR) ATMOSPHERIC LOSSES ANGLE OF ATTACK	12	12	12	12
PROBE DYNAMICS EFFECTIVE ANTENNA GAIN OSCILLATIONS DUE TO CHUTE	20	0	20	0
MODULATION INPUT VOLTAGE VARIATIONS FROM DATA SYSTEMS (POWER IN DATA CHANNEL)	7	7	12	12
GROUND STATIONS SYSTEM NOISE TEMPERATURE ANTENNA GAIN	35	35	35	35

The stability of the probe is an important factor in the communications subsystem design, and probably creates more uncertainty than such atmospheric parameters as pressure and temperature. Measurements to determine the probe attitude and attendant probe signal fluctuations could be used in future probe design. At present, an attitude measurement is not specified.

Concerning turbulence induced multipath propagation and fading rates, better analyses of these phenomena as a function of depth of the planetary atmosphere may aid in lowering the associated atmospheric uncertainties. Knowledge of the water content of the Venus atmosphere might lower some of the absorption uncertainties, but really represents only a very small percent of the total problem. Better planetary surface roughness numbers for reflectivity could aid in reducing uncertainties associated with the planet reflected signal multipath; however, this effect is presently considered negligible and no specific measurements appear warranted.

A better defined radius of the planet (or its equivalent) might prove useful in signal return modeling. The present design is based on a nominal planet surface, and "holes" or depressions may well exist.

The transmitter weight penalty that may result from any overdesign due to the above uncertainties is perhaps on the order of a pound or two; however, thermal, battery, and structural weight also are affected by transmitter power. Minimum engineering measurements that are needed to supply required information for system evaluation include the power amplifier temperature and output, current for the amplifier and receiver input, driver power output and current for the driver input, and temperature for the auxiliary oscillator and driver output stage. Other measurements include such items as receiver mode indication and static phase error, receiver AGC and VCO temperature.

Pressure Vessel, Aeroshell, and Auxiliary Structure

The current structural design for the pressure vessel is based on a 766°K planetary surface temperature and a 93 atmospheres planetary surface pressure. The pressure vessel is designed to this pressure on the Thor/Delta configuration. The capability of the probe to withstand these requirements will be demonstrated during the testing phase to provide assurance that the probe is good for a minimum of 80 percent of the surface pressure at the expected shell temperature.

A primary structural concern is the high (~350 g) inertia load resulting from aeroshell forebody pressure at time of entry. A better definition of the entry environments, such as obtained by the accelerometers and by temperature and pressure measurements, will provide valuable data for design of subsequent planetary probes. In a like manner, the weight penalty in the current design, using the established baseline limits, can be assessed only in terms of entry environment data returned from the present probe. These data could then be used to reduce structural margins for subsequent Venus probes. It is anticipated that no additional engineering measurements (e.g., strain gauges) can be effectively incorporated to provide useful structural data for subsequent probe mission designs.

Power

The present design philosophy for the power subsystem is to allow an 80 percent depth of discharge with a 20 percent margin or reserve. A 5 percent load uncertainty is now carried in the design (reserved for load growth). The 5 percent factor is not included in the 20 percent margin. Any overdesign in the power subsystem, using the baseline power loads is simply a built-in redundancy that is based upon reliability requirements.

One specific area of concern in the present power system design is the need for better definition for the science instrument window heating requirement. The present estimate is that an average of 15 watts per window is required for entry to impact (~53 minutes) just for heating the windows. For battery weight, a general rule-of-thumb is ~66 W-hr/kg, and hence for rough estimates the weight could be reduced proportionately with any reduction in the power requirements. The battery weight could be reduced by perhaps several kilograms if the heating requirements are reduced.

To provide an evaluation of the window heater's engineering temperature measurement will be made on the small probe nephelometer collector window at the outer lens element and at the Inconel 718 tube near the pressure vessel penetration. If the large probe carries the same nephelometer, then the same measurements would be made on the large probe. If not, the planetary flux radiometer window could be similarly instrumented.

With regard to a direct measurement of dust and condensate buildup on window surfaces, it should be noted that the attenuated total reflectance spectrometer (ATRS) experiment was originally conceived to evaluate deposition buildup on the nephelometer window. It was then decided that this was an interesting experiment in its own right and it was expanded accordingly to give an analysis of the deposition constituents. However, in view of their original efforts it may be desirable for NASA/ARC to request the nephelometer PI's to reconsider incorporating a dust and condensation measurement into the nephelometer.

3.3 PROBE BUS SCIENCE

The science objectivies of the probe bus mission were defined in "Report of a Study by the Science Steering Group," June 1972. The major science objective of the probe bus mission is to study the structure and composition of the upper atmosphere and ionosphere of Venus. NASA/Ames defined and described the scientific instruments which should be used in this study as the probe bus instruments in two Pioneer Venus Science definition reports: 1) for a Thor/Delta launched mission (Payload Version I), 22 September 1972; and 2) for an Atlas/Centaur launched mission (Payload Version II), 20 October 1972. Table 3-27 lists the scientific instruments defined in these documents and the role performed by each in satisfying the mission objectives.

On 13 April 1973, NASA redefined the Pioneer Venus missions to consist of Atlas/Centaur launches for both the probe mission and the

Table 3-27. Specified Scientific Instruments and Their Use

INSTRUMENT	OBJECTIVES/MEASUREMENTS
MAGNETOMETER	PRIMARY - MEASURE IONOSPHERIC MAGNETIC FIELD. SECONDARY - STUDY SOLAR WIND/VENUS ATMOSPHERE INTERACTIONS AND INTERPLANETARY FIELDS.
ELECTRON TEMPERATURE PROBE	TEMPERATURE AND DENSITY OF IONOSPHERIC THERMAL ELECTRONS.
NEUTRAL MASS SPECTROMETER	COMPOSITION OF NEUTRAL ATMOSPHERE PARTICULARLY He^4, O, CO, N_2, A, CO_2
ION MASS SPECTROMETER	NUMBER DENSITY OF THERMAL IONS IN UPPER ATMOSPHERE.
ULTRAVIOLET FLUORESCENCE	CO AND O DENSITY IN UPPER ATMOSPHERE
OTHER CANDIDATE INSTRUMENTS	
DAY GLOW PHOTOMETER	NEUTRAL ATMOSPHERE COMPOSITION.
SOLAR WIND PROBE	PRIMARY - STUDY SOLAR WIND/VENUS ATMOSPHERE INTERACTIONS. MEASURE DENSITY, VELOCITY AND TEMPERATURE. SECONDARY - STUDY INTERPLANETARY SOLAR WIND.

orbiter mission, and provided a new (Version IV) scientic instrument payload. This payload was similar to that shown in Table 3-27 with the following exceptions:

- The magnetometer was replaced by a retarding potential analyzer which will determine the ion and electron temperature and concentration in the Venus ionosphere.
- The ultraviolet (UV) fluorescence experiment was replaced by a UV spectrometer which will study the neutral atmosphere composition. In particular it will aid in determining the small concentration of CO and Ó, as well as the upper limits on other gases.

3.3.1 Science-Related System Requirements Analysis

3.3.1.1 Target Considerations

The following factors influencing the selection of the probe bus target have been identified:

- Maximize atmospheric experiment time
- Maximize bus earth/antenna pattern
- Minimize angle of attack
- Remain above atmosphere and be in same field of view as probes during first hour of probe entry
- Enter close to entry point of large probe
- Enter on dark side because of the UV fluorescence experiment
- Have bus penetrate as low as possible in atmosphere.

The primary factor affecting the selection of a target for the probe bus is the small amount of time available for in situ measurements to be made. For this reason a flight path angle, γ, as small as possible should be chosen, where flight path angle is defined as the angle between the velocity vector and the local horizontal at any altitude. For example, for the 1977 launch opportunity a trajectory with a flight path angle of $\gamma =$ 0.35 radian (20 degrees) at 250 km the bus spends 3 minutes in this region; and for $\gamma = 0.79$ radian (45 degrees) the bus spends 1.5 minutes in this region. Similar times apply also to the 1978 launch opportunity.

The mass spectrometers on the probe bus will require that the instrument point within 0.17 radian (10 degrees) of the spacecraft velocity vector on entry. If these instruments are mounted so that their ram direction is parallel to the bus spin axis, then it is also required that the bus angle of attack be less than 0.17 radian (10 degrees) on entry where angle of attack is defined as the angle between the velocity vector and the bus spin axis. Figure 3-83 shows the bus communications angle for entry with zero angle of attack for the 1977 launch opportunity. Also shown in the figure is the flight path angle defined at 250 kilometers and the selected bus target for the 1977 mission.

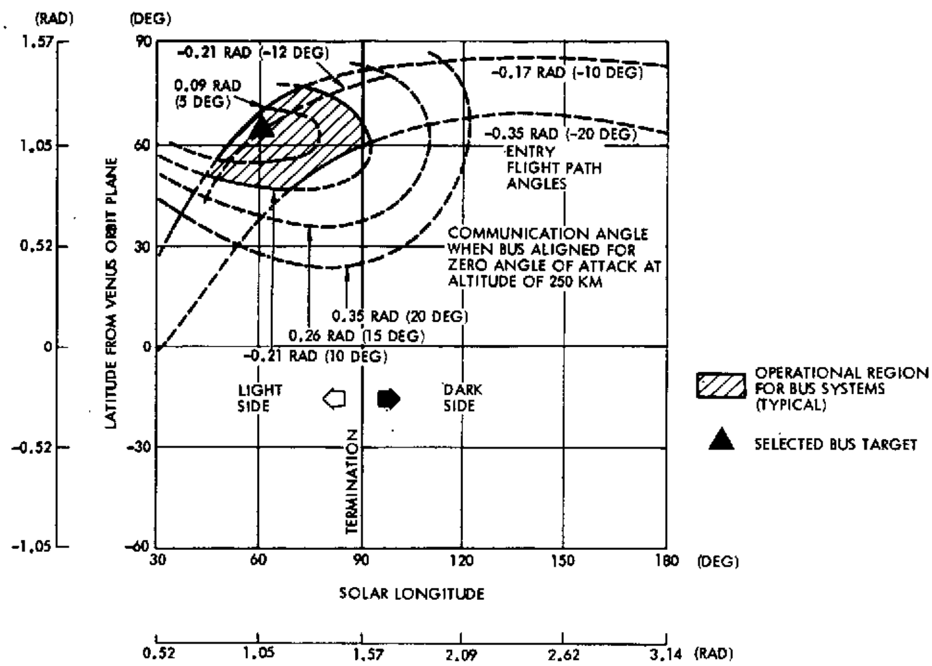

Figure 3-83. 1977 Probe Mission Bus Targeting

The selected bus target site satisfies the first four target selection factors identified previously. Selection of a much smaller flight path angle is prohibited to assure that the bus does not skip out at the Venus atmosphere without penetrating to about 130 kilometers.

We note from Figure 3-83 that, if the bus target is changed to the dark side, an increase in bus communication angle to 0.17 radian (10 degrees) or greater would be required if the angle of attack is to remain zero. Even if the angle of attack were permitted to be as high as 0.17

radian (10 degrees), a dark side entry would require a compromise in communications or an increased flight path angle or both.

The Science Steering Group recommended that the large probe enter near the equator and not closer than 0. 35 radian (20 degrees) from the terminator so that the solar radiometer could obtain data. Entry of the probe bus at the same target site would necessitate an increase in flight path angle of the probe bus to about 0. 70 radian (40 degrees). This would decrease the time in the atmosphere by more than half, and would also result in a large communication angle with severe communication degradation or an angle of attack much greater than 0. 17 radian (10 degrees).

3. 3. 1. 2 Targeting Update for 1978 Probe Mission

Figure 3-84 shows the 1978 probe bus targeting. The contours shown are the earth aspect angle for zero angle of attack and the flight path angle. The selected flight path angle (at 250-km altitude) is 0. 20 radian (11. 5 degrees), the smallest angle and therefore the longest bus probe time in the atmosphere consistent with 3σ assurance of penetrating the Venus atmosphere to at least 130-kilometer altitude. The large earth aspect angle of 0. 21 radian (12 degrees) necessitates a degradation in communication performance (and thus the science data rate) over that obtained for 1977 missions. However, as will be seen in Section 3. 3. 2. 1, the science data requirements will still be satisfied. For the target selected, the angle of attack will remain below 0. 17 radian (10 degrees) at all altitudes below 2000 kilometers. Selection of a smaller communication angle would necessitate a larger angle of attack or a greater probability of "skipout" about 130 kilometers. Details of the analysis leading to the conclusions above are given in Section 4. 2. 5.

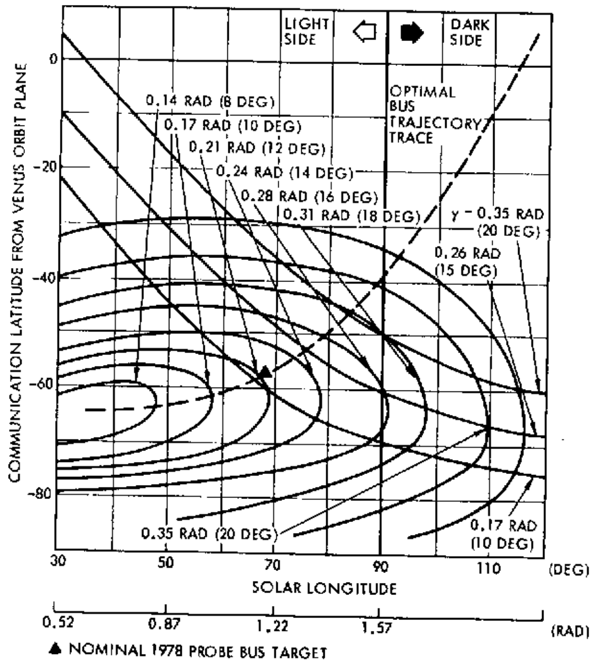

Figure 3-84. 1978 Bus Targeting (Mercator Projection)

Figure 3-85 shows the time it takes for the probe bus to descend from 1000 kilometers altitude. Note that for the nominal $\gamma = 0.20$ radian (11.5 degrees) the probe bus takes about 4.75 minutes to fall from 1000 to 130 kilometers.

As in the case of the 1977 mission the selected target satisfies most of the targeting requirements. Targeting on the dark side and at the large probe site are not recommended for the same reasons discussed in the 1977 probe mission targeting section.

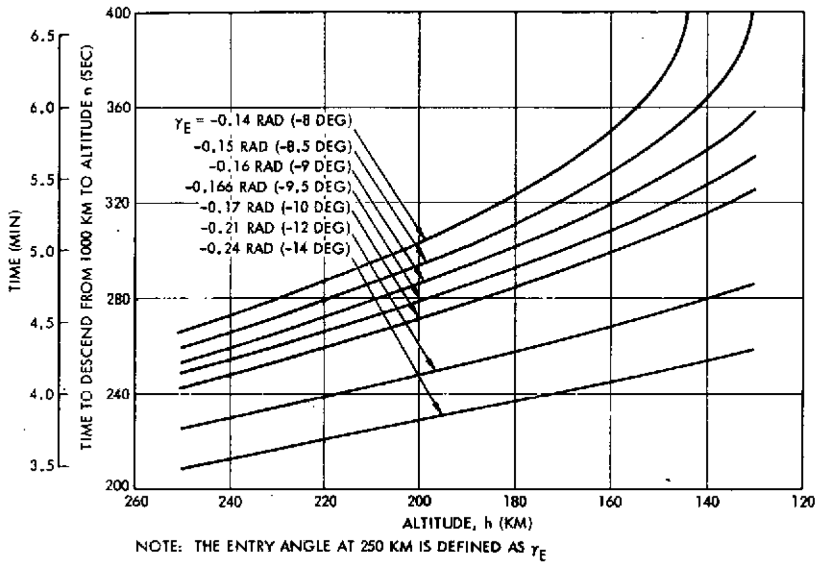

Figure 3-85. Time to Descend from 1000 KM

3.3.1.3 Spin Axis Orientation

The preferred orientation of the probe bus spin axis on entry is in the direction of the probe bus velocity vector. With any other orientation the ram instruments (those which must view along the veloicty direction to obtain valid data) will obtain data only for a fraction of the spin perioed. Furthermore, this orientation will permit the use of an earth-pointing antenna dish, adding to the downlink data capability during entry.

There is some advantage, particularly for those instruments which obtain data in interplanetary flight as well as on entry, if the spin axis orientation is the same during both regimes. For example, if a solar wind probe is used on the probe bus, two different sensors would be required if the spacecraft spin axis were normal to the ecliptic plane during interplanetary cruise and earth pointing during entry. The magnetometer data reduction (in the case of the 1977 Thor/Delta mission) would also be complicated by a change in axes of the sensor on entry.

We therefore recommend that the probe bus spin axis be earth pointing during interplanetary cruise and entry.

3.3.1.4 Demise of the Bus

As the probe bus enters the Venusian atmosphere, various phenomena will affect the performance of the scientific instruments. These phenomena are summarized and are discussed in detail in Section 4.

Below an altitude of approximately 155 kilometers the scientific instruments will be increasingly influenced by flow disturbances ahead of the entering bus. Data obtained by the mass spectrometers below this altitude will require detailed analysis for interpretation in this flow regime. At approximately 146 kilometers, teflon thermal control surfaces will begin to deteriorate. Outgassing from teflon surfaces could contaminate mass spectrometer readings. This problem can be somewhat alleviated if the spectrometer incorporates a velocity selector set at the ram velocity.

Just below 130 kilometers the bus high-gain antenna diverges from earth pointing to 0.105 radian (6 degrees) from earth pointing due to destabilizing aerodynamic forces. This change in attitude is about the limit for high data rate communications. The antenna points at an angle greater than 0.52 radian (30 degrees) from earth by the time the 122 to 119 kilometers altitude region is reached, effectively terminating all communications. This behavior occurs for the Thor/Delta bus, which spins at 0.524 rad/s (5 rpm). In the case of the Atlas/Centaur mission, the bus is spun up to 6.283 rad/s (60 rpm) prior to entry. The higher spin rate delays angle of attack divergence down to the 120 to 115 kilometers altitude range.

3.3.1.5 Probe Bus Measurement Resolution for the 1977 Probe Mission

Figure 3-86 shows the radial distance the probe bus falls between measurements at altitudes below 1000 kilometers. Also shown on the ordinate are the number of minutes of fall from the given altitude to 150 kilometers. The entry trajectory used in this computation has a flight

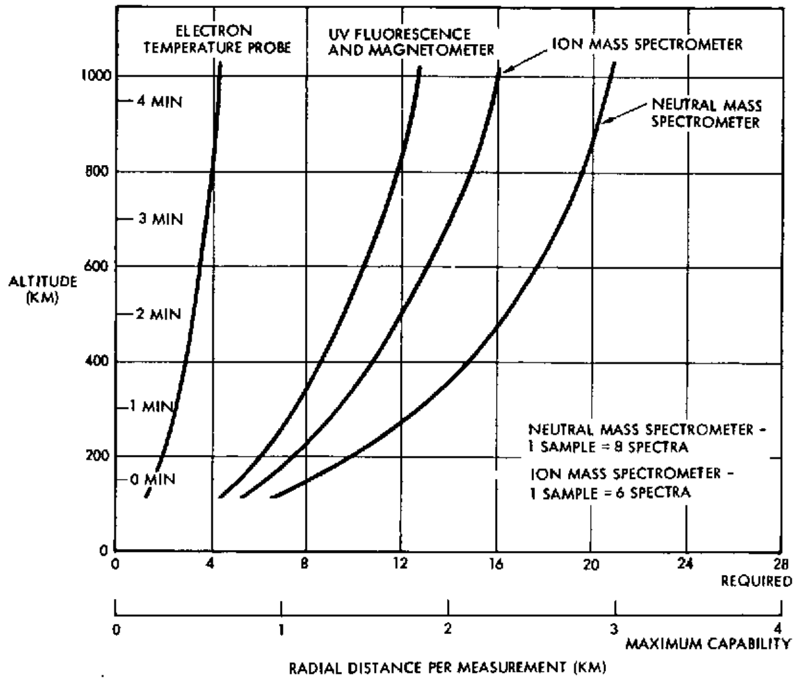

Figure 3-86. 1977 Probe Bus Measurement Resolution

path angle of 0.17 radian (10 degrees) at 150 kilometers, and was selected to obtain an angle of attack of zero on entry and an earth aspect of 3.14 radians (180 degrees). The "required" resolution is based on the data requirements given in the NASA/Ames Pioneer Venus Definition Report of 22 September 1972. It was assumed that the neutral mass spectrometer 2500-bit samples consisted of eight complete mass spectra and that the ion mass spectrometer 2000-bit sample consisted of six complete mass spectra.

Also shown in the figure is the radial distance per measurement that could be achieved with the maximum bit rate available in the baseline probe bus. As can be seen in the figure, the data capability can lead to a 600-percent improvement in measurement resolution if the additional capability is allocated among the scientific instruments in proportion to the baseline data rate allocations. This measurement resolution is obtained for the probe bus target recommended in the description of target considerations.

3.3.1.6 Probe Bus Measurement Resolution for the 1978 Probe Mission and New Atlas/Centaur Science Payload Version IV

Figure 3-87 shows the radial distance the probe bus falls per measurement at altitudes below 1000 kilometers for the 1978 trajectory with the nominal flight path angle, γ = -0.20 radian (-11.5 degrees), and for the bus trajectory with a 3σ flight path angle of γ = -0.24 radian (-14 degrees). The resolutions in Figure 3-87 are for the Version IV science payload.

The density scale height in the region above 140 kilometers is 6 kilometers. The requirements for the Version IV science payload state that in the altitude regime between 146 and 140 kilometers (one scale height) the number of measurements per scale height will exceed the following:

Neutral mass spectrometer Electron temperature probe Ultraviolet spectrometer	one per scale height
Ion mass spectrometer Retarding potential analyzer	Three per scale height

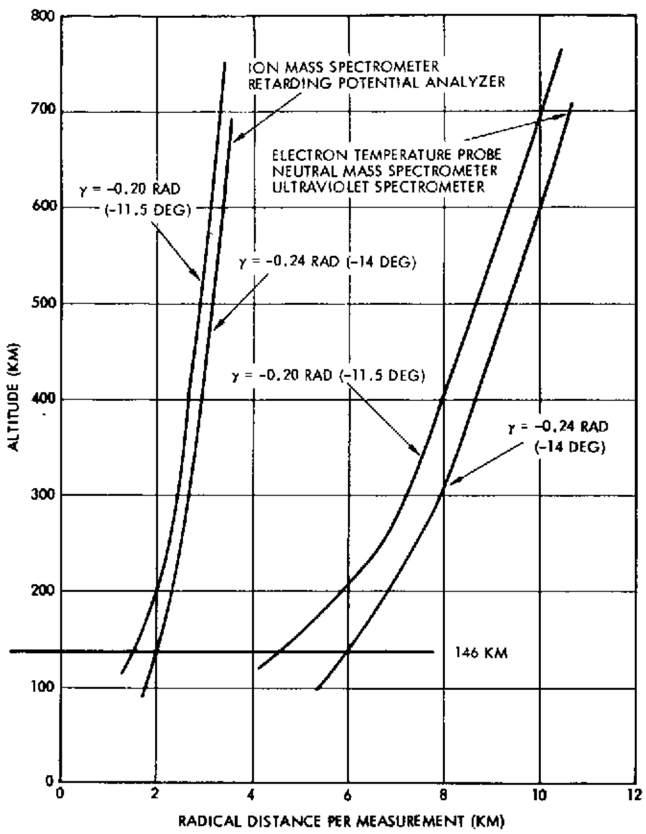

Figure 3-87. 1978 Mission and Version IV Payload Probe Measurement Resolution

We can see from Figure 3-87 that these requirements are met for the nominal fight path angle and up to the -0.24 radian (-14 degrees) flight path angle. Further details of the analysis of this requirement is given in Section 3.3.2.1.

3.3.1.7 Spacecraft Differential Charging ALL CONFIGURATIONS

Measurements of low energy electrons by a retarding potential analyzer and electron temperature probe can be deleteriously affected by spacecraft charging. In this section we examine the charging of the Pioneer Venus spacecraft due to its immersion in the solar wind and the Venus ionosphere.

Review of Charging Theory

A portion of a spacecraft immersed in an ambient plasma will come into electrical equilibrium with that plasma by developing surface charges of the proper sign and magnitude to reduce the net (surface-integrated) current between plasma and spacecraft to zero. The total current is computed from all of the partial currents contributed by the ambient electrons and ions, the back-scattered electrons and ions, secondary electrons and ions, and photo-electrons from any illuminated areas.

The sheath formed around a spacecraft immersed in a partially ionized gas will depend on whether the electron-neutral collison frequency is small, large, or comparable with respect to the local electron plasma frequency. On the basis of the standard atmospheric models for Venus as given in NASA SP-8011 (September 1972), one can show that at altitudes above about 140 kilometers the electron-on-neutral collision frequency $\nu_{e,n} = \sigma_{e,n} n_o \bar{v}_e$ is much less than the local electron plasma frequency $\omega_{pe} = (4 \pi n_e e^2/m_e)^{1/2}$. (In these expressions, $\sigma_{e,n}$ is the collision cross-section, n_o the neutral molecule number density, $\bar{v}_e$ the electron mean thermal speed, n_e the electron number density, e the electronic charge, and m_e the electronic mass.) Below 140 kilometers, the collision frequency rapidly becomes very much larger than the local plasma frequency. Thus, we will restrict our attention to the region above 140 kilometers, since collisions very effectively keep charging to lower potentials than those we shall compute in the "collisionless" regime above 140 kilometers. Furthermore, the bus and orbiter craft will be restricted in their data-gathering functions to these higher altitudes.

The very simplest of theories will be used here for the "collisionless" plasma regime. In this simplest of treatments, all current-carrying charged particles are considered to be Maxwellian with temperature T_α, that is, they have distribution functions in velocity space

$$f_\alpha(\underline{v}) = (m_\alpha/2\pi\kappa T_\alpha)^{3/2} \exp(-m_\alpha \underline{v}\cdot\underline{v}/2\kappa T_\alpha) \qquad (1)$$

where κ is Boltzmann's constant, m_α the species mass. The partial current densities then have the general form

$$j_\alpha = N_\alpha q_\alpha \,(m/2\pi\kappa T_\alpha)^{3/2} \int d^3v \; \underline{v}\cdot\underline{n} \; \exp\,(-m_\alpha v^2/2\kappa T_\alpha) \qquad (2)$$

where N_α is the partial number density, q_α is the signed charge, and we compute the current density j_α perpendicular to a surface of unit normal $\underline{n}$.

Let us use a geometrical model of a cylindrical spacecraft with covered ends, define a coordinate system with $v_{||}$ along the axis of the cylinder and $v_\perp$ normal thereto. Then, the current density incident on the wall of the cylindrical spacecraft may be written

$$j_{\alpha\perp} = N_\alpha q_\alpha \left(\frac{m_\alpha}{2\pi\kappa T_\alpha}\right)^{3/2} \int_{-\infty}^{\infty} dv_{||} \exp\left(\frac{-m_\alpha v_{||}^2}{2\kappa T_\alpha}\right) \int_{v_o}^{\infty} 2\pi v_\perp^2 dv_\perp \exp\left(\frac{-m_\alpha v_{||}^2}{2\kappa T_\alpha}\right) \quad (3)$$

where $v_o = 0$ if we expect a surface potential of zero, or an accelerating potential for particles of charge $q_\alpha = \pm e$, and $v_o > 0$ if the surface potential is expected to retard the α-species. For the end covers of the cylinder, one has

$$j_{\alpha||} = N_\alpha q_\alpha \left(\frac{m_\alpha}{2\pi\kappa T_\alpha}\right)^{3/2} \int_{v_o}^{\infty} v_{||} dv_{||} \exp\left(\frac{-m_\alpha v_{||}^2}{2\kappa T_\alpha}\right) \int_{0}^{\infty} 2\pi v_\perp dv_\perp \exp\left(\frac{-m_\alpha v_\perp^2}{2\kappa T_\alpha}\right) \quad (4)$$

for each end, with v_o having similar meaning as before.

In eclipse or shadow, a net negative surface potential causes total escape of all secondary electrons, and suppression of secondary ions. Thus the current balance equation will require currents to the unilluminated wall of the spacecraft to satisfy

$$N_e e \left(\frac{2\kappa T_e}{m_e}\right)^{1/2} \frac{2}{\sqrt{\pi}} \int_{e\Phi/\kappa T_e}^{\infty} t^{1/2} e^{-t} dt - N_p e \left(\frac{2\kappa T_p}{m_p}\right)^{1/2} - N_* e \left(\frac{2\kappa T_*}{m_e}\right)^{1/2} = 0 \quad (5)$$

where N_* and T_* are the number density and effective temperature of secondary electrons, respectively. Similarly, for the end currents one has for eclipsed or shadowed surfaces

$$N_e e\left(\frac{2\kappa T_e}{m_e}\right)^{1/2} e^{-e\Phi/\kappa T_e} - N_p e\left(\frac{2\kappa T_p}{m_p}\right)^{1/2} - N_* e\left(\frac{2\kappa T_*}{m_e}\right)^{1/2} = 0 \tag{6}$$

An equivalent photoelectron term $-N_{ph} e\left(\frac{2\kappa T_{ph}}{m_e}\right)^{1/2}$ can be added to both of these equations under illuminated conditions. The two densities N_* and N_{ph} must be computed from the appropriate yield factors for the surface materials in question, as pointed out by K. Knott (Reference 1) and R. J. L. Grard (Reference 2). For spherical geometry, one has only a $j_{\alpha\perp}$ given by

$$j_{\alpha\perp} + 2N_\alpha q_\alpha\left(\frac{2\kappa T_\alpha}{\pi m_\alpha}\right)^{1/2} \int_{v_o/\langle v_\alpha\rangle}^{\infty} t^2 e^{-t^2} dt, \quad [v_\alpha] = \left(\frac{2\kappa T_\alpha}{m_\alpha}\right)^{1/2} \tag{7}$$

which leads to the current balance condition

$$N_e e\left(\frac{2\kappa T_e}{m_e}\right)^{1/2} \left(1 + \frac{e\Phi}{\kappa T_e}\right) e^{-e\Phi/\kappa T_e} - N_p e\left(\frac{2\kappa T_p}{m_p}\right)^{1/2} - N_* e\left(\frac{2\kappa T_*}{m_e}\right)^{1/2} = 0 \tag{8}$$

to which a term $-N_{ph} e\left(\frac{2\kappa T_{ph}}{m_e}\right)^{1/2}$ for photoelectrons may be added, as before.

If we write the saturation current density to the spacecraft (in the conventional sense) as

$$j_+^{(S)} = N_p e\left(\frac{2\kappa T_p}{m_p}\right)^{1/2} + N_* e\left(\frac{2\kappa T_*}{m_e}\right)^{1/2} + N_{ph} e\left(\frac{2\kappa T_{ph}}{m_e}\right)^{1/2} \tag{9}$$

and away from the spacecraft as

$$j_-^{(S)} = N_e \, e \left(\frac{2\kappa T_e}{m_e} \right)^{1/2} \tag{10}$$

then for the planar (Equation 6), cylindrical (Equation 5), and spherical (Equation 8) surfaces, the equilibrium potential Φ assumed by that surface is, within the simple theory, given by the solution to the transcendental equation of the general form

$$\psi_g \, (e\Phi/\kappa T_e) = j_+^{(S)}/j_-^{(S)} = R \tag{11}$$

where the geometry-dependent function ψ_g is

$$\psi_g \, (e\Phi/\kappa T_e) = \begin{cases} \exp(-e\Phi/\kappa T_e), \text{ for the plane} \\[2ex] \dfrac{2}{\sqrt{\pi}} \displaystyle\int_{e\Phi/\kappa T_e}^{\infty} t^{1/2} \, e^{-t} dt = \dfrac{\Gamma(3/2, \, e\Phi/\kappa T_e)}{\Gamma(3/2)}, \text{ for the cylinder} \\[2ex] (1 + e\Phi/\kappa T_e) \, e^{-e\Phi/\kappa T_e}, \text{ for the sphere.} \end{cases} \tag{12}$$

These three functions are plotted in Figure 3-88 as a function of the normalized energy $|e\Phi/\kappa T_e|$. Since the saturation current densities are functions of the thermal properties of the ambient plasma, of the secondary and photoelectron yield factors of the surface material, and of the direction of incidence of solar photons on the local surface, it is not true that the ratio R in Equation 11 is independent of geometry. However, if we assume that the ratio R is a constant, then the intersection of horizontal lines R = constant ≤ 1 with the ψ_g yield three different values of $|e\Phi/\kappa T_e|$. Since our initial assumption was $\Phi \leq 0$, for the example R = 0.3 shown in Figure 3-88, one obtains potentials

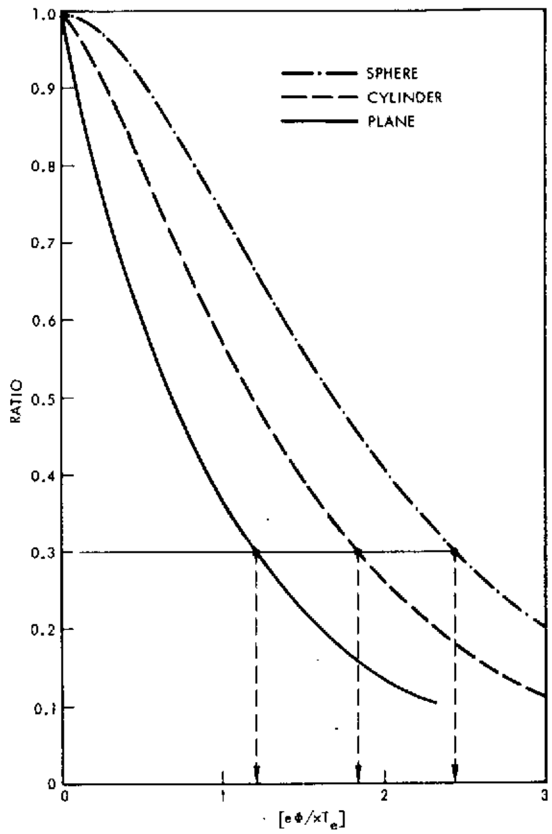

Figure 3-88. Ratio of Saturation Current Densities to and from Surface versus Potential Function $[e\Phi/\kappa T_e]$

$$\Phi = -1.2\ \kappa T_e/e\ \text{(plane)}$$
$$= -1.84\ \kappa T_e/e\ \text{(cylinder)}$$
$$= -2.42\ \kappa T_e/e\ \text{(sphere).}$$

Because actual spacecraft surfaces are complex and inhomogeneous, the practical case of spacecraft charging is probably well beyond hope for adequate theoretical treatment. However, the above treatment does provide some guidance concerning orders of magnitude of surface potentials.

As an example of the efficacy of the above estimates for spacecraft surface potential, let us examine a well-documented case of measured spacecraft charging on the NASA synchronous orbiter ATS-5 during magnetospheric substorm events, reported by S. E. DeForest (Reference 3).

If we apply the simple theory to the experimental results of Reference 3 during eclipse of ATS-5, we can estimate the ratio $R = j_+^{(S)}/j_-^{(S)}$. Let us take the example of Figure 3-88, where $\Phi = -4.2$ kV. According to DeForest, the density of injected protons and electrons was ~1 cm^{-3}, with T_p ~10 keV and T_e = 5 keV. If there were no secondary emission, then $R = (m_e T_p/m_p T_e)^{1/2} = 0.033$. In this case, for the three geometries of spacecraft surface, the curves in Figure 3-88 yield the results

$$\Phi = -(3.4)(\kappa T_e/e) = -17\ \text{kV (plane)}$$
$$\Phi = -(4.4)(\kappa T_e/e) = -22\ \text{kV (cylinder)}$$
$$\Phi = -(5.25)(\kappa T_e/e) = -26\ \text{kV (sphere)}$$

These voltages, especially that of the plane, are consistent with DeForest's comments that extrapolation of his curve labeled "without secondaries" in Figure 7 of his 1972 paper would yield a predicted potential about three times the measured one.

If we draw a vertical line at $|e\Phi/\kappa T_e| = 0.84$, which is the value of 4.2 kV divided by electron voltage of 5 kV, then the intersections yield

$$R = 0.425 \text{ (plane)}$$
$$R = 0.64 \text{ (cylinder)}$$
$$R = 0.80 \text{ (sphere)}.$$

In all geometries, then, secondary emission currents and backscattered electron currents from the surface materials of ATS-5 during eclipses must be a significant fraction (40 to 80 percent) of the incident currents.

Of course, the Pioneer Venus configuration differs largely from the ATS-5 geometry, and the Venus atmosphere and ionosphere present much different environmental parameters to be used in the formulas for spacecraft potential. As an example, one has a relatively low-energy plasma ($\sim$ 2500 to 10 000°K electron temperature) compared to the energetic plasmas impinging on ATS-5 (electron energies of 5 to 20 keV, or $T_e \sim 6$ to 20×10^{7} $^{\circ}$K). This obviously enters in the factor $\kappa T_e/e$ and also in the ratio R, since in the latter the influence of secondary electrons may be negligible, because of the relatively small secondary-per-primary electron yield factor for primary electron energies of $\sim$ 0.25 eV (2500°K). The saturation current density $j_+^{(S)}$ then is dominated by the photoelectron term in sunlight, and by the combination of the positive ion and secondary electron terms in shadow. This latter case is the most likely to produce elevated potentials on the surfaces in shadow, since the ratio R tends to a very small number, implying that $\ln(R)$ is a fairly large negative number. We will make some estimates subsequently and this point will become clear.

Differential Charging

One should recall that the surfaces of different spacecraft vary widely. For example, many spacecraft are cylindrical in shape, and have solar cells with glass covers coating the entire cylindrical surface. Some of these are open on one or both ends, with both dielectric and conducting surfaces bearing instrumentation exposed to both sunlight and plasma environment. Others have one end open in this manner, and the other end with a thermal closure surface covering it. Still others having cylindrical geometry have varying materials (dielectrics, thermal balance surfaces, conductors, paint, openings, etc.) distributed over all surfaces. Some spin at 1.57 rad/s (15 rpm), some at 6.28 rad/s (60 rpm) and some, including ATS-5, at as much as 10.47 rad/s (100 rpm). Still others, usually with solar paddles, are attitude-stabilized, and do not spin at all.

At Venus, the solar photon flux exceeds that at the orbit of earth 150 gigameters (1 AU) by roughly the inverse square of the ratio of the Venus-sun distance in AU. Thus, a typical value of photoelectron emis sion current can be scaled approximately by multiplying the fairly well-known value of this current from earth orbiters by the inverse square factor. Thus we use the scaling

$$j_{ph}\ (\text{Venus}) \approx \frac{j_{ph}\ (\text{earth})}{(0.723)^2} \sim 1.9\ j_{ph}\ (\text{earth}).$$

Now j_{ph} (earth) is known to range over values from about 10^8 electrons/cm^2-sec-ster up to 3.4×10^9 elec/cm^2-sec-ster, i.e., current densities $\sim 1.6 \times 10^{-11}$ amp/cm^2 up to $\sim 8.2 \times 10^{-10}$ amp/cm^2. Thus, at Venus one expects the range

$$j_{ph} \sim 3.2 \times 10^{-11} \text{ to } 1.7 \times 10^{-9} \text{ amp/cm}^2$$

or

$$n_{ph}\bar{v}_{ph} \sim 2 \times 10^8 \text{ to } 7 \times 10^9 \text{ elec/cm}^2\text{-sec-ster.}$$

To estimate the magnitude of secondary emission fluxes from the spacecraft surfaces, we use the semi-empirical equation of E. J. Sternglass (Reference 4), which seems to be in adequate agreement with experimental results for a variety of surface materials

$$f(E) = 7.4\ f_{max}\ (E/E_{max})\ \exp\left[-2\ (E/E_{max})^{1/2}\right]$$

where E_{max} is the primary electron energy at which $f(E) = f_{max}$. These parameters take on different values for various surface materials, and a table of such values for typical spacecraft surfacing materials is given in the ESTEC Working Paper by Grard, Knott, and Pedersen (Reference 5).

For a plane surface of potential ϕ relative to plasma ground, the secondary electron flux is

$$\langle n_* v_* \rangle = \int_{v_o(\phi)}^{\infty} dv\, v\, F_e(v)\, f(E)\, (E = 1/2\, m_e v^2)$$

where $F_e(v)$ is the velocity distribution of primary electrons and $v_o = 0$ for spacecraft potentials $\phi \geq 0$, and $v_o > 0$ for $\phi < 0$. For a Maxwellian $F_e(v) = n_e \left(\frac{m_e}{2\pi\kappa T_e}\right)^{1/2} \exp\left(-\frac{1}{2} m_e v^2/\kappa T_e\right)$ one obtains

$$\langle n_* v_* \rangle = \langle n_e v_e \rangle_{sat} \frac{7.4\, f_{max}}{\sqrt{\pi}} \left(\frac{\kappa T_e}{E_{max}}\right)^{1/2} \int_{m_e^{1/2} v_o(\phi) 2\kappa T_e^{1/2}}^{\infty} dt\, t^2\, e^{-t^2 - 2\left(\frac{\kappa T_e}{E_{max}}\right)^{1/2} t}$$

which integral can be evaluated exactly in terms of error functions as follows. First, one completes the square to obtain

$$\langle n_* v_* \rangle = \langle n_e v_e \rangle_{sat} \frac{7.4\, f_{max}}{\sqrt{\pi}} \beta\, e^{-\beta^2} \int_{(m_e)^{1/2} v_o(\phi)/(2\kappa T_e)^{1/2}}^{\infty} dt\, t^2\, e^{-(t-\beta)^2} \quad \beta \equiv \left(\frac{\kappa T_e}{E_{max}}\right)^{1/2}$$

and changes the integration variable to $u = t - \beta$. Thus one obtains

$$\langle n_* v_* \rangle = \langle n_e v_e \rangle \frac{7.4\, f_{max}}{\sqrt{\pi}} \beta\, e^{-\beta^2} \int_{\left(\frac{m v_o^2}{2\kappa T_e}\right)^{1/2} - \beta}^{\infty} du\, (u+\beta)^2\, e^{-u^2}$$

For a negatively charged spacecraft, $m v_o^2/2 = -e\phi$ so that the limit can be written $(-e\phi_o/\kappa T_e)^{1/2} - (\kappa T_e/E_{max})^{1/2}$.

As an example, consider the quartz solar cell surfaces. The values are $E_{max} = 420$ eV and $f_{max} = 2.5$. For $\kappa T_e \sim 1$ eV, then $\beta = (\kappa T_e/E_{max})^{1/2} = (1/420)^{1/2} \sim 0.05$. On the other hand one expects $-e\phi_o/\kappa T_e > 1$. Thus we can ignore β in the lower limit and obtain numerically

$$<n_* v_*> = <n_e v_e> (0.88) \frac{1}{\sqrt{\pi}} \int_{(-e\phi_o/\kappa T_e)^{1/2}}^{\infty} du\, (u^2 + 2\beta u + \beta^2) e^{-u^2}.$$

Now the integral is less than its value for $\phi_o = 0$, i.e., it has a value less than

$$\frac{1}{2}\,\Gamma(3/2) + \beta + \frac{\Gamma(\frac{1}{2})}{2} \approx \frac{3}{4}\sqrt{\pi}$$

It follows that, in the absence of photoelectron emission one obtains a secondary flux from quartz

$$<n_* v_*> \leq 0.66 <n_e v_e>.$$

Suppose we assume an eclipse at "perigee" of say, 200 kilometer. The ion (CO_2^+) density according to models based on Mariner 5 indicates that

$$n_+(200 \text{ km}) \sim 3 \times 10^3 \text{ cm}^{-3} \text{ (night-side)}.$$

Using a ram speed of 11 km/s = 1.1×10^6 cm/s, an ion ram current of

$$n_+ v_{ram} = 3.3 \times 10^9 \text{ ions/cm}^2\text{-s}$$

is available, while at $T_e \sim 1$ eV

$$<n_e v_e> \sim 1.7 \times 10^{11} \text{ electrons/cm}^2\text{-s}.$$

Thus, it is easily seen that the spacecraft must charge to a sufficiently negative potential so that

$$\phi \simeq \frac{\kappa T_e}{e} \ln \frac{3.3 \times 10^9}{1.7 \times 10^{11}} = \frac{\kappa T_e}{e} \ln (0.02) \simeq -4 \text{ volts (eclipse).}$$

One should note that the ion ram current is on the order of the maximum expected photoelectron current. Thus, the potential may be as low as

$$\phi \sim \frac{\kappa T_e}{e} \ln 0.1 = -\frac{\kappa T_e}{e} \ln 10 = -2.3 \frac{\kappa T_e}{e} \sim -2.3 \text{ volts (sunlight).}$$

Another region of interest is the solar wind, there one expects $\kappa T_e \sim 20$ to 40 eV (at times) with densities on the order of $n_e \sim 10$ to 30 cm^{-3}. On the shadowed solar panel surface there will be no neutralizing ion ram current. In this case, one has in effect only the solar wind thermal ion current to balance the incident solar wind electron flux. Thus flux. Thus

$$\phi \sim \frac{\kappa T_e}{e} \ln \left(\frac{T_i m_e}{T_e m_i} \right)^{1/2} .$$

For $T_e \sim 20$ eV and $T_i \sim 10$ eV one has

$$\phi \sim \frac{\kappa T_e}{e} \ln \left(\frac{1}{3686} \right)^{1/2} = -\frac{1}{2} \frac{\kappa T_e}{e} \ln (3686)$$

or

$$\phi \sim -\frac{1}{2} (20 \text{ eV})(8.21) \sim -80 \text{ volts (dark side).}$$

On the illuminated solar array surface, on the other hand, one has a photoelectron flux say $7 \times 10^9 cm^{-2}\text{-}sec^{-1}$ and an ion ram flux on the order of $10^9 cm^{-2}\text{-}sec^{-1}$, while the thermal electron flux will be $\sim 4.4 \times 10^9 \ cm^{-2}\text{-}sec^{-1}$. This leads to

$$\phi = \frac{\kappa T_e}{e}\, \ln\left(\frac{8\times10^9}{4.4\times10^9}\right) = \frac{\kappa T_e}{e}\, \ln\,(1.82) = (20V)(0.5988) \sim= 12\text{ volts.}$$

Estimates of Pioneer Venus potentials are summarized in the table below.

Night-side 200 km		Solar Wind	
Eclipse or Shadowed Insulators	Sunlit Insulators	Shadowed Insulators	Illuminated Insulators
$\phi \sim -4$ V	$\phi \sim -2.3$ V	$\phi \geq -80$ V	$\phi \leq +12$ V

Solar Cell Conductive Coating

An indium-oxide 95 percent transparent conductive coating on the solar cell cover glasses will be helpful in minimizing the effect of the spacecraft charging on the scientific instruments. This will equalize the shadow-sunlit potential differences, thus aiding the performance of some of the low energy particle detectors, provided the estimated potentials are considered deleterious by the experimenters. Of course, solar array voltages of ±28 volts from spacecraft ground must also be considered in addition to the floating potentials calculated here. A conductive coating may be of value in shielding out this solar array voltage wherever it can affect the probe operations.

Conductive coating has been extensively studied by ESTEC for use on the GEOS (ESRO) synchronous scientific satellite. The conductive coating is also a high-priority modification of the solar array structures on the International Magnetospheric Explorer (formerly Mother/Daughter Heliocentric) project at Goddard. At the recent IME Science Working Team meeting, 28 to 30 March 1973 at GSFC, plasma wave experiment team members as well as the plasma science team (plasma probe) members strongly recommended that the IME project put on the indium oxide conductive coating to achieve a maximum resistance per square of 10^5 Ω/sq. The project reported at that time that the cost of uncoated IMP-type solar arrays was about $185 K per spacecraft, while their data indicate that with conductive coating the price would be approximately doubled, to $350 K. The cost for conductive coating for the Pioneer Venus program could easily be coubled this value because of the larger array and need for development. The conductive coating will also cost 3 to 4 percent in power. For these reasons it is not included in the baseline spacecraft.

3.3.1.8 Considerations to Minimize Instrument Contamination

The outgassing of spacecraft material has been cited as, or has been suspected of being, the cause of several experiment anomalies or failures. Details of these cases and a summary of the possible sources of contamination are given in a NASA/Ames memorandum by D. M. Chisel (Reference 6). Some of the sources of contamination are:

- Gases evolved from the desorption of gases absorbed on the surface of spacecraft materials
- Evaporation of gases in solution in the materials
- Sublimation or evaporation of materials
- Outgassing of wet space lubricants
- Outgassing from thruster and retromotor cases
- Exhaust products from hydrazine thrusters
- outgassing of pump oils absorbed during spacecraft testing.

The problems of defining the outgassed environment of spacecraft in interplanetary as well as planetary (earth) environment have been discussed by Pressman, Meyers, and Lillienfeld (Reference 7) of the GCA Corporation. The contamination problem for the scientific experiments may be broken down into several parts:

- Prelaunch and post-launch contamination of spacecraft surfaces.
- The rate of outgassing from the spacecraft
- The density of the evolved products around the spacecraft
- Backscatter of evolved products towards scientific instrument apertures.

Both the GCA report (Reference 7) and an OGO-6 report (Reference 8) by D. McKeown and W. E. Corbin, Jr. quote early outgassing rates of

10^{-10} gauss/cm^2-s. The cloud density surrounding the spacecraft is dependent on initial ejection velocity (temperature), as well as the various forces which act on it. Thruster mass flow rate computations result in velocities in the order of 10^5 cm/s, and thermal ($\sqrt{3KT/m}$) velocities of gas molecules are also in this range. Aerodynamic drag is the controlling force in the planetary environment whereas solar radiation pressure is stated to be dominant in the interplanetary regime. Residence times during which a particle may be considered a part of the cloud are reported to vary from the order of 10 seconds for a few hundred kilometer altitude (Gemini) orbiter to about 1 day for a synchronous orbiter for particle sizes in the order of 3μ. According to the GCA report these residence times are directly proportional to particle size and density.

Diffusion of neutral gas molecules away from a pulsed point source is described by:

$$\rho(r,t) = N(\beta/\pi)^{3/2}\, t^{-3} \exp(-\beta r^2/t^2)$$

where ρ = gas density at distance r and time t

N = total number of molecules released

$\beta = \frac{m}{kT}$ = (average thermal molecular velocity)$^{-2}$.

This equation, which assumes that there are no drag forces, shows that the gas density decreases as the inverse cube of time and exponentially with distance. For continuous desorption the equation is

$$\rho(r,t) = q_o\, (\beta/\pi)^{3/2}\, (2\beta r^2)^{-1} \exp(-\beta r^2/t^2)$$

where q_o = total efflux per unit time. In both cases the residence time should be less than that for the 3μ particles.

In general, the GCA report provides no answers to the final part of the problem — that of estimating the backscattered flux. Some indication is provided of the theoretical-analytical collision problems which involve spacecraft velocity, effusing flux density and velocity distribution, and the mean free paths. The main thrust of that report as indicated by its title is to define experiments to measure these contamination effects.

Our approach to the problem of minimizing contamination of the scientific instruments on Pioneer Venus is:

- Optimized layout of spacecraft with particular care in defining instrument sensor locations and orientations
- Selection of materials for minimum outgassing
- Procedural controls to prevent contamination.

Solid Rocket and Thruster Exhaust

Recent test at the JPL Molsink facility reported by Chirivella, Moynihan, and Simon (Reference 9) show the presence of exhaust plume turning angles much larger than the Prandtl-Meyer limit predicted by calculations in which nozzle boundary layer friction is neglected. An analysis of the exhaust plume of the retromotor is given in Section 8.6.2.4. The results of that analysis also show that exhaust gases may impinge on parts of the spacecraft. The solid particles, however, will be confined in a 0.35 radian (20-degrees) cone and will not hit any part of the spacecraft.

It is at the large turning angles that the boundary layer effects become important because the exhaust gases may directly affect the operation of scientific experiments. At these angles the gas is in the free molecular flow regime and the molecular flow begins near the exhaust nozzle, then it is possible to prevent any direct or spacecraft scattered emissions from the nozzle from entering an instrument aperture by mounting the instrument so that the plane containing the aperture does not intersect any portion of the spacecraft. As discussed in Section 3.2.1.1, the layout of the instruments on the Pioneer Venus probe bus satisfies this criterion.

Some of the scientific experiments may be extremely sensitive to retromotor or repeated thruster firings. For these instruments we recommend the use of "captured" contamination covers or heaters. The covers would be closed for each firing. Heaters are being employed on the Atmosphere Explorer Electron Temperature Probe to boil off contaminants which may have absorbed onto its sensor.

After orbit insertion the thrusters on the orbiter will be fired only near apoapsis. Therefore, about 12 hours will elapse before the spacecraft reaches an atmosphere sufficiently dense to cause any significant backscatter of any exhaust products being evolved from contaminated spacecraft surfaces towards the instrument apertures. Outgassed constituents from the solid rocket propellant prior to motor firing are precluded from exiting the central cylinder by the thermal insulation that completely encases the motor. Any outgassing products evolving from the motor case materials are likewise controlled. In addition to the protection provided by the thermal insulation, propellant outgassing is inhibited by a weather seal located in the motor nozzle. Outgassing of the motor case insulation will occur after the orbit insertion burn of the solid rocket motor. This outgassing, however, will be directed out the nozzle and most likely be in the free molecular flow regime. Few, if any, of these molecules will reverse their translational velocities and impinge on the spacecraft.

Selection of Organic Outgassing Materials for Pioneer Venus

Many recent spacecraft programs have utilized rigid selection criteria for nonmetallic materials in order to minimize the potential outgassing problem. Since the mean free path of molecules leaving the spacecraft surface is very large, and recondensation can only occur on relatively colder surfaces, it is actually possible through analysis of the spacecraft geometry, and knowledge of location of critical surfaces, to be selective in specification of those areas requiring special material selection. However, in the interest of reliability it has generally been considered more desirable to impose a general minimum outgassing requirement on all materials. In most cases this has been accomplished by one of two similar techniques.

The NASA/Marshall specification (Reference 10) requires a minimum steady state outgassing rate for materials heated to 100°C, and in addition imposes a limitation on total weight loss and the quantity of outgassed products greater than atomic mass unit 44. The latter is determined by residual gas analysis. This approach was utilized in the design of the solar array system for the Skylab program at TRW and will also be a consideration in the construction of the HEAO spacecarft. Unfortunately, for a variety of reasons such as incomplete sample history, much of the information in the approved materials data bank is inconsistent. In addition, there is no qualification presented to allow comparison of marginal versus truly low outgassing materials.

The second technique commonly used to control outgassing of spacecraft materials is imposing maximum acceptable weight loss (1 percent) and condensible products (0.1 percent) upon materials when exposed to a temperature of 125°C in a vacuum. This method has been used by NASA/Goddard, NASA/Houston and SAMSO, and is based on a test technique developed by Stanford Research Institute (Reference 11). The approach must be used judiciously, since large quantities of barely acceptable materials can be used adjacent to sensitive surfaces. In addition, the test is technique-sensitive as demonstrated by the fact that different test facilities do not always agree on acceptable materials. However, the data obtained is published (Reference 12 and 13), and this allows the use of some judgment in comparing the degree of outgassing for various materials and material treatments.

Equipment carried on board the OGO-6 spacecraft (Reference 8) has shown that outgassed materials were primarily associated with "epoxy" (actually silicone) materials used in the solar array system and with contamination of the spacecraft during thermal-vacuum testing. These same tests demonstrated the directionality of these outgassed products, since the contamination rate dropped to near zero when the instruments were pointed away from the spacecraft. The authors further indicate that the rate of outgassing measured was extremely low and reflected appropriate care in materials selection.

Since the design of OGO-6, a number of factors have emerged which would tend to reduce significantly the quantities of outgassed materials. Improved materials technology and data availability allow for more judicious selection of nonmetallic materials than was possible at that time. Silicone resin systems developed specifically for space application have been made available and are currently utilized routinely. Spacecraft cleanliness is more carefully controlled through assembly of critical components in controlled areas. In addition, prebaking of suspect ancillary test materials, such as insulation and wiring, combined with "cold fingering" and bakeout procedures have been utilized to preclude spacecraft contamination dui ng thermal-vacuum testing.

The above procedures, i.e., appropriate materials selection to a weight loss/VCM criterion, coupled with improved spacecraft handling techniques, should be more than adequate to eliminate problems from recondensation of outgassing products on sensitive surfaces. In Pioneer Venus, the on-board presence of mass spectrometers creates additional concern over potential distortion of experimental data. To assure that real data are acquired, the sensitivity of the experiments to various molecular species must be established. With this information, it then becomes possible to select materials for those areas which are critical for providing uncontaminated spectrometer measurements. This would be accomplished through the use of the thermal gravimetric analysis and residual gas analysis techniques utilized by Martin Marietta to screen materials for such programs as the Viking Biological Experiment and others (Reference 14). Using this technique it is possible to determine total weight loss, condensible materials, weight loss rate at use temperatures, and mass numbers of outgassed species. Those materials demonstrating significant amounts of interfering species could then be eliminated entirely for critical areas.

The approach to materials selection for contamination control for the Pioneer Venus spacecraft would specifically:

- Utilize the NASA/Goddard or NASA/Houston criteria of 1 percent weight loss and 0.1 percent VCM for selection of all nonmetallic materials to be used in the construction of the spacecraft. Materials used would either be selected from published data of materials already tested and approved using the SRI technique (Reference 6) or the Martin Marietta technique which provides the same information (Reference 9), through thermal gravimetric analysis. Any materials not already tested would be submitted to Martin Marietta to obtain pertinent data.

- Request experimenters to specify the limits of contamination sensitivity of their equipment. Using this information and knowledge of the geometry of the spacecraft, submit to Martin Marietta any materials in critical areas that have not already been tested for residual gas analysis testing to determine mass numbers of outgassed constituents. Materials which might contaminate instrumentation would then be preconditioned or eliminated from consideration.

Procedural Controls

Contamination controls begun at the manufacturer for science black boxes must be continued after delivery to the spacecraft contractor. The individual instrument black boxes must be transported only in the approved shipping containers, which use packing materials compatible with the sensitive detectors within the instruments. Each packaged instrument is delivered to the spacecraft test area by the instrument representative using an approved mobile service dolly.

Mechanical inspection of each instrument is performed by the spacecraft contractor Quality Assurance personnel. All instrument handling operations are done by personnel using white, nonstatic, cotton gloves. A detailed inspection is made of mounting surfaces and connector interfaces and discrepancies noted on the receiving inspection form. Unit level weight, and center of gravity information is also recorded at this time. Nonflight red tag or protective covers are removed for this operation only with the approval of the instrument test representative. Prior to the mechanical installation of the instrument on the spacecraft, the instrument case surfaces are cleaned with a lintless cloth and methyl alcohol. All paper tags are removed from the instrument at this time. The unit is mechanically mounted to the spacecraft by spacecraft test personnel, again using white cotton gloves. Careful attention to sensors and detectors is observed throughout this operation. Spacecraft test crew personnel including scientific instrument test representatives who are performing mechanical or electrical test operations around the spacecraft are required to wear white, nonstatic smocks.

The transfer of airborne particulate contamination to the surfaces of the various black boxes is reduced significantly through the use of high density filters in the closed-loop air conditioning system in the assembly and test areas. During the transportation of the spacecraft between test facilities the spacecraft is sealed in its shipping container and a positive GN_2 purge to the container is provided during the entire transfer operation. Instruments whose detectors are subject to degradation in the presence of high ambient humidity conditions can be provided individual GN_2 purge at low flow rates. This requirement, however, significantly limits the routine day-to-day spacecraft test and handling operations at the contractor and at the launch site.

During thermal vacuum testing of the spacecraft, precautions are taken with the chamber control personnel to assure that all spacecraft structural elements (including black boxes) are kept warmer than the chamber cold wall during the entire thermal vacuum test, including pumpdown and pumpback to atmosphere. Test chamber personnel use formal procedures documenting these control techniques. Thermal vacuum chambers are equipped with automatic valve operation to preclude back flowing of silicone vacuum pump oil into the chamber in the event of pump or power failure.

During the thermal vacuum test of Pioneer 11, special plates were mounted in the chamber to determine the extent and type of contaminants present during the test. A NASA/Ames memorandum by F. G. Gross, dated 20 November 1972, reports that, "The analyses of the residues on the plates by IR spectroscopy and gas chromatography-mass spectrometry indicated the presence of mostly polyvinyl acetate and DEHP (di-2-ethylhexyl phthalate) in approximately the same quantity on each plate. The total amount on each plate may be described as moderate (a few milligrams). The polyvinyl acetate could have come from some protective film, or lacquer, or adhesive; DEHP is the most common plasticizer in use today, and therefore, it is one of the most frequently found contaminants in thermal vacuum testing. There was no evidence of vacuum pump oil in any of the samples." It has been subsequently determined that the poly-vinyl acetate and DEHP detected on the plates were due to emission from surfaces on the spacecraft and not from the thermal vacuum system.

We recommend a similar monitoring during the Pioneer Venus thermal vacuum test. If the plates show the presence of a significant amount of contaminants, which in view of the above memorandum does not appear to be likely, the spacecraft should have an additional bake out with a cold wall in the thermal vacuum chamber, following thermal vacuum test.

3.3.2 Probe Bus Instrument Interfaces

The scientific instrument interface requirements and accommodations for the probe bus are presented in the following two subsections.

- Section 3.3.2.1 presents the preferred Atlas/Centaur-launched probe bus accommodations for the Version IV science payload (without supporting detail).
- Section 3.3.2.2 presents: 1) chronologically the requirements and tradeoffs leading up to the preferred accommodations, and 2) the requirements and details of the preferred accommodations. The requirements and accommodations are presented first for the nominal instrument complement and then for the other candidate instruments as given by NASA in the Pioneer Venus Science Definition Reports of 22 September 1972, for a Thor/Delta-launched mission (payload Version I); and of 20 October 1972 for an Atlas/Centaur-launched mission (payload Version II). Late in December 1972, a set of "Preliminary Experiment Interface Descriptions" were received (ASD: 244-9/22-349). At that time the probe mission was planned for 1977 launch; the instrument accommodations were designed from the analyses and tradeoff studies of alternate trajectory and orbit configurations for those mission dates.

On 13 April 1973, NASA redefined the Pioneer Venus missions to consist of dual 1978 launches for both the probe mission and the orbiter mission using the Atlas/Centaur launch vehicle, and provided a new scientific instrument payload with more detailed instrument descriptions and parameters. New lists of baseline instruments and other candidate instruments were given for the probe mission; these are referred to as the Version IV instruments. Their requirements and accommodations are presented in separate sections following the sections describing the earlier instrument payloads. For brevity, the requirements and accommodations of the Version IV science payload instruments are described whenever possible by comparison with the earlier versions and by noting the nature and significance of the changes. Instrument parameters in addition to those provided by NASA have been chosen by discussions with possible experimenters and by consulting the literature.

3.3.2.1 Summary of Preferred Science Accommodations for New Atlas/Centaur Version IV Science Payload

This section summarizes the accommodations of the preferred configuration Atlas/Centaur launched bus with the Version IV payload. The requirements, tradeoffs, justifications, and studies leading to the selection of these preferred accommodations are given in Section 3.3.2.2.

Mechanical ALL VERSION IV SCIENCE PAYLOAD

Mechanical instrument layout and mounting configurations are shown in Figures 3-89 and 3-90 for the nominal payload instruments and the nominal plus other candidate instruments, respectively. The neutral and ion mass spectrometers are mounted to view parallel to the spin axis and the electron temperature probe to lie perpendicular to the spin axis in order to employ the ram direction upon Venus entry with maximum effectiveness. In the nominal payload (Figure 3-89), the retarding potential analyzer sensor head is similarly oriented for the same reason. The ultraviolet spectrometer is mounted to view at 0.14 radian (8.2 degrees) to the spin axis for the 1978 launch trajectory and has a 0.02 x 0.003 radians (1.2 x 0.17 degrees) field of view with the long slit dimension perpendicular to the spin axis to permit viewing in the direction of the local horizon at 150 kilometers, which is approximately the latitude of the maximum day glow. The retarding potential analyzer, the electron temperature probe, and the ion mass spectrometer are instruments that are sensitive to the effects of spacecraft charging and electrical potential variation from the ambient plasma, as is discussed in the paragraph titled "Spacecraft Charging Considerations for the New Science Payload (Version IV Redirection)." The ion mass spectrometer is located sufficiently far from the spacecraft solar array compared with the Debye length of the plasma at 200 kilometers so that the electric field from the array should not affect the instrument. The retarding potential anal zer and the electron temperature probe further require that a spacecraft surface area of at least 1.5 m^2 be conducting. During entry the conducting surface should not be in the wake of the spacecraft. This requirement is satisfied in the preferred configuration, as shown in the figures.

The field of view of the neutral mass spectrometer is a 0.35-radian (20-degree) full cone angle while the ion mass spectrometer may have a considerably wide field of view, up to a 1.57-radian (9-degree) full cone angle, as shown, thus easily satisfying the requirement that the view direction should lie within ±0.26 radian (±15 degrees) to the velocity vector, while the retarding potential analyzer requires a full 2π solid angle field

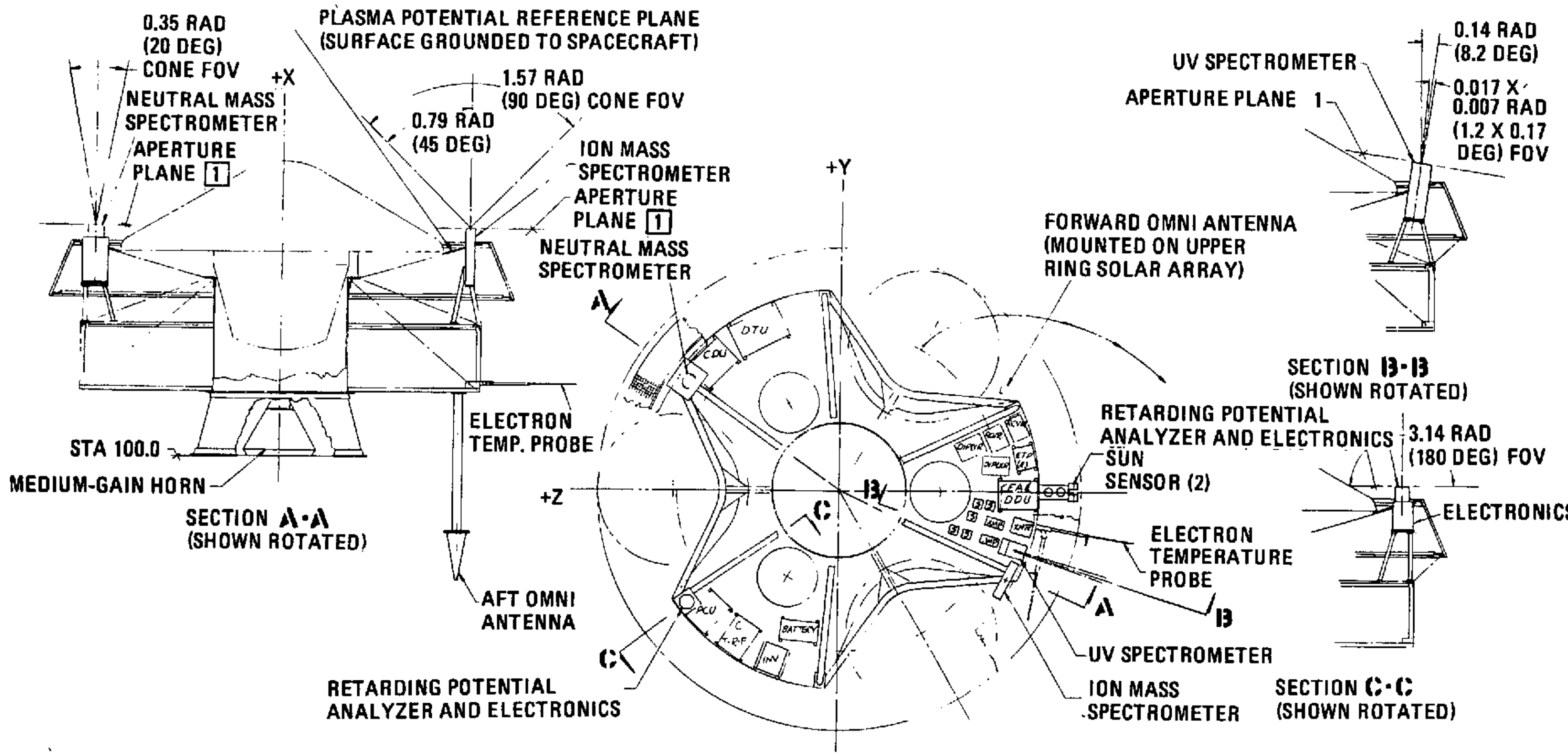

VIEW EQUIPMENT PLATFORM
LOOKING AFT

NOTES:

1 APERTURE PLANE DOES NOT INTERSECT ANY PART OF SPACECRAFT BUS THEREFORE EMISSIONS FROM SPACECRAFT OR THRUSTERS CANNOT ENTER DIRECTLY INTO APERTURE.

Figure 3-89. Atlas/Centaur Probe Mission Nominal Science and Equipment Layout, Version IV Science Payload

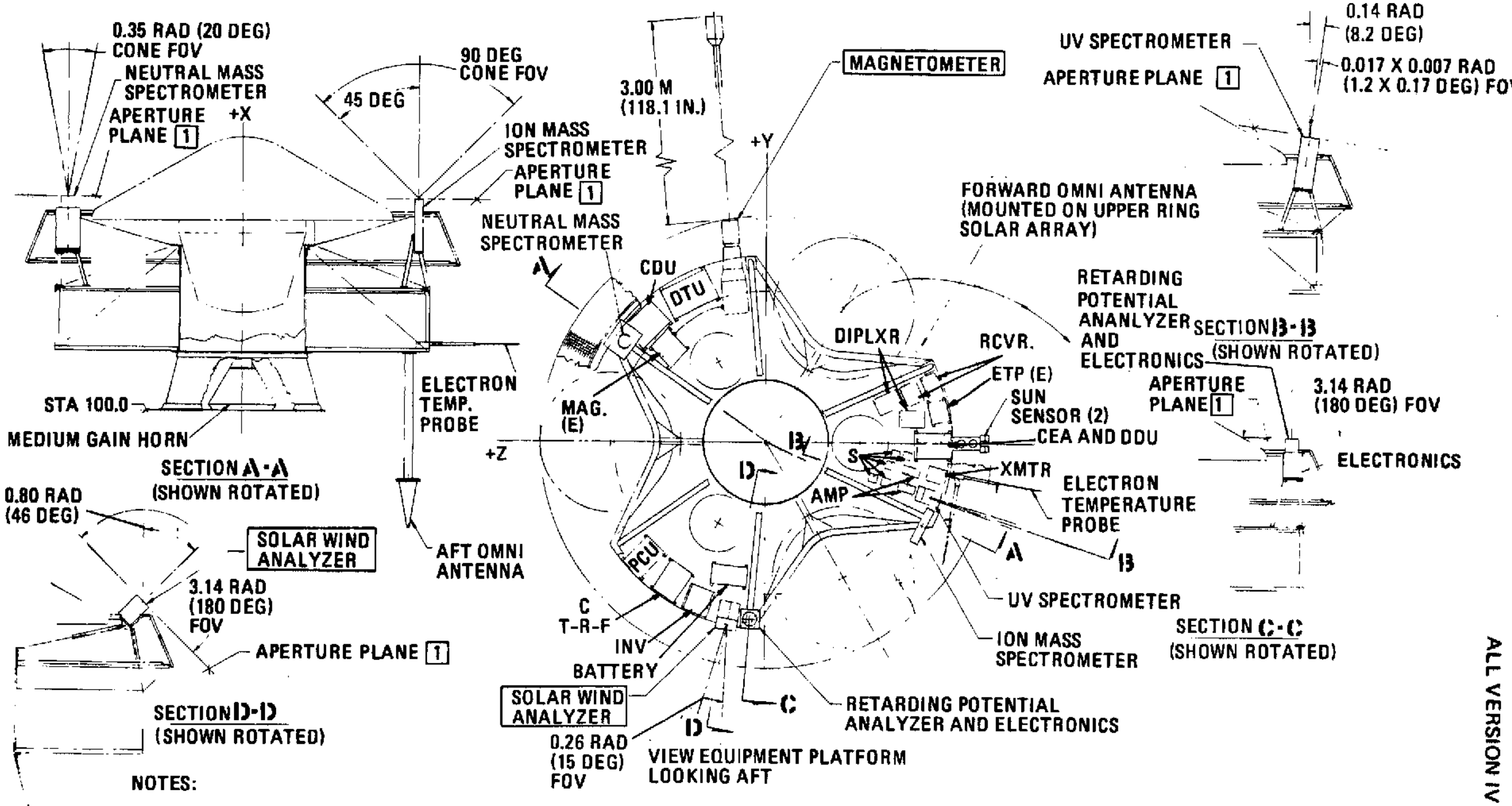

NOTES:

[1] APERTURE PLANE DOES NOT INTERSECT ANY PART OF SPACECRAFT BUS THEREFORE EMISSIONS FROM SPACECRAFT OR THRUSTERS CANNOT ENTER DIRECTLY INTO APERTURE.

2. [ITEM] DENOTES OTHER CANDIDATE INSTRUMENTS.

Figure 3-90. Atlas/Centaur Probe Mission Science Equipment Layout with Other Candidate Instruments of view. These conditions are all met, since these instruments and the ultraviolet spectrometer (and the solar wind analyzer, in the other candidate instrument category) are located to have 2π unobstructed access (after ejection of the probes) so that in each case the instrument aperture plane does not intersect any part of the spacecraft, and therefore emissions from the thrusters or from outgassing of spacecraft materials cannot enter directly into the aperture.

Additional mechanical accommodations for the other candidate instruments are as follows:

- The magnetometer sensor is mounted on a boom with a length of 3 meters (10 feet) to achieve a spacecraft magnetic field in space less than 5 NT at the sensor
- The field of view requirement of the solar wind analyzer is satisfied by an unobstructed 0.35 x 2.09 radians (20 x 120 degrees) fan-shaped acceptance angle within which the solar direction is included as centrally as possible. For the 1978 probe mission the angle between the solar direction and the spin axis (sun aspect angle) varies between about 0.35 and 1.13 radians (20 and 65 degrees) with angles less than 0.52 radian (30 degrees) occurring for the first 80 days of the mission. Since the instrument operates with maximum effectiveness throughout cruise as well as at Venus entry, the instrument is mounted with the axis of its field of view at about 0.70 radian (40 degrees) to the spin axis and with the ±1.05-radian (±60-degree) wide fan angle parallel to the spin axis in order to accept particles along and near to the solar direction at all times.

Data Handling and Signals to Instruments

The preferred data handling system is very similar to the Pioneer 10 and 11 data system. Four mainframe science formats are provided for science data. The availability of four formats provides a convenient way to change science instrument data rate allotments between cruise and entry. Each mainframe format provides 704 bits for scientific measurements. Inputs to the mainframe format may be digital or analog that is converted in the telemetry unit to 10-bit digital. Any bit length bit train for the science instrument is acceptable.

Two subcommutated science formats are available for use for low rate science housekeeping data. The inputs may be either analog or digital. The length of the words in these formats is either 1 bit in groups of 10 bits for accepting as input signals bilevel status bits; or 10 bits for accepting as input signals analog or digital data from the scientific instruments. The two formats are telemetered in a subcommutated science word of the main frame. Up to 40 10-bit or analog words can be accepted. The analog words must be normalized from 0 to +5 volts. Up to 48 bilevel status words can also be accepted from the science instruments.

The probe bus will be capable of providing at least 50 discrete commands to the science instruments for performing these functions, leaving a large number of commands available for growth.

The following signals will be generated and provided to the scientific instruments as required for timing, changing modes, and roll azimuth determination:

Bit rate signals
Word rate pulses
Frame rate pulses
Subframe rate pulses
Clock pulses
Shift clock pulse
Mode signals
Format signals
Roll index and spin period sector pulses
Word gate signal

The roll index pulse will provide for view direction control. A pulse is sent to the instruments when a fixed reference line on the spacecraft perpendicular to the spin axis passes through the ecliptic plane. A spin period sector generator will also provide as-required pulses at the following rates:

One pulse each 1/8 of roll index pulse period
One pulse each 1/64 of roll index pulse period
One pulse each 1/512 of roll index pulse period.

3.3.2.2 Details of Science Requirements and Accommodations

Mechanical, Thermal, and Power

ALL VERSION III SCIENCE PAYLOAD

Requirements for the probe bus baseline instruments are shown in Table 3-29 for the Thor/Delta configuration and in Table 3-30 for the Atlas/Centaur configuration. The Thor/Delta probe bus and the Atlas/Centaur probe bus accommodate these requirements in each case.

The maximum power for science instruments, 15.9 and 24.5 watts (at 28 volts ±2 percent), are provided in the Thor/Delta and Atlas/Centaur

Table 3-29. Thor/Delta Configuration Probe Bus Science Instruments (Nominal Payload)

INSTRUMENT	WEIGHT [KG (LB)]	VOLUME [M^3 (IN.^{3})]	TEMPERATURE (°C)	POWER (WATT)
NEUTRAL MASS SPECTROMETER	5.0 (11.0)	5.75×10^{-3} (350)	-30 TO +60	5.9
ION MASS SPECTROMETER	1.36 (3.0)	3.43×10^{-3} (240)	-30 TO +60	2.0
ELECTRON TEMPERATURE PROBE				2.0
SENSOR	0.14 (0.3)	8.65×10^{-7} (.055=18" X 1/16" DIA)		
ELECTRONICS	1.00 (2.2)	1.77×10^{-3} (108=6" X 6" X 3")	-30 TO +60	
ULTRAVIOLET FLUORESCENCE	1.36 (3.0)	1.97×10^{-3} (120)		2.5
ELECTRONICS			-30 TO +40, OPERATING	
MAGNETOMETER				3.5
SENSOR	0.50 (1.1)	1.03×10^{-3} (63)	-20 TO +20, OPERATING -40 TO +60, NONOPERATING	
ELECTRONICS	1.81 (4.0)	3.28×10^{-3} (200)	0 TO 60, OPERATING -20 TO +80, NONOPERATING	
TOTAL	11.2 (24.6)	17.7×10^{-3} (1073)		15.9

Table 3-30. Atlas/Centaur Configuration Probe Bus Science Instruments (Nominal Payload)

INSTRUMENT	WEIGHT [KG (LB)]	VOLUME [M^3 (IN.^{3})]	TEMPERATURE (°C)	POWER (WATT)
NEUTRAL MASS SPECTROMETER	5.45 (12.0)	8.195×10^{-3} (500)	-30 TO +60	12.0
ION MASS SPECTROMETER	1.45 (3.2)	3.934×10^{-3} (240)	-30 TO +60	2.0
ELECTRON TEMPERATURE PROBE	1.0 (2.2)	1.639×10^{-3} (100)	-30 TO +60	2.5
ULTRAVIOLET FLUORESCENCE	1.6 (3.5)	1.967×10^{-3} (120)		
ELECTRONICS			-30 TO +40, OPERATING	4.0
MAGNETOMETER	2.5 (5.5)	3.937×10^{-3} (240)		4.0
SENSOR			-20 TO +20, OPERATING -40 TO +60, NONOPERATING	
ELECTRONICS			0 TO +60, OPERATING -20 TO +80, NONOPERATING	
TOTAL	12.0 (26.4)	19.672×10^{-3} (1200)		24.5

configurations, respectively. Both configurations provide platform-mounted instruments with a thermal environment limited to the temperature range of 4 to 27°C. The boom-mounted magnetometer sensor is exposed to varying solar intensities. Preliminary analysis given in the thermal control section of this report indicates that the sensor can be thermally controlled to the required operational range of -20 to +20°C; a carefully designed passive system is used that employs both multilayer insulation and radiator surface in respective fractional parts of the housing surface area determined by the internal power dissipation.

Instrument mounting configurations are shown in Figures 3-91 and 3-92 for the Thor/Delta and the Atlas/Centaur probe bus, respectively. Magnetometer boom lengths of 3 meters (10 feet) are provided for the Thor/Delta and Atlas/Centaur probe bus spacecraft. In each case the degaussed spacecraft magnetic field at the magnetometer sensor is less than 5 nT. A closed cross-section deployable/retractable boom, based on a Viking design, has been selected. Since the boom is in the plane of the small probes' paths after their release, it is necessary to retract the magnetometer before the release of small probe No. 3; following probe release the boom is then deployed again.

Two additional booms are provided. One is 0.915 meter (3 feet) long and is designed to support the grating for the ultraviolet fluorescence experiment, with the orientation of the grating known relative to a spacecraft-fixed coordinate system during that portion of the entry in which data can be obtained. The other boom is a 0.458 meter (1.5 feet) long, 0.00159 meter (0.00529 foot = 1/16 inch) diameter probe for the electron temperature probe experiment. Both the grating boom and the electron temperature probe fold down on the surface of the spacecraft, and are spring-loaded to deploy after all spacecraft maneuvers exceeding 1 G are performed; when deployed both of these small booms have their long dimension perpendicular to the probe bus spin axis and hence nearly perpendicular to the spacecraft velocity vector.

The scientific instrument and spacecraft subsystem packages have been located on the spacecraft instrument platform as shown in Figures 3-91 and 3-92. The Thor/Delta and Atlas/Centaur configurations are very

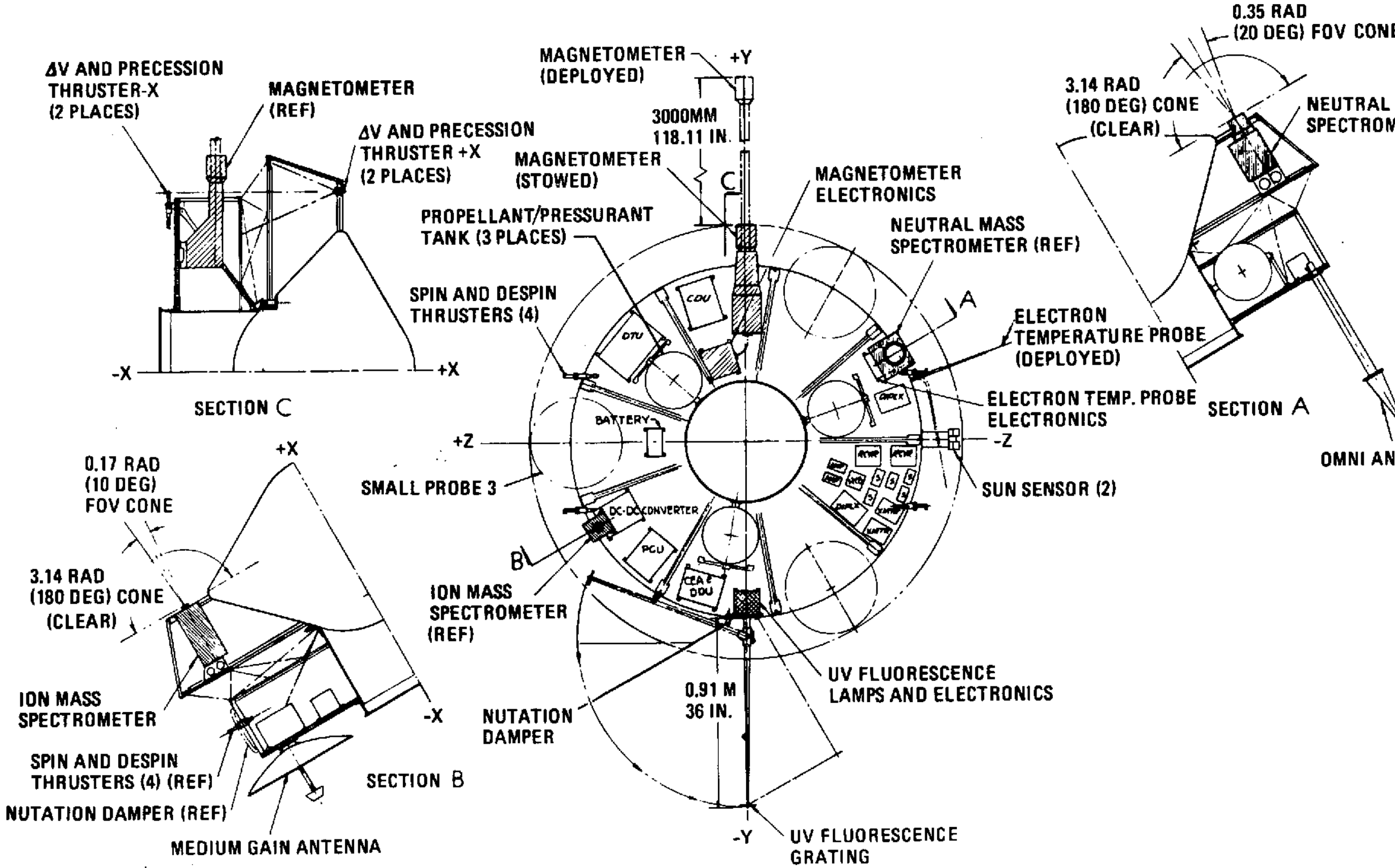

Figure 3-91. Thor/Delta Probe Mission Science and Equipment Layout

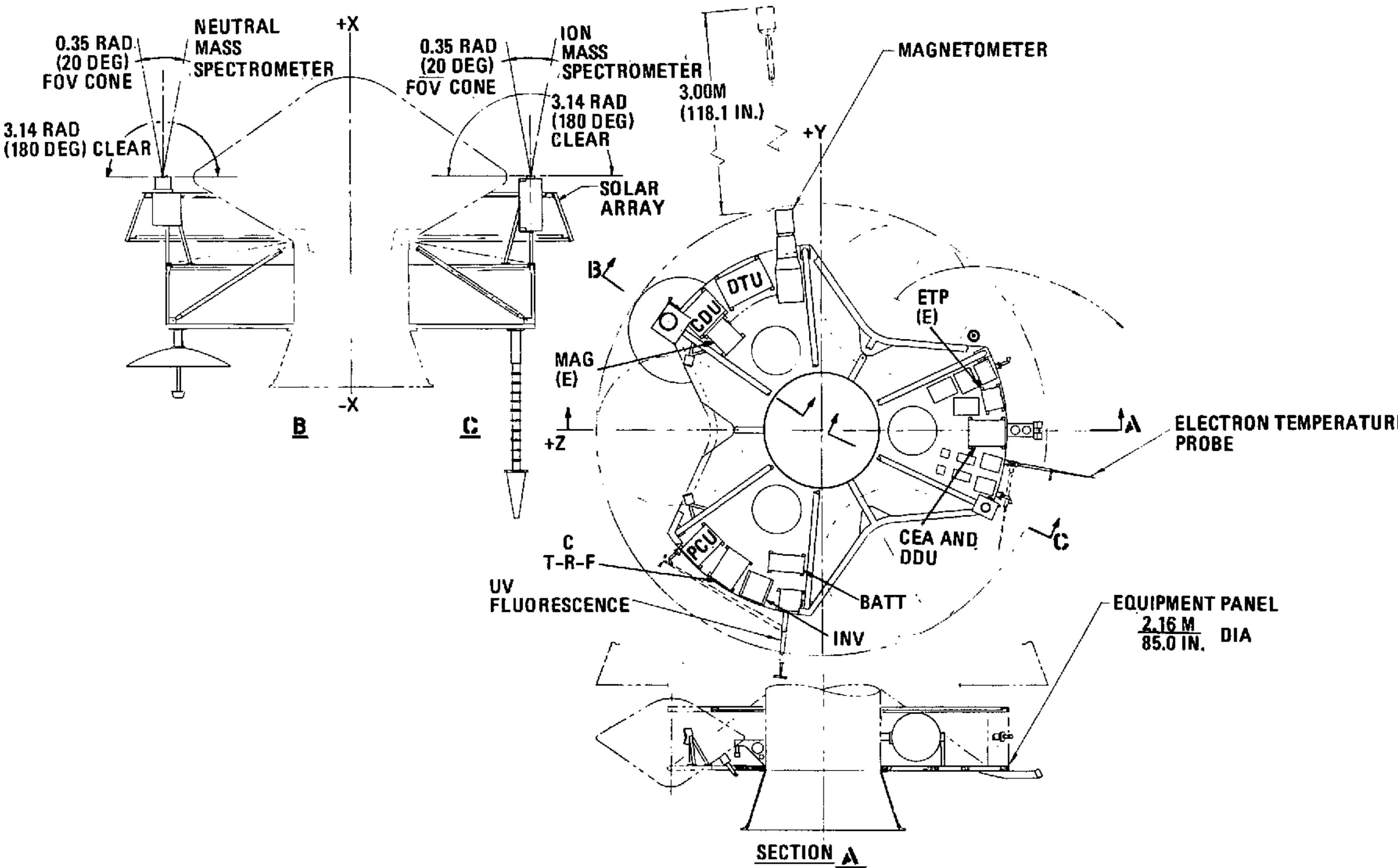

Figure 3-92. Atlas/Centaur Probe Mission Science and Equipment Layout, Version III Science Payload

similar, and each satisfies all identified experiment requirements and desirable characteristics as follows:

- Batteries and power system units are located on the opposite side of the platform from the magnetometer boom in order to minimize the stray field at the magnetometer sensor and hence the boom length as given above.
- The ultraviolet fluorescence lamp radiates a beam at 87 degrees to the spin axis to the boom-mounted grating.
- The neutral mass spectrometer and the ion mass spectrometer view along the spacecraft spin axis for ram orientation on entry; both instruments have 0.35-radian (20-degree) full-cone field of view and are located to have 2π unobstructed access (after ejection of the probes) so that the aperture plane does not intersect any part of the spacecraft and therefore emissions from the thrusters or from the spacecraft materials cannot enter directly into either aperture.
- Similarly, the ultraviolet spectrometer and the infrared radiometer have been located so that the apertures are clear of direct spacecraft emissions.

In addition to the five instruments discussed above which comprise the nominal, or baseline, probe bus payload, NASA listed two other candidate instruments in the Science Definition Reports of 22 September and 20 October 1972 for the Thor/Delta and Atlas/Centaur Version III payload configurations, respectively. These were a dayglow photometer and a solar wind probe. Figure 3-93 shows the capability of the baseline probe

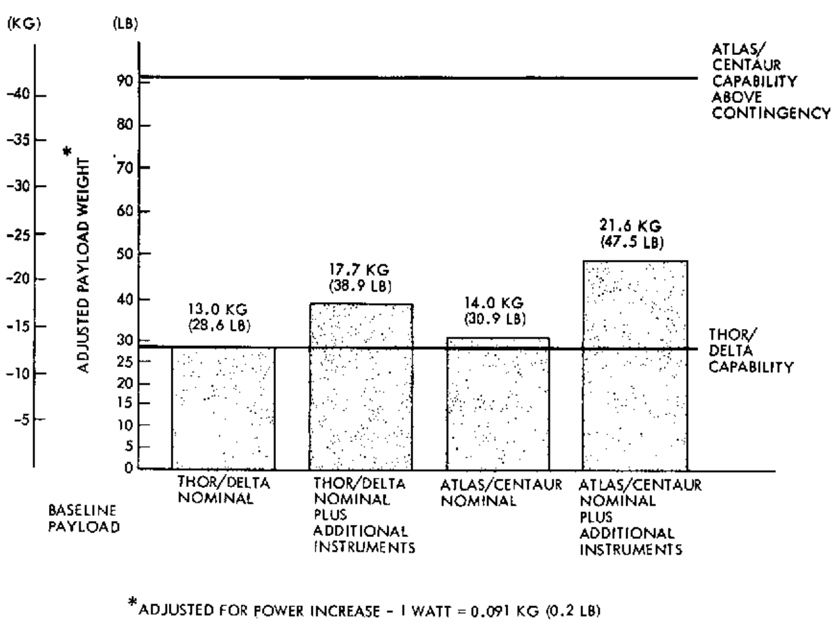

Figure 3-93. Baseline Probe Bus Capability for Additional Instruments

bus to accommodate the weight and power requirements of these instruments. It is possible to generate a watt of power at Venus at a weight cost of 0.091 kilogram (0.2 pound); the power requirements of the additional instruments are thus shown in terms of weight and labeled "adjusted" payload weight. The Thor/Delta and Atlas/Centaur probe bus capabilities are also shown in the figure, expressed in terms of total adjusted payload weight. The Thor/Delta baseline payload has no additional capability for other candidate instruments, while the Atlas/Centaur configuration has ample capability to accommodate both instruments as well as others that might be considered.

The equipment layout diagram, including these two instruments in addition to the baseline payload, is shown in Figure 3-94. The dayglow photometer is mounted to view in a direction at 0.70 radian (40 degrees) to the spin axis with a 0.02-radian (1-degree) full cone field of view centered within a 0.26-radian (15-degree) unobstructed cone which should be free of scattered light; this view direction will look at the planet at least once per rotation starting at an altitude of 700 000 kilometers (2.3×10^9 feet). The solar wind probe requires an unobstructed field of view 0.35 by 2.09 radians (20 by 120 degrees) with the solar direction included as centrally as possible within the field of view. The earth-vehicle-sun angle varies between 1.61 and 3.07 radians (92 and 176 degrees) during the 1977 probe mission. The geometry is simpler and more advantageous for an earth-pointing spacecraft than for the normal-to-Venus orbit plane (NVOP) case. For the earth-pointing spacecraft, the angle between the solar direction and the spin axis (sun aspect angle) varies between about 0.21 and 1.15 radians (12 and 66 degrees); hence, the solar wind probe may be mounted with the axis of its field of view at 0.70 radian (40 degrees) to the spin axis and with the ±1.05-radian (±60-degree) wide fan angle parallel to the spin axis in order to accept particles along and near to the solar direction at all times. The instrument operates with maximum effectiveness throughout cruise as well as at Venus entry. For the NVOP spacecraft, a different instrument design is required. In this case the instrument must view normal to the spin axis and will look in the solar direction once per revolution. A more nearly summetrical, rather than a thin fan, field of view is required to

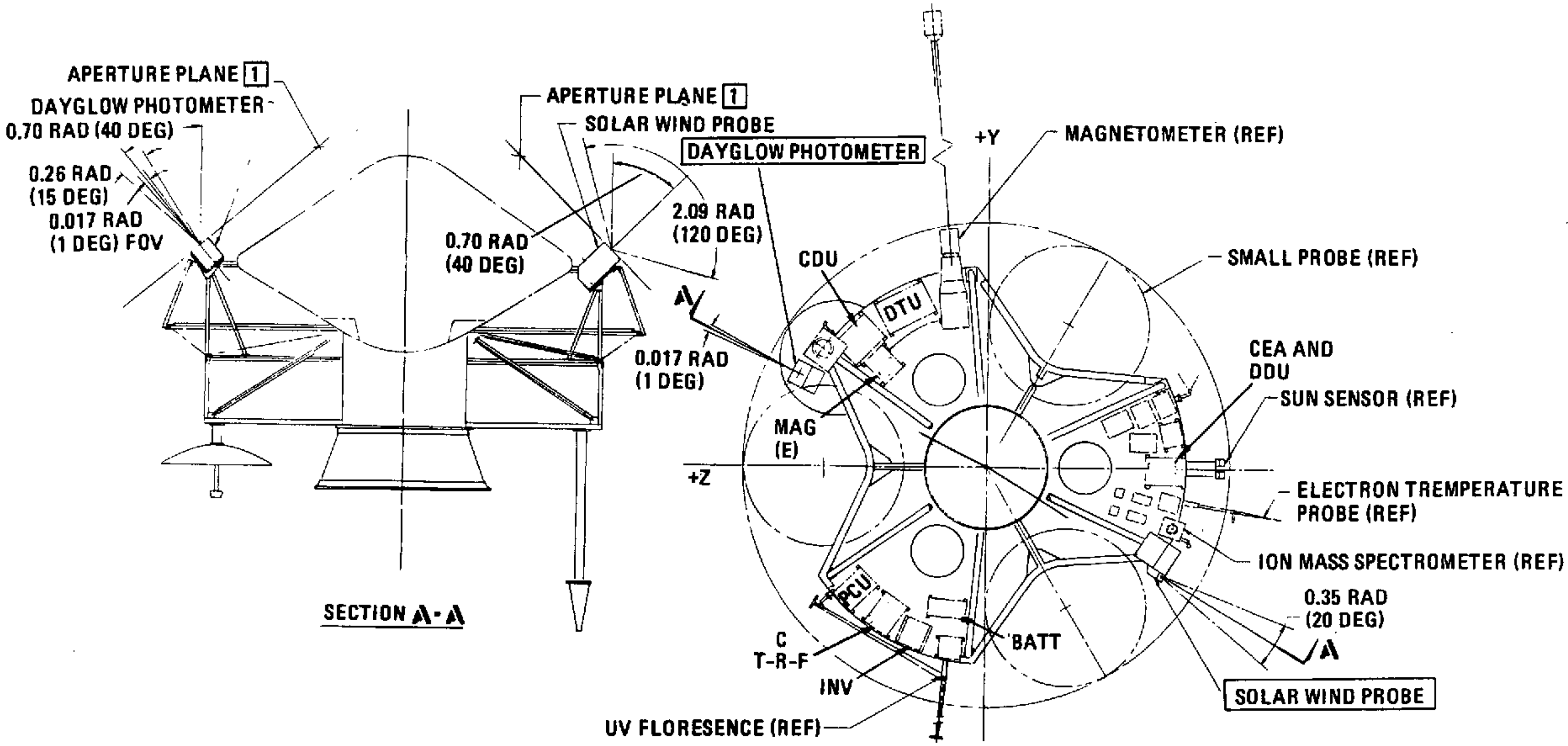

NOTE:

1 APERTURE PLANE DOES NOT INTERSECT ANY PART OF SPACECRAFT BUS THEREFORE EMISSIONS FROM SPACECRAFT OR THRUSTERS CANNOT ENTER DIRECTLY INTO APERTURE.

Figure 3-94. Atlas/Centaur Probe Mission Science and Equipment Layout (Including Other Candidate Instruments) Version III Science Payload measure particles at directions near the solar direction. If the spacecraft is reoriented to earth-pointing at Venus entry, a second instrument is required to view at the proper angle to the spin axis [1.13 radians (65 degrees) for the 1977 mission, 0.80 radian (46 degrees) for the 1978 mission] to look in the solar direction at that time in the mission. Thus, the earth-pointing spacecraft all the way is easiest for the solar wind probe design, and the layout configuration in Figure 3-94 is appropriate to the earth-pointing mode. These instruments have also been located so that their apertures are clear of direct spacecraft emissions, as shown in Figure 3-94.

Thermal requirements for these instruments are taken to be within the approximate range of -30 to +40°C met by other equipment-platform mounted instruments; no special thermal problem is anticipated at this time.

Mechanical, thermal, and power requirements of the two "other candidate instruments" as additions to the nominal, or baseline, instruments are easily met within the growth capability of the Atlas/Centaur probe bus design.

Effect of New Science Payload (Version IV) on Instrument Mechanical and Power Requirements and Accommodations. The redirected science payload (Version IV) substituted an ultraviolet spectrometer for the former ultraviolet fluorescence instrument and a retarding potential analyzer for the magnetometer in the nominal, or baseline instrument list; it included the magnetometer and a solar wind analyzer as other candidate instruments in place of the dayglow photometer and the solar wind probe. Nominal values were given by NASA of weight, volume, and power for each of the five nominal payload instruments and two other candidate instruments, with instruction to assume tolerances of +15 percent, -5 percent in weight, +15 percent in volume, and +20 percent, -10 percent in power. Accommodation of the new science payload has been provided for the worst-case condition given by using weight, volume, and power values for each instrument equal to the nominal plus the maximum positive tolerance.

Table 3-31 compares the values for the Version IV science payload with the values for the corresponding previous Atlas/Centaur Version II payload. It will be noted that the Version IV nominal payload represents

Table 3-31. Probe Bus Experiments, Version IV, Atlas/Centaur Only

	WEIGHT (W) [KG (LB)]			VOLUME (V) [CC (IN.^{3})]			POWER (P) (WATT)		
	W_{IV} (NOMINAL)	W_{IV}' (W_{IV}+15%)	ΔW ($W_{IV}'-W_{II}$)	V_{IV} (NOMINAL)	V_{IV}' (V_{IV}+15%)	ΔV ($V_{IV}'-V_{II}$)	P_{IV} (NOMINAL)	P_{IV}' (P_{IV}+20%)	ΔP ($P_{IV}'-P_{II}$)
<u>NOMINAL PAYLOAD INSTRUMENTS</u>									
NEUTRAL MASS SPECTROMETER	5.5 (12.0)	6.3 (13.8)	+0.85 (+1.80)	8195 (500)	9423 (575)	+1228 (+75)	12.0	14.4	+2.4
ION MASS SPECTROMETER	1.6 (3.5)	1.84 (4.03)	+0.39 (+0.83)	2459 (150)	2828 (173)	-1106 (-67)	2.5	3.0	+1.0
ELECTRON TEMPERATURE PROBE	1.0 (2.2)	1.15 (2.53)	+0.15 (+0.33)	1500 (91.5)	1725 (105.2)	+86 (+5.2)	3.0	3.6	+1.1
ULTRAVIOLET SPECTROMETER (VERSUS UV FLUORESCENCE)	2.7 (6.0)	3.1 (6.9)	+1.5 (+3.4)	2295 (140)	2639 (161)	+672 (+41)	1.5	1.8	-2.2
RETARDING POTENTIAL ANALYZER (VERSUS MAGNETOMETER)	1.2 (2.7)	1.38 (3.1)	-1.12 (-2.4)	1967 (120)	2262 (138)	-1675 (-102)	2.5	3.0	-1.0
TOTAL NOMINAL PAYLOAD IV VERSUS II	12.0 (26.4)	13.77 (30.4)	+1.77 (+3.96)	16416 (1002)	18879 (1152)	-793 (-48)	21.5	25.8	+1.3
<u>OTHER CANDIDATE INSTRUMENTS</u>									
SOLAR WIND ANALYZER (VERSUS SOLAR WIND PROBE)	1.36 (3.0)	1.57 (3.45)	-3.43 (-7.55)	2100 (128)	2415 (147)	-3092 (-189)	2.5	3.0	-2.0
MAGNETOMETER (VERSUS DAY GLOW PHOTOMETER)	2.25 (5.0)	2.59 (5.75)	+0.8 (+1.75)	3934 (240)	4524 (276)	+2557 (+156)	3.0	3.6	+0.6
TOTAL NOMINAL + OTHER INSTRUMENTS, VERSION IV VERSUS II	15.61 (34.4)	17.93 (39.60)	-0.86 (-1.84)	22450 (1370)	25818 (1575)	-1328 (-81)	27.0	32.4	-0.1

a weight increase of 1.8 kilograms (4.0 pounds), a volume decrease of 793 cm^3 (48 $in.^3$), and a power increase of 1.3 watts, the total of the nominal payload plus the other candidate instruments gives a weight decrease of 0.86 kilogram (1.8 pound), a volume decrease of 1328 cm^3 (81 $in.^3$), and a power decrease of 0.1 watt, using upper tolerance limits for the revised payload instruments, as mentioned above. The Version IV payload and the two other candidate instruments are easily accommodated within the payload weight, volume, and power capability of the baseline (1978 Atlas/Centaur launched) probe bus. Ample weight capability exists as indicated by Figure 3-92 and the fact that there has been no large change for the baseline probe bus. The power system is designed for the required capability and, as mentioned, the require payload volume actually decreases.

The location and mounting provisions of the individual instruments to satisfy experiment requirements and desires in optimal fashion are more significant than the total volume. Instrument layout and mounting configurations are shown in Figures 3-89 and 3-90 for the Version IV nominal payload instruments and the nominal plus other candidate instruments, respectively. In comparison with Figures 3-92 and 3-94 for the previous Atlas/Centaur probe bus instrument configurations, the location and orientation of the neutral and ion mass spectrometers to view parallel to the spin axis end of the electron temperature probe to lie perpendicular to the spin axis are unchanged in order to employ the ram direction upon Venus entry with maximum effectiveness. In the nominal payload (Figure 3-89), the retarding potential analyzer sensor head is similarly oriented for the same reason. The ultraviolet spectrometer is mounted to view at 0.14 radian (8.2 degrees) to the spin axis for the 1978 launch trajectory and has a 0.02 x 0.003 radian (1.2 x 0.17 degree) field of view with the long slit dimension perpendicular to the spin axis to permit viewing in the direction of the local horizontal at 150 kilometers, which is approximately the altitude of the maximum dayglow. This experiment also wishes to scan the planet at high altitudes, particularly when the disc fills the field of view. This occurs at about 4 days out, and to accommodate this operating mode of the ultraviolet spectrometer, the spacecraft will be reoriented so that the spectrometer views directly at the planet once per revolution. It should be noted that the retarding potential analyzer, electron temperature probe, and ion mass spectrometer are instruments that are sensitive to the effects of spacecraft charging and electrical potential variation from the ambient plasma. The ion mass spectrometer is located sufficiently far from the spacecraft solar array, compared with the Debye length of the plasma at 200 kilometers, that the electric field from the array should not affect the instrument. Although a conductive coating over the solar array is not recommended in the baseline design, further consideration might be given to it if this distance does not prove adequate.

The field of view of the neutral mass spectrometer is a 0.35-radian (20-degree) full cone angle, as before, while the ion mass spectrometer may have a considerably wider field of view, up to a 1.57-radian (90-degree) full cone angle (as shown in the figures), thus easily satisfying the requirement that the view direction should lie within ±0.26 radian (±15 degrees) to the velocity vector, while the retarding potential analyzer requires a full 2π solid angle field of view. These conditions are all met since these instruments and the ultraviolet spectrometer (and the solar wind analyzer, in the other candidate instrument category) are located to have 2π unobstructed access (after ejection of the probes) so that in each case the instrument aperture plane does not intersect any part of the spacecraft; therefore emissions from the thrusters or from outgassing of spacecraft materials cannot enter directly into the aperture. Backscattering due to intermolecular collisions is negligible, and only straight line paths are present in thruster emissions even for the outer portions of the plumes found at angles beyond the Prandle-Meyer limit, as applied in the discussion of contamination control in Section 3.3.1.8.

Additional considerations for the other candidate instruments are as follows. The magnetometer is similar to the instrument previously considered in the Atlas/Centaur Version II payload. The electronics box dimensions have been increased by 5 percent to accommodate the +15 percent volume tolerance, and the boom is of the same type and mounting as before, with a length of 3 meters (10 feet), to achieve a degaussed spacecraft magnetic field less than 5 nT at the magnetometer sensor. The field of view requirement of the solar wind analyzer is satisfied as with the previous earth-pointing Atlas/Centaur configuration by an unobstructed 0.35 x 2.09 radian (20 x 120 degrees) fan-shaped acceptance angle within which the solar direction is included as centrally as possible. For the 1978 probe mission the angle between the solar direction and the spin axis (sun aspect angle) varies between about 0.35 and 1.13 radians (20 and 65 degrees) with angles less than 0.52 radian (30 degrees) occurring for the first 80 days of the mission. Since the instrument operates with maximum effectiveness throughout cruise as well as at Venus entry, the instrument may be mounted with the axis of its field of view at about 0.70 radian (40 degrees) to the spin axis and with the ±1.05-radian (±60-degree) wide fan angle parallel to the spin axis in order to accept particles along and near to the solar direction at all times.

Data Handling

Most of the probe bus data will be obtained during entry at altitudes below 1000 kilometers. It is therefore important to optimize the downlink bit rate during this period and to select a trajectory that maximizes atmospheric experiment time. The data handling requirements for the probe bus science instruments are shown in Figure 3-95.

During entry into the Venus atmosphere, the probe bus will be capable of transmitting science data at a rate of 1536 bits/s for the 1977 launch opportunity. The data handling capability for the 1978 probe mission is discussed in the following section titled "Effect of 1978 Probe Mission and New Science Payload (Version IV) on Science Data Requirements." All the science instrument requirements shown in Figure 3-95 are easily met.

Figure 3-95. Science Instrument Requirements

INSTRUMENT	BITS/SAMPLE	SAMPLES/MIN	BITS/S	OPERATING TIME
ION MASS SPECTROMETER	2000	2	67	DURING ENTRY
ELECTRON TEMPERATURE PROBE	30	60	30	DURING ENTRY
NEUTRAL MASS SPECTROMETER	2500	2	84	DURING ENTRY
ULTRAVIOLET FLUORESCENCE	72	20	24	DURING ENTRY
MAGNETOMETER	32	20	11	DURING CRUISE AND ENTRY
TOTAL RATE TOTAL AVAILABLE			216 1536*	

*FOR 1977 LAUNCH OPPORTUNITY.

The data handling system recommended is very similar to the Pioneer 10 and 11 data system. Other data handling systems have been studied as well as an additional interface module for buffering scientific instruments and providing a 10-bit analog to digital conversion. The details and conclusions of these studies are given in Section 8.3.

Two mainframe science formats (A and B) are provided for science data. The availability of two formats provides a convenient way to change science instrument data rate allotments between cruise and entry. Each mainframe format provides 48 3-bit words for scientific measurements. All inputs to the mainframe format must be digital. Any bit length bit train for the science instrument is acceptable, but the telemetry unit will format it into 3-bit groups for transmission to earth.

Two subcommutated science formats are available for use for low rate science housekeeping data. The inputs may be either analog or digital. The length of the words in these formats is either 1 bit in groups of 6 bits for accepting as input signals bilevel status bits; or 6 bits for accepting as input signals analog or digital data from the scientific instruments. The two formats are telemetered in a subcommutated science word of the main frame. Up to 40 6-bit or analog words can be accepted. The analog words must be normalized from 0 to +3 volts. Up to 48 bilevel status words can also be accepted from the science instruments.

Further details concerning the telemetry system are given in Section 8.3.

Effect of 1978 Probe Mission and New Science Payload (Version IV) on Science Data Requirements. The Version IV science payload imposed new data handling requirements on the probe bus. These are given in Table 3-32.

The column marked "bit rate" has been computed in the following manner. The reference scale height was selected according to the NASA requirements to be the first scale height above 140 kilometers. With the aid of Table 5 of NASA SP-8011, revised September 1972, this was computed by determining the attitude at which the atmospheric density was reduced to e^{-1} of its value at 140 kilometers. The 3σ bound on the steep side of our baseline entry flight path angle for the 1978 launch is $\gamma = -024$ radian (-14 degrees), defined at 250 kilometers. Using the trajectory

Table 3-32. Version IV Science Payload Data Handling Requirements

INSTRUMENT	MEASUREMENT			MINIMUM MEASUREMENTS		INSTRUMENT POWER – ON	BIT RATE (BITS/S)
	DESCRIPTION	ANALOG OR DIGITAL	SIZE (BITS)	PER REFERENCE SCALE HEIGHT	PER TIME INTERVAL (SECOND)		
NEUTRAL MASS SPECTROMETER	SCIENCE AND HOUSEKEEPING	D	520	1	NA	ENTRY – 1 HOUR	195
ION MASS SPECTROMETER	SCIENCE	D	210	3	NA	ENTRY – 1 HOUR	236-1/4
	HOUSEKEEPING	A	2	NA	60		
	HOUSEKEEPING	A	10	NA	5		
	HOUSEKEEPING	A	10	NA	5		
ELECTRON TEMPERATURE PROBE	SCIENCE	D	90	1	NA	ENTRY – 1 HOUR	33-3/4
	HOUSEKEEPING	A	8	NA	30		
	HOUSEKEEPING	A	8	NA	30		
RETARDING POTENTIAL ANALYZER	SCIENCE AND HOUSEKEEPING	D	125	3	NA	ENTRY – 1 HOUR	140-5/8
ULTRAVIOLET SPECTROMETER	SCIENCE	D	7200	NA	600	ENTRY– 4 DAYS	12
	HOUSEKEEPING	A	8	NA	300		
	HOUSEKEEPING	A	8	NA	300		
	SCIENCE	D	720	1	NA	ENTRY – 1 HOUR	270
	HOUSEKEEPING	A	8	NA	60		
	HOUSEKEEPING	A	8	NA	60		

corresponding to this flight path angle, the radial velocity in the reference regime was determined to be between 2.22 and 2.25 km/s. Since this is constant to within 2 percent, the higher velocity was used to determine the bit rates required in Table 3-32 to satisfy the minimum number of measurements in the reference regime.

In this manner it was determined that the nominal science instruments require a total of 12 bits/s from entry minus 4 days and a total of 875 bits/s from entry minus 1 hour. A small additional amount of housekeeping data of less than 1 bit/s from entry minus 4 days and less than 10 bits/s for entry minus 1 hour will also be required.

Comparison of these requirements to those in the previous section shows that the bit rate during entry has increased from 216 to 875 bits/s, and a requirement has been identified for analog housekeeping data with 10-bit resolution.

The change to 1978 probe bus launch changed the downlink capability from 2048 to 1024 bits/s. With a 25-percent fixed word frame requirement, this reduces the data available for science from 1536 in 1977 to 768 in 1978, which does not satisfy the new science requirements.

To accommodate the new requirements the following changes were made to the DTU design:

- Science subcommutator increased from 6 to 10 bits
- 10-bit analog-to-digital converter added into DTU, with routing to mainframe. This permits not only the 10-bit resolution analog housekeeping but also 10-bit resolution analog in mainframe
- Change length of word in mainframe from 3-bit to 1-bit increments, permitting variable size science words without bit penalty
- Quadrupled the size of format without a corresponding increase in fixed words.

The first two changes are designed to provide the 10-bit resolution analog housekeeping, and the last two increase the efficiency of the mainframe formats to permit a science utility of 91-2/3 percent instead of 75 percent.

The pre-Version IV telemetry unit provided two mainframe formats for science. One of these formats was used during cruise and the other during entry. After the removal of the magnetometer, the only instrument requiring data during cruise, the cruise format has been assigned to the ultraviolet spectrometer for use around 4 days prior to entry. At this time the spacecraft will be reoriented so that the spectrometer field of view subtends the planet once per revolution. The earth will not fall in the beam of the high-gain antenna, and the data will be transmitted by an omnidirectional antenna. This will permit a data rate of 16 bits/s and will accommodate the required ultraviolet spectrometer rate of 12 bits/s plus housekeeping. These changes permit 997 bits/s on entry to be available for science, and one 10-bit subcommutator word every 3/8 second. This satisfies the April 13 data handling requirements for a 1978 probe bus launch. Further details of these changes are described in Section 8.3.

Signals to Instruments

The following real-time ground command requirements have been identified for the probe bus instruments:

- Power on/off: two commands for each experiment
- Calibrate on/off: two commands for each experiment

- Ultraviolet fluorescence experiment: four commands for furnace current control
- Neutral mass spectrometer: eject ion source cover.

The probe bus will be capable of providing at least 50 discrete commands to the science instruments for performing these functions, leaving a large number of commands available for growth.

The following signals will be generated and provided to the scientific instruments as required for timing, changing modes, and roll azimuth determination:

Bit rate signals	Mode signals
Word rate pulses	Format signals
Frame rate pulses	Roll index and spin period sector pulses
Subframe rate pulses	Word gate signal
Clock pulses	
Shift clock pulse	

The roll index pulse will provide for view direction control. A pulse is sent to the instruments when a fixed reference line on the spacecraft perpendicular to the spin axis passes through the plane defined by the spin axis and the sun. A spin period sector generator will also provide as-required pulses at the following rates:

One pulse each 1/8 of roll-index pulse period
One pulse each 1/64 of roll-index pulse period
One pulse each 1/512 of roll-index pulse period.

<u>Consideration of Probe Bus 14 February 1973 Science-Briefing Instruments</u>. On 14 February 1973 ARC gave a briefing on the science instruments which had been proposed for the probe bus. Brief descriptions of the proposed instruments were given to TRW. The impact of the proposed instruments on the baseline probe bus design is discussed in this section.

We assume that a "nominal" probe bus payload consists of a magnetometer, an electron temperature probe, an ultraviolet fluorescence experiment, and a neutral and ion mass spectrometer. At the science briefing, more than one neutral mass spectrometer and ion mass spectrometer were described. By iterating the choices of the spectrometers it has been possible to define five different "nominal" payloads from the proposed instruments. These are shown in Table 3-33. The neutral/ion mass spectrometer shown in Payload 1 is a combination instrument capable of determining the masses of both neutral molecules and ions.

Table 3-33. Probe Bus Science Briefing Payloads

	1	2	3	4	5
MAGNETOMETER	x	x	x	x	x
ELECTRON TEMPERATURE PROBE	x	x	x	x	x
ULTRAVIOLET FLUORESCENCE	x	x	x	x	x
NEUTRAL/ION MASS SPECTROMETER	x				
MAGNETIC NEUTRAL MASS SPECTROMETER		x	x		
QUADRUPLE NEUTRAL MASS SPECTROMETER				x	x
MAGNETIC ION MASS SPECTROMETER		x		x	
BENNETT ION MASS SPECTROMETER			x		x

In Figure 3-96 we examine the capability of the baseline probe bus to accommodate the weight and power requirements of the five payloads. Since it is possible to generate a watt of power at Venus at a weight cost of 0.091 kilogram (0.2 pound) the power requirements of the payloads are shown for convenience as additional weight requirements in the figure and

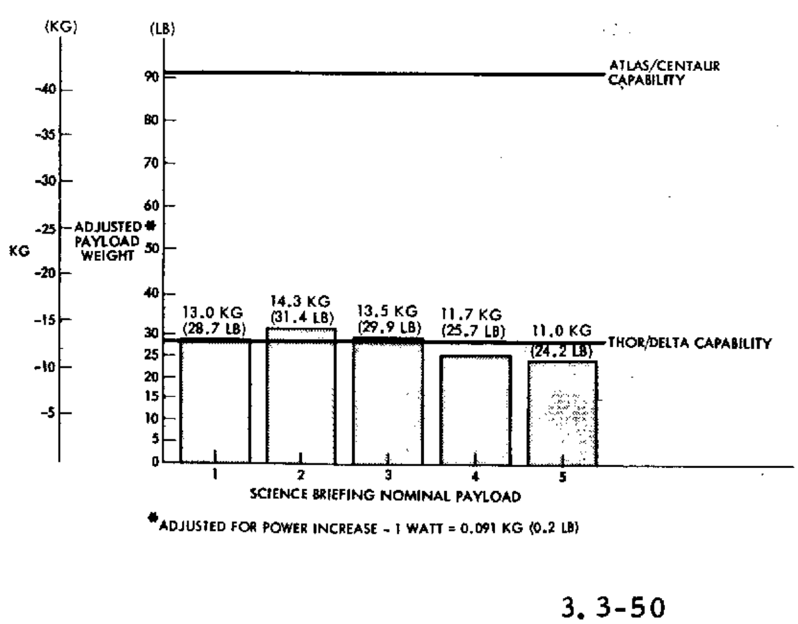

Figure 3-96. Payload Capability of Baseline Bus

labeled "adjusted" payload weight. Also shown in the figure are the Atlas/Centaur as well as the Thor/Delta launched probe bus capabilities.

Descriptions were also given at the same briefing of four scientific instruments which were not of the type included in the nominal probe bus instrument lists. The additional instruments and these adjusted weights are given below:

	Weight [kg (lb)]
Ultraviolet spectrometer	3.0 (6.5)
Extreme ultraviolet spectrometer	1.1 (2.4)
Retarding potential analyzer	1.40 (3.0)
Exospheric and ionospheric probe	2.5 (5.4)

The baseline Thor/Delta probe bus capability is marginal for accommodating the first three science briefing "nominal" payloads. The Thor/Delta bus can accommodate additional instruments with each of the five nominal payloads as long as the adjusted weight required by the additional instruments is less than the values shown below:

Payload	Adjusted Weight [kg (lb)]
1	None
2	None
3	None
4	1.3 (2.9)
5	2.0 (4.4)

On the other hand, the baseline Atlas/Centaur probe bus can accommodate all additional instruments with any of the nominal payloads identified, thus providing an important growth capability.

The data handling requirements of the instruments described at the science briefing have been examined. The total required bit rate during entry for each of science briefing payloads and also the required bit rate for the additional instruments are shown below.

	Total Required Bit Rate During Entry (bits/s)
Science briefing nominal payload No. 1	215
Science briefing nominal payload No. 2	268
Science briefing nominal payload No. 3	255
Science briefing nominal payload No. 4	202
Science briefing nominal payload No. 5	199
Science briefing additional instruments	144
Maximum total (No. 2) plus additional	411
Baseline bus maximum capability during entry	1536

The baseline probe bus maximum science bit rate capability can readily accommodate any one of the science briefing payloads along with all of the additional science briefing instruments.

Most of the scientific instrument requirements identified at the 14 February 1973 science briefing are readily satisfied by the baseline probe bus. However, some requirements have been identified which could have significant impact on the design of the probe bus as envisioned at the time of the briefing. These are tabulated in Tables 3-34 and 3-35.

The ultraviolet fluorescence experiment required that the probe bus enter the Venus atmosphere on the dark side. As discussed in Section

Table 3-34. Probe Bus, Impact of Other Requirements from Science Briefing on Probe Bus (Nominal Instruments)

NOMINAL INSTRUMENTS	REQUIREMENTS	IMPACT
ULTRAVIOLET FLUORESCENCE	ENTER ON NIGHT SIDE	• RETARGETING MAY DECREASE TIME IN ATMOSPHERE DUE TO INCREASED FLIGHT PATH ANGLE • ANGLE OF ATTACK INCREASES ABOVE 0.17 RAD (10 DEG) • COMMUNICATIONS WILL BE COMPROMISED
BENNETT ION MASS SPECTROMETER	POSITIVE (+) GROUND	• CHANGES TO PIONEERS 10 AND 11 EQUIPMENT REQUIRED
ELECTRON TEMPERATURE PROBE	NO POSITIVE POTENTIAL EXPOSED	• COATING OF EXPOSED POSITIVE TERMINALS • MAY ALSO REQUIRE POSITIVE (+) SOLAR ARRAY GROUND • INSTRUMENTS WITH THIS REQUIREMENT MAY BE INCOMPATIBLE WITH EACH OTHER

Table 3-35. Probe Bus, Impact of Other Requirements from Science Briefing on Probe Bus (Additional Instruments)

ADDITIONAL INSTRUMENTS	REQUIREMENT	IMPACT
RETARDING POTENTIAL ANALYZER	NO POSITIVE POTENTIAL EXPOSED	• COATING OF EXPOSED POSITIVE TERMINALS • MAY ALSO REQUIRE POSITIVE (+) SOLAR ARRAY GROUND • INSTRUMENTS WITH THIS REQUIREMENT MAY BE INCOMPATIBLE WITH EACH OTHER
RETARDING POTENTIAL ANALYZER	SPACECRAFT TO HAVE AT LEAST 1.5 M^2 (2325 $IN.^2$) CONDUCTING AREA	• SPACECRAFT CAN HAVE UPWARDS OF 2.8 M^2 (30 FT^2) OF THERMALLY SELECTED CONDUCTING SURFACE. CAREFUL CONSIDERATION OF THERMAL DESIGN IS REQUIRED.
ULTRAVIOLET SPECTROMETER	ANGLE OF ATTACK 0.35 RAD (20 DEG)	• ANGLE OF ATTACK INCOMPATIBLE WITH OTHER INSTRUMENTS

3.3.1.1, retargeting for dark side entry would necessitate an increased flight path angle on entry with a subsequent decrease in time in the atmosphere.

The most costly of the requirements identified is the requirement imposed by the Bennett ion mass spectrometer that the electrical power system have a positive ground. An estimate of the weight and cost impact of incorporating a positive ground electrical system on the baseline probe is given below:

Item		Cost ($K)	Weight [kg (lb)]
1	DC/DC converter for S-band amplifier or additional +28 VDC windings	420	3.5 (7.8)
2	CDU electronic switches in ground return change from NPN to PMP for	18	
	• Thrusters		
	• Transfer switches		
	• Heaters		
	• Internal relay drivers (safe/arm)		
3	DC/DC converter front end redesign		
	• Pressure transducer	10	
	• Transmitter drivers	10	
	• Receivers	10	
	• Probes	30	

Item		Cost ($K)	Weight [kg (lb)]
4	Shield all interface lines including DC power (secondary)		
5	Revise ordnance capacitors/SCR circuits		
6	Revise CEA thruster firing circuits internal relay drivers, etc.		
7	Mechanical repackage of most boxes as the solid grounds (structure) are isolated and powered at -28 VDC CEA DEA PCU CDU DMA Battery		
8	Reverse all capacitors referenced to chassis ground (tantalum) on the +28 VDC bus		

Total extra cost for + ground $468K and extra weight 3.5 kg (7.8 lb).

<u>Spacecraft Charging Considerations for New Science Payload (Version IV)</u>. A spacecraft immersed in an ambient plasma will come into electrical equilibrium with that plasma by developing surface charges. A review of the charging theory and an estimate of the resulting potentials for Pioneer Venus is given in Section 3.2.1.1.

Because of spacecraft charging and due to the fact that the electrons are more mobile than positive ions in a neutral plasma, low energy electron measuring instruments on a spacecraft require that conducting surfaces, electrically tied to the spacecraft structure, be exposed to the plasma. The purpose of this conducting surface is to provide a known reference "ground" for the instrument during its electron measuring modes. The area of the conducting surface is determined from the fact that it should be large compared to the surface area of the sensor.

The retarding potential analyzer added to the nominal payload by the Version IV science payload redirection requires an exposed conducting reference surface of 1.5 m^2. The electron temperature probe also requires a reference conducting surface but because of its much smaller sensor surface area, it requires a surface less than 10 percent of that required by the retarding potential analyzer. Thus, the spacecraft conducting surface requirement is determined by the retarding potential analyzer requirement.

On entry into the Venus ionosphere, the plasma is driven out of the wake of the probe bus. Therefore, the reference conducting surface must not be located on those portions of the bus lying in the wake during entry.

Another effect of the greater mobility of plasma electrons is that if positive charged conductors are exposed to the plasma, large currents will flow which will tend to change the spacecraft potential. Therefore, if the solar array has a negative ground, these instruments, as well as the ion mass spectrometer, also require that all cells have cover glasses and that any exposed array wires be insulated from the plasma. Similarly, any other positive exposed spacecraft potentials should be insulated. This problem is somewhat alleviated if the solar array has a positive instead of a negative ground. The cost of this alternative is high and is discussed in Section 3.3.2.2 under "Consideration of 14 February 1973 Science Briefing Instruments."

Conversations with Dr. A. Nagy of the University of Michigan for the electron temperature probe, Dr. W. Knudsen of Lockheed for the retarding potential analyzer, and Dr. K. K. Harris of Lockheed have indicated that a positive grounded array is not required if the aforementioned precautions are taken.

Magnetic Control

The magnetometer on the probe bus imposes a magnetic cleanliness requirement on the probe bus and the probes which are carried on it. The total field at the magnetometer sensor must be less than 5.0 nT while magnetic field measurements are being made. Since the probes will not be energized during this time, their stray fields are of no concern.

The magnetic cleanliness requirements for the Pioneer Venus probe bus will be met by:

- Defining a minimum magnetometer boom length
- Instituting a magnetic control program
- Final spacecraft magnetic test with compensation, if required.

A tradeoff must be made between the length of the magnetometer boom and the degree of magnetic controls imposed on the spacecraft fabrication program. The baseline data for defining the minimum magnetometer boom length is provided by the Pioneer 10 spacecraft magnetic field measurements. TRW's experience in the Pioneer, Apollo Lunar Particles and Field Subsatellite, and OGO programs shows that the moderate particles and fields type magnetic control program with the appropriately selected magnetometer boom length would be the optimum for the Pioneer Venus spacecraft. Such a program consists of:

- The use of an approved parts list
- Spot screening of incoming parts and materials
- Magnetic consultation in subsystem design and layout
- Solar cell array backwiring
- Subassembly testing of selected units.

Our experience indicates that, with a moderate magnetic control program, the hard remanence plus stray fields constitute at least 50 percent of the spacecraft fields obtained after launch. The remainder is due to soft remanence fields which are induced by exposure to incidental magnetizing fields after the last demagnetization. Compensation during the final spacecraft magnetic test may be used to eliminate the predictable components of the spacecraft fields.

Baseline Data for Magnetic Field Computation. The estimates of the magnetic fields of the Pioneer Venus spacecraft are based on the extrapolation of prelaunch vector field measurements of the Pioneer 10 spacecraft. It was assumed that the permed and depermed spacecraft fields were proportional to the spacecraft mass, and that the stray field was proportional to the steady load.

Figures 3-97 and 3-98 show the radial variation of the spacecraft magnetic field after exposure to a 25×10^{4} tesla and after deperming in a quasi-exponentially decaying field having a maximum of 50×10^{-4} tesla. Figure 3-99 shows the spacecraft stray field variation with radial distance. The distance is measured from the spacecraft center, i.e., half the distance from one end of the spacecraft to the other measured along

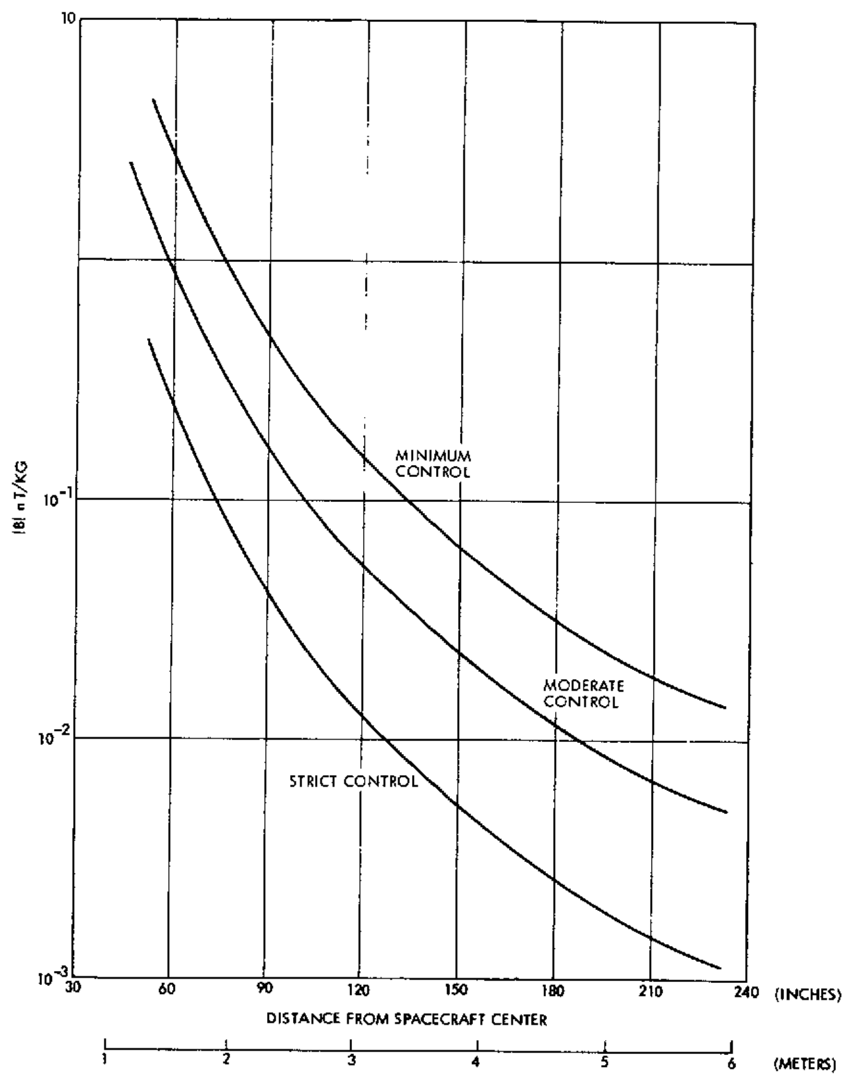

Figure 3-97. Magnetic Field of Spacecraft After 25×10^{-4} Tesla Perm

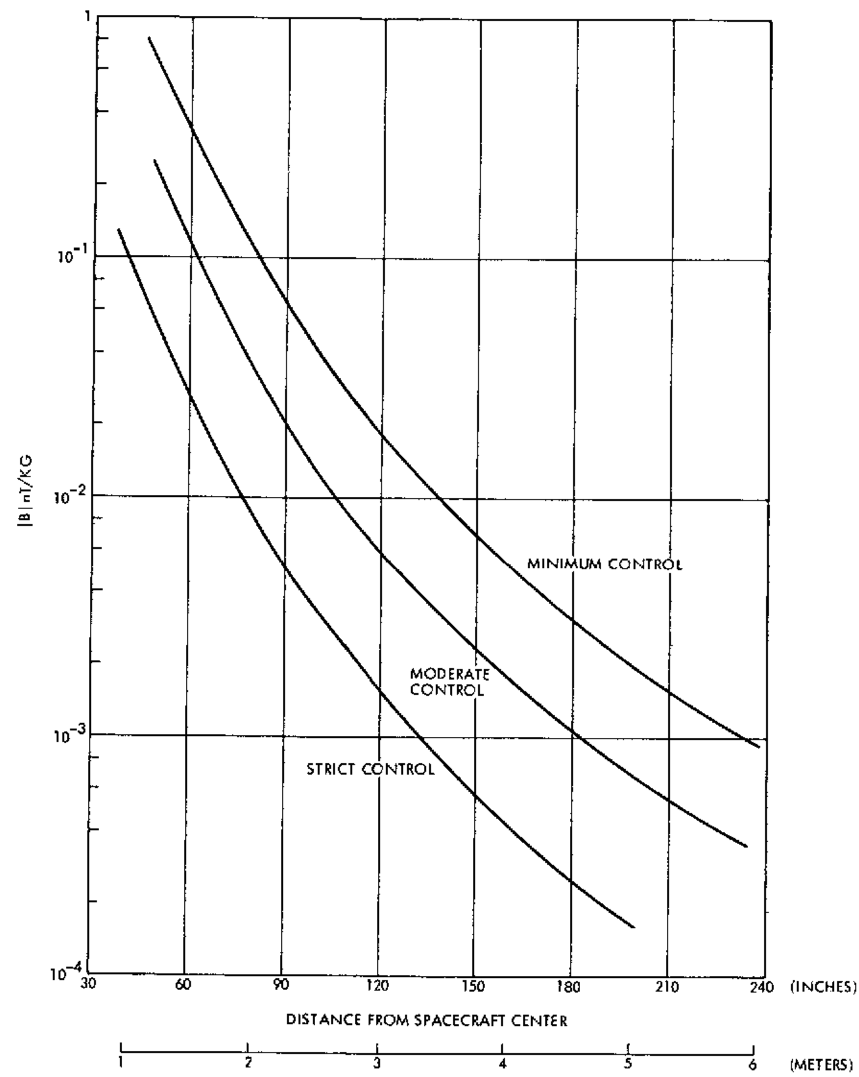

Figure 3-98. Magnetic Field of Spacecraft Post Deperm

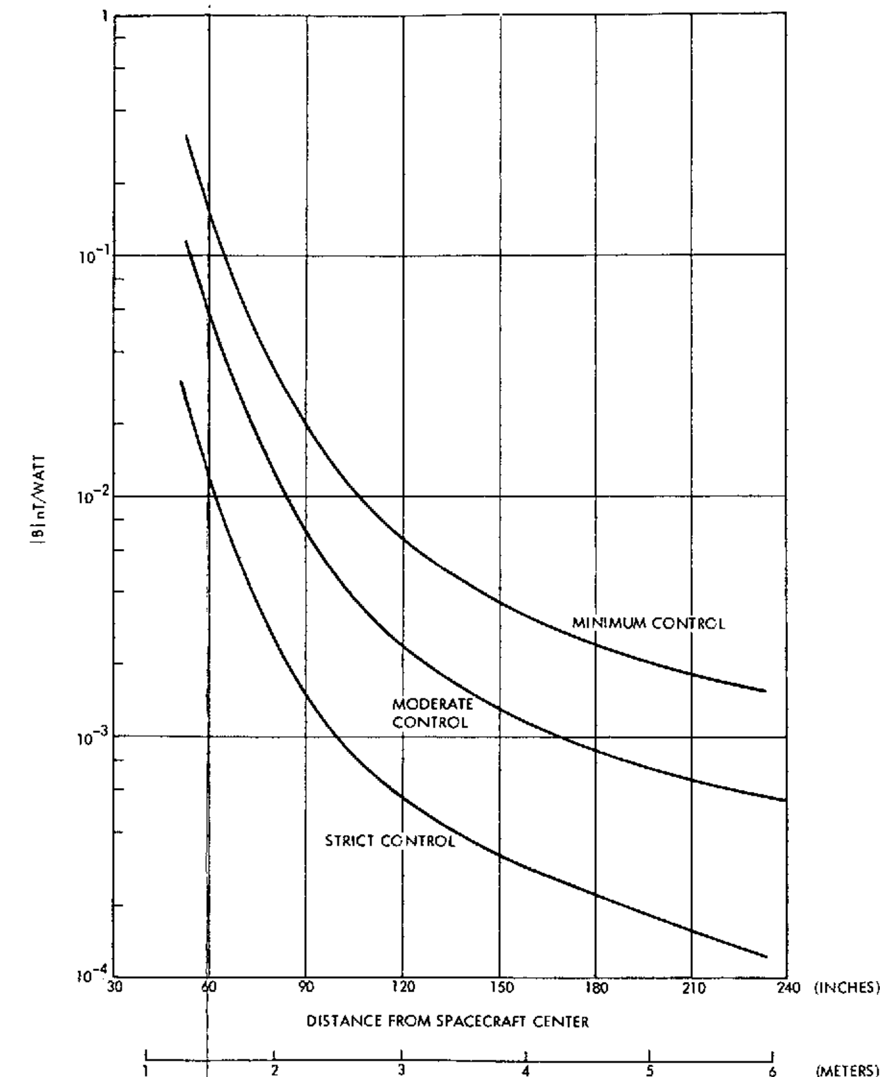

Figure 3-99. Magnetic Field Due to Currents

FOLDOUT FRAME 1

FOLDOUT FRAME 2

the line containing the magnetometer boom. The baseline parameters for the various spacecraft discussed are as follows:

	Spacecraft Radius [m (in.)]	Weight [kg (lb)]	Power Dissipation (Watts)
Pioneer 10	0.76 (30)	200 (440)*	100
Thor/Delta probe bus (with probes)	0.86 (34)	385 (849)	80
Atlas/Centaur probe bus (with probes)	1.08 (42.5)	771 (1700)	90

*Does not include weight of RTG power sources.

The data for these figures are normalized to unit weight and power for convenience in application to the present program. The data shown are for three cases:

- Strict magnetic control (data obtained from Pioneer 10 magnetic tests)
- Moderate magnetic control (data based on measurement of the magnetic field of the Apollo Lunar Particles and Fields subsatellites)
- Minimum magnetic control (data based on magnetic field measurement of the Orbiting Geophysical Observatory).

The reason for presenting these curves is that they contain the higher order multipole effects which are important at close-in radial distances. Otherwise, a statement of the assumed dipole moments would have sufficed.

All the magnetic control programs were carried out at TRW. In the case of Pioneer a strict control program was followed. In the case of the Particles and Field subsatellite a moderate control program not requiring 100 percent inspection and test was performed. In the case of the OGO the control consisted of identifying and controlling specific problem areas, with provisions for fields compensation during spacecraft magnetic tests. The "moderate control" curves, which are a factor of four higher than those for "strict controls," were used in the following calculations in order to permit the use of a reduced cleanliness control program for Pioneer Venus as compared to the one instituted for the Pioneer 10 spacecraft.

The spacecraft field after launch depends on the magnetic environment to which it is exposed after its last demagnetization. Surveys of the post-demagnetization field for the earlier Pioneer spacecraft programs have shown this to be less than 2×10^{-4} tesla if reasonable caution is exercised. Using a linear approximation for the remanent magnetization curve:

$$B_{remanent} = \frac{2}{25-0.5}(P-D) + D$$

where P is the post 25×10^{-4} tesla permed field, and D is the spacecraft field at the magnetometer sensor after demagnetization and subsequent exposure to the 0.5×10^{-4} tesla geomagnetic field. Generally, the magnetization curve is very flat up to $3\text{-}5 \times 10^{-4}$ tesla, showing little remanence increase due to exposures below these magnitudes. The linear approximation therefore provides a margin of safety in estimating the post-launch spacecraft field. Figure 3-100 shows the resulting field obtained by applying the above equation to Figures 3-97 and 3-98. These curves are about 80 percent higher than those for the demagnetized spacecraft at large radial distances. At closer-in distances the percentage increase is somewhat less because the induced remanence decreases the proportionate effects of the higher order miltipolar moments.

Scaling of Spacecraft Magnetic Fields. The problem addressed here is that of scaling the results of the Pioneer Jupiter spacecraft magnetic tests to other proposed spacecraft. In the past we have extrapolated prior test data by taking the field at the sensor and computing a corresponding dipole moment for the spacecraft, using the radial distance of the magnetometer sensor from the center of the spacecraft. Different spacecraft, e.g., Pioneer, Particles and Fields, and OGO, were compared on the basis of dipole moment per unit weight and power dissipation, and appropriate per unit values were selected to estimate the new required boom lengths.

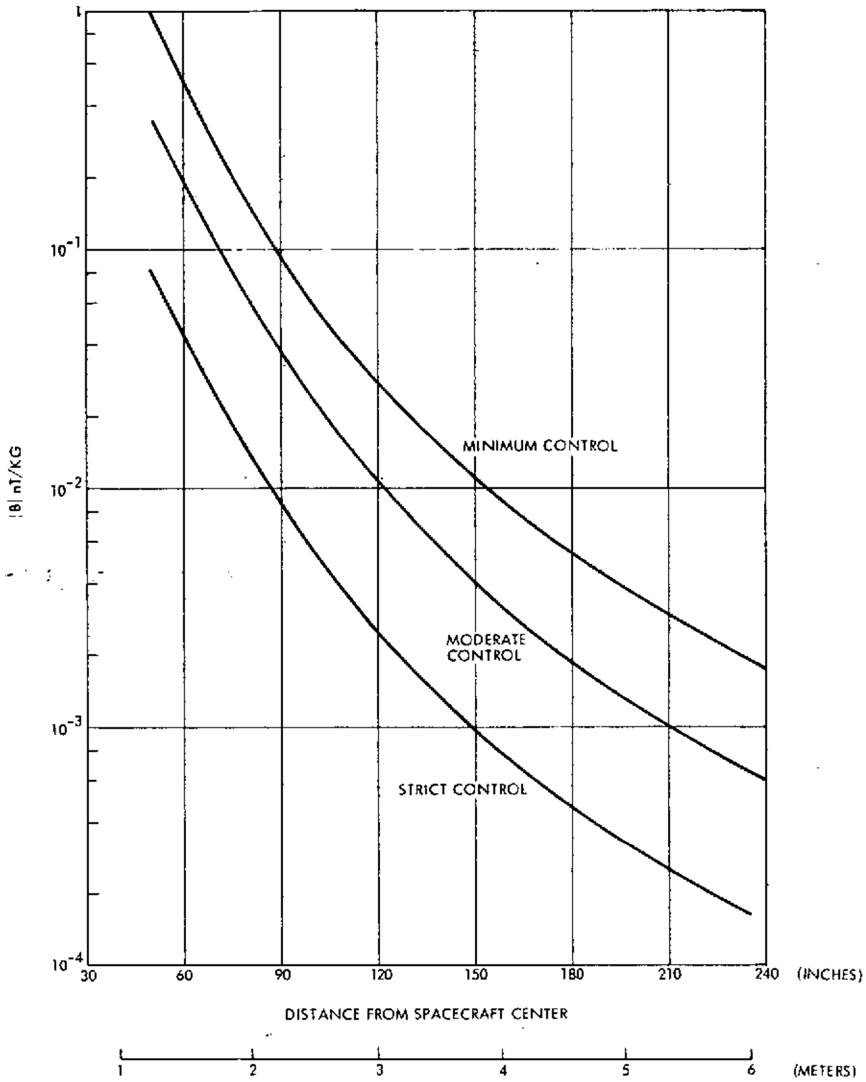

Figure 3-100. Post-Launch Magnetic Field Due to Magnetized Material on Spacecraft

For the Pioneer Venus study, it was realized that the dipole assumption was not realistic in view of the relatively shorter boom lengths compared to the size of the spacecraft. The Pioneer Jupiter test data taken at a number of different radial distances provides the information to make a more accurate estimate of required boom lengths. In those tests the data at varying radial distances were used to determine the quadrupole, octupole and hexadecapole moments in addition to the dipole moment in order to permit the computation of the field at the magnetometer sensor location. This method was used because the specified and actual field levels were lower than those attainable with the available instrumentation and the existing ambient noise levels.

One method of scaling, then, is to take the Pioneer Jupiter data versus radial distance and multiply them by the appropriate weight and power factors. In effect this adjusts each multipolar moment by the same multiplicative factor and maintains the original proportions of the various moments.

Another factor that should be taken into account in scaling is the size of the spacecraft. The equation for the magnetic field from currents is

$$B = \frac{\mu_o}{4\pi} \int \frac{i d\vec{l} \times \hat{r}}{r^2}$$

so that

$$\frac{B_2}{B_1} = \frac{i_2}{i_1} \times \frac{r_1}{r_2}$$

if all linear dimensions in system 2 are obtained by scaling system 1 by the factor r_2/r_1. If we assume that the fields are due to dipole moments (M):

$$\frac{B_2}{B_1} = \frac{i_2 a_2^2}{i_1 a_1^2} \times \left(\frac{r_1}{r_2}\right)^3 = \frac{M_2}{M_1}\left(\frac{r_1}{r_2}\right)^3.$$

With the weight (W) and power (P) corrections:

$$\left(\frac{B_2}{B_1}\right)_{weight} = \frac{W_2}{W_1}\left(\frac{r_1}{r_2}\right)^3, \text{ and } \left(\frac{B_2}{B_1}\right)_{power} = \frac{P_2}{P_1}\left(\frac{r_1}{r_2}\right)^3.$$

The dipole moment assumption $M = ia^2$ does not preclude the existence of higher order moments due to the spatial distribution of dipole moments.

If we express the field at a distance r as

$$B = \frac{D}{r^3} + \frac{Q}{r^4} + \frac{O}{r^5} + \frac{H}{r^6} \ldots,$$

then

$$\frac{B_2}{B_1} = \frac{D_2}{D_1}\left(\frac{r_1}{r_2}\right)^3 \frac{\left(1 + \frac{Q_1}{r_1 D_1} + \ldots\right)}{\left(1 + \frac{Q_2}{r_2 D_2} + \ldots\right)}$$

where D, Q, O, H are the dipole and higher order moments. We obtain the same expression for the scaling law as from the original argument

$$\frac{B_2}{B_1} = \frac{D_2}{D_1}\left(\frac{r_1}{r_2}\right)^3 ,$$

if we assume

$$\frac{D_2}{D_1} = \frac{W_2}{W_1} \text{ and } \frac{Q_2}{r_2} \Big/ \frac{Q_1}{r_1} = \frac{W_2}{W_1}, \quad \frac{O_2}{r_2^2} \Big/ \frac{O_1}{r_1^2} = \frac{W_2}{W_2} \ldots,$$

because then

$$\frac{Q_1}{r_1 D_1} = \frac{Q_2}{r_2 D_2}, \frac{O_1}{r_1^2 D_1} + \frac{O_2}{r_2^2 D_2}, \ldots$$

The scaling law, then, assumes that dipole moments scale directly as the weights and power dissipations, but the higher order moments as

$$\frac{Q_2}{Q_1} = \left(\frac{r_2}{r_1}\right)\frac{W_2}{W_1}, \frac{O_2}{O_1} = \left(\frac{r_2}{r_1}\right)^2 \frac{W_2}{W_1} \ldots$$

It is the usual practice in the design of the layout of subassemblies on the spacecraft to locate those units which are highly magnetic as far as possible from the magnetometer sensor. This technique is more effective in larger spacecraft, such as the Atlas/Centaur configuration of the Pioneer Venus orbiter, than in smaller spacecraft. The scaling law derived above may therefore be too pessimistic, and direct scaling by weight and power of all of the multipole moments may be adequate. For the Atlas/Centaur probe bus with the 5.0 nT specification, the comparative results for the required boom lengths are as follows:

	Boom Lengths [meters (ft)]
With size scaling	3.10 (10.19)
Without size scaling	2.84 (9.31)
With only dipole scaling	2.03 (6.65)

Note that scaling with only the dipole extrapolation is too optimistic. Compared with the size-scaled boom, it would give a field which is too large by a factor of 2.45. The boom length computations in this study are based on the scaling with size, weight, and power dissipation taken into account.

Magnetometer Boom Lengths. Using Figures 3-97 and 3-98 we find that the post-launch field of 5 nT can be obtained easily with a moderate magnetic control program similar to that used for the Particles and Fields satellite as long as the magnetometer sensor is placed on a boom having the values shown below:

Thor/Delta launch	2.19 meters (7.19 ft)
Atlas/Centaur launch	2.75 meters (9.03 ft).

The above results were obtained assuming the use of a silver-cadmium battery as on Pioneer 10. The requirement that a nickel-cadmium battery be used increases the boom length. The field of a typical 12 AH 22-cell nickel-cadmium battery is 3000 nT at 1 foot. These boom lengths would be increased to:

Thor/Delta launch	2.71 meters (8.88 ft)
Atlas/Centaur launch	3.10 meters (10.91 ft)

For commonality of design it is recommended that the boom lengths for both booster configurations be fixed at 3 meters.

Requirements on Probe Magnetic Fields. The magnetic fields discussed above include the fields of the probes as well as the bus. An estimate was made of the effect of the magnetic fields of the large and small probes on the probe bus magnetometer to define a magnetic field requirement for the probes. The magnetic fields considered here are separate from those which must be imposed on the small probes due to the fact that they also carry magnetometers. No stray field limits for the probes were considered since it was assumed that they will not be operated on the probe bus while the probe bus magnetometer is taking data.

The requirements for the magnetic fields of the large probes were computed by using the data shown on Figures 3-97 and 3-98 for a moderate magnetic control program. Figures 3-97 and 3-98 were not directly used for the computation of the small probe fields, since that data from the Pioneer 10 spacecraft was not expected to be valid for a body as small as the small probes. At the distances of interest it is reasonable to approximate small probes by dipoles and to allot to each dipole a field proportional to the ratio of the small probe mass to the total probes and probe bus mass. The probe magnetic field allotments are shown in Table 3-36.

Table 3-36. Probe Magnetic Field Requirements at 1.82 Meters*

	AFTER 25×10^{-4} T EXPOSURE (nT)	POST-DEPERM (nT)
THOR/DELTA LAUNCH		
EACH SMALL PROBE	4.2	0.31
LARGE PROBE	29.0	3.2
ATLAS/CENTAUR LAUNCH		
EACH SMALL PROBE	10.1	0.74
LARGE PROBE	50.0	5.0

*THE NUMBERS SHOWN ARE THE MAGNITUDE OF THE FIELD AT 1.82 METERS (6 FEET) FROM THE CENTER OF EACH PROBE IN THE DIRECTION DEFINED BY THE LINE SEGMENT FROM THE CENTER OF EACH PROBE TO THE PROBE BUS MAGNETOMETER SENSOR.

Solar Array. The Pioneer 10 data used here does not include the effects of the RTG power supplies used in that spacecraft. The solar cell array is not expected to contribute significantly to the Pioneer Venus spacecraft stray field. The maximum stray field measured for the Pioneers 6 through 9 spacecraft solar cell array under all normal and failure modes was $B_{solar\ array}$ = 0.013 nT per watt at 1 meter.

Using the dipolar extrapolations, this results in

$B_{solar\ array}$ = 0.020 nT for 90 watts at 3.86 meters (3.0-meter boom)

$B_{solar\ array}$ = 0.014 nT for 190 watts at 5.67 meters (4.59-meter boom).

These values are negligible compared to the 5 nT and 0.5 nT requirements for the probe bus and orbiter respectively. Backwiring techniques developed for the earlier Pioneers will be used.

Effect on Magnetic Control of New Science Payload (Version IV). The removal of the magnetometer from the probe bus by the Version IV redirection eliminates all need for magnetic control on the probe bus and the need for the probe bus to impose magnetic constraints on the probes. Since the orbiter still contains a magnetometer, elimination of the entire magnetic control effort will not be possible. The bus will still "inherit" a certain amount of magnetic cleanliness due to the commonality of experiments with the orbiter and the use of the Pioneers 10 and 11 equipment. Furthermore the nonrecurring costs associated with the magnetometer boom and testing still must remain. The following are estimates of the cost savings resulting from the removal of the probe bus magnetometer:

Boom cost (recurring)	\$50,000
Integration and test costs include: Alignment tests Deployment test Probe bus magnetic test	30,000
Magnetic control	10,000
Total	\$90,000

These costs do not include the cost savings realized on the probes due to the removal of the bus magnetometer.

SECTION 3.3 REFERENCES

1. R. J. L. Grard, "Properties of the Satellite Photoelectron Sheath Derived from Photoemission Laboratory Measurements," ESTEC Internal Working Paper No. 663, March 1972.

2. K. Knott, "The Equilibrium Potential of a Magnetospheric Satellite in an Eclipse Situation," Planet. Space Sci. (late 1972 either in or after September).

3. S. E. DeForest, "Spacecraft Charging at Synchronous Orbit," J. Geophys. Res., 77, 651, 1972.

4. E. J. Sternglass, Phys. Reve., 80, 925, 1950.

5. R. J. L. Grard, K. Knott, and A. Pedersen, "The Influence of Photoelectron and Secondary Electron Emission on Electric Field Measurements in the Magnetosphere and Solar Wind," ESTEC Internal Working Paper No. 733, February 1973.

6. NASA/Ames: 242.3 PV-03-72, "Investigation of Spacecraft Outgassing Problems," from D. M. Chisel.

7. J. Pressman, J. Meyers and P. Lillienfeld, GCA Corporation Final Report on Contract NASW-1745, "Definition of Experimental Studies for Determining Gaseous and Particulate Cloud Environment of Manned Spacecraft and Applications to Cometary Physics," May 1970.

8. D. McKeown and W. E. Corbin, Jr., "Space Measurements of the Contamination of Surfaces by OGO-6 Outgassing and Their Cleaning by Sputtering and Desorption, "NBS Special Publication 336, pp. 113-127, October 1970.

9. J. E. Chirivella, P. I. Moynihan and W. Simon, "Small Rocket Exhaust Plume Data, "JPL Quarterly Technical Review, Vol. 2, No. 2, July 1972.

10. NASA/Marshall – 50M02442, "Material Control for Contamination Due to Outgassing."

11. Stanford Research Institute, "Polymers for Spacecraft Applications."

12. MSC 0752, "List of Materials Meeting MSC Vacuum Stability Requirements," Manned Spacecraft Center, Houston, Texas.

13. X-764-71-314, "A Compilation of Low Outgassing Materials Normally Recommended for GSFE Cognizant Spacecraft," Goddard Space Flight Center, Greenbelt, Maryland.

14. Harold Papazian, "Prediction of Polymer Degradation Kinetics at Moderate Temperatures from T.G.A. Measurements," J. Applied Polymer Sci., Vol. 16, 11. 2503-2510, 1972.

3.4 ORBITER SCIENCE, ATLAS/CENTAUR AND THOR/DELTA

The principal objectives of the orbiter mission are to perform global mapping of the planetary surface, ionosphere, and atmosphere by remote sensing. The orbiter mission will also supplement the probe mission by global and temporal in situ measurements of the upper atmosphere, ionosphere, and solar wind.

Table 3-37 lists the Version III science payload nominal orbiter instruments and the measurements performed by each.

On 13 April 1973, NASA redefined the Pioneer Venus missions to consist of 1978 Atlas/Centaur launches for both the probe mission and orbiter mission. New (Version IV) scientific instrument payload complements were provided. For the orbiter mission, the solar wind analyzer and the X-band occultation were transferred from the list of other candidate instruments to the nominal payload, with the following objectives:

- The solar wind detector will measure the flux and energy distribution of the solar plasma during cruise and in orbit, and aid in investigating the solar wind-ionospheric interface.
- The X-band addition to the occultation experiment will measure the frequency dependence of the absorption in the dense clouds, and calibrate the effects of interplanetary electrons.

Table 3-37. Version III Science Nominal Orbiter Science Instruments Payload

INSTRUMENT	OBJECTIVES/MEASUREMENTS
MAGNETOMETER, ELECTRON TEMPERATURE PROBE, NEUTRAL MASS SPECTROMETER, ION MASS SPECTROMETER	SAME AS PROBE BUS MISSION. WILL EXTEND AND SUPPLEMENT PROBE MISSION DATA
ULTRAVIOLET SPECTROMETER	DETECT PREVIOUSLY UNIDENTIFIED CONSTITUENTS IN VENUS ATMOSPHERE. REPEAT LYMAN-α PROFILE (MARINER V).
INFRARED SPECTROMETER	THERMAL STRUCTURE OF ATMOSPHERE ABOVE THE CLOUDS.
OCCULTATION	LOWER ATMOSPHERE TEMPERATURE AND PRESSURE MEASUREMENTS.
RADAR ALTIMETER	GRID MAPPING OF SURFACE HEIGHT VARIATIONS. STUDY REFLECTIVITY AND ROUGHNESS.

3.4.1 Science-Related System Requirements Analysis

3.4.1.1 Orbit and Spin Axis Orientation

The orbiter spin axis and orbit were selected on the basis of science instrument considerations. The requirements listed in Table 3-38 for each Version III science nominal payload instrument also affect the instrument configuration.

All the scientific instruments benefit from a periapsis altitude as low as possible. Other requirements are based on the needs of specific instruments.

The neutral mass spectrometer should point within 0.17 radian (10 degrees) of the spacecraft velocity vector (ram direction) at periapsis at least once per revolution. The same applies to the ion mass spectrometer, but measurements should be made from periapsis to high altitudes (1000 kilometers). Latitude coverage and diurnal effects are also of interest but probably secondary importance.

Table 3-38. Parameters Affecting Orbit and Configuration Selection for Version III Science Payload

REQUIREMENT	EXPERIMENT								AFFECTS	
	NMS	IMS	IR	UV	RADAR ALTIMETER	OCC.*	MAG.	ETP	CONFIGURATION	ORBIT
MINIMIZE PERIAPSIS ALTITUDE	X	X	X	X	X		X	X		X
VIEW ALONG RAM VELOCITY AT PERIAPSIS	X	X							X	X
RAM VELOCITY ALTITUDE COVERAGE (TO 1000 KM)		X							X	X
NEAR-PERIAPSIS LATITUDE COVERAGE (TO 1000 KM)	X	X					X	X		X
SPIN AXIS VIEW:										
FREQUENCY			X	X					X	X
RESOLUTION (ALTITUDES)			X	X					X	X
LATITUDE COVERAGE			X	X					X	X
TERMINATOR CROSSING				X					X	X
DARK SIDE LATITUDE COVERAGE			X						X	X
DARK SIDE FREQUENCY			X						X	X
PERIAPSIS TERMINATOR CROSSING		X					X	X		X
SUBORBITAL VIEW:										
POINTING BELOW 1000 KM				X	X				X	X
LATITUDE COVERAGE BELOW 1000 KM				X	X					X
BOW SHOCK AND PLASMA TAIL CROSSING							X			X
NORMAL LIMB SCAN AT FIXED ANGLE**										
FREQUENCY BELOW 1000 KM			X						X	X
LATITUDE COVERAGE			X						X	X
EARTH OCCULTATION:										
FREQUENCY						X				X
VIEW THROUGH REFRACTED RAY						X			X	

*NASA/AMES GROUNDRULE S-BAND ONLY, NO WEIGHT OR POWER ALLOTMENT. X-BAND IS ADDITIONAL INSTRUMENT.
**SPIN SCAN. REQUIREMENT DEPENDS ON IR INSTRUMENT SELECTED.

The infrared (IR) radiometer will require either a normal spin limb scan or a despun view of the planet. In the former case, the instrument will have a long, narrow entrance slit with the requirement that (once or twice per revolution near periapsis) the length of the slit be parallel to the planetary surface and scan the atmosphere vertically. In the latter case, if the IR radiometer is of the IRIS type (i.e., a Michelson interferometer), it requires a despun view of the planet. This can be accomplished by mounting it to view along the spacecraft spin axis. It also requires that the planet be viewed on the dark side.

The ultraviolet (UV) spectrometer may require a view along the spin axis or a suborbital view. Both sides of the terminator are of interest. The spatial resolution for both the UV and IR instruments is improved if measurements are made at low altitudes. Improved latitude coverage also benefits these experiments.

The radar altimeter requires that its antenna point at the Venus aspect angle, below 1000 kilometers range, for a suborbital view of the planet. Maximum latitude coverage is desired.

The magnetometer experiment is enhanced by maximizing the range of altitudes at which it passes through the Venus plasma tail as well as going through the bow-shock region. A good orbit for the magnetometer will also have good latitude coverage near periapsis.

The electron temperature probe should be in an orbit in which periapsis crosses the terminator after a reasonable length of time to permit study of day/night effects. Latitude coverage near periapsis may be of interest also.

The occultation experiment should experience a reasonably large number of occultations, and should cover a range of latitudes. The rays refracted at the lowest layers of the atmosphere are of the greatest interest, but are at the same time subject to the most attenuation. For example, a ray that is refracted 0.30 radian (17 degrees) is attenuated by about 40 dB. The antenna should be programmed to minimize the effects of this attenuation by moving to keep the refracted ray in the high-gain portion of the dish. The earth-pointing configuration simply requires prepointing the spacecraft in the direction of the deepest refracted ray to be measured. This complies with the requirement that the occultation experiment should place a minimum burden on the spacecraft.

Detailed studies, presented below, have been made of the requirements identified in Table 3-38. The studies are summarized numerically later in this section, under "Science Relevant Orbit Parameters."

View Along Ram Velocity Angle of Attack

The angle from the spacecraft positive spin axis to the instantaneous vehicle velocity vector is defined as the angle of attack. The range covered by this angle at periapsis and from periapsis to 1000 kilometers has been computed for a variety of orbits and for a spacecraft with spin axis normal-to-Venus orbit plane (NVOP) and a spacecraft with an earth-pointing (EP) spin axis.

Figure 3-101 shows the variations in the angle of attack for two Type II orbits, θ_{AIM} = 1.57 radian (90 degrees) and θ_{AIM} = 2.09 radian (120 degrees). The EP angle of attack near periapsis changes continually and requires a rotatable ram platform for those instruments which must be pointed in the ram direction. Once, however, the ram platform is provided, the instruments can be pointed in the ram direction once per revolution over a wide range of altitudes and latitudes. This is of particular value to the ion mass spectrometer, since the height of the Venus ionosphere has not been determined to date.

The NVOP angle of attack is essentially constant at any given point in the orbit, such as periapsis, but gimballing the instruments might be required to accommodate the change in angle of attack between periapsis and the 1000-kilometers altitude.

Spin View Coverage and Range

A study was performed to determine the frequency with which Venus is viewed along the spacecraft spin axis for various orbits and the EP and NVOP spin axis configurations. The latitude, solar longitude ranges covered, as well as the altitude range to the surface for a spin axis view were also determined.

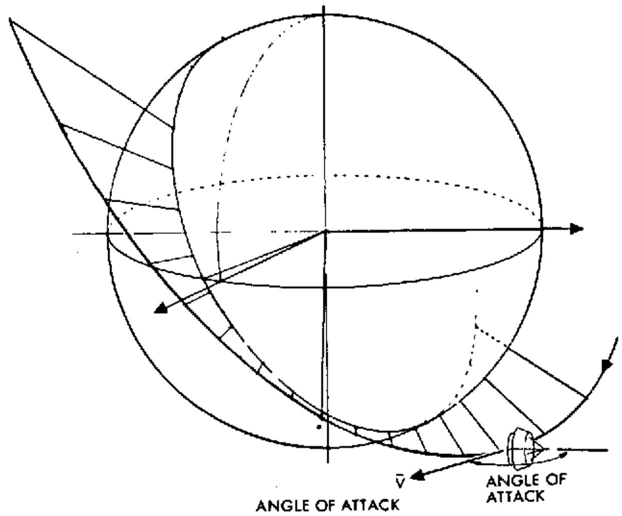

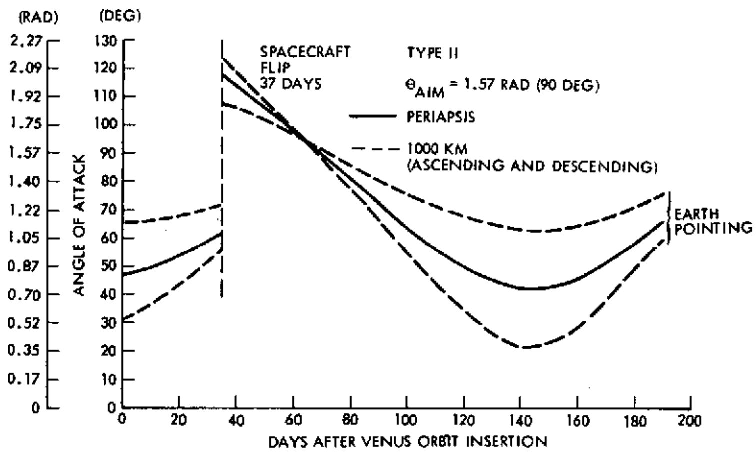

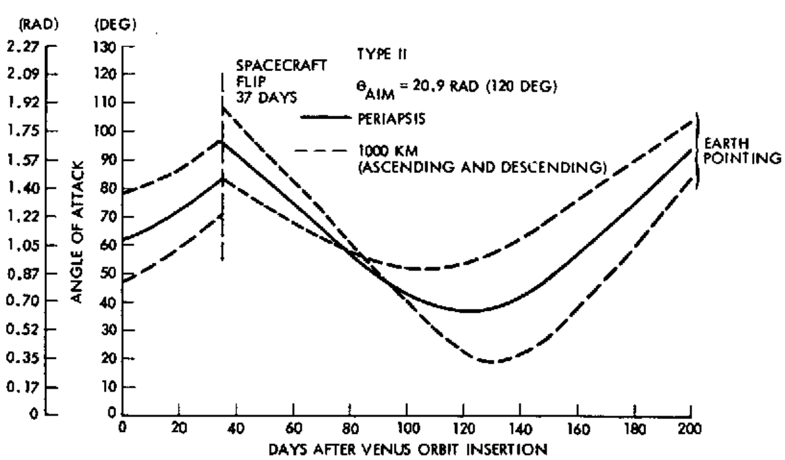

Figure 3-101. Angle of Attack

Figures 3-102A and 3-102B show the range of latitudes covered by the EP and NVOP spin axis view. Figures 3-102C and 3-102D show the corresponding ranges of longitude covered, measured from the terminator. Figure 3-103 plots the EP and NVOP spin axis projections on the surface of Venus. The EP gives almost pole to pole latitude coverage, while the NVOP coverage is limited to the southern hemisphere. Both provide adequate longitude coverage.

Figure 3-104 shows the spin axis view range variation for each day in Venus orbit. The ranges from the spacecraft to the planet surface during each pass determine the viewing resolution of the instruments. Long duration viewing periods at low ranges are desired.

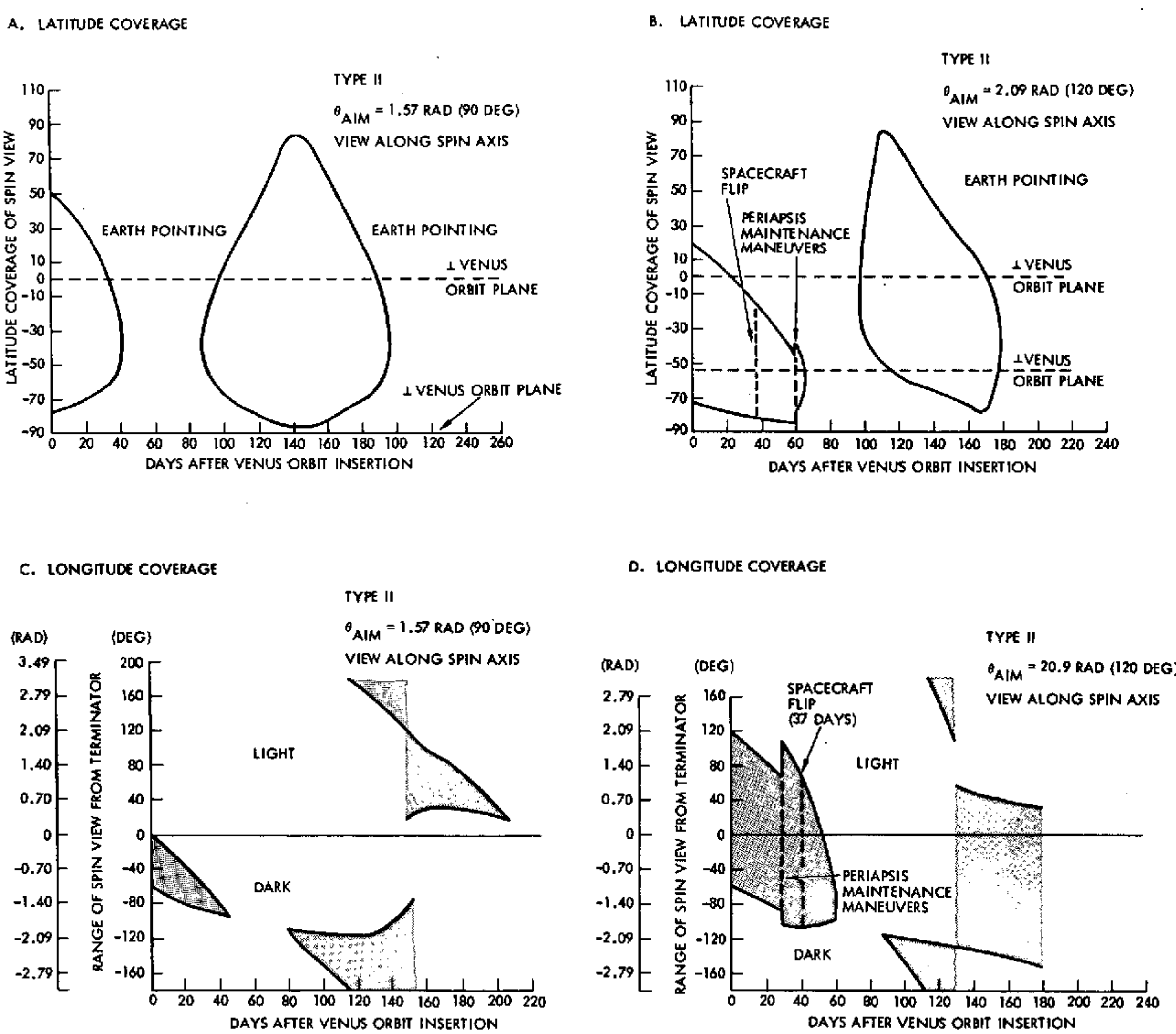

Figure 3-102. Spin View Planetary Considerations

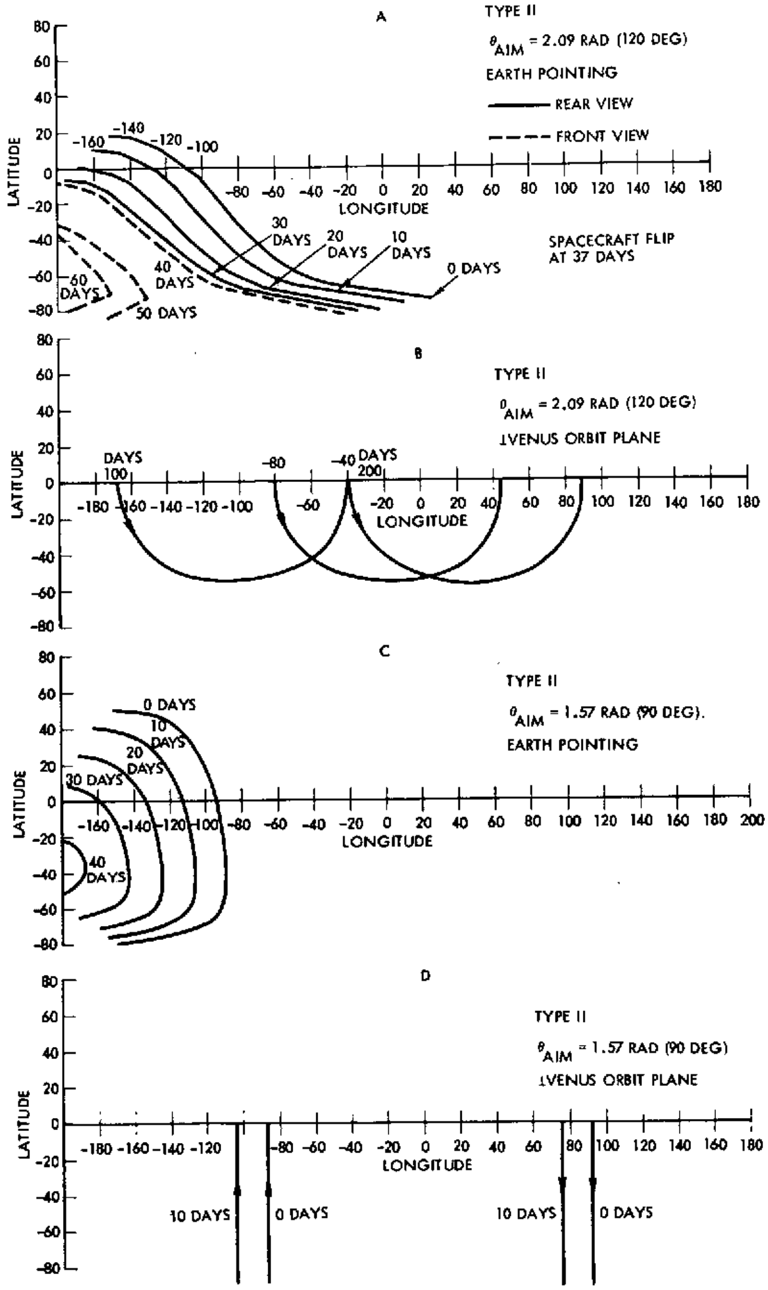

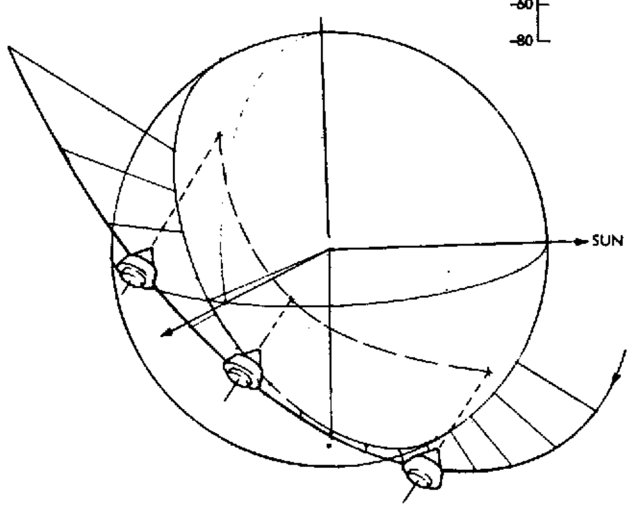

SPIN VIEW

Figure 3-103. Spin View Coverage

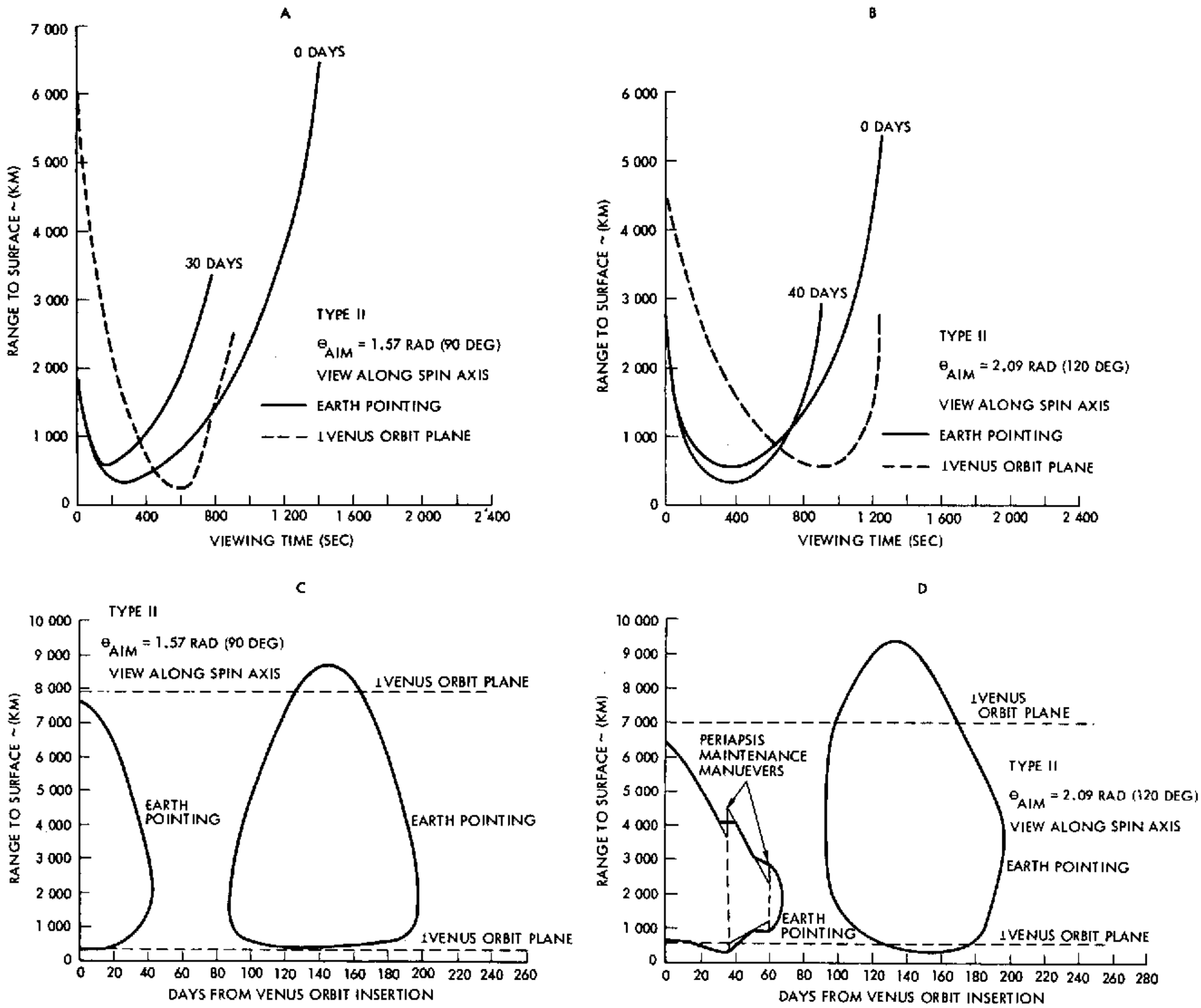

Figure 3-104. Spin View Range Considerations

During each pass a minimum range to the surface is encountered which produces the maximum resolution. The EP viewing range varies considerably during the course of the mission. The NVOP viewing range is constant.

Venus Aspect Angle Suborbital View

The Venus aspect angle, which is defined as the angle from the vehicle's positive spin axis to the radius vector pointing at the planet's center, is the angle at which an instrument must be placed from the spin axis in order to obtain a suborbital view of the planet once per spin cycle. Both the radar altimeter and the UV spectrometer may require a suborbital view.

Figure 3-105 shows the variation in Venus aspect angle at periapsis and at 1000 kilometers for two Type II orbits and both the EP and NVOP.

The EP Venus aspect angle at any point in the orbit varies from periapsis altitude to 1000 kilometers, which determines the range through which an instrument will have to be gimballed to produce optimum surface resolution. The NVOP Venus aspect angle is constant at periapsis, but gimballing would be required from periapsis to 1000 kilometers.

Normal Limb Scan

A normal limb scan occurs when an instrument having a long, thin entrance slit views the planet limb. The long dimension of the slit must be perpendicular to the planet radius vector at the limb. The frequency and latitude coverage of normal limb scans depends on the view direction and the slit angle. The slit angle is the angle between the direction of the long dimension of the slit, which lies in a plane normal to the view direction, and the plane defined by the spacecraft spin axis and the view direction.

Normal limb scan near periapsis (to 1000 kilometers) is desirable to obtain good spatial resolution. If an instrument is mounted at a fixed angle on the spacecraft, normal limb scans will always occur at the same altitude and latitude for the NVOP. The slit angle and view direction can be chosen so that the normal limb scan occurs at periapsis. If latitude coverage is desired, this can be obtained by rotating the slit about the view direction. The latitude coverage obtained in this manner is shown in Figure 3-106.

The upper bound in Figure 3-106 indicates the altitude limit, the lower bound indicates the 1.57 radian (90-degree) slit angle. View aspect angle, as used in the figure, is measured from the North pole of the Venus orbit plane. The regions indicated are favorable from a range point of view.

For the earth-pointing configuration a range of latitudes will be covered depending on the slit angle and the view direction chosen. This is a distinct advantage of the EP over the NVOP for normal limb

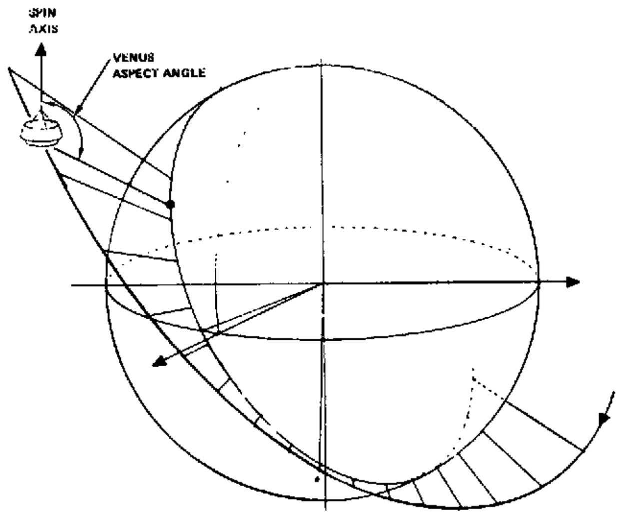

VENUS ASPECT ANGLE

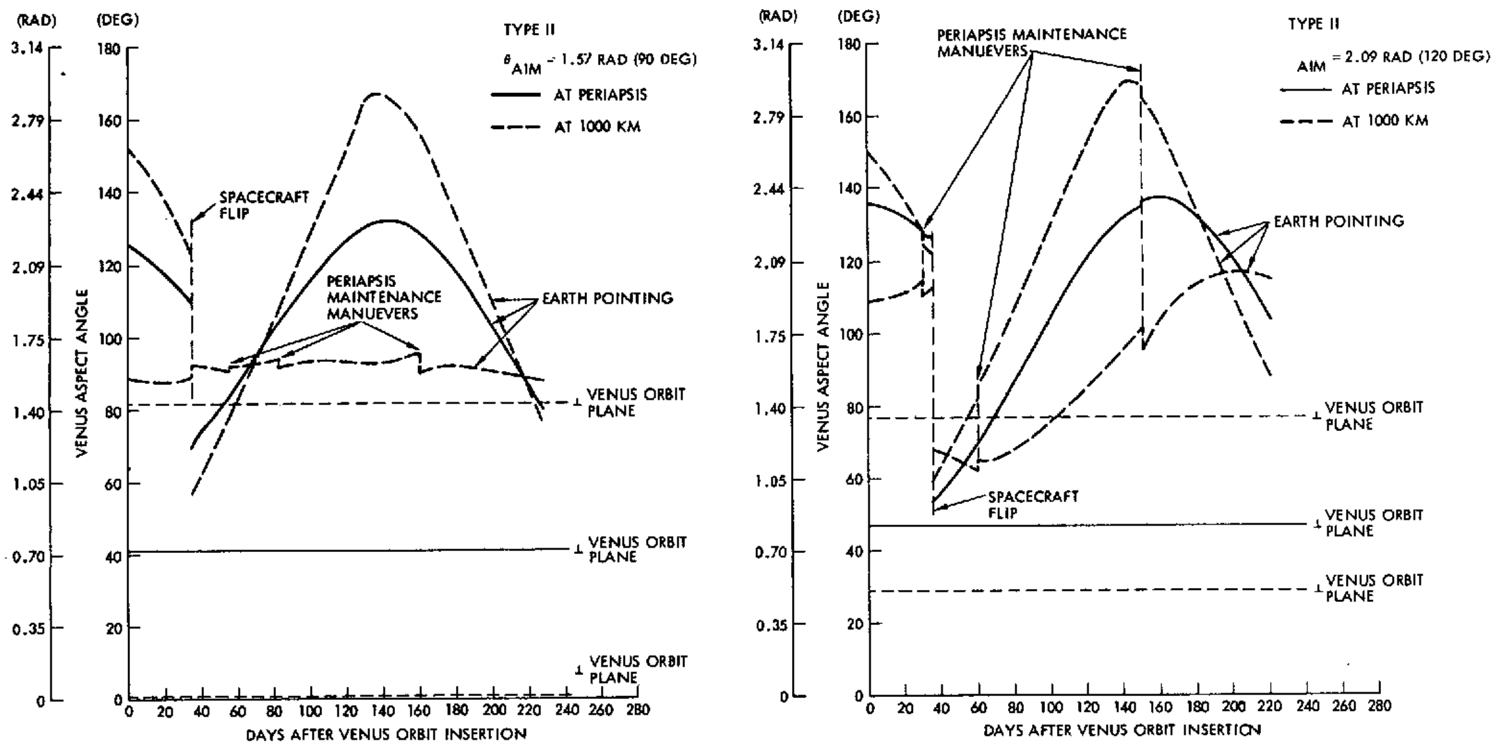

Figure 3-105. Venus Aspect Angle

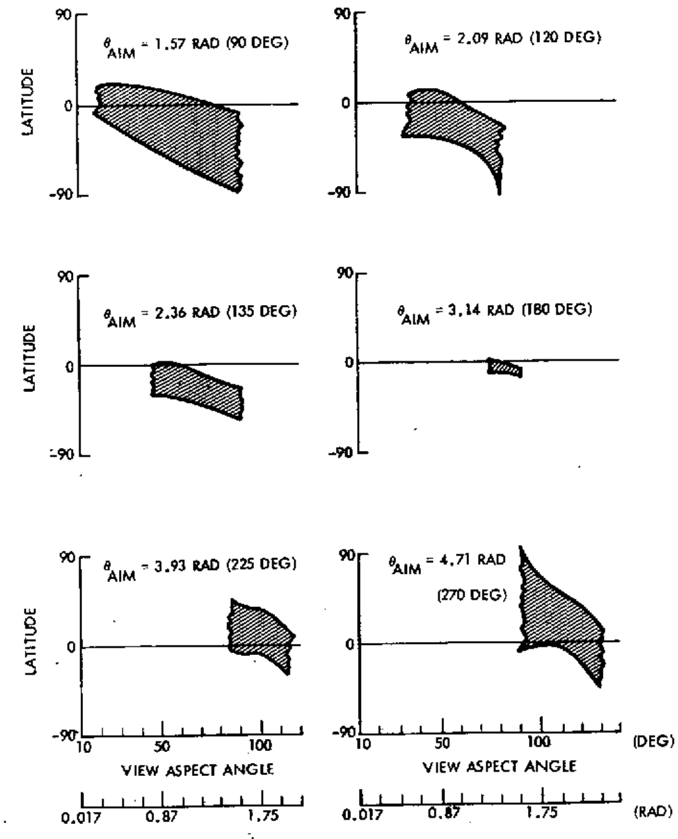

Figure 3-106. NVOP Latitude Coverage of Normal Limb Scan if Slit is Rotatable ±1.57 Radians (±90 Degrees) (1000 KM and Lower)

scanning. In order to determine the frequency and latitude coverage for normal limb scan for an earth pointer, it is necessary to specify the direction and slit angle. The optimum view direction and slit angle has been chosen as those angles for which a maximum number of normal limb scans occurs through the mission at altitudes below 1000 kilometers. A computer program was generated that determined the slit angle, altitude and latitude for normal limb scans when the instrument view is in the optimum direction.

The method of determining the optimum EP view direction is discussed in the following subsection.

Determination of Optimum View Direction for Normal Limb Scan. A method to determine the optimum view direction is summarized here with the necessary charts and two example orbit cases.

As an aid to visualizing the trigonometric relationships in Figure 3-107, a sphere is generated with its center at the spacecraft

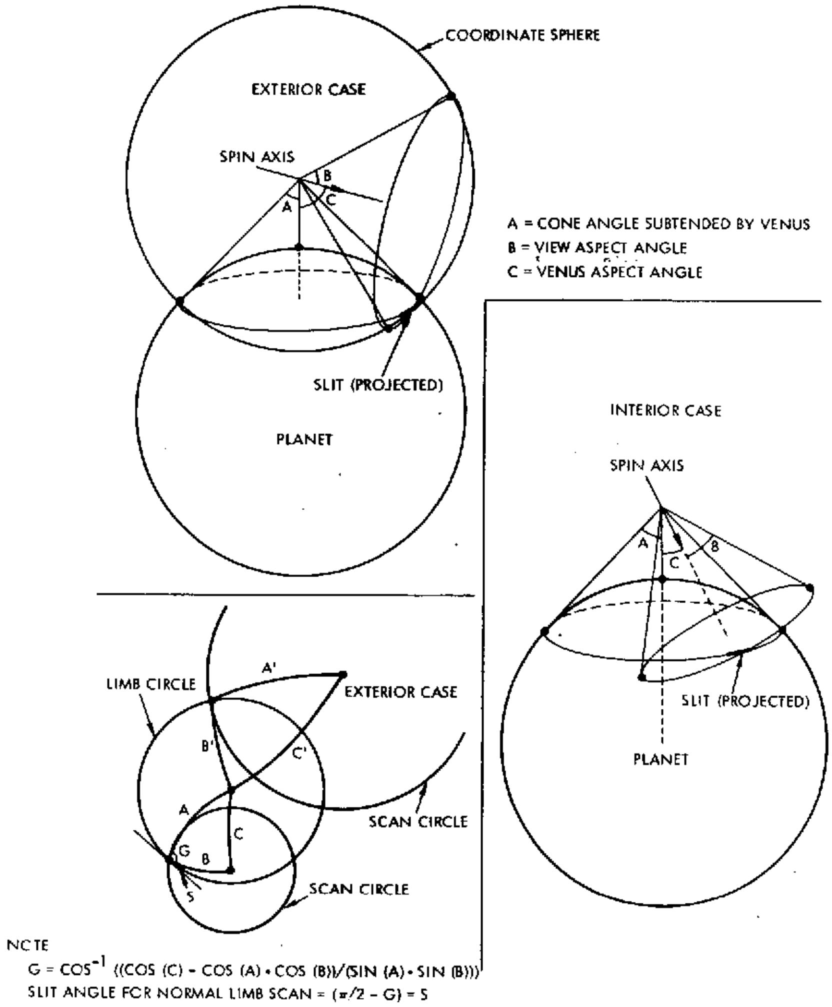

Figure 3-107. Limb Scan Geometry

and intersecting the planet at the points of tangency, i.e., limb points. On this coordinate sphere, the Angles A, B and C form the sides of a spherical triangle. The limb crossing of the instrument view axis occurs at the A, B apex of the spherical triangle. The angle formed by A and B is G. The central angle B defines a plane containing the view axis and the spin axis. This plane is the plane of reference for the angle of the slit about the view axis. Note that if the slit is aligned with this reference plane and G = 1.57 radian (90 degrees), a normal limb scan occurs. Any time the view aspect of the instrument intersects cone A, a normal limb scan can occur if the slit angle is chosen properly. The slit angle in the diagram is designated as S where $S = \pi/2 - G$. Note that by spherical trigonometry

$$\cos G = [\cos c - \cos a \cos B] / [\sin A \sin B]$$

providing A + B + C 6.28 radians (< 360 degrees).

The view angle, B, and the slit angle, S, are parametrically related to the Venus aspect angle C for any given altitude. The relationships between S, G, and C are shown in Figures 3-108, 3-109 and 3-110 for altitudes 200, 600 and 1000 kilometers, respectively.

Note the 3.14-radian (180-degree) symmetry of the curves in that B relates to C as the supplement of B relates to the supplement of C. Now if the view angle and slit angle are fixed, only two values of Venus aspect angle at a given altitude will result in a normal limb scan. For example, if the slit angle is fixed at 0.70 radian (40 degrees) and the view aspect at 1.92 radian (110 degrees), a normal limb scan will occur at a Venus aspect of 1.05 and 2.30 radians (60 and 132 degrees) at 200 kilometers altitude.

Optimization. The altitude of interest for normal limb scans is less than 1000 kilometers. The optimum values for slit angle and view aspect are such that a normal limb scan can occur at all altitudes from 200 to 1000 kilometers. The curves of Figures 3-108

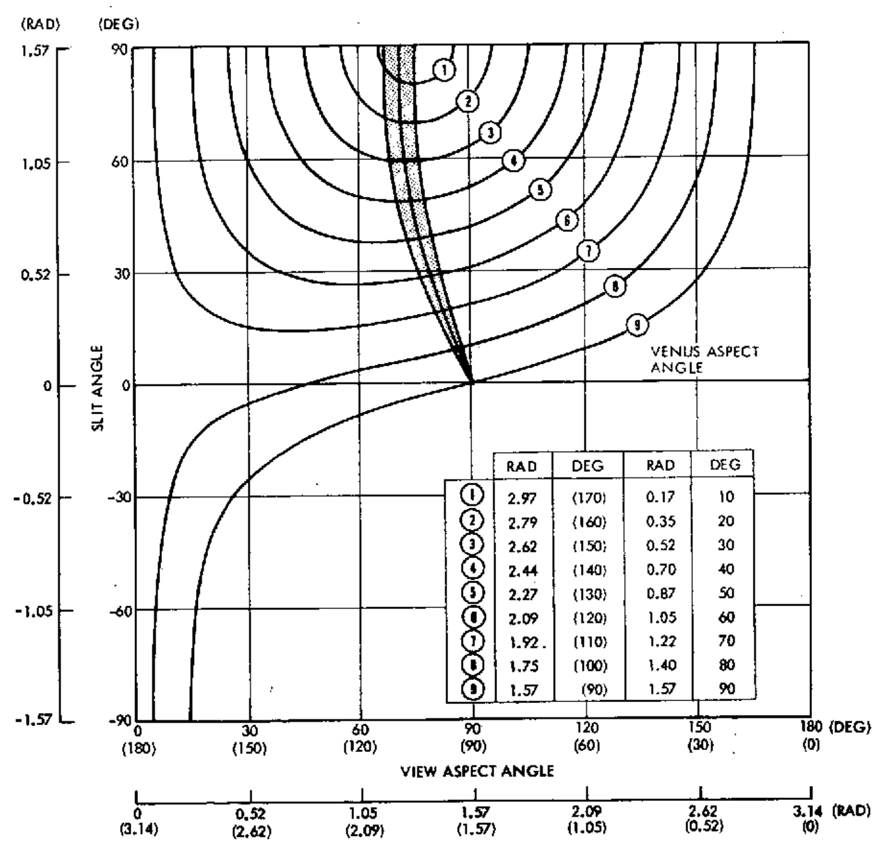

	RAD	DEG	RAD	DEG
1	2.97	(170)	0.17	10
2	2.79	(160)	0.35	20
3	2.62	(150)	0.52	30
4	2.44	(140)	0.70	40
5	2.27	(130)	0.87	50
6	2.09	(120)	1.05	60
7	1.92	(110)	1.22	70
8	1.75	(100)	1.40	80
9	1.57	(90)	1.57	90

Figure 3-108. Angles for Normal Limb Scan (200 Kilometers Altitude)

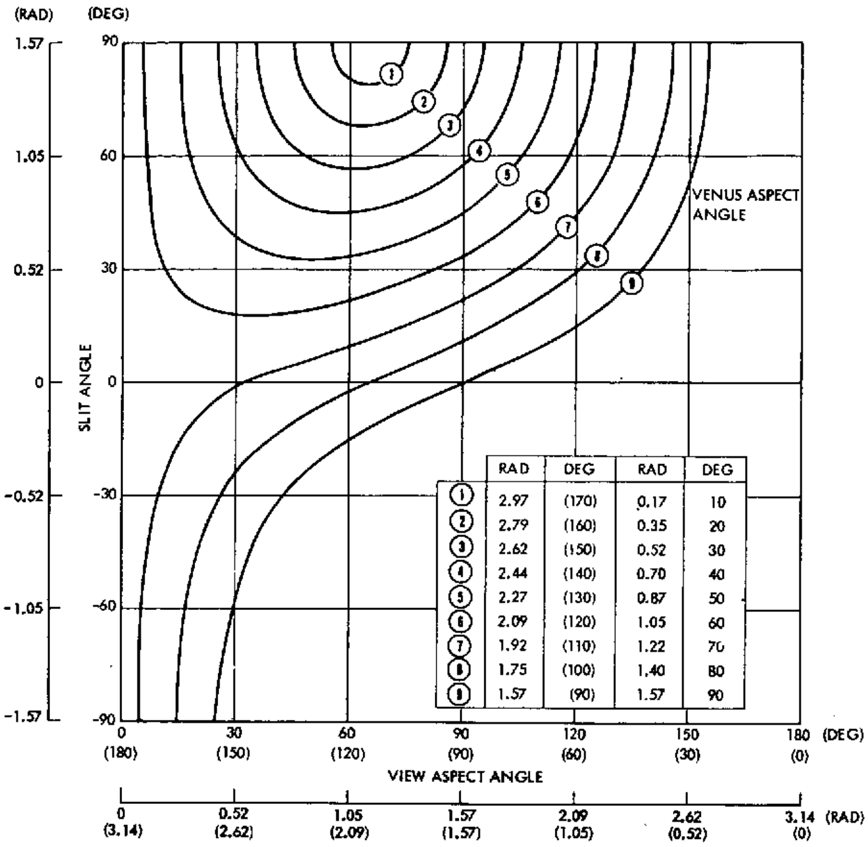

	RAD	DEG	RAD	DEG
1	2.97	(170)	0.17	10
2	2.79	(160)	0.35	20
3	2.62	(150)	0.52	30
4	2.44	(140)	0.70	40
5	2.27	(130)	0.87	50
6	2.09	(120)	1.05	60
7	1.92	(110)	1.22	70
8	1.75	(100)	1.40	80
9	1.57	(90)	1.57	90

Figure 3-109.
Angles for Normal Limb Scan
(600 Kilometers Altitude)

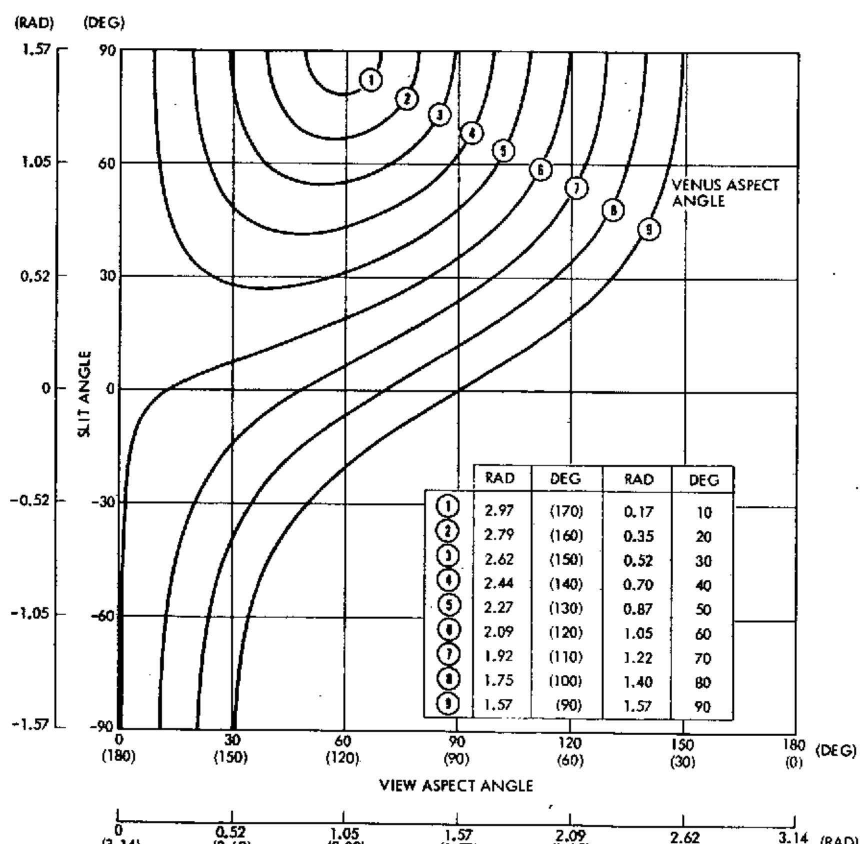

	RAD	DEG	RAD	DEG
1	2.97	(170)	0.17	10
2	2.79	(160)	0.35	20
3	2.62	(150)	0.52	30
4	2.44	(140)	0.70	40
5	2.27	(130)	0.87	50
6	2.09	(120)	1.05	60
7	1.92	(110)	1.22	70
8	1.75	(100)	1.40	80
9	1.57	(90)	1.57	90

Figure 3-110.
Angles for Normal Limb Scan
(1000 Kilometers Altitude)

through 3-110 are centered at the subtended cone angles [1.33, 1.15, and 1.05 radian (75.5, 65.5, and 59.1 degrees), respectively]. The effect of raising altitude is to shift the curves to the left. For the values of B and S to be most universal for altitudes from 200 to 1000 kilometers, the point which defines B and S must lie in a region that is insensitive. This region is shaded in Figure 3-108 and is bounded by the intersection of the corresponding Venus aspect angle curves as altitude is varied from 200 to 1000 kilometers.

To maximize the number of normal limb scans throughout the mission, a Venus aspect angle value must be chosen which occurs most frequently. This value then determines the view angle and slit angle by the constraints of Figures 3-108, 3-109 and 3-110. The maximum and minimum EP Venus aspect angles at less than 1000 kilometers are plotted for the mission duration for the θ_{AIM} = 2.09 and 2.36 radians (120 and 135 degrees) in Figures 3-111 and 3-112. On each periapsis pass, all values of Venus aspect angle between the maximum and minimum are encountered. For the

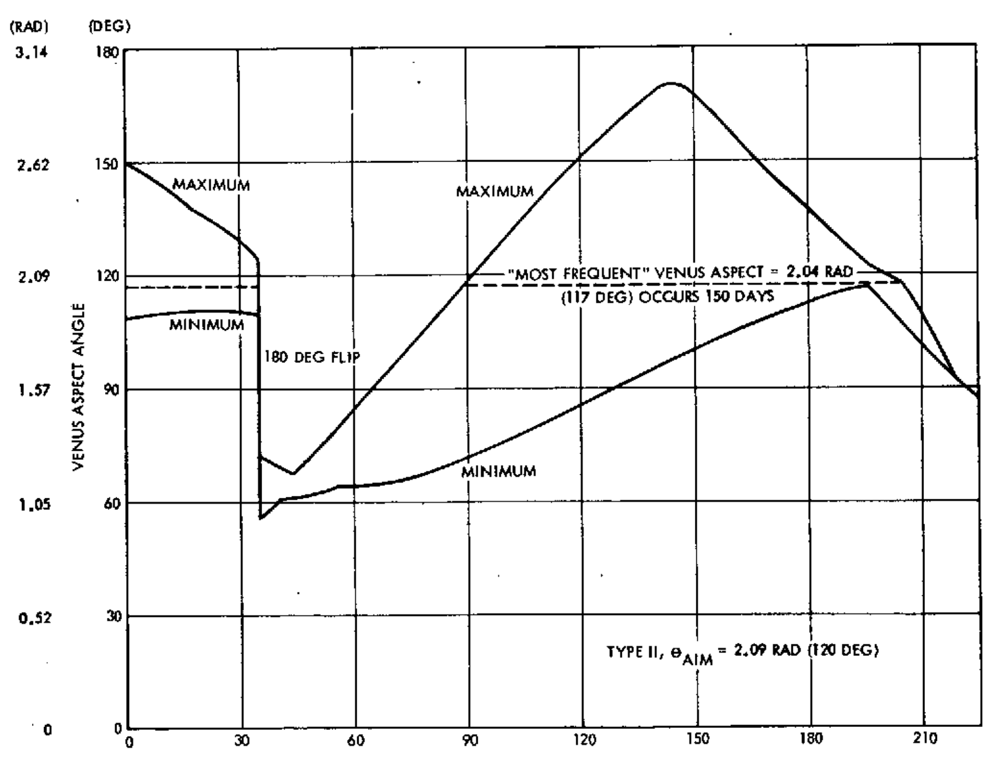

Figure 3-111. Maximum and Minimum Venus Aspect, Earth-Pointing Configuration (Type II, θ_{AIM} = 2.09 Rad (120 Deg))

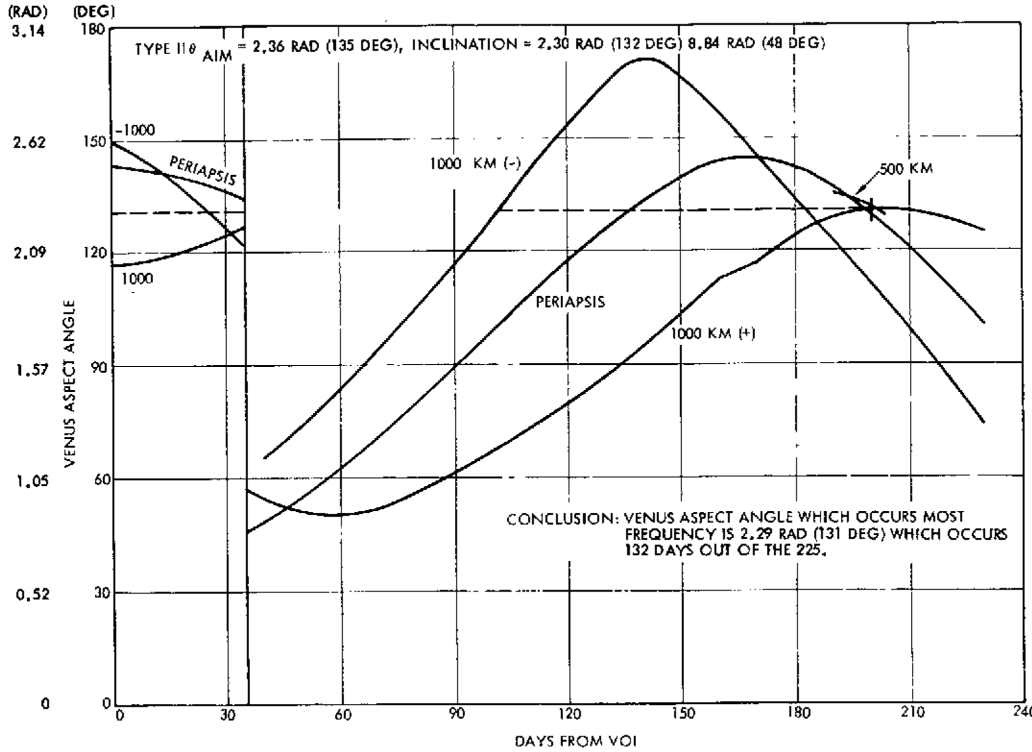

Figure 3-112. Maximum and Minimum Venus Aspect Earth-Pointing Configuration (Type II, θ_{AIM} = 2.36 Rad (135 Deg), Inclination = 2.30 Rad (132 Deg) 8.84 Rad/48 Deg)

θ_{AIM} = 2.094 radians (120 degrees) orbit, the most frequent Venus aspect if 2.04 radians (117 degrees) which occurs 150 days out of the 225-day mission. Referring to Figure 3-108, the optimum slit angle and view angle are 0.44 and 1.71 radian (25 and 98 degrees), respectively. For the θ_{AIM} = 2.36 radians (135 degrees) case, the most frequent Venus aspect is 2.29 radians (131 degrees) which occurs 132 days out of the 225. The 2.29 radians (131 degrees) yields an optimum slit angle of 0.61 radian (35 degrees) and a view angle of 1.78 radian (102 degrees). These values of slit angle and view angle guarantee a normal limb scan for every occurrence of a Venus aspect of 2.29 radians (131 degrees).

For a chosen view direction and slit angle a normal limb scan may occur for two different Venus aspect angles. For this reason the number of days discussed above is the minimum number. The actual number of days of normal limb scans was computed using the optimum view direction.

Slit Angle Studies. If the normal limb scan instrument has a fixed view direction and slit angle, a normal limb scan will usually occur during only one spin revolution per orbit period at altitudes below 1000 kilometers. It is of interest to determine the angular deviation from the normal limb scan that occurs for the remainder of the low altitude portion of the pass.

The slit angle is defined as the angle between the direction of the long dimension of the slit, which lies in a plane normal to the view direction, and the plane defined by the spacecraft spin axis and the view direction. The following curves show the slit angles at which normal limb scans occur for altitudes below 1000 kilometers for the Type II orbit with θ_{AIM} = 2.09 radians (120 degrees). One of the two limbs observed per spin period will have a normal limb scan at the negative of that angle.

In Figure 3-113, the NVOP view direction was chosen at 1.57 radian (90 degrees). A single curve is approximately valid for every pass. However, a normal limb scan will occur at only one

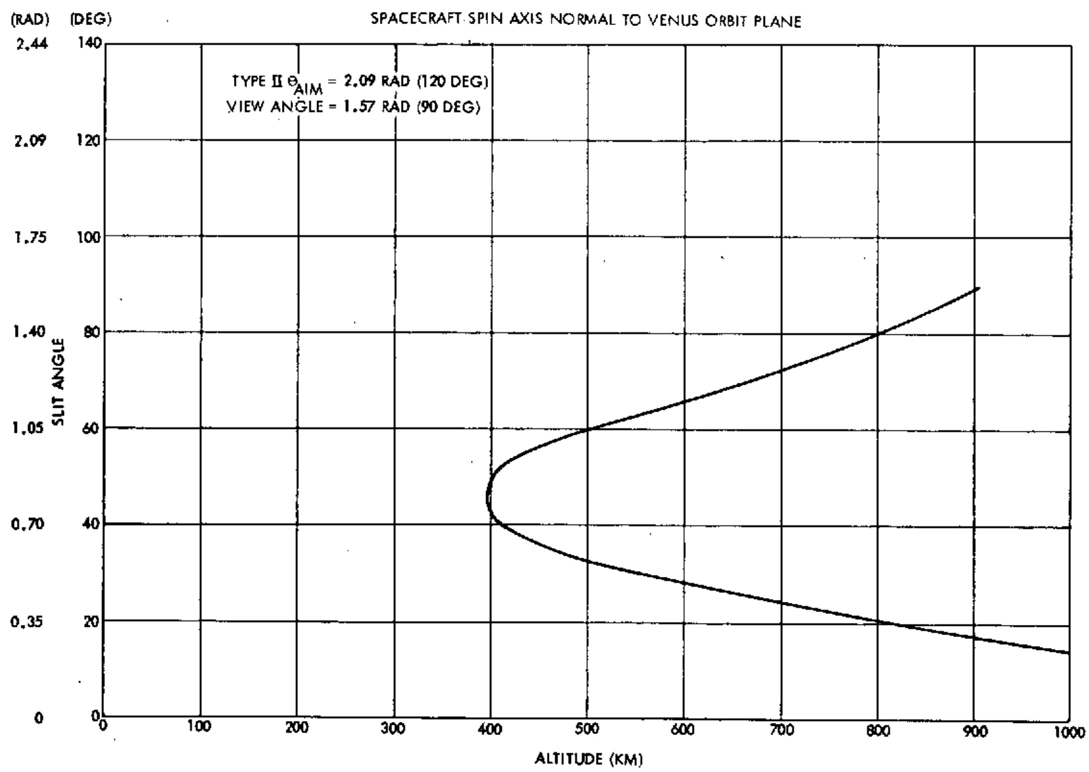

Figure 3-113. Slit Angle for Normal Limb Scan

latitude for a fixed slit angle. If the slit angle is chosen at 0.7 radian (45 degrees), the normal limb scan will occur at periapsis and for the remainder of the low altitude pass the slit will be within 0.52 radian (30 degrees) of normal on one of the limbs.

For the EP spacecraft (Figures 3-114 through 3-118), the view direction chosen in this study was 1.71 radian (98 degrees) to the spin axis (optimum for frequency of normal limb scan). In this case a normal limb scan will occur with a 0.44-radian (25-degree) slit angle almost every day. These scans will occur over a large range of latitudes.

In either the EP or NVOP, if a fixed slit angle at 0.79 radian (45 degrees) is chosen, the slit will be within 0.79 radian (45 degrees) of normal to the vertical of one of the limbs throughout every pass between periapsis and 1000 kilometers. Fixed crossed 0.79-radian (45-degree) slits will ensure that this occurs for both limbs.

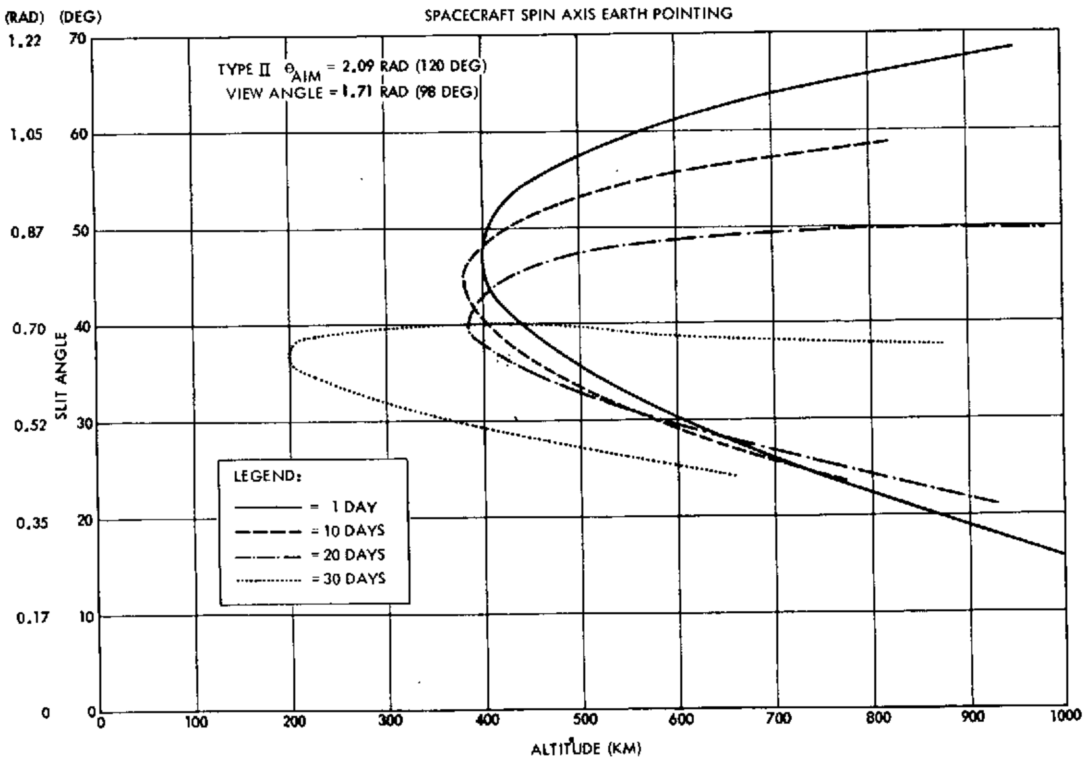

Figure 3-114. Slit Angle for Normal Limb Scan

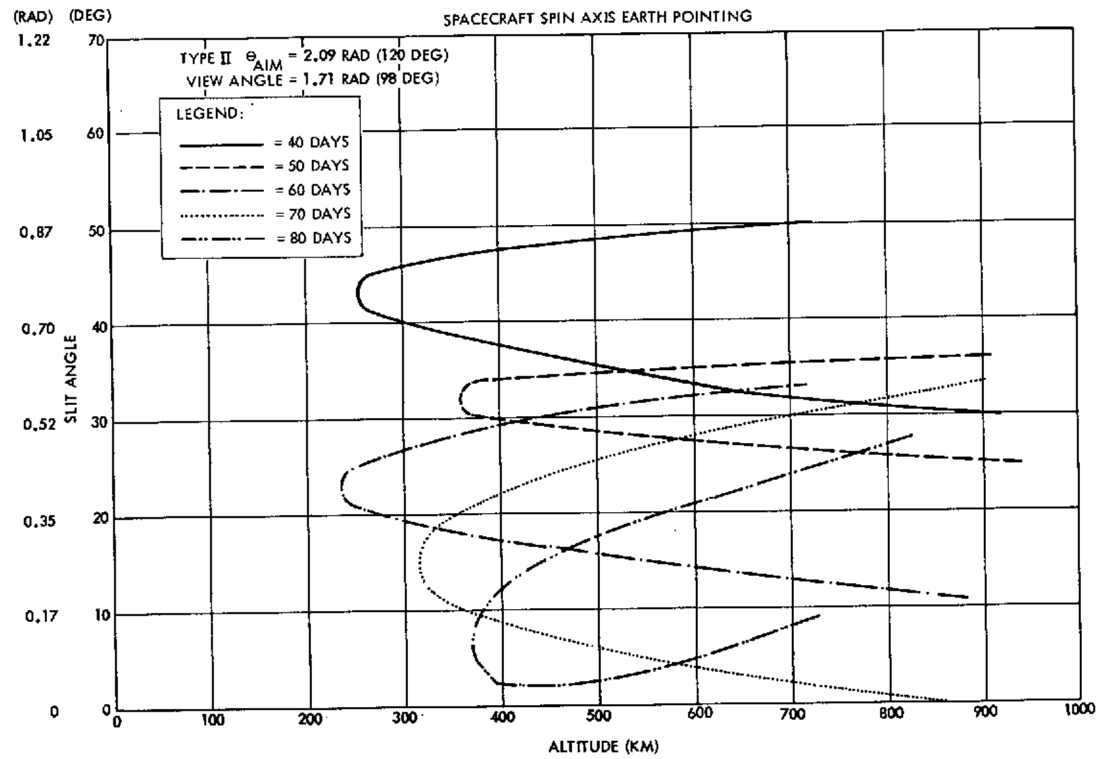

Figure 3-115. Slit Angle for Normal Limb Scan

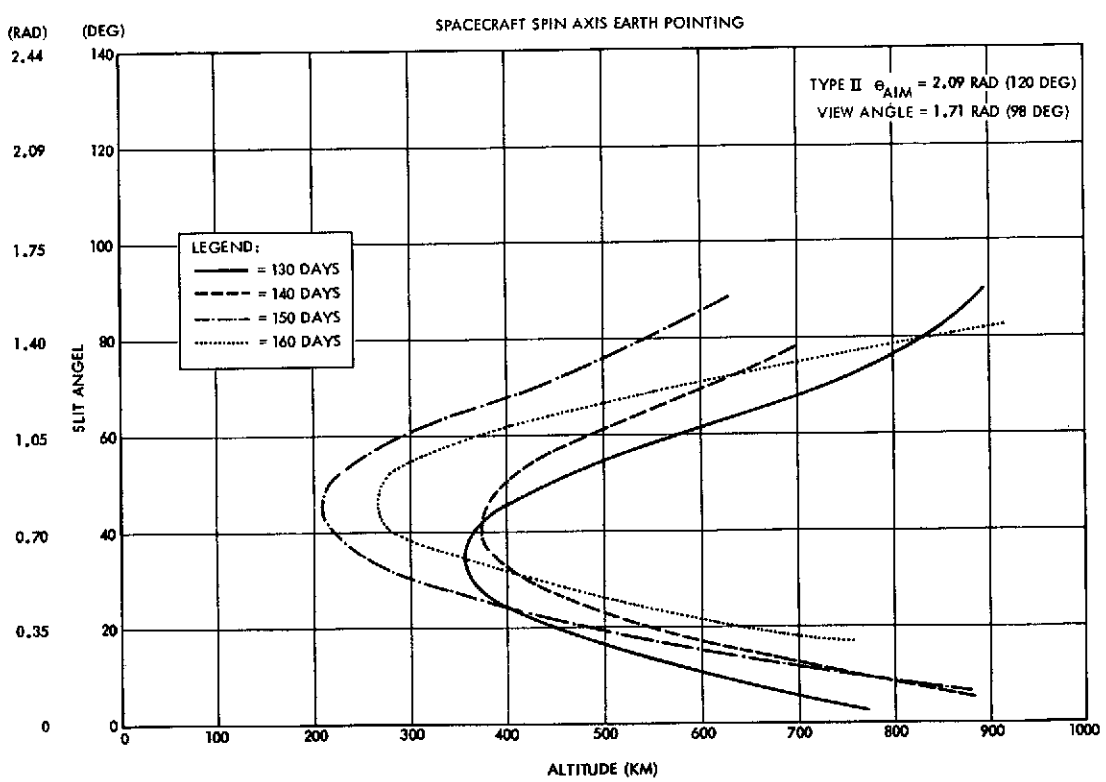

Figure 3-117. Slit Angle for Normal Limb Scan

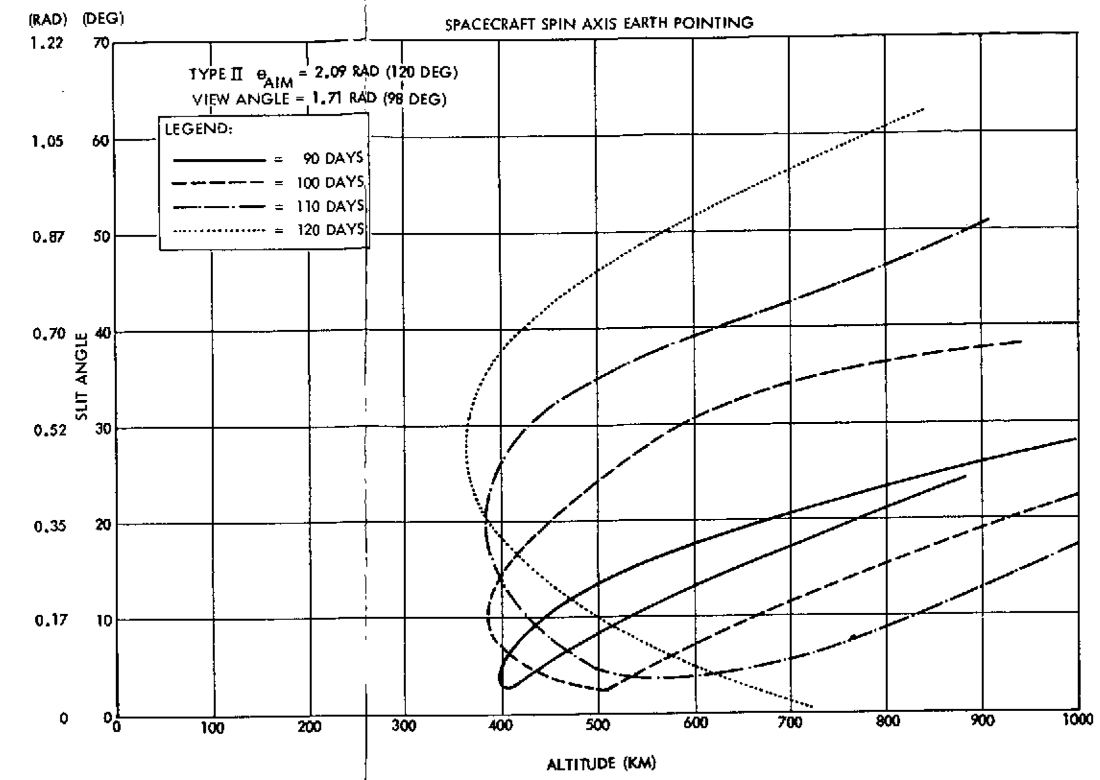

Figure 3-116. Slit Angle for Normal Limb Scan

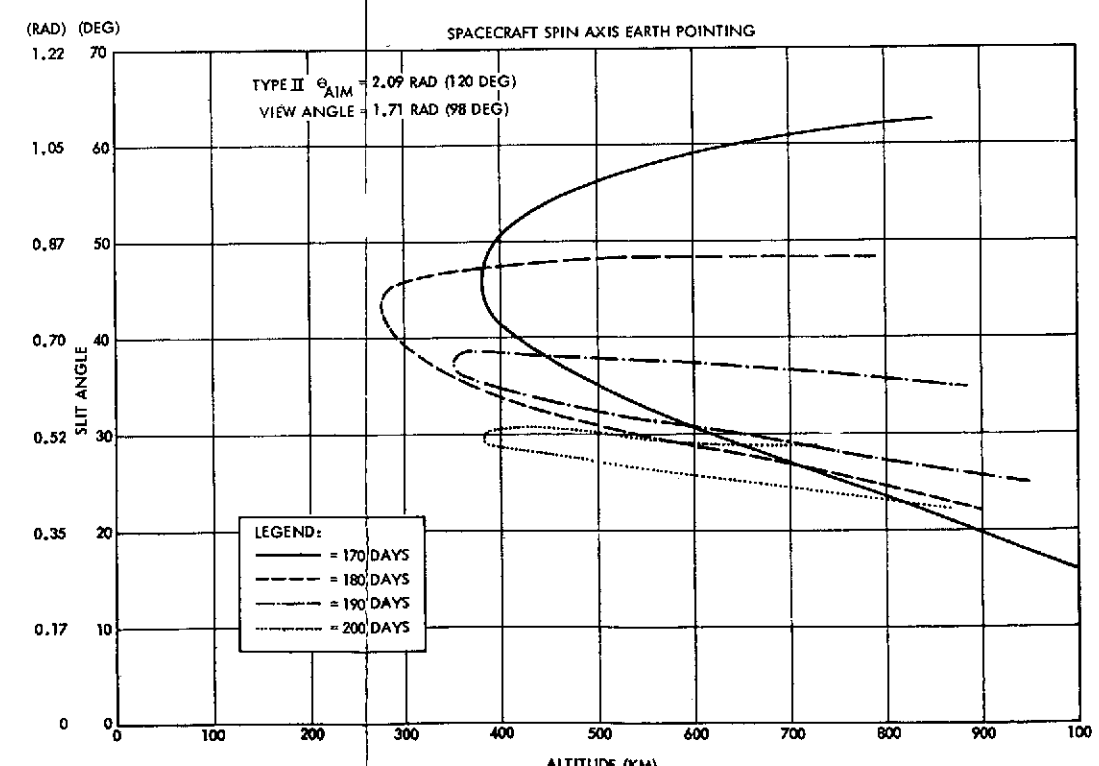

Figure 3-118. Slit Angle for Normal Limb Scan

FOLDOUT FRAME 1

FOLDOUT FRAME 2

Science-Relevant Orbit Parameters

The orbit parameters discussed in the previous sections and identified in Table 3-38 were computed for the EP and NVOP for six Type II and four Type I orbits. For the EP it is assumed that the spacecraft has a gimballed platform on which ram pointing instruments can be mounted, so the mass spectrometers can view in ram direction at periapsis each orbit.

The results of these compilations are included in Tables 3-39, 3-40, and 3-41.

The angular range figures are the smallest and largest angles that the instruments must make with the spacecraft spin axis to point in the desired directions. If the spacecraft spin axis is normal to the Venus orbit plane, the ram velocity and Venus aspect angles are constant at periapsis from orbit to orbit. The small changes shown are due to changes in periapsis altitude. Significant ranges must be covered in high inclination orbits for both EP and NVOP for instruments to make measurements up to 1000 kilometers.

An instrument viewing along the spacecraft spin axis does not necessarily view the planet during each orbit. For each orbit, if the planet is observed, a minimum range is recorded. The averages of the minimum ranges are shown in Tables 3-39 to 3-41 under "Average Minimum for View Along Spin Axis." (For good instrument resolution, it is desirable that these ranges be as small as possible.) Also shown under "Range" is the range of altitudes in which an instrument remains within 0.017 radian (10 degrees) of the "ram direction" if it is set at the "ram direction" at periapsis. This is only shown for the NVOP since, for the EP, a ram platform is required and can be used to point in the ram direction at any altitude.

Under "Plasma Tail Crossings" the spacecraft radial distance throughout the mission for entering and leaving solar eclipse is given.

If an instrument is mounted at a fixed angle on the spacecraft, NVOP normal limb scans will always occur at the same altitude and latitude. The EP range of latitudes covered and the frequency of normal limb scans shown in the table are for the slit angle and view direction which correspond to the maximum number of normal limb

Table 3-39. Science Relevant Orbit Parameters

θ (AIM)(TYPE)	2.36 RAD (135-DEG) TYPE I		3.14 RAD (180-DEG) TYPE I		3.93 RAD (225-DEG) TYPE I		4.71 RAD (270-DEG) TYPE I	
	EARTH POINTING	NVOP	EARTH POINTING	NVOP	EARTH POINTING	NVOP	EARTH POINTING	NVOP
ANGULAR RANGE [RAD (DEG)]								
VENUS ASPECT ANGLE AT PERIAPSIS	1.03 TO 2.06 (59 TO 118)	0.58 TO 0.59 (33 TO 34)	0.56 TO 2.62 (29 TO 150)	1.10 TO 1.12 (63 TO 64)	0.104 TO 3.09 (6 TO 177)	1.50 TO 1.54 (86 TO 88)	0.087 TO 3.09 (5 TO 177)	1.66 TO 1.69 (95 TO 97)
VENUS ASPECT ANGLE TO 1000 KM	0.63 TO 2.34 (36 TO 134)	0.58 TO 0.94 (33 TO 54)	0.105 TO 2.58 (6 TO 148)	0.84 TO 1.57 (48 TO 90)	0.104 TO 3.09 (6 TO 177)	0.91 TO 1.57 (52 TO 121)	0.087 TO 3.09 (5 TO 177)	0.96 TO 2.41 (55 TO 138)
RAM VELOCITY DIRECTION AT PERIAPSIS (ANGLE OF ATTACK)	0.122 TO 2.37 (7 TO 136)	1.68 TO 1.73 (96 TO 99)	0.45 TO 2.06 (26 TO 118)	2.04 TO 2.00 (117 TO 120)	0.98 TO 1.73 (56 TO 99)	2.57 TO 2.60 (147 TO 149)	1.47 TO 1.64 (84 TO 94)	3.02 TO 3.05 (173 TO 175)
RAM VELOCITY DIRECTION TO 1000 KM (ANGLE OF ATTACK)	0.122 TO 2.65 (7 TO 152)	1.68 TO 2.04 (96 TO 117)	0.24 TO 2.29 (14 TO 131)	1.87 TO 2.25 (107 TO 129)	0.84 TO 2.08 (48 TO 119)	2.44 TO 2.60 (140 TO 149)	1.12 TO 2.02 (64 TO 116)	2.62 TO 3.12 (151 TO 179)
RANGE (KM)								
AVERAGE MINIMUM FOR VIEW ALONG SPIN AXIS	960	330	728	1000	1850	1960	319	1270
RAM WITHIN 0.17 RAD (10 DEG)	---	300 TO 500	---	200 TO 1000	---	300 TO 1300	---	200 TO 400
PLASMA TAIL CROSSINGS, R_V	1.04 TO 3.29		1.04 TO 7.7		1.04 TO 1.4 7.52 TO 12		1.08 TO 1.31 11 TO 12	
LATITUDE RANGE [RAD (DEG)]								
VIEW ALONG SPIN AXIS ON DARK SIDE	-1.17 TO 1.31 (-67 TO 75)	0 TO 0.98 (0 TO -56)	+1.48 TO -1.40 (+85 TO -80)	0 TO -0.56 (0 TO -32)	+1.48 TO 1.48 (+85 TO -85)	0 TO -0.52 (0 TO -30)	+1.48 TO -1.48 (+85 TO -85)	0 TO -1.57 (0 TO -90)
VIEW ALONG SPIN AXIS	-1.17 TO -1.50 (-67 TO 86)	0 TO -0.98 (0 TO -56)	-1.40 TO -1.05 (-80 TO -60)	0 TO -0.56 (0 TO -32)	+1.48 TO -1.48 (+85 TO -85)	0 TO -0.52 (0 TO -30)	+1.48 TO -1.48 (+85 TO -85)	0 TO -1.57 (0 TO -90)
VENUS ASPECT ANGLE BELOW 1000 KM	-1.01 TO -0.58 (-58 TO -33)		-0.72 TO -0.017 (-41 TO -1)		-0.66 TO 0.54 (-38 TO 31)		-0.61 TO 0.82 (-35 TO 47)	
PERIAPSIS TO 1000 KM	-1.01 TO -0.58 (-58 TO -33)		-0.72 TO -0.017 (-41 TO -1)		-0.66 TO 0.54 (-38 TO 31)		-0.61 TO 0.82 (-35 TO 47)	
NORMAL LIMB SCAN AT FIXED ANGLE BELOW 1000 KM	+0.31 TO 0.79 (+18 TO +45) -0.45 TO -0.86 (-26 TO -49)	NONE	+0.54 TO +1.03 (+31 TO +59) -0.89 TO -1.33 (-51 TO -76)	NONE	+0.56 TO +1.15 (+32 TO +66) -1.06 TO -1.33 (-61 TO -76)	NONE	+0.73 TO +1.26 (+42 TO +72) -0.79 TO -1.26 (-45 TO -72)	NONE
FREQUENCY (DAYS)								
VIEW ALONG SPIN AXIS ON LIGHT SIDE	140	100	100	150	60	80	40	225
VIEW ALONG SPIN AXIS ON DARK SIDE	130	90	110	150	40	50	30	225
VIEW ALONG SPIN AXIS	140	120	110	150	70	110	40	225
NORMAL LIMB SCAN BELOW 1000 KM AT FIXED ANGLE*	(25) (83) 225	225	(35) (77) 200	150	(45) (74) 160	225	(45) (106) 110	225
EARTH OCCULTATION (DAYS)	188		162		137		106	
DAY OF PERIAPSIS EVENING TERMINATOR CROSSING	76		65		51		31	
DAY OF PERIAPSIS MORNING TERMINATOR CROSSING	189		178		164		144	

*THE FIRST FIGURE IN PARENTHESES IS THE OPTIMUM SLIT ANGLE YIELDING THE INDICATED NUMBER OF DAYS OF NORMAL LIMB SCAN. THE SECOND IS THE CORRESPONDING VIEW ASPECT ANGLE.

FOLDOUT FRAME 1

FOLDOUT FRAME 2

Table 3-40. Science Relevant Orbit Parameters Affecting Orbit and Spin Axis Selection

θ (AIM) (TYPE)	3.14 RAD (180-DEG) TYPE II		3.93 RAD (225-DEG) TYPE II		4.71 RAD (270-DEG) TYPE II	
	EARTH POINTING	NVOP	EARTH POINTING	NVOP	EARTH POINTING	NVOP
ANGULAR RANGE [RAD (DEG)]						
VENUS ASPECT ANGLE AT PERIAPSIS	0.49 TO 2.93 (28 TO 168)	1.36 TO 1.38 (78 TO 79)	0.63 TO 2.93 (36 TO 168)	1.73 TO 1.76 (99 TO 101)	1.08 TO 2.76 (62 TO 158)	1.90 TO 1.94 (109 TO 111)
VENUS ASPECT ANGLE TO 1000 KM	0.139 TO 2.91 (8 TO 167)	1.40 TO 1.71 (80 TO 98)	0.56 TO 2.93 (32 TO 168)	1.22 TO 2.23 (70 TO 128)	1.22 TO 2.83 (70 TO 162)	1.19 TO 2.65 (68 TO 152)
RAM VELOCITY DIRECTION AT PERIAPSIS (ANGLE OF ATTACK)	0.069 TO 1.95 (4 TO 112)	1.68 TO 1.73 (96 TO 99)	0.73 TO 2.36 (42 TO 135)	2.34 TO 2.39 (134 TO 137)	1.20 TO 1.75 (69 TO 100)	2.78 TO 2.81 (159 TO 161)
RAM VELOCITY DIRECTION TO 1000 KM (ANGLE OF ATTACK)	0 TO 2.30 (0 TO 132)	1.59 TO 1.78 (91 TO 102)	1.08 TO 2.36 (62 TO 135)	2.18 TO 2.41 (125 TO 138)	0.77 TO 1.88 (44 TO 108)	1.94 TO 2.65 (111 TO 152)
RANGE (KM)						
AVERAGE MINIMUM FOR VIEW ALONG SPIN AXIS	540	NONE	580	1620	470	740
RAM WITHIN 10 DEG	---	200 TO 10,000	---	200 TO 10,000	---	200 TO 300
PLASMA TAIL CROSSINGS, R_V	1.04 TO 6.21		1.05 TO 1.58 8.87 TO 11.1		1.06 TO 1.43 7.77 TO 10.2	
LATITUDE RANGE [RAD (DEG)]						
VIEW ALONG SPIN AXIS ON DARK SIDE	-0.35 TO 0.35 (-20 TO 20)	NONE	-1.55 TO 1.47 (-89 TO 84)	0 TO +0.35 (0 TO +20)	-1.48 TO 1.52 (-85 TO 87)	0 TO -1.57 (0 TO -90)
VIEW ALONG SPIN AXIS	-0.35 TO 0.35 (-20 TO 20)	NONE	-1.55 TO 1.47 (-89 TO 84)	0 TO +0.35 (0 TO +20)	-1.48 TO 1.52 (-85 TO +20)	0 TO -1.57 (0 TO -90)
VENUS ASPECT ANGLE BELOW 1000 KM	-0.24 TO -0.069 (-14 TO -4)		-0.35 TO 0.65 (-20 TO 37)		-0.38 TO 1.06 (-22 TO 61)	
PERIAPSIS TO 1000 KM	-0.24 TO -0.069 (-14 TO -4)		-0.35 TO 0.65 (-20 TO 37)		-0.38 TO 1.06 (-22 TO 61)	
NORMAL LIMB SCAN (SPIN) AT FIXED ANGLE BELOW 1000 KM	0.37 TO -0.65 (21 TO -37)	NONE	0.80 TO -0.70 (46 TO -40)	NONE	-0.66 TO +0.98 (-38 TO +56)	NONE
FREQUENCY (DAYS)						
VIEW ALONG SPIN AXIS ON LIGHT SIDE	160	NONE	180	120	100	225
VIEW ALONG SPIN AXIS ON DARK SIDE	160	NONE	160	150	100	225
VIEW ALONG SPIN AXIS	160	NONE	180	225	160	225
NORMAL LIMB SCAN BELOW 1000 KM AT FIXED ANGLE*	(45) (106) 190	225	(45) (105) 190	225	(35) (109) 150	225
EARTH OCCULTATION (DAYS)	164		100		61	
DAY OF PERIAPSIS EVENING TERMINATOR CROSSING	21		16		2	
DAY OF PERIAPSIS MORNING	134		129		115	

*THE FIRST FIGURE IN PARENTHESIS IS THE OPTIMUM SLIT ANGLE YIELDING THE INDICATED NUMBER OF DAYS OF NORMAL LIMB SCAN. THE SECOND IS THE CORRESPONDING VIEW ASPECT ANGLE.

FOLDOUT FRAME 3

Table 3-41. Science Relevant Orbit Parameters Affecting Orbit and Spin Axis Selection

θ (AIM)(TYPE)	1.57 RAD (90-DEG) TYPE II		2.09 RAD (120-DEG) TYPE II		2.36 RAD (135-DEG) TYPE II	
	EARTH POINTING	NVOP	EARTH POINTING	NVOP	EARTH POINTING	NVOP
ANGULAR RANGE [RAD (DEG)]						
VENUS ASPECT ANGLE AT PERIAPSIS	1.27 TO 2.32 (73 TO 133)	0.70 TO 0.72 (40 TO 41)	0.99 TO 2.39 (57 TO 137)	0.80 TO 0.82 (46 TO 47)	0.86 TO 2.50 (49 TO 143)	0.93 TO 0.94 (53 TO 54)
VENUS ASPECT ANGLE TO 1000 KM	1.06 TO 2.91 (61 TO 167)	0 TO 1.43 (0 TO 82)	0.99 TO 2.95 (57 TO 169)	0.47 TO 1.36 (27 TO 78)	0.36 TO 2.98 (49 TO 171)	0.72 TO 1.40 (41 TO 80)
RAM VELOCITY DIRECTION AT PERIAPSIS (ANGLE OF ATTACK)	0.82 TO 1.99 (47 TO 114)	0.84 TO 0.87 (48 TO 50)	0.63 TO 2.27 (36 TO 130)	0.96 TO 0.99 (55 TO 57)	0.51 TO 2.46 (29 TO 141)	1.08 TO 1.12 (62 TO 64)
RAM VELOCITY DIRECTION TO 1000 KM (ANGLE OF ATTACK)	0.37 TO 2.08 (21 TO 119)	0.44 TO 1.26 (25 TO 72)	0.33 TO 2.27 (19 TO 130)	0.70 TO 1.27 (40 TO 73)	0.23 TO 2.46 (13 TO 141)	0.86 TO 1.41 (49 TO 81)
RANGE (KM)						
AVERAGE MINIMUM FOR VIEW ALONG SPIN AXIS	580	370	750	490	760	592
RAM WITHIN 10 DEG	---	200 TO 400	---	200 TO 450	---	250 TO 800
PLASMA TAIL CROSSINGS, R_V	1.04 TO 5.5		1.05 TO 5.53		1.05 TO 5.6	
LATITUDE RANGE [RAD (DEG)]						
VIEW ALONG SPIN AXIS ON DARK SIDE	-1.52 TO 1.47 (-87 TO 84)	0 TO -1.57 (0 TO -90)	-1.34 TO 1.47 (-77 TO 84)	0 TO -1.01 (0 TO -58)	-0.84 TO +1.19 (-48 TO +68)	0 TO -0.70 (0 TO -40)
VIEW ALONG SPIN AXIS	-1.52 TO 1.47 (-87 TO 84)	0 TO -1.57 (0 TO -90)	-1.34 TO 1.47 (-77 TO 84)	0 TO -1.01 (0 TO -58)	-0.84 TO +1.19 (-48 TO +68)	0 TO -0.70 (0 TO -40)
VENUS ASPECT ANGLE BELOW 1000 KM	-1.57 TO -0.139 (-90 TO -8)		-1.08 TO -0.157 (-62 TO -9)		-0.84 TO -0.157 (-48 TO -9)	
PERIAPSIS TO 1000 KM	-1.57 TO -0.139 (-90 TO -8)		-1.08 TO -0.157 (-62 TO -9)		-0.84 TO -0.157 (-48 TO -9)	
NORMAL LIMB SCAN (SPIN) AT FIXED ANGLE BELOW 1000 KM	0.122 TO -1.57 (7 TO -90)	NONE	0.24 TO -1.15 (14 TO -66)	NONE	0.24 TO 1.05 (14 TO -60)	NONE
FREQUENCY (DAYS)						
VIEW ALONG SPIN AXIS ON LIGHT SIDE	80	225	90	190	130	160
VIEW ALONG SPIN AXIS ON DARK SIDE	100	225	130	160	140	170
VIEW ALONG SPIN AXIS	160	225	130	225	140	225
NORMAL LIMB SCAN BELOW 1000 KM AT FIXED ANGLE*	(5) (92) 210	225	(25) (98) 200	225	(35) (102) 225	225
EARTH OCCULTATION (DAYS)	64		109		148	
DAY OF PERIAPSIS EVENING TERMINATOR CROSSING	2		15		19	
DAY OF PERIAPSIS MORNING TERMINATOR CROSSING	115		138		132	

*THE FIRST FIGURE IN PARENTHESES IS THE OPTIMUM SLIT ANGLE YIELDING THE INDICATED NUMBER OF DAYS OF NORMAL LIMB SCAN. THE SECOND IS THE CORRESPONDING VIEW ASPECT ANGLE.

scans. These optimum angles are shown in parentheses in the tables alongside the frequency entry labeled "Normal Limb Scan Below 1000 Kilometers at Fixed Angle." The slit angle is shown first.

The latitude range covered by the spacecraft at periapsis and the Venus aspect angle below 1000 kilometers do not depend on spacecraft configuration. These tables have been used in selecting an orbit for maximum science return.

For many of the cases examined, the planet can be viewed along the spin axis through both ends of the spacecraft. The number of days an instrument views the planet along the spin axis is shown in the table for that direction giving maximum coverage. All the numbers under "Frequency" correspond to a 225-day mission.

Summary of Spin Axis Orientation Trades

Both spin axis orientations are adequate for the orbiter, each having specific advantages and disadvantages from the point of view of the scientific instruments. A comparison is given below:

- Advantages of normal-to-Venus orbit plane:
  - Fixed angle for nadir view, normal limb scan and ram direction at periapsis
  - Angular range for Venus aspect pointing near periapsis relatively small
  - Nadir view, normal limb scan, ram pointing obtained at periapsis every orbit
  - View along spin axis obtained every orbit.
- Advantages of earth pointing with ram platform:
  - Ram direction at different latitudes and altitudes
  - Normal limb scans and nadir viewing at various latitudes
  - Two-hemisphere coverage along spin axis at low altitudes.

The potential orbiter experimenters contacted showed no marked preference for either orientation.

Science Orbit Selection. Of the six Type II and four Type I orbits considered (see Tables 3-39, 3-40, 3-41), Type II $\theta_{AIM} = 2.09$

and 2.36 radians (120 and 135 degrees) best satisfy the science mission parameters. These orbits have inclinations of 1.05 and 0.82 radian (61 and 47 degrees), respectively.

These orbits were selected since they permit good planetary latitude coverage and frequent earth occultations.

Another advantage of these orbits is that periapsis remains on the light side in each case for more than 2 weeks after Venus orbit insertion, permitting a convenient comparative study of light and dark side science measurements.

The reasons for the elimination of the other orbits considered are given below:

	Type	θ_{AIM} [rad (deg)]
Poor near-periapsis latitude coverage	I II	2.36 (135) 3.14 (180)
Poor periapsis terminator crossing time	I II	2.36 (135) 4.71 (270)
Poor normal limb scan latitude coverage (fixed angle)	I	2.36, 3.14, 4.71 (135, 180, 270)
Poor bow shock and plasma tail crossing ranges	I II II	3.93 (225) 3.93 (225) 4.71 (270)
Poor frequency of occultation	II	1.57 (90)
Poor spin axis view frequency on dark side	I	3.93 (225)

3.4.1.2 Gimballing of Scientific Instruments

Some of the scientific instruments may require programmed gimballing in order to permit samples to be taken at various altitudes and latitudes. Gimballing has been stated as a requirement only for the radar altimeter. Because of the present state of uncertainty in the definition of the orbiter scientific instruments, it is recommended that the programs and gimbals, where required, be part of the scientific instruments, but that the program control signals such as stored commands and sun reference pulses be provided by the spacecraft.

Table 3-42 lists possible gimballing requirements and type of gimballing control that might be required.

The programs to control the gimbals need not be complex. Figures 3-119 and 3-120 show the gimbal time history for tracking the spacecraft velocity direction (ram) once per revolution near periapsis. Figure 3-119 shows the EP ram gimbal angles, while in Figure 3-120 the NVOP angles are shown. These curves can be satisfactorily approximated by linear ramps. For the EP a different linear ramp would be required each day.

Figure 3-120 also shows (for NVOP) that a linear approximation can be used by the radar altimeter program to track the nadir near periapsis once per revolution. In this case a peak error of ±0.061 radian (±3.5 degrees) occurs.

3.4.1.3 Spacecraft Differential Charging

The same charging considerations which apply to the probe bus and were discussed in Section 3.3.1.7 also apply to the orbiter. For the detailed discussion of the problem, refer to that section.

Table 3-42. Gimbal Requirements and Control

INSTRUMENT	REASON FOR GIMBAL	TYPE OF GIMBAL CONTROL
ION MASS SPECTROMETER NEUTRAL MASS SPECTROMETER	VIEW ALONG RAM DIRECTION AT MORE THAN ONE ALTITUDE AND LATITUDE	PROGRAM
RADAR ALTIMETER	TRACK NADIR ONCE/REVOLUTION BELOW 1000 KM	PROGRAM
INFRARED RADIOMETER* ULTRAVIOLET SPECTROMETER*	PERMIT NORMAL LIMB SCAN OVER A RANGE OF LATITUDES AT LOW ALTITUDES	COMMAND OR PROGRAM

*ONLY IF NORMAL LIMB SCAN IS REQUIRED

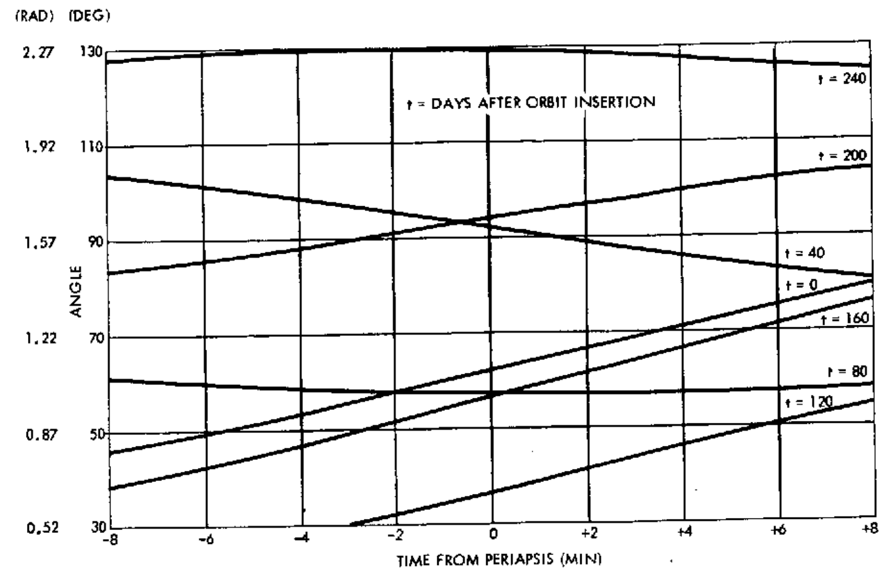

Figure 3-119. Science Interface Ram Gimbal Angles, Earth-Pointing Configuration

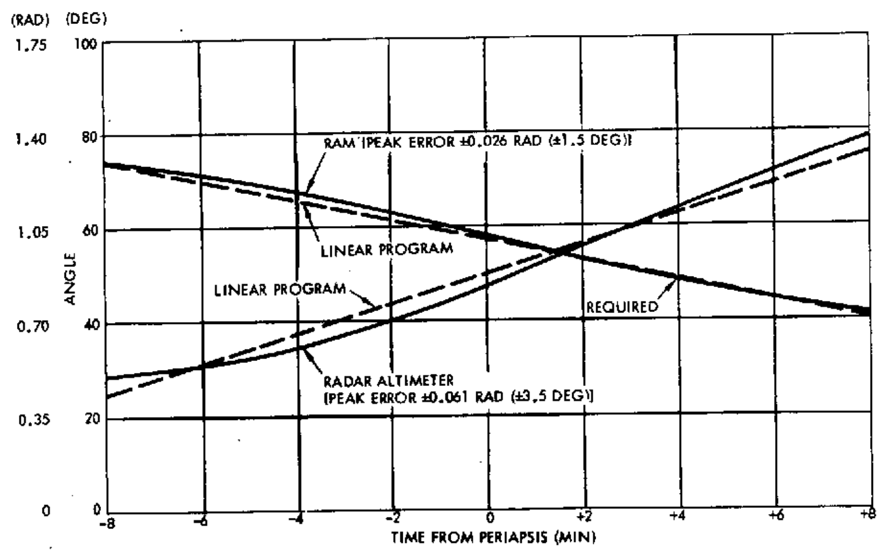

Figure 3-120. Gimbal Angles, Spin Axis Normal-to-Venus Orbit Plane

3.4.1.4 Considerations to Minimize Instrument Contamination

The same considerations which apply to the probe bus and were discussed in Section 3.3.1.8 also apply to the orbiter.

As shown in Figure 3-122 of Section 3.4.2.1, the layout of the instruments on the orbiter satisfies the criterion that no aperture plane can intersect any portion of the spacecraft.

3.4.2 Orbiter Instrument Interfaces

The following sections present the preferred Version IV science payload instrument interface requirements and accommodations, and the requirements and tradeoffs performed for the previous payloads which led to the preferred accommodations. In all cases, requirements and accommodations are presented first for the nominal payload instruments, then for the other candidate instruments.

Section 3.4.2.1 summarizes the preferred Version IV science accommodations. Section 3.4.2.2 through 3.4.2.7 describe the requirements, tradeoffs, and accommodations for the Thor/Delta Version I science payload, the Atlas/Centaur Version II science payload, and the Thor/Delta and Atlas/Centaur Version III science payloads. Definitions of the science payloads are in Section I. The detailed impact of the preferred Atlas/Centaur Version IV science payload is presented at the end of each section.

Instrument parameters in addition to those provided by NASA have been chosen by discussion with possible experimenters, and by consulting the literature.

3.4.2.1 Summary of Preferred Science Accommodations for the Atlas/Centaur Orbiter, Version IV Science Payload

The Version IV science payload mechanical instrument layout and mounting configurations are shown in Figure 3-121 for the nominal payload instruments and Figure 3-122 for the nominal plus other candidate instruments.

The neutral and ion mass spectrometers are mounted together on a deployable boom (ram platform) to view in a direction making an angle of 2.2 radians (126 degrees) with the boom. The boom can be rotated about its axis and set at any desired position so that the instrument view direction with respect to the spacecraft spin axis can be varied from 0.63 to 2.51 radians (36 to 144 degrees) during the mission in order to employ the ram direction with maximum effectiveness at periapsis and and to 1000 kilometers altitude. This covers the operating requirements of both instruments throughout the mission. The electron temperature probe is mounted at 2.62 radians (150 degrees) to the spin axis to lie nearly perpendicular to the ram direction at low altitudes around periapsis.

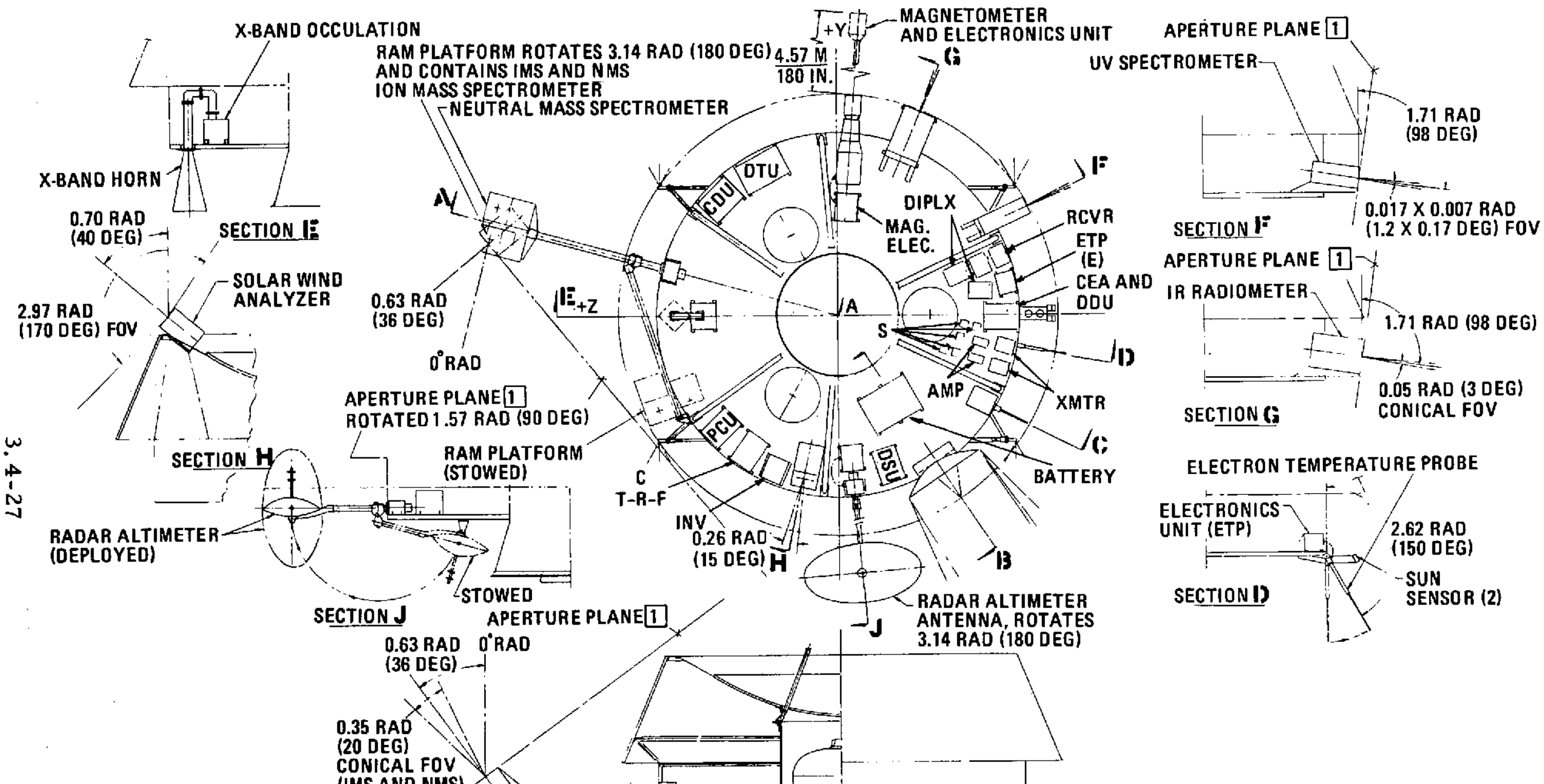

NOTES:

1 APERTURE PLANE DOES NOT INTERSECT ANY PART OF SPACECRAFT THEREFORE EMISSIONS FROM SPEACECRAFT OR THRUSTERS CANNOT ENTER DIRECTLY INTO APERTURE.

Figure 3-121. Atlas/Centaur Orbiter Instruments and Equipment, Version IV Science Payload

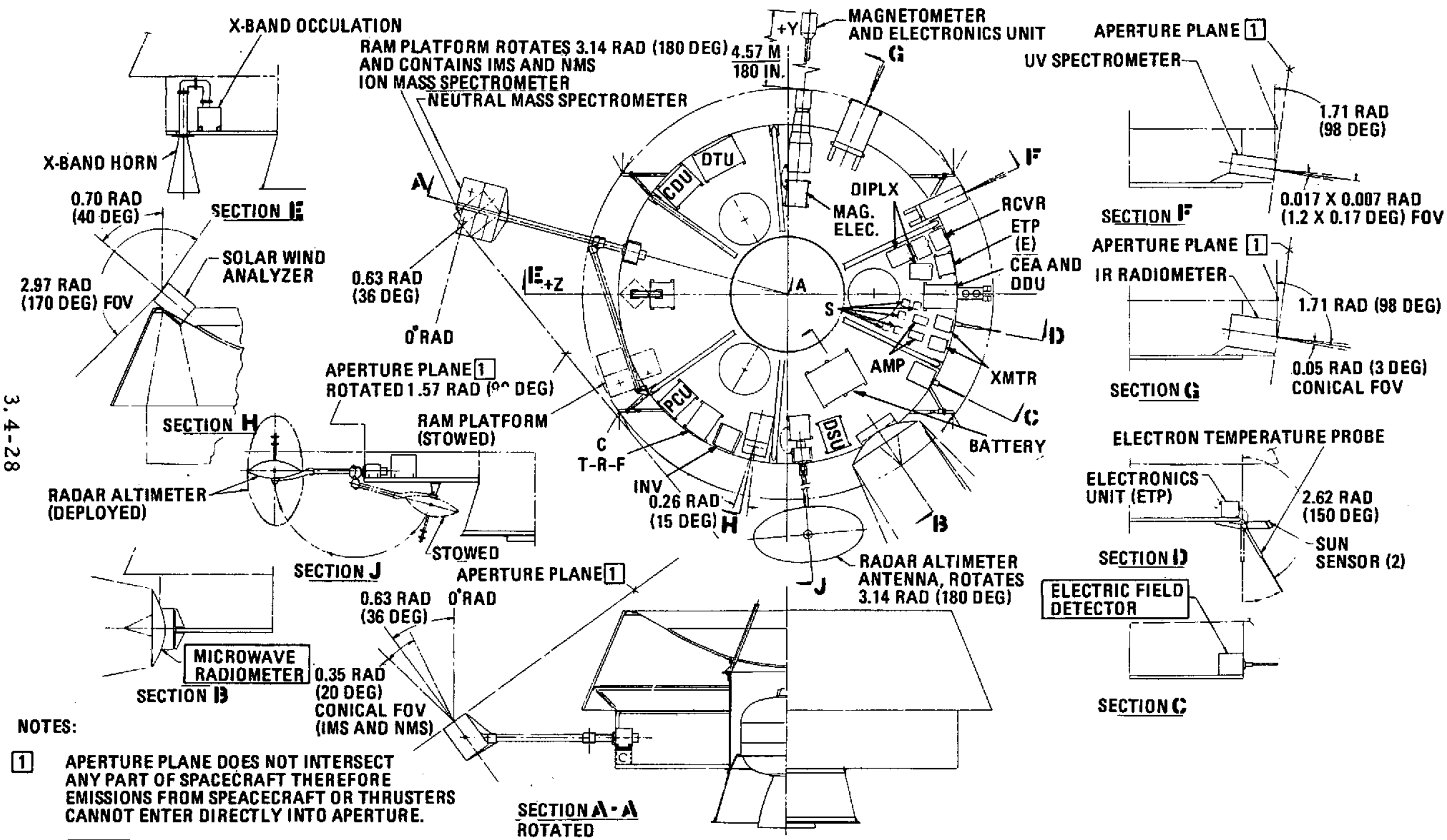

NOTES:

1 APERTURE PLANE DOES NOT INTERSECT ANY PART OF SPACECRAFT THEREFORE EMISSIONS FROM SPEACECRAFT OR THRUSTERS CANNOT ENTER DIRECTLY INTO APERTURE.

2. ▭ DENOTES OTHER CANDIDATE INSTRUMENTS.

Figure 3-122. Atlas/Centaur Orbiter Instruments and Equipment (plus Other Candidate Instruments), Version IV Science Payload

The ultraviolet (UV) spectrometer and infrared (IR) radiometer are mounted to view at 11.71 radians (98 degrees) to the spin axis to provide normal limb scan operation over a large range of latitudes at altitudes below 1000 kilometers. The radar altimeter antenna is mounted on a short boom perpendicular to the spin axis; the antenna views perpendicular to the boom and is gimballed for a full 3.14 radian (180-degree) rotation about the boom to provide nadir view of the planet at all operating times during the mission. S-band occultation is provided by the spacecraft medium-gain communication horn. The X-band occultation instrument has an additional horn antenna directed parallel to the spin axis; beam tracking to various accuracies during occultation measurements is provided by precessing the spacecraft. The solar wind analyzer is oriented to look at 0.70 radian (40 degrees) to the spin axis with a 0.26 by 2.97 radians (15 by 170 degrees) fan field of view, the wide fan angle being parallel to the spin axis; this provides acceptance of solar particles throughout the mission, during both cruise and orbital phases. The magnetometer sensor is mounted on a boom with a length of 4.6 meters (15 feet) to achieve a spacecraft magnetic field in space less than 0.5 nT at the sensor.

The fields of view of the neutral and ion mass spectrometers are taken to be 0.35 radian (20 degrees) full cones, and that of the solar wind analyzer to be 0.26 by 2.97 radians (15 by 170 degrees) as just described; both the UV spectrometer and the IR radiometer have small fields of view, 0.003 by 0.021 radian (0.17 by 1.2 degrees) and 1 by 10 milliradians, respectively. These conditions are all met with wide margin for possible increase, since these instruments (and the spin scan photometer, in the other candidate instrument category) are located to have 2π unobstructed access so that in each case the instrument aperture plane does not intersect any part of the spacecraft, and therefore emissions from the thrusters or from outgassing or desorption from spacecraft materials cannot enter directly into the aperture.

Additional mechanical accommodations (for the other candidate instruments) are as follows. A 50-centimeter diameter parabolic dish receiver for the microwave radiometer is mounted directly on its electronics package and views perpendicular to the spin axis with a 0.07 radian (4.2-degree) beamwidth and 0.36 radian (21-degree) full cone unobstructed view; this provides nadir view of the planet up to 1000 kilometers altitude during most of the mission time in orbit. The AC electric field detector is provided with a small stub antenna normal to the spin axis; for example a quarter-wave antenna for 500 MHz is 0.15 meters (6 inches) long. The spin scan photometer is mounted to have a 0.05 radian (3-degree) full cone field of view normal to the spin axis. This experiment requires measurements near both periapsis and apoapsis, the latter being of greater importance. Viewing normal to the spin axis is midway between the typical Venus aspect angles of 1.22 and 1.92 radians (70 and 110 degrees) at apoapsis and periapsis, respectively. It is probable that the photometer will include a movable mirror or telescope to accommodate both observation periods, otherwise the photometer may be gimballed.

Data Handling and Signals to Instruments

The preferred data handling system is the same as that for the probe bus discussed in Section 3.3.2.1 with the exception that a data storage capability is provided. The data storage system can provide 1,228,000 bits of storage at input rates up to 10,000 bits/s. There are five units of 245,760 bits each. Each unit can be shared at half the bit capability by two scientific instruments simultaneously. During normal operation the IR radiometer, radar altimeter, and both mass spectrometers are connected to the DTU through storage units. Sufficient storage is provided for these instruments to satisfy the requirements (see Section 3.4.2.3). This uses up the capability of 2-1/2 units. An additional half of a unit is connected to the DTU and is used to store preformatted data from the remaining scientific instruments when periapsis is occulted. The additional storage unit provides redundancy, and can by ground command replace any of the other four units.

The signals provided by the orbiter to the scientific instruments are identical to the signals provided on the probe bus (Section 3.3.2.1) with the addition of an end-of-memory signal. This signal is sent to a scientific instrument that is shifting data to the storage unit when the storage unit is full.

The orbiter will be capable of providing up to 50 discrete commands and six stored commands to the scientific instruments.

3.4.2.2 Mechanical, Thermal, and Power Requirements and Accommodations

Details of Version I, II, III Science Payload

Requirements for the orbiter baseline instruments are shown in Table 3-43 for the Thor/Delta configuration and in Table 3-44 for the Atlas/Centaur configuration.

For science instruments (exclusive of the radar altimeter), 32 and 34.5 watts maximum power at 28 volts ±2 percent are provided in the Thor/Delta and the Atlas/Centaur configurations, respectively. In addition, a nominal 25 watts average during transmitter operation is shown in each case for the radar altimeter; analysis of its power requirements is given in detail in Section 3.4.2.5 "Radar Altimeter Pulse Load." The total power requirements are provided by the Thor/Delta and Atlas/Centaur power systems.

Instrument mounting configurations are shown in Figure 3-123 for the Thor/Delta and Figure 3-124 for the Atlas/Centaur. As with the probe bus, both configurations provide platform-mounted instruments with a thermal environment limited to the temperature range from 4 to 27°C and the magnetometer boom, sensor, and associated thermal control are the same and are satisfactorily accommodated. The magnetometer sensor is on a 3-meter (10-foot) boom, if the spacecraft magnetic field at the sensor is required to be less than 5n T degaussed; if the magnetic field requirement in 0.5n T, the boom length is 4.6 meters (15 feet). Batteries and power system units are located on the opposite side of the instrument platform from the magnetometer boom, in order to minimize the stray field at the magnetometer sensor. A special problem has been identified, however, with respect to the 12°C upper operating temperature limit of the IR radiometer; this requirement is not met with the present spacecraft thermal control design. Since this requirement was obtained from the Mariner IR interferometer spectrometer (IRIS) requirements and since the Pioneer Venus IR instrument may be significantly different, further thermal analysis was delayed until more instrument definition is provided.

Table 3-43. Orbiter Versions I/III Science Instruments (Nominal Payload) Weight, Volume, Temperature, and Power Requirements – Thor/Delta Configuration

INSTRUMENT	WEIGHT [KG (LB)]		VOLUME M^3	VOLUME (IN^3)	TEMPERATURE (°C)	POWER (WATTS)
NEUTRAL MASS SPECTROMETER	4.5	(10)	8.195×10^{-3}	(500)	-30 TO +60	12.0
ION MASS SPECTROMETER	1.4	(3)	3.278×10^{-3}	(200)	-30 TO +60	1.0
ELECTRON TEMPERATURE PROBE						
A) SENSOR	0.14	(0.3)	8.65×10^{-7}	(0.055 = 18 X 1/16 DIAM.)		2.0
B) ELECTRONICS	1.0	(2.2)	1.770×10^{-3}	(108 = 6 X 6 X 3)	-30 TO +60	
ULTRAVIOLET SPECTROMETER	5.4	(12.0)	9.834×10^{-3}	(600)	0 TO +40, OPERATING -20 TO +75, NONOPERATING	8.0
MAGNETOMETER						
A) SENSOR	0.5	(1.0)	0.655×10^{-3}	(40)	-20 TO +20, OPERATING -40 TO +60, NONOPERATING	3.0
B) ELECTRONICS	1.81	(4.0)	3.28×10^{-3}	(200)	0 TO +60, OPERATING -20 TO +80, NONOPERATING	
INFRARED RADIOMETER	4.1	(9.0)	6.556×10^{-3}	(400)	-30 TO +12, OPERATING -45 TO +60, NONOPERATING	6.0
RADAR ALTIMETER	9.5	(21)				
A) ELECTRONICS			1.970×10^{-3}	(120)	-30 TO +60	25, AVERAGE DURING TRANSMITTER OPERATION
B) ANTENNA				APPROXIMATELY 1 X 2 FT PARABOLOID		
TOTAL	28.3	(62.5)	35.538×10^{-3}	(2168) EXCLUDING RADAR ANTENNA		57

Table 3-44. Orbiter Versions II/III Science Instruments (Nominal Payload) Weight, Volume, Temperature, and Power Requirements – Atlas/Centaur Configuration

INSTRUMENT	WEIGHT [KG (LB)]		VOLUME M^3	VOLUME (IN^3)	TEMPERATURE (°C)	POWER (WATTS)
NEUTRAL MASS SPECTROMETER	5.4	(12.0)	8.195×10^{-3}	(500)	-30 TO +60	12.0
ION MASS SPECTROMETER	1.45	(3.2)	3.278×10^{-3}	(200)	-30 TO +60	2.0
ELECTRON TEMPERATURE PROBE	1.0	(2.2)	1.639×10^{-3}	(100)	-30 TO +60	2.5
ULTRAVIOLET SPECTROMETER	5.4	(12.0)	9.834×10^{-3}	(600)	0 TO +40, OPERATING -20 TO +75, NONOPERATING	8.0
MAGNETOMETER						
A) SENSOR	0.5	(1.1)	0.655×10^{-3}	(40)	-20 TO +20, OPERATING -40 TO +60, NONOPERATING	4.0
B) ELECTRONICS	2.0	(4.4)	3.28×10^{-3}	(200)	0 TO +60, OPERATING -20 TO +80, NONOPERATING	
INFRARED RADIOMETER	4.5	(10.0)	6.556×10^{-3}	(400)	-30 TO +12, OPERATING -45 TO +60, NONOPERATING	6.0
RADAR ALTIMETER	12.7	(28)				
A) ELECTRONICS			1.970×10^{-3}	(120)	-30 TO +60	25, AVERAGE DURING TRANSMITTER OPERATION
B) ANTENNA				APPROXIMATELY 1 X 2 FT PARABOLOID		
TOTAL	33.0	(72.9)	35.407×10^{-3}	(2160) EXCLUDING RADAR ANTENNA		59.5

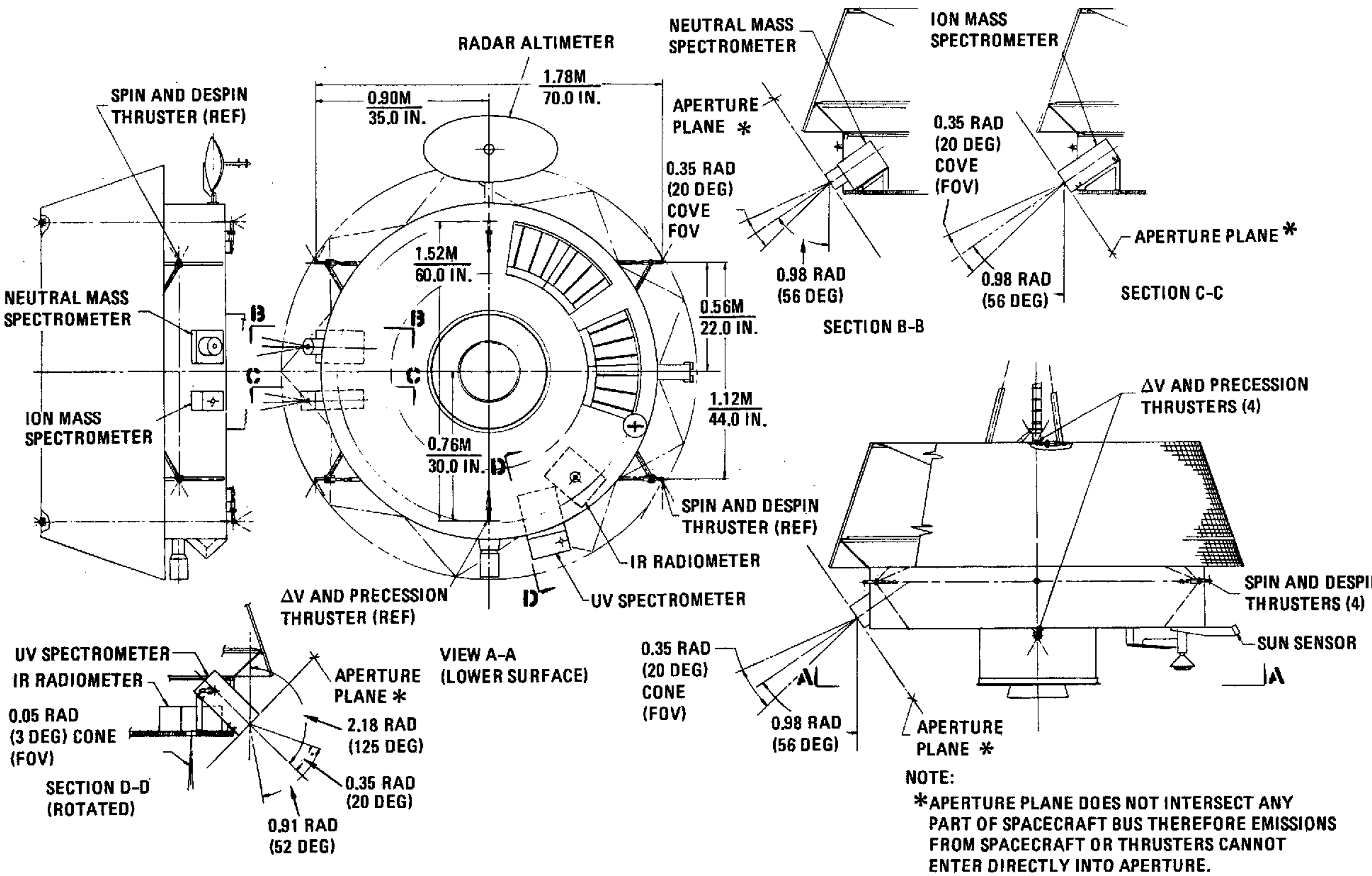

Figure 3-123. Thor/Delta Orbiter, Version I Science Payload and Equipment Layout

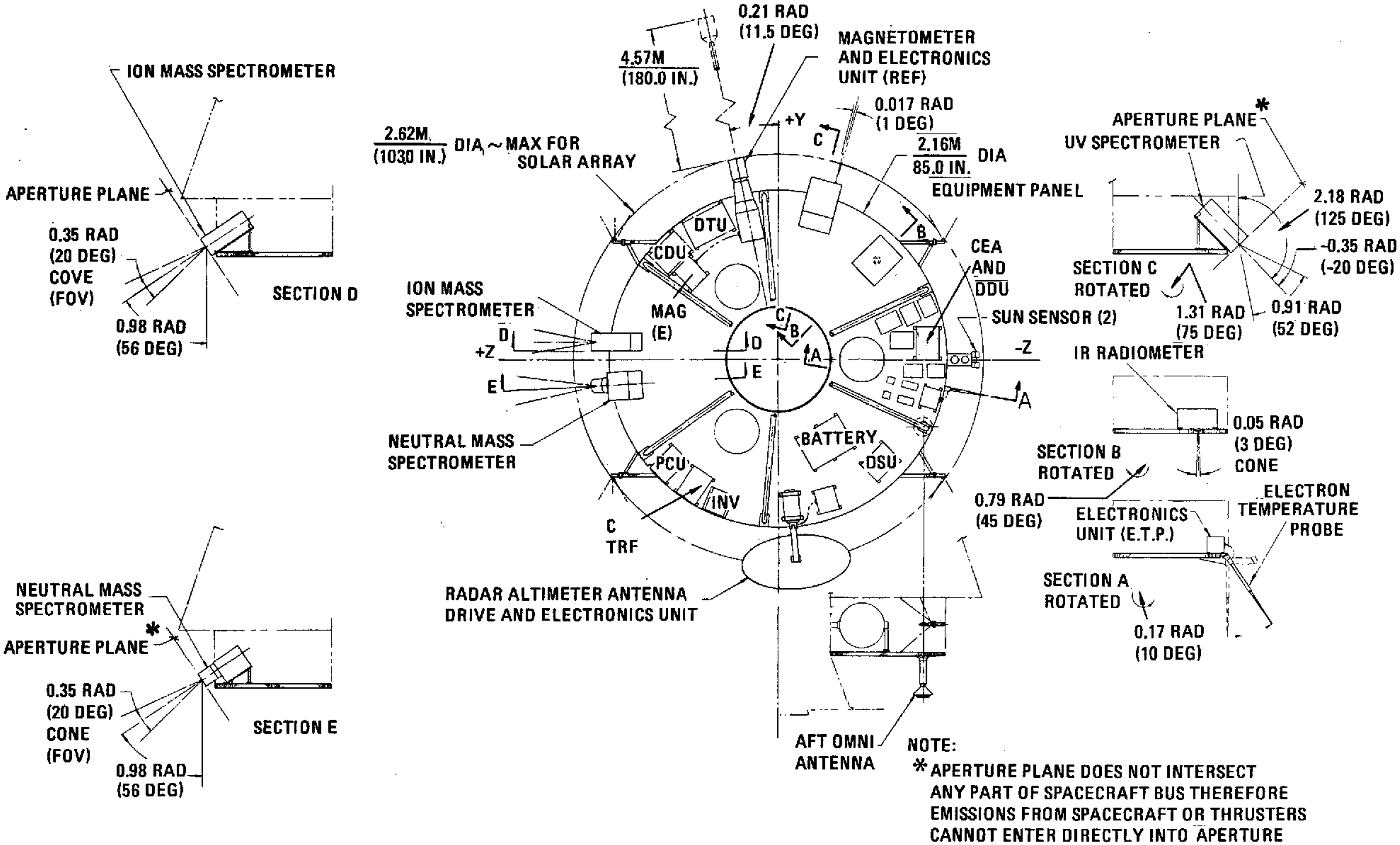

Figure 3-124. Atlas/Centaur Orbiter, Version II Science Payload and Equipment Layout

Instrument mounting provisions of the configurations shown in Figure 3-123 and 3-124 are given below for a spacecraft with spin axis normal to the Venus orbit plane in a Type II trajectory with θ_{aim} = 2.09 radians (120 degrees).

- Ram Instruments: Neutral Mass Spectrometer, Ion Mass Spectrometer, and Electron Temperature Probe. The view direction of both spectrometers is at 0.98 radian (56 degrees) to the spin axis in order to look in the ram direction once per revolution at periapsis. If gimballed to look from 0.70 to 1.27 radians (40 to 73 degrees) to the spin axis, the ram condition may be satisfied between periapsis and 1000 kilometers altitude both when entering and when leaving the Venus atmosphere. Both instruments are located so that the apertures are clear of direct spacecraft emissions. The electron temperature probe is mounted at 0.59 radians or 2.55 radians (34 degrees or 146 degrees) to the spin axis in order to be normal to the ram direction once per revolution at periapsis; the probe is stowed parallel to the spin axis and deployed in orbit.

- Nadir View Instruments: UV Spectrometer and Radar Altimeter. Both of these instruments are mounted to have a nominal view direction at 0.80 radian (46 degrees) to the spin axis to provide nadir view of the planet once per revolution at periapsis. Gimballing from 0.47 to 1.36 radians (27 to 78 degrees) with respect to the spin axis would permit nadir view between periapsis and 1000 kilometers altitude. The UV spectrometer has a 0.01 radian (1 degree) full cone true field of view, with a 0.91 radian (52 degrees) unobstructed outlook to allow for the possible gimballing. The radar altimeter has a dedicated antenna providing a beamwidth 0.52 radian (30 degrees) in azimuth by 0.24 radian (14 degrees) in altitude and gimballed to provide the necessary nadir view along the line of minimum distance to the planet surface during the observation period. An alternate type instrument described in the NASA supplementary letter of 2 November 1972 employs an electronically phased planar array antenna with peak power of 10 watts and gain at 0.76 radian (45 degrees) scan of 18 dBi.

- Spin Axis Viewing Instrument: IR Radiometer. An IRIS type instrument similar to that flown on Mariner 9 has been assumed for the orbiter spacecraft. It requires approximately 18 seconds to take a complete spectrum and hence it is mounted to view along the spin axis. Not only does this avoid the complexities of a despun platform or mirror, but for the favored 2.09 radians (120 degrees) NVOP orbit, the periapsis region in which measurements will be made affords a good cut of the southern hemisphere, and a variety of transits across the light and dark surfaces due to the orbital motion of the spacecraft and the varying position of the terminator as the mission progresses.

- Possible Normal Limb Scan Operating Mode. If the UV spectrometer and the IR radiometer desire normal limb scan operation near periapsis, they can be mounted on the instrument platform with a view direction excluding 1.57 radians (90 degrees) to the spin axis to avoid looking at the sun. The fields of view of the entrance slits would be 0.011 by 0.05 radian (0.5 by 3 degrees) and 0.0012 by 0.012 radian (0.06 by 0.6 degrees), for the UV spectrometer and the IR radiometer, respectively. In each case, the long dimension of the slit is normal to the view direction and may be gimballed to vary from θ = 0 to 1.57 radians (0 to 90 degrees) where θ is the angle between the slit length and the plane containing the spin axis and the view direction. For the vew direction chosen, the latitude coverage and corresponding slit angle for attitudes below 1000 kilometers are shown in Section 3.4.1.1, "Normal Limb Scan" subsection.

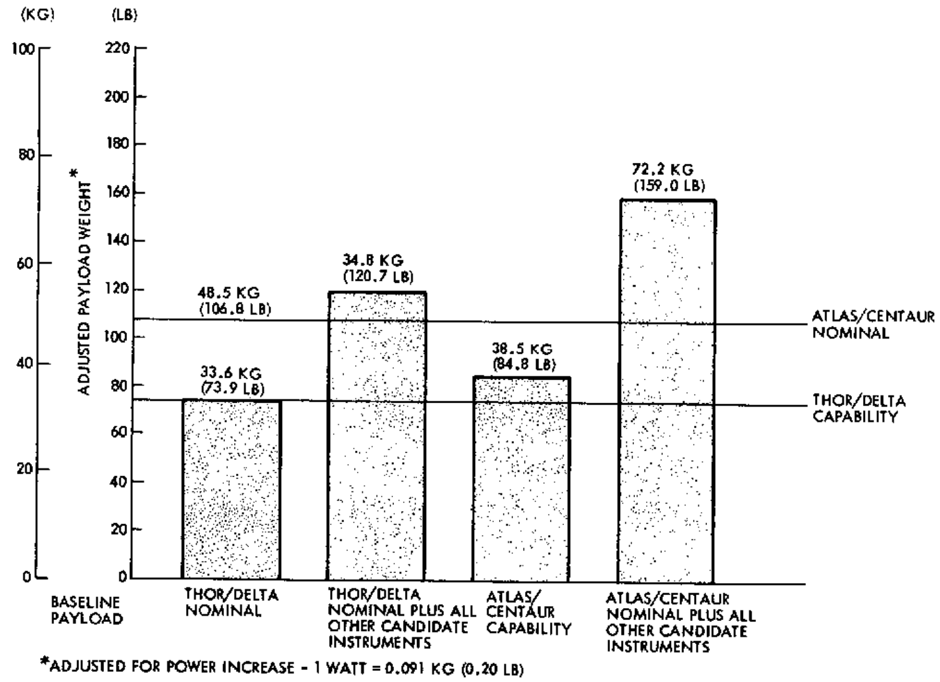

Figure 3-125. Baseline Orbiter Capability for Additional Instruments

Figure 3-125 shows the capability of the baseline orbiter spacecraft to accommodate the weight and power requirements of the other candidate instruments. As in the analysis of the growth capability for experiments for the probe bus, the figure includes the power requirements of the additional instruments expressed as the associated weight requirements. Since it is possible to generate a watt of power at Venus at a weight cost of 0.091 kilograms (0.20 pounds), the weight equivalent of the power requirement added to the weight requirement is labeled "adjusted" payload weight, and the figure shows the total Thor/Delta and Atlas/Centaur orbiter spacecraft capabilities expressed as total adjusted payload weight. The Thor/Delta baseline payload has no additional capability for other candidate instruments, while the Atlas/Centaur configuration has additional capability for 10 kilograms (22 pounds) adjusted weight.

Table 3-45. Version III Science, Other Candidate Instruments

	POWER (WATTS)	WEIGHT [KG (LB)]	ADJUSTED WEIGHT [KG (LB)]
SOLAR WIND PROBE	5.0	5.0 (11.0)	5.4 (12.0)
THERMAL/SUPRATHERMAL PARTICLE DETECTOR	3.5	2.7 (6.0)	3.0 (6.7)
ELECTRIC FIELD DETECTOR	3.0	2.3 (5.0)	2.5 (5.6)
SOLAR ELECTRON DETECTOR	1.5	1.4 (3.0)	1.5 (3.3)
MICROWAVE RADIOMETER	15.0	11.3 (25.0)	12.7 (28.0)
X-BAND OCCULTATION	10.0	3.0 (6.6)	3.9 (8.6)

The requirements of the six other candidate instruments in the Atlas/Centaur configuration are shown in Table 3-45.

Comparison of Table 3-45 and Figure 3-124 shows that it is not possible to accommodate the microwave radiometer, and that sets of the remaining instruments can be formed by iterating choices from the five other instruments such that the total adjusted weight of each possible set is within the 10 kilograms (22 pounds) limit for extra capability.

Table 3-46. Orbiter Version III Science Instruments (Other Candidate Instruments Excluding Microwave Radiometer) Weight, Volume, Temperature, and Power Requirements - Atlas/Centaur Configuration

INSTRUMENT	WEIGHT [KG	(LB)]	VOLUME M^3	(IN^3)	TEMPERATURE (°C)	POWER (WATTS)
SOLAR WIND PROBE	5.0	(11.0)	5.507×10^{-3}	(336)	-15 TO +50, OPERATING -40 TO +60, STORAGE	5.0
THERMAL/SUPRATHERMAL PARTICLE DETECTOR	2.7	(6.0)	3.937×10^{-3}	(240)	-30 TO +50	3.5
ELECTRIC FIELD DETECTOR	2.3	(5.0)	2.950×10^{-3}	(180)	-30 TO +60	3.0
SOLAR ELECTRON DETECTOR	1.4	(3.0)	1.967×10^{-3}	(120)	DETECTOR = IN CRYOSTAT AT 77°K ELECTRONICS = -30 TO +50	1.5
X-BAND RF OCCULTATION	3.0	(6.6)	4.255×10^{-3}	(260)	-30 TO +60	10.0
TOTAL	14.4	(31.6)	18.616×10^{-3}	(1136)		23.0

A summary of the weight, volume, temperature, and power requirements of the five other candidate instruments that can be accommodated in various sets in the Atlas/Centaur configuration is given in Table 3-46 and an equipment layout diagram including these instruments in addition to the baseline payload is shown in Figure 3-126. It is possible to include

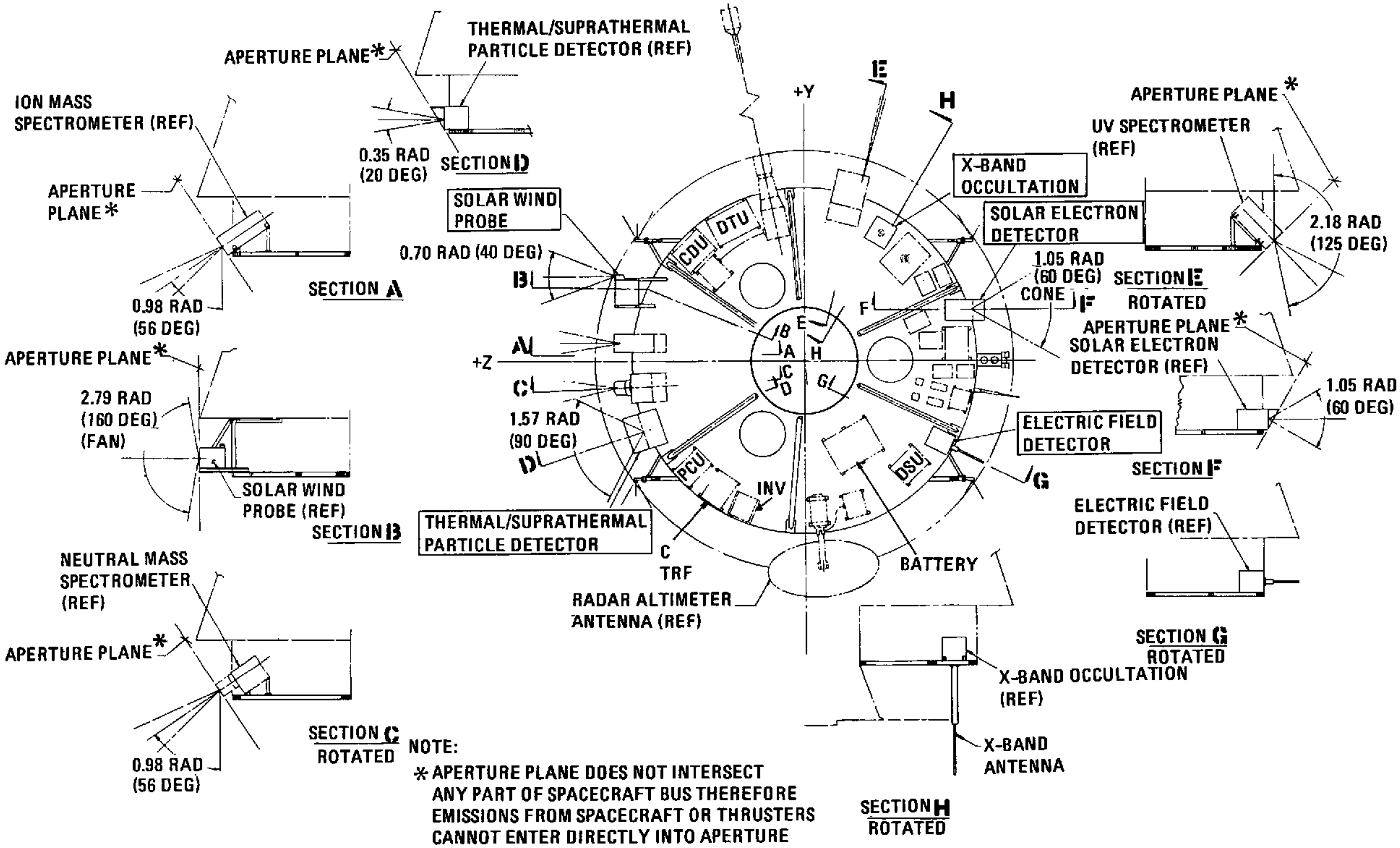

Figure 3-126. Atlas/Centaur Orbiter Equipment Layout (plus Other Candidate Instruments)

all of the five other candidate instruments of Table 3-46 in the available space on the equipment platform with proper locations and view directions, as shown, but it must be remembered that only these sets whose adjusted weight is less than 10 kilograms (22 pounds) can be accommodated within the available weight/power capability. Mounting orientations shown are for the NVOP configuration. Hence, the solar wind probe, the thermal/suprathermal particle detector, and the solar electron detector are mounted to view normal to the spin axis, with clear fields of view as shown in the diagram. The electric field detector has a small stub antenna 0.15 meters (6 inches) long, corresponding to the requirement of a $\lambda/4$ whip antenna at a typical frequency of 500 MHz, while the X-band occultation experiment requires a transmitter package and a pole antenna colinear with the spacecraft axis; it is mounted on the bottom of the spacecraft, and its length is 0.30 to 0.38 meters (12 to 15 inches) beyond a pedestal section long enough so that the radiation beam clears the insertion engine and the bottom of the spacecraft structure.

Thermal requirements for these instruments are taken to be less stringent than the range of 4 to 27°C provided for platform instruments; no special thermal problem is anticipated for these instruments.

Effect of Version IV Science Payload on Instrument Mechanical and Power Requirements and Accommodations

The Version IV science payload transferred the solar wind analyzer and the X-band occultation experiment from the other candidate instruments category to the nominal (baseline) instrument list. A spin scan photometer replaced the thermal/suprathermal particle detector and the solar electron detector on the other candidate instrument list. The remainder of the payload instrument lists were not changed by name. Revised instrument parameters were specified, as well as tolerances of +15 percent, -10 percent in weight; ±15 percent in volume; and +20 percent, -10 percent in power.

Table 3-47 compares the Version IV science payload with the earlier payloads. For the nominal payload; weight increases by 12 kilograms, volume by 10 681 cm^3, and power by 53.4 watts. The total payload, nominal plus other candidate instruments, increases power by 12.7 kilograms, volume by 6 357 cm^3, and power by 55 watts.

Table 3-47. Orbiter Experiments, Version IV, Atlas/Centaur Only

INSTRUMENT	WEIGHT (W) [KG (LB)]				VOLUME (V) ($IN.^3$)				POWER (P) P			
	W_{IV} (NOMINAL)	W_{IV}' (W_{IV} + 15%)	ΔW ($W_{IV}' - W_{II/III}$)		V_{IV} (NOMINAL)	V_{IV}' (V_{IV}+15%)	ΔV ($V_{IV}' - V_{II/III}$)		P_{IV} (NOMINAL)	P_{IV}' (P_{IV}+20%)	ΔP ($P_{IV}' - P_{II/III}$)	
<u>NOMINAL PAYLOAD INSTRUMENTS</u>												
NEUTRAL MASS SPECTROMETER	5.4 (12.0)	6.21 (13.8)	+0.81 (+1.8)		8,195 500	9,423 (575)	+1,228 (+75)		12.0	14.4	+2.4	
ION MASS SPECTROMETER	1.5 (3.2)	1.73 (3.68)	+0.28 (+0.48)		3,278 (200)	3,769 (230)	+491 (+30)		2.0	2.4	+0.4	
ELECTRON TEMPERATURE PROBE	1.4 (3.0)	1.61 (3.45)	+0.61 (+1.25)		1,967 (120)	2,262 (138)	+623 (+38)		2.5	3.0	+0.5	
ULTRAVIOLET SPECTROMETER	5.5 (12.0)	6.33 (13.8)	+0.93 (+1.8)		6,556 (400)	7,540 (460)	-2,294 (-140)		6.0	7.2	+4.7	
MAGNETOMETER	3.5 (7.7)	4.03 (8.86)	+1.53 (+3.36)		3,937 (240)	4,528 (276)	+591 (+36)		4.0	4.8	+0.8	
INFRARED RADIOMETER	5.5 (12.0)	6.33 (13.8)	+1.83 (+3.8)		6,556 (400)	7,540 (460)	+984 (+60)		6.0	7.2	+1.2	
RADAR ALTIMETER	9.0 (20.0)	10.35 (23.0)	-2.35 (-5.0)		9,824 (600)	11,309 (690)	-1,803 (110)		40.0	48.0	+23.0	
SOLAR WIND ANALYZER	5.0 (11.0)	5.75 (12.65)	+5.75 (+12.65)	+0.75* (+1.65)	5,507 (336)	6,333 (384)	+6,333 (+384)	+826* (+48)	5.0	6.0	+6.0	+1.0*
X-BAND OCCULTATION	2.7 (6.0)	3.11 (6.90)	+3.11 (+6.90)	+0.11* (0.30)	3,937 (240)	4,528 (276)	+4,528 (+276)	+273* (+16)	12.0	14.4	14.4	+4.4*
TOTAL NOMINAL PAYLOAD IV VERSUS II/III	39.5 (86.9)	45.45 (99.94)	+12.00 (+28.0)		49,767 (3,036)	57,232 (3,489)	+10,681 (+649)		89.5	107.7	+53.4	
<u>OTHER CANDIDATE INSTRUMENTS*</u>												
MICROWAVE RADIOMETER	11.4 (25.0)	13.11 (28.25)		+1.71 (+3.75)	9,834 (600)	11,309 (690)		+1,475 (+90)	15.0	18.0		+3.0
AC ELECTRIC FIELD DETECTOR	2.3 (5.0)	2.65 (5.75)		+0.35 (+0.75)	2,950 (180)	3,393 (207)		+443 (+27)	3.0	3.6		+0.6
SPIN SCAN PHOTOMETER (VERSUS THERMAL/SUPRATHERMAL PARTICLE DETECTOR PLUS SOLAR ELECTRON DETECTOR)	9.0 (20.0)	10.35 (23.0)		+6.25 (+14.0)	8,195 (500)	9,424 (575)		+3,520 (+215)	15.0	18.0		+13.0
TOTAL NOMINAL PLUS OTHER INSTRUMENTS, VERSION IV VERSUS II/III	62.2 (136.9)	71.56 (157.4)		+12.31 (+27.9)	70,746 (4,316)	81,358 (4,961)		+6,357 (+385)	122.5	147.3		+55.0

*NOTE: SOLAR WIND PROBE AND X-BAND OCCULTATION WERE OTHER CANDIDATE INSTRUMENTS IN VERSION II/III OF ATLAS/CENTAUR PAYLOAD

As explained in Section 3.4.2.2, the weight increase required to generate the power increase for each instrument is added to the instrument weight to arrive at an adjusted weight increase. Adjusted weight increases by 17.5 kilograms for the nominal payload, and 29.8 kilograms for the nominal plus other candidate instruments payload.

The Atlas/Centaur orbiter can easily accommodate this adjusted weight increase, because of its additional weight capability.

	Kilograms
Version II/III Weight Margin	10
Additional Weight Margin from Atlas/ Centaur Performance Increase	38
Total Weight Margin	48

Instrument mounting configurations were shown in Figure 3-121 for the Version IV nominal payload instruments and in Figure 3-122 for the addition of the three other candidate instruments. An earth-pointing spacecraft configuration has been selected for the orbiter mission for reasons discussed in detail in Section 5 of this report; the chief impact of this decision on the scientific instrument payload is that instrument view directions are changed in comparison with those shown in Figures 3-124 and 3-126 for the Versions II/III instrument payload and a spacecraft with spin axis normal to the Venus orbit plane. Instrument mounting considerations for the layouts shown in Figures 3-121 and 3-122 are given below for an earth-pointing spacecraft in a Type II trajectory with $\theta_{aim} = 2.09$ radians (120 degrees).

- Ram Instruments: Neutral Mass Spectrometer, Ion Mass Spectrometer and Electron Temperature Probe. The two spectrometers, each with a 0.35 radian (20 degrees) full cone field of view, are mounted together on a deployable boom 0.79 meters (31 inches) long (to the center of gravity of the combined mass) which is normal to the spin axis when deployed. The spectrometers are mounted to view outward at an angle of 2.20 radians (126 degrees) to the boom. The boom can be rotated about its axis and set at any desired angular position by command so that the view direction of the spectrometers with respect to the spacecraft spin axis can be varied from 0.63 to 2.51 radians (36 to 144 degrees, depending on the rotational setting of the boom), in order to view in the ram direction once per revolution at periapsis throughout the mission. In addition, from 70 to 100 days the ram direction will stay within ±0.17 radians (±10 degrees) from 1000 kilometers to periapsis and back to 1000 kilometers. Further, throughout the entire mission it will be possible to make continuous measurements either from periapsis to 1000 kilometers or from 1000 kilometers to periapsis with a single setting for the pass. As before, the aperture plane of both instruments does not intersect any part of the spacecraft so that no emissions from the spacecraft or thrusters can enter directly into the apertures. The electron temperature probe is mounted at 2.62 radians (150 degrees) to the (positive) spin axis so that it is out of the spacecraft wake and nearly perpendicular to the ram direction once per revolution at low altitudes around periapsis most of the time, especially early in the mission. As before, it is stowed parallel to the spin axis and deployed in orbit.

- Planetary Viewing Instruments: UV Spectrometer, IR Radiometer, and Radar Altimeter. These instruments are mounted to view essentially normal to the spin axis to provide nadir view of the planet once per revolution around periapsis, but there are small differences in the optimum view directions to accommodate most effectively the different experiment requirements. The UV spectrometer and IR radiometer are mounted to view at 1.71 radians (98 degrees) to the spin axis to provide normal limb scan operation at altitudes below 1000 kilometers for approximately 200 orbits out of the 225 in the specified mission life, if the instrument slit is at 0.44 radian (25 degrees) to the plane defined by the view direction and the spacecraft spin axis. An advantage of this mounting configuration with the earth-pointing spacecraft is that these normal limb scans will occur over a large range of latitudes on Venus. The field of view of the UV spectrometer is taken to be approximately 0.003 by 0.021 radians (0.17 by 1.2 degrees), and that of the IR radiometer slit to be 1 by 10 millirad (0.06 by 0.6 degrees), with the slit angle oriented as just stated. Both instruments are mounted so that the apertures are clear of direct spacecraft emissions. The Version IV payload requires no change in the mounting of the radar altimeter dedicated dish antenna on, and perpendicular to, a short boom normal to the spin axis and gimballed for a full 3.14 radian (180 degree) rotation about the axis of the boom. This more than encompasses the range of 0.99 to 2.95 radians (57 to 169 degrees) between the antenna axis and the spacecraft spin axis to provide nadir view along the line of minimum distance to the planet surface during the observation period. The electronically phased planar array antenna alternative is probably no longer viable, however, because of this range of angle associated with the earth pointer.

- Spin Axis Viewing Instrument: X-Band Occultation. This instrument consists of the transmitter and the X-band horn antenna directed parallel to the spin axis out the bottom of the spacecraft. Procedures for orienting the spacecraft during occultation measurements are discussed in Sections 8.5.6 and 3.4.1.1.

- Solar Viewing Instrument: Solar Wind Analyzer. This instrument has a field of view 0.26 by 2.97 radians (15 by 170 degrees) with its axis at 0.70 radians (40 degrees) to, and the wide fan angle parallel to, the spacecraft spin axis. This orientation provides acceptance of particles from, and near to, the solar direction once per revolution throughout both interplanetary cruise and Venus orbit portions of the mission. The mounting location at the upper edge of the solar array provides that the aperture plane does not intersect any part of the spacecraft so that emissions from the spacecraft or thrusters cannot directly enter the aperture.

- Magnetometer. The accommodation of the magnetometer is unchanged from that of the Version II/III Atlas/Centaur payload except for considerations of the length of the boom. At the briefing accompanying the redirection, TRW was notified that the requirement for the orbiter magnetic field in space was to be 0.5n T at the magnetometer sensor. For this reason a magnetometer boom length of 4.6 meters (15 feet) was chosen for the baseline Atlas/Centaur orbiter spacecraft. A detailed study of the methods of determining required boom length under various spacecraft conditions is given in Section 3.2.2.2. It should be noted again here that care has been taken in the layout of the orbiter subassemblies, as shown in Figure 3-122, to locate those units which are relatively highly magnetic as far as possible from the magnetometer sensor and that in the case of a larger spacecraft such as the Atlas/Centaur configuration of the Pioneer Venus orbiter, this technique is more effective than in smaller spacecraft.

In addition to the nine instruments discussed above which comprise the nominal payload shown in Figure 3-121, there are the three other candidate instruments, all of which can be accommodated within the weight and power capability of the Atlas/Centaur orbiter, as discussed previously, and with the layout configuration shown in Figure 3-122. Instrument mounting considerations for these three instruments are as follows:

- Microwave Radiometer. This instrument may consist of a 50 centimeter (19.5 inch) diameter parabolic dish receiver about 8 centimeters (3.1 inches) deep with a 1.9 centimeter (3/4 inch) diameter feed located 15 centimeters (5.9 inches) above the center of the dish. Such a configuration is characterized by a 10.7 centimeter (4.2 inch) beam width [0.037 radian (2.1 degree) divergence] and should have a 0.37 radian (21 degree) full cone unobstructed view. The dish is most satisfactorily mounted directly on the associated electronics box, with the view direction normal to the spacecraft spin axis. This provides nadir view of the planet once per revolution near periapsis and up to 1000 kilometers altitude during most of the mission time in orbit.

- AC Electric Field Detector. This instrument is the same as that included in the other candidate instruments for the Version II/III Atlas/Centaur orbiter payload, except that the 15 centimeter (6-inch) stub antenna ($\lambda/4$ for 500 MHz) is now normal to the spin axis.

- Spin Scan Photometer. This instrument has a 0.05 radian (3 degree) full cone field of view and is mounted to view normal to the spin axis in order to look at Venus both near apoapsis and near periapsis. The best average Venus aspect angle near periapsis is approximately 1.92 radians (110 degrees) while near apoapsis, it is approximately 1.22 radians (70 degrees). Distant measurements in which the whole planet is within the field of view are of the greatest importance. Hence, the view direction is chosen at 1.57 radians (90 degrees), and the folded optical system of the photometer may include a movable mirror or telescope of minimum angular range to view the planet at the desired observation times.

There are no new thermal requirements for the instruments of the new science payload (Version IV redirection). All mechanical, thermal, and power requirements for the 12 nominal and other candidate instruments have been accommodated.

3.4.2.3 Data Handling Requirements and Accommodations

Details of Version I/II/III Science Payload

Figure 3-127 shows the regions of space where data is obtained by the scientific instruments on the orbiter for the orbit with θ_{aim} = 2.09 radians (120 degrees) and a Type II trajectory. It is clear that most of the scientific data is obtained near periapsis. It has been assumed that the IR radiometer is of the IRIS type and views along the orbiter spin axis. The data shown in this figure is for the NVOP case.

Figure 3-128 shows the earth occultation history for the same orbit. For the first 70 days of the mission periapsis is in occultation. It therefore will be necessary to provide adequate storage on the orbiter to permit the science measurements to be made during this period.

Table 3-48 shows the orbiter science data handling and storage requirements. Many of the science instruments require high data rates for relatively short periods of time. In the same table, "special mode" shows typical data storage requirements that would be needed to permit these high data rates to be accommodated.

The data handling system for the orbiter will be identical to that for the probe bus, as described in Section 3.3.2.2, with the exception that a data storage capability is provided. The data storage system can store 737,280 bits at input bit rates as high as 10,000 bits/s. This number of

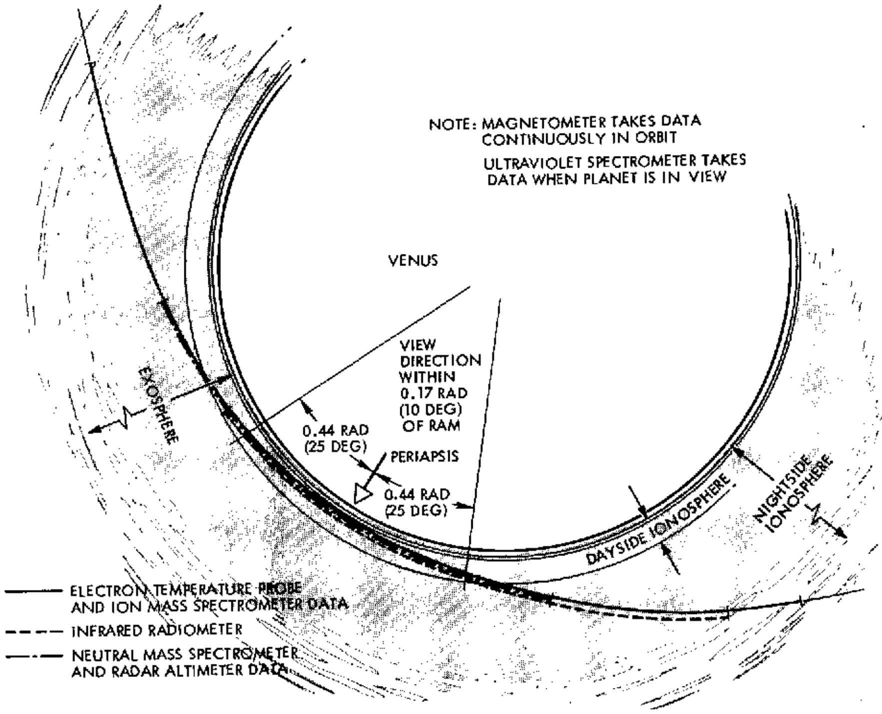

Figure 3-127. Orbiter Data Acquisition

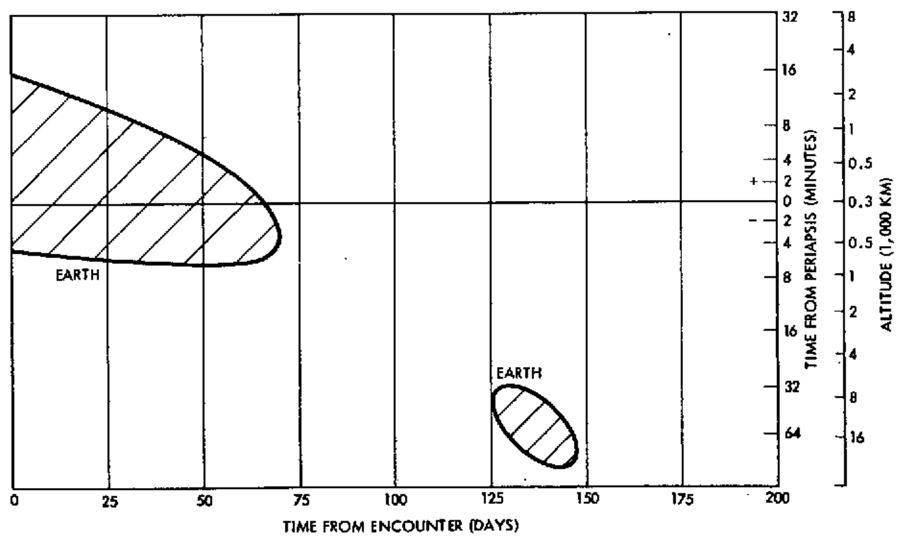

Figure 3-128. Earth Occultation History

bits permits all the data obtained in earth occultation to be stored and also provides storage for the high bit rate experiments. The storage capability is provided by three storage units. Each unit can be shared by use of two inputs. These units provide simultaneous storage access to three scientific instruments and also to the data handling unit for preformatted storage

Table 3-48. Orbiter Data Handling and Data Storage Requirements, Version III Science Nominal Instrument Payload

INSTRUMENT	DATA HANDLING REQUIREMENTS			DATA STORAGE REQUIREMENTS			
				OCCULTATION MODE		SPECIAL MODE*	
	BITS/ SAMPLE	SAMPLES/ MIN	OPERATING TIME	STORAGE BITS/MIN	TOTAL BITS	STORAGE BITS/S	TOTAL BITS
MAGNETOMETER	24	5	DURING CRUISE AND ORBIT	120	DURING PERI-APSIS OCCUL-TATION		
ELECTRON TEMPERATURE PROBE	30	60	PERIAPSIS ±20 MINUTES (3800 KM)	1800			
NEUTRAL MASS SPECTROMETER	5000	0.2	PERIAPSIS ±10 MINUTES (1500 KM)	1000			
ION MASS SPECTROMETER	2000	0.4	PERIAPSIS ±20 MINUTES (3800 KM)	800			
ULTRAVIOLET SPECTROMETER	400	2	DURING ORBIT WHEN VIEWING NADIR AND ZENITH	800		1600	250,000
INFRARED RADIOMETER	40	10	DURING ORBIT WHEN VIEWING DARK SIDE MAXIMUM DATA PERIOD PERIAPSIS -18 MIN +4 MIN	400		2300	40,960
RF ALTIMETER	280	5	PERIAPSIS ±10 MINUTES	1400		3500	120,000

*BY COMMAND, WHEN AVAILABLE

during periapsis earth occultation. In case of failure of one storage unit, it is possible by ground command to rearrange the inputs to the remaining storage units. Further details of the data handling accommodations for the orbiter are discussed in Section 8.3.

Effect of Version IV Science Payload

Tables 3-49 and 3-50 give the orbital experiment data requirements imposed by the Version IV science payload.

There are several differences between these measurements and earlier parameters which have significant impact on the orbiter design.

- The addition of the solar wind experiment increases bit rate requirements at high altitudes
- Bit rate increases were required for all instruments except the electron temperature probe.

An overall increase in bit rate required at higher altitudes from 2 to 7.6 bits/s and an increase in peak bit rate at periapsis from 105.7 to 440 bits/s necessitates a large increase in storage requirements and also in real-time downlink requirements.

Table 3-49. Data Handling Requirements, Version IV Science Nominal Instrument Payload

INSTRUMENT	DATA DESCRIPTION	ANALOG OR DIGITAL	DATA ACQUISITION RANGE*	APPROXIMATE ACQUISITION INTERNAL (MINUTES)	TYPICAL MINIMUM DATA REQUIREMENTS: BITS PER MEASUREMENT	TOTAL BITS PER PASS	DATA RATE (BITS/S)	ANALOG WORDS
MAGNETOMETER	SCIENCE	D	CRUISE		32	----	3	3
	HOUSEKEEPING	A&D	ORBIT >4000 KM	1400	32	252,000	3	
			ORBIT <4000 KM	42	32	80,000	32	
SOLAR WIND ANALYZER	SCIENCE	D	CRUISE		32	----	3	4
	HOUSEKEEPING	A&D	ORBIT >4000 KM	1400	32	252,000	3	
			ORBIT <4000 KM	----	--	0	0	
ELECTRON TEMPERATURE PROBE	SCIENCE	D	ORBIT >4000 KM	----	--	0	0	2
	HOUSEKEEPING	A&D	ORBIT <4000 KM	42	24	60,000	24	
NEUTRAL MASS SPECTROMETER	SCIENCE	D	ORBIT >4000 KM	----	--	0	0	3
	HOUSEKEEPING		ORBIT 500<R<4000 KM	30	--	45,000	25	
		A&D	ORBIT <500 KM	12	--	72,000	100	
ION MASS SPECTROMETER	SCIENCE	D	ORBIT >4000 KM	----	--	0	0	2
	HOUSEKEEPING	A&D	ORBIT 500<R<4000 KM	30	--	45,000	25	
			ORBIT <500 KM	12	--	72,000	100	
ULTRAVIOLET SPECTROMETER	SCIENCE	D	ORBIT >4000 KM	1400	--	144,000	1.67	2
	HOUSEKEEPING	A&D	ORBIT <4000 KM	42	--	85,000	34	
INFRARED RADIOMETER	SCIENCE	D	ORBIT >3000 KM	----	--	0	---	3
	HOUSEKEEPING	A&D	ORBIT <3000 KM	30	--	180,000	100	
RADAR ALTIMETER	SCIENCE	D	ORBIT >1000 KM	----	--	0	0	3
	HOUSEKEEPING	A&D	ORBIT <1000 KM	16	--	96,000	50	

*DATA RATES SHOWN ARE FOR PERIODS OF ACQUISITION INDICATED; NOT AVERAGES OVER ENTIRE ORBIT; INCLUDE BOTH SCIENCE AND DIGITAL HOUSEKEEPING DATA

Table 3-50. Data Handling Requirements, Version IV Science Other Candidate Instruments Payload

INSTRUMENT	DATA DESCRIPTION	ANALOG OR DIGITAL	DATA ACQUISITION RANGE	APPROXIMATE ACQUISITION INTERNAL (MINUTES)	TYPICAL MINIMUM DATA REQUIREMENTS: BITS PER MEASUREMENT	TOTAL BITS PER PASS	DATA RATE (BITS/S)	ANALOG WORDS
AC ELECTRIC FIELD DETECTOR	SCIENCE	D	CRUISE	----	24	----	2.25	2
	HOUSEKEEPING	A&D	ORBIT >4000 KM	1400	24	195,000	2.25	
			ORBIT <4000 KM	----	24	5,600	2.25	
MICROWAVE RADIOMETER	SCIENCE	D	ORBIT >2000 KM	----	--	----	0	3
	HOUSEKEEPING	A&D	ORBIT <2000 KM	26	--	250,000	---	
SPIN SCAN PHOTOMETER	SCIENCE	D	ORBIT >4000 KM	1400	--	3,600,000	---	3
	HOUSEKEEPING	A&D	ORBIT <4000 KM	42	--	378,000	---	

To accommodate the new bit rate requirements the changes made to the DTU for the probe bus will also be made to the orbiter DTU. This, of source, also provides commonality. These changes are listed below.

- Science subcommutator increased from 6 to 10 bits.

- 10-bit analog-to-digital converter added to DTU, with routing to mainframe. This permits not only the 10-bit resolution analog housekeeping but also 10-bit resolution analog in mainframe.
- Change length of word in mainframe from 3-bit increment to 1-bit increments, permitting variable size science words without bit penalty.
- Quadrupled the size of format without a corresponding increase in fixed words.

As was the case in the probe bus these changes permit 91 2/3 percent of the transmitted data to be used for science data instead of 75 percent, effectively increasing the science bit rate capability.

An increase in storage capability is also required. Since the data rate required at periapsis was increased, the storage capability to permit data taking when periapsis is in occultation must also increase. Furthermore, the higher required bit rates at altitudes up to 4000 kilometers exeed the downlink capability at the end of the mission and therefore storage is also required to buffer these data.

The new storage requirements are satisfied by increasing the size of the storage system to 1 228 800 bits. These come in five units of 245 760 bits each. Each unit can be shared at half the bit capability by two scientific instruments simultaneously. During normal operation the IR radiometer, radar altimeter, and both mass spectrometers are connected to the DTU through storage units. Sufficient storage is provided for these instruments to satisfy the requirements in Table 3-49. This uses up the capability of 2-1/2 units. An additional half of a unit is connected to the DTU and is used to store preformatted data from the remaining scientific instruments when periapsis is in occultation. The additional storage unit provides redundancy, and can by ground command replace any of the other four units. This unit can be assigned to any one or two scientific instruments to store high data rate data if desired.

Details of the data handling system are given in Section 8.3.

Even with all the above changes to the data handling systems, the increase in science bit rate requirements from 2 to 7.6 bits/s at high altitudes, and the need to dump the increased stored data acquired at low altitudes, invalidated the use of the fanbeam antenna version of the orbiter studied earlier. All the science requirements in Table 3-49 are met with the above changes and the downlink capability of an earth pointing orbiter.

3.4.2.4 Signals to Instruments Requirements and Accommodation for All Versions of the Science Payload

The following real-time ground commands have been identified for the orbiter science instruments:

- Power on/off, two for each experiment
- Calibrate on/off, two for each experiment
- UV spectrometer, two high/low data rate select
- Magnetometer, two high/low range select
- Ion mass spectrometer, four mode select
- Neutral mass spectrometer, one eject ion source cover
- Solar wind probe, two mode select.

The orbiter will be capable of providing up to 50 discrete commands and six stored commands to the scientific instruments for performing these functions.

The stored command capability permits a command to be sent to the orbiter for execution at a later time. This capability is valuable for instrument functions that must be performed when the spacecraft is in earth occultation.

The signals provided by the orbiter to the scientific instruments are identical to the signals provided on the probe bus (Section 3.3.2.2) with the addition of an end-of-memory signal. This signal is sent to a scientific instrument shifting data to the storage unit when the storage unit is full.

Many of the scientific instruments on the orbiter obtain useful data during only a small portion of the spin cycle or the orbit period. When these instruments use large amounts of power or take large amounts of data during these short periods, control of the instrument turn-on and/or data taking will be desirable. The spacecraft signals required by the instruments for control are similar to those on Pioneer 10, consisting of a sun reference pulse and/or sector generator pulses, and stored ground commands.

3.4.2.5 RF Science Requirements, Studies, and Accommodations

Versions I/II Science Payload Requirements and Accommodations

The Versions I/II science payload requirements included a dual frequency occultation, a radar altimeter, and bistatic radar. Accommodations for these experiments had to consider refracted ray tracking for the occultation experiment, an antenna to track the Venus nadir for the radar altimeter and suppression of its noise pulses, and use of the telemetry antenna to view targets of opportunity for the bistatic radar. This package of RF experiments was allocated a budget of 9.07 kilograms (20 pounds) and 20 watts.

Studies of the use of the telemetry antenna for the RF science experiments resulted in the following conclusions.

Earth-Pointing Spacecraft. For the occultation experiment, a programmed spin axis precession of about 0.30 radians (17 degrees) is required to track the refracted ray to earth. At 0.0002 rad/s (0.1 deg/s) either 0.05 kilogram (0.1 pound) of gas per pass, or 0 to 35 watts peak with reaction wheel control is required. Conscan feed would require redesign to provide two positions, i.e., conscan or concentric. Addition of an X-band occultation would require the addition of an X-band feed.

It would not be practical to use the telemetry antenna for either the altimeter or the bistatic radar because of the excessive gas weight or power required.

Normal to Venus Orbit Plane Spacecraft with Despun Antenna Dish. A despun telemetry antenna would be useful for the occultation experiment but would require gimballing to permit tracking the refracted ray to earth by a programmed combination of a despin angle and gimbal angle. Addition of an X-band occultation would require a new dual frequency rotary joint design and addition of an X-band feed. A despun gimballed telemetry antenna could occasionally be used for both the radar altimeter and bistatic radar, but both would require an increased gimbal angle range.

In all of the cases above, spacecraft precession can replace gimballing.

Version III Science Payload Requirements and Accommodations. The Version III science payload removed consideration of bistatic radar and provided a dedicated gimballed antenna for the radar altimeter. It relegated the X-band occultation to the other candidate instruments list. This redirection, along with cost factors, led to the consideration of fanbeam telemetry antenna with and without a despun reflector on a spacecraft with the spin axis normal to the Venus orbit plane.

Normal to Venus Orbit Plane Spacecraft with Fanbeam Antenna. Programmed spin axis precession would be required to track refracted rays to earth. As a minimum accommodation, the spacecraft should be offset prior to occultation to partially compensate for the bending. Because of the low gain, the experiment would be limited in performance. If X-band were added to the occultation experiment, an additional antenna would be required.

Normal to Venus Orbit Plane Spacecraft with Fanbeam Antenna and Despun Reflector. Programmed spin axis precession would be required to track refracted rays to earth. Spacecraft offset prior to occultation would partially compensate for refractive bending. Addition of X-band to the occultation experiment would require an additional antenna and despun reflector.

Occultation Experiment Considerations with Narrow Antenna Patterns, Version III Science Payload

The time duration of useful occultations will be severely limited if the refracted ray cannot be tracked. The occultation data will be limited to spacecraft locations where the direction of the refracted ray to earth is within the antenna beamwidth. For that reason, the requirements for tracking the refracted ray were investigated.

A ray tracing program for the study of refracted ray tracking during occultation was developed. The formulation is essentially that given in the reference below with minor modification. The basic problem is shown in Figure 3-129. A ray from earth entering the atmosphere of a planet is refracted according to Snell's law. In terms of the quantities shown, Snell's law is given by:

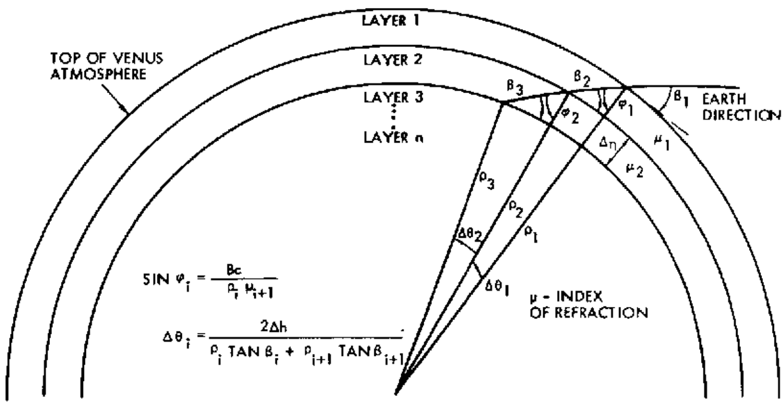

Figure 3-129. Basic Refracted Ray Tracing Program

$$\frac{\cos \beta_i}{\sin \phi_i} = \frac{\mu_{i+1}}{\mu_i} \tag{1}$$

where μ_i and μ_{i+1} are the refractive indices of the two adjoining layers. For the purpose of the Pioneer Venus study, the Venus atmosphere was divided into spherical layers 20 meters thick and a refractive index assigned to each layer. The law of sines gives the additional relation

$$\frac{\sin \phi_1}{\cos \beta_{i+1}} = \frac{\rho_{i+1}}{\rho_i} \tag{2}$$

Equation (2) is solved for $\sin \phi_i$ and substituted into Equation (1) giving Bourger's law.

$$\rho_i\ \mu_i \cos \beta_i = \rho_{i+1}\ \mu_{i+1} \cos \beta_{i+1} = B_c \tag{3}$$

where B_c is Bourger's constant. From Equations (2) and (3) we can write

$$\sin \phi_i = \frac{B_c}{\rho_i\ \mu_{i+1}} \tag{4}$$

Reference: Croft, T. A., Eshelman, V. R., Marouf, E. A., Tyler, G. L., "Preliminary Review and Analysis of Effects of the Atmosphere of Venus on Radio Telemetry and Tracking of Entry Probes," Stanford University Center for Radar Astronomy, October 1972.

and thus the angle ϕ can be found at each altitude. However, to completely trace the ray, the angle $\Delta\theta_i$ must also be calculated at each layer. This angle may be accurately approximated by

$$\Delta\theta_i = \frac{2\Delta h}{\rho_i \tan \beta_i + \rho_{i+1} \tan \beta_{i+1}} \tag{5}$$

where Δh is the layer thickness.

The ray tracing technique is simple: calculate the required quantities at each layer using the values at the previous layer as initial conditions.

For a ray which exits the atmosphere the path is symmetric since the atmosphere model chosen is symmetric, hence the ray need be traced only to the point where ϕ = 1.57 radians (90 degrees). The final geometry of the ray is given by Figure 3-130, where θ is the sum of the $\Delta\theta_i$. An important quantity to be found is α, the angle the ray makes with the earth direction on existing the planet's atmosphere. Results show that this angle can be as large as 0.35 radians (20 degrees) indicating that communications are possible during a considerable portion of occultation. This angle is also needed for correct orientation of the antenna. In terms of the quantities previously discussed

$$\alpha = \theta - 2\beta_i \tag{6}$$

The results from the ray tracing program were coupled with an orbit program to get the α true anomaly history for typical orbits. Also of interest is the second angle needed to define the spacecraft orientation for communication during occultation. This angle called γ is the angle between the plane defined by the earth, Venus and the spacecraft and the Venus orbit plane. The configuration is shown in Figure 3-131.

α and γ versus true anomaly for a Type II orbit, θ_{aim} = 2.09 radians (120 degrees) at 30 days from VOI are shown in Figures 3-132 and 3-133.

Figure 3-134 shows the two angles that should be tracked during occultation for those orbits for which earth occultations occur.

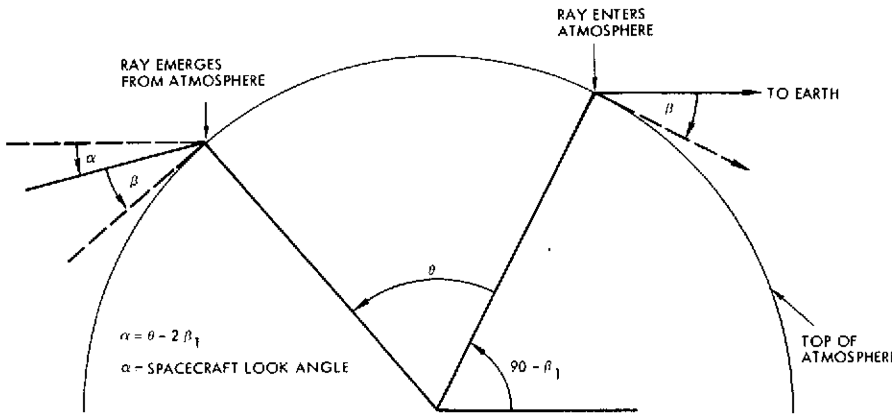

Figure 3-130. Final Geometry of Ray Where θ is the Sum of the Δv_i

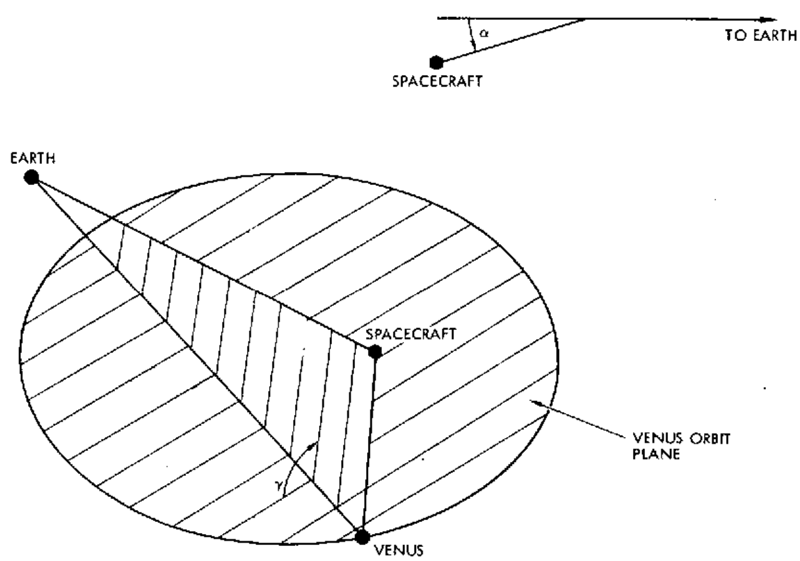

Figure 3-131. α Measured in Earth-Venus-Spacecraft Plane

Although the RF attenuation was not computed, data was obtained from Dr. A. J. Kliore and Dr. G. Fjeldbo of JPL showing the loss due to defocusing to be expected as well as the direction to the image of earth as seen from the spacecraft for a polar orbit with θ_{aim} = 4.71 radians (270 degrees) and a Type II trajectory. This data is shown in Figures 3-135 and 3-136. Besides being computed for a different orbit than the TRW data it is also presented in a different coordinate system. The cone angle is measured from the spacecraft earth vector and is the same as the angle α discussed previously, but the clock angle is defined as the angle between

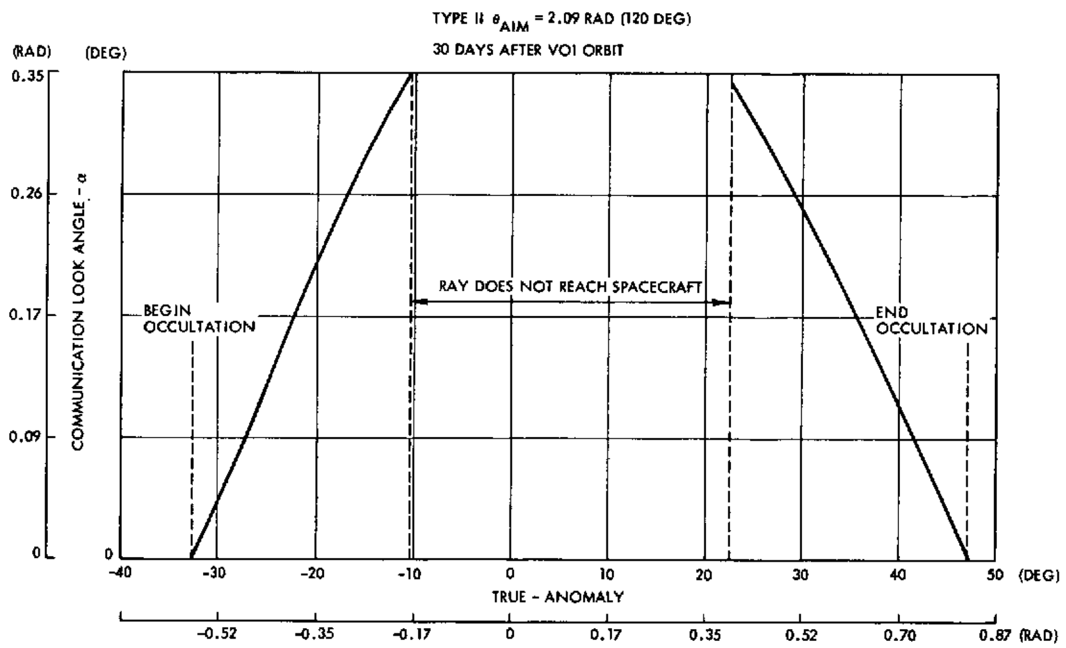

Figure 3-132. α Versus True Anomaly

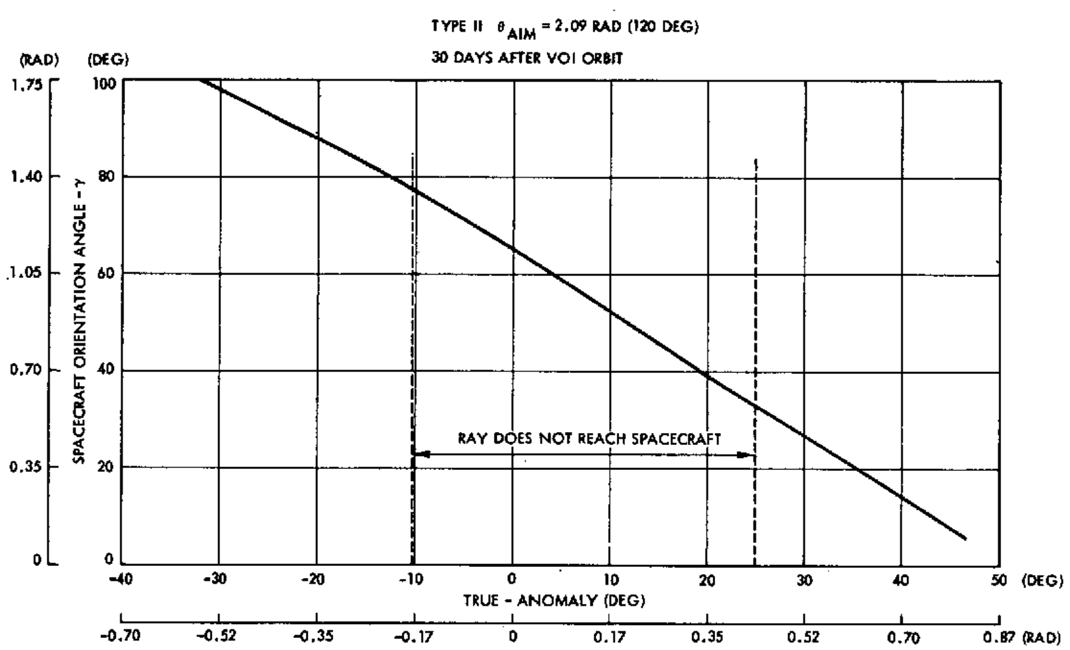

Figure 3-133. γ Versus True Anomaly

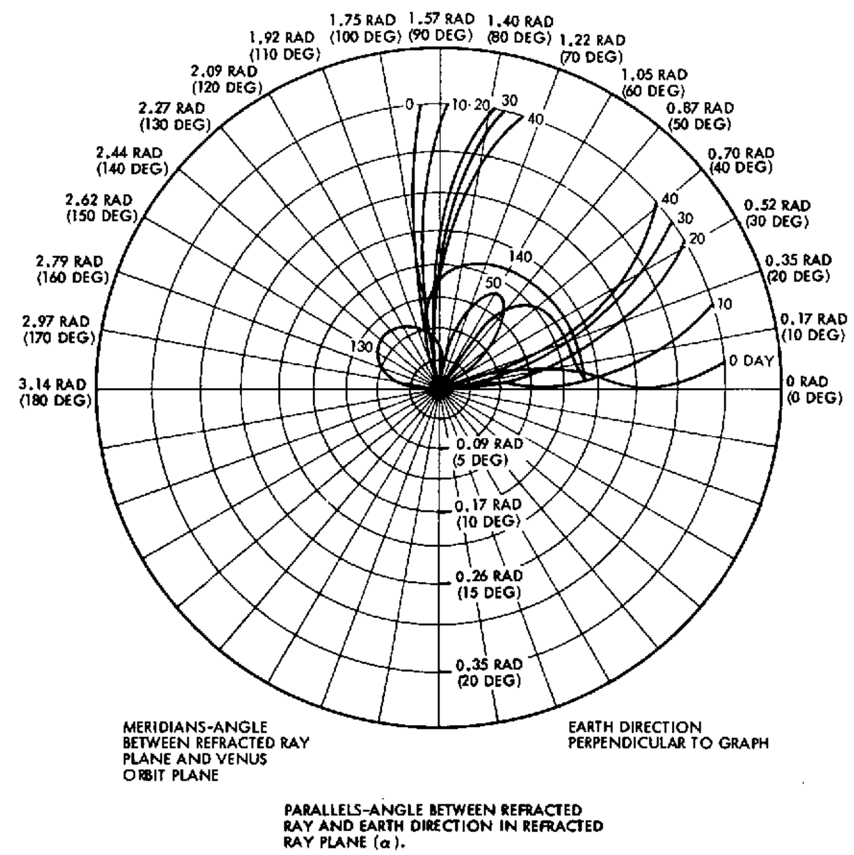

Figure 3-134. Orbiter Occultation Experiments Refraction Tracking Angles

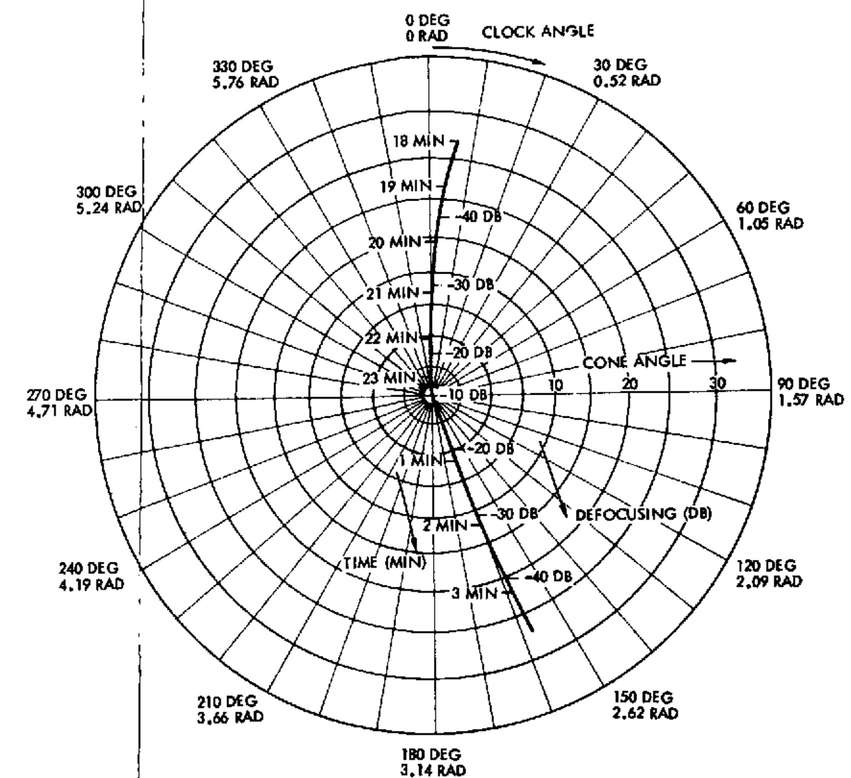

Figure 3-135. RF Attenuation Data (Insertion + 0 Days) from Dr. A. J. Kliore and Dr. G. Fjeldbo of JPL

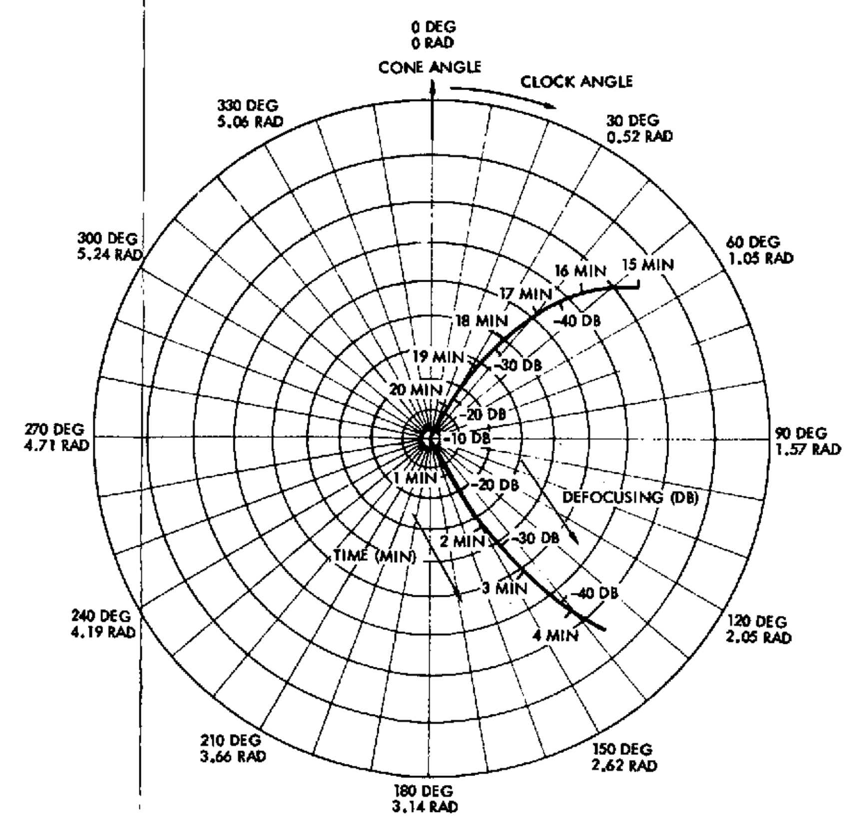

Figure 3-136. RF Attenuation Data (Insertion + 35 Days) from Dr. A. J. Kilore and Dr. G. Fieldbo of JPL

FOLDOUT FRAME 1

FOLDOUT FRAME 2

the projection of the spacecraft-Canopus vector on a plane perpendicular to the spacecraft-earth vector and the projection of the position vector on the same plane. The data in these figures are valid for both X- and S-band. The defocusing is essentially a function of the cone angle and not the clock angle. These curves were used in evaluating the behavior of the baseline system for the RF occultation experiment for all orbiter configurations, Version III science payloads.

Radar Altimeter Pulse Load

The effect of the radar altimeter pulse loads on the spacecraft power has been evaluated. Three operational modes were considered for the altimeter.

1) 110 watts continuously for 1 second per spacecraft revolution

2) 150 pulses each 50 μsec long and 110 watts peak load during 1 second per revolution

3) 100 pulses each 1 millisecond long and 110 watts peak load during 1 second per revolution.

For mode 1), the 110-watt peak load represents a current requirement of 3.93 amperes at 28 VDC. Since the power subsystem bus regulation method is similar to Pioneers 10 and 11, the Pioneer 10 and 11 design review package was reviewed for test data which showed the PCU transient response. The engineering model PCU was tested for step changes in loads of 35, 42 and 63 watts. Photographs of the PCU output voltage response for the 63-watt load change are shown in Figure 3-137. The top photograph shows the application of the 63-watt load with 1-ampere shunt current plus 0.25-ampere charge current before load turn-on and 1 ampere discharge current after load turn-on. The PCU operating mode changes from shunting to discharge due to the increased load. This is a worst-case situation insofar as transient response is concerned. The bottom photograph shows the bus response to a load reduction of 63 watts. In this case the PCU switches from a discharge to a shunt/charge mode. Note that the duration of the transient is approximately 5 milliseconds in both cases.

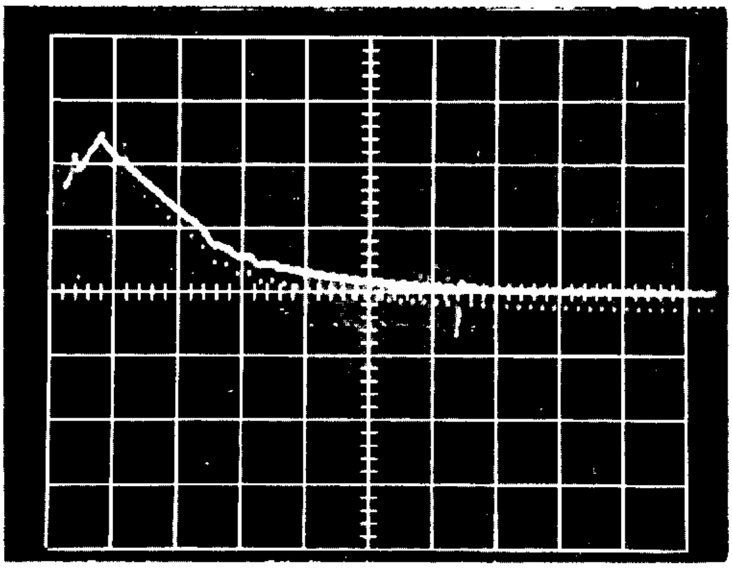

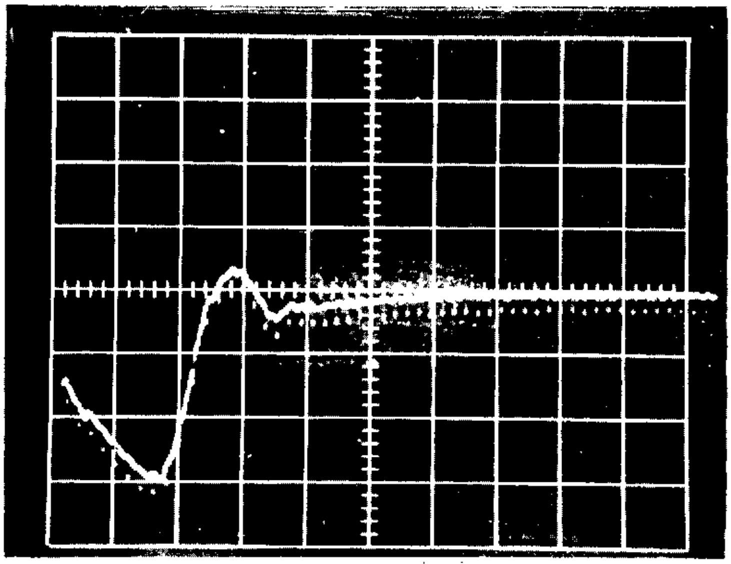

Figure 3-137. Transient Response of Pioneer 10 and 11 Power Control Unit

Similar test data for peak transient voltage for the 35- and 42-watt load together with the 63-watt load are shown graphically in Figure 3-138. The dotted line is an extrapolation to the 110-watt transient case (mode 1). For 110 watts the bus would drop to approximately 22.7 volts and return to 28 volts within 5 milliseconds. Reciprocal data would apply for the turn-off transient. This transient is considerably in excess of present Pioneers 10 and 11 EMC specification limits. An energy storage filter for this mode of operation will require an extremely large capacitor.

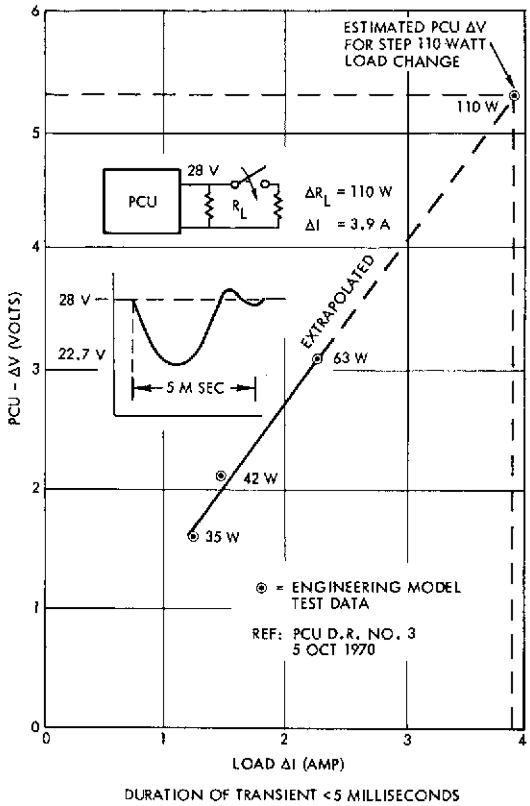

Figure 3-138. Mode 1 Transient Amplitude (Shunt to Discharge)

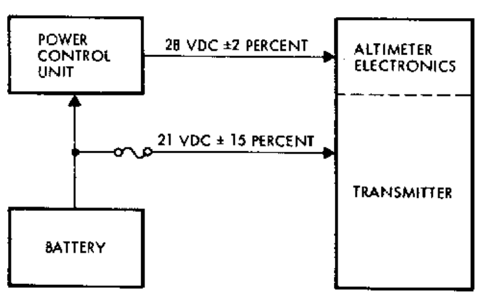

Figure 3-139. Radar Altimeter Electronics as Steady Load

In order to prevent the 1-second pulse transients from appearing on the main DC bus, the radar altimeter transmitter can be connected directly to the battery. With this arrangement the battery voltage will only drop approximately 0.5 volt during each 110-watt pulse. However, the battery voltage varies from 18 to 24 volts as a function of battery state of charge and temperature. If the radar altimeter transmitter can operate within this battery voltage range and with proper fault protection, a direct battery connection is recommended for mode 1) conditions. The radar altimeter electronics will be treated as a steady load and will be connected to the main 28-VDC bus. Figure 3-139 shows this arrangement.

The mode 2) transient load duration is less than mode 3) which is discussed below, but the amplitude is the same. Since mode 3) is the worst case, mode 2) is not covered in detail.

For mode 3), the engineering model test data for the PCU was used to estimate the PCU response to 3.51 ampere load transients of 1 millisecond duration. Figure 3-140 shows the predicted PCU output response. The effect of user input filters on total bus response is neglected in this analysis. If user input filtering were to be included, the transient peaks would be less than shown, and the data presented is for a worst case.

It can be seen that the transient voltage excursions are roughly ±4 volts about the 28-VDC nominal bus voltage. Filtering is required to reduce these transients to acceptable levels.

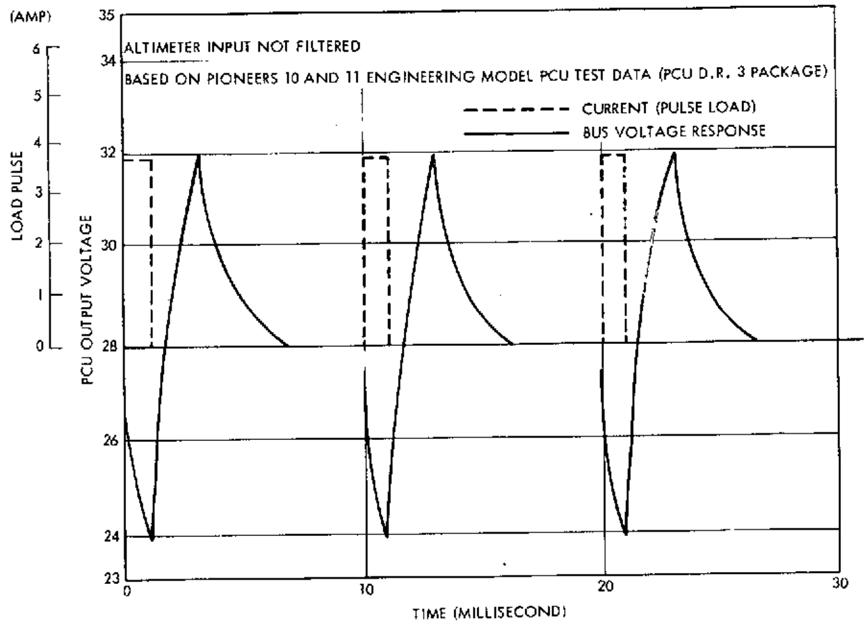

Figure 3-140. Pioneers 10 and 11 Type PCU Response to Transients

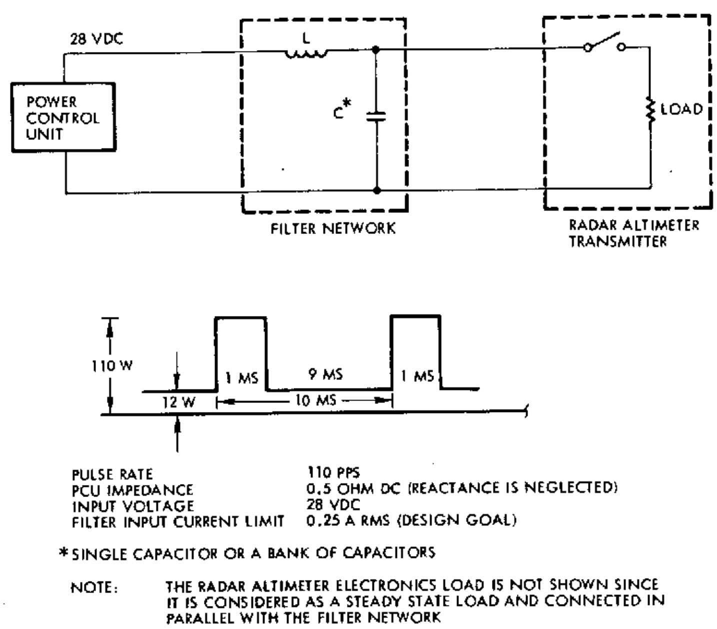

Figure 3-141. Filter Circuit and Design Criteria

The results of an analysis using the conditions of mode 3) provide a means of choosing a filter network to meet a range of input voltage requirements of the radar transmitter. Figure 3-141 represents the circui and criteria used in determining the filter designs.

A transient simulation of the above circuit was conducted using the TRW Interactive Circuit Analysis Program (ICAP). The results indicate that the input current to the filter is held relatively constant by effectively suppressing transients from appearing on the main 28-VDC bus. However, the output voltage variation is a function of capacitor size. Larger capacitance provides smaller voltage variations at the input to the radar transmitter at the expense of increased weight. The results of the different LC filter networks were plotted as three points on Figure 3-142 which provide the means of selecting the required filter.

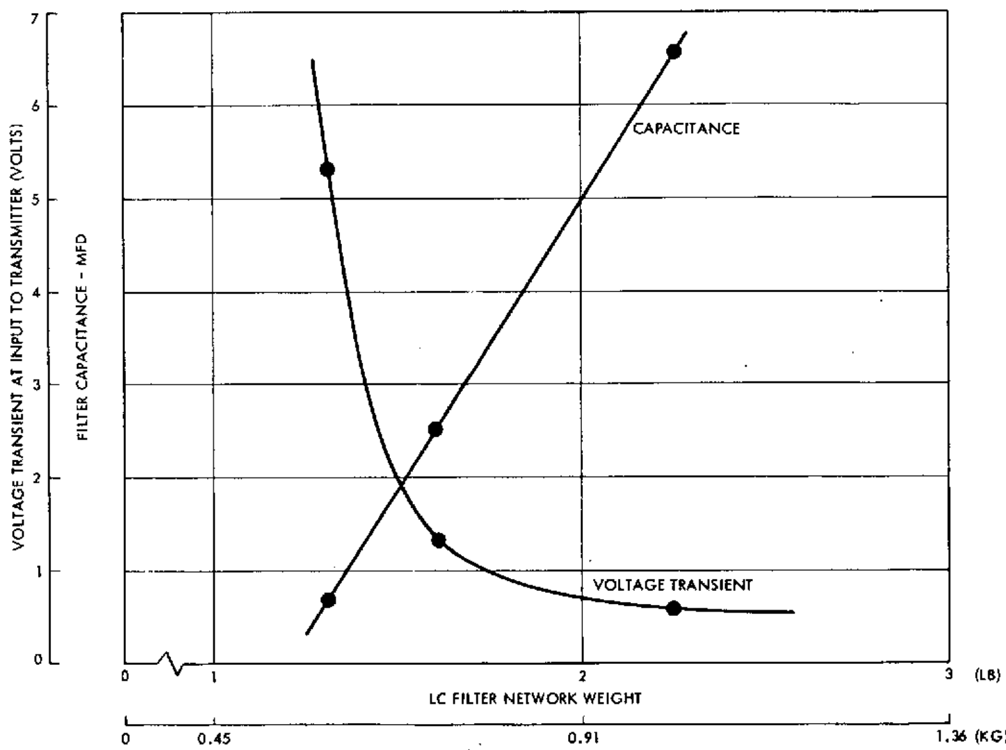

Figure 3-142. Filter Network Design Selection Delta V and Capacitance Versus Filter Weight

In implementing the design, the H-field effects due to the 3.93-ampere current at the input to the transmitter can be minimized with twisted shielded wire pairs. The high-frequency components of the radar RF can be decoupled from entering the spacecraft power lines by using small ceramic capacitors in parallel with the large capacitors. Inrush current transients can be avoided by allowing the filter to be connected to the power bus at all times.

In conclusion, a filter network can be provided as an integral part of the radar experiment or as a separate box attached to or located near the experiment. For TRW to provide this network as a separate box will cost approximately $58K for three units. It is recommended that the filtering be included in the experiment.

Effects of Version IV Science Payload on RF Science Accommodations

Two changes affecting the RF science were made: the decision to change the baseline spacecraft to an earth pointer and the addition to the nominal payload of the X-band occultation experiment with a dedicated 200 milliwatt transmitter.

The preferred implementation for the occultation experiment consists of the use of the S-band communication horn and an additional X-band horn mounted parallel to the spin axis on the rear of the spacecraft. The horns view toward earth during the first 35 days after orbit insertion before the spacecraft flip maneuver. The broad beams of these antennas eliminates the need to track refracted rays. Prepointing toward the final refracted ray is adequate.

During this period earth occultations occur while the spacecraft is near periapsis and also while the earth is closest to Venus, thus permitting maximum margin for use in the occultation experiment.

The S-band horn has a 0.27 radian (30 degree) 15.5 dB peak gain and a beamwidth of 0.52 radians (30 degrees). It is identical to the Pioneers 10 and 11 medium gain antenna. The X-band horn has a 20 dB peak gain and a beamwidth of 0.30 radian (17 degrees). It is derived from DSP.

In this implementation the spacecraft will be offset by about 12 degrees in cone angle before the start of occultation. The occultation measurement will not be obtained on leaving occultation.

The communication system has a dual modulation index capability. In one mode all but one dB of the power appears in the carrier. This mode is optimally suited for the occultation experiment. On day zero (the first day in orbit) a received carrier power of -143 dBm is received at the S-band horn peak gain prior to occultation. Dr. G. Fjeldbo at JPL estimated that the occultation processing could be performed down to -180 and -190 dBm. Therefore on day zero at least 36 dB margin is available for S-band occultation. On day 35, at least -147.2 dBm is received at S-band and the occultation margin would be at least 31.8 dB. We see from Figures 3-135 and 3-136 that with these margins bending of more than 0.31 radians (18 degrees) and 0.26 radians (15 degrees) respectively can be examined at S-band.

The corresponding margins with a 200 mW X-band transmitter and the medium-gain horn are 25 dB on day zero and 21 dB on day 35 which corresponds to bending angles of 0.17 and .12 radian (10 and 7 degrees), respectively.

3.4.2.6 Spacecraft Charging Considerations, Version IV Science Payload

The same considerations apply to the orbiter that apply to the probe bus; they are discussed at the end of Section 3.3.2.2. On the orbiter, however, there is no retarding potential analyzer and thus the 1.5 m^2 reference conducting plane requirement does not apply. However, a large exposed conducting reference surface would prove valuable to the solar wind experiment, when that instrument is in an electron measurement mode. Although no specific requirement has been imposed, as large an area as possible out of the wake of the spacecraft should be provided. This would also satisfy the requirements of the electron temperature probe.

For the orbiter all portions of the spacecraft are at some time in the wake of the spacecraft. Since the solar wind analyzer obtains data throughout the mission, it would be beneficial if the exposed conducting surfaces cover as much as the spacecraft surface as feasible.

3.4.2.7 Magnetic Control

Details of Version I/II/III Science Payload Magnetic Control

The magnetometer on the orbiter imposes a requirement that the in-flight magnetic field of the orbiter at the sensor be less than 5n T, as suggested by the Pioneer Venus science steering group in June 1973.

Using the methods discussed in Section 3.3.2.2, this requirement can be met without stringent magnetic controls if the magnetometer sensor is placed on a boom having a length greater than the following:

Thor/Delta launch orbiter [0.864 meter (34-inch) radius, 292.6 kilograms (645 pounds), 175 watts]	2.16 meters (7.08 feet)
Atlas/Centaur launch orbiter [1.080 meter (42.5-inch radius, 435.4 kilograms(960 pounds, 190 watts]	2.37 meters (7.79 feet)

With a nickel-cadmium battery, the minimum boom lengths become:

Thor/Delta launch orbiter	2.68 meters (8.80 feet)
Atlas/Centaur launch orbiter	2.80 meters (9.17 feet)

For commonality of design with the probe bus the recommended boom length is 3 meters.

Effect of Version IV Science Payload on Magnetic Control

The Pioneer Venus ESRO Joint Working Group, January 1973, has suggested that a field of 0.5n T could be achieved without special cleaning of the spacecraft with a 3-meter boom on a Thor/Delta launch orbiter.

At the ARC briefing associated with the Version IV, April 13th re-direction, notification was given that the magnetic requirement for the orbiter was 0.5n T. Using the methods discussed in Section 3.3.2.2 we find that a conservative estimate of the boom length for the Atlas/Centaur orbiter using the size scaling correction would be:

Atlas/Centaur launch orbiter	5.20 meters (17.07 feet)
Atlas/Centaur launch orbiter with Ni-Cd battery	5.34 meters (17.53 feet)

As discussed in Section 3.3.2.2 about 50 percent of the field in space is due to hard remanence and strays. If we assume we can compensate 90 percent of this we can reduce the estimated field by about a factor of two by compensation. Furthermore, using the arguments of that section we can reduce the field even more by carefully laying out assemblies. We therefore recommend that the boom lengths computed without size scaling be used:

Atlas/Centaur launch orbiter	4.41 meters (14.46 feet)
Atlas/Centaur launch orbiter with Ni-Cd battery	4.59 meters (15.06 feet)

4. MISSION ANALYSIS AND DESIGN

The effective design of a planetary mission requires satisfaction of the scientific objectives of the mission, while ensuring cost-effective yet reliable hardware and mission operations design. The scientific considerations involved in the Pioneer Venus missions were discussed in detail in Section 3. The probe, bus, and orbiter system and subsystem descriptions and the mission operations considerations are summarized in the following sections. This section presents the studies that were made to blend the two goals into an effective system design, one that satisfies the mission objectives.

The final profiles of the preferred 1978 Atlas/Centaur missions are documented in Section 4.1. It serves as a convenient tabulation of the mission definition data on which the configurations of the probes, bus, and orbiter are based.

Sections 4.2, 4.3, and 4.4 discuss the broad trades that led to the final preferred mission designs detailed in Section 4.1. Section 4.2 summarizes the mission opportunity assessment, demonstrating the rationale for selecting the 1978 Type I opportunity for the probe mission and the early 1978 Type II opportunity for the orbiter mission. Also included are discussions of alternative mission profiles (broken plane and looper transfers) and launch vehicle considerations applicable to the Pioneer Venus missions.

Section 4.3 provides a survey of the major trades involved in the design of the probe mission. Critical studies summarized here include an in-depth comparison of sequential versus simultaneous release, detailed analyses of the behavior of the probes during entry and descent, and a complete assessment of the entry and demise of the probe bus. Data on both the 1977 and 1978 probe missions and both the Thor/Delta and Atlas/Centaur configurations will be included, with the preferred 1978 Atlas/Centaur combination discussed first in each section.

Section 4.4 summarizes the studies leading to the definition of the preferred orbiter mission. Highlights of this section include the selection and sensitivities of the preferred orbit (Type II transfer, 24-hour period, 120 degree θ_{AIM}) and the determination of the strategy and requirements for the insertion and trim maneuvers of the mission.

4.1 MISSION ANALYSIS SUMMARY

This section details the preferred mission profiles for the preferred probe orbiter missions and summarizes the major mission impact of the launch vehicle selection. The following sections then discuss the major trades that influenced the design of the two missions reported herein.

4.1.1 Probe Mission Profile

The preferred probe mission is flown by an Atlas/Centaur launch vehicle with the 1978 Type I transfer. The mission profile features sequential release at 10 rpm, permitting zero angles of attack for each of the probes while obtaining good planet coverage. The sequential release is designed to achieve a staggered entry of the probes so that the second and third small probes enter 15 minutes after the large and first small probe have completed their mission. The bus, targeted for a shallow entry angle, reaches an altitude of 1000 km 18 minutes after the second set of probes impact the surface. The large probe mortars a drogue parachute 21 seconds after a 50-g switch is tripped, releases the aeroshell 5 seconds later, remains on the large parachute for 39.5 minutes, and impacts the surface 34 minutes later. The small probes enter at entry angles between 60 and 25 degrees and, employing only their aerodynamic shape to control entry and descent, impact the surface 65 minutes after entry. The bus obtains about five minutes of entry science before contamination of science instruments terminates the useful mission.

4.1.1.1 Launch Profile

The launch window for the probe mission is relatively constant from day to day, providing a window of approximately 160 minutes per day throughout the 10-day opportunity. The coast time for the Centaur prior to trans-Venus injection also varies little throughout the 10-day period. The departure geometry is shown in Figure 4-1. Although liftoff occurs on the night side of earth, the injection from parking orbit is within 0.52 radian (30 degrees) of the morning terminator. Following injection, the Centaur orients the spacecraft into the desired cruise position prior to separation. This orientation is such that the spacecraft is aft-earth pointing at 5 days after launch. This procedure minimizes propellant consumption aboard the probe mission spacecraft.

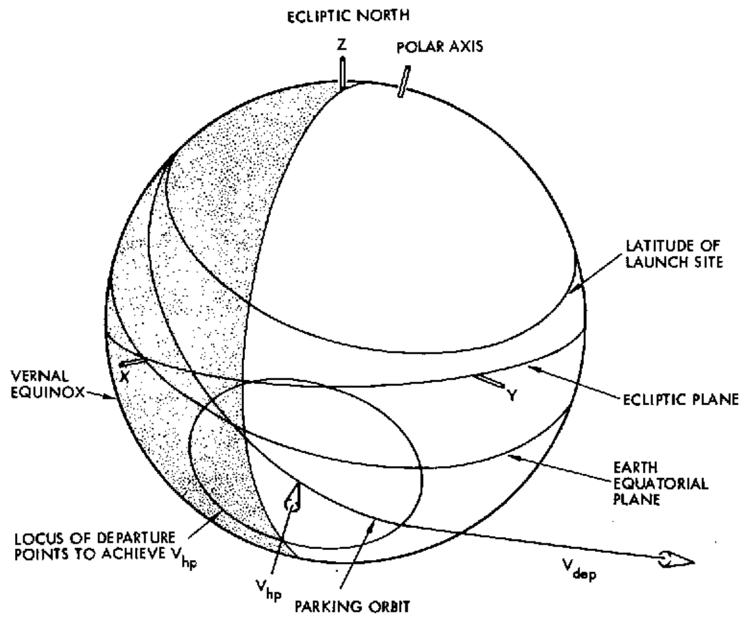

Figure 4-1. Probe Mission Departure Geometry

4.1.1.2 Interplanetary Cruise

The interplanetary trajectory is a 1978 Type I transfer summarized in Table 4-1. The launch period and arrival date were chosen to maximize the injected payload while constraining entry velocities to be less than 11.33 km/s (37 200 fps) throughout a 10-day launch period. The interplanetary transfer is illustrated in Figure 4-2 in two views: a standard heliocentric plot where the trajectories of Venus, earth, and the spacecraft are projected onto the ecliptic plane and a view as seen from the moving earth. Points are indicated at 10-day intervals. The second view clearly illustrates the point of syzygy, which causes special concerns to the attitude determination and control systems.

Table 4-1. Interplanetary Trajectory Summary

LAUNCH PERIOD	20-29 AUGUST 1978
ARRIVAL DATE	17 DECEMBER 1978
TRIP TIME (DAYS)	119-110
LAUNCH ENERGY C_3 (KM^2/S^2)	9.76
ARRIVAL VELOCITY V_{HP} (KM/S)	5.04
ENTRY VELOCITY V_E (KM/S (FPS))	11.33 (37,200)

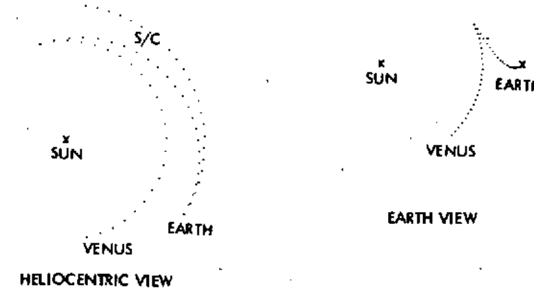

Figure 4-2. Interplanetary Transfer

Midcourse maneuvers are scheduled at five and fifteen days after launch and at 30 days before Venus arrival. The midcourse requirements are summarized in Section 4.1.1.3 below.

4.1.1.3 Probe Release and Planetary Approach

The approach geometry for the 1978 probe mission is illustrated in Figure 4-3. The large probe is targeted for the equator 65 degrees from the subsolar point. The small probes are deposited within boundaries defined by entry flight path angles of -25 to -60 degrees and earth communication angles of 55 degrees. One small probe is deposited on the equator as far from the large probe as practical. A second small probe is located as far from the equator as possible while meeting the above constraints. The third small probe is then placed at an intermediate location. The bus entry site is selected to lie on the greater circle defined by the hyperbolic excess velocity vector V_{HP} and the subearth point at an entry angle of -11.5 degrees. These entry sites are illustrated in Figure 4-3 and detailed in Table 4-2.

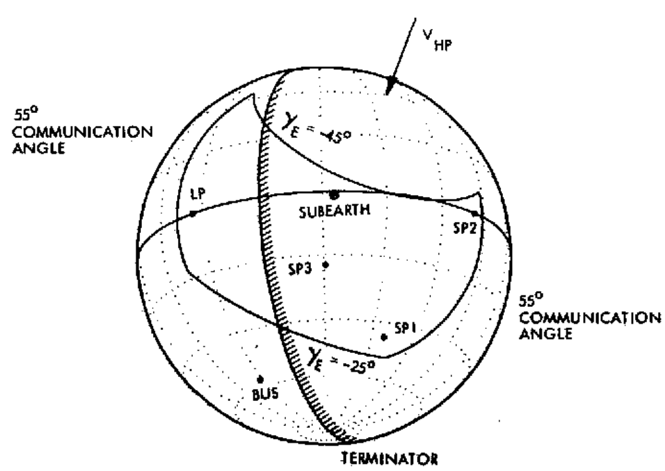

Figure 4-3. Preferred Target Sites for 1978 Probe Mission

The release sequence used to attain these entry sites is summarized in Figure 4-4. The release sequence is initiated 50 days before encounter (E-50) with tracking for the final midcourse. Tracking continues for 20 days at which time (E-30) the final midcourse is performed. Five days later the large probe is released at 10 rpm in the attitude required for zero angle of attack. The small probes are then sequentially released at four day intervals, with retarget maneuvers midway between releases as

Table 4-2. Coast Phase Parameters from Release to Entry

	LP	SP1	SP2	SP3	BUS
RELEASE PARAMETERS					
TIME BEFORE LP ENTRY [(a)] (DAYS)	25	21	17	13	11
VENUS RANGE (10^6 KM)	10.7	9.0	7.3	5.6	4.8
SOLAR RANGE (10^6 KM)	116	115	113	112	111
EARTH RANGE (10^6 KM)	37.8	41.7	45.8	50.2	66.2
VENUS ASPECT ANGLE	23	26	14	20	10
SOLAR ASPECT ANGLE	40	15	28	36	44
EARTH ASPECT ANGLE	138	139	125	145	136
ENTRY PARAMETERS [(b)]					
TIME AFTER LP ENTRY [(a)] (MIN)	0	0	90	90	180
ENTRY ANGLE (DEG)	-35	-30	-56	-41	-11.5
ANGLE OF ATTACK (DEG)	0	0	0	0	6
DESCENT COMMUNICATION ANGLE (DEG)	49	48	52	22	-
LATITUDE (DEG)	0	-45	0	-23	-57
LONGITUDE (DEG)	65	135	165	110	69.5
SOLAR ASPECT ANGLE (DEG)	72	45	43	55	67
PRE-ENTRY COMMUNICATION ANGLE (DEG)	35	29	45	28	6

(a) LARGE PROBE ENTRY TIME = 17 HOURS 46 MINUTES ON 12/17/78.
(b) ENTRY RADIUS = 6300 KM. SOLAR RANGE AT ENTRY = 107.5×10^6 KM, EARTH RANGE = 65.3×10^6 KM.

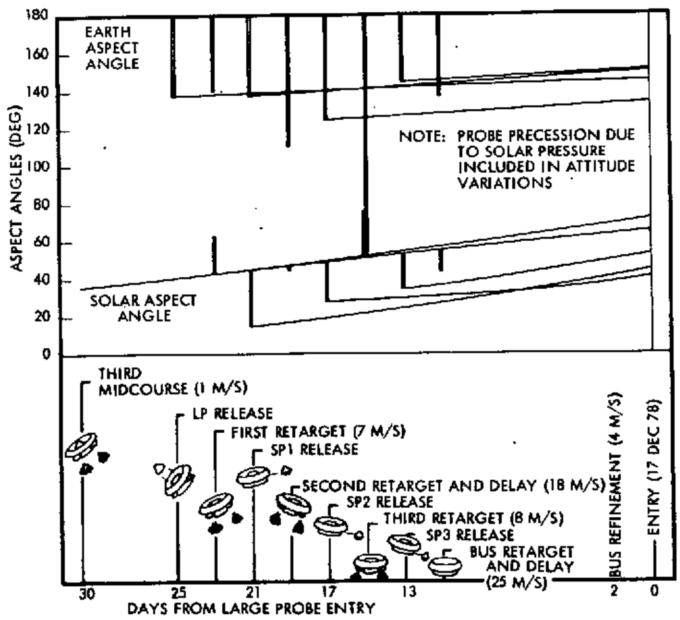

Figure 4-4. Release Sequence and Approach Profile

indicated in Figure 4-4. The attitudes required for the various releases and retarget maneuvers are also illustrated. The targeting and release sequence is summarized in Table 4-3. The sequence is designed to release the shallowest probe first to most effectively limit dispersions (see Section 4. 3. 2. 4). At E-11 days the bus is retargeted to the desired entry site. A final midcourse maneuver is scheduled at E-2 days to refine the bus trajectory if necessary. The maneuver budget allocated in Table 4-3

Table 4-3. Bus Maneuver Budgets for Probe Mission

TIME	MANEUVER	ΔV BUDGET (M/S)	PRECESSION BUDGET PRECESSION (DEG)	SPIN RATE (RPM)
L+5	FIRST MIDCOURSE (c)	14 (c)	360	4.8
L+15	SECOND MIDCOURSE	1	300	4.8
E-30	THIRD MIDCOURSE	1	300	4.8
E-25	LP RELEASE	-	90	10
E-23	FIRST RETARGET	7	220	10
E-21	SP1 RELEASE	-	100	10
E-19	SECOND RETARGET (a)	18	150	10
E-17	SP2 RELEASE	-	120	10
E-15	THIRD RETARGET	8	320	10
E-13	SP3 RELEASE	-	80	10
E-11	BUS RETARGET (a)	25	90	10
E-2	BUS REFINEMENT	4	300	60
	TOTAL MANEUVER REQUIREMENTS	78	2430	55.2 (b)

(a) INCLUDES ΔV NECESSARY TO DELAY BUS 90 MINUTES FOR STAGGERED ENTRY.
(b) TOTAL SPIN RATE CHANGE
(c) INCLUDES 9 M/S FOR INJECTION COVARIANCE PLUS 5 M/S FOR INJECTION FIGURE OF MERIT

is slightly larger than necessary for these specific sites to accommodate the acquisition of any set of small probe entry sites within the design constraints indicated above. Also included is sufficient ΔV to successively delay the bus by 90 minutes at the second probe and bus retarget maneuvers to obtain a staggered entry of the probes and bus, discussed in more detail in Section 4.1.1.4 below.

The probe attitudes variations during the coast period are caused by changing trajectory geometry and by the precession of the probes resulting from solar pressure effects. Solar pressure results in a 4 degree attitude precession for the large probe and less than 2.2 degrees for each of the small probes. The probes are released at attitudes designed so that they precess into the zero degree angle of attack attitude at entry. The time histories of the critical coast phase parameters are detailed in Table 4-2 for the large and small probes and the bus.

4.1.1.4 Probe Mission Entry and Descent Sequence

The probe mission entry times were selected to allow coverage of all probes and the bus from the DSN stations at Goldstone and Canberra. The nominal entry time for the large probe and first small probe (SP1) is 17 hours 45 minutes (GMT) on December 17, 1978. The large probe and SP1 will reach the Venus surface before the remaining two small probes enter 90 minutes after large probe entry. This separation of the probe entry and descent allows each of the first set of probes to be tracked with two receivers at each DSN station. The second set of probes can also be tracked with two receivers at each station for the first 24 minutes of descent. At this time one receiver at each station will be tuned to cover the bus since bus science data rates during the last hour of the bus mission require 64-meter antenna gain. The bus is targeted to reach 1000-km altitude 18 minutes after the second set of probes reach the surface. The bus mission is completed approximately five minutes later.

Figure 4-5 illustrates the entry and descent sequence. Time is referenced to the nominal large probe entry time given above. The dual station coverage period of 3 hours 20 minutes indicated in Figure 4-5 assumes 15-degree elevation angle constraints. The large probe entry time was selected to occur 10 minutes after the beginning of the overlap period. The last event of the probe mission, bus demise, takes place 10 minutes before the end of the overlap period.

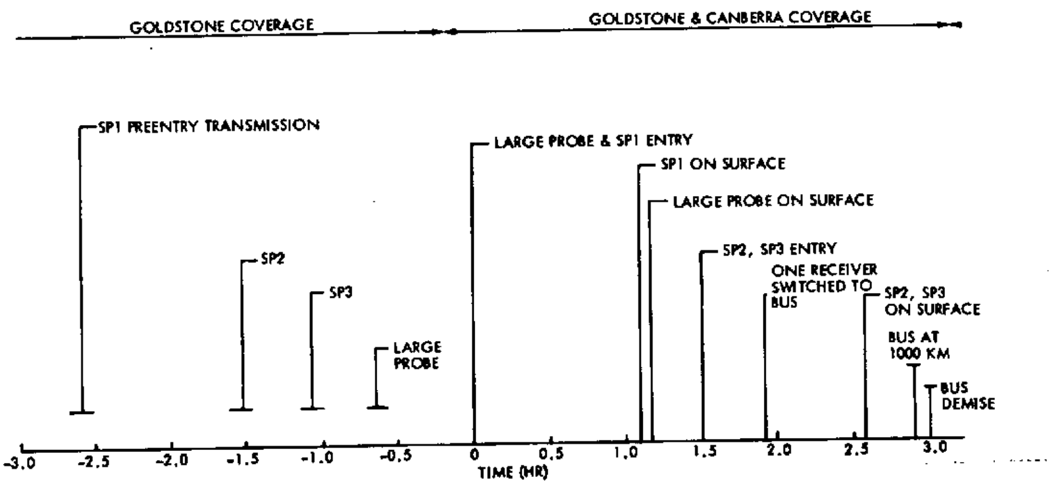

Figure 4-5. Probe Mission Entry and Descent Sequence

Figure 4-5 also illustrates the probe preentry transmission sequence. Each probe will transmit for 10 minutes with individual transmissions separated by at least 15 minutes. The last preentry transmission is completed 35 minutes before nominal large probe entry to allow time for the DSN stations to set up for entry of the large probe and first small probe.

4.1.1.5 Probe Entry and Descent Profiles

This section presents the detailed entry and descent profiles for the Atlas/Centaur baseline probe configurations. Table 4-4 lists the ballistic coefficients. Entry ballistic coefficients are hypersonic values while the descent coefficients are subsonic.

Table 4-4. Baseline Configuration Ballistic Coefficients

	LARGE PROBE	SMALL PROBE
ENTRY PHASE [KG/M^2(SLUG/FT^2)]	86.4(0.55)	141.4(.90)
PARACHUTE PHASE [KG/M^2(SLUG/FT^2)]	7.85(0.05)	--
DESCENT PHASE [KG/M^2(SLUG/FT^2)]	549.8(3.5)	198.0(1.26)

The large probe entry profile is shown in Figure 4-6. By definition the entry phase begins when the probe altitude is 250 km. At this altitude the atmospheric density is too low to produce significant drag forces. Drag forces begin to decelerate the probe at an altitude of approximately 110 km. The 50-g accelerometer switch trips 24.5 seconds after entry when the probe altitude is 92.20 km. The 50-g sensor trip starts the data handling system descent timer which controls all timed events through the remainder of the mission. The 50-g trip is also used to begin acquisition and storage of four-axis accelerometer data. Prior to this time only axial accelerometer data are taken and stored. Peak deceleration of 330 g occurs 2.2 seconds after the 50-g trip time. The dynamic pressure profile has the same shape as the deceleration profile shown in Figure 4-6. Maximum dynamic pressure of 2.8 x 10^5 N/m^2 (5848 psf) occurs at the same time as peak deceleration.

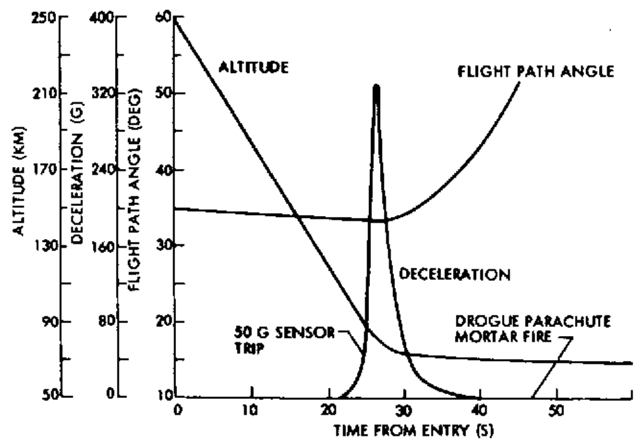

Figure 4-6. **Large Probe Entry Profile**

The large probe drogue parachute is deployed by mortar 21 seconds after 50-g increasing deceleration. At this time the probe altitude is 70.44 km and velocity is 187 m/s (Mach 0.78). The dynamic pressure is 1695 N/m^2 (35.4 psf). Figure 4-7 illustrates the parachute deployment and aeroshell separation phase of the large probe descent. Descent capsule velocity remains near the deployment value of 180 m/s until the parachute becomes inflated about 1 second after drogue parachute mortar fire. The aeroshell is released 5 seconds after mortar firing causing the slight slope change in the velocity curve. The altitude, velocity, and dynamic pressure at aeroshell release are 70.08 km, 43.2 m/s, and 95.8 N/m^2 (2.0 psf), respectively.

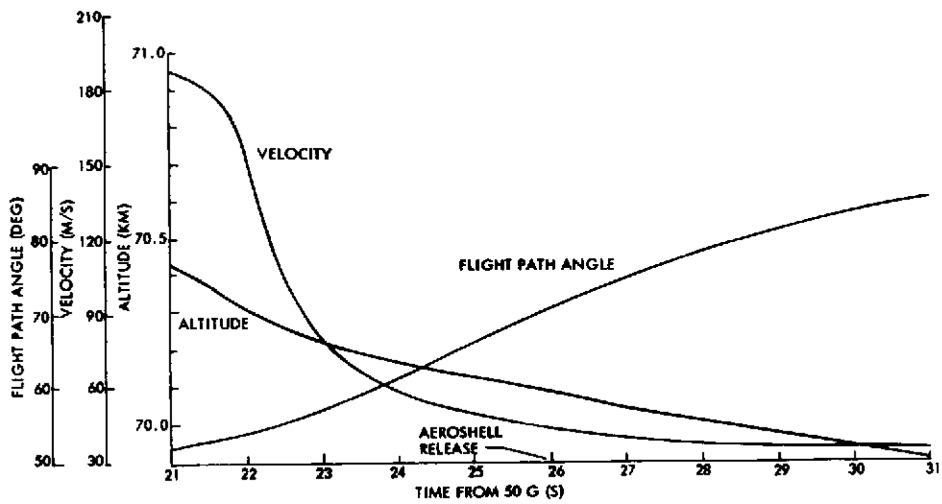

Figure 4-7. **Large Probe Parachute Deployment and Aeroshell Release**

The aeroshell release time of 5 seconds after drogue parachute mortar fire is based on the descent capsule dynamic response shown in Figure 4-8. The descent capsule pitch rate due to drogue parachute mortar fire, and main parachute opening load is well damped by 5 seconds after mortar fire. Figure 4-8 also shows the aeroshell/descent capsule separation distance. The increased pitch rate at 5 seconds is induced by aeroshell separation.

The large probe science instruments will be exposed to the atmosphere a few seconds after aeroshell release. The exact time depends on the descent capsule/aeroshell separation distance required for those instruments which are subject to contamination from ablative aeroshell material. At

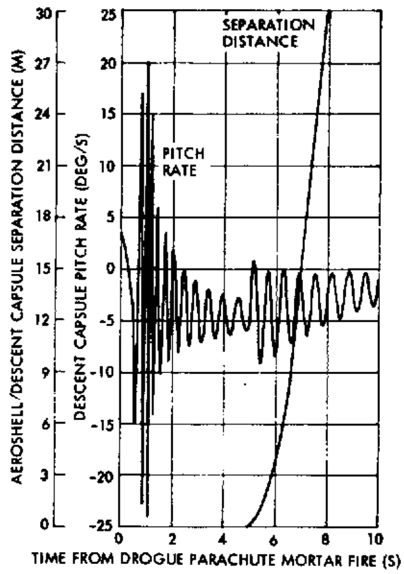

Figure 4-8. **Aeroshell Release Dynamics**

10 seconds after mortar fire the descent capsule altitude 69. 9 km and velocity is 33. 7 m/s. The separation distance between the aeroshell and descent capsule is approximately 73 meters at this time. The descent capsule flight path angle is 85 degrees and increases to 90 degrees (vertical descent) about 10 seconds later.

The remainder of the large probe descent trajectory is shown in Figure 4-9. The descent capsule remains on the parachute for 39. 5 minutes. Parachute release takes place at an altitude of 42. 9 km causing the descent velocity to increase from 5. 8 to 48 m/s. Approximately 34 minutes later, the descent capsule impacts the surface at a velocity of 12 m/s.

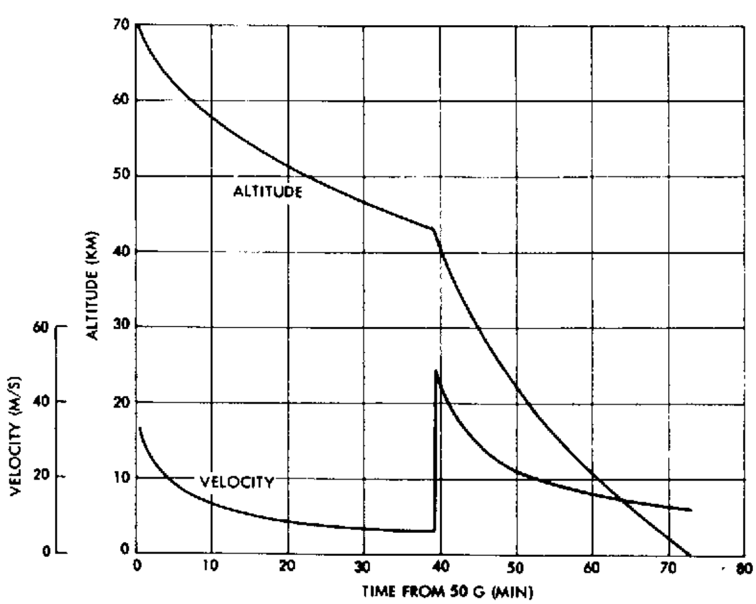

Figure 4-9. **Large Probe Descent Profile**

Small probe entry profiles for entry flight path angles $\left(\gamma_E\right)$ of -25 and -60 degrees are shown in Figures 4-10 and 4-11. These values of γ_E bound the small probe design range.

The small probes employ the same 50-g accelerometer switch used in the large probe to start the data handling system timer. The 50-g deceleration level occurs 16.2 seconds after entry for the γ_E = -60 degrees small probe and at 34.6 seconds after entry for the γ_E = -25 degrees small probe. Peak deceleration and dynamic pressure values are 486 g and 674×10^2 N/m^2 for the γ_E = -60 degrees probe, while the γ_E = -25 degrees probe values are 232 g and 322×10^2 N/m^2.

Small probe descent science instruments (pressure, temperature, and nephelometer) are exposed to the atmsophere 16 seconds after the 50-g deceleration level. The altitude and Mach number at this time are 66.0 km and 0.70 for the γ_E = -60 degrees probe, and 71.4 km and 1.5 for the γ_E = -25 degrees probe.

The descent trajectory profile for the γ_E = -60 degrees small probe is shown in Figure 4-12. The profile for the γ_E = -25 degrees small probe is virtually identical except for the first minute when the altitude and descent velocity are slightly higher. The small probe impacts the Venus surface 65 minutes after entry at a velocity of 7.4 m/s.

4.1.1.6 Probe Mission Doppler Profiles

Figure 4-13 shows the large probe preentry Doppler rate profiles for the DSN tracking stations. The preentry Doppler rate profiles for the small probes and bus are very similar to the large probe profiles. The 10-minute preentry probe communication will take place between 3 hours before entry to 0.5 hours before entry. The Doppler rate is less than 7 Hz/s for all probes during this time interval.

The large probe Doppler rates during descent are shown in Figure 4-14. As soon as the large probe parachute becomes inflated (near 70-km altitude) the Doppler rates drop to less than 0.6 Hz/s. The spikes in the rates near 40 minutes are caused by the step increase in descent velocity at parachute release. Figure 4-15 shows the Doppler rate profiles for small probe 3 as a function of time from 70-km altitude. The profiles for the other two small probes are similar. The rates decrease to less than 1 Hz/s after 3 minutes. The small probe altitude at this time is approximately 54 km. The Doppler rates change from positive to negative values near 10 minutes after 70 km altitude causing the Doppler rate magnitude variation shown in Figure 4-15.

4.1.2 Orbiter Mission Profile

The preferred orbiter mission is flown during the 1978 Type II (early) opportunity to reduce the size of the insertion burn and to simplify the launch operational sequence. The orbit selected for the mission is a posigrade (with respect to Venus rotation) orbit having a 24-hour period at an inclination of 62 degrees to the Venus orbit plane. The periapsis altitude is maintained between 200 and 400 km nominally during the 225-day mission, requiring four trim maneuvers and 44 m/s total trim budget. The orbiter is flown in an earth-pointing attitude throughout the mission to facilitate the required data rates of the mission.

4.1.2.1 Accommodation with Probe Mission

Some minor adjustments must be made in the orbiter mission sequence to accommodate the probe mission, which arrives five days after the orbiter mission. The separation (86 days) between launch periods allows a very comfortable interval to refurbish the launch pad and prepare for the probe mission launch. The arrival times of the two missions are unavoidably close to each other, necessitating a rather intense period of operational activity in mid-December 1978. The details are summarized in Figure 4-16. The third midcourse for the orbiter mission is scheduled on November 12, 1978, before the probe mission approach activity begins. Three days of tracking follow the probe bus retargeting maneuver before a final orbiter trajectory refinement maneuver is performed three days before Venus orbit insertion. This is an attractive time to schedule such a maneuver since the spacecraft tracking improves significantly about 10 days before arrival. After insertion the bus is tracked and placed into a "safe" orbit at the initial trim (IT) for the preentry through descent portion of the probe mission. After the bus entry all operational attention is returned to the orbiter mission for the remainder of its 225-day mission.

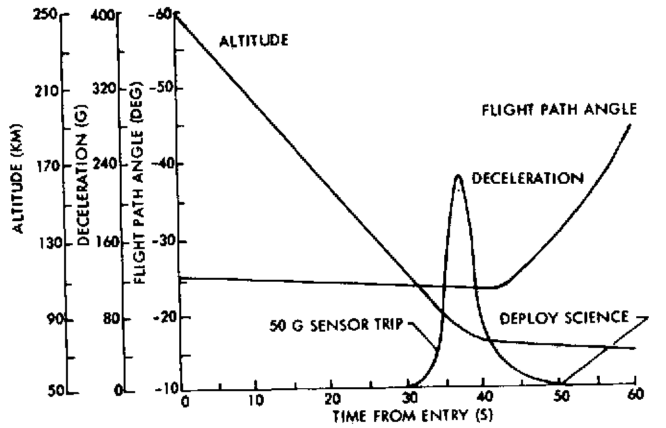

Figure 4-10. Small Probe Entry Profile ($25^0 \gamma_E$)

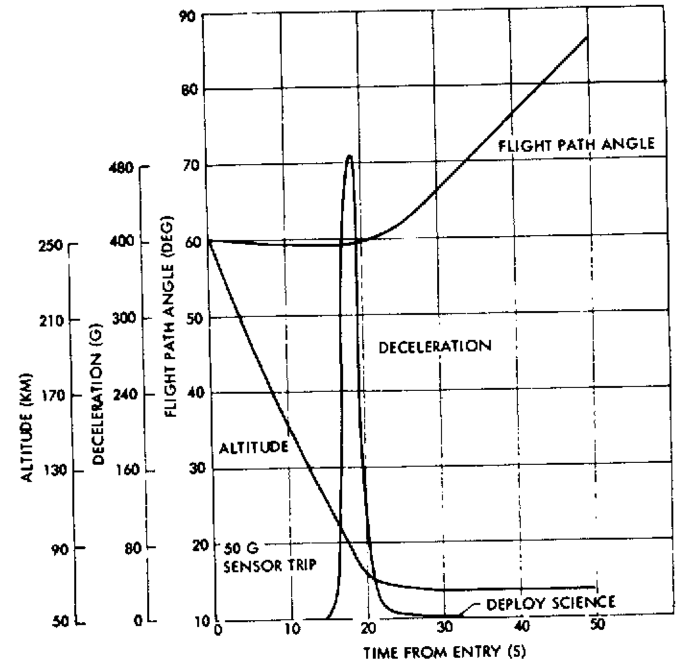

Figure 4-11. Small Probe Entry Profile ($60^0 \gamma_E$)

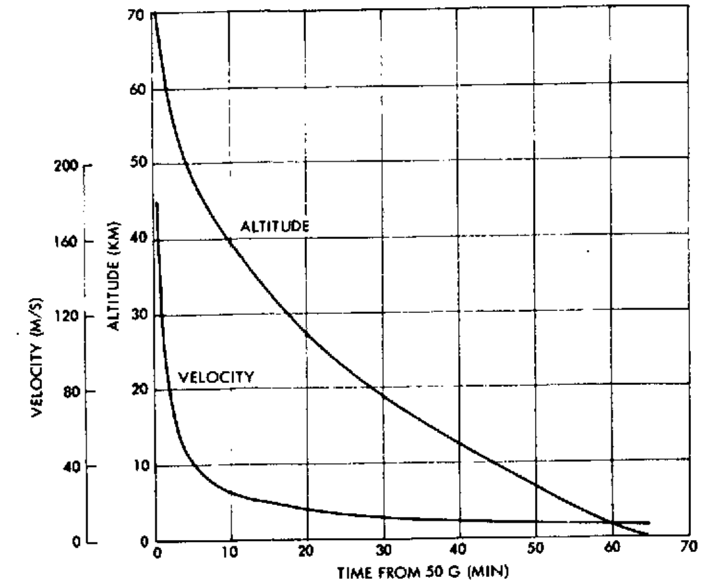

Figure 4-12. Small Probe Descent Profile, γ_E = -60 Degrees

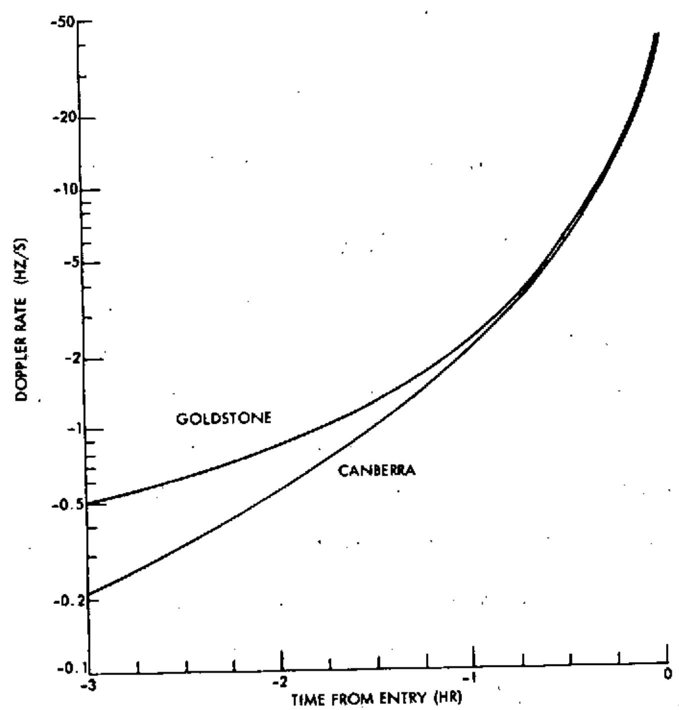

Figure 4-13. Large Probe Preentry Doppler Rates

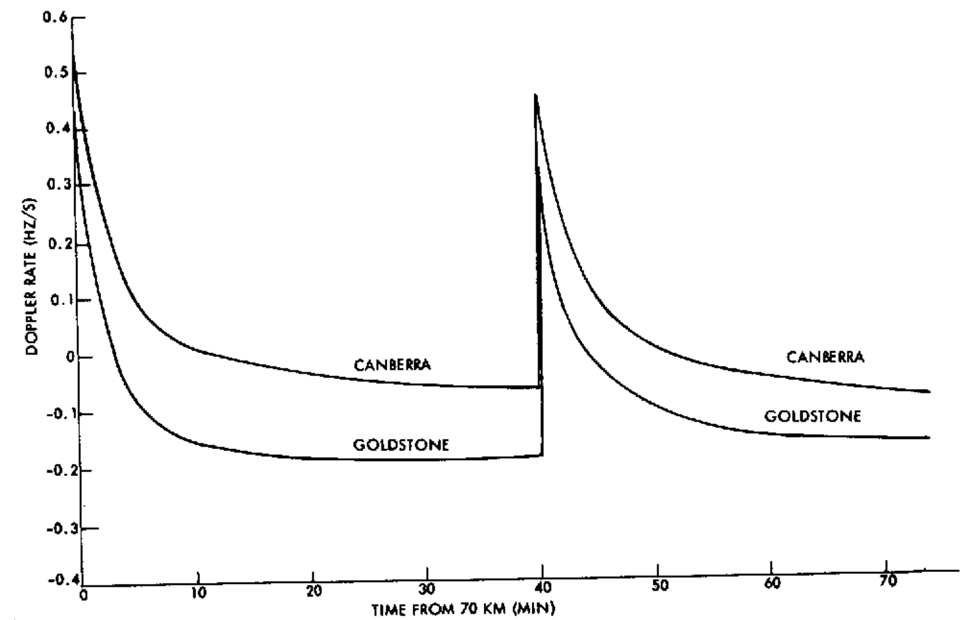

Figure 4-14. Large Probe Descent Doppler Rates

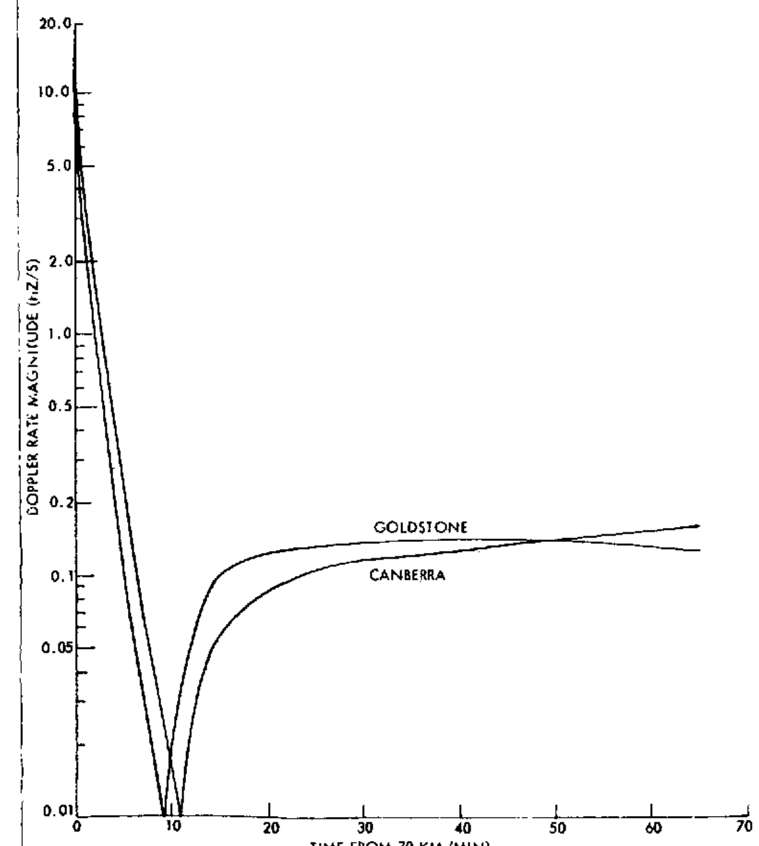

Figure 4-15. Small Probe 3 Descent Doppler Rates

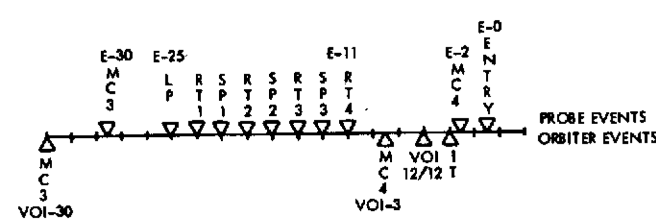

Figure 4-16. Dual Mission Sequencing

FOLDOUT FRAME

FOLDOUT FRAME

4.1.2.2 Launch Profile

The departure geometry for the 1978 Type II orbiter mission is shown in Figure 4-17. Note that injection occurs very near the subsolar point with the departure velocity vector nearly normal to the sun line. The higher launch C_3 results in a wider angle between the V_∞ line and the departure point, compared to the Type I launch (Section 4.1.1.1). With the Atlas/Centaur launch the vehicle orients the spacecraft to an attitude that will be earth pointing after about 5 days of an inertially fixed cruise attitude.

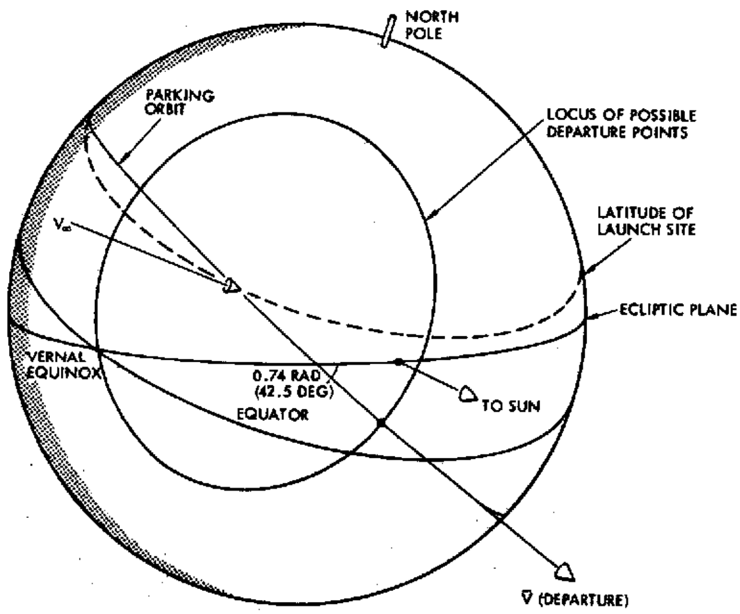

Figure 4-17. 1978 Orbiter Type 2 Departure Geometry (May 26 Launch 14:15:00 GMT)

4.1.2.3 Interplanetary Phase

The interplanetary trajectory is summarized in Table 4-5 and illustrated in 5-day increments in Figure 4-18. Relevant interplanetary parameters are profiled in Figure 4-19. The launch and arrival dates were selected on the basis of optimizing final weight in orbit. The arrival time of 1900 GMT (on December 12, 1978) is selected to obtain maximum elevation from both Canberra and Goldstone as indicated in Figure 4-20.

The nominal midcourse sequence is included in Table 4-6, which supplies the maneuver budget for the entire orbiter mission. The very accurate Atlas/Centaur vehicle results in a very small midcourse budget. The trim budgets are discussed in more detail below.

Table 4-5. Interplanetary Trajectory

LAUNCH PERIOD	5/24/78 TO 6/2/78
ARRIVAL DATE	12/12/78
TRIP TIME	202 TO 193 DAYS
C_3	19.99 KM^2/SEC^2
V_{HP}	3.29 TO 3.22 KM/SEC
RANGE AT VOI	59.9×10^6 KM

Table 4-6. Maneuver Budget for Orbiter Mission

TIME	MANEUVER	ΔV (M/S)	PRECESSION (DEG)	SPIN RATE (RPM)
L + 5	FIRST MIDCOURSE (a)	13	300	4.8
L + 15	SECOND MIDCOURSE	1	300	4.8
VOI-30	THIRD MIDCOURSE	2	300	4.8
VOI-3	FOURTH MIDCOURSE	1	300	4.8
VOI	INSERTION (SRM)	(923)	160	TBD*
VOI + 1	INITIAL TRIM	10	320	TBD
VOI + 30	FIRST PERIAPSIS MAINTENANCE (PM) TRIM	13	160	TBD
VOI + 60	SECOND PM TRIM	10	150	TBD
VOI + 148	THIRD PM TRIM	13	100	TBD
VOI + 175	FOURTH PM TRIM	9	140	TBD
	TOTAL (b)	72	2230	TBD

(a) INCLUDES 8 M/S FOR INJECTION COVARIANCE PLUS 5 M/S FOR INJECTION FIGURE OF MERIT

(b) TOTAL ΔV EXCLUDES VOI BUDGET (SRM)

*TO BE DETERMINED

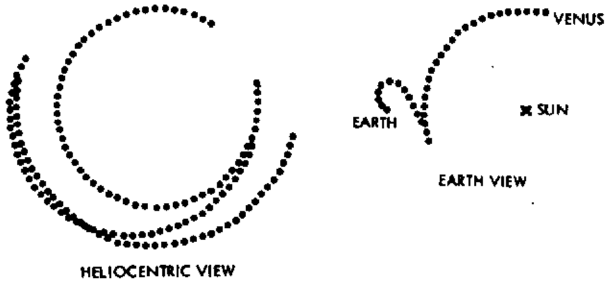

Figure 4-18. Interplanetary Transfer

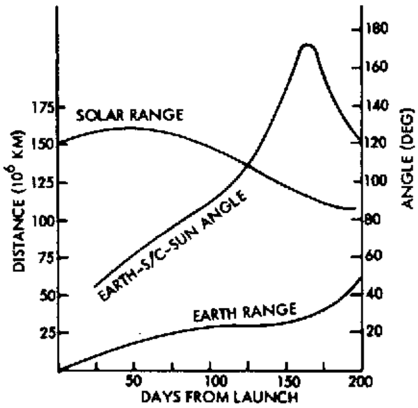

Figure 4-19. Interplanetary Cruise Parameters

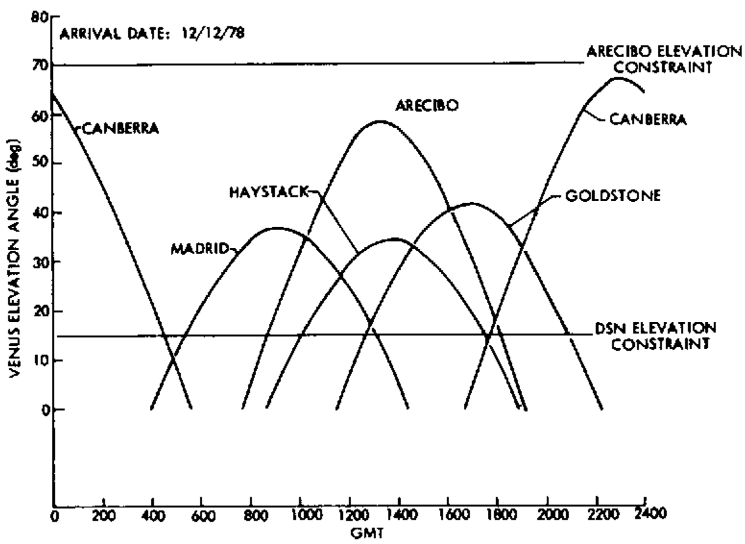

Figure 4-20. Tracking Station Coverage for Orbiter Mission

4.1.2.4 Orbit Insertion

The nominal pariapsis time on the approach hyperbola is 1900 hours on December 12, 1978. The solid rocket retro burn is sized to decrease the periapsis velocity by 923 m/s. The insertion fuel is sized to provide the ΔV required to insert the orbiter into a 24-hour orbit if launch occurs on the last day of the launch period (having the least excess approach velocity of 3.22 km/s) and if the spacecraft arrives with the entire midcourse budget exhausted. The orbiter enters earth occultation 4.4 minutes prior to periapsis (see Figure 4-21) and reappears to earth 15.2 minutes after periapsis.

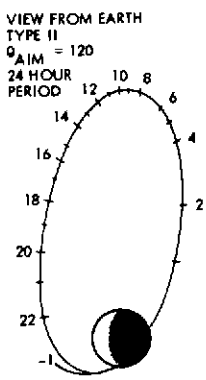

Figure 4-21. Initial Orbit

4.1.2.5 Insertion Dispersions and Initial Trim

An additional orbit trim budget must be allocated because of approach condition variations and insertion maneuver dispersions. If launch occurs on the day having the largest V_{HP} of 3.29 km/s (first day of launch period) the orbiter will be inserted into a 26.1-hour orbit. If all the midcourse budget remains (an orbiter weight increase of 2.9 kg) and launch occurs on the first day of the period, the initial period will be increased to 26.7 hours. The initial orbit dispersions (99 percent) caused by tracking uncertainties prior to the final midcourse, tracking uncertainties prior to loading the insertion burn, and execution errors during the burn itself (assuming three-sigma errors in the delivered ΔV of 1 percent proportionality, 2-degree pointing, and 0.5 degrees velocity degradation caused by coning) are 85 km in periapsis altitude and 0.55 hours in initial period. An initial trim budget of 10 m/s is allocated to correct the initial orbit variations caused by the variation in arrival V_{HP} and dispersions. The trim required to correct for any extra weight in midcourse fuel may be performed with the excess fuel.

4.1.2.6 Orbiter Profiles

The selected orbit is based on the Type I transfer with θ_{AIM} = 120 degrees and having a period of 24 hours, summarized in Table 4-7. The hyperbolic approach and initial orbit as viewed from earth at the date of encounter is illustrated in Figure 4-21 with time ticks representing one

Table 4-7. Preferred Orbit Elements

SEMIMAJOR AXIS	39 457 KM		
ECCENTRICITY	0.83653		
PERIAPSIS RADIUS	6450 KM (UPPER BOUND)		
APOAPSIS RADIUS	45 907 KM		
	SUBSOLAR ORBITAL PLANE	EQUATORIAL PRIME MERIDIAN	ECLIPTIC VERNAL EQUINOX
INCLINATION (DEG)	119.0	64.5	117.8
LONGITUDE OF ASC NODE (DEG)	-94.5	-171.6	-173.1
ARGUMENT OF PERIAPSIS (DEG)	-51.0	129.1	-47.4

hour intervals from VOI. The entire mission geometry for 243 days is illustrated in Figure 4-22. The view is from a point 30 degrees above the ecliptic plane and opposite the earth position at VOI. The orbit and its projection onto the Venus surface are indicated; the evolving positions of the earth and sun are illustrated at 30 day intervals. The earth and solar distances may be compared from the figure as they are illustrated with common scales; the planet and spacecraft orbit are pictured with a different scale. Periods during which portions of the spacecraft orbit are occulted by the planet from the earth and sun are also illustrated.

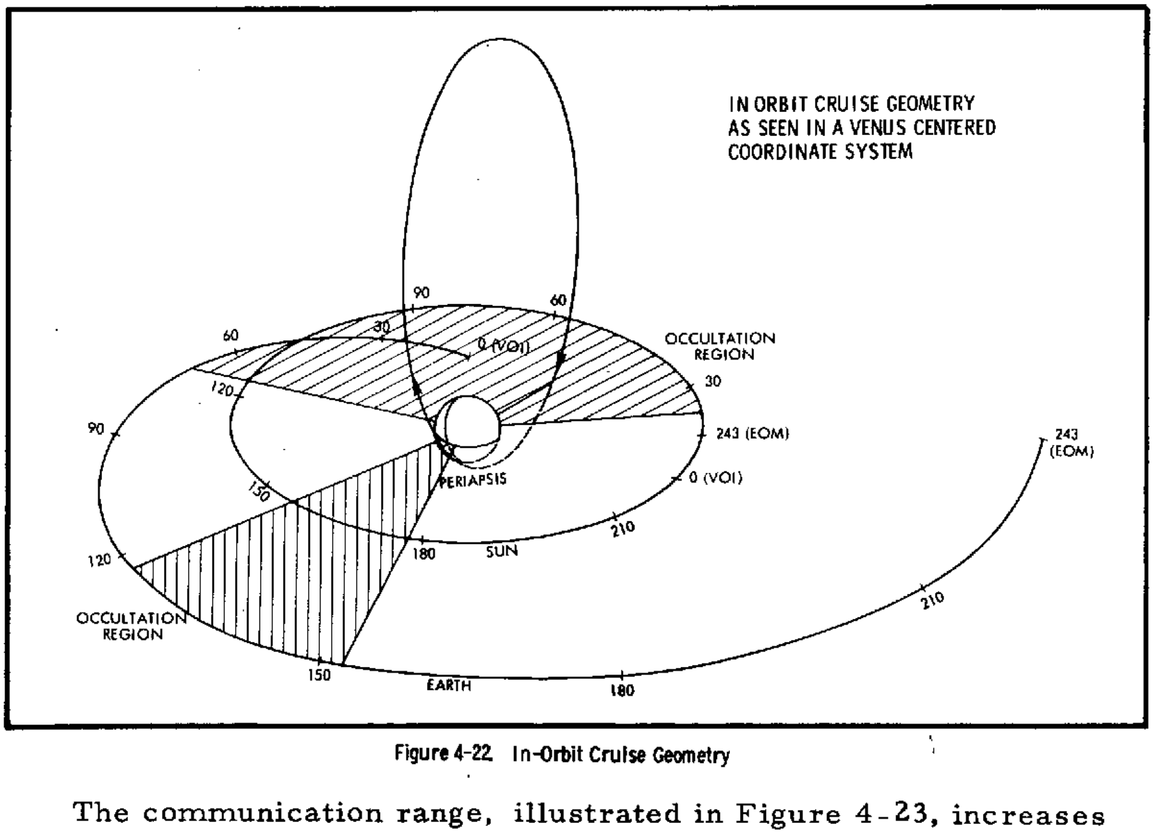

Figure 4-22 In-Orbit Cruise Geometry

The communication range, illustrated in Figure 4-23, increases from 0.4 to 1.7 AU during the in-orbit cruise. The geocentric declination of Venus during the course of the mission is also demonstrated there.

The periapsis altitude profile is summarized in Figure 4-24. The periapsis altitude is controlled between 200 and 400 km, requiring a trim ΔV budget of 44 m/s with trims nominally scheduled for 30, 60, 148 and 175 days after VOI.

The attitude profile is provided in Figure 4-25. The nominal cruise attitude is earth pointing. The attitudes required for axial thrusting during the periapsis maintenance maneuvers are also depicted in terms of solar and earth aspect angles. All maneuvers are designed to keep the sun in the forward hemisphere of the orbiter. The angle of attack at periapsis and at 1000 km on both sides of periapsis are indicated in Figure 4-26.

The occultation profiles are illustrated in Figures 4-27 and 4-28. In the first figure the portions of the orbit within occultations are noted; in the second the durations of the occultations are indicated. Periapsis begins in earth occultation but moves out after 68 days, two days before the earth occultation period ends. Periapsis is initially in the sun, moving into solar occultation after 32 days and remaining there for the next 82 days. Short periods of larger peak values of earth and solar occultations occur late in the mission as indicated.

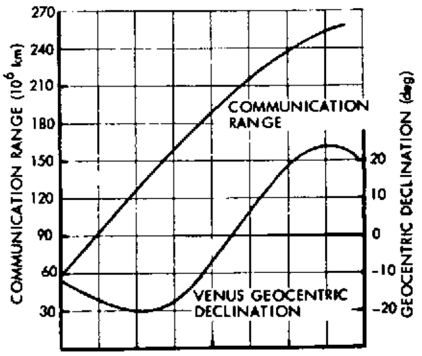

Figure 4-23. **Earth-Venus Parameters During Orbit Phase**

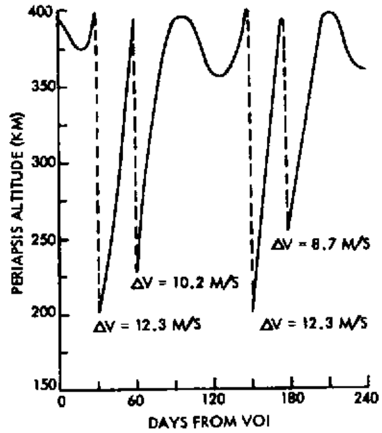

Figure 4-24. **Periapsis Altitude Profile**

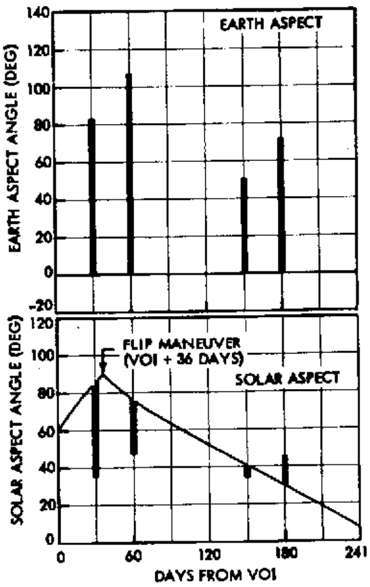

Figure 4-25. **Orbiter Attitude Profile**

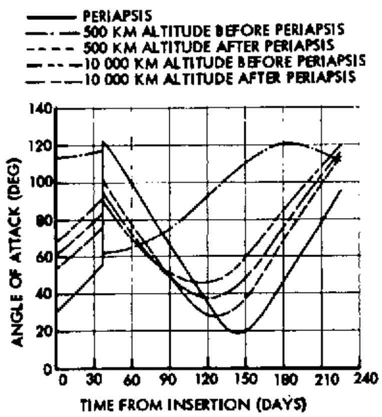

Figure 4-26. **Angle-of-Attack Profile**

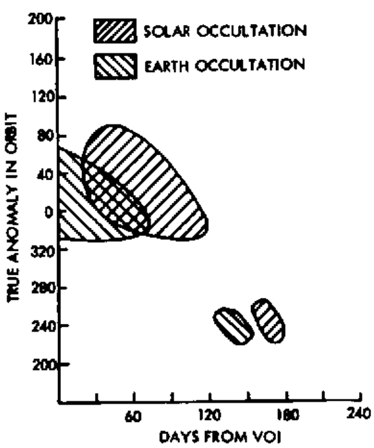

Figure 4-27. **Occulted Regions**

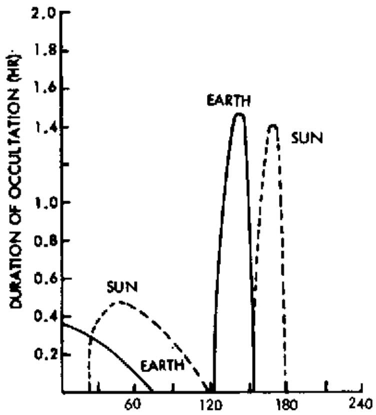

Figure 4-28. **Occultation Duration**

4.2 MISSION OPPORTUNITY ANALYSIS

The critical features of probe or orbiter missions are established by the selection of the launch date/arrival date (LD/AD) combination. This section reviews the characteristics of probe and orbiter missions to Venus in 1977 and 1978 with emphasis on dual-launched missions in 1978. Both standard ballistic transfers and nonstandard transfers (broken-plane and looper trajectories) are considered in the analysis. In addition, the mission impact of using the Thor/Delta or the Atlas/Centaur launch vehicle is compared.

4.2.1 Standard Ballistic Transfers

The optimal ballistic transfer for either probe or orbiter missions would be a 180-degree transfer between rays representing earth at the launch data and Venus at the arrival date. This transfer would have a launch energy C_3 of 6.25 km^2/s^2 and an arrival excess velocity V_{HP} of 2.66 km/s. Such a transfer is rarely possible since it would require an LD/AD combination in which the arrival date has Venus passing through the ecliptic plane and the launch date 147 days earlier (the Hohman transfer time) has earth 180 degrees from the arrival ray. Normally, near 180-degree transfers are impractical because slight out-of-plane effects at arrival cause the transfer plane to be highly inclined to the ecliptic plane, resulting in excessive launch energy requirements. However, a knowledge of the optimal values of C_3 and V_{HP} does give perspective to the actual values achieved in the 1977 and 1978 launch opportunities.

The launch vehicle performance for the Thor/Delta and Atlas/Centaur vehicles is summarized in Figure 4-29. The relative steepness of the performance curves should be noted as it affects the LD/AD trades for the two vehicles.

4.2.1.1 1978 Probe Mission

The launch energy and approach velocity contours for the 1978 opportunity are illustrated in Figure 4-30. An important feature of the 1978 opportunity is that a large portion of the Type II missions is eliminated by the contraint on the declination of launch azimuth (DLA) to less than 36 degrees in absolute value without overflying Brazil or using dogleg boost trajectories. This constraint divides the Type II opportunity into two

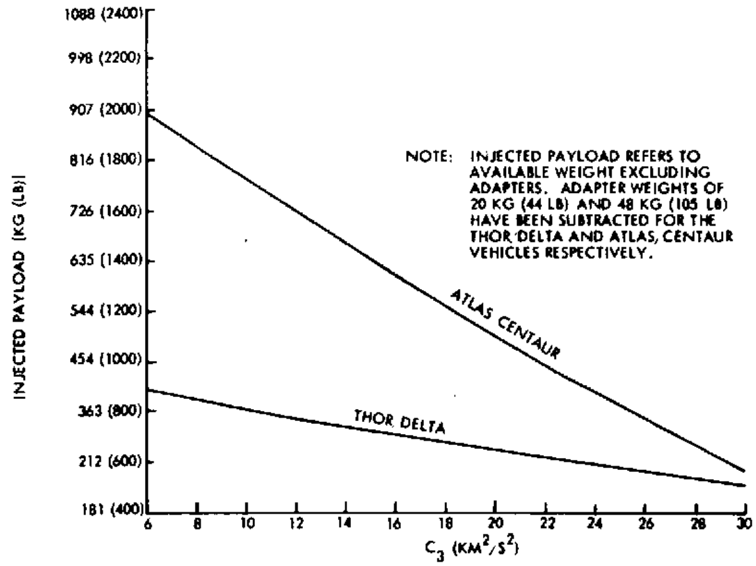

Figure 4-29. Launch Performance for Thor/Delta and Atlas/Centaur Vehicles

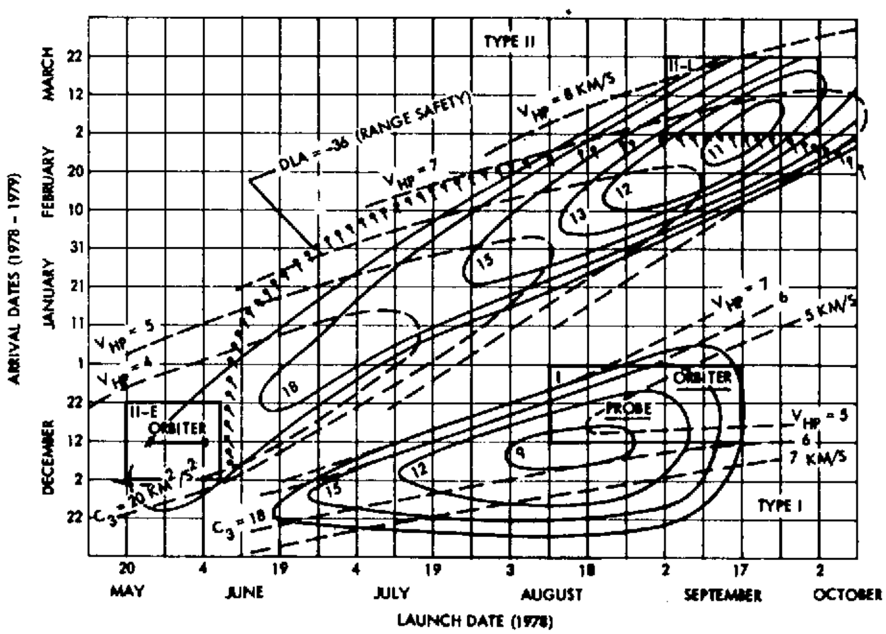

Figure 4-30. 1978 Mission Contours

candidate regions abutting the DLA = 36 degrees contour: the Type II-Early (II-E) region in the lower left hand corner and the Type II-Late (II-L) area in the upper right hand corner.

The primary considerations for the probe mission are to maximize the injected weight (minimize C_3) and minimize the entry velocity V_E $\left(\text{related to the approach velocity by } V_E = \sqrt{2\mu / r_E + V_{HP}^2}\right)$. The entry velocity is of critical importance since it directly affects the peak entry load factor (proportional to V_E^2) and the peak entry heating rates (convective approximately proportional to V_E^3 and radiative proportional to V_E^{α}, $\alpha > 7$). In addition, non-equilibrium radiative heating starts becomming important at $V_E \sim 12$ km/s (40 000 ft/s). The considerations have led to the imposition of a constraint limiting entry velocities to less than 11.3 km/s (37 200 ft/s).

The mission performance for the three candidate opportunities are compared in Table 4-8. The Type II-E mission may be immediately eliminated from consideration since it obtains 238 kg (525 lb) less injected weight (Atlas/Centaur) than the other two opportunities. Of the remaining candidates, the Type I mission is clearly preferred because it results in acceptable entry velocities while obtaining comfortable injected weight performance. The Type II-L mission has both larger entry velocities (12.1 vs 11.3 km/s) and poorer weight performance than the Type I. In addition the earth-Venus communication range at entry for the Type II-L opportunity is more than twice that of the other missions, resulting in severe penalties in RF transmitter power, associated battery weight, and internal thermal control.

Table 4-8. 1978 Probe Mission Performance

	TYPE I	TYPE II-E	TYPE II-L
LAUNCH PERIOD	8/20-8/29	5/26-6/4	9/16-9/25
ARRIVAL DATE	12/17/78	12/12/78	3/6/79
TRIP TIME	119-110	200-191	171-162
MAXIMUM C_3 $(KM/S)^2$	9.8	19.6	11.2
MAXIMUM V_{HP} (KM/S)	5.0	3.3	6.8
MAXIMUM V_E [KM/S (FT/S)]	11.3 (37 200)	10.7 (35 000)	12.1 (39 400)
COMMUNICATION RANGE (10^6 KM)	64.9	59.9	153.6
INJECTED WEIGHT [KG (LB)]			
THOR/DELTA	366 (805)	291 (640)	355 (780)
ATLAS/CENTAUR	781 (1730)	508 (1120)	746 (1645)

The probe targeting characteristics of the 1978 Type I and Type II-L opportunities are illustrated in Figure 4-31. Contours of entry flight path angles γ_E of -25 and -45 degrees and earth communication angles (during descent) of 55 degrees are illustrated on the figure for reference. The targeting capability for either opportunity is quite acceptable, offering good latitude and longitude coverage for reasonable entry angles. The Type I mission has good southern hemisphere coverage in both sunlight and darkness, while the Type II-L mission has good sunside coverage.

The preferred opportunity for the probe mission is thus the Type I opportunity; the selected launch and arrival dates were noted on Figure 4-30.

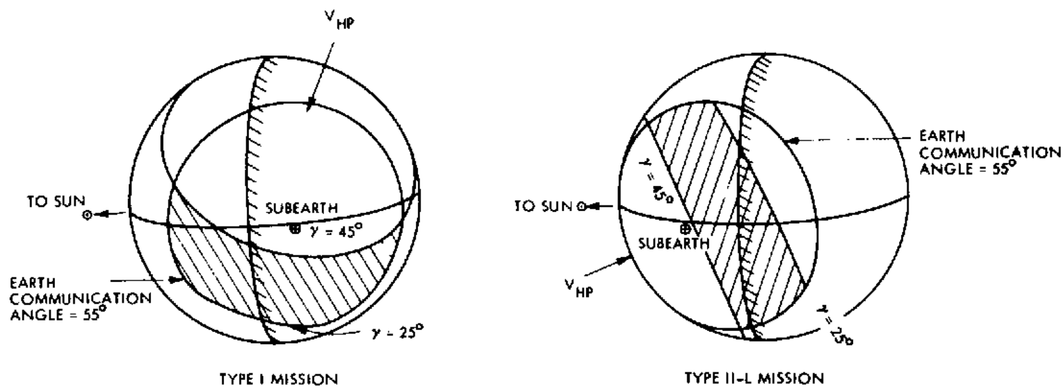

Figure 4-31. 1978 Mission Probe Targeting

4.2.1.2 1978 Orbiter Mission

The selection of the LD/AD combination for the orbiter mission must consider not only the performance of the orbiter mission but also the accommodation with the probe mission to be launched in the same year. The candidate regions for LD/AD selection in 1978 are again the Type I, the Type II-Early, and the Type II-Late opportunities identified in Figure 4-30. The performance of the optimal mission of each region is compared in Table 4-9.

Table 4-9. 1978 Orbiter Mission Performance

	TYPE I	TYPE II-E	TYPE II-L
LAUNCH PERIOD	9/4-9/13	5/26-6/4	9/20-9/29
ARRIVAL DATE	12/25/78	12/12/78	3/7/79
TRIP TIME (DAYS)	112-103	200-191	150-159
LAUNCH SEP./ARRIVAL SEPARATION[a] (DAYS)	+6/+8	-86/-5	+31/+70
MAXIMUM C_3 $(KM/S)^2$	15.9	19.6	11.0
V_{HP} VARIATION (KM/S)	4.66/4.41	3.29-3.22	6.76-6.74
ΔV_{VOI}[b] (M/S)	1344	921	2482
COMMUNICATION RANGE (10^6 KM)	73.3	59.9	153.8
WEIGHT IN ORBIT[c] [KG (LB)]			
THOR/DELTA	183 (404)	190 (418)	120 (265)
ATLAS/CENTAUR	342 (755)	342 (755)	247 (545)

(a) SEPARATION REFERS TO TIME SEPARATION RELATIVE TO THE 1978 PREFERRED PROBE MISSION WHICH HAS A LAUNCH PERIOD OF 8/20-8/29 AND AN ARRIVAL DATE OF 12/17/78.

(b) INSERTION ΔV SIZED FOR MINIMUM V_{HP} OVER 10 DAY LAUNCH PERIOD

(c) WEIGHT IN ORBIT BASED ON VOI MOTOR HAVING I_{SP} = 286 SECONDS, λ = 0.88 AND ORBIT PERIOD OF 24 HOURS, PERIAPSIS ALTITUDE OF 400 KM.

The LD/AD combinations selected for the Type II-Early and Late missions produce the maximum weight-in-orbit (injected weight minus the total of midcourse budget and orbit insertion fuel and tankage) consistent with the range safety constraint. The optimal Type II-Late mission suffers from inferior performance relative to the other types providing 95 kg (210 lb) less weight-in-orbit than the other opportunities. It is therefore dismissed from further discussion. The optimal Type I orbiter mission was selected with recognition of the complexity and cost associated with simultaneous launch and arrival of the probe and orbiter missions if both are flown on Type I missions. The Type I mission was therefore selected to obtain the maximum separation in launch and arrival dates from the preferred probe mission while achieving the same weight-in-orbit performance as the Type II early mission.

Both the Type I and Type II-E opportunities offer attractive possibilities for the orbiter mission. Section 3 discussed the science performance of both missions and the rationale for the preference of the Type II-E mission from science considerations. As explained above, the net weight-in-orbit is identical for the two missions assuming an Atlas/Centaur vehicle. The lower V_{HP} associated with the Type II-E orbit does produce a 40 percent decrease in the insertion magnitude, resulting in slight decreases in mission risk and structural requirements. The communication range at Venus orbit insertion is 20 percent less for the Type II-E mission, resulting in another advantage for that option. The geometry of the Type II-E mission also results in better tracking during approach for that mission (discussed in more detail in Section 4.4). The Type II-E does have a hidden insertion for all orbits (see Section 4.4) while the Type I insertion is visible from earth for θ_{AIM}'s between 30 and 210 degrees. However, the hidden insertion is comfortably accommodated for the Type II mission. Another advantage to the Type I mission is its nearly halved trip time relative to the Type II-E option.

The mission operations comparison of the surviving candidates indicates a significant advantage in going Type II-E in terms of launch operations while a slight advantage accrues to the Type I mission because of planetary encounter operations. The Type II-E mission launch period is separated from the preferred probe mission (Type I) launch period by three months, thereby obtaining a comfortable interval to refurbish the launch pad and prepare the second vehicle for launch. However if both the probe and orbiter missions are flown with Type I trajectories there is no way to obtain a reasonable separation between launches and get reasonable injected weights. Thus selection of the Type I mission would require two separate pads at launch plus much overlapping activity to accommodate the nearly simultaneous launches.

Typical schedules for the planetary encounter operations (assuming sequential release) are compared in Figure 4-32. The operational activity will be intense for either mission at encounter because probe entry and orbiter VOI occur within 5 or 8 days of each other. The Type II-E orbiter mission is slightly more complicated because the orbiter arrives first, requiring the orbiter final midcourse, VOI, and initial trim operations to be performed between the bus retarget maneuver at E-11 days and probe entry. These maneuvers and the tracking for them therefore must be performed in a fairly tight schedule. The Type I orbiter mission alleviates some of the problems by delaying most of the orbiter activity until after the probe mission is completed.

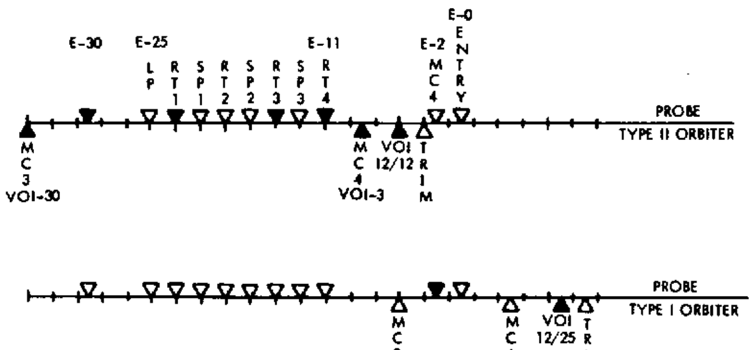

Figure 4-32. Operational Time Lines for Type I and Type II-E Options

In summary, the Type II-E mission is preferred for the orbiter mission because it has the better science, smaller VOI ΔV magnitude, smaller communication range at VOI, better tracking characteristics, essentially identical weight-in-orbit, and has simpler launch support requirements (single launch pad). However the Type I opportunity is also acceptable and may provide a convenient back-up to the Type II launch.

4.2.1.3 1977 Probe Mission

The Earth departure (C_3) and Venus approach (V_{HP}) energy contour for the 1977 launch opportunity are shown in Figure 4-33. Comparison of the Type I and Type II contours in Figure 4-33 shows that the Type I miss is clearly preferable based on the lower C_3 and V_{HP} within the desired en velocity V_{HP} constraint.

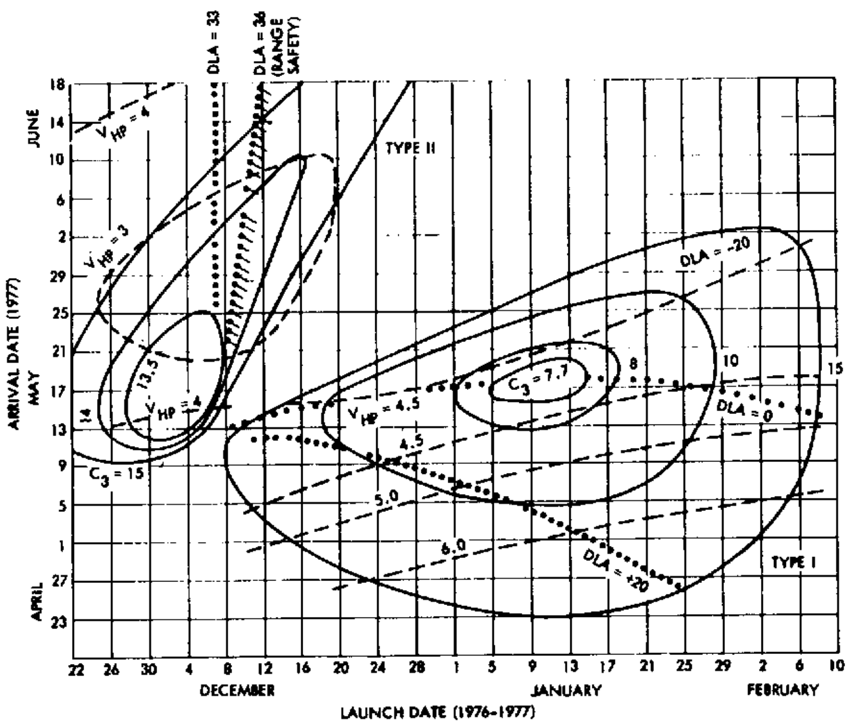

Figure 4-33. 1977 Mission Contours

The performance capability and optimum 10-day launch period is summarized in Table 4-10 for both the Type I and Type II missions. The Type I mission provides 13 percent more injected weight for the Thor/Delta launch vehicle and 25 percent more for the Atlas/Centaur. The cost is an increase in entry velocity of 300 m/s, an acceptable number.

Table 4-10. 1977 Probe Mission Performance

	TYPE I	TYPE II
LAUNCH PERIOD	1/5-1/14	11/28-12/7
ARRIVAL DATE	5/17/77	5/17/77
TRIP TIME (DAYS)	132-123	
MAXIMUM C_3 $(KM/S)^2$	7.7	13.5
MAXIMUM V_{HP} (KM/S)	4.4	3.6
MAXIMUM V_E [KM/S (FT/S)]	11.1 (36 300)	10.8 (35 400)
COMMUNICATION RANGE (10^6 KM)	70.8	70.8
INJECTION WEIGHT [KG (LB)]		
THOR-DELTA	386 (850)	336 (740)
ATLAS/CENTAUR	850 (1870)	680 (1495)

The relative approach geometries and allowable targeting areas for the Type I and Type II missions are summarized in Figure 4-34. The constraints used in defining the targeting area indicated are entry flight path angles between 25 and 45 degrees and Earth communication angle of 55 degrees. With these constraints, the Type I targeting area is a crescent' which satisfies all science targeting requirements. The corresponding Probe-bus targeting area is discussed in detail in Section 4.4.5.2.

The Type II mission targeting analysis shown in Figure 4-34 shows no targeting area which satisfies the above constraints. Use of the Type II mission would require entry flight path angles up to approximately -60 derees with the associated increase in entry load factor, heating rates and shear, and lower descent science deployment altitudes.

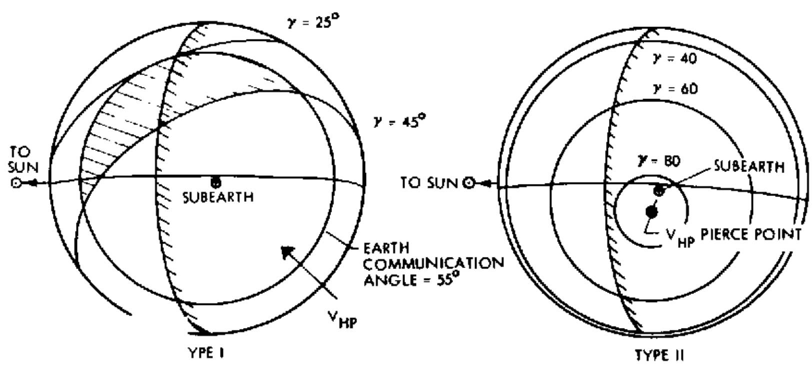

Figure 4-34. 1977 Mission Probe Targeting

All of the above considerations result in the preference for the Type I mission for the 1977 probe mission. It provides both good science coverage and higher allowable system weight than the most favorable Type II mission.

4.2.2 Nonstandard Transfers

The values of launch and arrival energy of the 1977 and 1978 ballistic transfers discussed above demonstrates the degradation in performance (relative to the Hohman transfer - Section 4.2.1) caused by non-optimal geometry. In certain cases nonstandard transfers have better energy characteristics than the simple ballistic transfers available at a given time. Broken plane and looper trajectories have been evaluated for possible enhancement of the Pioneer Venus missions.

A broken plane transfer is used to obtain a near 180-degree transfer without the large launch energy penalty associated with a high inclination transfer. The spacecraft is injected onto a nearly ecliptic transfer and a maneuver is performed approximately midway from earth to Venus to target the spacecraft for Venus at the arrival date. Thus, both legs of the transfer have relatively low inclinations. Both the 1977 and 1978 opportunities were assessed for potential gains of a broken plane transfer. The results are summarized in Figure 4-35 for the 1978 opportunity with similar conclusions holding for the 1977 mission. The analysis demonstrates the performance for a fixed arrival date (16 December 1978) and launch dates spanning the Type I and Type II opportunities. As indicated, the optimal broken plane performance never exceeds either the Type I or Type II maxima. However, it offers significant improvement in the near - 180 degree region where the ballistic transfers are severely degraded. However, since there is no necessity to extend the launch period, broken plane trajectories offer no substantial advantages for the current mission definition.

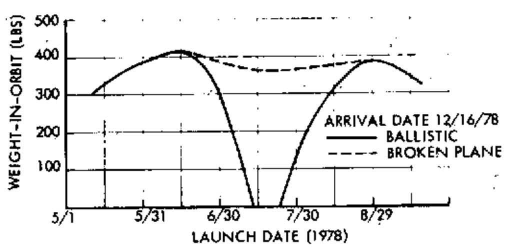

Figure 4-35. **Broken Plane Performance**

A second possibility of improving mission performance is through the use of a "looper" trajectory. In a looper trajectory the spacecraft is injected onto an ellipse intersecting the Venus orbit. Instead of encountering Venus at the first opportunity (as in a standard ballistic transfer) the spacecraft "waits" in the heliocentric ellipse one period until the second encounter when Venus also arrives at the intersection point. The possibility then exists to have an arrival date at which Venus is near the ecliptic plane and earth is 180 degrees from that arrival radius approximately 441 days earlier. Transfers with more than one phasing orbit are also possible. Figure 4-36 illustrates the 1978 "Type II" single looper opportunity. The corresponding "Type I" opportunity has much inferior characteristics.

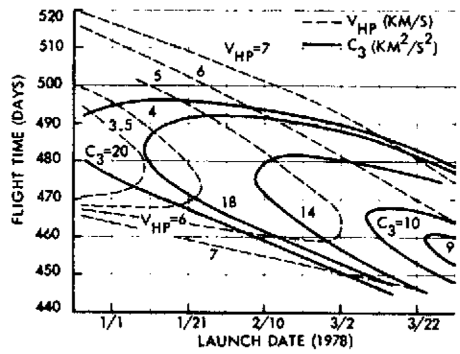

Figure 4-36. 1978 Looper Mission

Comparison with Figure 4-30 indicates that the looper transfers offer no improvement over the standard ballistic transfers in 1978. In addition, the longer time of flight degrades mission reliability.

4.2.3 Launch Vehicle Constraints and Flight Profiles

4.2.3.1 Thor/Delta

The Thor/Delta launch vehicle configuration consists of an extended long tank Thor first stage with nine strap-on solid motors, a 96-inch diameter second stage and fairing with the Aerojet General AJ10-118F propulsion system, and a Thiokol TE-364-4 third stage. A sequence of events is shown in Table 4-11.

Table 4-11. Thor/Delta Sequence of Events

EVENT	APPROXIMATE TIME (SECONDS)
SOLID MOTOR INJECTION	0
LIFTOFF	0
SOLID MOTOR BURNOUT	38
SOLID MOTOR SEPARATION	95
MAIN ENGINE CUTOFF (MECO)	219
BLOW STAGE I/II SEPARATION BOLTS	227
START STAGE II IGNITION	231
FAIRING SEPARATION	267
SECOND STAGE ENGINE CUTOFF (SECO 1)	544
STAGE 2 ENGINE RESTART	SECO I + PARKING ORBIT COAST
STAGE 2 ENGINE CUTOFF (SECO 2)	RESTART 2 + 27

Table 4-12. Thor/Delta Launch Vehicle Performance

C_3 (KM^2/SEC^2)	WEIGHT [KG (LB)]
6	401.0 (884)
8	383.0 (844)
10	365.0 (806)
12	349.0 (769)
14	333.5 (735)
16	318.0 (701)
18	304.0 (670)
20	290.5 (640)
22	277.0 (611)
24	264.5 (583)
26	243.0 (556)
28	241.0 (531)
30	230.0 (507)

The performance characteristics of the Thor/Delta shown in Table 4-12 are given as useful payload weight at injection as a function of energy, C_3. The useful payload weight accounts for an adapter weight of 20 kg (44 lb). The C_3 for the 1978 Type I mission is approximately 10.0 km^2/sec^2 and for 1978 Type II is 20.0 km^2/sec^2.

4.2.3.2 Atlas/Centaur

The Atlas SLV-3D/Centaur D-1A launch system consists of the two-stage Atlas booster and Centaur upper stage. A nominal sequence of events for the Atlas/Centaur is given in Table 4-13.

Table 4-13. Atlas/Centaur Sequence of Events

EVENT	APPROXIMATE TIME (SECONDS)
LIFTOFF	0
ROLL PROGRAM	2-15
BOOSTER ENGINE CUTOFF (BECO)	153
BOOSTER PACKAGE JETTISON	156
JETTISON INSULATION PANELS	198
SUSTAINER ENGINE CUTOFF (SECO)	251
SEPARATION	253
MAIN CENTAUR ENGINE START 1	263
JETTISON NOSE FAIRING	275
MAIN CENTAUR ENGINE CUTOFF 1 - MECO 1	586
MAIN CENTAUR ENTINE START 2	MECO 1 + PARKING ORBIT COAST
MAIN CENTAUR ENGINE CUTOFF 2	START 2 + 114
SEPARATION	(MECO 2 + ΔT (VARIES)

The performance characteristics of the Atlas/Centaur, given in Table 4-14, are given as useful payload weight at injection as a function of energy, C_3. The useful payload weight accounts for an adapter weight of 47.5 kg (105 lb). The C_3 for the 1978 Type I mission is 10.0 km^2/sec^2 and for the 1978 Type II mission is 20.0 km^2/sec^2.

C_3 (KM^2/SEC^2	WEIGHT [KG (LB)]
6	901.0 (1986)
8	840.0 (1751)
10	780.0 (1719)
12	721.0 (1590)
14	663.0 (1462)
16	607.0 (1338)
18	551.5 (1216)
20	497.5 (1096)
22	444.5 (980)
24	394.5 (869)
26	347.0 (765)
28	300.0 (661)
30	256.5 (565

Table 4-14. Atlas/Centaur Launch Vehicle Performance

4.3 PROBE MISSION STUDIES

4.3.1 Launch, Cruise and Midcourse Corrections

This section summarizes the results of trade studies concerning those phases of the mission resulting in the delivery of the bus and probes to the vicinity of Venus. The nominal profiles are provided in Section 4.1.

4.3.1.1 Launch Analysis

Each day during the launch opportunity an adequate firing window is needed to insure a high probability of launching the vehicle. The length of the daily window depends on the latitude of the launch site, the launch azimuth spread, the declination of the departure asymptote (determined by the arrival date at Venus), and any tracking and/or telemetry related constraints. The launch and powered flight parameters used for the Delta 2914 and Atlas/Centaur launch vehicles are presented in Table 4.15. The Centaur can extend its current nominal 25-minute coast time limit, but the resultant payload penalty could be prohibitive, so the indicated limit will be imposed.

Table 4-15. Launch and Powered Flight Parameters

PARAMETER	DELTA 2914	ATLAS/CENTAUR
PERMISSIBLE LAUNCH AZIMUTHS, [RAD (DEG)]	1.65 TO 1.92 (95 TO 110)	1.57 TO 2.01 (90 TO 115)
MAXIMUM PARKING ORBIT COAST TIME (MIN)	NO LIMIT	25
POWERED FLIGHT TO PARKING ORBIT (MIN)	10	10
CENTRAL ANGLE RAD (DEG)	0.30 (17)	0.36 (20.5)
INJECTION INTO INTERPLANETARY TRAJECTORY (SEC)	44	1.33
CENTRAL ANGLE [RAD (DEG)]	0.14 (8)	0.24 (14)

The daily windows for the 1978 Type I opportunity are shown in Figure 4-37. Daily launch intervals for the Atlas/Centaur range from 3.5 to 2.5 hours in duration with the Delta launch intervals slightly shorter Parking orbit coast times are of 15 to 25 minutes duration. Geocentric locations of the interplanetary injection burn are shown in Figure 4-38. Because the Centaur has the capability to orient the spacecraft to any

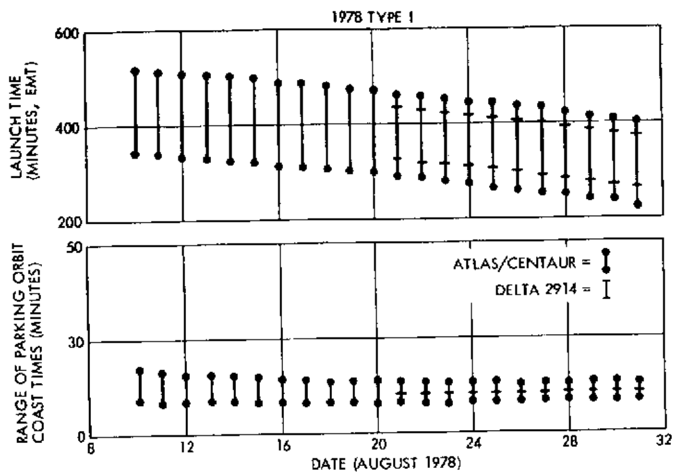

Figure 4-37. Launch Windows and Parking Orbit Coast Times

desired attitude prior to separation, the separation attitude and the resultant near earth aspect history can be selected to provide minimum reorientation prior to the first midcourse correction maneuver five days after injection.

The Delta-launched spacecraft will maintain the inertial attitude of the injection burn maneuver. Time histories of earth and solar aspect angles and altitude for the Delta-launched spacecraft are presented in Figure 4-39.

4.3.1.2 Cruise Analysis

The spacecraft is to be oriented so that the solar aspect angle remains below 0.52 radian (30 degrees) for a major portion of the cruise. As indicated in Figure 4-40, the spacecraft attitude, after the first midcourse maneuver, produces solar aspect angles less than 0.52 radian (30 degrees) until the time of the second midcourse maneuver, 50 days after injection. Following the second midcourse maneuver, the spacecraft is oriented in an earth-pointing attitude for the remainder of the interplanetary cruise.

4.3.1.3 Midcourse Analysis

The midcourse requirements and effectiveness are functions of many variables including the launch vehicle injection covariance matrix, sequencing of maneuvers, confidence levels of propellant loading, execution errors and tracking uncertainties, and magnitudes of unmodelled accelerations

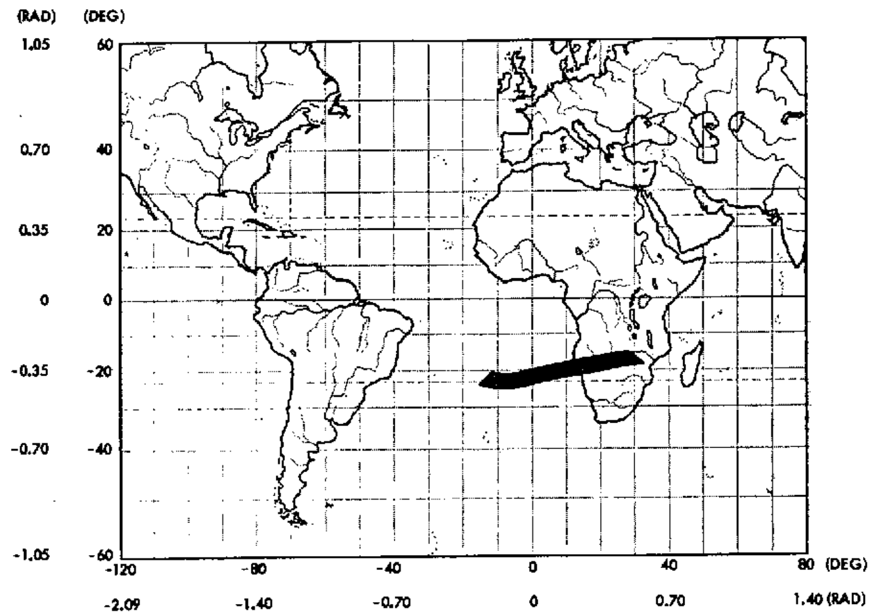

Figure 4-38. Injection Locations for 1978 Type II Window

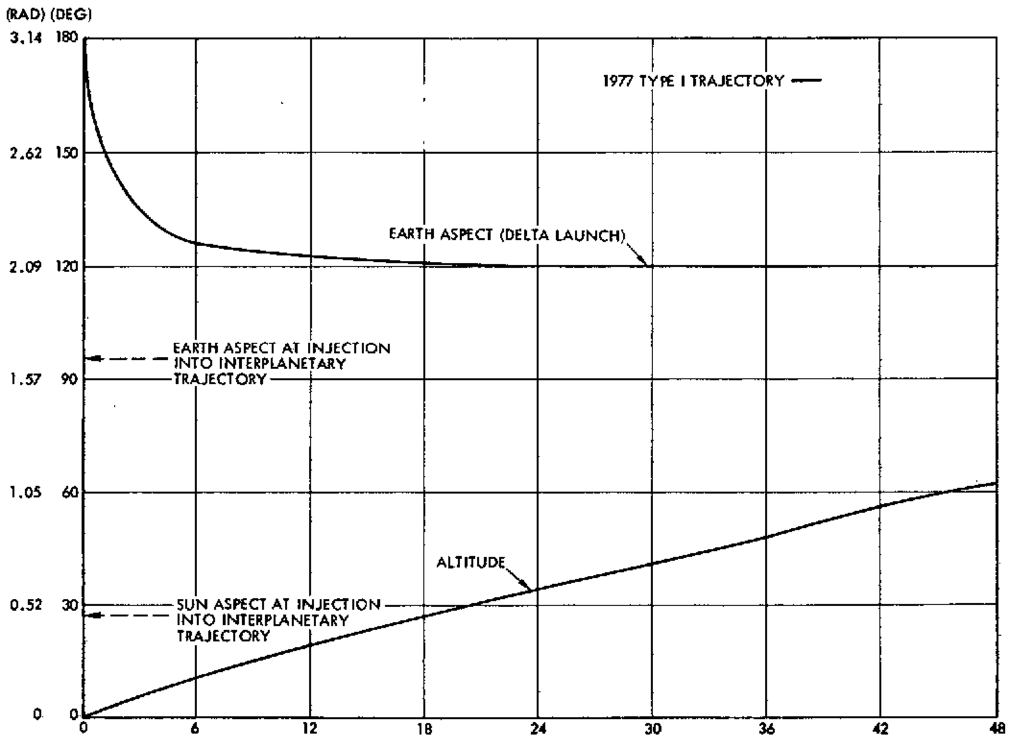

Figure 4-39. Time History of Earth Aspect and Altitude for Near-Earth Trajectory

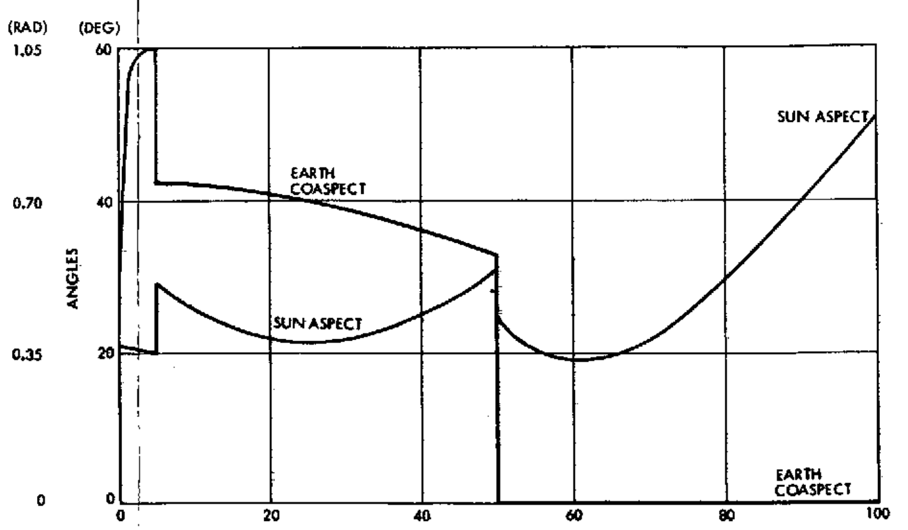

Figure 4-40. 1978 Probe Mission

FOLDOUT FRAME

FOLDOUT FRAME

and solar pressure uncertainties throughout the mission. A detailed parametric analysis of the midcourse sensitivities is included in Section 4.4.1.3, where the study is centered on the Type II orbiter mission (which has the longest trip time). This section focuses on the specifics of the 1978 and 1977 probe missions.

1978 Atlas/Centaur Mission

The first midcourse maneuver size normally dominates the total midcourse budget so this maneuver merits special attention.

The Atlas/Centaur injection covariance (supplied in Reference 1) is detailed in Table 4-16. X is downrange, R is geocentric radius, V is inertial velocity, Γ is the flight path angle, and W and $\dot{W}$ are the magnitude of the position and velocity components normal to the nominal flight plane, respectively.

Table 4-16. Atlas/Centaur Injection Covariance (C_3 = 7.6 km^2/sec^2)

	X(M)	R(M)	V(M S)	Γ(M RAD)	W(M)	$\dot{W}$(M S)
X	7.410 E-6	-1.749 E-6	2.638 E-3	-9.117 E-2	2.623 E-4	-8.168 E-2
R		1.024 E-6	-9.480 E-2	2.670 E-2	-2.930 E-4	1.876 E-2
V			1.177 E-0	-3.460 E-1	1.971 E+1	-2.506 E-1
Γ				1.251 E-1	-3.861 E+0	9.386 E-2
W		(SYMMETRIC)			1.071 E-6	-8.023 E-2
$\dot{W}$						4.194 E+0

The procedure used in generating the first midcourse requirements will be described in detail to indicate the assumptions. The midcourse ΔV covariance matrix $S = E[\Delta V \Delta V]^T$ is computed by standard linear techniques (Reference 2, for example) from $S = \Gamma(\Phi P_o \Phi^T)\Gamma^T$ where n-body integrated state transition matrices are used in Φ and the guidance matrix Γ. The guidance policy used in a fixed time of arrival policy with target parameters B · T, B · R, and time-of-arrival. The ΔV magnitudes for the various probability levels are then computed exactly using the recently published formulation of Reference 3. Thus the results are valid even for high probability levels of the order of 99.99 percent.

The first midcourse requirements for the 1978 probe mission, assuming a fixed time of arrival guidance policy, are summarized in Figure 4-41 as functions of the confidence level and time of maneuver.

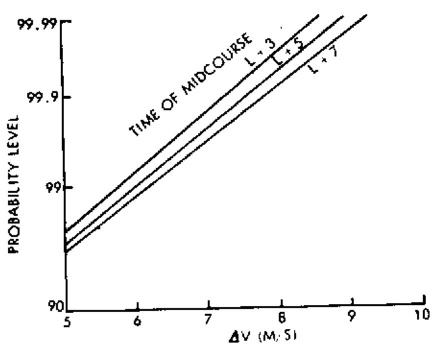

Figure 4-41. 1978 First Midcourse Requirements

The preferred mission schedules the first midcourse at E + 5 days and loads for the 99.99 percent probable magnitude of 9 m/s. The period of 5 days between launch and the first midcourse is long enough for comfortable tracking and operations scheduling, yet short enough to result in a reasonable ΔV penalty, even for such a high probability level. An important conclusion from Figure 4-41 is that the time of execution of the first midcourse correction is not critical; that is, the system is flexible with respect to this mission operation.

The second and third midcourses are quite small relative to the first midcourse (9 m/s) and the retargeting maneuvers (total of 50 m/s) performed during the probe release sequence. However, they are critical events in determining the accuracy of the control of the approach trajectories. This accuracy is measured by giving the semimajor (SMAA) and semiminor (SMIA) axes of the one-sigma uncertainty ellipse of the pierce point in the impact plane and the one-sigma time-of-flight accuracy.

The midcourse requirements and effectiveness for the 1978 probe mission are summarized in Table 4-17. Each midcourse ΔV is based on propagating the knowledge and execution errors at the previous midcourse maneuver (assuming the nominal ΔV was performed) to the appropriate maneuver time and including unmodelled accelerations of magnitude 2×10^{-12} km/sec^2. The execution errors assumed are 2 degree pointing, 1 percent proportionaltiy, 0.03 m/s resolution (three sigma). These error levels for the unmodelled accelerations and execution errors represent current estimates of the bus capability.

Table 4-17. 1978 Atlas/Centaur Midcourse Analysis

MANEUVER	TIME	$\Delta V_{99.99}$ (M/S)	SMAA (KM)	SMIA (KM)	TOF
INJECTION	L+0	-	43000	4600	2.19 HR
FIRST M/C	L+5	9.0	245	73	50 S
SECOND M/C	L+15	0.2	180	20	34 S
THIRD M/C	E-30	0.8	161	20	12 S

1977 Probe Mission

Both the Thor/Delta and Atlas/Centaur launch vehicles were considered in the assessment of the 1977 mission midcourse requirements and effectiveness. Table 4-18 details the Thor/Delta 2914 injection covariance as it was received (Reference 4) where V is inertial velocity, γ_1 and γ_2 are inertial flight path elevation and azimuth angles respectively, μ and ρ are longitude and latitude, respectively, and R is geocentric radius.

Table 4-18. Thor/Delta Inspection Covariance for 1977 Probe Mission

	V (FT/S)	γ_1 (DEG)	γ_2 (DEG)	μ (DEG)	ρ (DEG)	R (FT)
V	3.933E+2	2.566E-2	-9.953E-2	2.266E-1	-9.113E-2	-4.227E+4
γ_1		1.788E-2	-1.868E-4	6.318E-4	-2.538E-4	-4.541E+1
γ_2			1.788E-2	-5.169E-4	2.587E-4	6.886E+1
μ				1.853E-3	-6.367E-4	-2.325E+2
ρ					5.016E-4	9.358E+1
R						5.200E+7

The midcourse requirements and effectiveness for the two launch vehicles are compared in Table 4-19. The ΔV load numbers for the first midcourse represent the 99 and 99.9 percent levels for the Thor/Delta and Atlas/Centaur vehicles respectively; this variation was caused by the high weight penalty associated with using the 99.9 percent probable values in the weight-limited Thor/Delta mission. The ΔV load represents the mean-plus-three-sigma values for the less significant second and third midcourse numbers. The execution errors used in the 1977 analysis were slightly larger than the 1978 mission due to preliminary estimates of the bus capability, being 3 percent proportionality, 0.03 m/s resolution and 1-degree pointing (three-sigma). The 1977 Atlas/Centaur numbers are approximately equal to the 1978 Atlas/Centaur results and an order of magnitude lower than the 1977 Thor/Delta values.

Table 4-19. 1977 Probe Mission Midcourse Requirements Comparison

	THOR/DELTA	ATLAS/CENTAUR
INJECTION		
SMAA (KM)	568 000	50 200
TOF (MIN)	2300	213
FIRST MIDCOURSE		
ΔV_{LOAD} (M/S)	73.3	8.8
SMAA (KM)	5217	511
TOF (MIN)	21.5	2.15
SECOND MIDCOURSE		
ΔV_{LOAD} (M/S)	0.8	0.2
SMAA (KM)	183	173
TOF (MIN)	0.72	0.70
THIRD MIDCOURSE		
ΔV_{LOAD} (M/S)	0.9	0.6
SMAA (KM)	104	104
TOF (MIN)	0.24	0.24

4.3.2 Probe Targeting and Separation Sequence

A key task in probe mission design is the selection of the small probe target sites and the release scheme required to attain them. The target site selection is based on both the scientific objectives of the mission and the requirements imposed on the hardware by those sites. The release sequences investigated include both simultaneous and sequential release of the small probes. The selection of the preferred sequence is based on the impact of four major areas: mission design, bus requirements, probe requirements, and operations requirements. Either release strategy has totally acceptable performance characteristics; however, sequential release is selected as the preferred approach primarily for its reduced probe entry environment (angle of attack and spin rate) and targeting flexibility. The nominal sequential release profile is detailed in Section 4.1.1.3. Bus entry site selection and acquisition is a related problem and is discussed in Section 4.3.5.

4.3.2.1 Probe Targeting for 1978

The approach geometry of the preferred 1978 Type I mission is illustrated in Figure 4-42. The figure focuses on the southern hemisphere of Venus where the preferred target sites are located. Contours of the important systems design parameters of entry flight path angle and descent communication angle are illustrated on the figure. The selection of entry flight path angle impacts the altitude at which the small probe science may be deployed (see Section 3.1) and the entry environment seen by the probe (see Section 4.3.3). The implications of communication angle on the probe RF system is discussed in Section 7.6. A communication limit of 55 degrees has been imposed on the selection of small probe entry sites to control the RF power requirements to acceptable limits.

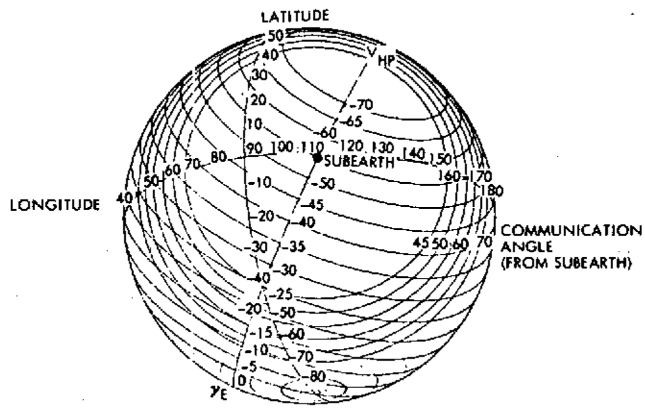

Figure 4-42 1978 Probe Mission Targeting Geometry

Several sets of candidate entry sites have been investigated. Three possible sets are illustrated in Figure 4-43 where the sites are indicated on Mercator projections of the planet. Set A of target sites was selected to satisfy the following requirements. The large probe entry site is at the equator within 70 degrees of the subsolar point. One small probe is deposited on the equator as far from the large probe as practical. A second small probe is placed as far from the equator as possible. The third probe is located at an intermediate latitude. Systems constraints limiting descent communication angles to less than 55 degrees and entry flight path angles between 25 and 60 degrees are imposed. Set B of target sites is directed toward meeting the science objectives as outlined in the Science Steering Group report (Reference 5). These science objectives require the large probe entry site to be at the equator within 70 degrees of the subsolar point, and the small probes to be deployed for greatest practical hemispheric coverage with latitude coverage of at least 30 degrees and longitude coverage of at least 90 degrees. System requirements limiting earth communication angles to less than 55 degrees and entry flight path angles between 25 and 45 degrees were imposed on the Set B sites.

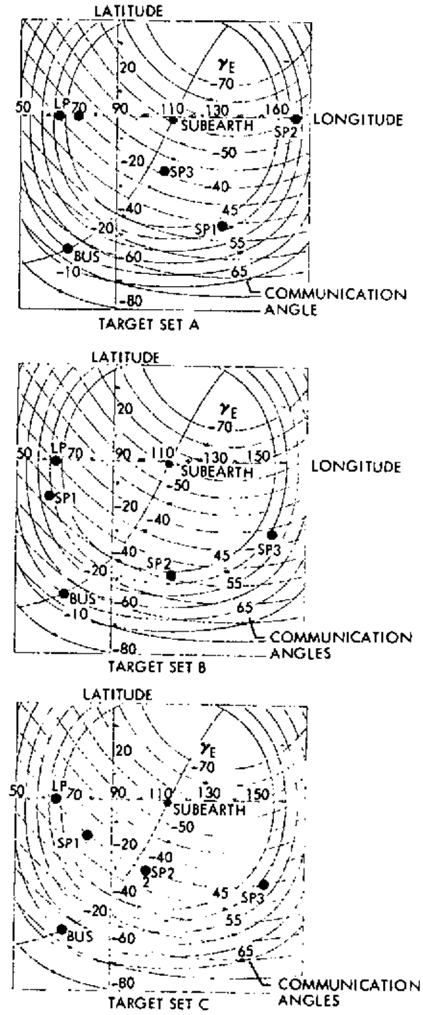

Figure 4-43. 1978 Candidate Target Site Sets

The third set of target sites has the three nominal entry sites lying along a line of constant entry angle. This targeting approach is made possible by the fortuitous geometry of the 1978 mission. Using this set reduces the size of the design entry corridor, which in turn could reduce design, hardware, and testing costs. The important objective of having a wide coverage of the planet with the small probes is still met with an entry flight path angle of 35 degrees. The candidate entry site sets are described in Table 4-20. The bus entry site selection is discussed in Section 4.3.5.

Table 4-20. Candidate Probe Target Sets

	LATITUDE	LONGITUDE	ENTRY ANGLE (°)	COMMUNICATION ANGLE (°)
LARGE PROBE	0	65	-35	48
BUS	-57	70	-12	66
TARGET SET A				
SP1	-45	135	-30	48
SP2	0	165	-56	52
SP3	-22.5	110	-41	22
TARGET SET B				
SP1	-15	63	-27	52
SP2	-47	115	-27	46
SP3	-30	158	-38	51
TARGET SET C				
SP1	-15	80	-35	36
SP2	-30	105	-35	30
SP3	-35	155	-35	52

4.3.2.2 Sequential vs Simultaneous Release

We have investigated two general categories of sequences to separate the small probes from the bus onto trajectories impacting the desired entry sites. In either case the separation velocity is derived from the tangential velocity acting on the probes at the instant they are released from the spinning spacecraft. In simultaneous release the bus is targeted toward a point interior to the three desired probe entry sites and the three probes are released simultaneously with a tangential velocity due to spin rate sufficient to attain the sites. In sequential release the probes are released in distinct maneuvers with the bus retargeted between each small probe release.

The prime characteristics of simultaneous release are a relatively straightforward operational sequence, a generally higher spin-rate requirement, and non-zero angles of attack for the small probes at entry. All three features result from the fact that both the small probe trajectory and attitude are determined by the single release maneuver. In sequential release each small probe entry site is largely obtained by an intermediate bus retarget maneuver. Then at each small probe release the bus is placed in an attitude that results in zero angle of attack at entry for that probe. Thus a flexible targeting scheme is obtained along with small entry angles of attack at a cost of slightly increased operational complexity. The two release schemes will now be compared in more detail for their mission implications, bus requirements, probe impact, and DSN and mission operations requirements.

4.3.2.3 Mission Implications

The mission implications of the two release schemes is in the area of targeting flexibility and contingency planning. Sequential release provides significantly more flexibility in targeting. Generally, either scheme may obtain any set of three target sites. However, practical limits on bus spin rates or entry angles of attack prevent simultaneous release from effectively attaining certain combinations of entry sites.

Figure 4-44 illustrates the general nature of site acquisition for simultaneous release. The bus attitude has been selected to obtain maximum coverage consistent with minimum angles of attack. The resulting spin rate and angles of attack are then illustrated. The general feature of probe entry sites approximately 120 degrees apart is apparent. By tilting the spin axis the figures may be somewhat warped, however, the general feature of 120-degree separation remains.

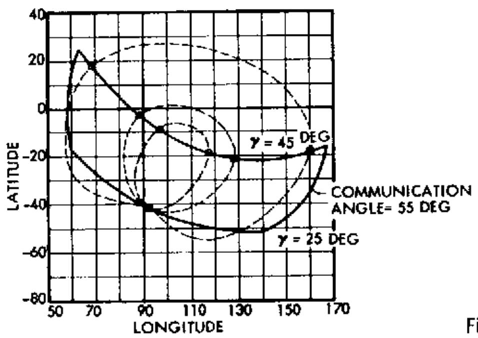

SYMBOL	SPIN RATE (RPM)	ANGLE OF ATTACK (DEG)		
		SP1	SP2	SP3
O	20	20	4	20
Δ	34	40	27	40
□	68	50	38	50

Figure 4-44. Simultaneous Release Parametrics

In contrast, sequential release opens the entire planet surface while putting no limits on spin rate or angle of attack. The bus can always be oriented to result in zero angle of attack at entry, and an intermediate bus impact point may be determined so that a release at a given spin rate and at the desired attitude acquires the entry point. The ΔV necessary to move the bus impact point from its initial point to the required target point is then obtained by a retargeting maneuver.

Besides flexibility in entry site selection, the entry times may be easily adjusted with sequential release. The ΔV to retarget the bus between releases may be adjusted to also speed up or delay any of the probe entry times. Thus in the current preferred sequence (see Section 4.1) the second retargeting event is designed to delay the second and third small probes to enter after the large probe and first small probe have completed their missions. In contrast, to achieve the Set A target sites in 1978 using simultaneous release would result in all three small probes entering within 30 minutes of each other.

Thus, introducing the extra retargeting maneuvers provides extra degrees of freedom that can be used to obtain increased target site selection and entry sequence flexibility that may be required at some point in the evolving mission requirements.

This targeting flexibility is also helpful in terms of contingency planning. If, in checkout, a single probe is discovered to be inoperable, the other two probes may be placed in the optimal two-site combination with no increased complexity. The practical limits of simultaneous release may preclude obtaining two widely separated sites.

4.3.2.4 Bus Requirements

The implications of the release sequence on the bus design may be divided into three areas: bus configuration, maneuver capability (ΔV magnitude, precession requirements, spin rate, and changes), and maneuver accuracy.

Bus Configuration

The interface requirements imposed on the bus by the probe mission are generally more severe for simultaneous release with one exception: mass properties control. The use of sequential release does require that the center of gravity (c.g.) of each probe be in the plane of the bus c.g. (without the large probe) with fairly small tolerance. The variations of c.g. location (and spin axis location) as the small probes are sequentially released does not impact the bus design as long as the spin rates are kept low (~10 rpm).

The use of the simultaneous release requires a combination spin rate, probe separation springs (or other mechanical separators), and separation distance from Venus to satsify reasonable small probe coverage requirements. Representative simultaneous releases for the Set A and Set B target sites (defined in Figure 4-43) performed 20 days from the planet would require spin rates of 60 and 40 rpm respectively (see the discussion of maneuver capability below). The higher spin rate makes bus attitude at probe release more critical and more difficult to achieve accurately, thereby jeopardizing both the probe communications angle limit and entry flight path angle. The spin rate requirements can be halved by releasing the probes twice as far out. However, doubling the coast times of the probes increases the intervals the probes are away from the protective environment of the spacecraft and subject to solar heating and pressure (see Section 4.3.2.5). The use of springs to supply part or all of the probe separation ΔV also may reduce the spin rate requirement, but again introduce other problems. Spring forces to 2224 to 4448 Newtons (500 to 1000 lb) for strokes of 10.1 to 5 cm (4 to 2 inches) respectively are required to compensate for 60 rpm. These springs must be very accurately aligned with the probe c.g. to minimize separation tipoff errors which are specified as 1 degree probe wobble per 1 percent uncertainty of spin rate in the pitch/yaw direction.

Maneuver Capability

A second area of impact on the bus systems caused by the release scheme is in the number of engine restarts and amount of hydrazine required. Table 4-21 summarizes the maneuver capability requirements of the two release sequences for the three candidate target site sets. Nominal sequence assumed for sequential release includes retargeting the bus impact point before each small probe release and a final retarget to acquire the desired bus entry site. The retarget maneuver preceding the second small probe release delays the bus trajectory by 1.5 hours so that the large probe and first small probe complete their descent before the second and third small probe enter (see Figure 4.5). This typically increases the second retarget maneuver (at E-19 days) by 10 m/s over the case with no delay. The final retarget maneuver to acquire the bus entry site and delay bus entry by 1.5 hours (at E-11 days) requires about 25 m/s. The simultaneous release needs

Table 4-21. Maneuver Capability Requirements

	SET A		SET B		SET C	
	SEQ	SIM	SEQ	SIM	SEQ	SIM
RETARGET MANEUVERS						
NUMBER	4	2	4	2	4	2
TOTAL ΔV (M/S)	56.8	21.6	52.7	19.8	52.8	35.7
HYDRAZINE [KG (LB)]	11.7 (25.7)	4.5 (9.8)	10.9 (23.9)	4.1 (9.0)	10.9 (23.9)	7.4 (16.2)
PRECESSION MANEUVERS						
NUMBER	16	8	16	8	16	8
ANGLE PRECESSED (DEG)	1144	534	983	488	976	459
HYDRAZINE [KG (LB)]	1.53 (3.4)	0.71 (1.6)	1.31 (2.9)	0.65 (1.4)	1.30 (2.9)	0.61 (1.3)
SPIN RATE CHANGES						
NUMBER	2	2	2	2	2	2
TOTAL CHANGE (RPM)	10.4	70.4	10.4	122.4	10.4	90.2

but two retargeting maneuvers: the maneuver to move the bus impact point from the large probe entry site to the required release impact point, and the maneuver to move it from there to the bus entry site. The second retarget maneuver including a delay of 1.5 hours requires about three-quarters of the total ΔV budget.

As demonstrated in Table 4-21, the sequential release requires about 50 m/s compared to the 20 m/s needed by simultaneous release. The mid-course budget for the Atlas/Centaur launch vehicle and 1978 mission is about 15 m/s so that the total requirements are typically 65 vs 35 m/s. However, since the fuel tanks are common for both the probe and orbiter missions, and since the orbiter mission requires more than 65 m/s for midcourses and trims (see Section 4.4.4), the fuel tank size will not be totally determined by the probe mission. The only penalty for sequential release will be the amount of fuel loaded for the mission.

The number and size of precession maneuvers is about twice as large for sequential release as for simultaneous release. The hydrazine weights for typical bus weights is 0.205 kg per m/s. Finally, the spin rate changes are roughly comparable. The bus nominally has a spin rate of 4.8 rpm and spins up to 10 rpm during the release sequence for the sequential strategy. For the simultaneous release the bus must spin up to 40 rpm at the time of the small probe release.

Maneuver Accuracy Requirements

A third area of impact on the bus by the choice of small probe release sequence is maneuver accuracy requirements. Entry dispersions are caused by navigation errors (Section 4.3.2.6), solar pressure uncertainties (Section 4.3.2.5), and of prime concern here, execution errors during the bus retarget and probe release maneuvers.

The dispersion sensitivities associated with simultaneous release (for the Set A target sites) are summarized in Table 4-22. The navigation uncertainty is quite significant (although tolerable) because of the relatively poor tracking characteristics of the 1978 Type I opportunity. The retarget errors represent the errors in the delivered ΔV relative to the desired ΔV at the retarget maneuver. Thus the pointing error includes the attitude determination uncertainty, attitude control and resolution errors, and thrust

Table 4-22. Simultaneous Release Dispersion Sensitivities (Set A Sites)

SMALL PROBE	ERROR SOURCE	3σ MAGNITUDE	THREE SIGMA DISPERSIONS γ (DEG)	t_E (MIN)	α (DEG)
1	NAVIGATION ERRORS	3 x SMAA = 480 KM	3.93	1.08	1.32
	RETARGET - PROPORTIONALITY	1%	0.57	0.27	0.39
	POINTING	1.5°	1.80	1.05	0.58
	RELEASE - BUS POINTING	1.5°	0.77	0.47	1.43
	RELEASE ANGLE	2.0°	0.57	0.36	0.03
	SPIN RATE	1 RPM	0.10	0.05	0.05
	TIP-OFF ERRORS	3°	-	-	3.00
	SOLAR PRESSURE UNCERTAINTY	A/C CONFIGURATION (40 RPM)	-	-	0.63
	RSS TOTAL		4.47	1.64	3.70
	MONTE CARLO TOTAL		4.77	1.59	3.74
2	NAVIGATION ERRORS	3 x SMAA = 480 KM	1.14	0.18	0.66
	RETARGET - PROPORTIONALITY	1%	0.63	0.24	0.24
	POINTING	1.5°	0.45	0.77	0.29
	RELEASE - BUS POINTING	1.5°	0.11	0.26	1.06
	RELEASE ANGLE	2.0°	0.51	0.50	0.18
	SPIN RATE	1 RPM	0.02	0.03	0.02
	TIP-OFF ERRORS	3.0°	-	-	3.00
	SOLAR PRESSURE UNCERTAINTY	A/C CONFIGURATION (40 RPM)	-	-	1.83
	RSS TOTAL		1.47	1.00	3.33
	MONTE CARLO TOTAL		1.83	0.97	3.34
3	NAVIGATION ERRORS	3 x SMAA = 480 KM	3.24	0.81	0.69
	RETARGET - PROPORTIONALITY	1%	0.06	0.09	0.24
	POINTING	1.5°	1.54	0.95	0.29
	RELEASE - BUS POINTING	1.5°	1.38	0.26	0.92
	RELEASE ANGLE	2.0°	0.97	0.16	0.15
	SPIN RATE	1 RPM	0.06	0.09	0.02
	TIP-OFF ERRORS	3.0°	-	-	3.00
	SOLAR PRESSURE UNCERTAINTY	A/C CONFIGURATION (40 RPM)	-	-	1.83
	RSS TOTAL		3.97	1.29	3.30
	MONTE CARLO TOTAL		4.40	1.28	3.32

dynamics (coning, misalignment) errors. The release errors are the errors induced during the spinning release maneuver itself. Probe attitude errors result from trajectory variations caused by the execution errors at retarget and release, as well as the pointing error at release, the tip-off error at release, and solar pressure uncertainties during coast.

Several of the dispersion sensitivities indicated in Table 4-22 warrant comment. For the simultaneous release, the navigation errors, retarget errors, and release errors all make significant contributions to the entry dispersions with the navigation uncertainties highly dominating. Generally the dispersions are related to entry angle as $(\sin\gamma)^{-1}$ so that, with nominal γ's of 30, 56, and 41 degrees for small probe sites 1, 2, and 3 respectively, the ratio of dispersions is approximately predicted to be 1, 0.6, and 0.8. This simple relationship does indicate the proper trends. The pointing error at both retarget and release is the dominant maneuver execution error; the proportionality, resolution, release angle, and spin rate errors are relatively minor contributors. The probe attitude error is evenly distributed over the bus pointing, tipoff, and solar pressure uncertainty errors. The errors are approximately independent of each other as demonstrated by the agreement between the RSS and Monte Carlo sums of the errors.

The sequential release dispersion sensitivities are summarized in Table 4-23. Several characteristics of the dispersion analysis are quite different than for simultaneous release. The navigation uncertainty at the start of each small probe targeting sequence (retarget maneuver and release maneuver) is a function of the execution errors at the previous retargeting maneuvers and the tracking effectiveness during the deployment period. The pointing error in the delivered ΔV at each probe release is also a variable as the thrust misalignment errors will increase as one and two small probes are removed from the bus configuration. Since dispersions increase with $(\sin\gamma)^{-1}$ it is best to deploy the shallowest probe first (so the retarget maneuver is performed with all three probes on the bus, resulting in the smallest thrust misalignment errors) and then have the larger execution errors associated with the steeper-entering probes. As indicated in Table 4-23, the result is that the first entry site dispersions are still largest even though the pointing errors are least for this site. With the sequential deployment method the release errors are clearly dominated by the other two major error sources.

Table 4-23. Sequential Release Dispersion Sensitivities (Set A Sites)

SMALL PROBE	ERROR SOURCE	3σ MAGNITUDE	THREE-SIGMA DISPERSIONS γ (DEG)	t_E (MIN)	α (DEG)
1	NAVIGATION ERRORS	3 x SMAA - 550 KM	3.84	1.26	1.38
	RETARGET ERRORS	1.5° POINTING	2.07	1.08	0.86
	RELEASE ERRORS	1.5° POINTING	1.04	0.02	1.50
	TIP-OFF ERRORS	3.0	-	-	3.00
	SOLAR PRESSURE UNCERTAINTY	A/C CONFIGURATION (10 RPM)	-	-	2.50
	RSS TOTAL	-	4.48	1.66	4.48
	MONTE CARLO TOTAL	-	4.51	1.68	4.49
2	NAVIGATION ERRORS	3 x SMAA = 500 KM	1.47	.33	0.57
	RETARGET ERRORS	2.0° POINTING	3.27	1.47	0.90
	RELEASE ERRORS	1.8° POINTING	0.30	0.08	1.80
	TIP-OFF ERRORS	3.0° ERROR	-	-	3.00
	SOLAR PRESSURE UNCERTAINTY	A/C CONFIGURATION (10 RPM)	-	-	2.50
	RSS TOTAL		3.60	1.50	4.42
	MONTE CARLO TOTAL		3.60	1.51	4.42
3	NAVIGATION ERRORS	3 x SMAA = 480 KM	3.15	1.04	.62
	RETARGET ERRORS	2.5° POINTING	1.38	1.08	.48
	RELEASE ERRORS	2.0° POINTING	0.10	.05	2.00
	TIP-OFF ERRORS	3.0° ERROR	-	-	3.00
	SOLAR PRESSURE UNCERTAINTY	A/C CONFIGURATION (10 RPM)	-	-	5.50
	RSS TOTAL		3.44	1.47	4.45
	MONTE CARLO TOTAL		3.45	1.47	4.46

The entry requirements (Set A sites) established to control the design of the small probes are summarized in Table 4-12. The small probes are designed to operate if deposited within 55 degrees of subearth and within an entry flight path angle corridor between 25 and 60 degrees. The probes must be designed to survive entry angles of attack up to 60 degrees if simultaneous release is used, and up to 10 degrees if sequential release is used. For the design of the acquisition process the small probe entry times are to be known to within two minutes. To allow a clear comparison of accuracy requirements, an additional constraint to limit the dispersions in entry angle to less than 5 degrees has also been imposed.

Maneuver accuracy requirements that comfortably satisfy the targeting criteria of Table 4-24 are compared in Table 4-25 for sequential and simultaneous release. The accuracies listed represent three-sigma requirements. The first three entries refer to errors in the delivered ΔV of retargeting events. The pointing error is the error in the direction of the velocity increment imparted to the probe because of attitude determination and control errors as well as thrust dynamics errors (coning, thrust misalignment, etc). Because of the increased misalignment errors as first one and then two small probes are released from the bus, sequential release allows an incremental increase in the pointing errors. This may be done for sequential release because the errors at release have significantly less impact in dispersions than do the corresponding errors in simultaneous release (see the sensitivities of Tables 4-22 and 4-23). The error levels quoted are significant as they may be met without the inclusion of star sensors. The star sensors would enable the attitude determination process to be accurate to tenths of degrees but would have no influence on the thrust dynamics errors which contribute approximately an equal share to the final pointing error. The other retargeting errors (proportionality and resolution) result in errors in the magnitude of the delivered ΔV and again represent reasonable requirements on the system.

The other accuracy requirements refer to the small probe release maneuver itself. The release pointing error represents the error in the final bus attitude at release due to bus attitude determination and control.

Table 4-24. Small Probe Entry Accuracy Requirements

PARAMETER		NOMINAL VALUE	THREE-SIGMA DISPERSIONS	DESIGN RANGE
ANGLE OF ATTACK (DEG)	(SEQ)	0	< 10	10
	(SIM)	41,50,50	< 10	60
FLIGHT PATH ANGLE (DEG)		29,56,41	< 5	25-60
COMMUNICATION ANGLE (DEG)		49,52,20	NR	< 55
LATITUDE, LONGITUDE (DEG)		-45, 135 0, 165, -22.5, 110	NR	NR
SPIN RATE (RPM)	(SEQ)	10	< 1	10
	(SIM)	40	< 1	40
COAST TIME (A)	(SEQ)	21, 17, 13D	2M	13-21D
	(SIM)	21D	2M	21D ± 2M
ENTRY TIME (B)	(SEQ)	0, +90M, +90M	2M	2M
	(SIM)	-11M +3M +15M	2M	2M

(A) COAST TIME REFERS TO TIME FROM RELEASE TO ENTRY FOR EACH SMALL PROBE.
(B) ENTRY TIME REFERS TO TIME OF ACTUAL ENTRY OF EACH SMALL PROBE REFERENCED TO NOMINAL LARGE PROBE ENTRY TIME OF 1746 GMT ON 12/17/78

Table 4-25. Bus Maneuver Accuracy Requirements

	SEQUENTIAL	SIMULTANEOUS
1. DELIVERED ΔV POINTING ERROR	1.5° (MC RT1) 2.0° (RT2) 2.5° (RT3)	1.5°
2. DELIVERED ΔV PROPORTIONALITY	1.0%	1.0%
3. RESOLUTION ERROR	0.03 M S	0.03 M/S
4. RELEASE POINTING ERROR	1.5° (LP, SP1) 1.8° (SP2) 2.0° (SP3)	1.5°
5. RELEASE SPIN RATE ERROR	1 RPM	1 RPM
6. RELEASE ANGLE ERROR	2°	2°
7. TIPOFF ERROR AT RELEASE	1.0° (LP) 3.0° (SP)	1.0 (LP) 3.0 (SP)

Because of difficulties in the precession engine alignment these errors are increased depending upon the bus configuration as in the retargeting pointing errors. None of the release accuracy requirements are difficult to attain. However, the fact that the simultaneous release requires higher spin rates at release (40 vs 10 rpm for the Set A Sites) does imply more difficulty for that scheme in meeting the identical accuracy requirement (2-degree release angle error for example).

4.3.2.5 Small Probe Requirements

The requirements on the small probes are significantly more severe for simultaneous release than for sequential release. The attainment of widely separated small probe entry sites with simultaneous release requires large angles of attack at entry and either high spin rates or long coast times

Conversely, sequential release allows zero angles of attack and any combination of spin rate and coast time at the cost of an insignificant increase in thermal control protection to account for the distinct probe attitudes during coast. Reducing the planet coverage of the small probe sites can limit the problems of simultaneous release at the cost of somewhat decreased small probe science return.

<u>Entry Environment</u>

The variations in entry conditions caused by the two release sequences are primarily in entry angle of attack and entry spin rate. Figure 4-44 demonstrated the angles of attack and spin rates required to obtain various levels of planet coverage with simultaneous release. Sequential release can obtain the sites with zero angle of attack for each probe and any spin rate. Spin rates of 10 rpm or higher are desirable because of solar pressure considerations (see below).

The acquisition of the Set A target sites by a simultaneous release maneuver at 23 days from encounter requires a 40 rpm spin rate and results in entry angles of attack (including dispersions) of 60 degrees. The same entry sites can be attained with sequential release with a 10 rpm spin rate and angles of attack less than 10 degrees. The higher spin rate and angle of attack required by simultaneous release results in lateral load factors of ± 44 g at approximately 119 rad/s (19 cps) for the second small probe (at $\gamma = 60$, 488 g peak longitudinal deceleration) compared to ± 5 g at the same frequency for the comparable sequential release using the preferred Atlas/Centaur configuration. Details of the entry analyses are provided in Section 4.3.3.

These considerations imply a more severe entry environment for the simultaneous strategy and increased requirements on both probe system design and system tests.

<u>Coast Phase</u>

The important considerations in the coast phase include the duration of the coast time, solar pressure effects, and the thermal control characteristics of the two release methods.

The length of the coast phase determines the interval that the probes are away from the protective environment of the spacecraft and under the perturbative influence of the sun. Therefore, it is desirable to keep the coast time as short as practical. The limiting factor is in the retargeting ΔV requirements, which increase as the inverse of the coast time.

An important consideration associated with solar effects during the coast phase is probe thermal control. In simultaneous release the small probes have identical attitudes relative to the sun and coast times resulting in identical thermal control requirements. In sequential release, however, each probe is released in a different attitude (determined to obtain zero angle of attack at entry), suggesting a possible problem in obtaining identical small probes. Figure 4-45 illustrates the solar aspect angles corresponding to the zero angle-of-attack attitudes for possible entry sites. Figure 4-46 demonstrates the variations in solar aspect angles during coast for the Set A target sites. The range of solar aspect angles demonstrated in those two figures are easily accommodated by using special (identical) paint patterns on the small probes, resulting in essentially no thermal control penalty attributed to sequential release.

A second solar influence on the probes during coast is caused by solar pressure effects. Solar pressure creates a torque on each probe causing the spin axis to precess about the sun line. This precession is directly related to probe spin rate and thereby raises concern over the minimum spin rate sufficient to limit precession angles and uncertainties to tolerable limits. Figure 4-47 illustrates the probe precession angles caused solely by solar pressure. The configuration assumed are the Atlas/ Centaur large and small probes (including afterbodies) assuming the surface reflectivity properties discussed in Section 7.4. The analysis is based on the preferred sequential release mode having a spin rate of 10 rpm and acquiring the Set A target sites. Total precession angles are indicated for both the nominal surface properties and a worst-case analysis assuming minimum absorbtivity and completely specular reflection. The large probe nominal precession is 4 degrees with a maximum expected precession of 7.5 degrees over the 25-day coast period. The small probes have about a 2-degree nominal precession angle with worst-case precession of about 4 degrees. Neither the nominal values nor the uncertainties associated with them cause any problems in mission design, even for spin rates as low as

10 rpm. The simultaneous release with its spin rate of 40 rpm would have solar precessions one-fourth as large.

For completeness the probe attitude time histories in terms of earth aspect angle are illustrated in Figure 4-48. The earth aspect angle profiles are especially important in analyzing the characteristics and requirements of preentry communication links with the probes. Both the solar and earth aspect angle profiles of Figures 4-46 and 48, respectively, include the solar pressure precession effects discussed above.

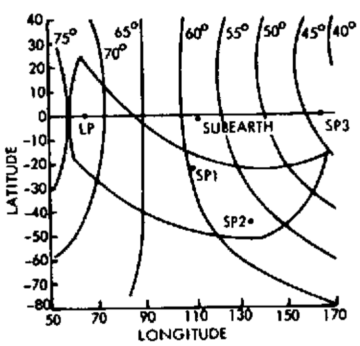

Figure 4-45. Solar Aspect Angles at Entry at Zero Angle of Attack

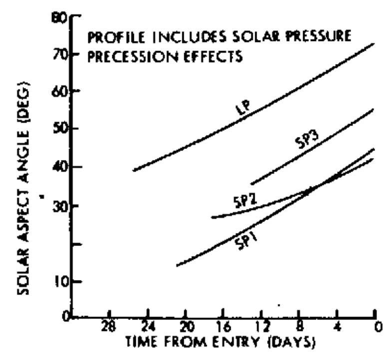

Figure 4-46. Solar Aspect Angles During Coast

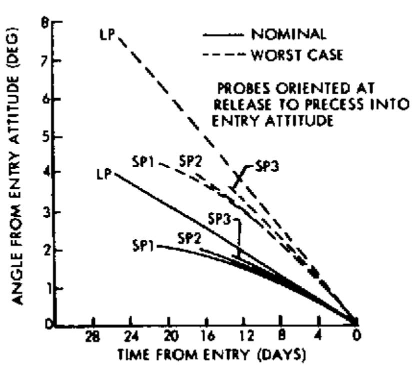

Figure 4-47. Solar Pressure Precession

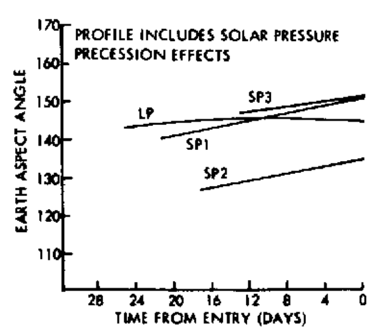

Figure 4-48. Earth Aspect Angles During Coast

4.3.2.6 Tracking and Operational Considerations

The final area of comparison for the sequential versus simultaneous release trade involves the requirements related to tracking accuracies, mission operations, and operational software. Here a very slight advantage accrues to simultaneous release, but it is not considered sufficient to offset the more numerous advantages of sequential release summarized above.

Tracking Requirements

The tracking characteristics of the approach trajectory are critical in selecting the preferred release scheme since the dispersions are significantly affected by navigational uncertainties. They are especially important if the sequential release method is used because the uncertainties due to execution errors at each of the retargeting maneuvers could cascade and become intolerable if the tracking were ineffective. Table 4-26 summarizes the assumptions of the tracking analysis. The analysis was conducted using the Space Trajectories Error Analysis Program (STEAP) computer program developed by Martin Marietta for NASA under Contracts NAS8-21120, NAS1-8745, NAS5-11795, and NAS5-11873. Tracking is initiated at (E = 50) days prior to encounter (E - 50). Tracking continues for 20 days, at which time the nominal final midcourse is performed. The knowledge uncertainty at this point is combined with the execution errors to determine the bus trajectory control uncertainty following the midcourse. The process is continued for each of the retargeting maneuvers.

Table 4-26. Tracking Model Definition

		POSITION	VELOCITY
A PRIORI UNCERTAINTIES (1σ)		1000 KM	100 M/S
VENUS EPHEMERIS UNCERTAINTIES (1σ)		20 KM	-
DOPPLER NOISE (1σ): 1 MM/S FOR 1 MINUTE COUNT TIME			
EQUIVALENT STATION LOCATION ERRORS	σ_{R_S}	σ_λ	ρ
CALIBRATED	1.0 M	2.0 M	0.97
UNCALIBRATED	4.5 M	5.0 M	0.97
TRACKING SIMULATED FROM GOLDSTONE, MADRID, CANBERRA AT 10 PER DAY			
NOTE: σ_{R_S} IS THE UNCERTAINTY IN DISTANCE FROM SPIN AXIS, σ_λ IS THE UNCERTAINTY IN LONGITUDINAL LOCATION, AND ρ IS THE CORRELATION COEFFICIENT BETWEEN STATION LONGITUDE ERRORS.			

The results for the 1978 probe mission are summarized in Figure 4-49. The bus trajectory uncertainty is measured by the semi-major axis of the one-sigma uncertainty ellipse in the impact plane (SMAA). For simultaneous release the SMAA at the retargeting event is 160 km. For sequential release the bus trajectory uncertainty is 160 km before the first retargeting maneuver, the execution errors at that maneuver increase the SMAA to 177 km, and tracking prior to the second retargeting event decreases the uncertainty to 162 km. No Doppler tracking is performed for 0.3 day during the small probe release maneuver and the predictions for the next retargeting maneuver are based on tracking terminating 0.7 day prior to the retargeting event. As indicated, the tracking is capable of eliminating most of the uncertainties introduced by the retargeting execution errors, leading to progressive SMAA at retargeting events of 158, 162, 184, and 172 km. Without effective tracking the dispersions would be intolerable as indicated by the SMAA of 360 km immediately after the second retargeting event. However, as indicated in Tables 4-23 and 4-24, the tracking is sufficient to control the entry dispersions to acceptable levels, even without requiring charged particle calibration. For comparison purposes the time histories of the SMAA are also included on Figure 4-49 for cases in which no maneuver execution errors were added. The figure indicates that calibration of charged particles could double the tracking accuracy. In summary, standard tracking arcs should be sufficient to ensure successful missions with either release scheme.

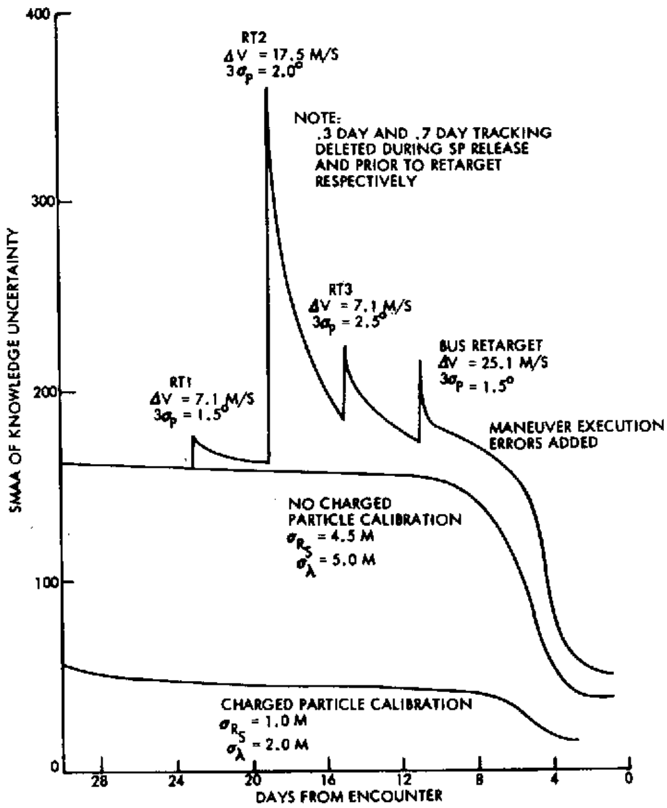

Figure 4-49. Tracking Characteristics, 1978 Probe Mission

Operational Software

The operational ground software requirements for both release strategies are virtually identical. The requirements include software for orbit determination, maneuver design, maneuver command, and bus attitude determination. The orbit determination software is required to determine the bus trajectory following the midcourses and retargeting events. The maneuver design software must convert the orbit determination information, bus and probe hardware status, and targeting objectives into the desired precession and ΔV maneuver definition. The command software must define, verify, and transmit the required commands to the bus. The attitude determination software must compute the attitude of the bus from bus sensor and ground-received Doppler information. These same functions must be accomplished for either release strategy. The only difference is in the requirements on the bus spin rate, release attitude, or bus aim point and these differences have a negligible effect on software complexity.

Existing Pioneer 10/11 software can be used unchanged for the maneuver design, and with very minor modifications for the maneuver command and bus attitude determination. New software will have to be written for the orbit determination.

Operational Time Lines

The operational time lines of the two schemes are essentially the same with sequential release requiring a repetition of several of the events. The ground system operational time lines (conservatively estimated) must cover the following functions:

1) Orbit determination: a 4-hour task for both the orbit determination task and propagation of the best estimate state vector.

2) Bus targeting analysis: conservatively a one-hour task to derive the timing, ΔV's, attitudes if tracking data are available.

3) Detail sequence and command generation: a 6-hour task to generate detailed command sequences, validate the sequences against system performance capabilities, validate actual command structure, and hold command conferences, as required. This will normally be done the day before command execution.

4) Release and validate commands: 1-hour to release commands, validate, transmit, and verify and retransmit if required.

5) Spacecraft implementation: 6-hours to precess, verify attitude, correct attitude, execute ΔV (or probe release), and unwind to to cruise attitude. Assume 4-hours from start precess to execute.

Excluding the orbit determination function, the remaining functions take a total of 15 hours, assuming conservative time spans. These same basic functions must precede each spacecraft maneuver event. The required events are:

Simultaneous	Sequential
Last M/C (E - 30 days)	Last M/C (E - 30 days)
Release large probe	Release large probe
Retarget spacecraft	Retarget spacecraft
Release small probes	Release SP 1
	Retarget spacecraft
	Release SP 2
	Retarget spacecraft
	Release SP 3
Retarget Bus	Retarget bus

The major difference in the targeting strategies is five events for simultaneous release, and nine events for sequential release. The total nominal time spans are 11 days for simultaneous release, and 19 days for sequential release. The minimum time span between events in either case is 48 hours to accomplish a series of functions requiring 15 hours. Thus, the time lines are not tight, nor do they require resources that are not already available. They need only be repeated an additional four times for the sequential release as opposed to the simultaneous release strategy over an additional 8 days.

In contingency situations the probe release or retarget maneuver times can be delayed, comfortably for up to a day. The ΔV trims to compensate for the delay can be done in arbitrary directions while in the release attitude, if desired.

4.3.2.7 1977 Mission Considerations

The probe targeting sensitivities indicated in the previous subsections for the 1978 mission also apply for the 1977 mission initially studied in this contract. The prime targeting differences in the 1977 mission are Northern instead of Southern hemisphere coverage and a decrease in approach hyperbolic excess velocity (4.4 vs 5.0 km/s), resulting in slightly lower deflection and entry velocities.

Probe Targeting

The probe targeting area of the 1977 mission is illustrated in Figure 4-50. The area within the crescent indicates the region available for targeting using the Set B criteria (see Section 4.2.2.1) of 25- to 45-degrees flight path angles and less than 55-degree descent communication angles. The specific target sites illustrated were chosen to obtain the widest practical latitude and longitude coverage. Comparison with Figure 4-43 indicates that the targeting in 1977 is nearly the mirror image of the 1978 mission with the only difference being in the hemisphere in which the probes are deposited. The entry sites are compared in Table 4-27.

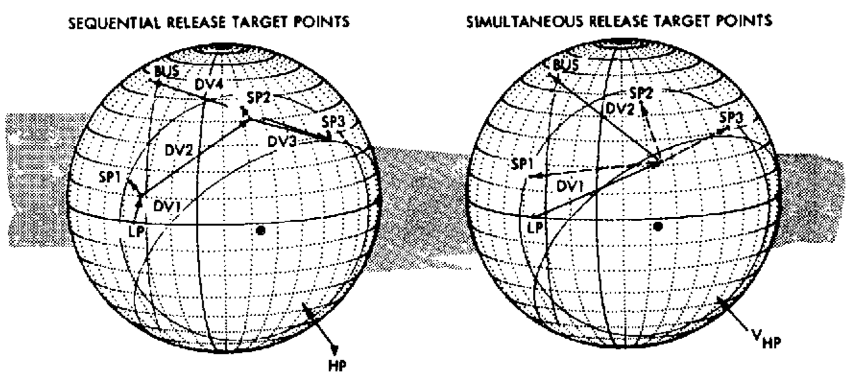

Figure 4-50. 1977 Reference Probe Mission

Table 4-27. 1977 Mission Probe and Bus Parameters

	LARGE PROBE	SEQUENTIAL RELEASE SP1	SEQUENTIAL RELEASE SP2	SEQUENTIAL RELEASE SP3	SIMULTANEOUS RELEASE SP1	SIMULTANEOUS RELEASE SP2	SIMULTANEOUS RELEASE SP3	BUS
AT RELEASE:								
SOLAR ASPECT ANGLE (DEG)	37.7	40.8	23.9	19.6	46.2	46.2	46.2	---
EARTH ASPECT ANGLE (DEG)	149.9	157.2	153.3	138.7	145.9	145.9	145.9	---
RANGE TO VENUS (10^6 KM)	9.57	8.05	6.53	5.01	8.05	8.05	8.05	---
RANGE TO SUN (10^6 KM)	116.0	114.8	113.5	112.3	114.8	114.8	114.8	---
AT ENTRY (6300 KM RADIUS):								
LATITUDE (A)	0	15.0	48.0	30.0	15.0	48.0	30.0	56.9
LONGITUDE (A)	65.0	63.0	110.0	158.0	63.0	110.0	158.0	42.8
FLIGHT PATH ANGLE	37.5	30.4	29.9	42.5	30.4	29.9	42.5	8.3
COMMUNICATION ANGLE	48.3	52.8	50.7	53.8	52.8	50.7	53.8	81.5
ANGLE OF ATTACK	0	0	0	0	54.2	43.3	56.5	0
SOLAR ASPECT ANGLE	71.0	71.8	51.2	37.4	70.7	70.7	70.7	67.0
EARTH ASPECT ANGLE	153.1	159.2	162.4	146.0	146.1	146.1	146.1	180.0
RANGE TO EARTH (10^6 KM)	70.5	70.5	70.5	70.5	70.5	70.5	70.5	70.5
RANGE TO SUN (10^6 KM)	108.7	108.7	108.7	108.7	108.7	108.8	108.7	108.7
TIME OF FLIGHT (DAYS)	25.0	21.0	17.0	13.0	21.0	21.0	21.0	---
TIME OF ENTRY WITH RESPECT TO LP (MIN)	0	0	0	0	+19.6	-27.6	+23.7	+90.0

(A) MEASURED IN VENUS ORBIT PLANE, SUN REFERENCED COORDINATES.

Probe Release Maneuvers and Dispersions

The release maneuvers necessary to attain the Set B target sites in 1977 are summarized in Table 4-28. The sequential release targeting requirements do not include a ΔV to delay entry of the second and third small probes by 1.5 hours, because that requirement was not imposed until after attention shifted to the 1978 mission. The operational sequences are otherwise identical to the 1978 mission.

The dispersion analysis for the 1977 mission is very similar to the 1978 mission. The three-sigma error sources and resulting entry dispersions are summarized in Table 4-29. The larger dispersions for the simultaneous release are due to the large spin rate (62.6 rpm) necessary to acquire the Set B target sites.

Table 4-28. 1977 Mission Probe Release Operations Sequence

TIME (DAYS)	MANEUVER	DELTA V (M/S)	PRECESSION (DEG, ONE-WAY)	SPIN RATE CHANGES (RPM)
OPERATIONS SEQUENCE FOR SEQUENTIAL RELEASE				
ENTRY-25	RELEASE LP	1	30.7	0
E-23	FIRST RETARGET	1.21	75.1	0
E-21	RELEASE SP 1	0	23.1	0
E-19	SECOND RETARGET	6.78	108.7	0
E-17	RELEASE SP 2	0	27.0	0
E-15	THIRD RETARGET	6.13	145.3	0
E-13	RELEASE SP 3	0	43.4	0
E-11	FOURTH RETARGET	26.54	27.6	0
E-4	FIFTH RETARGET (IF REQUIRED)	0.8	100	0
OPERATIONS SEQUENCE FOR SIMULTANEOUS RELEASE				
E-25	RELEASE LP	0	30.7	0
E-23	FIRST RETARGET	5.53	109.0	0
E-21	RELEASE ALL SP'S	0	34.6	115.6 (4.8 TO 62.6 RPM)
E-19	SECOND RETARGET	14.19	44.6	0
E-4	THIRD RETARGET (IF REQUIRED)	0.8	100	0

Table 4-29. 1977 Mission Bus/Probe Error Sources and Resultant Dispersions

ERROR SOURCES		RESULTING 3σ DISPERSIONS									
			SEQUENTIAL RELEASE				SIMULTANEOUS RELEASE				
PARAMETER	3σ ERROR	PARAMETER	LP	SP1	SP2	SP3	SP1	SP2	SP3	BUS
BUS AXIS POINTING (DEG)	1	ENTRY SITE ELLIPSE								
BUS DELTA V POINTING (DEG)		SEMI-A (DEG)	1.66	2.30	6.47	4.10	4.12	5.36	3.91	7.58
DV1	0.3	SEMI-B (DEG)	0.55	0.62	2.23	1.94	1.94	2.42	1.73	0.68
DV2	2.0	FLIGHT PATH ANGLE (DEG)	0.72	1.25	3.80	2.71	2.63	3.15	2.57	4.71
DV3	2.5	COMMUNICATION ANGLE (DEG)	0.55	1.31	5.61	2.96	3.69	4.74	3.03	7.86
DV4 (APPLIES TO DV2 FOR SIMULTANEOUS RELEASE)	0.5	ANGLE OF ATTACK (DEG)	1.64	3.20	3.29	3.35	3.20	3.79	3.23	1.90
BUS DELTA V PROPORTIONALITY	0.03	FLIGHT TIME (MIN)	0.69	0.59	2.05	1.75	1.24	1.38	1.25	1.27
BUS DELTA V GRANULARITY (M/S)	0.03	ENTRY VELOCITY (M/S)	1.55	1.64	3.25	1.85	3.47	3.96	4.59	0.07
BUS SPIN RATE (RPM)	1									
PROBE RELEASE ANGLE (DEG)	1									
BUS POSITION UNCERTAINTY AT E-23 DAYS (KM)	334									
BUS VELOCITY UNCERTAINTY AT E-23 DAYS (M/S)	0.10									

Tracking Considerations

The tracking characteristics of the 1977 mission (Figure 4-51) are slightly superior to those of the 1978 mission (Figure 4-49). Both the 1977 and 1978 Type I trajectories have near-zero geocentric declination on the planetary approach, resulting in difficulty in solving for the z-component of position. However, improved geometry in the 1977 mission results in a position uncertainty after the probe release sequence of 150 km for the 1977 mission, compared to 170 km for the 1978 mission. The effect of the larger second retargeting event (to obtain sequential entry of the probes) in the 1978 analysis should be noted.

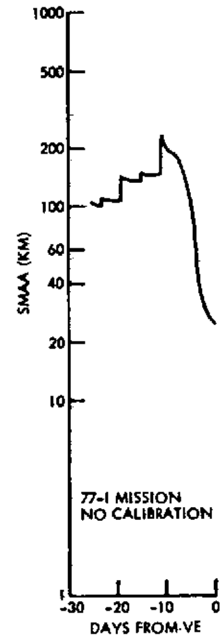

Figure 4-51. Tracking Characteristics of 1977 Mission

4.3.3 Probe Entry Analyses

The key mission design parameters associated with the probe entry phase are ballistic coefficient (B), entry flight path angle (γ_E), entry angle of attack (α_E), parachute deployment time, and small probe science deployment time. This section discusses the system design and performance implications of these parameters and presents the design values.

This section is divided into two parts. The first presents the results generated for the 1978 Atlas/Centaur mission, while the second part contains 1977 mission Atlas/Centaur and Thor/Delta configuration results. The 1978 mission Atlas/Centaur configuration analyses differ from the 1977 in that entry velocities are higher (11.33 vs 11.06 km/s) and the γ_E upper limit for the small probes has been increased to 60 degrees to accommodate target Set A (Section 4.3.2). The 1978 analyses also reflect minor changes from the 1977 configuration: two-stage parachute instead of single stage and 50 g deceleration sensor instead of 0.5 g.

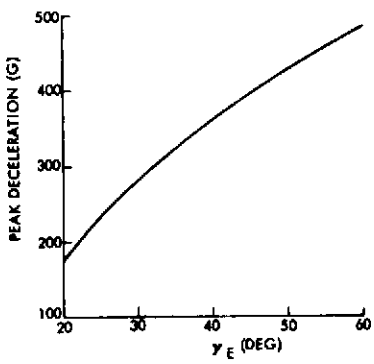

Figure 4-52. Peak Entry Deceleration, 1978 Mission

4.3.3.1 Peak Entry Deceleration, 1978 Mission

Figure 4-52 shows the peak deceleration in earth g's during entry as a function of γ_E. The deceleration levels shown are valid for both large and small probes. The nominal large probe γ_E of 35 degrees results in a peak deceleration of 330 g, while the small probe peak deceleration levels reach 464 g for small probe target Set A (nominal γ_E = 42 degrees).

4.3.3.2 Entry Dynamics Analysis, 1978 Mission

The dynamic characteristics of the large and small probes during entry are evaluated to define mass properties control requirements and resultant entry environment requirements on subsystem design. Entry conditions corresponding to both simultaneous and sequential release targeting strategies are compared for the small probes.

The high dynamic pressure build-up gradient for the Venus entry results in excellent angle-of-attack convergence between entry and maximum dynamic pressure, particularly if nominal or idealized parameters such as center of mass location are considered. Such results can be misleading relative to the definition of subsystem design environments as well as to potential angle-of-attack divergence between maximum dynamic pressure and science deployment when realistic parameter variations are considered. The analysis presented below investigates the impact of imperfect mass balance and high entry angle of attack and spin rates. The general conclusions are typical of those to be expected from other entry shapes in the broad class of blunt sphere/cone configurations.

The Atlas/Centaur small probe total angle of attack envelopes are summarized in Figure 4-53. The entry angle of attack, α_E, is varied from 10 to 20 degrees at 10 rpm spin rate, assuming sequential release targeting (typical 3σ uncertainty, and 60 degrees at 40 rpm for a representative simultaneous release condition. All entries assume a flight path angle of -60 degrees, worst case for loads analysis.

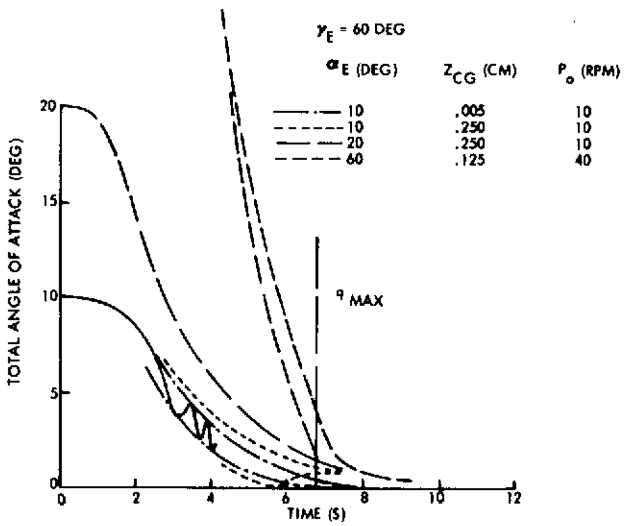

Figure 4-53. Atlas/Centaur Small Probe Total Angle of Attack Envelope

The key factor in Figure 4-53 for the α_E of 10 and 20 degrees is that with no lateral c.g. offset ($z_{c.g.}$), the angle of attack converges to a few tenths of a degree at maximum dynamic pressure (q_{MAX}). Introduction of a lateral c.g. offset (actual c.g. to aerodynamic centerline) results in the low α_E, and low spin rate entries converging to the hypersonic trim angle of attack near q_{MAX}. For the small probe, the α_{TRIM} is approximately 0.95 degrees for an offset of 0.25 cm.

The high α_E, spin rate case (60 degrees and 40 rpm, respectively) introduces two more key factors. The first is that the short time between onset of entry to q_{MAX} does not allow complete angle of attack convergence by q_{MAX}. Secondly, the relatively high roll inertia of the Atlas/Centaur configuration further inhibits angle of attack convergence even at 40 rpm due to gyroscopic effects early in the entry.

The impact of these dynamics characteristics is summarized in the lateral load factors at the probe c.g. shown in Figure 4-54. The upper two curves show the low α_E, spin rate lateral loads in the Y and Z body fixed axes. (The total lateral loads are approximately the RSS of the two envelopes.) For virtually no c.g. offset, the lateral loads are low and symmetrical (less than 4 g). Introduction of c.g. offset in the Z-direction results in the nonsymmetric loading shown for the Z-body loads and increases the lateral load factor at the c.g. to 8 and 11 g (RSS'd) for the α_E of 10 and 20 degrees, respectively. These lateral loads are imposed at a frequency of approximately 22 cycles per second (near q_{MAX}). This high

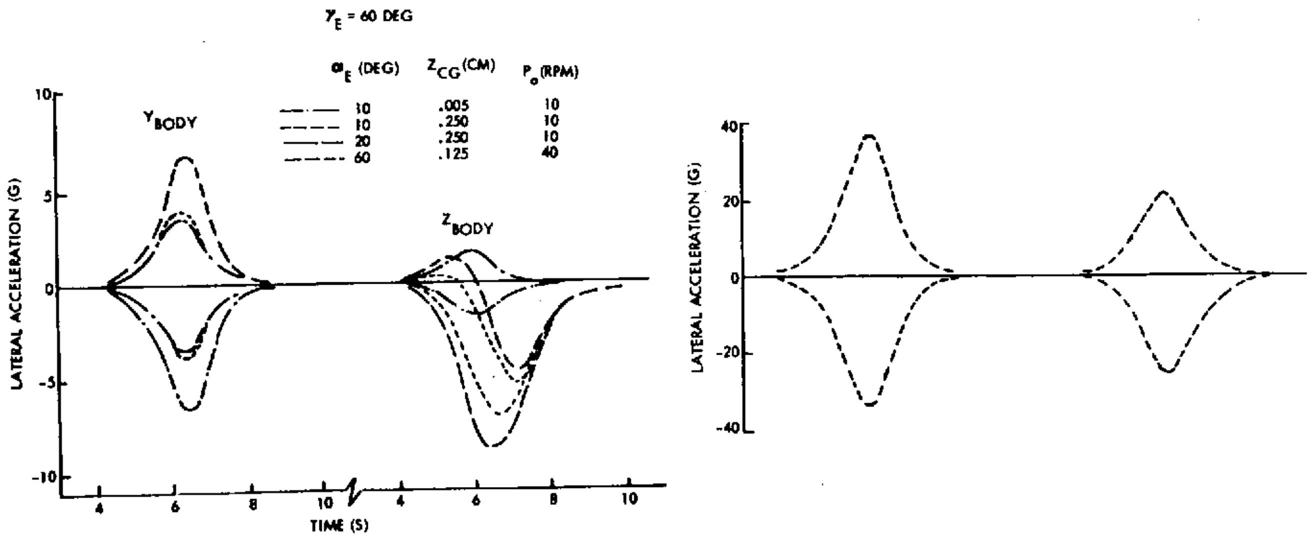

Figure 4-54. Atlas/Centaur Small Probe Lateral Acceleration Envelopes

frequency, coupled with the angle of attack near q_{MAX}, induce additional loads due to angular acceleration of 13 to 19 g per foot at 22 cycles per second at α_E of 10 and 20 degrees, respectively.

The corresponding loads for the high α_E, high spin rate case are approximately 40 g at the c.g. (Figure 4-54) and 60 g per foot due to angular accelerations.

These loads are small compared to the maximum longitudinal load factor of 490 g. Boxes, cabling, etc., designed for the high "static" load factor should be able to easily withstand the additional low α_E (10 to 20 degrees) "dynamic" loads as long as they are defined at an early point in the design. The dynamic loads induced by the high α_E, high spin rate condition will increase the design and test risk.

The above loads environment analysis shows the impact of lateral c.g. uncertainty and high spin rate. Other mass property characteristics investigated include different pitch-yaw inertias and principal axis offsets. Pitch-yaw inertia differences of 2 percent have no impact on the above results. Increasing the differences to 10 percent will increase the total angle-of-attack envelope a few tenths of a degree. Principal axis offsets between zero and 3 degrees have virtually no impact on the above results.

These mass properties uncertainties do impact spin rate, however. Spin rate envelopes for several conditions are shown in Figure 4-55. Although the spin acceleration contribution is small (spin rate variations of ± 3 percent at 22 cps), some degree of sensitivity to both c.g. offset and principal axis offset is indicated.

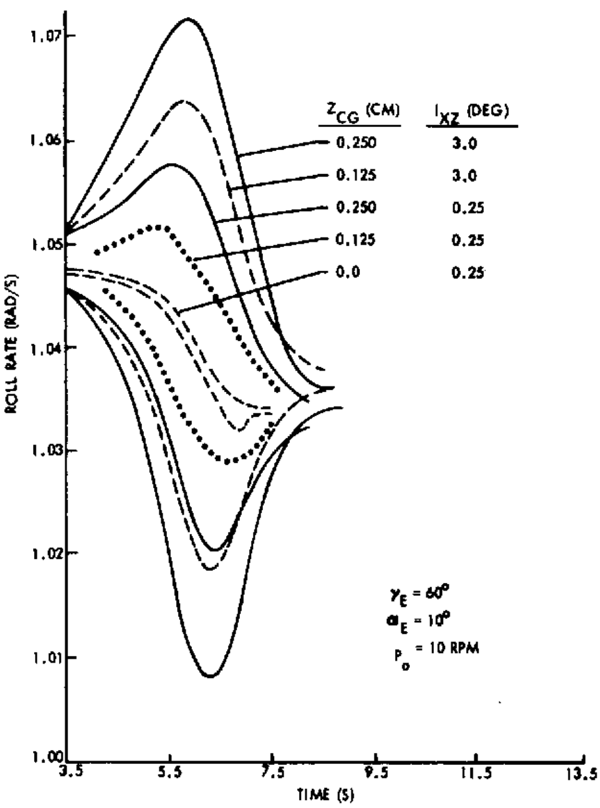

Figure 4-55. Atlas/Centaur Small Probe Roll Rate Variations

The Atlas/Centaur large probe dynamic environment is considerably less severe. The entry angle of attack (3σ uncertainty) can be kept low and the larger size of this probe results in lower natural frequencies (approximately 9 cps at q_{MAX}). The dynamic characteristics are summarized in Figure 4-56.

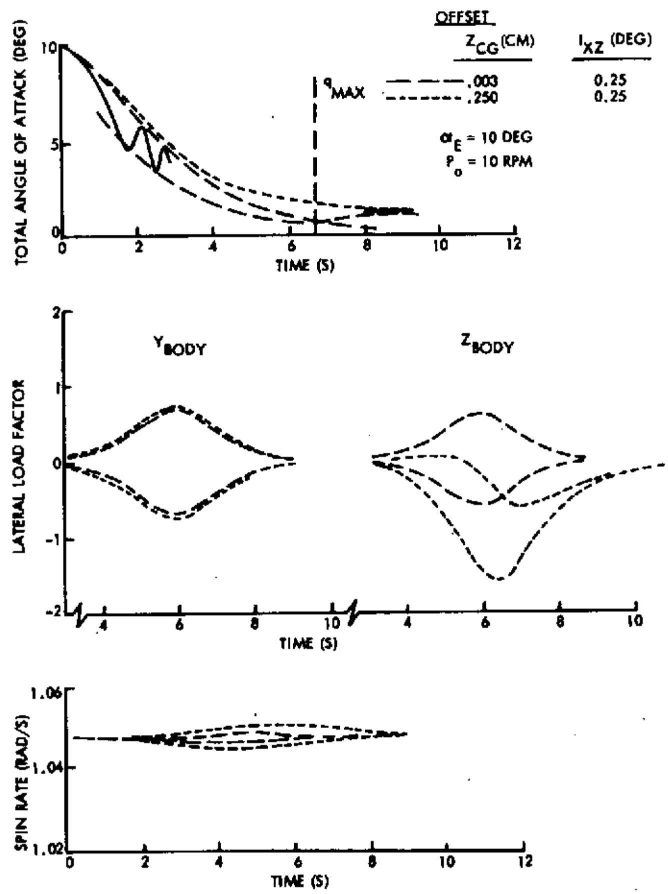

Figure 4-56. Atlas/Centaur Large Probe Entry Dynamics Summary

4.3.3.3 Large Probe Parachute Deployment Conditions, 1978 Mission

The large probe drogue parachute will be deployed by mortar at a fixed time after the 50-g deceleration sensor trips. A 50-g deceleration sensor rather than a low level (0.5 g) sensor is used to improve system reliability because the high-level sensor can remain armed throughout flight. If a low-level sensor is used it must be armed by the coast timer shortly before entry. The performance of a low-level deceleration sensor would therefore depend on the coast timer reliability.

A drogue parachute deployment time of 21 seconds after the 50-g deceleration sensor trip was selected to limit the worst-case dynamic pressure at drogue deployment to 1915 N/m^2 (40 psf). The dominant sources of variations in dynamic pressure at drogue parachute deployment are γ_E and B (ballistic coefficient) variations. Figure 4-57 shows the sensitivity of dynamic pressure, Mach number, and altitude to variations in these two parameters. The B and γ_E ranges indicated ($\pm$ 5 percent and $\pm$ 3 degrees, respectively) are the system design requirements. The nominal case dynamic pressure at drogue parachute deployment is 1695 N/m^2 (35.4 psf). If B is 5 percent above nominal and γ_E is 32 degrees, the dynamic pressure is 1834 N/m^2 (38.3 psf). The highest Mach number at deployment is 0.847 and the lowest altitude (leading to lowest descent science deployment altitude) is 69.71 km.

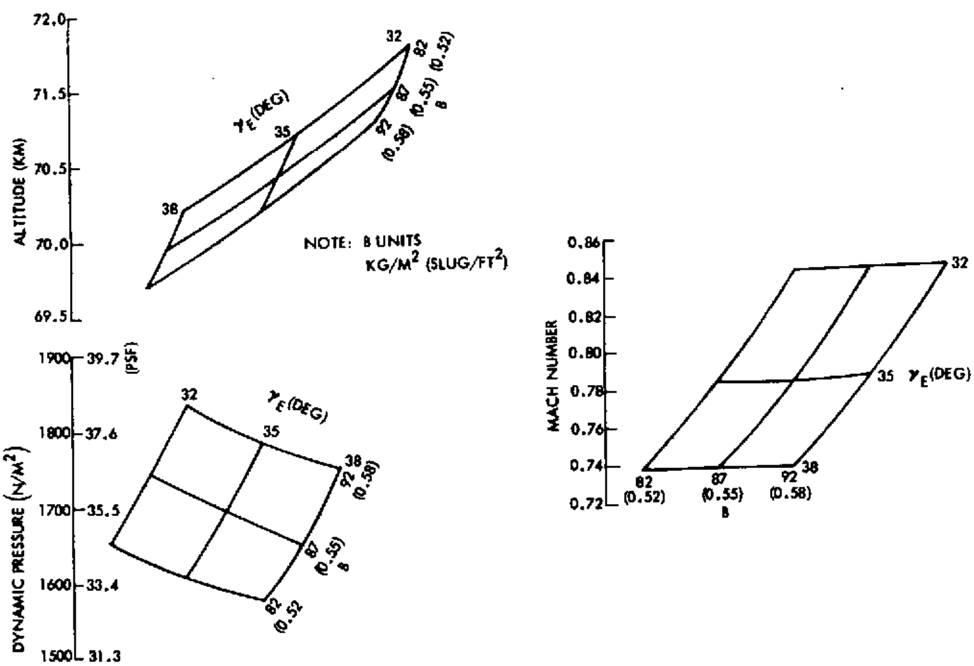

Figure 4-57. Large Probe Drogue Parachute Deployment Conditions

4.3.3.4 Small Probe Descent Science Deployment, 1978 Mission

Deployment exposure of small probe descent science instruments--temperature, nephelometer, IR flux detectors and pressure--is similar to the large probe drogue parachute deployment problem. The instruments must be deployed at a fixed time after the 50-g deceleration sensor trip point. Selection of this time is governed by the science objective to begin data acquisition near 70 km and no lower than 66 km altitude, and a preliminary limit on descent velocity at instrument deployment of Mach 1.5. The requirement that all three small probes be identical implies the science deployment time must be selected so that any γ_E within the design range will meet the deployment altitude and velocity objectives.

Figure 4-58 shows the variations in science deployment altitude, Mach number, and dynamic pressure as functions of γ_E for science deployment times of 15 to 25 seconds after 50 g increasing. Based on these data, a science deployment time of 16 seconds was selected. This time produces a minimum science deployment altitude of 66 km for the steepest entry (γ_E = 60 degrees) and a maximum Mach number at deployment of 1.487 for the shallowest entry (γ_E = 25 degrees). The science deployment conditions are relatively insensitive to ballistic coefficient variations. A 5 percent above nominal B variation decreases the 60 degree γ_E deployment altitude to 65.75 km and increases the Mach number at deployment to 1.49 for a 25 degree γ_E probe.

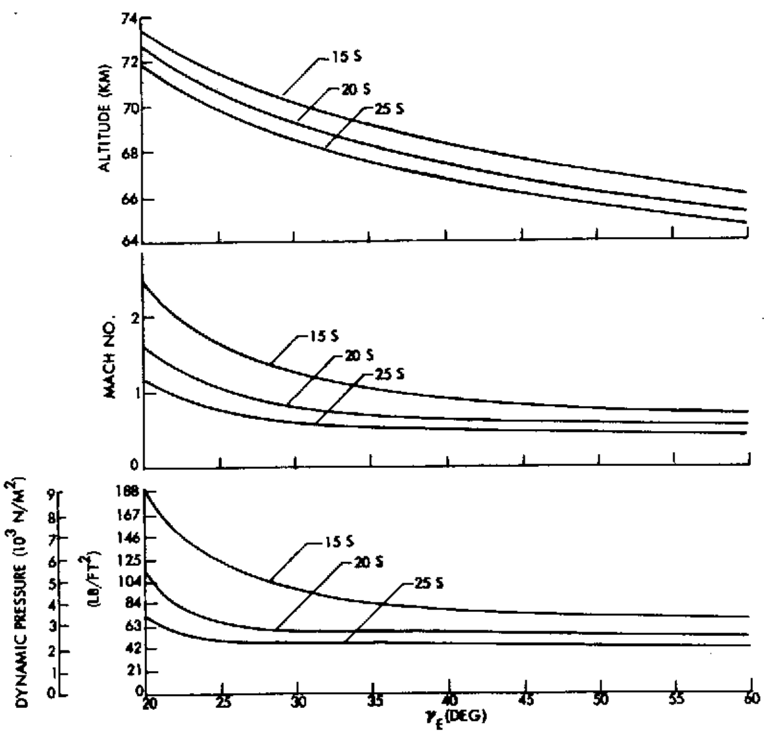

Figure 4-58. Small Probe Science Deployment Conditions

4.3.3.5 Entry Dispersion Analysis, 1978 Mission

Uncertainties in the probe approach trajectories, ballistic coefficient, g sensor trip level, parachute deployment time (T_{PD}), and small probe science deployment time (T_{SD}) produce variations in the peak deceleration, parachute deployment time, and small probe science deployment conditions. Table 4-30 shows the nominal values and accuracy requirements imposed on the entry trajectory and system design.

Table 4-30. 1978 Probe Mission Design Parameters and Accuracies

	LARGE PROBE	SMALL PROBE
B (KG/M^2)	86.4 ± 5%	141.4 ± 5%
γ_E (DEG)	35 ± 3	25 TO 60
V_E (KM/S)	11.330 ± 0.005	11.330 ± 0.005
G SENSOR TRIP POINT	50 G ± 20%	50 G ± 20%
T_{PD} (S)	21 ± 0.5	
T_{SP} (S)		16 ± 0.5

Table 4-31 presents the large probe entry design parameter nominal values and worst-case variations. The maximum axial deceleration is 358 g while the dynamic pressure maximum variation is 331 000 N/m^2. The maximum dynamic pressure at drogue parachute deployment is 1884 N/m^2, well below the design goal of 1915 N/m^2 (40 psf). Drogue parachute deployment altitude varies from 70.19 to 70.79 km.

Table 4-31. Large Probe Entry Design Parameters

	NOMINAL	RANGE
PEAK G	330	304 TO 358
MAXIMUM DYNAMIC PRESSURE (N/M^2)	280 000	246 000 TO 331 000
DROGUE PARACHUTE DEPLOYMENT		
DYNAMIC PRESSURE (N/M^2)	1 695	1 577 TO 1 884
MACH NUMBER	0.786	0.739 TO 0.847
ALTITUDE (KM)	70.45	70.19 TO 70.79

The small probe dispersion study results are shown in Table 4-32. The wide variations in these parameters are due to the relatively wide γ_E design range (25 to 60 degrees) required by target Set A. Tolerances in g sensor trip point and science deployment time are minor contributors to the science deployment variations.

Table 4-32. Small Probe Entry Design Parameters

	RANGE
PEAK G	231 TO 488
MAXIMUM DYNAMIC PRESSURE (N/M^2)	306 200 TO 705 600
SCIENCE DEPLOYMENT	
DYNAMIC PRESSURE (N/M^2)	3 046 TO 5 066
MACH NUMBER	0.697 TO 1.493
ALTITUDE (KM)	65.74 TO 71.61

4.3.3.6 Entry Ballistic Coefficient Range, 1977 Mission

Table 4-33 gives the range of entry ballistic coefficients examined. The probe weights and aeroshell diameters shown resulted from probe system configuration trade studies and are conservative bounds for the respective final configurations. The Thor/Delta configuration drag coefficient ranges

Table 4-33. Entry Ballistic Coefficient Range

	THOR/DELTA		ATLAS/CENTAUR	
	LARGE PROBE	SMALL PROBE	LARGE PROBE	SMALL PROBE
MASS (KG)	147 TO 164	20 TO 30	272 TO 296	64 TO 74
AEROSHELL DIAMETER (M)	1.32 TO 1.42	0.41 TO 0.51	1.60 TO 1.75	0.69 TO 0.81
HYPERSONIC DRAG COEFFICIENT	1.5 TO 1.6	1.0 TO 1.1	1.3 TO 1.4	1.3 TO 1.4
ENTRY BALLISTIC COEFFICIENT	58.1 TO 80	89.5 TO 173	80.0 TO 113	86.5 TO 151
(KG/M^2, (SLUGS/FT^2))	(0.37 TO 0.51)	(0.57 TO 1.1)	(0.51 TO 0.72)	(0.55 TO 0.96)

correspond to 60 and 45 degrees half angle cone aeroshell shapes for the large and small probes respectively. Atlas/Centaur drag coefficient ranges correspond to a common 55 degree half angle cone aeroshell. The ballistic coefficient ranges shown represent the maximum possible variations corresponding to the mass, drag area and drag coefficient ranges.

4.3.3.7 Entry Flight Path Angle Implications, 1977 Mission

Three major considerations establish the design range of entry flight path angles. The first is related to probe targeting, described in Section 4.3.2.7. The entry environment, load factor, and aerodynamic heating, is the second consideration. The final major consideration is the altitude at which the atmospheric science instruments can begin collecting data. The ranges of γ_E given in Section 4.3.2.7 (34.5 to 40.5 degrees for the large probe and 25 to 45 degrees for the small probes) are compatible with load factor, heating, and science deployment altitude.

Figure 4-59 shows the peak deceleration during entry for the range of ballistic coefficients given in Section 4.4.2.1 and γ_E's ranging from 20 to 60 degrees. Peak deceleration is primarily a function of γ_E with a slight dependence on B as shown. The 45-degree upper limit on γ_E generated by probe targeting requirements limits peak deceleration to 400 g.

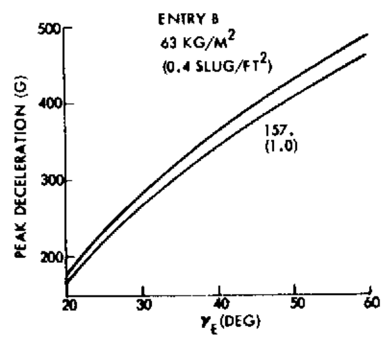

Figure 4-59. Peak Entry Deceleration-1977 Mission

For a given design range of γ_E, the probe heat shield must be designed to withstand the maximum integrated heat pulse, which is associated with the shallowest γ_E. The heat shield material, on the other hand, must be selected for its ability to withstand the maximum entry heating rates and aerodynamic shear, which occur at the steepest γ_E. Thus, the design range of γ_E has a major impact on the test facility requirements for entry heating simulation. Figure 4-60 shows the variation of peak stagnation pressure with γ_E for the expected range of probe ballistic coefficients. The capability of the Martin Marietta 5 MW Arc Jet Facility is super-imposed to illustrate the difficulty that will be encountered in testing to the full γ_E range.

Altitude at Mach 1 (Figure 4-61) gives an indication of the variations in science deployment altitude due to B and γ_E variations. Descent science measurements will commence near Mach 1. The large probe parachute will be deployed near Mach 0.8 while the small probe pressure, temperature, and other sensors will be deployed near Mach 1.5.

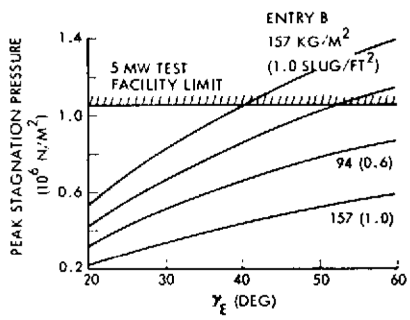

Figure 4-60. Peak Stagnation Pressure

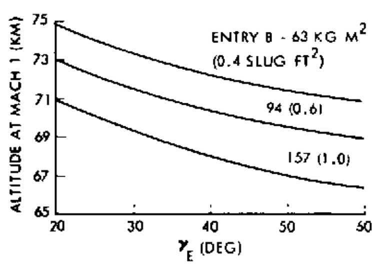

Figure 4-61. Altitude at Mach 1

4.3.3.8 Entry Dynamics Analysis, 1977 Mission

The Thor/Delta large and small probe entry dynamic characteristics have been evaluated as a function of angle of attack (α_E) and spin rate at entry (P_o). The differences between these results and those presented for the 1978 mission Atlas/Centaur configuration are primarily related to physical size and lower inertias.

The maximum total angle-of-attack envelope during the entry of the small probe is shown in Figure 4-62 for several α_E and P_o of 5 and 60 rpm. The base characteristics at P_o = 5 rpm show that the angle of attack has almost converged to its minimum value at maximum dynamic pressure for α_E = 5 degrees. At higher entry angles of attack, the convergence is not completed at maximum dynamic pressure. This leads to a peak lateral load factor approximately 1/2-second before peak longitudinal load factor. The angle-of-attack sensitivity at this time to α_E and P_o is also shown in

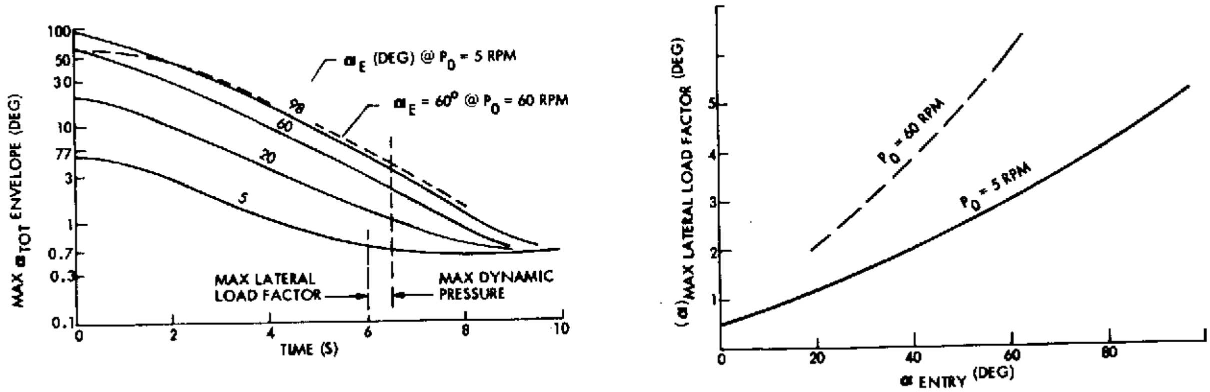

Figure 4-62. **Small Probe Entry Dynamics**

Figure 4-62. (These data assume a lateral c.g. offset of 0.05 cm, giving a trim angle of attack of 0.47 degrees at maximum dynamic pressure.)

The impact of these dynamic characteristics on lateral load factor are summarized in Figure 4-63. High α_E or P_o results in lateral load factors at the c.g. between ± 10 to ± 20 g at approximately 160 rad/s (25 c/s). Superimposed on this is an additional load factor of ± 30 to $+60$ g per foot from the c.g. due to the angular acceleration and ± 3.5 to ± 7.0 g per foot from the c.g. radially due to the angular velocity.

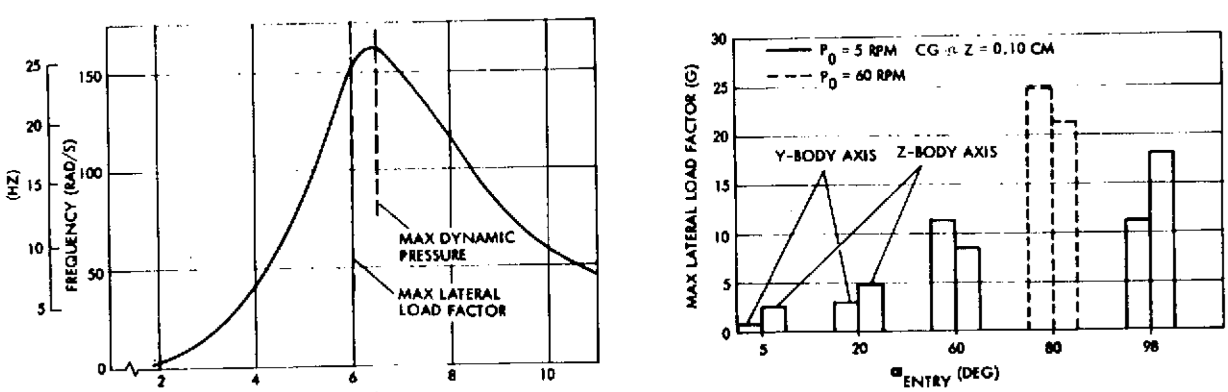

Figure 4-63. **Small Probe Entry Dynamic Environment**

The combination of lateral c.g. offset, slightly different pitch and yaw inertias, and principal axis offset results in some roll coupling, which becomes significant at high α_E values. Spin rate time histories for the high α_E and P_o conditions are shown in Figure 4-64. At α_E = 60 degrees and P_o = 5 rpm the spin rate essentially goes to zero during the entry for the c.g. offset direction used in the run. At P_o = 60 rpm, the spin rate fluctuates approximately ±3 rpm at high frequency. The α_E = 98 degrees, P_o = 5 rpm case has fairly violent spin rate oscillations between approximately ±10 rpm. At lower α_E, the spin rate variations are relatively small, 0.1 to 0.4 rpm for α_E of 5 and 20 degrees.

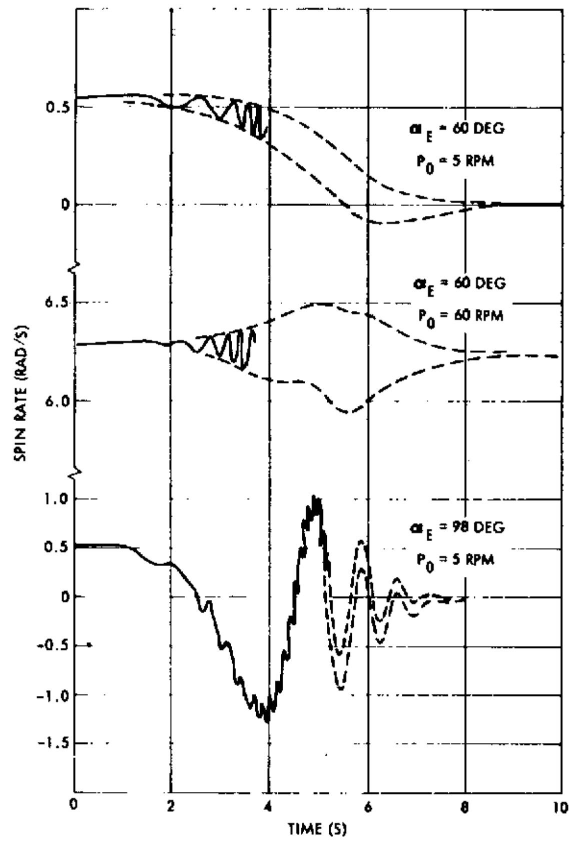

Figure 4-64. Small Probe Entry Spin Rate Dynamics

The large probe entry dynamics result in a relatively passive environment compared to the small probe because the entry angle of attack can be controlled to a low value (nominally zero). Angle of attack convergence is similar to the α_E = 5 degrees shown in Figure 4-63 for the small probe. Maximum lateral accelerations at the c.g. vary from 0.5 to 0.6 g for spin rates between 5 to 15 rpm. The maximum frequency is 50 rad/sec (8 c/s).

4.3.3.9 Large Probe Parachute Deployment, 1977 Mission

The large probe parachute is deployed by mortar at a fixed time after 0.5 g increasing deceleration is sensed. The time from 0.5 g was selected to limit the velocity at deployment to subsonic values and limit dynamic pressure to 1900 N/m^2 (40 psf). This dynamic pressure limitation is more restrictive than the subsonic deployment requirement. As long as dynamic pressure is below 1900 N/m^2, parachute deployment will take place at subsonic velocity. These parachute deployment restrictions are consistent with the science objective of beginning descent science data acquisition near 70 km altitude.

Figure 4-65 shows the time from 0.5 g increasing deceleration to the time when dynamic pressure has decreased to 1900 N/m^2, as a function of γ_E and B. The values of B shown bound the large

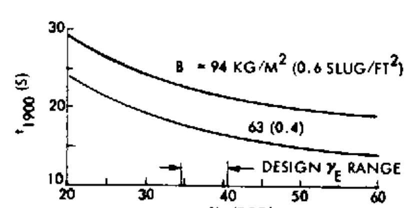

Figure 4-65. Large Probe Parachute Deployment

probe B range given in Table 4-33. A parachute mortar fire time of 24 seconds was selected. Dynamic pressure will be less than 1900 N/m^2 for this parachute deployment time as long as γ_E is within the design range.

4.3.3.10 Small Probe Descent Science Deployment, 1977 Mission

The small probe temperature, nephelometer, IR flux radiometer, and pressure sensors will be exposed to the atmosphere by nonexplosive devices actuated at a fixed time from 0.5 g increasing deceleration. Selection of this time is governed by the science objective to begin data acquisition near 70 km and a preliminary limit on descent velocity at deployment of Mach 1.5. The final descent velocity deployment limit will be established when detailed instrument design information is available.

The time between 0.5 g increasing deceleration and the time at which descent velocity decreases to Mach 1.5 is shown as a function of γ_E in Figure 4-66. This relationship is valid for entry ballistic coefficients from 78 kg/m^2 (0.5 $slug/ft^2$) to 157 kg/m^2 (1 $slug/ft^2$). Since the small probes will be identical, all three must have the same science deployment time. Thus, deployment time must be selected for the limiting γ_E over the design range. The design science deployment time selected (20 seconds) corresponds to a γ_E of 25 degrees. For a small probe entering with a γ_E of 45 degrees, science will be deployed approximately 8 seconds after the Mach 1.5 limit. The common deployment time of 20 seconds gives science deployment altitudes ranging from 72 to 67 km for the design γ_E range.

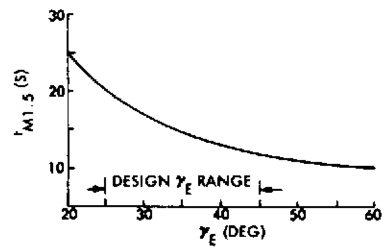

Figure 4-66. Small Probe Science Deployment

4.3.3.11 Entry Dispersion Analysis, 1977 Mission

Entry dispersion analyses were conducted to establish the variations in peak deceleration, maximum dynamic pressure, parachute deployment environment, and small probe science deployment environment. These dispersions were due to entry trajectory uncertainties, B uncertainty, g sensor trip point accuracy and timer accuracy. The γ_E and entry velocity uncertainties shown in Table 4-34 are consistent with probe targeting uncertainties given in Section 4.3.2.7. The g sensor trip point accuracy, parachute deployment time (T_{PD}), and small probe science deployment time (T_{SD}) accuracies shown are the system performance specifications.

Table 4-34. 1977 Reference Mission Design Parameters and Uncertainties

	LARGE PROBE	SMALL PROBE
B (KG/M^2)	71 ± 5% (A)	142 ± 5% (A)
	87 ± 5% (B)	114 ± 5% (B)
γ_E (DEG)	37.5 ± 3	25 TO 45
V_E (KM/S)	11.063 ± .005	11.063 ± .005
G - SENSOR TRIP POINT	0.5 G ± 20%	0.5 G ± 20%
T_{PD} (S)	24 ± 0.5	
T_{SP} (S)		20 ± 0.5

(A) THOR/DELTA CONFIGURATION
(B) ATLAS/CENTAUR CONFIGURATION

Table 4-35 gives the nominal values and worst-case variations in the large probe design parameters associated with the entry phase for the Thor/Delta and Atlas/Centaur configurations. The peak deceleration and dynamic pressure ranges given are system d sign parameters for the aeroshell,] eat shield, and probe structure. The maximum dynamic pressure at parachute deployment is well below the design goal of 1900 N/m^2 (40 psf) for both configurations. The subsonic parachute deployment velocity is satisfied since the maximum Mach number at deployment is 0. 8. Altitude at parachute deployment varies from 69. 2 to 71. 7 km.

Table 4-35. Large Probe Entry Design Parameters

	THOR/DELTA		ATLAS/CENTAUR	
	NOMINAL	RANGE	NOMINAL	RANGE
PEAK G	341	365 TO 311	338	362 TO 309
MAXIMUM DYNAMIC PRESSURE (N/M^2 x 10^3)	237	266 TO 206	286	321 TO 250
PARACHUTE DEPLOYMENT				
DYNAMIC PRESSURE (N/M^2)	1334	1439 TO 1239	7671	1791 TO 1571
MACH NUMBER	0.73	0.78 TO 0.69	0.75	0.80 TO 0.70
ALTITUDE (KM)	70.95	71.69 TO 70.21	70.05	70.80 TO 69.23

The small probe dispersion study results are shown in Table 4-36. Velocity at science deployment is limited to Mach 1. 5 while the maximum dynamic pressure is 5263 N/m^2 (110 psf). The 4. 6 km spread in science deployment altitude is primarily due to the common science deployment time. Tolerances in g sensor trip point and science deployment time are minor contributors to this variation.

Table 4-36. Small Probe Entry Design Parameters

	THOR/DELTA	ATLAS/CENTAUR
PEAK G	393 TO 215	388 TO 216
MAXIMUM DYNAMIC PRESSURE (N/M^2 x 10^3)	553 TO 282	454 TO 231
SCIENCE DEPLOYMENT		
DYNAMIC PRESSURE (N/M^2)	5263 TO 2813	4466 TO 2428
MACH NUMBER	1.49 TO 0.75	1.50 TO 0.77
ALTITUDE (KM)	71.60 TO 66.94	72.54 TO 67.90

4.3.4 Probe Descent Analysis

This section summarizes the descent phase studies relating to Atlas/Centaur and Thor/Delta weight sensitivity, descent trajectory sensitivity, probe dynamic response to winds, and descent trajectory tracking. The descent phase of the probe mission is essentially independent of the mission year. The descent rate through the Venus atmosphere depends on the probe ballistic coefficient and the atmospheric density and is independent of the entry velocity variations associated with changes in launch/arrival dates.

4.3.4.1 Probe Weight Sensitivity

Analyses were conducted to obtain weight sensitivity of the Atlas/Centaur large probe and Thor/Delta large and small probes preferred designs to variations in the descent parameters. The large probe key descent trajectory parameters are parachute phase ballistic coefficient (B_{CH}), parachute jettison or staging altitude (H_s), and the descent capsule ballistic coefficient (B_{DC}). The small probe descent trajectory is described by the subsonic ballistic coefficient (B_{SP}).

The large probe battery, thermal control, and parachute weights vary with the descent trajectory parameters. Battery weight is proportional to total descent time which is a function of all three descent trajectory parameters. Thermal control weight is sensitive to the descent rate through the lower portion of the Venus atmosphere where the temperature is high. The lower atmosphere descent rate depends on B_{DC}. The parachute size and hence weight depends on B_{CH}.

Figure 4-67 shows the relationship between large probe total descent time, B_{CH}, and B_{DC}, assuming the staging altitude is fixed at 43 km. This altitude is used since the Version IV science payload specifies science data rates that set the maximum staging altitude at 44 km. The preferred Atlas/Centaur configuration average battery load during descent is 322 watts. Since the battery energy density is 56 w-hr/kg, the battery weight sensitivity to total descent time for the Atlas/Centaur large probe is 0.096 kg/min. This factor can be used in conjunction with Figure 4-67 to estimate the Atlas/Centaur battery weight variations due to changes in large probe ballistic coefficients. The relationship between ballistic coefficients and science data rate capability is discussed in Section 3.1.1. The other

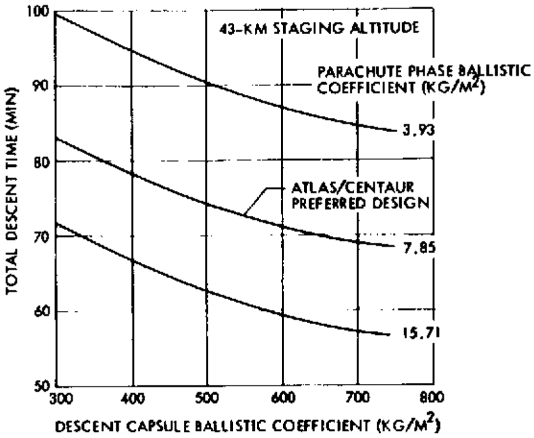

Figure 4-67. **Large Probe Total Descent Time**

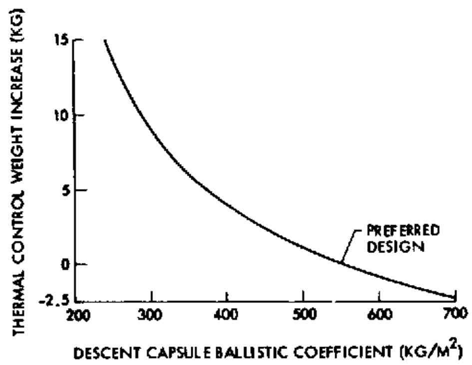

Figure 4-68. **Atlas/Centaur Large Probe Thermal Control Weight Sensitivity**

major Atlas/Centaur large probe weight variation with B_{DC} is shown in Figure 4-68. The thermal control system weight is quite sensitive to the descent capsule ballistic coefficient.

Figure 4-69 shows the Thor/Delta large probe weight variations due to B_{CH} and H_s assuming the descent capsule ballistic coefficient is fixed at 550 km/m^2 (3.5 slug/ft^2). The parachute ballistic coefficient must be less than 31 kg/m^2 in order to separate the aeroshell from the descent capsule. As B_{CH} is reduced, the probe weight increases due to longer total descent time and increased parachute weight. Reducing the staging altitude also increases weight due to longer descent times. Figure 4-70 shows that a 5 kg weight savings could be realized by increasing the descent capsule ballistic coefficient to 1256 kg/m^2 (8 slug/ft^2). Thermal control weight is the major source of this reduction. However, this change in B_{DC} would significantly reduce the amount of science data acquired since the descent velocity would be increased by about 50 percent.

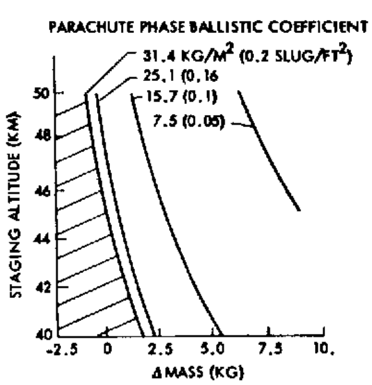

Figure 4-69. **Weight Sensitivity to B_{CH}**

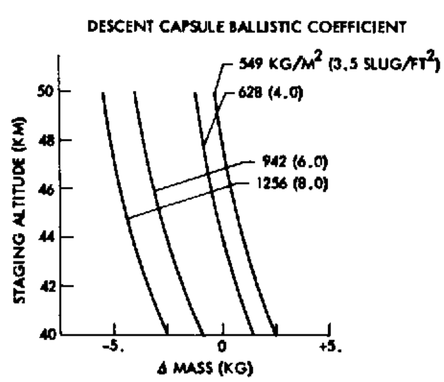

Figure 4-70. **Weight Sensitivity to B_{DC}**

The Thor/Delta small probe weight sensitivity to B_{SP} is shown in Figure 4-71. The small probe weight sensitivity is much greater than the large probe because the diameter of the small probe aeroshell must be altered to produce the change in B_{SP}. The variations in battery and thermal control weight due to descent time and velocity are minor when compared to structural and heat shield weight variations associated with changes in aeroshell diameter.

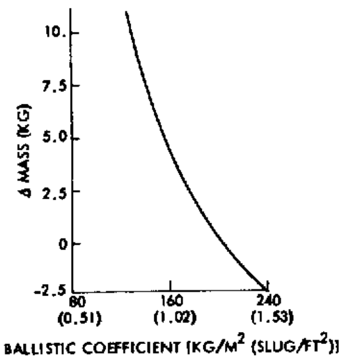

Figure 4-71. Small Probe Weight Sensitivity

4.3.4.2 Descent Trajectory Sensitivity

The preliminary system design specifications on ballistic coefficient tolerance have been set at ± 7 percent for the parachute phase of the large probe descent and ± 5 percent for the descent capsule and small probe. The other major source of descent trajectory variations in atmosphere uncertainty. Descent trajectory sensitivity to the current NASA set of engineering models of the Venus atmosphere (Reference 6) have been evaluated. The variations associated with Model III (maximum molecular mass and maximum solar activity) and Model IV (minimum molecular mass and minimum solar activity) bound those produced by the other models.

The variations in Atlas/Centaur staging altitude and total descent time (time from 50 g to mean surface) due to the ballistic coefficient uncertainty and atmospheres discussed above are given in Table 4-37. The worst-case large probe staging altitude error (ballistic coefficient plus atmosphere variation) is 890 meters. The worst case error in descent time is less than 6 percent of the normal value. Table 4-38 gives similar results for the Thor/Delta probes.

Table 4-37. Atlas/Centaur Descent Trajectory Uncertainty

	STAGING ALTITUDE (KM)	DESCENT TIME (MIN) LARGE PROBE	DESCENT TIME (MIN) SMALL PROBE
NOMINAL	42.9	73.0	65.0
VARIATION DUE TO BALLISTIC COEFFICIENT	+0.48	+1.0	+1.6
	-0.45	-0.9	-1.6
VARIATION DUE TO ATMOSPHERE	+0.22	+0.5	+0.7
	-0.44	-1.3	-2.2

Table 4-38. Thor/Delta Descent Trajectory Uncertainty

	STAGING ALTITUDE (KM)	DESCENT TIME (MIN)	
		LARGE PROBE	SMALL PROBE
NOMINAL	49.7	50.1	62.4
VARIATION DUE TO BALLISTIC COEFFICIENT	+0.4	+1.0	+1.6
	-0.3	-0.9	-1.5
VARIATION DUE TO ATMOSPHERE	+0.1	+0.4	+0.7
	-0.3	-1.3	-2.1

4.3.4.3 Dynamic Response to Winds

The probe response to wind shear has been evaluated for a wind shear of 0.05 s^{-1} (NASA SP-8011). The analysis has been performed using both approximate solutions and six-degree-of-freedom (6DOF) computer simulations (small probe and descent capsule) and two-body, 3DOF computer simulation for the parachute phase.

The approximate solutions are compared to the computer simulation results in Figure 4-72, 4-73, and 4-74 for the parachute and descent capsule/small probe configurations, respectively. The first-order approximation for the parachute case (Figure 4-72) shows reasonable agreement with the computer output, at least for the final trim attitude. The dynamic response is somewhat different, primarily since the computer simulation is a two-body problem (parachute and capsule).

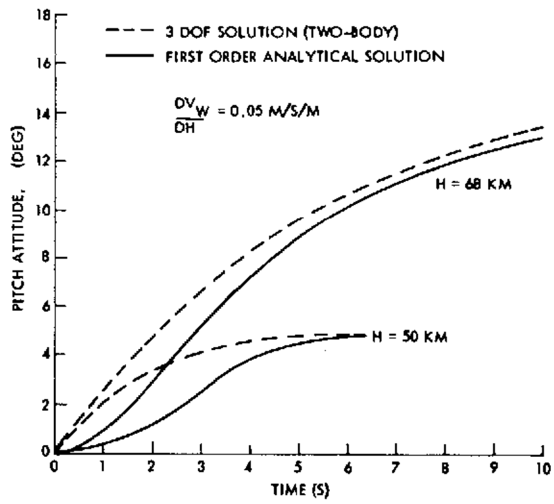

Figure 4-72. Parachute Response to Wind Shear

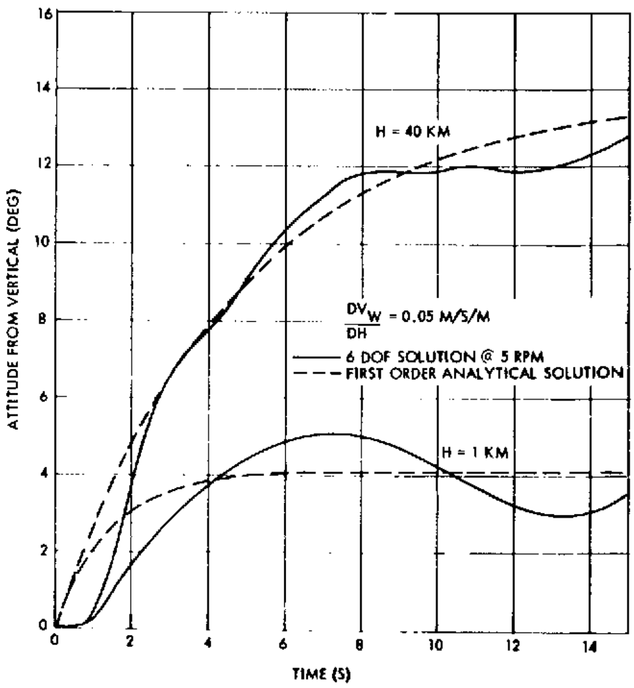

Figure 4-73. Descent Capsule Response to Wind Shear

The comparison of the descent capsule and small probe analytical and 6DOF response to the 0.05 s^{-1} wind shear is shown in Figures 4-73 and 4-74, respectively. The 6DOF run has a spin rate of 5 rpm. The only significant difference between the two solutions is the 5 rpm "beat" which shows up on the 6DOF solution.

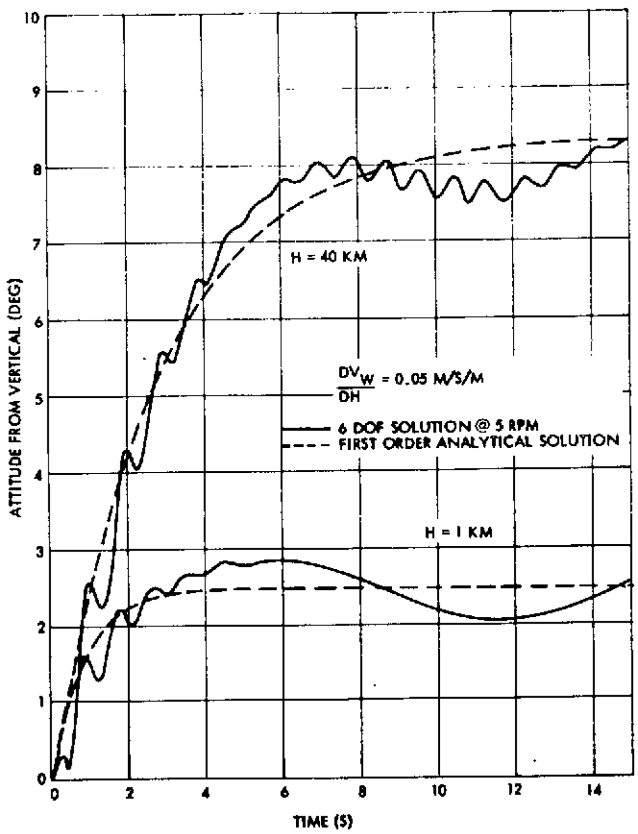

Figure 4-74. **Small Probe Response to Wind Shear**

These results show that the first-order analytical solution given below can be used to evaluate vehicle attitude in response to wind shears.

$$\theta(t) = \theta_T \left(1 - e^{-t/\tau}\right)$$

where

$$\sin \theta_T = \frac{dV_w}{dh} \frac{V_T}{g}$$

$$\tau = \frac{V_T}{g}$$

The angle of attack variation during the response is small (less than 1 degree).

The resultant attitude variation with altitude and corresponding time constant for the Atlas/Centaur large and small probes is shown in Figure 4-75. This attitude variation represents an increased (adverse) communication aspect angle if an increasing wind as the vehicle descends is blowing away from earth. Conversely, a wind blowing towards earth results in an improved communication aspect angle.

The large time constant for the small probes at high altitude results in a slow attitude change with time. The data in Figure 4-75 show the maximum attitude change that will be experienced if the gradient is maintained until velocities of 10, 20, 50, or 100 m/s are reached and then the wind is kept constant. Typically, a gradient with a wind velocity change of 25 m/s (at altitudes over 50 km) can be handled with ease. There should be no problems at lower altitudes for the small probe.

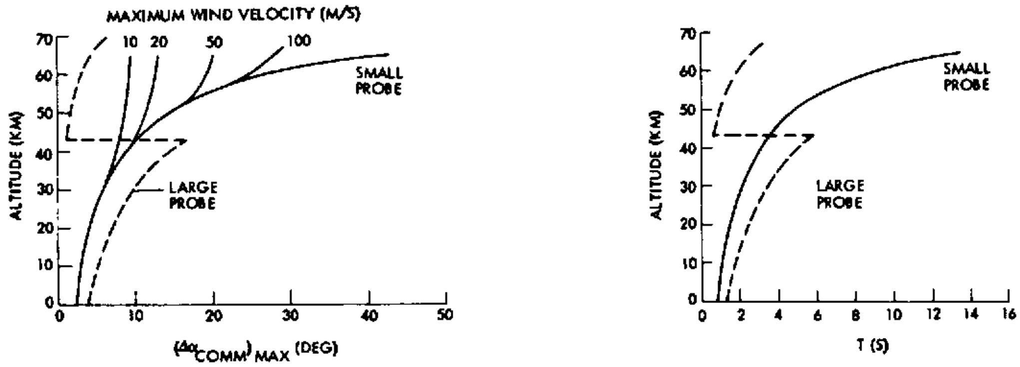

Figure 4-75. Large and Small Probe Attitude Variations to 0.05 m/s/m Wind Shear

The Atlas/Centaur large probe maximum attitude variation is less than 15 degrees at all altitudes except 43 to 40 km. Changing the staging altitude to 40 km would limit the attitude variation to 15 degrees for all altitudes.

4.3.4.4 Probe Descent Tracking

One of the scientific objectives of the Pioneer Venus probe mission is to determine the circulation patterns on the planet. This requires tracking of the probes during their descent in the Venusian atmosphere. Both standard Doppler tracking (one- and two-way) and DLBI (doubly-differenced very long baseline interferometry) have been suggested as possible means of doing this descent tracking. This mission and systems implications of these tracking schemes have been assessed for their impact on the mission design.

Standard Doppler tracking measures the velocity component of the probe along the line of sight to earth. The DLBI measurement (Reference 7) is obtained by making the differencing measurements from two vehicles (generally a probe and the spacecraft) at two ground-based tracking stations. The processed measurement determines the relative velocity component of the two vehicles in the direction formed by projecting the baseline vector (the vector from the first station to the second) onto the plane normal to the earth-Venus line. Thus the DLBI measurement always furnishes complementary data to the Doppler measurement. The two measurement types in combination can furnish an effective means of measuring the horizontal velocity of the probes. The knowledge of the probe response to winds (discussed in the previous section) combined with the time history of the probe horizontal velocity then yields the wind profile encountered by each probe.

Assumptions of Study

The probe descent tracking study was performed using the following assumptions:

1) A linear error analysis is conducted using a Kalman-Schmidt recursive filter to compute the accuracy of the probe velocity determination at the surface.

2) The tracking is initiated with an a priori state uncertainty of the probe of 10 km position and 500 cm/s velocity (one-sigma spherical).

3) The probe is assumed to move as a point mass at terminal velocity in the Venusian atmosphere. The probe descent trajectory begins at 70-km altitude and has a two-stage descent with ballistic coefficients of 25 and 550 kg/m^2 (0.16 and 3.5 $slug/ft^2$). The atmospheric parameters are those of the NASA SP-8011 (September 1972) most probable profile.

4) DLBI measurements are modeled as alternative measurements from Goldstone/Madrid, and Goldstone/Arecibo. Perfect knowledge is assumed of the bus. The bus is assumed to move on a hyperbolic approach trajectory with bus entry delayed 90 minutes from probe entry.

The efficiency of the tracking process is characterized by the minimum and maximum eigenvalues of the one-sigma uncertainty ellipse of the (local) horizontal velocity of the probes at the surface. The minimum and maximum eigenvalues correspond to the velocity uncertainties in the most and least favorable directions respectively.

Mission Implications

Figure 4-76 illustrates several of the important mission characteristics of DLBI. The progressive velocity uncertainty in the best direction is plotted for a variety of descent conditions. Case A is the reference case, representing the large probe configuration and entry site of the 1977 mission and assuming a 2.5 percent uncertainty in ballistic coefficient and a DLBI noise corresponding to one electrical degree. The tracking for Case D, in which the ballistic coefficient uncertainty was reduced to zero, is essentially identical to Case A, demonstrating the relative insensitivity of tracking to ballistic coefficient uncertainties of the expected magnitude. For comparison purposes the uncertainty in the worst direction is also plotted for these cases. Case B demonstrates the effect of a slower descent; the tracking uncertainties are essentially identical, but the aerodynamic

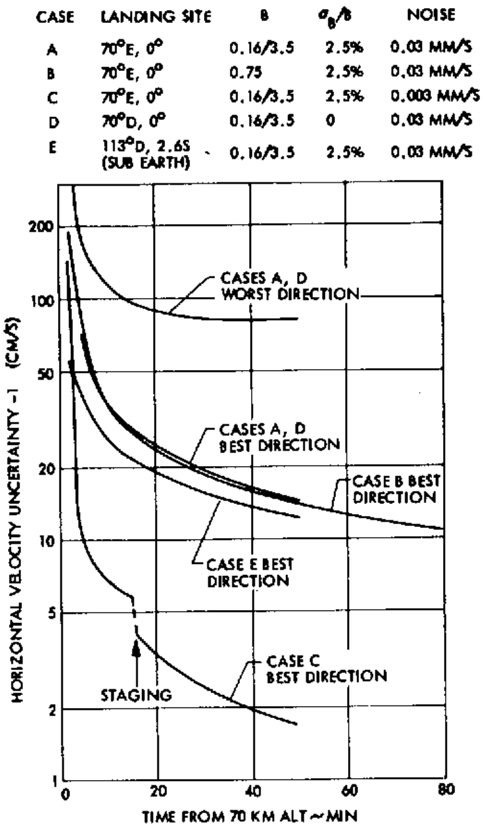

Figure 4-76. Probe Descent Tracking with DLBI

response would be different. Case E illustrates the improvement that could be obtained by moving the entry site to the subearth point. The subearth point is the optimal probe location for determining the probe horizontal velocity by DLBI alone. In contrast, using Doppler tracking, the horizontal velocity is best determined at sites 90 degrees from subearth. Dramatic improvement is obtained for Case C where the DLBI measurement noise is decreased by an order of magnitude. Thus the tracking effectiveness is relatively insensitive to the general-mission parameters of entry site location or descent rate, but is dominated by the measurement noise.

Measurement Noise Parametrics

Because of the importance of the measurement noise on probe descent tracking and because of the relative uncertainty of the actual noise levels of the measurements, a parametric study of measurement noise has been conducted with the results summarized in Table 4-39.

The prime characteristic of Doppler tracking is that it determines only one component of velocity. The semimajor axis remains at the a priori uncertainty level while the semiminor axis is reduced to a level compatible with the measurement noise. For Doppler noise levels of less than 100 mm/s the semiminor axis of velocity uncertainty is less than 2 cm/s.

A significant feature of DLBI tracking is that it always reduces the semimajor axis well below the a priori value. This is caused by the rotation of the baseline vector during the hour-long descent of the probe. Two station DLBI (single baseline) results in semimajor and semiminor axes of 94 and 46 cm/s while three station DLBI (two baselines) reduces the values to 81 and 14 cm/s. The semiminor horizontal velocity errors increase approximately linearly with increasing DLBI measurement noise.

Table 4-39. Descent Tracking Sensitivities

EFFECT OF DOPPLER NOISE ON DOPPLER TRACKING		
NOISE LEVEL (MM/S)	EV_{MAX} (CM/S)	EV_{MAX} (CM/S)
10	499.0	0.58
100	500.0	1.92
1000	500.0	16.6
2000	500.0	32.2

EFFECT OF DLBI NOISE ON DLBI TRACKING (3 STATIONS: GOLDSTONE/MADRID/ARECIBO; 2 STATIONS: GOLDSTONE/MADRID)		
NOISE LEVEL (ELECTRICAL DEG)	EV_{MAX} (CM/S)	EV_{MAX} (CM/S)
1 (2 STATIONS)	94.0	45.8
1 (3 STATIONS)	80.6	14.3
5 (3 STATIONS)	240.4	66.6
10 (3 STATIONS)	365.0	128.3

EFFECT OF COMBINED DOPPLER/DLBI TRACKING			
DOPPLER NOISE (MM/S)	DLBI NOISE (ELECTRICAL DEG)	EV_{MAX} (CM/S)	EV_{MAX} (CM/S)
10	1 (2 STATIONS)	45.8	0.56
10	1 (3 STATIONS)	15.0	0.56
1000	10 (3 STATIONS)	143.8	16.6

Combined tracking produces the best aspects of each type of tracking: the error is reduced significantly in the best direction and the error in the worst direction is very significantly reduced over the a priori value. Even for very conservative error levels of 1000 mm/s Doppler noise and 10 electrical degrees DLBI noise the horizontal velocity is well determined.

One-Way vs Two-Way Tracking

Because of the penalties associated with including a two-way transponder on the large probe (cost, weight, volume, power, false lock possibilities) discussed in Section 7.6.3, an important consideration is the tracking improvement it affords. Table 4-40 summarizes the current estimates of the noise levels associated with one- and two-way Doppler tracking. The Doppler noise in millimeters per second is approximately 10^7 times the oscillator accuracy (Section 7.6.3). In a two-way system

Table 4-40. One- and Two-Way Uncertainties

	ONE-SIGMA DOPPLER NOISE LEVELS (MM/S)	
	TWO-WAY	ONE-WAY
OSCILLATOR INSTABILITY	10^{-5}	1
PROCESS NOISE	1	10
VENUS ATMOSPHERIC EFFECTS	10 TO 100	10 TO 100
RSS TOTAL	10 TO 100	14 TO 101

the instability is about 10^{-12}, resulting in a negligible Doppler uncertainty. The oscillator instability in a one-way system is in the range 10^{-5} to 10^{-10}. The value recommended in Section 7.6.5 is ± 4 parts in 10^7 (three-sigma) or a frequency accuracy (one sigma) of 1.3×10^{-7} and a Doppler noise of 1.3 mm/s.

The standard two-way Doppler noise for interplanetary analysis is 1 mm/s. Because the oscillator instability is negligible for two-way Doppler, this contribution is assigned to process noise (assumed to include earth atmosphere medium effects, interplanetary medium, processing errors, etc.). The corresponding one-way noise is estimated to be one order of magnitude worse because of the inability to use the standard Doppler extractor equipment.

The effects of the Venus atmosphere are extremely difficult to assess without a detailed study. Assuming that the standard two-way noise (1 mm/s) is due mainly to earth atmosphere effects and assuming that the Venus atmosphere effects are similar to those of the earth, the Venus contribution is estimated to be in the 10 to 100 mm/s range (since the descent is to 100 bars).

Thus the oscillator instability is seen to be a minor contributor to the total Doppler noise and Venus atmospheric effects appear to dominate.

Since wind drift radar is now a large probe science instrument, it will provide information on the lower altitude winds. Thus earth-based tracking will be most important in the upper regions where the lower estimates of Venus atmospheric effects (10 mm/s) would be expected. For this error level the one-way tracking would be expected to be about 40 percent worse than the two-way transponder. However, for such error levels the Doppler tracking would be able to solve for horizontal velocities in the direction along the earth line to less than a couple centimeters per second for either tracking system (Table 4-39). Combining Doppler with DLBI tracking (at a conservative error level of 10 electrical degrees) would reduce the uncertainty in the worst direction to less than a couple of meters per second, which should be adequate for the upper winds. It should be emphasized that these DLBI results should be equivalent for either one-way or two-way Doppler because of the differencing out of oscillator errors.

4.3.5 Probe Bus Targeting

The selection of the bus entry target site is based on scientific objectives and hardware constraints. The science objectives summarized in Section 3.3.1 discussed the need for 4 or 5 minutes of bus measurements below 1000 km altitude. Shallow bus entry angles (less than about 15 degrees) are necessary to satisfy this requirement. The preferred bus attitude is determined by two desires: the bus should be aligned for small angles of attack to facilitate science instrument operation (Section 3.3.1) and the bus axis should be pointed directly at the earth to optimize the communication link to earth (Section 8.2.4). Since the attitude required for zero angle of attack is a function of the particular entry site selected, that impact must be considered in the entry site selection. Finally the trajectory uncertainties must be considered in choosing the bus entry site. At entry angles shallower than -8 degrees, the bus skips out before reaching an acceptable altitude (Section 4.2.6). Therefore, the entry angle must be chosen so that, even with three-sigma dispersions, entry angles shallower than -8 degrees will be avoided.

4.3.5.1 1978 Bus Targeting

The approach geometry for the 1978 probe mission was illustrated in Figure 4-42. The diagonal line running from the upper right corner to the lower left corner represents the trace of the orbit passing through the V_{HP} vector and the subearth point. For a given entry flight path angle, the entry site having the least earth aspect angle will lie on this trace. Figure 4-77 presents the 1978 bus targeting characteristics in slightly more detail. The flight path angle contours and the optimal bus trajectory trace are plotted on a Mercator projection of the planet along with contours of the bus entry degradation (BED) angle. The BED angle is the angle between the zero angle-of-attack direction for a given entry site and the direction to earth. Thus, the bus may be aligned for zero angle of attack (resulting in an earth aspect angle of BED degrees), for zero earth aspect angle (resulting in an angle of attack of BED degrees), or for any combination in between so that the sum of the angles is BED degrees. As indicated in the figure, the combination of shallow entry angles and low BED angles is met in the sunlit portion (solar longitude less than 90 degrees) of the southern hemisphere of the planet.

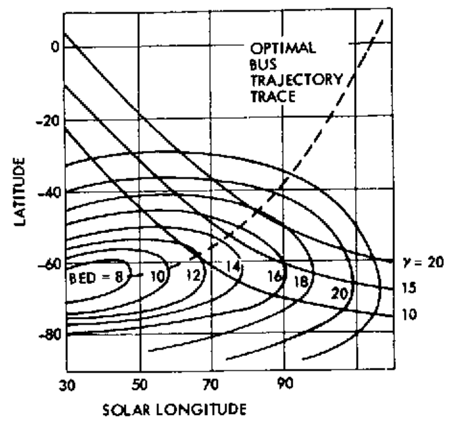

Figure 4-77. 1978 Bus Targeting (Mercator Projection)

The optimal bus mission design for science performance would have as shallow a flight path angle as possible (simultaneously ensuring low BED angles). The practical limit is determined by bus skip-out considerations. Entry analyses (Section 4.2.6) have indicated that for entry angles shallower than -9.5 degrees the bus is not captured, but skips back out of the atmosphere. For an entry angle of -8 degrees, the bus reaches a minimum altitude of 144 km; this is considered the shallowest entry angle acceptable for science considerations. A bus entry site selection ground-rule is to insure that even with three-sigma dispersions this limit will not be exceeded.

The bus entry footprint is dominated by the knowledge uncertainty in tracking the bus. Figure 4-49 illustrated the tracking characteristics of the bus following the probe release sequence. The one-sigma uncertainty in the magnitude of the impact parameter B immediately following the nominal retarget maneuver is 216 km. Nine days of tracking is sufficient to reduce this uncertainty to 50 km. The tracking is based on Doppler only using a noise of 1 mm/s for a one-minute count time and equivalent station location errors (ESLE's) corresponding to no-charged particle calibration (see Table 4-26).

The relation between B and γ for the 1978 mission ($B = 14\,263 \cos \gamma$ km) is plotted in Figure 4-78. If a final midcourse is scheduled at E - 2 days, the three-sigma knowledge uncertainty of B at that point is 150 km. The nominal value of B for the shallowest allowable entry angle (8 degrees) is $B_{MAX} = 14\,130$ km. Thus to limit the possibility of skipout the nominal B should be selected at $B_{NOM} = B_{MAX} - 3\sigma_B = 13\,980$ km. This corresponds to a nominal entry angle of 11.5 degrees. The minimum B magnitude (three sigma) is then $B_{MIN} = B_{NOM} - 3\sigma_B = 13\,830$ km, corresponding to a three-sigma steepest entry angle of 14 degrees. Thus the nominal entry site for the bus is selected as $\gamma = 11.5$ degrees; the bus however must be designed for an entry corridor of $8 < \gamma < 14$ degrees. The fact that the entry corridor

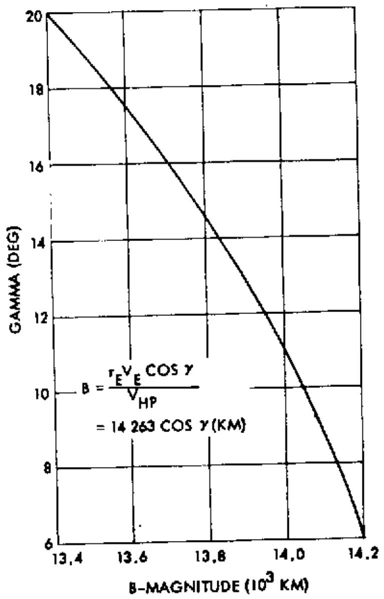

Figure 4-78. Gamma versus B-Magnitude

is not centered on the nominal entry angle is caused by the greater sensitivity of shallower entry angles to dispersions as evidenced by the nonlinearity of the entry angle-impact parameter relationship (Figure 4-78).

The statistical ΔV required for the final midcourse at E - 2 days may be estimated by forming the quotient of the B-magnitude uncertainty at the bus retargeting event over the time from encounter. The three-sigma velocity increment is then approximated by (648 km/ 2 days) or 3.8 m/s. An intermediate refinement maneuver at E - 4 days of 1.9 m/s would reduce the three-sigma B uncertainty to 240 km (see Figure 4-49), decreasing the size of the maneuver at E - 2 days to 1.4 m/s.

4.3.5.2 1977 Bus Targeting

The approach geometry for the 1977 mission was illustrated in Figure 4-50. The detailed description of the bus targeting is given in Figure 4-79. The region of the planet having shallow entry angles and low BED angles is in the sunlit portion of the northern hemisphere. The lower BED angles in 1977 (for comparable entry flight path angles) resulted in an easier design of the bus RF system.

The tracking characteristics of the 1977 were illustrated in Figure 4-50. The tracking is slightly more effective in 1977 and this combined with the improved geometry results in a nominal bus entry angle of 10.5 degrees and an entry corridor of $8 < \gamma < 13$ and BED angles of under 4 degrees.

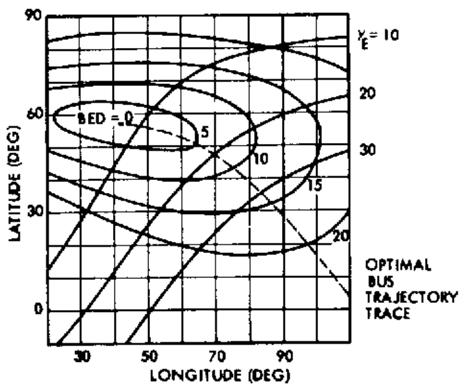

Figure 4-79. 1977 Bus Targeting

4.3.6 Entry and Demise of the Probe Bus

As discussed in the previous section, the bus target site selected represents a rational compromise between the science requirements presented in Section 3.3.1.1 and the instrument ram angle and earth communication angle limitations imposed by the bus. In Section 3.3.1, the trajectory of the bus was projected from approximately 2000 km above the planet's surface down to the turbopause, which occurs at a nominal altitude of 130 km. The effects of the atmosphere were ignored in this projection. At 250 km, the atmospheric portion of the bus trajectory is assumed to commence, with initial conditions (flight path angle and angle of attack) established by the Venus-approach geometry and the selected target site. This section describes the atmospheric portion of the bus trajectory.

The mission of the probe bus is to provide a platform for science sensors to take data in the ionosphere and upper atmosphere of Venus. It must penetrate the atmosphere to enable samples to be taken at altitudes the orbiter cannot reach, i.e., below about 200 km. It would be desirable for the bus to continue functioning at least down to the turbopause, 130 km. Two aspects of the bus' entry and descent through the atmosphere are addressed here: 1) what altitude does the bus reach before it no longer can perform its function of acquiring and transmitting scientific data; and 2) at what altitude do the science measurements begin to become contaminated by the presence of the bus.

Potential causes for the demise of the bus are: deceleration loads, aerodynamic heating, communications blackout, and communication loss due to change in bus attitude with respect to the earth line. These effects are discussed and illustrated below. Brief consideration is also given to the aerodynamic flow regimes that the bus encounters as it penetrates deeper into the atmosphere, and the potential impact of the flow field on atmospheric sampling by the bus mass spectrometers. The atmospheric model used in the analysis of bus entry phenomena is the 1972 Venus Atmosphere Model I (most probable molecular mass and mean solar activity) defined in NASA SP-8011, September, 1972.

In the following discussion, the 1977 Thor/Delta probe bus is used to illustrate how the various entry phenomena affect the bus' performance. The analysis was performed for a trajectory corresponding to an entry flight path angle of γ_E = -0.244 radian (-14 degrees); this value of γ_E was estimated early in the Phase B study, before targeting uncertainties were included in the mission analysis. It now appears that this is a more comfortable trajectory than can be achieved realistically in the 1977 mission. Nevertheless, the results are considered to be representative of the relative order in which the various entry phenomena occur as the bus descends. A brief examination was also made of the 1978 Atlas/Centaur bus, using a trajectory with the appropriate nominal entry flight path angle, γ_E = -0.201 radian (-11.5 degrees). It will be seen that the causes of the demise of the bus are substantially unchanged, with minor shifts in their altitudes of occurrence.

4.3.6.1 Bus Aerodynamic Characteristics

The configuration of the Thor/Delta bus as it enters the Venusian atmosphere is illustrated in Figure 4-80. At low angles of attack the oncoming flow encounter surfaces (A), (B), and (C). After the thermal control blankets (A) and (B) burn through, the flow encounters the equipment platform (D) and the inner surface of the central cylinder (E). Note that there is no covering over the aft end of the central cylinder. At large angles of attack [approaching 1.57 radians (90 degrees)], the oncoming flow encounters surfaces (C), (F), and (G). Various subsystem equipment and science instruments have been ignored in defining the aerodynamic configuration. The only exception is the magnetometer boom (J), which is nominally

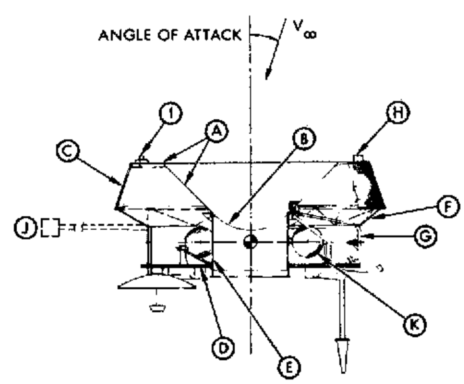

LEGEND:

A THERMAL SHIELD: ONE OUTER LAYER 2 MIL TEFLON, ALUMINIZED ON ITS INNER SURFACE, LAMINATED TO ONE INNER LAYER OF 2 MIL CLEAR MYLAR.
B THERMAL SHIELD: 22 LAYERS 1/4 MIL ALUMINIZED MYLAR SANDWICHED BETWEEN TWO 2 MIL ALUMINIZED MYLAR COVER SHEETS.
C SOLAR ARRAY: SOLAR CELLS ON ALUMINUM HONEYCOMB PANEL.
D EQUIPMENT PLATFORM: 3/4-INCH ALUMINUM HONEYCOMB PANEL.
E CENTRAL CYLINDER: 0.040-INCH ALUMINUM SHEET.
F SAME AS A
G SAME AS B
H NEUTRAL MASS SPECTROMETER
I ION MASS SPECTROMETER
J MAGNETOMETER AND BOOM (ROTATED 2.09 RAD (120 DEG) FROM ACTUAL POSITION)
K HYDRAZINE TANK

Figure 4-80. 1977 Thor/Delta Probe Mission Bus Entry Configuration extended during cruise and entry of the bus. The positions of the two mass spectrometers (H) and (I) are also shown in Figure 4-80.

Free molecular flow was assumed for determining the aerodynamic characteristics of the bus. It will be shown subsequently that this is a reasonable assumption from entry at 250 km down to about 110 km where the bus mission will have ended. The equations for the normal and tangential aerodynamic stresses in free molecular flow (Reference 8) are functions of the speed ratio and temperature ratio,

	Altitude h = 250 km	Altitude h = 150 km
speed ratio, $s = \dfrac{V}{\sqrt{2\,RT}} =$	15	29
temperature ratio $= \dfrac{T_{Body}}{T} =$	0.44	0.83

where V and T are the velocity and temperature of the oncoming flow, R is the atmospheric gas constant, and T_{Body} is the surface temperature of the bus. The values of the speed ratios shown above were based on a nominal entry velocity of 11.06 km/s. This velocity is virtually unchanged as the bus descends from 250-km altitude to about 100 km. Also, surface temperatures on the bus are relatively cool at entry, 294 to 327°K (70 to 130°F), and remain unaffected by aerodynamic heating down to about 150 km. Thus, for the ranges of speed ratio and temperature ratio shown above, aerodynamic characteristics of flat plates, cones, and cylinders at angle of attack were obtained from existing computer simulation data. Accommodation coefficients of 1 for the normal and tangential momentum of reemitted molecules were assumed for this analysis, implying that all atmospheric molecules impacting the bus give up their kinetic energy and are reemitted after accommodating to the bus temperature.

Bus aerodynamic coefficients for a range of angles of attack from 0 to 1.57 radians (0 to 90 degrees) were generated from the aero coefficient data of simple geometric shapes, as described in the previous paragraph. The effects of shadowing were included. Results are shown in Figure 4-81 for the axial and normal force coefficients and the pitching

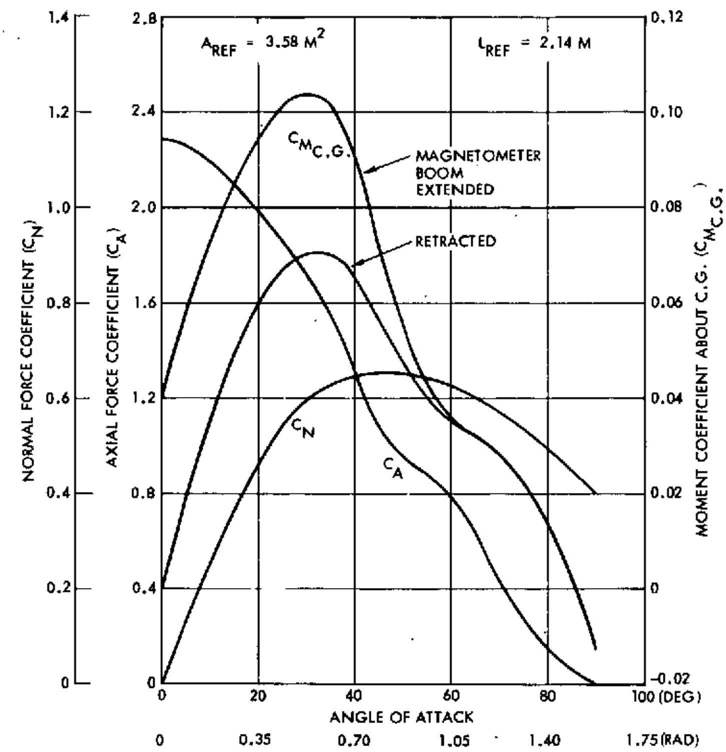

Figure 4-81. Free Molecular Flow Aerodynamic Coefficients of Thor/Delta Probe Bus

moment coefficient about the bus center of gravity. The pitch damping derivative, $C_{m_q} + C_{m_{\dot{\alpha}}}$, was assumed to be zero. It is evident from the coefficient data that the bus is aerodynamically unstable at small angles of attack even with the magnetometer retracted. The vehicle does not become stable until reaching an angle of attack about 1.48 radians (85 degrees).

4.3.6.2 Entry Trajectories

Point mass trajectories were computed for an entry velocity of 11.06 km/s and for various entry flight path angles (entry assumed to start at 250-km altitude). A ballistic coefficient of 15.7 kg/m^2 (0.100 slug/ft^2), corresponding to a bus mass of 126 kg (279 pounds) and the zero angle of attack drag coefficient, was used in the computer runs. The variation of flight path angle with altitude is shown in Figure 4-82 for entry path angles from -0.244 to -0.105 radian (-14 to -6 degrees). It is evident that, for entry angles shallower than -0.166 radian (-9.5 degrees), the bus is not captured and skips back out of the atmosphere. For γ_E = -0.166 radian (-9.5 degrees) and steeper, the bus is captured

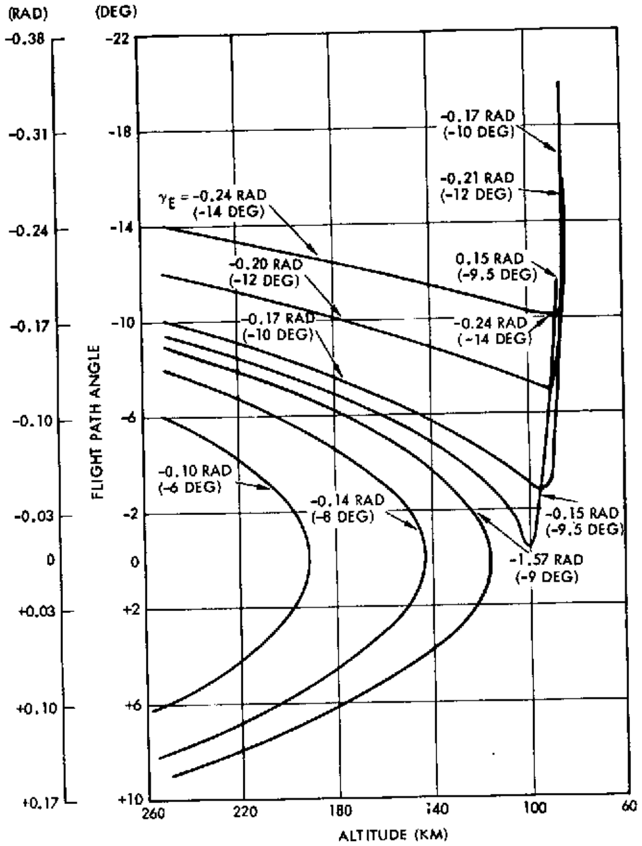

Figure 4-82. Thor/Delta Probe Flight Path Angle Variation

and plunges into its demise. At γ_E = -0.140 radian (-8 degrees), the bus reaches a minimum altitude of 144 km, which is probably the shallowest entry that can be allowed from the standpoint of science measurements. It would be desirable for the bus to penetrate (and function!) at least to the turbopause, which is postulated to occur at 130 km in the model of the Venus atmosphere used here.

The deceleration of the bus along its flight path is shown in Figure 4-83. The extended magnetometer boom can be expected to fail at 1/2 g (114 km); major structural damage to the bus itself will commence in the 25- to 30-g range (about 99 km). The altitudes at which these deceleration levels occur are essentially independent of entry flight path angle.

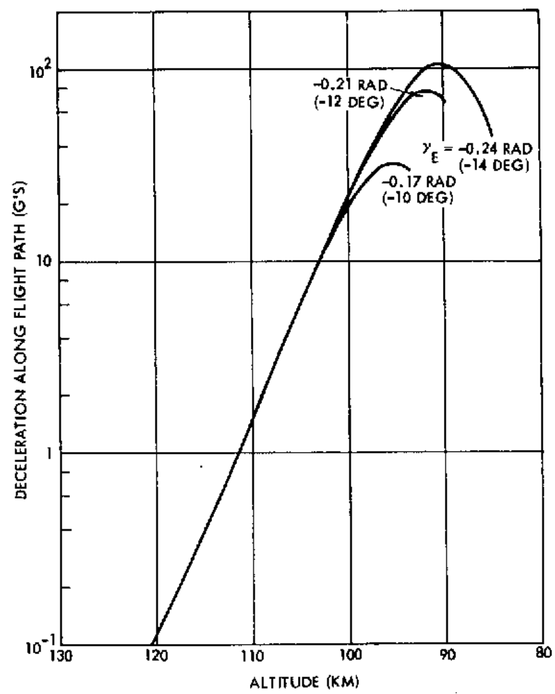

Figure 4-83. Thor/Delta Probe Bus Deceleration During Entry

A brief six-degree-of-freedom trajectory study was performed to investigate the divergence in angle of attack which will result from the unstable aerodynamic nature of the bus configuration. The following matrix of initial conditions was investigated; an entry velocity of 11.06 km/s and an entry flight path angle of -0.244 radian (-14 degrees) were used for all cases.

	Entry Angle of Attack [rad (deg)]	Spin Rate (rpm)	Magnetometer Boom
Case I	0 (0)	5	Extended
Case II	0.035 (2)	5	Extended
Case III	0.035 (2)	60	Extended
Case IV	0.035 (2)	5	Retracted

Results are shown in Figure 4-84 as the variation in angle of attack with altitude for Cases II and III. The increase in angle of attack from entry down to about 150 km is the result of the decrease in flight path angle over this altitude range (see Figure 4-82) since the bus spin axis remains fixed in inertial space in the absence of disturbing aerodynamic torques. Aerodynamic effects begin to be felt commencing at about 140 km. If the bus is targeted so that its spin axis is inertially aligned toward earth prior to entry [(earth aspect angle = 3.14 radians (180 degrees)], deviations from this alignment due to angle of attack buildup cause the bus high-gain antenna to point away from earth. The Thor/Delta probe bus can tolerate a 0.122 radian (7-degree) deviation from earth pointing before its communication performance starts to degrade. Figure 4-84 shows that an angle of 0.122 radian (7 degrees) is reached at 129 km if the bus enters at 0.035 radian (2 degrees) angle of attack and is spinning at its nominal rate of 5 rpm. If $\alpha_E = 0$, divergence to the communication angle limit occurs at about the same altitude. By spinning the bus up to 60 rpm prior to entry, the angle of attack divergence to 0.122 radian (7 degrees) can be delayed down to 112 km. With magnetometer boom retracted and a nominal 5 rpm spin rate, $\alpha = 0.122$ radian (7 degrees) is reached at 124 km.

4.3.6.3 Aerodynamic Heating

Under the assumption of free molecular flow, the rate of energy transfer to a body intercepting the free stream is represented by (Reference 9):

$$(\rho V \sin \theta) \left(\frac{1}{2} V^2\right)$$

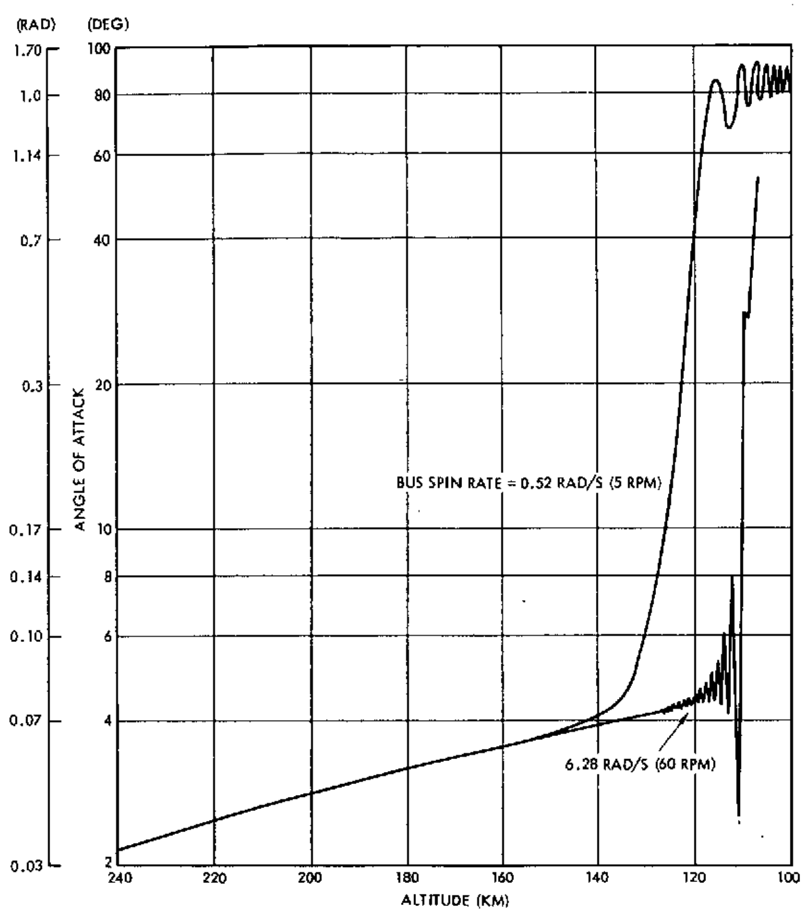

Figure 4-84. Thor/Delta Probe Bus Angle of Attack Divergence During Entry (Magnetometer Boom Extended)

where ρV is the free stream mass flow rate, θ is the inclination of the surface to the flow direction, and the $\frac{1}{2} V^2$ completes the expression for kinetic energy. Thus, for a surface perpendicular to the oncoming flow [(θ = 1.57 radians (90 degrees)], the free molecular heat transfer rate may be approximated by

$$\dot{q}_{FM} = \frac{\rho V^3}{2J}$$

where J is Joule's mechanical equivalent of heat constant. The heating of the thermal control surface A in Figure 4-80 was determined using these heat rates. This surface consists of one outer layer of 2-mil teflon aluminized on its inner surface, laminated to one inner layer of 2-mil clear mylar. The emissivity of the outer layer is ϵ = 0.66. It was assumed that the thermal capacity of this teflon-mylar laminate is zero, so that the aerodynamic heat input is continuously balanced by the emitted infrared radiation. Thus,

$$\frac{\rho V^3}{2J} = \sigma \epsilon (T_s{}^4 - T_o{}^4)$$

where σ is the Stefan-Boltzmann constant, T_s is the temperature of the thermal control surface, and T_o is the temperature of the medium receiving the radiation. For the purposes of this analysis, T_o was assumed to be 305°K (90°F). The resulting temperature rise of the teflon-mylar laminate is shown in Figure 4-85. Mylar turns brown and deteriorates when its temperature reaches 394 to 422°K (250 to 300°F). Teflon degrades and outgasses between 478 to 505°K (400 and 450°F). Thus, this surface is expected to begin sustaining thermal damage by the time the bus reaches an altitude of 145 to 143 km. The two mass spectrometers are located in the midst of this thermal control surface, and teflon outgassing products can contaminate their samples.

An approximate calculation was also made to determine the altitude range where thermal damage to the bus structure and its subsystems is expected to begin. A hydrazine propellant tank (K in Figure 4-80) was selected as a typical element for this analysis. It was assumed that the tank is shielded from the external flow until the thermal control surfaces forward of it are destroyed, which was considered to occur at 140 km. The spherical tank was then exposed directly to the oncoming flow, and all adjacent bus structure and subsystem equipment were ignored. The temperature, T_T, at the

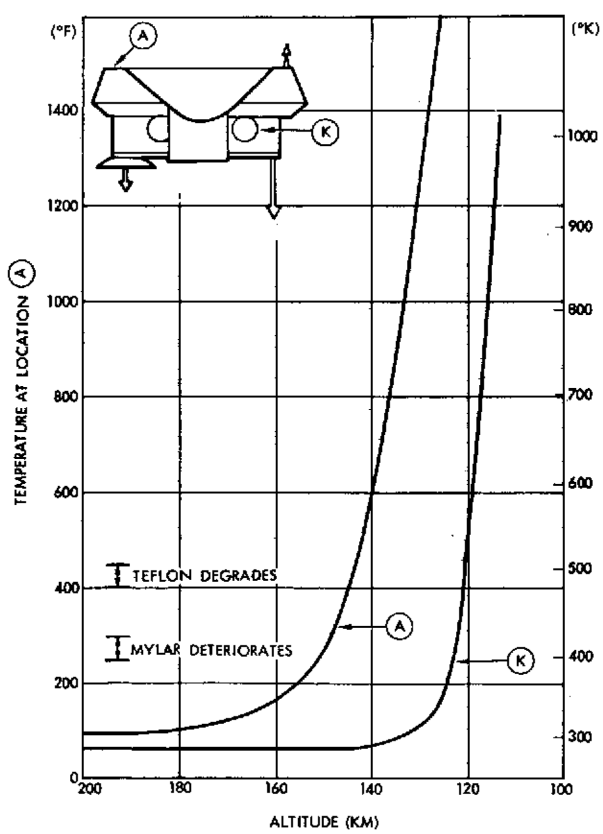

Figure 4-85. Aerodynamic Heating of Thor/Delta Probe Bus

stagnation point of the tank was calculated as follows:

$$(\rho\ c_p\ \tau)_T \frac{dT_T}{dt} = \dot{q}$$

where $\dot{q}$ is the aerodynamic heating rate. The reradiation term, $\sigma\epsilon\ (T_T{}^4 - T_o{}^4)$, was neglected in this equation since it was considered that the tank would be radiating to surroundings nearly at the same temperature as itself. The material properties of the tank are as follows:

Material: titanium
Diameter = 28 cm (11 inches)
Density, ρ_T = 4701 km/m^3 (294 lb/ft^3)
Specific heat, $(c_p)_T$ = 523 J/kg^{o}K (0.125 BTU/lb ^{o}R)
Wall thickness, τ_T = 0.15 cm (0.060 inch)

In determining the aerodynamic heat rate, the following highly simplified approach was used. Both free molecular flow and continuum flow stagnation point heating rates were calculated. The expression presented earlier was used for the free molecular case. The continuum heating was determined from a simplification of the expression for cold wall stagnation heating in air developed by Fay and Riddell (Reference 10):

$$\dot{q}_{STAG} = 0.84 \times 10^{-8} \left(\frac{\rho}{R}\right)^{\frac{1}{2}} V^{3.08}\ \text{BTU/ft}^2\ \text{sec}$$

where R is the radius at the stagnation point in feet and ρ and V are expressed in units of slug/ft^3 and ft/s, respectively. This expression was arbitrarily increased by 10 percent to account for higher convective heat transfer in CO_2 as compared to air. At higher altitudes (140 to 160 km), where free molecular flow is expected to be the case, the continuum heating equation overestimates the heat transfer rate. Similarly, in the 100- to 110-km region where continuum flow is expected to occur, the free molecular equation overestimates the heating rate. The approach adopted for this analysis was to use the lower of the two heating rates at every altitude.

The temperature rise at the stagnation point of the hydrazine tank is also shown in Figure 4-85. The temperature starts to rise rapidly below 130 km, and exceeds 538°C (1000°F) by 116 km. It is concluded that major thermal damage to the bus and its contents will commence in the 116- to 113-km altitude region.

4.3.6.4 Communications Blackout

The phenomenon of telemetry blackout is now a familiar one as the result of manned space flight. In fact, blackout is experienced by all blunt bodies entering the earth's atmosphere at velocities of about 5 km/s and greater. Furthermore, predictions of when blackout can be expected due to ionization of the air as it is heated behind the bow shock and passes around the body can be made with considerable accuracy.

Because the probe bus is a blunt body, it too will experience telemetry blackout at some point in its entry into the Venus atmosphere. Several aspects of the probe bus entry, however, make blackout predictions less accurate. One of these is the CO_2/N_2 composition of the Venus atmosphere, a chemical system which has been studied much less than the N_2/O_2 system making up the earth's atmosphere. Another difficulty comes from the irregular shape of the probe bus, thereby requiring simplifying assumptions about flow properties. Finally, the much higher entry velocity will result in a higher degree of ionization than usually associated with earth entry.

To make the blackout problem more tractable, the following simplifying assumptions have been made (the validity of these assumptions will be examined later to determine their effect on the predicted blackout altitudes):

- Body Geometry Ignored. It is assumed that a continuum normal shock is formed in front of the body.
- Chemical Equilibrium in the Stagnation Region. As the vehicle enters at 11.06 km/s and follows a ballistic trajectory into the Venus atmosphere, the stagnation pressure and enthalpy are calculated from the normal shock relations. The composition including the electron density is obtained (with TRW's Equilibrium Chemistry Computer Program) for a 97-percent CO_2, 3-percent N_2 atmosphere. Results of this calculation are shown in Table 4-41 for altitudes of 250, 200, 150, and 100 km.

- Frozen Expansion to Ambient Pressure. Because the antenna is located at the base of the vehicle and points backward toward the earth, it is necessary to estimate plasma properties in the base and wake regions. It is assumed that the species composition is frozen as the ionized gas flows around the body and expands from the very high stagnation pressure to the ambient pressure characteristic of the wake. Figure 4-86 shows the electron density in the stagnation region and in the wake after expansion.

- Electron Collision Frequency Based on Analysis for Equilibrium Air. Calculation of the electron collision frequency for the composition shown in Table 4-41 is complicated because the dominant collision partner of a free electron is another charged particle, resulting in very long range coulomb interactions. To obtain some estimate of the electron-ion collision frequency, a calculation of the electron-neutral collision frequency was made for equilibrium air at the ambient pressure and a temperature of 1000°K. This value was then increased by a factor of 100 to account for the coulomb interaction. The collision frequency used to characterize the plasma is shown in Table 4-42.

- Attenuation from a Plane Wave in a Semi-Infinite Plasma. The plasma is described by the electron number density shown in Figure 4-86 and the collision frequency given in Table 4-42. The attenuation is then obtained from a solution to Maxwell's equations for a plane electromagnetic wave propagating into a semi-infinite plasma slab. Typical results for a collision frequency of 10^8 per second (roughly the highest value encountered down to 100 km) are shown in Figure 4-87 in terms of the attenuation per meter of path length through the plasma.

Table 4-41. Equilibrium Flow Behind Normal Shock for Venus Atmosphere

ATMOSPHERE: 97-PERCENT CO_2, 3-PERCENT N_2

ENTRY VELOCITY: 11.06 KM/S

PROPERTY	ALTITUDE (KM)			
	250	200	150	100
PRESSURE (EARTH ATMOSPHERE)	1.6×10^{-9}	1.2×10^{-8}	6.5×10^{-7}	4.9×10^{-2}
ENTHALPY (KCAL/100 GM)	1.5×10^{3}	1.5×10^{3}	1.5×10^{3}	1.35×10^{3}
C (MOLE FRACTION)	0.018	0.024	0.063	0.135
C^+ (MOLE FRACTION)	0.227	0.222	0.195	0.144
O (MOLE FRACTION)	0.472	0.475	0.505	0.550
O^+ (MOLE FRACTION)	0.018	0.019	0.011	0.005
N (MOLE FRACTION)	0.011	0.011	0.013	0.015
N^+ (MOLE FRACTION)	0.004	0.004	0.002	0.001
e^- (MOLE FRACTION)	0.249	0.245	0.209	0.150
TOTAL NUMBER DENSITY (CM^{-3})	2.3×10^{9}	1.6×10^{10}	8.0×10^{11}	4.0×10^{16}
ELECTRON DENSITY (CM^{-3})	5.8×10^{8}	3.9×10^{9}	1.7×10^{11}	6.0×10^{-5}

Table 4-42. Electron Collision Frequency in the Wake Region

ALTITUDE (KM)	COLLISION FREQUENCY (SEC^{-1})
250	3.7×10^{1}
200	2.6×10^{2}
150	7.8×10^{3}
100	2.8×10^{8}

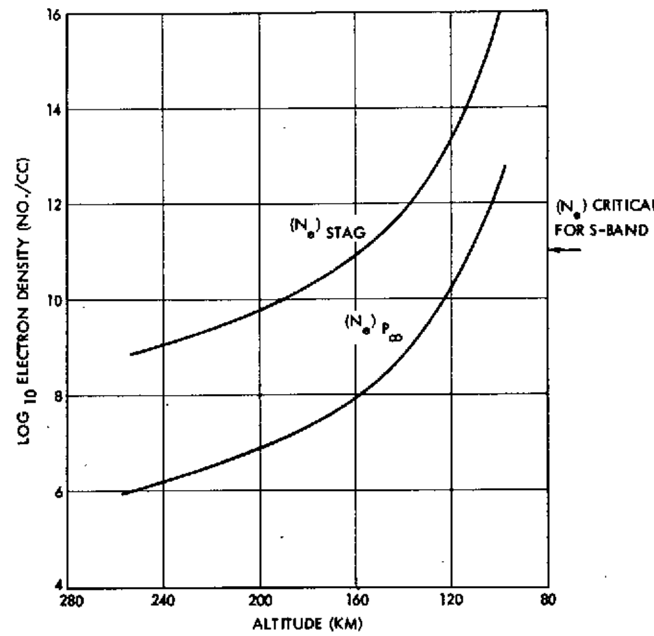

Figure 4-86. Electron Density in Stagnation Region Behind Normal Shock and in Wake After Expansion to Ambient Pressure

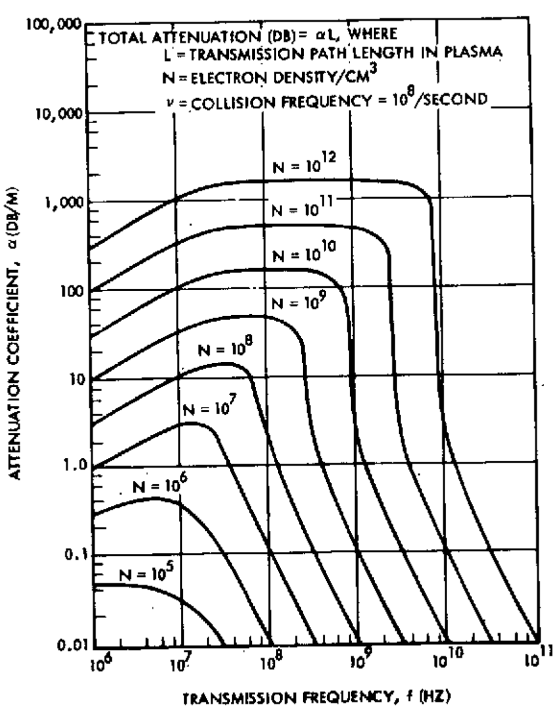

Figure 4-87. Plasma Attenuation of Electromagnetic Wave Propagation

Since a plasma depth of several meters can be expected in the wake, blackout will occur for plasma conditions which give rise to an attenuation coefficient of about 2 dB per meter or greater, resulting in a total attenuation of at least 4 or 5 dB. It can be seen from Figure 4-87 that, for S-band transmission at 2.3 gHz, this attenuation coefficient occurs when the plasma electron density is between 10^{10} and 10^{11} electrons per cc. This result is based on the plane electromagnetic wave solution for a collision frequency of 10^8 per second. Solutions for lower collision frequencies exhibit a more nearly vertical drop in attenaution coefficient with increasing transmission frequency. The implication of this is that the attenuation depends strongly on electron density only—the plasma appearing virtually transparent until the electron density reaches the critical value for S-band or approximately 10^{11} electrons per cc.

The probe bus will thus experience blackout when wake electron densities of about 10^{11} per cc are encountered by the telemetry transmission to earth. Reference to Figure 4-86 shows that 10^{11} electrons per cc will occur in the wake at an altitude of approximately 115 to 110 km, yielding blackout in roughly this altitude range.

An examination of the assumptions suggests that the predicted blackout altitude of 115 to 110 km is probably reasonable. Some of the assumptions employed result in electron densities higher than would be expected in reality at the higher altitudes. For example, application of the Monte Carlo direct simulation technique to the flow around the probe bus indicates that continuum flow with a thin shock is not attained until about 110 km (see Section 4.3.6.5). Above this altitude, there are not enough collisions to produce a strong, discrete bow shock. Furthermore, nonequilibrium chemical studies in air show that electron densities do not reach their equilibrium values until the product of ambient pressure and nose diameter is about 1×10^{-6} atm-meter, or an altitude of about 115 km for the probe bus (although the CO_2/N_2 composition requires a more detailed study of this point).

The assumption of a frozen expansion of the electrons from the stagnation region to the wake is probably correct above 100 km. Since the ions are all monatomic, the dominant recombination and attachment mechanisms require a third body and are thus very slow at the altitudes of interest. There is no analogue of the dissociative-recombination of NO^+ and e^-, which is important in air plasmas.

It has already been shown that the particular assumption used to obtain the electron collision frequency is not important for this situation since the attenuation is so weakly dependent on this parameter.

Finally, it is difficult to assess the validity of the EM-plasma interaction model with great certainty. There are other phenomena besides attenuation that may affect the transmission, such as near-field effects, plasma gradients and nonhomogeneities, etc. However, these effects are beyond the scope of this study. The simplified model employed here has been successfully used to predict plasma attenuation in the wake of ballistic missile nose cones.

If some of the assumptions suggest a lower electron density level as being more appropriate at high altitude, most of these assumptions are valid by 115 to 110 km, and electron density predictions below this altitude are probably reliable. This altitude, therefore, seems the correct one for the onset of blackout. Furthermore, the ambient pressure (and thus the wake electron density) is increasing so rapidly in this altitude regime that a drop of a few kilometers brings an order of magnitude increase in wake electron density and thus almost certain telemetry blackout.

4.3.6.5 Flow Regimes and Molecular Flux Identification

During its passage through the atmosphere, the probe bus encounters three different flow regimes. In the upper reaches of the atmosphere, the density is so low that molecules or other atmospheric particles that make contact with the bus excape from its vicinity without further collisions with oncoming molecules. This is the collisionless, or free molecule, flow regime. Science sensors, specifically the neutral particle and ion mass spectrometers, sampling the atmosphere in this regime will measure the actual constituency of the atmosphere. As the bus penetrates into the denser layers of the atmosphere, collisions between molecules dominate the flow structure, and a thin strong shock wave forms ahead of the body. This is the continuum flow regime. The collisions are so energetic that molecules are dissociated and ionized, chemical reactions occur, and radiation is a significant energy transfer mode. In this regime, science sensors located behind the strong shock wave sample a gas that has been radically changed from its original character. Any measurements taken in this flow regime while the bus is still traveling at hypersonic speeds will be virtually impossible to interpret. In between the free molecule and continuum flow regimes is the transition flow regime. Here the molecules that encounter the bus and are reflected into the oncoming stream sustain frequent collisions and many may be knocked back onto the bus. In this regime, mass spectrometers will sample a mixture of collision-free particles and particles that may have had sufficiently energetic collisions to change their nature. Interpretation of these "contaminated" measurements is difficult but can be accomplished if an accurate description of the flow field is provided.

As a first step in determining the altitude to which the bus can penetrate and still obtain meaningful data samples, the altitude bands in which each type of flow is expected to occur was estimated using the TRW Monte Carlo Direct Simulation Technique (Reference 11). This approach will describe rarefied gas flows in which the motion of a representative set of a few thousand simulated molecules flowing past the body is followed exactly by digital computation while collisions in the gas are determined by statistical sampling. Initially, a field of physical space surrounding the body is populated with molecules typical of the free stream. The subsequent evolution to a steady state is then computed as molecules flow into and through the field while interacting with each other and with the body. The motion of the molecules and the computation of collisions are uncoupled over an interval, which is small compared to the mean free time. To compute collisions in the gas, the field is divided into a number of cells (on the order of a thousand) whose dimensions are small compared to gradients in the flow. The molecules in each cell are taken to represent the distribution function for that region and collisions are prescribed by selecting pairs from each cell with the appropriate probabilities. This simulation method produces a solution of the Boltzmann equation; hence, the solution is valid at all density levels in the atmosphere. The output is a description of the flow field and fluxes at the surface of the body.

In applying this approach to the probe bus, the constituents of the atmosphere were assumed to be neutral monatomic species. Particles encountering the body accommodate completely to the body temperature and are subsequently reemitted diffusely. Results are presented in Figure 4-88 for two idealized bus geometries: a hemisphere-cylinder, and a flat-faced cylinder. Shown as a function of Knudsen number (ratio of mean free path in the atmosphere at a given altitude to a characteristic dimension of the bus) is the composition of the molecular flux to the front face of the body. Three types of molecular fluxes are identified:

Type 1 — free stream flux; i.e., collisionless flow before encountering the body

Type 2 — flux of molecules that had encountered the body, were immediately reemitted at low velocity, and were subsequently knocked back to the body by collisions with other molecules

Type 3 — flux of molecules that have had one or more collisions with other than Type 1 molecules before striking the body.

The altitude scale corresponding to the mean free paths in the Venusian atmosphere is shown under the Knudsen number scale. The Mach number range for which these analyses were performed is 20 to 55, covering the flight Mach numbers of the bus from entry at 250 km down to 100 km.

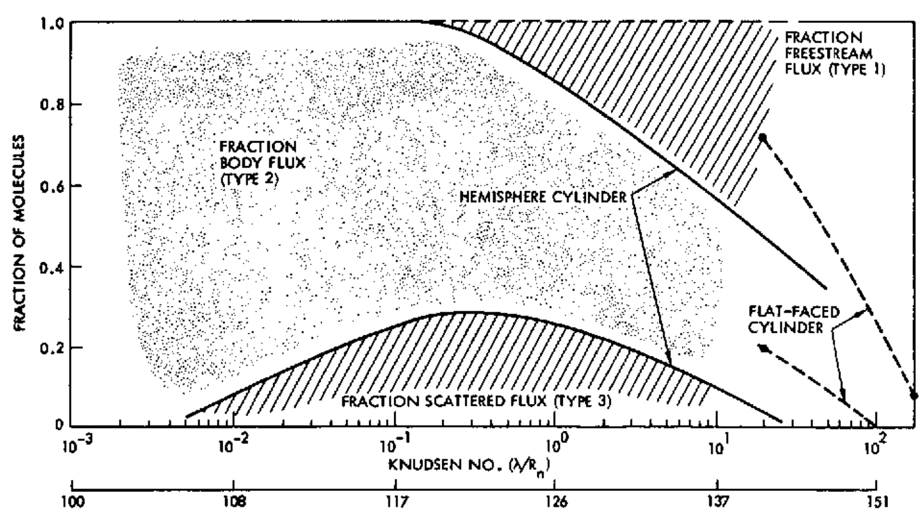

Figure 4-88. Pioneer Venus Bus Entry: Identification of Molecular Flux to Body Stagnation Point

Considering first the hemisphere-cylinder geometry, we see that, at a Knudsen number of 10 (altitude = 137 km), 45 percent of the flux to the stagnation point consists of molecules that hit the body previously and were knocked back onto it (Type 2's). Ten percent of the molecules were perturbed from the free state by collisions in the gas (Type 3's), and the remaining 45 percent were free stream molecules (Type 1's). Thus, at this altitude the flow differs significantly from a true free molecular (i.e., collisionless) flow. At 117 km ($Kn = 10^{-1}$), the free-stream flux to the body ceases and the flux consists entirely of back-scattered molecules. The flow for a hemisphere-cylinder probably becomes continuum at around 108 km and is entirely free molecular (~100 percent Type 1 flux) somewhere above 150 km.

The additional calculations performed for the flat-face cylinder, which is a closer approximation to the bus geometry than the hemisphere-cylinder, confirm the trends previously noted, and shift the flow regimes to slightly higher altitudes. Based on these results we estimate that, for the Thor/Delta probe bus free molecular flow will occur down to about 155 km, transition flow in the altitude band from there to about 115 km, and continuum flow below 115 km.

The distribution of the three types of fluxes across the fact of the flat-face cylinder is shown in Figure 4-89 at two altitudes, 141 km ($Kn = 20$) and 156 km ($Kn = 200$). The molecular flux coefficient

$$C_F = \frac{\text{flux per unit time}}{\text{free stream flux}}$$

is plotted against the normalized radial distance from the axis of the cylinder. Obviously, $C_F = 1$ in free-molecule flow. The key point to be noted from this figure is that the flux distribution across the face of the cylinder is nearly constant, so that there is no obvious optimum location to mount an instrument which samples the atmosphere. This conclusion may not be valid for the actual bus geometry.

Although not displayed here, the disturbance in the transition flow regime ($Kn = 20$) falls off rapidly forward of the body face. At 1/3 of a cylinder diameter forward, the particle number density is 1/5 that at the face; at one cylinder diameter forward, the number density has fallen

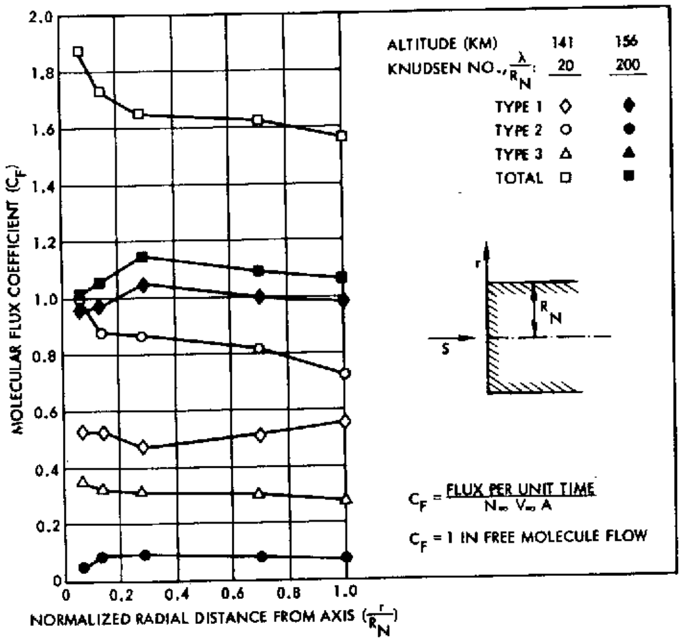

Figure 4-89. Distribution of Molecular Fluxes Across Face of Body

off by almost two orders of magnitude. Extending the sensor forward of the front face reduces the fraction of disturbed flow that it samples. The sensor will create its own disturbance field, although it will occur at a lower altitude than that arising from the body itself.

In the transition flow regime, it is highly probable that a portion of the molecules in Types 2 and 3 collisions will be dissociated and ionized. Thus, neutral particle and ion mass spectrometers taking samples in the disturbed region at the face of the probe bus will require an accurate description of flow field details to permit interpretation of instrument readings. Because the gas in the disturbed region will be in a highly nonequilibrium state, such a description will require the use of the methods of kinetic theory. In the free-molecule flow regime, above an altitude of about 155 km, the science instruments on the bus should be able to sense the undisturbed atmosphere.

4.3.6.6 Altitude History of Bus Entry Phenomena

The recapitulation of the various phenomena that affect the performance of the Thor/Delta probe bus during its descent through the

Venusian atmosphere is presented in Figure 4-90. In descending order of altitude, these phenomena are:

~155 km - roughly the end of the free-molecular flow regime and the beginning of the transition flow regime. The science instrument readings will be increasingly influenced by the flow disturbances ahead of the body as the bus descends below this altitude. Detailed analyses will be required to interpret the science data gathered in this flow regime.

145 to 143 km - thermal control surfaces on the bus begin to deteriorate and fail in this altitude range. Outgassing from teflon surfaces can contaminate mass spectrometer readings.

139 to 129 km - the bus, spinning at 5 rpm, diverges due to destabilizing aerodynamic forces, and reaches an angle of attack of 0.122 radian (7 degrees) in this altitude range. This change in bus attitude tips the high-gain, earth-pointing antenna to about its limit for high data rate communication. The divergence increases rapidly, and exceeds 0.524 radian (30 degrees) by the 121 to 120-km altitude band.

116 to 113 km - thermal damage to the bus structure and subsystems commences in this range of altitudes. Electronic equipment will begin to fail.

115 to 110 km - communications blackout is expected to start in this altitude range.

112 to 110 km - degradation of communications due to angle-of-attack divergence for bus spinning at 60 rpm.

99 km - major structural damage will start occurring at this altitude.

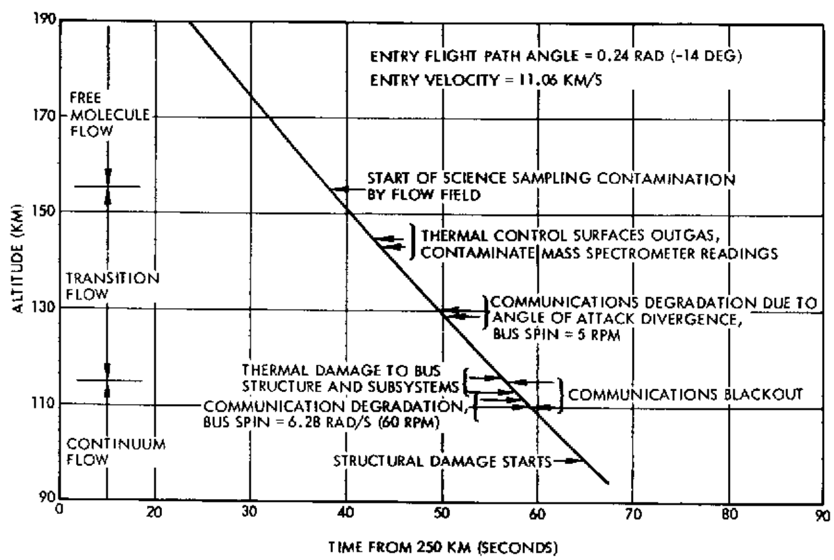

Figure 4-90. Altitude History of Bus Entry Phenomena

4.3.6.7 Entry Behavior of 1978 Atlas/Centaur Probe Bus

A brief investigation of the 1978 Atlas/Centaur probe bus entry into the Venusian atmosphere indicated that the phenomena which degrade the science measurements or lead to failure of the bus itself occur at very nearly the same altitudes as they do in the case of the 1977 Thor/Delta probe bus. Major results of this investigation are reported below.

Configuration

From an aerodynamic standpoint, the configuration differences between the Atlas/Centaur and Thor/Delta probe buses are minor. On the Atlas/Centaur bus, the magnetometer boom has been deleted and a medium-gain horn substituted for the Thor/Delta's high-gain antenna. In the Thor/Delta bus, the forward end of the central cylinder was closed over by a thermal shield (B in Figure 4-80). In the Atlas/Centaur bus, the central cylinder is open to the flow except for the blockage provided by the medium-gain horn. The maximum diameter of the Atlas/Centaur bus is 2.51 meters (8.24 feet) versus 2.14 meters (7.0 feet) for the Thor/Delta bus. The corresponding weights at entry are 220 kilograms (485 pounds) versus 126.6 kilograms (279 pounds).

Aerodynamic Coefficients

Free molecular flow force and moment coefficients were calculated for the Atlas/Centaur probe bus using the approach described in Section 4.3.6.1. The data are shown in Figure 4-91. As was the case for the Thor/Delta configuration, the Atlas/Centaur bus is aerodynamically unstable for angles of attack up to and exceeding ±1.57 radians (±90 degrees).

Trajectory and Flight Dynamics

A point mass trajectory was computed for the Atlas/Centaur bus for the following initial conditions:

V_E = entry velocity = 11.288 km/sec

γ_E = entry flight path angle = -0.200 radian (-11.5 degrees)

The ballistic coefficient based on the zero angle of attack drag coefficient is 21.2 kg/m^2 (0.134 $slug/ft^2$). Comparing the deceleration on this

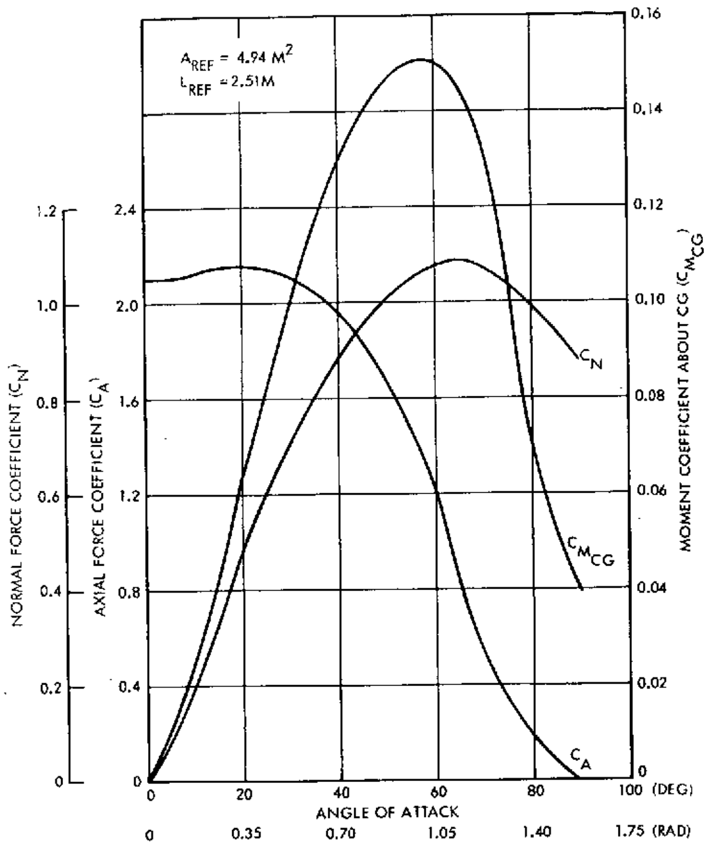

Figure 4-91. Free Molecular Flow Aerodynamic Coefficients of Atlas/Centaur Probe Bus

trajectory with that of Thor/Delta bus trajectory examined in Section 4.3.6.2 (V_E = 11.06 km/s, γ_E = -14 degrees) reveals that the altitude histories of deceleration are practically identical. Hence, structural breakup of the Atlas/Centaur bus will occur at about the same altitude (99 kilometers) as the Thor/Delta bus.

Six-degree-of-freedom trajectories were computed using the bus-alone mass properties given in Figure 4-14b. Initial angles of attack of +0.03 and -0.03 radian (+2 and -2 degrees) were assumed (bracketing the range of possible entry angle of attack dispersions) with the same entry velocity and flight path angle as for the point mass trajectory. The nominal Atlas/Centaur bus spin rate of 6.28 rad/s (60 rpm) was used. The results showed that the high spin rate effectively stabilizes the bus against the very light but destabilizing aerodynamic torques, until the buildup of dynamic pressure occurs in the 105 to 100 kilometer altitude range. Commencing at about 120 kilometers, a 1.8 Hz oscillation begins to build up; but at 110 kilometers the amplitude is only about $\pm$0.010 radian ($\pm$0.2 degree). The conclusion is that the angle of attack divergence which might cause the bus to lose communication with earth occurs below 110 kilometers altitude. The Thor/Delta bus, spinning at its nominal 0.52 rad/s (5 rpm) spin rate, experienced loss of its communication link with earth starting at about 129 kilometers altitude.

Heating and Blackout

Free molecular flow aerodynamic heating of a teflon-mylar thermal control surface on the probe bus (corresponding to location A in Figure

4-80) was calculated for the Atlas/Centaur entry trajectory described in the previous paragraph. The altitude at which teflon outgassing temperatures are reached is nearly identical to that predicted for the Thor/Delta bus. A similar check was made on the heating of the hydrazine propellant tank which, in the Atlas/Centaur bus, is the Model 777 tank. Other than minor shape differences, the only difference between this tank and the Thor/Delta hydrazine tank, which is of significance with respect to aerodynamic heating, is the wall thickness (0.075 cm for Atlas/Centaur versus 0.15 cm for Thor/Delta). The thinner wall Atlas/Centaur tank reaches temperatures where thermal damage may be expected about 2 km higher in altitude than the Thor/Delta tank, namely, starting at about 118 kilometers.

Within the accuracy of the blackout predictions, there will be no change in the altitude at which blackout occurs for the Atlas/Centaur trajectory. The higher entry velocity results in higher electron density in the flow around and behind the bus, but not enough to significantly change the results of the Thor/Delta analysis.

Flow Regimes

The Monte Carlo direct simulation analysis of the flow regimes at the forward face of the simplified geometrical shapes representing the bus (described in Section 4.3.6.5) is independent of entry trajectory. For this analysis, the atmospheric constituents were treated as chemically inert monatomic molecules, and the flow regimes are characterized by the Knudsen number, the ratio of the mean free path in the atmosphere to a characteristic dimension of the body. Since the Atlas/Centaur bus is about 17 percent bigger in diameter than the Thor/Delta bus, the Knudsen number at a given altitude is correspondingly reduced. Conversely, a given Knudsen number will correspond to a slightly higher altitude for the Atlas/Centaur bus in comparison to the Thor/Delta bus. Quantitatively, however, the altitude difference is about 1 kilometer, so that the altitude scale in Figure 4-88 essentially applies to the Atlas/Centaur bus as well.

In summary, the Atlas/Centaur probe bus will behave substantially the same as the Thor/Delta bus during its entry into the atmosphere. Figure 4-90 is therefore considered applicable to the Atlas/Centaur bus entry.

4.4 ORBITER MISSION STUDIES

4.4.1 Launch, Cruise, and Midcourse Corrections

This section summarizes trade studies dealing with the launch and interplanetary phases of the orbiter mission. The nominal profiles are given in Section 4.1.2.

4.4.1.1 Launch Analysis

Data associated with the launch and near-earth portion of the 1978 Type II orbiter mission are presented below. The launch and powered flight parameters used for the Delta 2914 and Atlas/Centaur launch vehicles were presented in Table 4-15.

The daily windows and parking orbit coast times for the 1978 Type II opporunity are shown in Figure 4-92. Daily launch intervals range from 10 minutes to 1.5 hour in duration. Parking orbit coast times range from

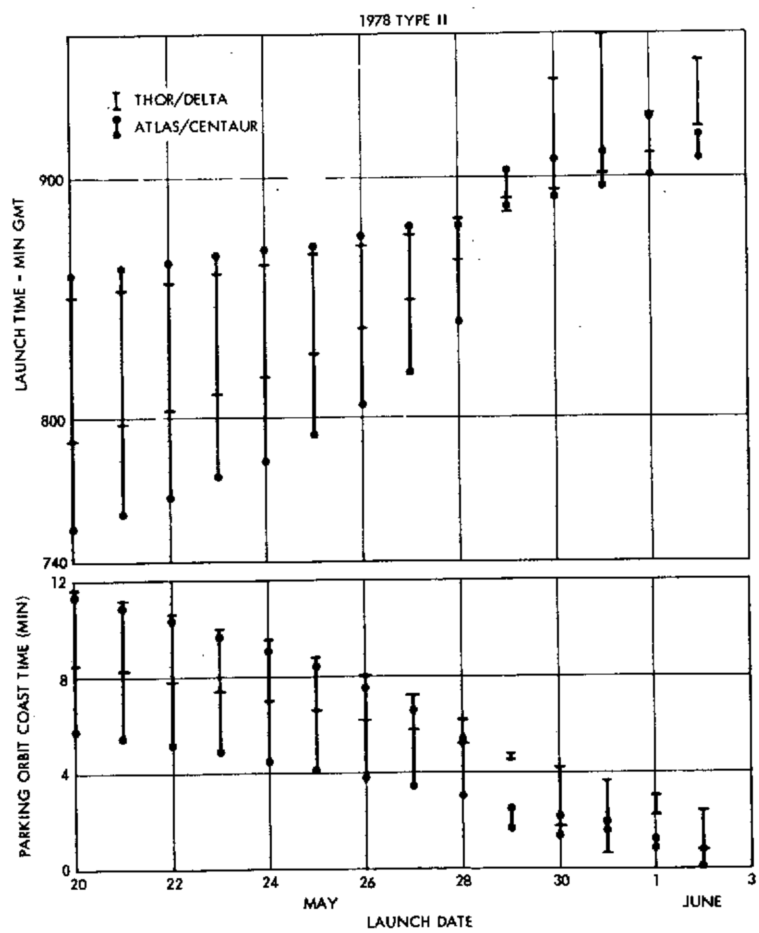

Figure 4-92. Launch Windows and Parking Orbit Coast Times

zero to 12 minutes in duration. Geocentric locations of the interplanetary injection burn are shown in Figure 4-93. Time histories of earth and solar aspect angles and altitude for the Delta launched spacecraft are presented in Figure 4-94. Injection attitude considerations were discussed in Section 4. 2. 1. 1 and are applicable here.

4. 4. 1. 2 Cruise Analysis

The nominal cruise attitude of the spacecraft from the first midcourse maneuver (5 days after injection) is earth pointing. To maintain the sun in the forward spacecraft hemisphere [solar aspect less than 1. 57 radian (90 degrees)], the spacecraft is flipped 3. 14 radians (180 degrees) approximately 110 days after launch. Thus the cruise attitude from 110 days until orbit insertion is anti-earth pointing. The solar aspect, range and earth range histories are presented in Figure 4-95.

4. 4. 1. 3 Midcourse Analysis

The general assumptions for the midcourse analysis were discussed in Section 4. 3. 1. 3. There are slight differences in the midcourse requirements and effectiveness for the probe and orbiter missions, primarily because of the longer flight time and different geometry associated with the Type II orbiter transfer. A second difference is in the timing of the final midcourse relative to Venus encounter (E - 30 days for probe mission, E - 15 days for orbiter mission) caused by mission requirements.

Atlas/Centaur Mission

Both the 1978 Type II and Type I orbiter missions have been analyzed for their midcourse requirements and effectiveness. The first midcourse requirements are compared in Figures 4-96 and 4-97. As in the probe mission the 99. 99 percent probability levels may be comfortably met (less than 8 m/s) with a first midcourse maneuver scheduled at five days after launch. The 1978 Type II mission (having the greatest transfer time) has the least Δ V requirements while the Type I orbiter mission requires values between the Type II and the Type I probe mission. The sensitivity to time of first midcourse is also demonstrated in the figure as requirements are indicated for midcourses 3, 5, and 7 days after launch.

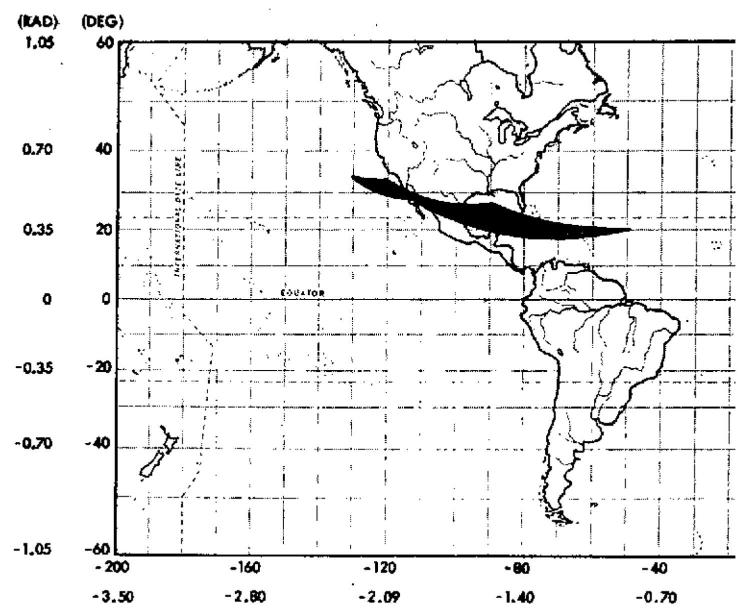

Figure 4-93. Ground Locations of Injection Points

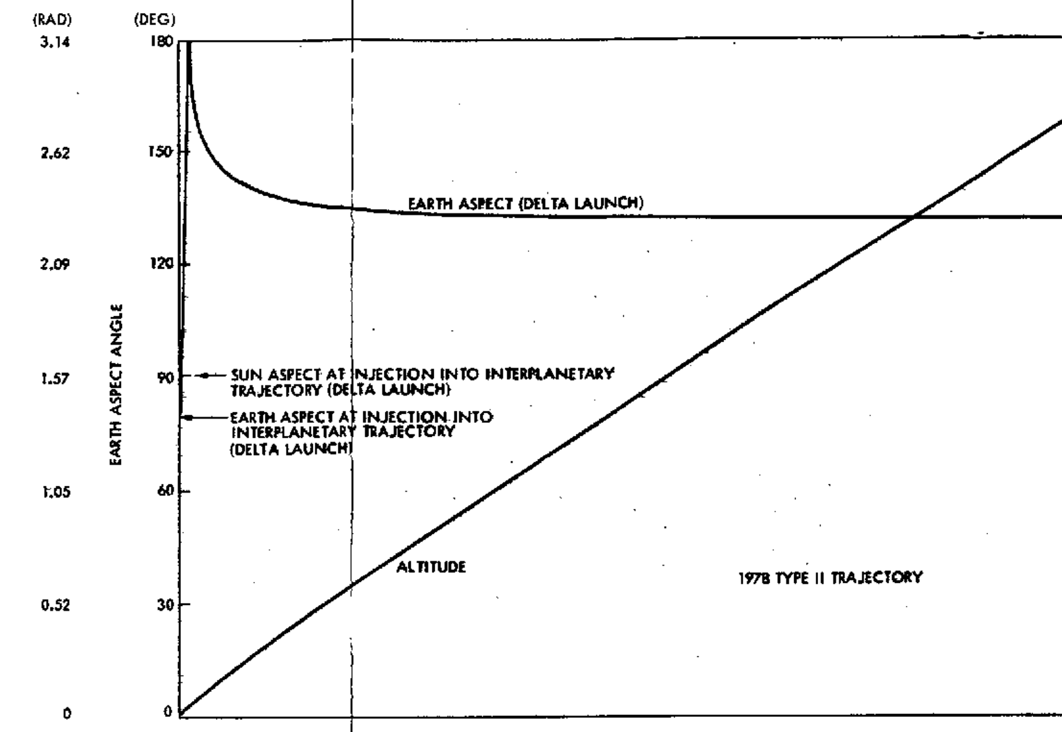

Figure 4-94. Time History of Earth Aspect and Attitude for Near-Earth Trajectory

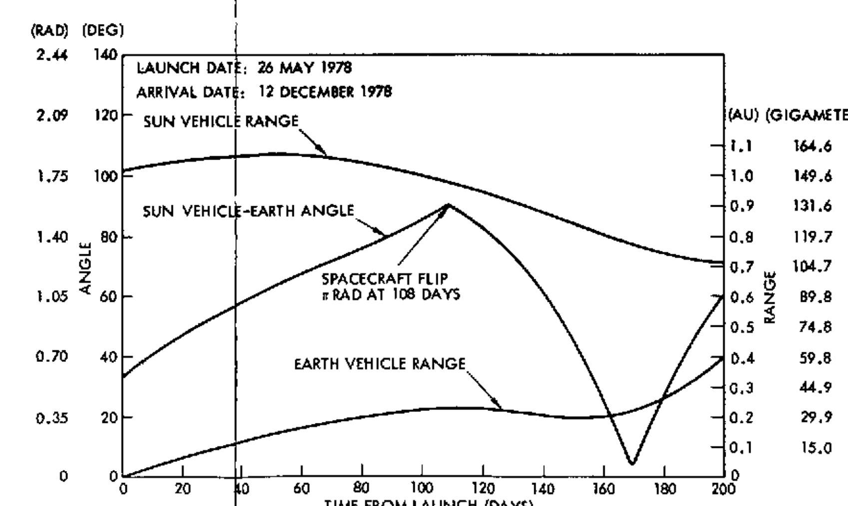

Figure 4-95. Transvenus Cruise Geometry, 1978 Type II Orbiter

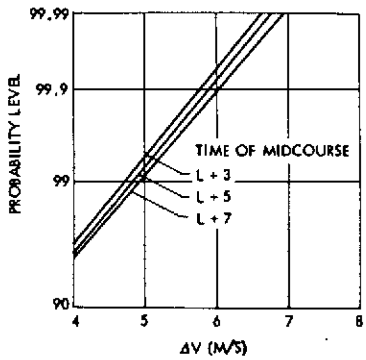

Figure 4-96. 1978 Type II Orbiter First Midcourse Requirements

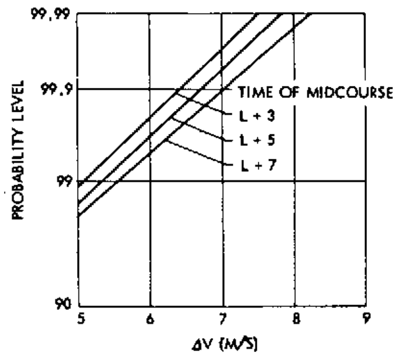

Figure 4-97. 1978 Type I Orbiter First Midcourse Requirements

The entire midcourse sequences are compared in Table 4-43. The midcourse ΔV numbers are approximately equal for the two missions. The important difference in the approach trajectory control accuracy following the last midcourse is due to the significantly superior tracking prior to that last maneuver, discussed in more detail in Section 4.4.1.4.

Table 4-43. Midcourse Requirements and Effectiveness for Atlas/Centaur Vehicle

	TYPE II	TYPE I
INJECTION		
SMAA (KM)	25 500	29 100
TOF (MIN)	445	14
FIRST MIDCOURSE		
ΔV_{LOAD} (M/S)	6.8	7.9
SMAA (KM)	252	241
TOF (MIN)	4.5	0.6
SECOND MIDCOURSE		
ΔV_{LOAD} (M/S)	0.2	0.2
SMAA (KM)	101	237
TOF (MIN)	1.6	0.4
THIRD MIDCOURSE		
ΔV_{LOAD}	1.4	1.2
SMAA (KM)	64	230
TOF (MIN)	0.1	0.1

Thor/Delta Considerations

The Thor/Delta launch vehicle is much less accurate than the Atlas/Centaur vehicle, resulting in first midcourse requirements an order of magnitude greater than the Atlas/Centaur, and affecting the second and third midcourses through the execution errors at that first maneuver. This section discusses the sensitivities of midcourse requirements and effectiveness along with a presentation of the Thor/Delta specifics.

The first midcourse requirements for the Type I and Type II missions are given in Figure 4-98. As indicated, the midcourse requirements are an order of magnitude greater than the corresponding Atlas/Centaur values, necessitating lower design margins (99 percent) in loading for the midcourses than is possible with the Atlas/Centaur vehicle. The injection covariance used in the study was supplied by the contractor and similar to that listed in Table 4-18 for the probe mission. The second and third midcourses have an almost negligible effect on the total midcourse budget for the Thor/Delta relative to the first. However, they are critical events in controlling the accuracy of the final approach trajectory. Table 4-44 illustrates the total midcourse budgets and effectiveness for the Thor/Delta Type II orbiter mission. The three-sigma execution errors used as a reference for this study are 1 degree pointing, 3 percent proportionality, and 0.03 m/s resolution.

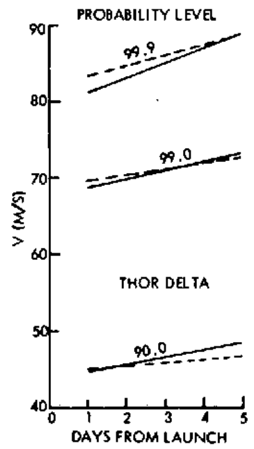

Figure 4-98. First Midcourse Requirement for Thor/Delta

Table 4-44. Thor/Delta Midcourse Analysis

MANEUVER	ΔV_L (M/S)	POST-MANEUVER DISPERSIONS SMAA (KM)	TOF (MIN)
INJECTION	-	414 000	7 000
FIRST M/C (I+5)	72.7	4 455	75
SECOND M/C (I+15)	0.9	141	2.4
THIRD M/C (VE-10)	1.6	70	0.12

A number of parametric studies associated with midcourse analyses have been conducted using the Type II orbiter mission with the Thor/Delta launch vehicle. Comparison of Tables 4-44 and 4-43 illustrates the effect of the launch vehicle. The launch vehicle has some effect on the magnitudes of the second and third midcourses because of the magnitude (and accompanying execution errors) of the first maneuver. However, because of the size of the third midcourse there is essentially no impact on the final approach trajectory control.

Execution errors made at each of the midcourses cause increases in the subsequent maneuvers. The error with the most variation is the pointing error (of the delivered ΔV) as it is a function of the attitude determination and control systems, the reaction control system, and thrust dynamics effects. Table 4-45 illustrates the sensitivities of trajectory control and second midcourse requirements to pointing error at the first midcourse.

Table 4-45. Effect of Pointing Error on Midcourses, One-degree (Two-degree)

MANEUVER	ΔV_L (M/S)	POST-MANEUVER DISPERSIONS SMAA (KM)	TOF (MIN)
INJECTION		414 000	7 000
FIRST M C (I+5)	72.7 (72.7)	4 455 (4970)	75 (87)
SECOND M/C (I+15)	0.9 (1.1)	141 (152)	2.4 (2.5)

Unmodeled accelerations are most dominant over large propagation intervals. The magnitude of their effect is summarized in Table 4-46 for the 78-II mission. A second midcourse was assumed to be performed 15 days after launch; the third, 175 days later (ten days before encounter). Nominal execution errors (3σ) of 1-degree pointing, 3 percent proportionality, and 0.03 m/s resolution error were assumed. Levels of unmodeled accelerations used represent a nominal value (2×10^{-12} km/s^2) and a conservative estimate based on twice the nominal value. The effect of unmodeled accelerations on trajectory control is indicated by the semimajor axis (SMAA) of the B-plane error ellipsis. Unmodeled accelerations of the magnitude studied have a significant effect when propagated over intervals of 170 days. For intervals of the order of ten days no appreciable effects are introduced.

Table 4-46. Effect of Unmodelled Accelerations on Third Midcourse

UNMODELED ACC (10^{-12} KM/SEC^2)	PREMANEUVER SMAA (KM)	DISPERSIONS TOF (MIN)	ΔV_L (M/S)
0	141	2.4	1.6
2	154	3.1	1.8
4	195	4.0	2.3

The midcourse requirements and effectiveness are insensitive to minor variations in sequencing. Moving the third midcourse to 15 days before arrival instead of 10 decreases the magnitude of the maneuver by

0.1 m/s and only increases the trajectory control errors from 70 to 71 km for SMAA and from 0.12 to 0.13 min for TOF. Delaying the second midcourse from 15 days after injection to 55 days after injection results in an increase of 1.3 m/s in the second maneuver, but a decrease of 0.8 m/s in the third, resulting in a net increase of 0.5 m/s. Again the final control errors are nearly identical.

The standard guidance policy proposed for the third midcourse is a fixed time of arrival (FTA) policy in which the arrival time and impact plane pierce point are controlled. If arrival time is not critical, a variable-time-of-arrival (VTA) policy may be used, decreasing the ΔV magnitude from 1.6 to 0.4 m/s, but increasing the TOF uncertainty from 0.12 to 2.43 minutes.

4.4.1.4 Approach Orbit Determination

The approach orbit determination is critical because it determines the accuracy with which the orbiter may be delivered to its designated target site. As indicated in Section 4.3.1.3, the third midcourse magnitude is on the order of meter per second. Thus, the maneuver execution errors at the final midcourse are dominated by the tracking uncertainty at the time of that maneuver. Further tracking after the maneuver enables accurate predictions for orbit insertion command loading.

Trajectory Characteristics

The trajectory parameters having greatest impact on the tracking effectiveness are compared in Figure 4-99 and Table 4-47 for the Type I and Type II trajectories. The geocentric declination δ is significant as the error $\Delta\delta$ in the declination is related to errors in the spin radius of the tracking station Δr_s as $\Delta\delta = \Delta r_s (r_s \tan \delta)^{-1}$. Thus low geocentric declinations results in large uncertainties in the Z-direction errors. The approach velocity magnitude is important because it determines the

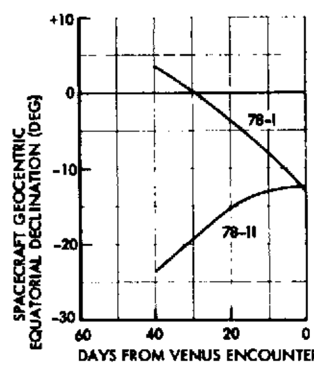

Figure 4-99. Geocentric Declinations of Approach

Table 4-47. Navigation Aspects of Approach Geometrics

PARAMETER	MISSION 78-I	78-II
δ (DEG)	+4 TO -14	< -13
V_{HP} (KM/S)	5.0	3.3
ZAE (DEG)	125	150

relative speed with which Venus is approached: the slower the speed, the more the gravitational effects of Venus may be felt and thus the stronger information content in the tracking. The ZAE angle is the angle between the V_{HP} vector and the line-of-sight to earth. A ZAE-angle of 180 degrees would result in the acceleration due to Venus acting directly along the line of sight, leading to maximum observability of planetary effects. From a comparison of the data the 78-II would appear to have the better approach geometry.

Table 4-48. Tracking Assumptions

STATIONS: GOLDSTONE, MADRID, CANBERRA			
DOPPLER NOISE: 1MM/S (FOR 1 MIN COUNT TIME)			
ESLE VALUES:	σ_{R_S}(M)	σ_{λ}(M)	ρ_{λ}
NO CALIBRATION	4.5	5.0	.97
CALIBRATION	1.0	2.0	.97
VENUS EPHEMERIS ERRORS: 20 KM SPHERICAL			
A PRIORI UNCERTAINTIES: POSITION: 1000 KM SPHERICAL; VELOCITY: 100 M/S SPHERICAL			

Tracking Model

Table 4-48 summarizes the assumptions used in the approach orbit determination analyses. Doppler tracking is simulated from Goldstone, Canberra, and Madrid at an assumed Doppler noise of 1 mm/s for a 1-minute count time. Equivalent station location errors correspond to current estimates, including both charged particle calibration and no calibration. The ephemeris errors are consistent with recently published results for the arrival conditions of the interplanetary trajectories. The arrival of both missions near inferior conjunction result in near-minimum values of ephemeris errors.

Tracking for Orbiter Missions

Figure 4-100 illustrate the tracking characteristics of the two orbiter missions. The final midcourse for orbiter missions was assumed to be 10 days before encounter. Tracking is initiated 30 days prior to that time. The significantly superior tracking of the 78-II mission confirms the predictions based on the trajectory characteristics discussed above. The tracking knowledge improves significantly 10 days before encounter as the gravitational effects of Venus begin to be sensed by the navigation algorithm (Kalman-Schmidt recursive filter). Again the possibility of performing a refinement maneuver nearer the planet is suggested.

Figure 4-100 compares the tracking effectiveness using different error levels. The top curve illustrates the results of tracking with equivalent station location errors (ESLE's) corresponding to no charged particle

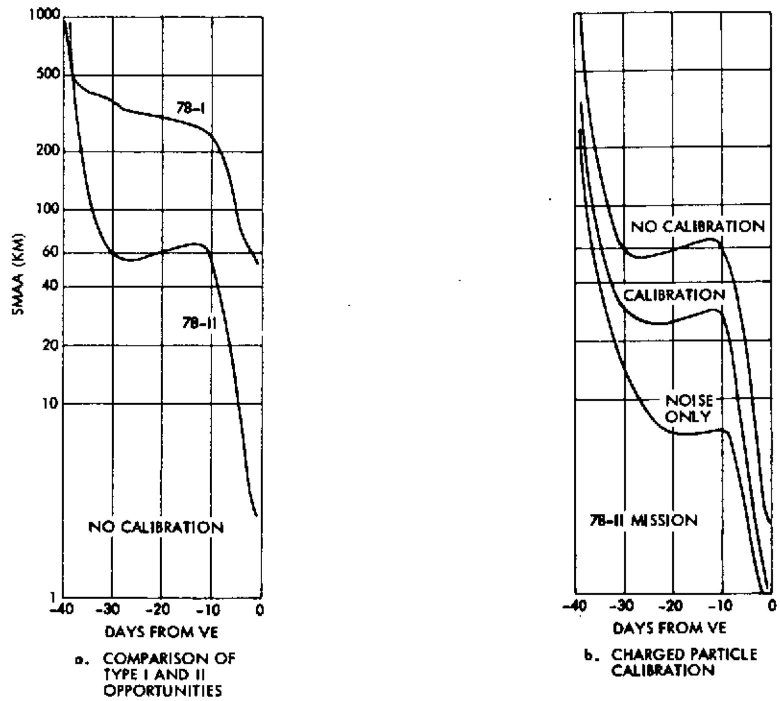

Figure 4-100. **Approach Orbit Determination**

calibration. The second curve indicates the results for calibration. For comparison the effectiveness using Doppler noise only (zero ESLE's) is also illustrated. The effect of these uncertainties is most strongly felt in the periapsis altitude dispersions. Assuming a final midcourse at VE - 10 days the 99 percent error in periapsis altitude is 83 and 46 km for no calibration and calibration, respectively. Thus calibration of charged particles is not necessary for the missions under consideration.

4.4.2 Orbit Selection

The selection of the orbit for the Pioneer Venus mission is dominated by scientific return considerations. This section indicated the sensitivities of mission parameters to that selection.

4.4.2.1 Type I Versus Type II

The mission opportunity analysis provided in Section 4.2 and the interplanetary trajectory assessment of Section 4.2.1 compared the Type I and Type II missions. The Type II mission provides competitive weights in orbit, requires a smaller insertion engine, and has superior tracking characteristics relative to the Type I. The penalties associated with the

Type II mission include the longer flight time (202 days versus 120 days) and an insertion hidden from view (Figure 4-101). This section emphasizes the preferred Type II mission.

4.4.2.2 Orbital Inclination

The possible suborbit traces are a function of the location of the approach velocity vector V_{HP}. Figure 4-101 illustrates the possible periapsis locations for the 1978 Type I and II opportunities. Figure 4-102 demonstrates the relation between θ_{AIM} and inclination. θ_{AIM} is the angle in the impact plane pierce point and the T axis. Since θ_{AIM} is a single valued function, it is convenient to discuss orbital selection in terms of θ_{AIM} instead of inclination.

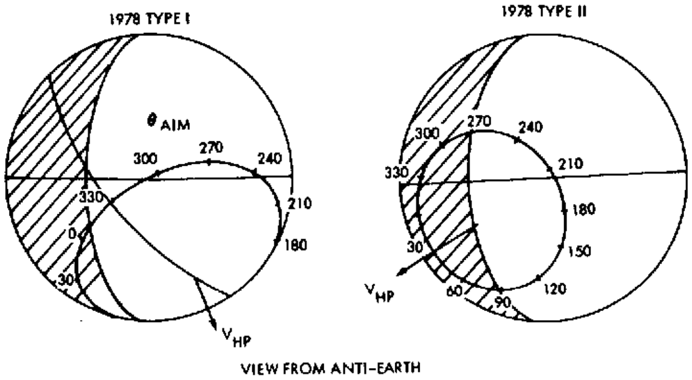

Figure 4-101. Comparison of Type I and II Orbit Geometries

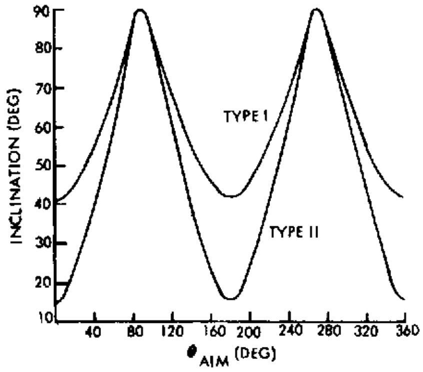

Figure 4-102. θ_{AIM} versus Inclination

The dominant tradeoffs concerning inclination for the Type II mission (24-hour period) are summarized in Figure 4-103. Three of the prime system considerations are indicated as a function of θ_{AIM}. The baseline mission selection of θ_{AIM} = 120 degree is also noted. The peak occultation time affects the design of the batteries and thermal control system. The current design limits peak solar occultation times to less than approximately 2 hours. As indicated this restricts θ_{AIM}'s to less than about 180 degrees.

The dominant perturbation force causing periapsis altitude variations is solar gravitation and its effect is a function of orbit geometry. The ΔV trim requirements to control periapsis for a 225-day mission are indicated in the second figure. The baseline mission inclination of 120 degrees results in an intermediate requirement of ΔV_{TRIM}. The trim budget could be reduced with θ_{AIM} selected nearer 180 degrees.

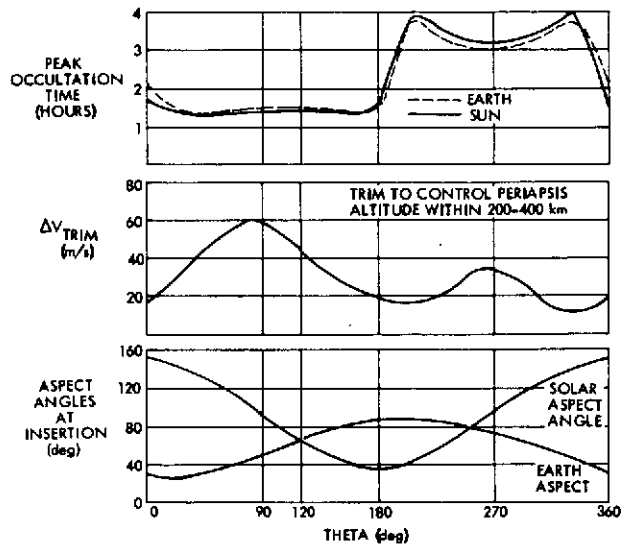

Figure 4-103. Orbit Inclination Sensitivities

The orbit attitude at insertion is also a consideration in orbit and mission design. Since the orbiter is put in its insertion attitude about 1 day before insertion, it must be capable of operating in that attitude during that time interval. The design of the solar arrays for the orbiter requires that the sun be kept approximately in the forward hemisphere of the spacecraft or solar aspect angles should be kept less than about 90 degrees. Thus, the current power design is compatible with θ_{AIM} in the range 80 to 280 degrees. The communication system is designed for optional operation at earth aspect angles near 90 degrees and is adequate at the insertion altitude.

4.4.2.3 Orbit Periapsis

The tradeoffs affecting periapsis altitude selection are indicated in Figure 4-104. For science purposes it would be advantageous to have as low a periapsis altitude as possible. Atmospheric drag becomes significant for altitudes much lower than 140 km as indicated in the figure. To allow a reasonable margin, a lower bound of 200 km has been imposed on the periapsis altitude. The insertion velocity requirements increase only slightly with increasing periapsis altitude as demonstrated in the figure. Therefore an initial periapsis altitude of 400 km has a small cost penalty in relation to the reliability margin it provides. The orbit insertion uncertainties are discussed in detail in Section 4.4.3.3. During the lifetime of the mission the periapsis altitude is controlled between 200 and 400 km.

4.4.2.4 Orbit Period

The selection of orbit period is summarized in Figure 4-105. The data depicted are based on the Type II trajectory with periapsis altitude of 400 km. The data are generated around the selected orbit period of 24 hours. The orbit period of 24 hours places the insertion velocity near the knee of that curve. The peak solar occulation time increases with period as the time spent near apoapsis (where the peak occultations would occur) increases with period. The trim ΔV also increases with period as the solar gravitation perturbations become more significant. Finally, the ability to solve for gravitational anomalies by tracking the orbiter motion becomes more effective as the orbit period decreases. The uncertainty in J_2 based on in-orbit tracking is illustrated in Figure 4-55 as a function of orbit period.

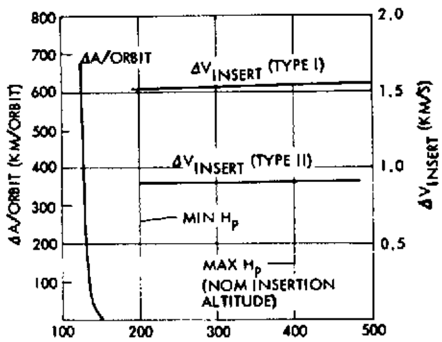

Figure 4-104. Periapsis Altitude Selection

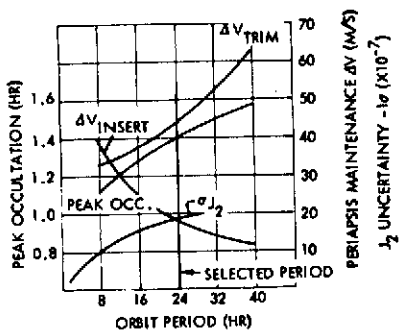

Figure 4-105. Orbit Period Selection

4.4.3 Orbit Insertion Analysis

The orbit insertion burn is the critical maneuver of the orbiter mission. This section summarizes the tradeoffs associated with that maneuver.

4.4.3.1 Nominal Requirements

The nominal requirements of the insertion maneuver are illustrated in Figure 4-106 for the nominal parameters of interest. The minimum V_{HP} is 4.9 and 3.2 km/sec for the Type I and Type II mission, respectively, with slight increases over the launch period. The periapsis altitude is nominally 400 km, but will vary with the accuracy of the approach trajectory

$\mathcal{V}$

control. The data illustrated are for a 24-hour period orbit. The requirements will vary with period as illustrated in Figure 4-105. The nominal ΔV insert is important because it has a significant impact on fuel weight and mission reliability.

4.4.3.2 Arrival Condition Variations

If a solid rocket motor (SRM) is used for the insertion burn, it must be sized before launch. Therefore variations in the arrival conditions will cause errors in the post-insertion period, even assuming no navigation or execution errors. The magnitude of these variations is illustrated in Figure 4-107. The result of these variations determines the strategy that should be used in sizing the SRM. The optimal policy is to size the orbit insertion motor for the minimum V_{HP} over the launch period and assume that no midcourse fuel remains. Then if the spacecraft arrives heavy or arrives on a date with higher than the minimum V_{HP}, it will be inserted into a higher than nominal period orbit. However, if it arrives heavy it will have extra midcourse fuel available for trims, so that even after trimming back to the desired period some of the extra midcourse fuel will be available for trim maneuvers. The trim fuel bedget must have adequate fuel to account for the V_{HP} variations.

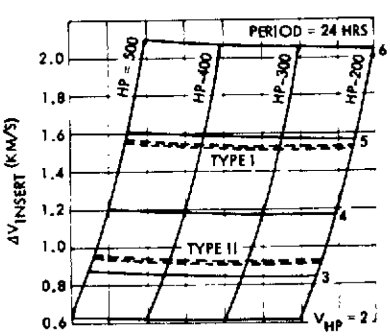

Figure 4-106. Nominal Insertion Requirements

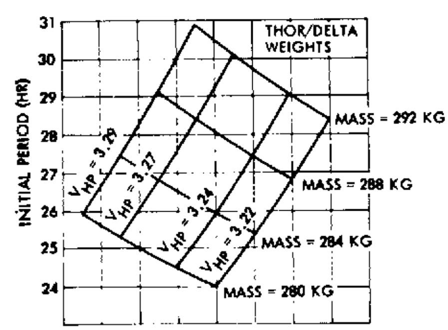

Figure 4-107. Arrival Condition Variations

4.4.3.3 Insertion Dispersions

Insertion dispersions are caused by two contributions: tracking erro and maneuver execution errors. Tracking errors before the final midcour dominate the errors in the control of the approach trajectory. Tracking uncertainties at the time of the insertion command (knowledge errors) result in errors in the timing and attitude of the burn. Execution errors at the insertion maneuver itself must be considered, although they may be ignored at the third midcourse because of the small size of that maneuver. The important tradeoffs are illustrated in Figure 4-108.

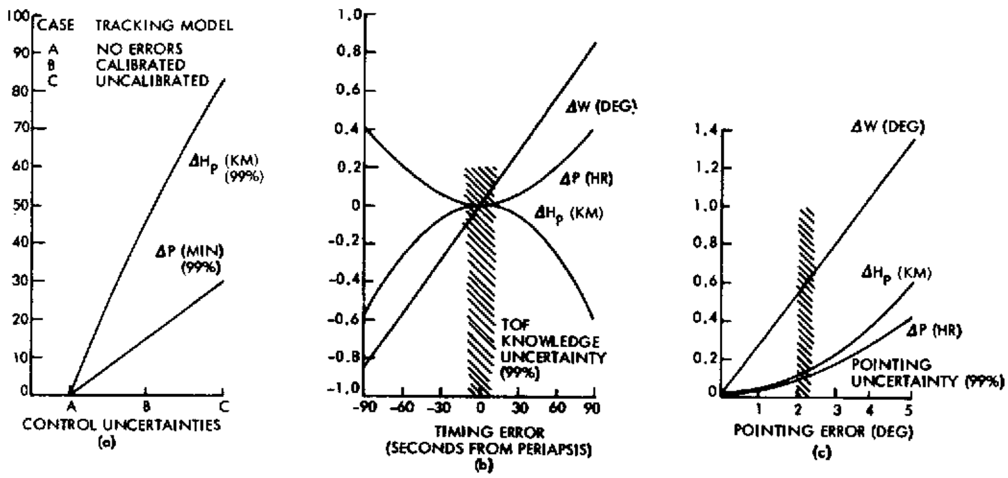

Figure 4-108. Insertion Dispersion Sensitivities

Orbit insertion dispersions are dominated by errors in the control of the approach trajectory, which in turn are determined by the tracking accuracy of the approach trajectory prior to the final midcourse. The tracking characteristics of the Type I and II approach trajectories are discussed in detail in Section 4.4.14. The results of the control error on orbit insertion parameters for the Type II mission are illustrated in Figure 4-108a. The prime parameter affected is periapsis altitude. If charged particle calibration is used, the 99% uncertainty in altitude is 47 km; if no calibration is used the corresponding uncertainty is increased to 84 km. Trajectory control errors contribute to the period errors through the periapsis altitude error: firing the fixed magnitude solid rocket motor at an incorrect periapsis altitude causes the period errors illustrated in the figure. The periapsis location error caused by control errors is less than 1 degree in all cases. For comparison, the control error impact is even greater in the Type I mission because of the worse tracking characteristics, resulting in periapsis altitude errors (99 percent) of 142 km and 421 km for calibrated and uncalibrated tracking, respectively, based on a θ_{AIM} of 110 degrees.

The insertion commands must be loaded prior to the actual insertion maneuver. Predictions based on tracking up to the loading of that maneuver therefore include errors caused by the accuracy of the tracking. The dominant error caused by these knowledge uncertainties in the error in the predicted time of periapsis passage. Figure 4-108b illustrates the results of timing errors of ± 90 seconds. Since the estimated knowledge uncertainty in periapsis time is ± 12 seconds (99 percent), its impact on dispersions is slight. Ignition system errors on the order of a minute also have a minor contribution to dispersions. The extremely small dispersions in periapsis altitude (< 1 km) should be noted.

Insertion maneuver execution errors also affect the period and periapsis location much more strongly than periapsis altitude. Figure 4-10 indicates dispersion sensitivities of pointing errors. Pointing errors are caused by attitude determination/control and by dynamic errors during firing and therefore may be controlled somewhat by the system design. The predicted design region is indicated on the figure. Again the dominant effects are in period and periapsis location. The well-established value of the proportionality error of the solid rocket motor is less than 1 percent; its effect is most strongly felt in the period error with a sensitivity of 0.8 hour per percent for a 24-hour orbit.

4.4.4 Orbit Perturbations and Trim Periapsis Maintenance

The trajectory of the orbiter following insertion is determined by the basic gravitational attraction of Venus perturbed by several smaller forces. In this section the effects of these perturbative forces are quantified and means of controlling them assessed.

4.4.4.1 Perturbative Forces

The major perturbative forces on the orbiter include planet non-sphericity, atmospheric drag, third body gravitational effects, and solar pressure. Solar gravity is by far the dominant perturbation with a magnitude of 10^{-3} relative to the Venus force at periapsis and producing periapsis variations of hundreds of kilometers during a 225-day mission for practical orbit periods. For 24-hour orbits the solar perturbation is one-sixth that of the Venus gravitational force at apoapsis. The three dominant zonal harmonics, J_2, J_3, and J_4, are of significantly lower magnitude producing periapsis variation in terms of kilometers. Atmospheric drag is essentially insignificant as long as periapsis altitudes of greater than 140 km are maintained (see Figure 4-104). The other perturbations may be safely ignored: the earth and Jupiter gravitational effects are each on the order of 10^{-8} while solar pressure results in a force 10^{-10} that of Venus.

4.4.4.2 Periapsis Altitude Maintenance

Because of the dynamical perturbations, the periapsis altitude will vary during the 225-day mission. To control this variation with acceptable limits, trims are performed at apoapsis periodically in the mission. The current strategy is based on controlling periapsis altitude between 200 and 400 km. The baseline mission periapsis altitude time history is illustrated in Figure 4-94.

In the preferred strategy, whenever the periapsis altitude is increasing and surpasses the upper limit, a trim maneuver lowers the next periapsis altitude to the lower limit unless a partial correction allows periapsis to have a (local) maximum exactly at the upper limit. Similar actions are taken on lower limit violations. The second and fourth trims in the baseline mission are partial trims allowing minimum trim level requirements. The periapsis altitude maintenance requirements for alternate inclinations and periods were summarized in Figures 4-103 and 4-105.

The trim budget is a function of the upper and lower limits placed on the periapsis altitude. Figure 4-109 demonstrates the trades. The lower altitude limit is kept at 200 km while the upper limit is allowed to vary from 225 to 400 km. The result is that the number of trims required increases significantly as the tolerance band is decreased, but with each maneuver being smaller the total ΔV budget does not increase significantly. The altitude tolerance band can be tightened at the prime penalty of an increase in mission operations complexity. The knee of the maneuver number curve occurs at the tolerance band of approximately 100 km.

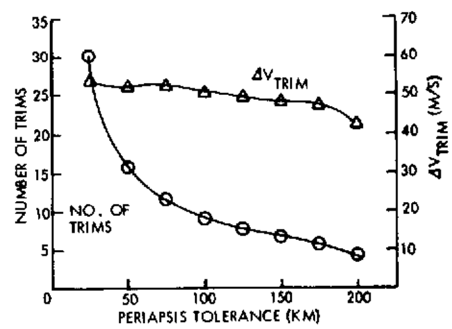

Figure 4-109. Periapsis Altitude Control

4.4.4.3 Initial Orbit Trims

Because of arrival condition variations (Section 4.4.3.2) and insertion dispersions (Section 4.4.3.3) the initial orbit achieved will not be the designed orbit. Trim budget allocations need not be made for the errors caused by extra midcourse fuel as the excess fuel will be used to trim out the errors. However, other initial orbit errors must be considered.

An adaptive policy is advisable for these trims. Again referring to Figure 4-94, if the initial periapsis altitude is high the first trim would be designed to drop the altitude immediately to about 225 km altitude and the periapsis maintenance trim originally scheduled for 30 days would be delayed. If the initial periapsis were low no initial trim would be necessary, as the solar perturbations would naturally raise it to the upper limit. Thus the initial orbit trim requirements are closely related to the periapsis maintenance strategy and trim budget allocated to them will likely form a trim budget reserve.

4.4.5 In-Orbit Tracking

Effective tracking of the orbiter is necessary for accurate predicts for the trim maneuvers and can yield instructive data on the gravitational field of the planet.

4.4.5.1 Maneuver Implications

Table 4-49 summarizes the assumptions used in the tracking analysis. The consider parameter uncertainties are based on the Lorell-Kaula dimensional analysis study. Figure 4-110 illustrates the behavior of the uncertainties in periapsis altitude and period during a single orbit of tracking for the preferred mission (Type II, 24-hour period, 400-km periapsis, $\theta_{AIM} = 120$). One full orbit of tracking produces one-sigma uncertainties of 0.07 km in altitude and 0.4 seconds in period. When the orbit parameter uncertainties are propagated forward, the dynamic parameter uncertainties cause them to increase only slightly. Predicting forward two orbits results in uncertainties in periapsis altitude of 0.07 km and period of 1.1 seconds when the Lorell-Kaula estimates of harmonic uncertainties are used. Even when those harmonic uncertainties are increased by an order of magnitude the uncertainties in altitude and period are increased to only 0.11 km and 1.2 seconds respectively. Thus the in-orbit tracking characteristics of the preferred orbit are acceptable for determining the evolving orbit perturbations and predicting times and magnitudes of trim maneuvers.

Table 4-49. In-Orbit Tracking Assumptions

NOMINAL MASS DISTRIBUTION:	SPHERICAL	
CONSIDER PARAMETER SIGMAS:		
	M:	$2.39\ KM^3/S^2$
	J_2:	6.8×10^{-6}
	J_3:	3.58×10^{-6}
	J_4:	2.28×10^{-6}
	C22, S22:	1.92×10^{-6}
	C31, S31:	1.46×10^{-6}
DOPPLER NOISE:	1 MM/S (1 MIN COUNT TIME)	
A PRIORI SIGMAS - POSITION:	10 KM	
VELOCITY:	1 M/S	
TRACKING STATIONS:	GOLDSTONE, MADRID, CANBERRA	

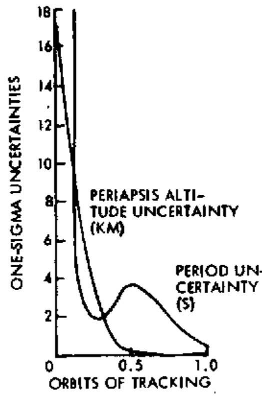

Figure 4-110. In-Orbit Tracking Effectiveness

Alternative orbits were analyzed to determine the sensitivity of in-orbit tracking to orbit selection. Orbits with θ_{AIM} = 90 and 135 degrees were analyzed with the tracking results differing from those of θ_{AIM} = 120 degrees by less than 10 percent.

4.4.5.2 Celestial Mechanics Measurements

The in-orbit tracking data may also be used to measure the gravitational parameters of the planet. Figure 4-111 illustrates the effectiveness of solving for J_2 from tracking of the orbiter motion. The most effective tracking is done near periapsis. The first periapsis passage is extremely helpful; subsequent passages add less information. The tracking ability improves significantly with shorter period as discussed in Section 4.4.2.4. If sufficient fule is available, it is recommended to trim to a short period orbit late in the mission.

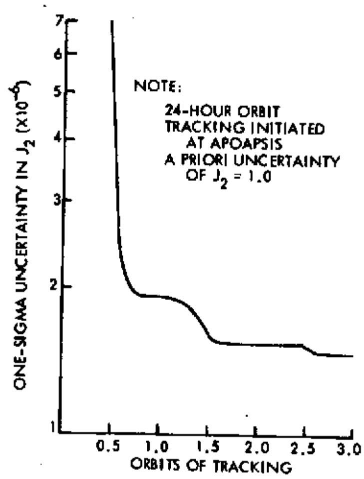

Figure 4-111. Evolving Solution for J_2

4.4.6 Mission Options

4.4.6.1 Drag Circularization

To improve the ability to solve for the gravitational harmonics, it would be desirable to have a low period orbit as discussed in the previous section. A method of accomplishing this at the end of the mission is to allow the spacecraft to continually dip into the Venus atmosphere. These repeated energy losses would eventually circularize the orbit. However, the atmospheric drag also causes a heat increase in the orbiter. Figure 4-112 indicates the number of days it would take to circularize the orbit as a function of the energy loss per orbit. For the maximum allowable heat input that can be tolerated the process would take 400 days. It would also require accurate maneuvers every orbit to control the periapsis altitude from becoming too low. It is impractical to reduce period in this way. Therefore, if lower period orbits are required, trim maneuvers are necessary.

4.4.6.2 Station Synchronous Orbits

Mission operations are simplified if the orbit is synchronized with the view times of DSN stations. For example, a single crew could be trained for all apoapsis activity such as loading for trim maneuvers. If earth and Venus were stationary, orbit periods commensurate with 24 hours (e.g., 8, 12, 24 hours) would result in such station synchronous orbits. However, because of the relative earth-Venus motion the optimal period actually varies during the mission. Figure 4-113 demonstrates the times that Venus enters and exits from view of Goldstone. It demonstrates that an orbit whose period is controlled at 24 hours would have the same orbit phase in view of Goldstone throughout the mission.

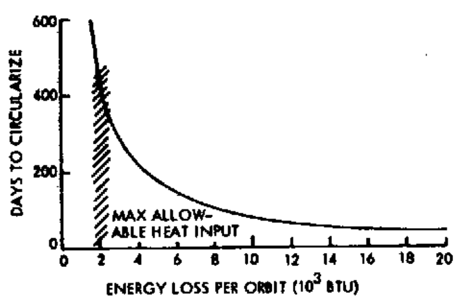

Figure 4-112. Drag Circularization

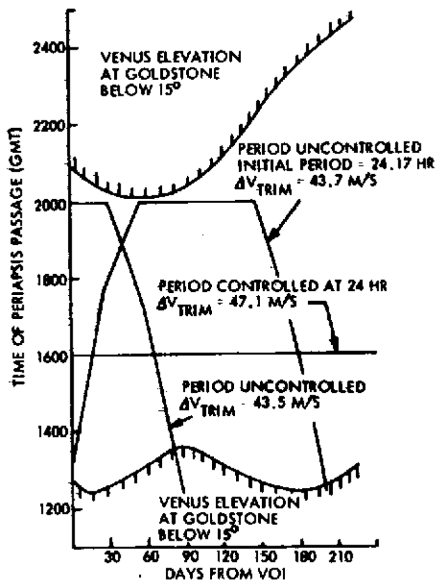

Figure 4-113. Station-Synchronous Orbits

The trim policy defined in Section 4.4.2.2 makes no attempt to control period and therefore loses synchronization after the first trim maneuver. An orbit with periapsis initially in view of Goldstone would have periapsis out of view of Goldstone in 80 days if the standard policy were used. If period trim maneuvers were made at periapsis following each periapsis maintenance trim (made at apoapsis) the period could be kept at 24 hours with four extra maneuvers and an additional ΔV of 4 m/s. Maneuvers near apoapsis that would control both period and periapsis increase each trim by about 25 percent. Another option would be to initially bias the orbit period to 24.17 hours. Then the standard periapsis maintenance trim strategy also adjusts the period to keep periapsis in view of a single station throughout the mission. It should be noted that at certain times earth occultations occur that preclude viewing by any station.

REFERENCES

1. Request for Proposal 2-18975 (JH-14) for a Systems Design Study of the Pioneer Venus Spacecraft using an Atlas Centaur Launch Vehicle, ARC, 13 October 1972, Appendix D.

2. E. D. Vogt et al., "Space Trajectories Error Analysis Programs," MCR-71-3, Contract NAS5-11795, Martin Marietta Report.

3. B. G. Lee and R. J. Boain, "Propellant Requirements for Midcourse Velocity Requirements," AIAA 11th Aerospace Sciences Meeting, Washington, D.C., January 1973. AIAA Paper 73-173.

4. Additional Delta 2914 Injection Covariances for 90 RPM Spin Rate, Letter dated 3 November 1972 from NASA/ARC, ASD: 244-9/22-277.

5. "Report of a Study by the Science Steering Group," Ames Research Center, NASA, Moffett Field, California (June 1972).

6. "Space Vehicle Design Criteria (Environment), Models of Venus Atmosphere," NASA SP-8011 (1972).

7. I. I. Shapiro, "Differential VLBI Tracking of Entry Probes," Report to Pioneer Venus Science Steering Group (May 1972).

8. Schaaf, S. A. and Chambré, P. L., "Flow of Rarefied Gases," Section H of Volume III, "Fundamentals of Gas Dynamics," in the High Speed Aerodynamics and Jet Propulsion Series, Princeton University Press, 1958.

9. Allen, H. J., "Gas Dynamics Problems of Space Vehicles," NASA Document SP-24, "Gas Dynamics in Space Exploration," December 1962.

10. Fay, J. A. and Riddell, F. R., "Theory of Stagnation Point Heat Transfer in Dissociated Air," Journal of the Aeronautical Sciences, February 1958.

11. Vogenitz, F. W., Broadwell, J. E., and Bird, G. A., "Leading Edge Flow by the Monte Carlo Direct Simulation Technique," AIAA Journal, Vol. 8, p. 504, 1970.